

Mathematical and Statistical Investigation of Steamflooding in Naturally Fractured Carbonate Heavy Oil Reservoirs

by

Ali Shafiei

A thesis

presented to the University of Waterloo

in fulfillment of the

thesis requirement for the degree of

Doctor of Philosophy

in

Earth Sciences

Waterloo, Ontario, Canada, 2013

© Ali Shafiei 2013

AUTHOR'S DECLARATION

I hereby declare that I am the sole author of this thesis. This is a true copy of the thesis, including any required final revisions, as accepted by my examiners.

I understand that my thesis may be made electronically available to the public.

Abstract

A significant amount of Viscous Oil (e.g., heavy oil, extra heavy oil, and bitumen) is trapped in Naturally Fractured Carbonate Reservoirs also known as NFCRs. The word VO endowment in NFCRs is estimated at ~ 2 Trillion barrels mostly reported in Canada, the USA, Russia, and the Middle East. To date, contributions to the world daily oil production from this immense energy resource remains negligible mainly due to the lack of appropriate production technologies. Implementation of a VO production technology such as steam injection is expensive (high capital investment), time-consuming, and people-intensive. Hence, before selecting a production technology for detailed economic analysis, use of cursory or broad screening tools or guides is a convenient means of gaining a quick overview of the technical feasibility of the various possible production technologies applied to a particular reservoir. Technical screening tools are only available for the purpose of evaluation of the reservoir performance parameters in oil sands for various thermal VO exploitation technologies such as Steam Assisted Gravity Drainage (SAGD), Cyclic Steam Stimulation (CSS), Horizontal well Cyclic steam Stimulation (HCS), and so on. Nevertheless, such tools are not applicable for VO NFCRs assessment without considerable modifications due to the different nature of these two reservoir types (e.g., presence and effects of fracture network on reservoir behavior, wettability, lithology, fabric, pore structure, and so on) and also different mechanisms of energy and mass transport. Considering the lack of robust and rapid technical reservoir screening tools for the purpose of quick assessment and performance prediction for VO NFCRs under thermal stimulation (e.g., steamflooding), developing such fast and precise tools seems inevitable and desirable.

In this dissertation, an attempt was made to develop new screening tools for the purpose of reservoir performance prediction in VO NFCRs using all the field and laboratory available data on a particular thermal technology (vertical well steamflooding). Considering the complex and heterogeneous nature of the NFCRs, there is great uncertainty associated with the geological nature of the NFCRs such as fracture and porosity distribution in the reservoir which will affect any modeling tasks aiming at modeling of processes involved in thermal

VO production from these types of technically difficult and economically unattractive reservoirs. Therefore, several modeling and analyses techniques were used in order to understand the main parameters controlling the steamflooding process in NFCRs and also cope with the uncertainties associated with the nature of geologic, reservoir and fluid properties data. Thermal geomechanics effects are well-known in VO production from oil sands using thermal technologies such as SAGD and cyclic steam processes. Hence, possible impacts of thermal processes on VO NFCRs performance was studied despite the lack of adequate field data.

This dissertation makes the following contributions to the literature and the oil industry: Two new statistical correlations were developed, introduced, and examined which can be utilized for the purpose of estimation of Cumulative Steam to Oil Ratio (*CSOR*) and Recovery Factor (*RF*) as measures of process performance and technical viability during vertical well steamflooding in VO Naturally Fractured Carbonate Reservoirs (NFCRs). The proposed correlations include vital parameters such as *in situ* fluid and reservoir properties. The data used are taken from experimental studies and also field trials of vertical well steamflooding pilots in viscous oil NFCRs reported in the literature. The error percentage for the proposed correlations is < 10% for the worst case and contains fewer empirical constants compared with existing correlations for oil sands. The interactions between the parameters were also considered. The initial oil saturation and oil viscosity are the most important predictive factors. The proposed correlations successfully predicted steam/oil ratios and recovery factors in two heavy oil NFCRs. These correlations are reported for the first time in the literature for this type of VO reservoirs.

A 3-D mathematical model was developed, presented, and examined in this research work, investigating various parameters and mechanisms affecting VO recovery from NFCRs using vertical well steamflooding. The governing equations are written for the matrix and fractured medium, separately. Uncertainties associated with the shape factor for the communication between the matrix and fracture is eliminated through setting a continuity boundary condition at the interface. Using this boundary condition, the solution method employed differs from

the most of the modeling simulations reported in the literature. A Newton-Raphson approach was also used for solving mass and energy balance equations. *RF* and *CSOR* were obtained as a function of steam injection rate and temperature and characteristics of the fractured media such as matrix size and permeability. The numerical solution clearly shows that fractures play an important role in better conduction of heat into the matrix part. It was also concluded that the matrix block size and total permeability are the most important parameters affecting the dependent variables involved in steamflooding.

A hybrid Artificial Neural Network model optimized by co-implementation of a Particle Swarm Optimization method (ANN-PSO) was developed, presented, and tested in this research work for the purpose of estimation of the *CSOR* and *RF* during vertical well steamflooding in VO NFCRs. The developed PSO-ANN model, conventional ANN models, and statistical correlations were examined using field data. Comparison of the predictions and field data implies superiority of the proposed PSO-ANN model with an absolute average error percentage $< 6.5\%$, a determination coefficient (R^2) > 0.98 , and Mean Squared Error (*MSE*) < 0.06 , a substantial improvement in comparison with conventional ANN model and empirical correlations for prediction of *RF* and *CSOR*. This indicates excellent potential for application of hybrid PSO-ANN models to screen VO NFCRs for steamflooding. This is the first time that the ANN technique has been applied for the purpose of performance prediction of steamflooding in VO NFCRs and also reported in the literature. The predictive PSO-ANN model and statistical correlations have strong potentials to be merged with heavy oil recovery modeling softwares available for thermal methods. This combination is expected to speed up their performance, reduce their uncertainty, and enhance their prediction and modeling capabilities.

An integrated geological-geophysical-geomechanical approach was designed, presented, and applied in the case of a NFCR for the purpose of fracture and *in situ* stresses characterization in NFCRs. The proposed methodology can be applied for fracture and *in situ* stresses characterization which is beneficial to various aspects of asset development such as well placement, drilling, production, thermal reservoir modeling incorporating geomechanics

effects, technology assessment and so on. A conceptual study was also conducted on geomechanics effects in VO NFCRs during steamflooding which is not yet well understood and still requires further field, laboratory, and theoretical studies. This can be considered as a small step forward in this area identifying positive potential of such knowledge to the design of large scale thermal operations in VO NFCRs.

“Ability is of little account without opportunity.” Napoleon Bonaparte

Acknowledgements

I would like to express my deepest gratitude and appreciation to my PhD thesis adviser, Professor Maurice B. Dusseault, first of all for inviting me to Canada and providing me with this great opportunity to work with him on “heavy oil recovery” which I found it really “heavy” at first especially for a pure Engineering Geologist by background but later extremely interesting and fascinating. Second, I thank him for his guidance, moral and financial support, inspiration, and encouragement during the term of my studies in uWaterloo.

I would also like to thank Professor Ioannis Chatzis, Professor Mario Coniglio, and Professor Stephen G. Evans, for serving as my committee members at various stages from comprehensive examination to the final examination in addition to providing me with useful and constructive comments for this dissertation.

I would like to express my sincere gratitude and appreciation to Professor Ian D. Gates, external examiner from University of Calgary, for his valuable comments.

I wish to acknowledge the financial support from the Natural Sciences and Engineering Research Council (NSERC) of Canada for parts of my studies.

I would like to thank Ms. Susan Fisher (Graduate Secretary) and Ms. Lorraine Albrecht (Secretary) of the Department of Earth & Environmental Sciences and Ms. Agnes Kolic (Administrative Assistant, Faculty of Science Graduate Studies) for their kind and timely administrative support during the term of my studies in uWaterloo.

I wish to thank Mr. Bahman Samimi Sadeh, former project manager of the Kuh-e-Mond Heavy Oil Field development project with PEDEC-NIOC, for providing me with available reservoir, geological, and geophysical logs and data which I used in developing part of this dissertation.

Special thank goes to Ken Schuldhuis and Poinciana Jear from Alberta Energy and Utilities Conservation Board (ERCB) for providing me with a number of progress reports on field pilots of Cyclic Steam Stimulation conducted in bitumen saturated Grosmont formation in Alberta back in the late 1970’s.

I had the opportunity to receive encouragement and support from many individuals at some point down the road in the past decade or so which helped me greatly to clarify and prioritize things, choose the right direction, and pave the road toward my academic goals. I wish to especially thank: Professor Mohammad Reza Kamali, Professor Mansour Gholami, Professor S. M. Farouq Ali, Professor Kambiz Sadaghiani, Professor Ebrahim Vasheghani Farahani, Professor Ali Suat Bağcı, Professor Hossein Memarian, Professor Sue Horton, and Mrs. Betty A. Dusseault.

I made so many great friends in Waterloo and had the opportunity to meet many brilliant men and women which made my life much more enjoyable. I would like to especially thank Dr. Keyvan Nowruzi, Mehdi Behnamjou, and Dr. Shahpour Moradi for their friendship and support during the course of my studies in uWaterloo.

I would like to express my sincere appreciation to my friend and colleague, Dr. Sohrab Zendejboudi, for his friendship and support in and out of the graduate school during the term of my studies in uWaterloo. I benefited greatly from his deep knowledge, understanding, and insight for my work.

Last, but not least, I would like to express my deepest gratitude, love, and appreciation to my dear parents: Manizheh and Yousef for their unflagging love, moral support, and encouragement throughout my life. I could not be standing at this point today without the freedom you provided me with from early in my life to pursue my dreams, for which I am always thankful, despite the ups and downs I encountered, failures experienced, and difficulties faced while discovering the true meaning of life, exploring new people and things, which made my life a wonderful and magnificent journey so far.

Dedication

To my dear parents: Manizheh and Yousef, for their unflagging love and support.

“What we call the beginning is often the end. And to make an end is to make a beginning. The end is where we start from.”

— T.S. Eliot

Table of Contents

AUTHOR’S DECLARATION.....	ii
Abstract.....	iii
Acknowledgements.....	vii
Dedication.....	ix
Table of Contents.....	x
List of Figures.....	xxi
List of Tables.....	xxix
Chapter 1 Introduction.....	1
1.1 Problem Statement.....	1
1.2 World Viscous Oil Endowment in NFCRs.....	4
1.3 Reservoir Technical Screening Criteria and Approaches.....	7
1.4 Thermal Reservoir Modeling.....	14
1.4.1 Mathematical Modeling and Experimental Work.....	14
1.4.2 Empirical Models or Correlations.....	16
1.4.3 Connectionist and Smart Techniques.....	16
1.5 Theoretical Orientation.....	17
1.6 Thesis Aims, Objectives, and Methodology.....	19
1.6.1 Aims and Objectives.....	19
1.6.2 Methodology.....	20
1.7 Organization and Presentation.....	22
1.7.1 Chapter 1: Introduction.....	23

1.7.2 Chapter 2: Viscous Oil Resource: From Genesis to Production and Upgrading....	23
1.7.3 Chapter 3: New Correlations for Prediction of Steam to Oil Ratio and Recovery Factor during Steamflooding in Naturally Fractured Carbonate Heavy Oil Reservoirs .	23
1.7.4 Chapter 4: A New Mathematical Model for Steamflooding in Naturally Fractured Carbonate Heavy Oil Reservoirs	24
1.7.5 Chapter 5: A New Smart Screening Tool for Evaluation of Steamflooding Performance in Naturally Fractured Carbonate Heavy Oil Reservoirs	24
1.7.6 Chapter 6: Geomechanics of Thermal Oil Production in Sandstones	25
1.7.7 Chapter 7: Geomechanics of Thermal Oil Production from Naturally Fractured Carbonate Reservoirs.....	25
1.7.8 Chapter 8: Fracture Characterization and In situ Stresses Inference in a Naturally Fractured Carbonated Heavy Oil Reservoir – An Integrated Geophysical-Geological Approach	26
1.7.9 Chapter 9: Major Contributions, Conclusions, and Recommendations	26
1.7.10 Bibliography	27
1.7.11 Appendices	27
Nomenclature	28
Chapter 2 Viscous Oil Resource: From Genesis to Production and Upgrading.....	30
2.1 Abstract	30
2.2 Definitions.....	31
2.3 Reservoir Definitions	34
2.4 Chemistry	36
2.5 Viscous Oil Origins, Geological Setting and Resource Base Estimates.....	40
2.5.1 Viscous Oil Origins	40

2.5.2 Geographical Distribution and Resource Base Estimates	42
2.5.3 Canadian Oil Sand Deposits	45
2.5.4 Venezuelan Viscous Oil Deposits	53
2.5.5 Other Major Viscous Oil Deposits	57
2.6 VONFCRs	63
2.6.1 Iran	63
2.6.2 Turkey	65
2.6.3 Oman	68
2.6.4 Egypt	70
2.6.5 Kuwait	71
2.6.6 Rest of the world	72
2.7 <i>In situ</i> Viscous Oil Production Technologies	72
2.7.1 Historical Development	72
2.7.2 Surface Mining	74
2.7.3 Viscous Oil Production Technologies	77
2.7.4 Technical Screening Criteria for VO Production	80
2.7.5 VO Production Cost Estimates	80
2.7.6 Non-Thermal Commercialized Methods	81
2.7.7 Cold Production	81
2.7.8 Commercialized Thermal Methods	85
2.7.9 Emerging Methods	97
2.7.10 Hybrid Approaches and Sequencing of Technologies	103

2.7.11 Steam Generation	105
2.7.12 Further Technical Issues.....	107
2.8 Upgrading and Transportation	108
2.8.1 Non-Catalytic Processes in VO Upgrading.....	110
2.8.2 Catalytic Processes in VO Upgrading	114
2.8.3 Future Developments in Upgrading	119
2.9 Viscous Oil Transportation	120
2.10 Environmental Issues	121
2.10.1 Surface Mining Solid Wastes	122
2.10.2 Surface Mining Liquid Wastes and Sludges.....	123
2.10.3 <i>In situ</i> Viscous Oil Recovery Processes	123
2.10.4 Sulfur and Coke	125
2.10.5 General Waste Management Options.....	125
2.10.6 Zero Emissions Targets	128
2.10.7 Greenhouse Gas Emissions	129
2.10.8 Water Issues.....	130
Nomenclature	131
Chapter 3 New Correlations for Prediction of Steam to Oil Ratio and Recovery Factor during Steamflooding in Naturally Fractured Carbonate Heavy Oil Reservoirs.....	135
3.1 Abstract	135
3.2 Introduction.....	135
3.2.1 Steamflooding.....	139

3.2.2 Production Mechanisms	142
3.3 CSOR and RF Prediction.....	143
3.4 Data collection.....	146
3.5 Methodology	155
3.5.1 Multivariable Regression Analysis.....	155
3.6 Results and Discussion.....	159
3.6.1 Regression Analysis	160
3.6.2 Screening of a HO Field for Steamflooding.....	188
3.7 Limitations and assumptions for the correlations of CSOR and RF	193
3.8 Concluding Remarks	194
Nomenclature	198
Chapter 4 A New Mathematical Model for Steamflooding in Naturally Fractured Carbonate Heavy Oil Reservoirs.....	202
4.1 Abstract	202
4.2 Introduction.....	202
4.2.1 Naturally Fractured Reservoirs.....	206
4.2.2 Steamflooding in NFCRs.....	212
4.3 Mathematical Formulation	213
4.3.1 Model Assumptions.....	214
4.3.2 Governing Equations	214
4.3.3 Auxiliary Equations.....	218
4.3.4 Fluid and Rock: Physical, Thermal, and Thermodynamic Properties.....	220

4.3.5 Boundary and Initial Conditions.....	224
4.4 Solution Method.....	227
4.4.1 Mesh Size and Configuration.....	231
4.4.2 Equations Discretization.....	232
4.4.3 Validation of of the Results.....	239
4.5 Results and Discussion.....	239
4.5.1 Effect of Matrix Permeability.....	240
4.5.2 Effect of Fracture Aperture.....	241
4.5.3 Effect of Matrix Size.....	242
4.5.4 Effect of Injection Rate.....	243
4.5.5 Effect of Formation Thickness.....	245
4.5.6 Effect of Reservoir Porosity.....	246
4.5.7 Effect of Oil Viscosity.....	247
4.5.8 Fractured Versus Unfractured Systems.....	249
4.6 Limitations.....	252
4.7 Concluding Remarks.....	253
Nomenclature.....	258
Chapter 5 A New Smart Screening Tool for Evaluation of Steamflooding Performance in Naturally Fractured Carbonate Heavy Oil Reservoirs.....	263
5.1 Abstract.....	263
5.2 Introduction.....	264
5.3 Steamflooding.....	268

5.4 Artificial Neural Network	270
5.5 Particle Swarm Optimization	273
5.6 ANN Model Development	275
5.6.1 Selection of Input Variables	275
5.6.2 Data Collection and Model Evaluation	276
5.6.3 Range of Parameters	277
5.7 Results and Discussion	278
5.7.1 Sensitivity Analysis	293
5.7.2 Case Study	295
5.8 Limitations	298
5.9 Concluding Remarks	299
Nomenclature	303
Chapter 6 Geomechanics of Thermal Oil Production in Sandstones.....	307
6.1 Abstract	307
6.2 Introduction	307
6.3 Thermally Induced Stresses in Reservoir Rocks.....	313
6.4 Thermal Reservoir Simulation and Numerical Modeling.....	313
6.5 Geomechanical Behavior of Reservoir Rocks at Elevated Temperatures.....	316
6.5.1 Thermal Characteristics of Rocks at Elevated Temperatures.....	317
6.5.2 Chemical Reactions	320
6.5.3 Ultrasonic Velocities of Unconsolidated Sandstones.....	320
6.5.4 Geomechanical Properties of Rocks at Elevated Temperatures.....	321

6.6 Thermal Geomechanics Effects in Sandstones/Oil Sands (SAGD Case)	327
6.7 Caprock Integrity and Thermally Induced Casing Shear Mechanisms.....	333
6.8 Concluding Remarks	335
Nomenclature	337
Chapter 7 Geomechanics of Thermal Oil Production from Naturally Fractured Carbonate	
Reservoirs	341
7.1 Abstract	341
7.2 Introduction	342
7.3 Viscous Oil in NFCRs.....	348
7.4 Thermal Methods in VO NFCRs	351
7.5 Commercialized Thermal VO Production Techniques in NFCRs	352
7.5.1 <i>In Situ</i> Combustion	354
7.5.2 Steam Processes.....	359
7.5.3 Thermally Assisted Gas Oil Gravity Drainage.....	361
7.5.4 SAGD	363
7.6 Thermally Induced Stresses in Reservoir Rocks.....	366
7.7 Thermal Reservoir Simulation and Numerical Modeling.....	366
7.8 Carbonate Rocks at High Temperature	371
7.8.1 Thermal Conductivity and Diffusivity	371
7.8.2 Physical Properties	373
7.8.3 Geomechanical Behavior.....	374
7.9 Discussion	378

7.9.1 Temperature, Stress, Shear, Dilation	378
7.9.2 Comparison to Unconsolidated Sandstone Behavior	379
7.9.3 Thermally Induced Casing Shear Mechanisms	383
7.9.4 Geomechanics Effects in NFCRs (Steamflooding Case)	384
7.10 Concluding Remarks	389
Nomenclature	392
Chapter 8 Fracture Characterization and <i>In situ</i> Stresses Inference in a Naturally Fractured Carbonated Heavy Oil Reservoir – An Integrated Geophysical-Geological Approach	396
8.1 Abstract	396
8.2 Introduction	396
8.2.1 Naturally Fractured Reservoirs	397
8.2.2 Natural Fractures Impacts on Field Development	398
8.2.3 Origin and Classification of Natural Fractures	400
8.2.4 Classification of Naturally Fractured Reservoirs	405
8.2.5 Evaluation of Fractures and Fields	406
8.2.6 Fluid Flow and Stress Coupling in NFRs	407
8.2.7 The Need to Characterize NFRs	408
8.2.8 Stresses	409
8.3 Fracture Characterization Techniques	411
8.3.1 Outcrop Studies and Core Analysis	411
8.3.2 Seismic Techniques	412
8.3.3 FMI and UBI	415

8.4 Earth Stresses – Geological Inference.....	415
8.4.1 Stresses and Effective Stresses.....	415
8.4.2 Stress Orientation Determination	416
8.4.3 Stress Magnitude Estimation.....	418
8.4.4 Pore Pressure	419
8.4.5 Geomechanical Implications	420
8.4.6 Anomalous Horizontal Stress Orientations	420
8.5 Kuh-e-Mond Heavy Oil Field	420
8.6 Results and Discussion.....	423
8.6.1 Field Geological and Core Studies	423
8.6.2 Seismic Surveys.....	424
8.6.3 FMI and UBI	432
8.6.4 Origins of Natural Fractures in the Study Area.....	439
8.7 Geological Inference of Stress State at the Kuh-e-Mond.....	441
8.7.1 Core Analysis	441
8.7.2 Borehole Images.....	442
8.7.3 Magnitude of the <i>In Situ</i> Principal Stresses.....	443
8.7.4 Orientations of the <i>In Situ</i> Stresses.....	444
8.8 Concluding Remarks	446
Nomenclature	450
Chapter 9 Major Contributions, Conclusions, and Recommendations.....	452
9.1 Major Contributions	452

9.2 Conclusions	453
9.3 Recommendations	454
9.3.1 Assemble a Database for World Disposition of VO in NFCRs	454
9.3.2 Conduct Systematic Numerical Modeling and Laboratory Investigations.....	454
Appendix A Multi-Variable Regression Analysis	457
Appendix B Numerical modeling program for steamflooding.....	467
Appendix C Artificial Neural Network and Particle Swarm Optimization program.....	494
Bibliography	524

List of Figures

Figure 1-1: Idealization of dual porosity reservoir (Modified from: Warren and Root, 1963).	6
Figure 1-2: Reservoir technical screening flow chart.	13
Figure 2-1: A typical T- μ plot for Athabasca bitumen (106 cP@10°C).....	32
Figure 2-2: A graphical demonstration of the oil definitions used in this dissertation.	33
Figure 2-3: A resources classification scheme proposed by the SPE/WPC/AAPG (Modified from: Ross, 2001).....	35
Figure 2-4: A proposed model for VO generation (From: Head <i>et al.</i> , 2003).....	40
Figure 2-5: Geographical distribution of VO in the world (Dusseault and Shafiei, 2011; GEA, 2012).	43
Figure 2-6: Geographical distribution of VO in the world in sandstones and/or oil sands (Dusseault and Shafiei, 2011; GEA, 2012).....	44
Figure 2-7: Geographical distribution of VO in carbonates (Dusseault and Shafiei, 2011; GEA, 2012).	44
Figure 2-8: Geographical distribution of the major VO deposits in Canada.	45
Figure 2-9: Resource based estimates of the major VO deposits in Canada (AERCB, 2010, with minor modifications).....	46
Figure 2-10: Technically recoverable oil with current technology and price in Canada (AERCB, 2010, with minor modifications).....	46
Figure 2-11: Viscosity-Temperature relationships for the major VO deposits in Canada and Venezuela (Modified from Meyer and Attanasi, 2004).....	48
Figure 2-12: VO production methods.	78
Figure 2-13: Cold Production using long horizontal wells and multilaterals.	82
Figure 2-14: The original concept of <i>In Situ</i> Combustion process.	86
Figure 2-15: Steam Drive concept.	88
Figure 2-16: Vertical well Cyclic Steam Stimulation process.....	90
Figure 2-17: Horizontal well cyclic steam stimulation.....	92
Figure 2-18: Steam Assisted Gravity Drainage (SAGD) concept.	94

Figure 2-19: Toe-to-Heel Air Injection (THAI™) concept.....	99
Figure 2-20: Schematic view of process zones in THAI™ (Adopted from M. Greaves, 2008).	100
Figure 2-21: CO ₂ injection (ideal condition).	103
Figure 2-22: Using PPT to accelerate steam chamber growth in SAGD.....	104
Figure 2-23: Carbon rejection and hydrogen addition for viscous oils.	109
Figure 2-24: Simplified schematic of the delayed coking process (From: Gray, 1994).	112
Figure 2-25: Simplified schematics of fluid coking process (From: Gray, 1994).	113
Figure 2-26: Simplified schematics of visbreaking process (From: Gray, 1994).	114
Figure 2-27: Simplified schematics of fluid catalytic cracking (From Gray, 1994).	115
Figure 2-28: Simplified schematics of fixed bed catalytic process (From Gray, 1994).	116
Figure 2-29: Simplified schematics of ebullated bed catalytic process (From Gray, 1994).	117
Figure 2-30: The major Canadian and U.S. oil pipelines (From: ERCB, 2012).	121
Figure 2-31: SAGD Development, eastern Alberta. Courtesy David Dodge, Pembina Institute.	124
Figure 2-32: Permanent disposal methods for liquid and solid wastes.	127
Figure 2-33: Deep Injection Facility for Solid and Liquid Wastes, Duri Oilfield, Indonesia. The black area is a concrete pit for viscous fluids and solids in transit. Duri Oilfield has close to Zero Discharge status.	128
Figure 3-1. Steamflooding in NFCRs (Steamed zone is presented in red).	140
Figure 3-2: <i>CSOR</i> vs. oil viscosity for the database analyzed.	162
Figure 3-3: <i>CSOR</i> vs. steam injection rate for the database analyzed.	163
Figure 3-4: <i>CSOR</i> vs. fracture to matrix permeability ratio for the database analyzed.	164
Figure 3-5: <i>CSOR</i> vs. gross to net thickness ratio for the database analyzed.	165
Figure 3-6: <i>CSOR</i> vs. steam quality for the database analyzed.	166
Figure 3-7: <i>CSOR</i> vs. oil saturation for the database analyzed.....	167
Figure 3-8: <i>CSOR</i> vs. oil content for the database analyzed.....	168
Figure 3-9: <i>CSOR</i> vs. $1/K \times \phi$ for the database analyzed.	169

Figure 3-10: Residuals vs. porosity for the database analyzed.....	170
Figure 3-11: Residuals vs. gross to net thickness ratio for the database analyzed.	171
Figure 3-12: <i>RF</i> vs. steam flow rate for the database analyzed.....	172
Figure 3-13: <i>RF</i> vs. oil viscosity for the database analyzed.	173
Figure 3-14: <i>RF</i> vs. fracture permeability to matrix permeability ratio for the database analyzed.	174
Figure 3-15: <i>RF</i> vs. gross to net thickness ratio for the database analyzed.....	175
Figure 3-16: <i>RF</i> vs. steam quality for the database analyzed.	176
Figure 3-17: <i>RF</i> vs. oil saturation for the database analyzed.....	177
Figure 3-18: <i>RF</i> vs. Producibility factor for the database analyzed.	178
Figure 3-19: <i>RF</i> vs. oil content for the database analyzed.....	179
Figure 3-20: Residuals vs. product of steam injection rate and quality for the database analyzed.	180
Figure 3-21: Residuals vs. porosity for the database analyzed.....	181
Figure 3-22: Geographical location of the Kuh-e-Mond heavy oil field.....	189
Figure 4-1: Idealized dual porosity reservoir model (Modified from Warren and Root, 1963).	207
Figure 4-2: Idealistic view of Steamflooding in NFRCs (Steamed zone is presented in red).	213
Figure 4-3: A schematic of (a) differential element and (b) A side view of the physical model.....	215
Figure 4-4: The developed numerical model with two vertical wells as injector and producer (This is an aerial view).....	228
Figure 4-5: Flowchart of the numerical modeling study for VO NFRCs.....	231
Figure 4-6: Average oil saturation during steamflooding vs. PV in fractured reservoirs for different matrix permeabilities; fracture permeability (K_f) = 5 D.	241
Figure 4-7: Effect of fracture aperture on oil recovery before breakthrough during steamflooding; Matrix permeability (K_m) = 20 mD.....	242
Figure 4-8: Effect of matrix size on oil production during steamflooding.	243

Figure 4-9: Recovery factor vs. PV of injected steam for different injection rates.	244
Figure 4-10: Effect of formation thickness on SOR for fractured and homogeneous systems [Injection rate = 2000b/d, area = 8 acers, and fracture permeability = 20 D].....	245
Figure 4-11: Effect of oil saturation on recovery factor for different porosity values.	247
Figure 4-12: Steamflooding performance versus oil viscosity; a) Recovery Factor, b) Cumulative Steam Oil Ratio	249
Figure 4-13: <i>CSOR</i> vs. time for homogeneous and fractured reservoirs; Injection rate = 2000 b/d, area = 8 acers, fracture permeability = 20 D.	250
Figure 4-14: Variation of production rate for fractured and unfractured systems under steamflooding; Injection rate = 2000 b/d, area = 8 Acers, and fracture permeability = 20 D.	251
Figure 5-1: Resource estimates and worldwide distribution.....	265
Figure 5-2: Steamflooding in NFCRs (Steam zone is presented in red).....	269
Figure 5-3: A three layer ANN structure used for the purpose of this study.....	271
Figure 5-4: Particle Swarm Optimization method work flow.	275
Figure 5-5: Real field vs. predicted <i>RF</i> based on BP-ANN; a) Training, b) Testing.	283
Figure 5-6: Real field vs. predicted <i>RF</i> based on PSO-ANN; a) Training, b) Testing.	284
Figure 5-7: Measured vs. predicted <i>CSOR</i> based on BP-ANN; a) Training, b) Testing.	285
Figure 5-8: Measured vs. predicted <i>CSOR</i> based on PSO-ANN; a) Training, b) Testing....	286
Figure 5-9: Scatter diagrams for steamflooding - <i>RF</i> based on BP-ANN in terms of R^2 ; a) Training, b) Testing.	288
Figure 5-10: Scatter diagrams for steamflooding - <i>RF</i> based on PSO-ANN in terms of R^2 ; a) Training, b) Testing.	289
Figure 5-11: Scatter diagrams for steamflooding - <i>CSOR</i> based on BP-ANN in terms of R^2 ; a) Training, b) Testing.	290
Figure 5-12: Scatter diagrams for steamflooding - <i>CSOR</i> based on PSO-ANN in terms of R^2 ; a) Training, b) Testing.	291
Figure 5-13: Relative impacts of main independent variables on <i>RF</i> and <i>CSOR</i> during SF.	294
Figure 5-14: Geographical location of the Kuh-e-Mond heavy oil field.	296

Figure 6-1: Surface uplift (+ Δz) above a SAGD project in Canada.	311
Figure 6-2: A schematic model of stresses in a laterally extensive reservoir (Dusseault, 1993).	315
Figure 6-3: Thermal diffusivity of Bandera Sandstone.	318
Figure 6-4: Volume thermal expansion of three tested sandstones.	319
Figure 6-5: Compressional (V_p) and shear velocities (V_s) in VO saturated reconstituted sample.	321
Figure 6-6: Sandstone (compression); Young's modulus parallel and perpendicularly to the isotropic plane.	322
Figure 6-7: Stress-Strain curve obtained for the tested sandstone samples at elevated temperature.	323
Figure 6-8: Strain-time curves for the Felser sandstone under different differential stresses at 150°C to 250°C.	324
Figure 6-9: Shear test results for dense and loose sand: From left to right: Shear stress – lateral displacement, shear stress – normal effective stress (Mohr-Coulomb shear yield diagram), and volumetric strain – lateral strain.	328
Figure 6-10: Thermally induced shear dilation in SAGD. Phase A: Initial stage of a SAGD operation. Phase B: A mature SAGD operation. These sketches show how horizontal stresses increase during a thermal operation.	330
Figure 6-11: The geometry of the SAGD and thermally induced stresses. Typically, $H = 20$ to 35 m, $W/H \approx 3.5$ to 4 and $L = 750$ to 1000 m.	331
Figure 6-12: Schematic view of thermally induced shearing in unconsolidated sandstones.	335
Figure 7-1: Wedging, or crack opening strain from rotational displacements, increases fracture aperture (top) and flow capacity; shear of natural fractures leads to self-propping and permanent increases in flow capacity.	345
Figure 7-2: Volume change effects during slurried solids injection into a NFR.	346
Figure 7-3: World resource estimates and distribution of VO in both clastics and carbonates.	349
Figure 7-4: World resource estimates and distribution of VO NFCRs.	349

Figure 7-5: A basin-tectonic context for VO deposits (From: Eschard and Huc, 2008).	350
Figure 7-6: Viscous oil production methods.....	353
Figure 7-7: TA-GOGD in the Qarn Alam VO NFCR (From: Shahin <i>et al.</i> , 2006).....	362
Figure 7-8: A schematic model of stresses in a laterally extensive reservoir (Dusseault, 1993).	368
Figure 7-9: Thermal diffusivity of a limestone (Data from Somerton and Boozer, 1961)...	372
Figure 7-10: Stress-strain curve for limestones at elevated temperature (From Zhang <i>et al.</i> , 2009).	375
Figure 7-11: Effect of thermal shock on non-fractured carbonate core permeability (Data from Zekri and Chaalal, 2001).....	376
Figure 7-12: Effect of thermal shocks on fracture carbonates core permeability (Data from Zekri and Chaalal, 2001).....	377
Figure 7-13: Stress-Strain relationship before and after thermal shocks for different temperatures (Base case: TZ2 Specimen # 1 tested at 25°C. TZ6 Specimen # 2 tested at 300°C) (Data from Zekri and Chaalal, 2001).	378
Figure 7-14: Typical dilation potential (maximum) for a quartzose 30% porosity oil sand.	380
Figure 7-15: Schematic view of thermally induced shearing in unconsolidated sandstones.	383
Figure 7-16: Early-time steaming of a blocky NFCR at depth of ~ 250–300 meters.....	386
Figure 7-17: Favored slip directions for a regular orthogonal array of fractures subjected to a heating process in a strongly differential stress field.....	388
Figure 8-1: World stress map showing stress data compiled from various sources. In oil and gas regions, borehole measurements are an important source of present-day <i>in situ</i> stress information. This basic information is used in modeling to help understand fracture networks in fields worldwide (From: the World Stress Map Project, http://www-wsm.physik.uni-karlsruhe.de).....	399
Figure 8-2: Shear fracture on a shear joint surface in limestone from Iran.	401
Figure 8-3: Tensile fracture on a tensile joint surface in cordierite hornfels from Iran.....	402
Figure 8-4: Principal stresses and the creation of low angle conjugate fractures.	403
Figure 8-5: Naturally fractured reservoir classification system (From: Nelson, 2001).....	406

Figure 8-6: Side View Seismic Location technique (SVSL) (From: Kouznetsov <i>et al.</i> , 2001).	413
Figure 8-7: Geological cross-section of the Kuh-e-Mond anticline (x-section courtesy of PEDEC).....	421
Figure 8-8: Lithostratigraphic column of the reservoirs at the Kuh-e-Mond field (Modified from Bordenave and Burwood, 1990).	422
Figure 8-9: Vertical fractures and vugs infilled with heavy oil in a core sample from Kuh-e- Mond field (Photo courtesy of PEDEC).	424
Figure 8-10: 3-D view of open fracture distribution throughout the Kuh-e-Mond field (intensity) (Photo courtesy of PEDEC).....	425
Figure 8-11: Cross-line of open fractures distribution at azimuth 277 in Kuh-e-Mond field (Photo courtesy of PEDEC).	426
Figure 8-12: Variation of the mean value (a) and relative variance (b) of fracturing within horizontal (1) and lateral slices (2).	428
Figure 8-13: SVSL results (Photo courtesy of PEDEC).....	430
Figure 8-14: Summary plot of the features identified and picked out from FMI (track 2) and UBI (track 4) images in the Well MD-8 (Photo courtesy of PEDEC).....	433
Figure 8-15: Resistive fractures on the FMI (track 2) image indicated by magenta arrows (Figure 10). Minor open fractures on the UBI (tracks 4 and 6) image (cyan arrows, below) (Photo courtesy of PEDEC).	434
Figure 8-16: Two highly fractured zones in Sarvak I interval on FMI (track 2) and UBI (tracks 4 and 6) logs (Photo courtesy of PEDEC).	436
Figure 8-17: A good example of fractures that are seen both on UBI (tracks 4 and 6) and FMI (track 2) images (Photo courtesy of PEDEC).	437
Figure 8-18: Upper section: a snapshot from a section containing a number of bedding features and a minor open fracture (tracks 4 and 6). Below right is a 3-D view of the same section showing the orthogonal relationship between fractures and beddings. Below left is an azimuth rosette and dip histogram of bedding and open fractures showing an orthogonal relationship (Photo courtesy of PEDEC).	438

Figure 8-19: Orientation of regional stresses in the Arabian Peninsula based on borehole breakouts and drilling induced fracture data (Modified from Akbar and Sapru, 1994) (Photo courtesy of PEDEC).....	440
Figure 8-20: Rose diagram of trends of natural fractures from core analysis.	442
Figure 8-21: Rose diagram of trends of natural fractures measured in image logs.	443
Figure 8-22: The orientation of the <i>in situ</i> principal stresses in the study area.	444
Figure 8-23: World Stress Map generated for the study area to infer the orientation of the <i>in situ</i> stress field (Courtesy of the World Stress Map Project) (Heidbach <i>et al.</i> , 2008).....	445

List of Tables

Table 1-1: Technical screening criteria for VO production from oil sands	9
Table 2-1: Gross composition of bitumen from Alberta, Canada (From: Strausz, 1977).	38
Table 2-2: Properties and SARA fractionation results for Athabasca and Cold Lake bitumen (Rahimi and Gentzis, 2006).	38
Table 2-3: Some chemical and physical properties of viscous oils (averages) (From: Mayer and Attanasi, 2004).	39
Table 2-4: Average geologic, reservoir and fluid properties of the major VO deposits in Canada.....	47
Table 2-5: Average geologic, reservoir and fluid properties of the VO deposits in FPO and Maracaibo Basin.	56
Table 2-6: Average geologic, reservoir and fluid properties of selected VO deposits from Kuwait, Kazakhstan, China, and Iran.	59
Table 2-7: Major <i>in situ</i> production technologies for VO (Dusseault and Shafiei, 2011; GEA, 2012).	75
Table 2-8: Estimated production costs for VO production with various methods.	79
Table 3-1: Screening Criteria for SF/SD/CSS in oil sands (Dusseault, 2012).....	141
Table 3-2: Characteristics of the successful steamfloods conducted in fractured reservoirs.	153
Table 3-3: Regression model of the <i>CSOR</i> ($R^2 = 0.962$; $F = 196.645$).	183
Table 3-4: Information for the Linear Regression Model of the <i>RF</i> prediction ($R^2 = 0.964$; $F = 79.317$).	185
Table 3-5: ANOVA table for <i>CSOR</i> regression analysis.....	186
Table 3-6: ANOVA Table for <i>RF</i> during steamflooding.....	186
Table 3-7: Summary of the Statistical Linear Regressions.....	187
Table 3-8: Performances of previous predictive models, and statistical correlations obtained in the current study.....	188
Table 3-9: Reservoir and fluid properties of reservoirs at the Kuh-e-Mond HO field.	191

Table 3-10: Range of variables to estimate RF and CSOR	193
Table 5-1: Range of parameters to predict RF and $CSOR$	277
Table 5-2: Performance of the PSO-ANN model based on the number of hidden neurons.	279
Table 5-3: Performance of the PSO-ANN model for different values of c_1 and c_2	280
Table 5-4: Effect of number of particles on performance of the PSO-ANN model.	281
Table 5-5: Performances of the PSO-ANN model, BP-ANN model, and statistical correlations.....	292
Table 5-6: Reservoir and fluid properties of the Kuh-e-Mond HO reservoirs.	297
Table 7-1: Physical properties of limestone (Yavuz <i>et al.</i> , 2010).	373

Chapter 1

Introduction

1.1 Problem Statement

In this section, the problem and issues to be addressed throughout this research work are identified and defined. Then, methodologies and solutions are proposed to solve the defined problems. The major issues raised here are further delineated in the subsequent sections, subsections, and or chapters.

As a preliminary step toward a better understanding of the performance of complex reservoirs such as Viscous Oil (e.g., heavy oil, extra heavy oil, and bitumen) Naturally Fractured Carbonate Reservoirs (VO NFCRs) under thermal processes in the absence of appropriate reservoir screening tools, a number of questions needs to be addressed. Furthermore, various aspects of reservoir modeling and performance analysis in VO NFCRs still remain ill-understood or not well-addressed, mainly due to the fact that developing these reservoirs using thermal processes has attracted the attention of the oil industry as well as the scientific communities and the governments very recently, barely a decade ago, if we ignore the limited vertical well cyclic stimulation pilots attempted in Alberta back in the late 1970's:

Why does the contribution of VO NFCRs (almost 100% from primary cold production) to the world daily oil production remains negligible compared with conventional oil production or production from VO sandstones?

What are the major technical obstacles in the way of developing this vast energy resource? Are there any robust and rapid screening tools available for the purpose of preliminary technical screening schemes? Are there any appropriate models or modeling approaches available which take into account the effects of fracture network properties, permeability ratio, heat transfer, and rock/fluid interactions on fluid flow, production rates of the phases, and consequently the cumulative oil production?

Technical screening criteria exist for a variety of commercialized cold and thermal VO production techniques thanks to over six decades of VO production experience from oil sands (e.g., see [Dusseault \(2012\)](#) for a set of screening criteria suggested for various technologies for oil sands) and VO sandstone reservoirs mainly located in California, Canada, and Venezuela. How performance predictions can be made for VO NFCRs in the absence of sufficient good quality field data of various thermal VO exploitation techniques? The stage of technology application, maturity in terms of long runs of field experience, energy efficiency, process optimization level, and the number of active thermal operations (i.e., availability of large amounts of process data), in oil sands production is at least 50 years ahead of VO NFCRs. Clearly, application of thermal processes for the purpose of VO exploitation from VO NFCRs is in its infancy at this time.

Technical screening tools (economic screening tools are not examined herein despite the fact that technical feasibility study parameters also speak to economic viability) are available for the purpose of rapid evaluation of the reservoir performance parameters in oil sands for various thermal VO exploitation technologies such as Steam Assisted Gravity Drainage (SAGD), Cyclic Steam Stimulation (CSS), Horizontal well Cyclic steam Stimulation (HCS), and so on. Nevertheless, such tools are not applicable for VO NFCRs assessment without considerable modifications due to the different nature of these two reservoir types (e.g., presence and effects of fracture network on reservoir behaviour, wettability, lithology, fabric, pore structure, and so on) and also different mechanisms of energy and mass transport. The question yet to be answered here is how new screening tools can be developed in order to predict reservoir performance using all the available data on a particular thermal technology (e.g., steamflooding or cyclic steam processes) piloted or field implemented in VO NFCRs? Is it technically reasonable to include data from fractured sandstone reservoirs saturated with VO? Are such tools going to be capable of prediction of the reservoir performance for any types of VO reservoirs including the two major types (sandstones and NFCRs) assuming that the tools developed for VO NFCRs represent higher complexity tools compared with the

existing screening tools developed solely for oil sands (e.g., dual or triple porosity systems versus single porosity system) when some terms are simplified?

A few studies have been reported on modeling thermal processes in oil sands and VO saturated sandstones based on high-quality field data of full-field commercialized projects (the criteria for a full-field commercialized operation are steady production yielding over 10,000 b/d over several years). In such a case, reservoir performance can be predicted with an acceptable degree of precision, managed, and monitored to gradually achieve improved oil recovery and thermal efficiency (e.g., higher recovery factor (*RF*) and lower cumulative steam-oil ratio (*CSOR*)). Such thermal models are incapable of prediction of VO NFCRs performance during major thermal VO recovery methods. What types of models and modeling approaches can be developed and verified using the available actual data and laboratory data to develop robust screening and predictive tools for a particular thermal process applied to VO NFCRs?

There is great uncertainty associated with the geological nature of the NFCRs such as fracture and porosity distribution in the reservoir. This affects modeling of processes involved in thermal VO production from these types of reservoirs. What tools or techniques can be implemented to lower the degree of uncertainty when modeling reservoir performance for a particular thermal method (e.g., steamflooding) in VO NFCRs?

What are the effects of properties of oil and steam such as viscosity, temperature, and injection fluid quality on the performance of a VO NFCR during thermal oil recovery (e.g., steamflooding)?

Geomechanics effects are well-known in VO production from oil sands using thermal technologies such as SAGD and cyclic steam processes. What are the possible impacts of thermal processes on VO NFCRs performance? How do fracture properties affect reservoir performance during thermal oil recovery (e.g., steamflooding)? What are the major effects of introducing heat (steam) on fractured rock mass behaviour? Can we expect an enhancement in reservoir behaviour and quality (e.g., increase in reservoir permeability, increase in matrix

permeability, improvement in wettability and so on) similar to what has been observed and experienced in thermal operations in oil sands over the past few decades? What are the differences between the thermal effects in VO NFCRs compared to oil sands?

NFCRs are also known as stress-sensitive reservoirs, meaning a strong flow-stress dependency exists (i.e., fracture apertures change as stress changes), and therefore fluid flow and recovery mechanisms will be significantly affected by the presence of natural fractures. In thermal processes such as steam injection into an NFCR, large thermal stresses are generated in the reservoir. How can the possible impacts of such stress changes (geomechanics effects) on reservoir performance predictions be considered in technology assessment?

A few studies combining mathematical modeling and statistical investigation have been reported on steamflooding in VO NFCRs, but research works including experimental, pilot plant, and also full-field data are very rare in the open literature. Some experimental approaches and numerical models have been introduced but have not discussed and elaborated on practical field applications and their application to develop useful screening criteria for steamflooding processes in NFCRs. Hence, the technical feasibility of application of steam-based VO exploitation methods in NFCRs needs to be further investigated.

1.2 World Viscous Oil Endowment in NFCRs

Sedimentary rocks cover around 70% of the earth crust; one-third of this is different types of carbonate sedimentary rocks. Carbonate sedimentary rocks differ from terrigenous sedimentary rocks in several ways (Akbar *et al.*, 2000). As much as 50–60% of the world's present proven conventional petroleum reserves are in NFCRs (e.g., Roehl and Choquette, 1985). Hence, NFCRs evaluation has been a high priority for researchers in oil and gas production for many decades, but the challenges presented by these highly heterogeneous rocks seem to be never-ending.

The world endowment of VO in both clastic (consolidated or unconsolidated sandstones) and carbonate rocks (mostly limestone and dolomite) is estimated by the United States

Geological Survey (USGS) and others to be in the order of 9000×10^9 b [1430×10^9 m³] (Meyer and Dietzman, 1981; Meyer and Duford, 1989; Meyer and Attanasi, 2004; Meyer *et al.*, 2007; Schenk *et al.*, 2009, CAPP, 2009; BGR, 2009; IEA, 2009; Dusseault and Shafiei, 2011; GEA, 2012), over two times the conventional oil resource of about 4500×10^9 b [715×10^9 m³]. The world's VO resources in NFCRs are also estimated to be $1500\text{--}2200 \times 10^9$ b [$238\text{--}35 \times 10^9$ m³] (Briggs *et al.*, 1988; Shafiei *et al.*, 2007; Dusseault and Shafiei, 2011; GEA, 2012).

Almost 100% of the VO production from NFCRs comes from cold production operations in Oman, Iran, Iraq, Kuwait, Saudi Arabia, Turkey, and Mexico of mainly lower viscosity VO; mainly heavy oil with some degree of mobility under *in situ* reservoir conditions (Dusseault, 2001; Shafiei *et al.*, 2007; Dusseault *et al.* 2008; IEA, 2009; GEA, 2012). Productive VO NFCRs are characterized by low matrix permeability and high fracture permeability, giving high early production which declines rapidly, leading to *RF*s below 3–5% in many cases. Large-scale, early oil flux takes place through the high permeability, low volume fracture system, whereas the matrix-fracture interaction mainly controls the recovery efficiency and maintenance of longer-term smaller-scale production levels. VO production from NFCRs is in its very early days and is presenting major technical and economic challenges to the oil industry. These reservoirs are not yet widely commercialized and progress remains necessary for them to contribute a notable portion of the daily worldwide oil production.

Saidi (1987) defined a Naturally Fractured Reservoir (NFR) as a reservoir that contains fractures (planar discontinuities) created by natural processes (e.g., tectonic forces), distributed as a consistent connected network throughout the reservoir (Figure 1). NFRs are usually considered to be made of an interconnected fracture system that provides the main flow paths (high permeability and low storage volume), along with the reservoir rock or matrix that acts as the main source of hydrocarbons (low permeability and high storage volume). Thus, the matrix system contains most of the oil, but the oil transport to the wells is through the high permeability fracture system, implying that the matrix-fracture interaction mainly controls the fluid flow. Production from the matrix-fracture system is attributed to

various physical mechanisms including oil expansion or pressure diffusion, imbibition or saturation diffusion, gravity imbibition or drainage, mass diffusion and viscous displacement or convection. The first two mechanisms mentioned above are the predominant ones for most NFRs and the third is also important for certain reservoirs. The last two can be usually neglected, as their effect is insignificant compared to the others.

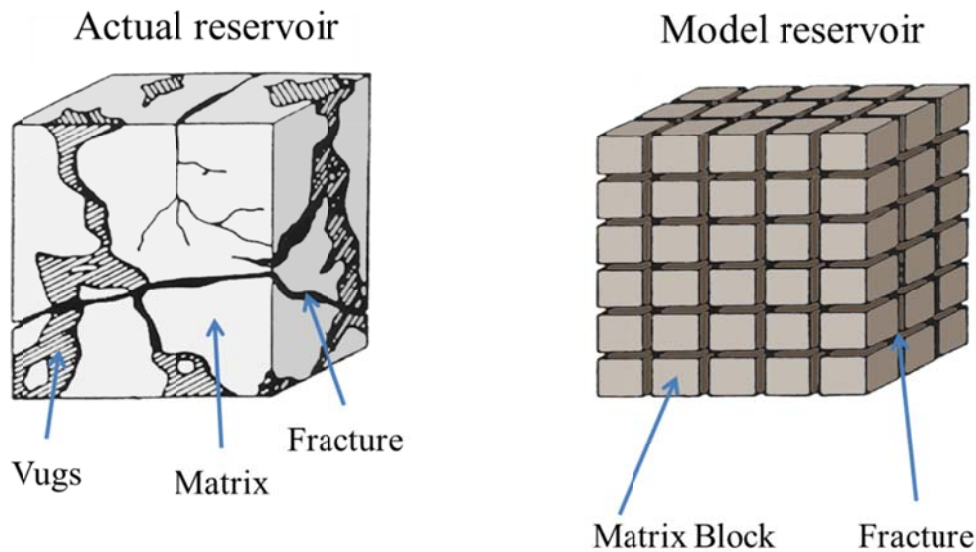


Figure 1-1: Idealization of dual porosity reservoir (Modified from: [Warren and Root, 1963](#)).

Most NFRs are actually highly fractured, and the flow behavior is controlled by this type of secondary porosity; hence, this dichotomy for NFRs seems justified. A dual porosity formulation superimposes the secondary or fracture media on the primary or matrix media and this superimposition is idealized as primary porosity coupled with the secondary porosity as shown in Figure 1-1. Also, it should be noted here that some of the NFRs contain vuggy and karst-related porosity in addition to the matrix and fracture porosity that makes flow simulation or well test interpretation in these reservoirs much more complicated than in unfractured reservoirs.

Herein, the acronym NFR is used intentionally when referring to a condition or process involving reservoir rock types other than carbonates (e.g, fractured sandstones), which is the

primary subject of interest in this research work. The term NFCRs is used when particularly referring to carbonate NFRs.

NFCRs usually demonstrate an unusual production history; initially they may appear highly productive, but then production declines rapidly. They are also well-known for early gas or water breakthrough as the low-viscosity phase migrates quickly through the fracture network. On the other hand, carbonates include some of the largest, most productive reservoirs on Earth (e.g., Ghawar oil field in Saudi Arabia which now produces $\sim 4 \times 10^6$ b/d). Also, NFCRs tend to have extremes in flow behavior with open channels and large vugs with permeabilities of many Darcies, yet with matrix permeability in the mD range. Only slow seepage is possible in the latter, yet a network of open fractures and cavities can have flow rates like a small river. Heterogeneity and scale effects also complicate the reservoir evaluation, modeling, technology screening, and oil recovery. The complicated nature of this class of reservoirs is the motivation behind the oil industry's current efforts to learn more about them and model them with a reasonable amount of certainty.

Almost all hydrocarbon reservoirs are affected in some way by natural fractures (e.g. naturally fractured sandstones), while the effects of fractures are often poorly understood and may be underestimated. [Maksimovich \(1958\)](#), using simple calculations, postulated that fractures alone contain insignificant volumes of oil and gas in carbonate reservoir rocks ([Chilingarian *et al.*, 1992](#)). This is why when the only oil present in the reservoir is that present in the fractures, then the reservoir will be depleted rapidly after initiation of the production. In NFCRs, natural fractures in the form of secondary porosity promote communication between reservoir blocks. However, these high-permeability conduits sometimes short-circuit the fluid flow within a reservoir, leading to premature water or gas production.

1.3 Reservoir Technical Screening Criteria and Approaches

Technologies required to economically extract VO *in situ*, particularly highly viscous bitumen and extra-heavy oil, have major differences compared to conventional oil. It is

usually recommended to reduce the viscosity. In practice, this can be achieved by three methods: heating, dilution, and reducing the molecular weight. Implementation of a production technology such as steam or solvent injection is expensive (high capital investment), time-consuming, and people-intensive. Hence, before selecting a production technology for detailed economic analysis, use of cursory or broad screening tools or guides is a convenient means of gaining a quick overview of the technical feasibility of the various possible production technologies applied to a particular reservoir (Taber and Martin, 1983; Taber *et al.*, 1997; Dusseault, 2012).

Technical screening criteria, largely for conventional oil or commercialized VO technologies, have been investigated comprehensively (King *et al.*, 1984; Taber *et al.*, 1997; Dusseault and El-Sayed, 2000; Dusseault, 2012). Nevertheless, technical screening criteria are not available yet for VO NFCRs as they are for oil sands due to very limited numbers of field cases and the general unavailability of adequate and sufficient data.

Some process and *in situ* parameters are vital for screening; without them, technology evaluation would be impossible or inadequate. These parameters are defined as “first order” (or “critical”) screening criteria. A “first-order” parameter potentially has a great effect (> 10%) on which technology is chosen and will directly affect the suitability ranking of feasible technologies during a general screening process applied to several development candidates. For example, viscosity certainly has > 10% “impact” on all non-thermal processes; it is vital, first-order screening parameter. First-order parameters may vary from one technology to another. For instance, reservoir depth, *in situ* oil viscosity, net pay thickness, and water/oil saturations are among first-order screening criteria for most VO production technologies. However, designing and operating a specific production approach for a specific set of conditions requires assessment of many factors, far more than in the list of first-order screening criteria. For example, thermal conductivity of the overburden will affect decisions, although it is not a first-order screening parameter. In early multiple-candidate screening phases, only first-order screening criteria including parameters related to the geological and lithostratigraphical disposition, fluid and petrophysical properties, and *in*

situ conditions required for each particular production technology are expected to be considered. First-order screening criteria are listed only for commercialized production technologies as shown in Table 1-1. It should be pointed out here that these criteria were generated for oil sands, not VO NFCRs.

Table 1-1: Technical screening criteria for VO production from oil sands.

Production Technology	Technical Screening Criteria	Reference(s)
CP (Cold Production)	Permeability > 2–4 D, but much less for lower viscosities Net pay thickness > 7–8 meters Porosity > 25% in current implementation, but lower porosities OK with high k Viscosity < 5000 cP Produceability factor (F) (kh/μ) > 15-20 mD-m/cP High solution gas content needed No free water zones (CP is a high-gradient approach)	Dusseault and El-Sayed, 2000; Chugh <i>et al.</i>, 2000; Dusseault, 2006
CHOPS (Cold Heavy Oil Production with Sand)	Permeability > 1 D average Net pay thickness > 5–6 m Viscosity < 15000 cP High solution gas content is needed Unconsolidated sandstones only (solids production is needed) Minimal free water zones	Dusseault, 2006
ISC (In situ Combustion)	Depth > 150 meters Permeability > 50 mD Porosity > 18% Oil Saturation > 50 % PV Net pay thickness > 10 meter Oil Content ($\phi \times S_o$) > 0.065 Produceability factor (F) (kh/μ) mD-m/cP (not a factor)	Greaves and Al-Shamali, 1995; Moore <i>et al.</i>, 1997; Prath, 1999

	<p>Viscosity < 5000 cP</p> <p>Local or no bottom water</p> <p>Local or no gas cap</p>	
<p>SF (Steamflooding)</p>	<p>Depth < 1400 meters</p> <p>Permeability > 200 mD</p> <p>Porosity > 20–25%</p> <p>Oil Saturation > 50% PV</p> <p>Net pay thickness > 6–10 m (100%), 20 m (80%), > 20 m (75%)</p> <p>Produceability factor (F) (kh/μ) > 15 mD-m/cP</p> <p>Oil Content > 0.065</p> <p>Current pressure < 1500 psi</p> <p>Viscosity < 2000-5000 cP</p> <p>No steam drive likely with active water</p> <p>Local or no gas cap present</p> <p>Low clay volume</p> <p>Thin shale beds < 2.5 m thick, lateral flow dominated process</p>	<p>Taber and Martin, 1983; King <i>et al.</i>, 1984; Taber <i>et al.</i>, 1997; Dusseault, 2006</p>
<p>CSS (Cyclic Steam Stimulation)</p>	<p>Depth < 1400 meters</p> <p>Permeability > 1 D</p> <p>Porosity > 20–25%</p> <p>Oil Saturation > 60% PV, preferably > 0.8</p> <p>Net pay thickness > 8–10 m (100% net-to-gross), 20 m (90%), > 20 m (85%)</p> <p>Viscosity < 500000 cP</p> <p>Formation must be unconsolidated</p> <p>No CSS possible if active water is present</p> <p>Thin shale beds only, < 1 m, or too slow recovery</p>	<p>Fialka <i>et al.</i>, 1993; Al-Qabandi <i>et al.</i>, 1995; Donnelly, 2000, Dusseault, 2006</p>

<p style="text-align: center;">HCS (Horizontal well Cyclic steam Stimulation)</p>	<p>Depth between 200–1400 meters Net pay thickness > 15 meters Oil Saturation > 60% PV Permeability > 0.5 D (k_h); > 0.25 D (k_v) Porosity > 20% Viscosity > 2000 cP No free water zones can be tolerated Low strength formation is better because of formation shearing</p>	<p>Smith and Perepelecta, 2002; Cline and Basham, 2002; Dusseault, 2006</p>
<p style="text-align: center;">SAGD (Steam Assisted Gravity Drainage)</p>	<p>Depth between 200–1000 meters Net pay thickness > 15 meters Oil Saturation > 60% PV Permeability > 2 D; k_h, > 1 D; k_v for oils >10000 cP Porosity > 20% Can handle mobile bottom water, whereas Δp methods cannot Low strength formation is better (shear enhancement of permeability) Viscosity – no limits have been identified</p>	<p>Edmunds and Sugget, 1995; Ito <i>et al.</i>, 1988; Singhal <i>et al.</i>, 1996; Llaguno <i>et al.</i>, 2002; Dusseault, 2006</p>

Typically, the following procedure is followed when screening a petroleum reservoir for a particular production technology, as summarized and presented in Figure 1-2:

- 1- Collect experimental and field data (analogues) of the petroleum reservoirs where the same production technology is applied at various scales from the laboratory to pilot plants and full-field implementation.
- 2- Extract “Technical Screening Criteria” (TSC), meaning that the economic viability of the operation is not essentially taken into account at this point, in order to determine the range of the parameters for which a particular technology works well or cannot work well. Compare the reservoirs in terms of important parameters contributing to

- the production performance (e.g., *RF* and *CSOR* in steam-flooding) determined based on the physics of the processes involved. Consider the presence of a wide variety of parameters such as fluids properties and formation characteristics. Needless to mention, such a comparative analysis relies on geological and reservoir parameters such as rock type, depth, thickness, oil saturation, presence of active aquifers, etc.
- 3- Carry out experimental studies in the laboratory and at pilot plant scales using the porous media and oils whose properties are close enough to real field cases or the target reservoirs. Clearly, an extensive Design of Experiments (DOE) is vital here in order to cover wide ranges of the process conditions (e.g., temperature and pressure), porous media characteristics, and also the physical properties of the oil samples. This phase of the study determines the most important factors affecting the target variables.
 - 4- Employ proper statistical and commercial software packages in order to evaluate the production performance of the target cases under various process and reservoir conditions. The tools usually include SAS software, and smart techniques (e.g., Artificial Neural Networks, Fuzzy Logic, Analytical Hierarchy Process) to delineate non-linear relationships between input and output variables. Such investigation also leads to generation of rank scores and importance percentages for the independent parameters.
 - 5- Combine the above stages in order to provide adequate technical guidelines to identify whether a certain production technology is can be considered as proper for a particular reservoir or not.
 - 6- Perform analytical and numerical simulations using linear programming and commercial software packages, depending on the quality and quantity of the available data, mathematical computation difficulties, and time restrictions.
 - 7- Assess the soft variables including operational expenses (OPEX), capital expenses (CAPEX), availability of the injection fluids, natural gas (for steam), and oil price.

Implementation of such a systematic study allows final decisions in terms of process both technical and economic feasibility for the production technology under question. Economic evaluation of most the feasible technologies for a particular reservoir is generally the last phase when assessing a reservoir for commercial development.

- 8- Take into account engineering considerations (e.g., safety and durability), management decisions, business opportunities and environmental concerns once a particular production technology is demonstrated to be the most effective for a particular reservoir, technically and economically, prior to full field implementation.

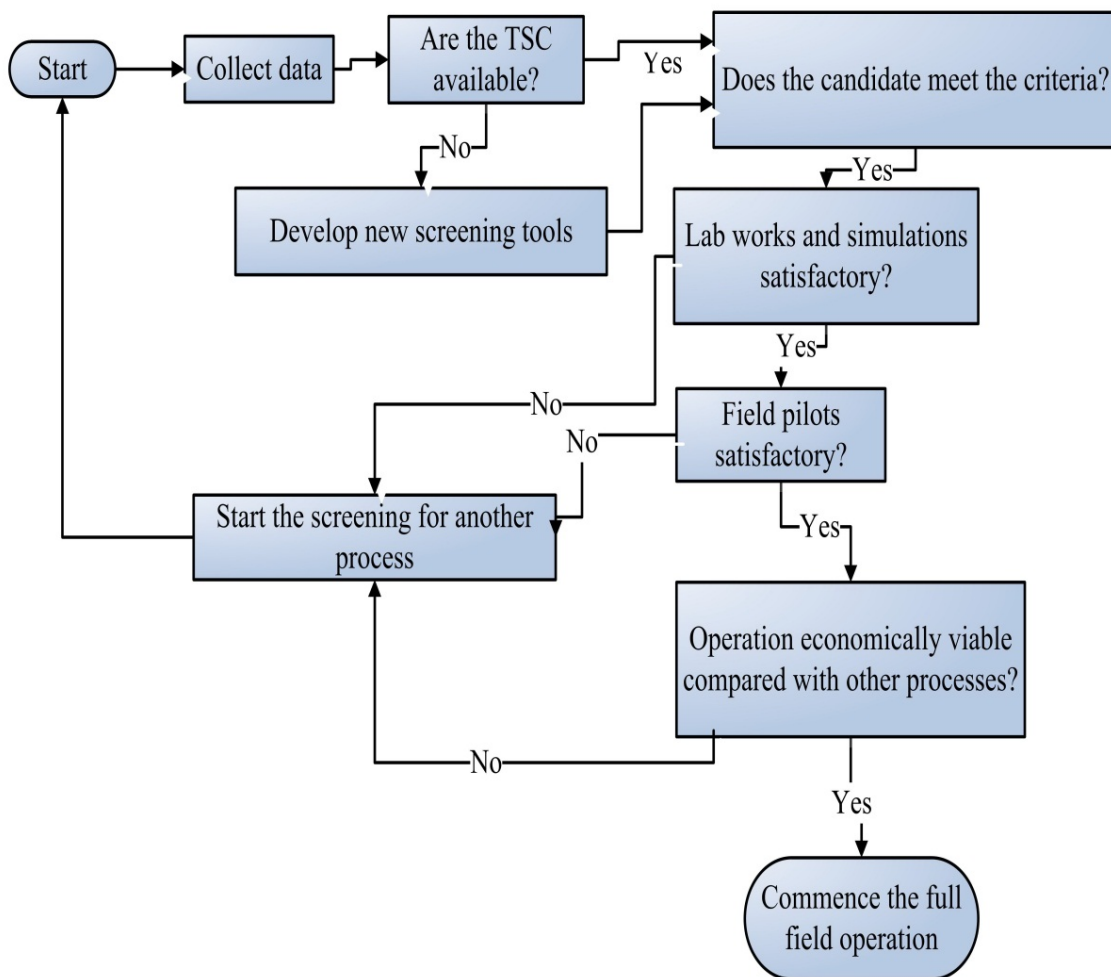


Figure 1-2: Reservoir technical screening flow chart.

1.4 Thermal Reservoir Modeling

1.4.1 Mathematical Modeling and Experimental Work

Several numerical modeling methods combined with experiments on thermal processes (e.g., steamflooding), mostly for oil sands and unconsolidated sandstones, are reported in the literature. For instance, [Miller and Leung \(1985\)](#) used a combination of a numerical modeling and software simulation runs for steam injection into a reservoir. They obtained cumulative production versus time and compared the results for both methods employed in their work; however, their model was unable to predict (or match) the production rate. In fractured systems, [Dreher *et al.* \(1986\)](#) conducted some steam and hot water injection tests; however, they did not simulate the process. [Jensen *et al.* \(1991\)](#) reported a number of core-flooding tests on fractured systems with some simulations to analyze the experimental results but a complete investigation was impossible as heat losses, temperature, and steam and oil saturation in various parts (e.g., matrix and fracture) were unknown. [Hong \(1994\)](#) studied the effects of rate and quality of steam on production performance for different situations and concluded that there is no single steam quality or injection rate that represents unequivocally optimal conditions because of the complex technical and economic aspects of steam consumption and oil prices. [Mohammadi *et al.* \(2012\)](#) conducted a study on steam injection in heavy oil reservoirs through numerical modeling; however, incorporating the fracture part into the matrix part to form a continuous model was not carried out properly.

Most of the models proposed to forecast the performance of VO reservoirs under steamflooding are based on the reservoir heating model developed by [Marx and Langenheim \(1959\)](#). The injection of hot fluid into a well is assumed to be taking place at constant injection rate and temperature according to their proposed method. The volume control considered in this model is composed of a radial flow system, with a well in the central point. The temperature in the heated zone was assumed to be constant, as well.

In the absence of appropriate models and predictive tools for VO NFCRs, all of the field pilots rely deeply on experimental work and simulations employing available commercial

petroleum engineering software such as CMGTM and ECLIPSETM. Nevertheless, only limited parameters involved in NFCRs over a narrow range of process and reservoir conditions can be examined using commercial softwares.

A number of experimental and mathematical models also are reported for performance prediction of steamflooding processes in VO sandstones. For instance, a 2-D model was introduced by [Shutler \(1970\)](#) to simulate oil, water, and gas phases in VO sandstones considering both heat conduction and convection terms in 2-D while determining the temperature profile. [Abdalla and Coats \(1971\)](#) developed a numerical model for steam injection in VO sandstones. They employed an implicit pressure-explicit saturation technique to obtain the pressure and saturation distributions of all three phases, assuming the fluids are compressible. Based on the results of their study, a model was developed to determine the rate of steam condensation. [Coats *et al.* \(1974\)](#) developed a 3-D model to conduct numerical simulations to model steam injection in VO sandstones. This model includes mass and energy balance in both reservoir and the overburden (conductive heat losses). Their solution does not require the iteration procedure while considering the condensation term.

Mass and heat transfer involved in multi-component flow were studied by [Ferrer and Farouq Ali \(1977\)](#) using a numerical model to simulate three-phase, 3-D flow during steam injection in VO sandstones. They concluded that the compositional constraints approach represents a good procedure for practical simulation purposes. [Coats \(1978\)](#) simulated distillation and solution gas phenomena in steamflooding through an implicit model. All the terms related to solution gas, distillation and capillary pressure were included in the model to investigate the variations of saturation and compositions during steamflooding. Beside the modeling studies, systematic experimental works were performed by a number of researchers such as [Sumnu *et al.* \(1996\)](#), [Mollaei *et al.* \(2007\)](#), and [Souraki *et al.* \(2011\)](#). These laboratory investigations were mostly focused on a parametric sensitivity analysis approach to capture major aspects of the steamflooding process (e.g., effects of temperature and steam quality on production mechanisms). It should be noted here that majority of the above research work is

considered to be flawed (e.g., insufficient measurements) or not applicable in real field conditions (e.g., inappropriate boundary conditions); especially for heterogeneous and dual- or triple-porosity systems such as VO NFCRs. For example, the reservoir models under laboratory study were treated as homogeneous because of their fairly small dimensions. Also, the numerical methods that were used generally faced divergence issues in attempting to incorporate the fluid/fluid and medium/medium interfaces.

1.4.2 Empirical Models or Correlations

Empirical models or correlations have not been yet developed to estimate *CSOR* and *RF* values as measures of process performance for steamflooding in VO NFCRs. However, various models and correlations are reported for performance prediction and analysis of various steam injection processes for VO production from oil sands and other unconsolidated sandstone VO reservoirs (e.g., Davidson *et al.*, 1967; Coats *et al.*, 1974; Chu and Trimble, 1975; Neuman, 1975; Myhill and Stegemeier, 1978; Farouq Ali, 1982; Gomaa, 1980; Yortsos and Gavalas 1981a and b; Neuman, 1985; Chu, 1990; Torabzadeh *et al.*, 1990; Jensen *et al.*, 1991; Gajdlca *et al.*, 1993; Jones, 1993; Donaldson and Donaldson, 1997; Edmunds and Peterson, 2007; Miura *et al.*, 2010). It is important to note that these models and correlations still suffer from high levels of error as there are some restricted applicability ranges for them in terms of operational conditions and petrophysical properties. Without modifications to account for the different production characteristics, such correlations or models cannot be used for VO NFCRs.

1.4.3 Connectionist and Smart Techniques

During the last two decades, advances in computer technology have improved the application of screening criteria via utilization of Artificial Intelligence (AI) techniques in the oil industry. The value of these programs depends on the accuracy of the input data used (For instance: Parkinson *et al.*, 1990; Parkinson *et al.*, 1991; Elemo and Elmahtab, 1993; Alvarado *et al.*, 2002; EL-M Shokir *et al.*, 2002; Ibatulin *et al.*, 2002). Artificial Neural Network (ANN) concept has been used extensively in geosciences and geophysics as well as in

reservoir engineering for prediction of reservoir and fluid properties ([Aminzadeh and De Groot, 2006](#)). This method is capable of modeling complex input-output relationships from a process with high uncertainty and still successfully identify reasonable patterns in the data.

Considering the lack of robust and rapid technical reservoir screening tools for the purpose of quick assessment and performance prediction for VO NFCRs under thermal stimulation (e.g., steamflooding), developing such fast and precise tools seems inevitable and desirable. Despite the notably smaller size of the database available for field implementation of thermal processes in VO NFCRs, such a work can be considered as the first logical step toward technical assessment of difficult and different VO reservoirs for particular processes (vertical well steamflooding in this research) until field data become more abundant so that other steps in way of developing more sophisticated tools can be taken.

1.5 Theoretical Orientation

In this section, various hypotheses associated with the proposed research are posed, providing a conceptual model of the project, identifying themes or trends that could be pursued from the literature or other data sources. The aim of this section was to demonstrate where this research project stands with respect to the topic, although this was an imprecise task at early stages of this project.

Here are the main considerations which guided this research:

In view of the past history of technology application and heavy oil production from NFCRs, it appears necessary to formulate new or modify existing screening tools for the application of particular thermal VO production technologies to VO NFCRs. Quantitative or semi-quantitative screening tools can be developed for NFCRs that permit more rational and scientifically based technology selection. In VO sandstone or oil sands, this has been partially accomplished, but apparently not in NFCRs, yet. This is quite challenging because of inadequate or insufficient data from the very few field-scale pilot projects available worldwide. Also, the complicated behavior of the fractured reservoirs in response to the fluid injection exacerbates this problem during the course of assessing and introducing

accurate predictive techniques. This issue appears not to have been addressed in the literature yet.

It is also hypothesized that these screening tools will be of a general, “first-order” nature. They will comprise geological, petrophysical, and possibly geomechanical criteria that can be quantified using seismic data, laboratory information, or borehole geophysics methods, without having recourse to the results of full-scale pilot projects (hence, they are “first-order” criteria only).

Refinement or application of some simple existing analytical models or numerical approaches for the prediction of efficiency of steam processes in VO NFCRs appears to be necessary in order to provide a better understanding of these processes in NFCRs where the volume of oil with respect to the rock mass is variable and of a dual nature (fractures versus matrix). This may lead toward establishment of more effective tools based on parameters such as thickness, initial oil saturation, *in situ* viscosity, fracture intensity, and so on. Then, assessment of the potential efficiency of a particular thermal process in NFCRs can be made. This may have particular value to the assessment of those NFCRs that appear to be economically or technically marginal, or far beyond the access of steam-based VO production technologies.

As reviewed in the literature, NFCRs have a reputation of a high flow-stress dependency (e.g. aperture of the fractures change as stress changes), and fluid flow and recovery mechanisms (gravity flow, pressure-driven flow, capillarity...) will be significantly affected by the natural fractures. It is hypothesized that new screening criteria, likely a first-order criterion or several second-order criteria, can be developed to express the sensitivity of an extraction process to the stress and fracture intensity. This will require engineering and structural geology information to be combined with geomechanical data. This represents quite a challenge but if a methodology can be developed and required data is collected then other steps can be taken toward considering geomechanical effects in thermal processes used for the purpose of VO exploitation from NFCRs. Nevertheless, to date no effect of geomechanics on reservoir performance is reported in VO NFCRs, mainly due to the small

scale (e.g., single well) nature of many field pilots to date. Additional data would be necessary to complete this task, although some of these effects can be considered in modeling tasks such as the effect of fracture properties such as aperture and length and etc. on reservoir performance.

To conduct a study on VO NFCRs, determination of some properties such as relative permeability for both matrix and fractures, communication of matrix and fracture media, and overall characteristics of the formation rocks imposes a high degree of difficulty to model development even if all the data about the fractured medium properties, production history and energy balance are provided. In this case, it is necessary to use proper techniques to cope with this high level of uncertainty and also consider the lumped properties. The current study introduces such a methodology to lower the number of unknown parameters (e.g., shape factor and total permeability) and consequently achieve good results through a more logical and straightforward method.

1.6 Thesis Aims, Objectives, and Methodology

1.6.1 Aims and Objectives

This section presents the main objectives for this dissertation. Based on the questions posed at the beginning of this chapter (Problem Statement), the following research objectives are intended to address important technical points for development of appropriate technical screening tools for steamflooding in VO NFCRs:

It is important to attain further understanding of oil production mechanisms, controlling parameters, technical issues involved in steamflooding to recover oil from VO NFCRs. To achieve this, a significant portion of public research studies regarding steamflooding in the form of theoretical, experimental, and pilot plant investigation were collected, studied, and analysed. This part of the study was intended to cover wide ranges of production data for porous media and fluids with various properties (e.g., physical and petrophysical). Collecting huge amounts of data and knowing important factors and mechanisms in steamflooding can pave the road for successful mathematical simulation of the production

behaviour of reservoirs. It is expected that an extensive mathematical model enables one to conduct a comprehensive sensitivity analysis, leading to forecasting of recovery performance of reservoirs operating under steamflooding using statistical, empirical, and neural network techniques.

New sets of screening tools for application of steamflooding in VO NFCRs depending on data availability and quality are proposed. The proposed screening tools consider the effects of the fracture network (dual-porosity system), communication between the matrix and fracture, and interrelationships between the main parameters of the fluids and rock. This has not been reported yet in the literature.

A database is established for VO NFCRs in Iran which includes: Fabric, geology (broad level geology only) and structural geology, reservoir parameters, fluid parameters, typical geophysical log response values (gamma ray, resistivity), *in situ* stresses inferred and stress history in the studied NFCRs from geological data, the origin and the characteristics of natural fractures. Probable *CSOR* and *RF* from application of steamflooding for specific reservoirs in the studies areas are presented. The predictive methods have high potential to technically and economically assess the feasibility of these practical cases prior to implementation of steamflooding technology.

Different VO production technologies and their mechanisms in various NFCRs are reviewed with special emphasis on the role of the natural fractures and overall petrophysical properties of formation rocks on the eventual success or failure of VO production technologies.

1.6.2 Methodology

In this section, procedures and research techniques employed to conduct this research are presented. It is clear that with some topics there may be several available alternative research methods, and an attempt was made to evaluate the advantages or disadvantages of the method(s) chosen and how this might affect the research process. Issues such as type of the parameters that should be collected, method(s) of data analysis, tools (e.g., software) required are addressed in this section.

The research conducted has different levels. New screening tools are developed for application of vertical well steamflooding to VO NFCRs (theory building), or to use to confirm data from actual field cases, if such cases exist (confirmation of the theoretical construct for the screening tools). Also, various topics related to the proposed hypotheses are investigated, and this is an exploratory phase to confirm the validity of the theory building aspect mentioned above, and to see if sufficient confirmatory cases exist. Finally, in an application phase, this led to evaluation of a series of Iranian HO NFCRs for steamflooding. In other words, a product of the research project is the application of the theoretical developments to practical cases (Iranian HO NFCRs).

Because of the uncertainty that characterizes geo-scientific data, this research had to be a combination of qualitative, semi-quantitative, and quantitative methods and data types. The research techniques used were also a combination of theoretical, field verification (from the literature), ANN models, and mathematical and statistical techniques at each stage. Modification and refinement of an existing model and its application for the purpose of this proposed research would be based on mathematical and statistical approaches.

Fracture characterization in the field or gathering litho-mechanical information, if field access is possible, requires application of field techniques (or special seismic or geophysical interpretations) as well. There are several methods of generating suitable data sets of this kind, and such work may in part be performed by others, or has been done already. Geomechanical characterization of a target NFCR could require implementation of experimental techniques involving detailed rock testing, but this also is likely to be done by others.

A wide variety of data were collected for the purpose of conducting this research. For example, to characterize each target NFCR from an engineering-geological point of view, data on general geology, stratigraphy, structural geology, porosity, fracturing in the target reservoir, lithologic controls, bed thickness, faulting, mineralization, subsurface structures (fractures, induced fractures, faults), fracture spacing versus bed thickness, outcrop studies to subsurface comparison and so on, was collected. Also, a wide variety of information was

collected regarding reservoir and fluids data and geophysical log data. This information was organized into a data base management environment (Excel™).

After the required data are gathered, important parameters and mechanisms for steamflooding in NFCRs are recognized. Statistical analysis of data reveals the significance order of variables and relationships between fluids and formation characteristics, and target variables (e.g., RF and $CSOR$). This stage can be a starting point to define dimensionless parameters (e.g., K_f/K_m) and also explore the interplay between various properties and/or processes. At this step, unimportant parameters (or effects) will be removed from the model under study.

Multivariable regression technique and ANN model are employed to correlate important parameters to the output variables. Wide ranges of data guarantee the validity of the developed models for different cases under steamflooding at various process and thermodynamic conditions

The statistical and ANN studies are followed by a numerical modeling simulation for both matrix and fractures. Mathematical modeling can be powerful for further investigation of steamflooding efficacy when changes in operating conditions are required to achieve greater oil recovery and further process optimization (e.g., lower $CSOR$ and higher RF during the life time of the operation).

Combination of these three deterministic approaches for steamflooding performance analysis can be used to examine the appropriateness of each computation method. If all three techniques are developed in effective ways, important decisions with regard to operational conditions of the process and their impact on oil production rate are possible to be made with high confidence, considering all restrictions present in the method.

1.7 Organization and Presentation

Each chapter represents approximately a stand-alone work but is also connected to the rest of the work; all chapters address various aspects of viscous production from naturally fractured carbonate reservoirs using steamflooding.

1.7.1 Chapter 1: Introduction

The aims and objectives of the research work are outlined in detail. It starts with problem statement, continues with literature review, theoretical concepts, delineation of the research objectives, explanation of the research methodologies, and ends with a brief overview of results.

1.7.2 Chapter 2: Viscous Oil Resource: From Genesis to Production and Upgrading

The petroleum engineering terminology for heavy oils used herein is introduced; then, chemical and physical properties of viscous oils are given and discussed. The production history and characteristics of the major VO fields in several countries are reviewed. Different types of reservoirs, and the nature and development of various *in situ* VO production technologies are described, followed by a review of refining techniques and transportation methods used in the VO industry. Finally, the environmental sustainability of viscous oil development is discussed in terms of health and pollution concerns.

1.7.3 Chapter 3: New Correlations for Prediction of Steam to Oil Ratio and Recovery Factor during Steamflooding in Naturally Fractured Carbonate Heavy Oil Reservoirs

New statistical reservoir screening tools in the form of non-linear regression correlations were developed using multivariate regression analysis for quick estimation of *CSOR* and *RF* in NFCRs. The relationships involve major parameters such as *in situ* fluid and reservoir properties, and process conditions (e.g., steam flow rate and quality). Previous modeling and experimental studies with the aid of a statistical method were used to determine the key variables that most strongly affect the *CSOR* and *RF* in homogeneous and fractured reservoirs experiencing steamflooding. The data used are mainly from field pilots and also some experimental test runs of steaming VO NFCRs. The correlations were then examined by statistical tests such as ANOVA, residual plots, and correlation coefficient, and qualitatively and quantitatively compared with existing correlations reported for oil sands and

unconsolidated sandstones. At the end, the new correlations are applied to predict *CSOR* and *RF* for a real VO NFCR. The statistical equations developed are superior compared to previous models because the newly introduced relationships consider parameters such as permeability ratios and interaction effects.

1.7.4 Chapter 4: A New Mathematical Model for Steamflooding in Naturally Fractured Carbonate Heavy Oil Reservoirs

A mathematical model for steamflooding in NFCRs is presented considering the matrix part and fracture part in the form of two subdomains, by writing separate governing equations. A continuity boundary condition is applied at the interface of the matrix and fractures to remove the uncertainties associated with the shape factor when determining the communication rate between the matrix and fractures. The proposed method uses fluid flow and heat transfer equations for all three phases (e.g., water, steam, and oil). A convective heat loss model was employed to calculate the heat transfer from the system to the surrounding environment via an overall convective heat transfer coefficient and temperature difference between two media. In addition, it was assumed that nonlinear relative permeability functions are valid for both matrix and fracture but with different coefficients. Applying mass and energy conservation laws, Partial Differential Equations (PDEs) were derived that relate saturation degree to pressure, time, and position. Given the numerical modeling solutions of the PDEs, the saturation, temperature, and pressure profiles along both matrix and fracture parts were obtained.

1.7.5 Chapter 5: A New Smart Screening Tool for Evaluation of Steamflooding Performance in Naturally Fractured Carbonate Heavy Oil Reservoirs

A predictive “screening tool” based on Artificial Neural Network (ANN) combined with Particle Swarm Optimization (PSO) for performance prediction of steamflooding in VO NFCRs is developed. PSO is applied to obtain the initial weights of the parameters in the ANN model. To avoid early convergence and permutation issues, the parameters required for construction of a network model are selected carefully. Training and testing phases are

conducted based on a statistical analysis to estimate *RF* and *CSOR*. The proposed PSO-ANN model is built using experimental and field data. To evaluate the appropriateness of the PSO-ANN model, a testing phase is performed employing new data that were not been used in the training phase. The predicted outputs are compared with the field data, and the results obtained from the conventional ANN system (e.g., Back Propagation-Artificial Neural Network (BP-ANN)) and regression correlations for *RF* and *CSOR*. Collection of fairly large amounts of input data and selection of important input variables appear to be important in developing any smart technique to predict target variables.

1.7.6 Chapter 6: Geomechanics of Thermal Oil Production in Sandstones

Despite the fact that this chapter is not directly related to NFCRs which is the main focus of this dissertation it provides a basis for better understanding and comparison of the behavior of NFCRs under high T as there is relatively large amount of data and field experience and modeling practice available on thermal geomechanics of oil sands or sandstones under high T. In this chapter, several methods to compute thermally induced stresses are provided. The temperature effects on reservoir rock properties during oil production are also discussed, and the geomechanical behavior of a practical example of reservoir rock during SAGD thermal oil production methods is illustrated, focusing on the improvement of oil recovery. As is well known, operational problems including thermally induced casing shear, cap rock breaching, and conductivity loss may happen during a thermal production process.

1.7.7 Chapter 7: Geomechanics of Thermal Oil Production from Naturally Fractured Carbonate Reservoirs

Some simple calculations are performed to allow estimation of thermally induced stress changes during thermal oil production from NFCRs. Mathematical modeling techniques to simulate thermal VO production methods are also discussed for further understanding of important parameters (e.g., shear and compressive stress) and mechanisms of geomechanics phenomena that occur during thermal production processes. Geomechanical behavior of NFCRs under high T is compared with geomechanical behaviour of oil sands / sandstones

under high T. At the end, a practical example of reservoir rock behavior during thermal oil production operations (steamflooding) is described, highlighting that thermal oil production methods change reservoir behavior in terms of static and flow characteristics, generally leading to production enhancement, although thermal stimulation can cause operational issues such as thermally induced casing shear and seal breaching.

1.7.8 Chapter 8: Fracture Characterization and In situ Stresses Inference in a Naturally Fractured Carbonated Heavy Oil Reservoir – An Integrated Geophysical-Geological Approach

This chapter is divided into two parts. In the first, fracture generation, classification, and characterization techniques applied in characterizing NFCRs are briefly described. Then, natural fractures are studied in a VO field in Iran using different geological, geomechanical, and geophysical data. Different seismic methods available for the purpose of estimation of fracture orientation and porosity in NFCRs are also reviewed, followed by an extensive discussion on geophysical and geological aspects. A field study of fractures at the surface and in the sub-surface is conducted and regional tectonic fracture systems are characterized. In the second part of this chapter, some of the techniques for *in situ* stress state determination are first described; then, a combination of geological, geomechanical, and log data is used to infer magnitude and orientation of the *in situ* stresses. Results obtained from this study can be used in field development, well placement, hydraulic fracture design, and reservoir simulation practices. Also, the methodology is generally applicable in the practical cases if enough geophysical and geological information are provided.

1.7.9 Chapter 9: Major Contributions, Conclusions, and Recommendations

The major contributions of this research work and also some recommendations for future studies are presented in Chapter 9.

1.7.10 Bibliography

This section contains a complete list of the citations including books, technical reports, referred journal papers, conference proceedings, patents, and so on.

1.7.11 Appendices

Appendices contain supplementary information such as computer programs used for the purpose of mathematical modeling, neural network modeling, and the statistical analysis.

Nomenclature

Acronyms, Symbols, Units

Acronyms: Production Technologies

CHOPS	=	Cold Heavy Oil Production with Sand
CP	=	Cold Production
CSS	=	Cyclic Steam Stimulation (vertical wells)
HCS	=	Horizontal well Cyclic steam Stimulation
SAGD	=	Steam-Assisted Gravity Drainage
SF	=	Steamflood

Symbols: Latin, then Greek

AI	=	Artificial Intelligence
ANN	=	Artificial Neural Network
ANOVA	=	Analysis of variance
b	=	Barrel of oil
BP-ANN	=	Back Propagation-Artificial Neural Network
CAPEX	=	Capital expenditures (pre-production)
CSOR	=	Cumulative Steam-Oil Ratio
D	=	Darcy
DOE	=	Design of Experiments
F	=	produceability factor - kh/μ (mD-m/cP)
HO	=	Heavy Oil
K_f	=	Fracture permeability (D, mD)

K_m	=	Matrix permeability (D, mD)
NFCR	=	Naturally Fractured Carbonate Reservoir
NFR	=	Naturally Fractured Reservoir
OOIP	=	Original Oil In Place
OPEX	=	Operating Expenses
PDEs	=	Partial Differential Equations
PSO	=	Particle Swarm Optimization
PV	=	Pore Volume
RF	=	Recovery Factor (% OOIP recovered)
S_o	=	Oil saturation degree (100%)
S_w	=	Water Saturation (%)
TSC	=	Technical Screening Criteria
USGS	=	Unites States Geological Survey
VO	=	Viscous Oil
ϕ	=	porosity in %

Metric Conversion Factors

$^{\circ}\text{F}$	=	$(^{\circ}\text{C} \times 1.8) + 32$
1 barrel oil	=	0.159 m ³
1 psi	=	6.8947 kPa
1 psi/ft	=	22.62 kPa/m or 22.62 MPa/km

Chapter 2

Viscous Oil Resource: From Genesis to Production and Upgrading¹

2.1 Abstract

There are $\approx 1.54 \times 10^{12} \text{ m}^3$ [$\sim 9.70 \text{ Tb}$ (Tb = trillion barrels of oil)] of viscous oil (VO) (e.g., heavy oil, extra heavy oil, and bitumen) known to exist in the world. By comparison, originally there were $\approx 0.75 \times 10^{12} \text{ m}^3$ [$\sim 4.7 \text{ Tb}$] of conventional oil, of which almost $0.19 \times 10^{12} \text{ m}^3$ [$\sim 1.195 \text{ Tb}$] have been produced to date. VO resources are not evenly distributed: Canada and Venezuela alone possess over one-third of the world endowment. Furthermore, the physical properties of these resources are variable, leading to differences in producibility from place to place. Only in Alberta, Canada, can significant amounts of VO be open-pit mined, but proven mineable oil reserves are small in the global context, constituting less than 1% of ultimate world VO reserves, estimated to be about $0.41 \times 10^{12} \text{ m}^3$ [$\sim 2.6 \text{ Tb}$], or 27% of the total OOIP (Original oil in place). The focus of this chapter is on *in situ* VO production methods, which will see increasing worldwide application in decades to come. The development of new oil production technologies in Canada since 1985 has played a major role in VO production growth. Canada is the only major oil producing country with more than 60% of total production from VO reserves, and is the world leader in the development of production technologies. Since 1990 the *in situ* VO production industry has seen a number of startling advances. New production technologies, combined with

¹ Materials presented in this chapter are in part contributed to the following publications:

Dusseault, M.B. and **Shafiei, A.** 2011. Oil Sands. Ullmann's Encyclopedia of Chemical Engineering, Wiley, 52 pages.

Rogner, H.-H., R. F. Aguilera, C. Archer, R. Bertani, S. C. Bhattacharya, M. B. Dusseault, L. Gagnon, H. Haberl, M. Hoogwijk, A. Johnson, M. L. Rogner, H. Wagner and V. Yakushev, 2012: Chapter 7 - Energy Resources and Potentials. In Global Energy Assessment - Toward a Sustainable Future, Cambridge University Press, Cambridge, UK and New York, NY, USA and the International Institute for Applied Systems Analysis, Laxenburg, Austria, pp. 423-512. (**Ali Shafiei** is a contributing author to this chapter)

developments in waste management, upgrading, monitoring, and transportation have changed expectations. Now, it is a widely held view that 15–20% of the world’s VO resource base can be profitably produced with current technology; this fraction will rise as further technological advances are implemented. For example, early in 2010, the United States Geological Survey estimated that $81 \times 10^9 \text{ m}^3$ [0.5 Tb] of VO in the Orinoco Heavy Oil Belt was technically recoverable (Schenk *et al.*, 2009). The Energy Resources Conservation Board of Alberta estimates over $50 \times 10^9 \text{ m}^3$ [0.315 Tb] of VO recoverable with current technology (CAPP, 2009). Together, this is almost 10% of the world’s VO. After introducing the terminology used herein and discussing the chemical and physical properties of VOs, this chapter then describes the major VO fields in several countries, the nature and development of different *in situ* VO production technologies, the refining techniques and transportation used in the VO industry. Finally, the environmental sustainability of VO development is discussed.

2.2 Definitions

There is not a universal definition for Viscous Oil (VO) in petroleum engineering literature. Many different definitions have been used to identify, classify, or rank and assess VO resources, including terms that allude to VO physical properties. For instance, heavy oil and extra-heavy oil have been defined as oil with a density (ρ) of 0.934–1.0 and $> 1.0 \text{ g/cm}^3$, respectively (Head *et al.*, 2003). ‘Heavy’ relates to the high density of VO, usually expressed with the American Petroleum Institute (API) gravity scale; however, the definition of heavy oil varies among different authors. Heavy oil has been defined as having an API gravity $< 20^\circ\text{API}$ (Meyer and Dietzman, 1979), but this does not describe the flow properties *in situ* (Gibson, 1982). Some crude oils may be dense (e.g., low API gravity) but with a modest viscosity because of reservoir temperature; for example, the deeper Faja del Orinoco oil in Venezuela is typically $8.5\text{--}9^\circ\text{API}$ with a viscosity of 1000–4000 cP at 40–45°C. In Canadian reservoirs at 5°C and 100 meters depth, similar oil has a viscosity of over 10^6 cP (Dusseault, 2001).

In production technology economic evaluation, definitions based on *in situ* viscosity are preferred because viscosity controls flow rate and is thus far more important than density or API gravity. Although each crude VO has a unique temperature–viscosity relationship, viscosity always decreases sharply with temperature increase, usually halving each 6.5–8°C increase, and the temperature sensitivity of VO is greater than for conventional oils. Figure 2-1 shows a typical T– μ plot for Athabasca bitumen that has a viscosity of $\sim 10^6$ cP at 10°C; to achieve a viscosity less than 10 cP in this case, $T > 200^\circ\text{C}$ is necessary.

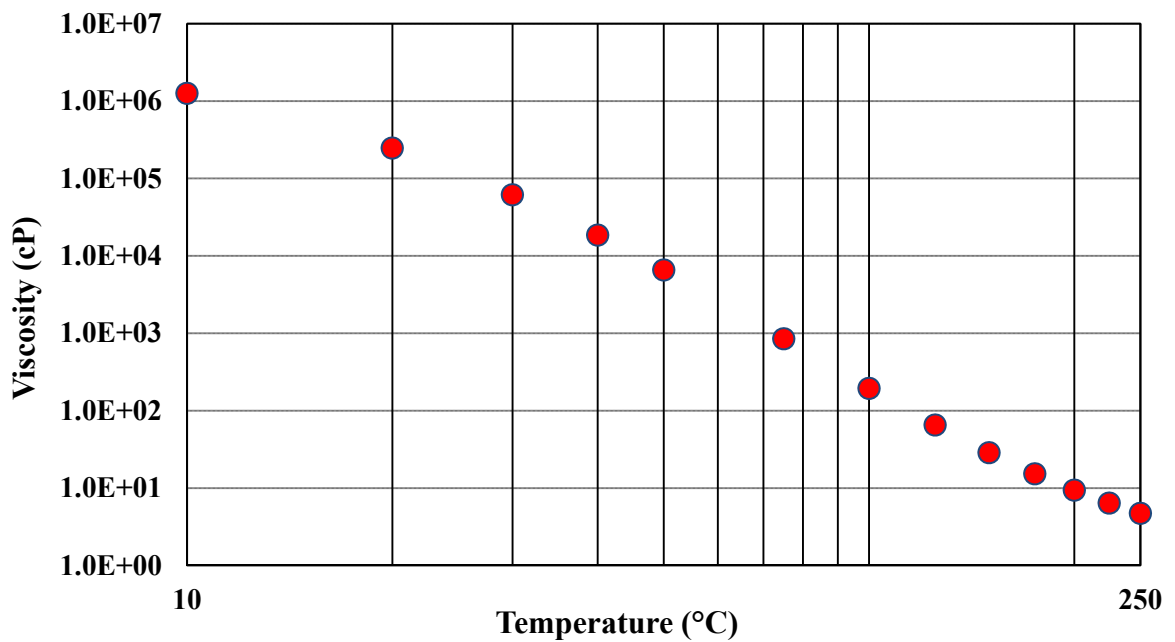


Figure 2-1: A typical T– μ plot for Athabasca bitumen (106 cP@10°C).

Many suggest that ‘heavy oil’ be defined as oil having a viscosity > 100 and < 10000 cP at reservoir conditions, as in Figure 2-2 (Briggs, *et al.*, 1988; Dusseault, 2006); then, ‘bitumen’ refers to oil having a reservoir viscosity > 10000 cP. Clearly, there is no single ‘correct’ set of definitions.

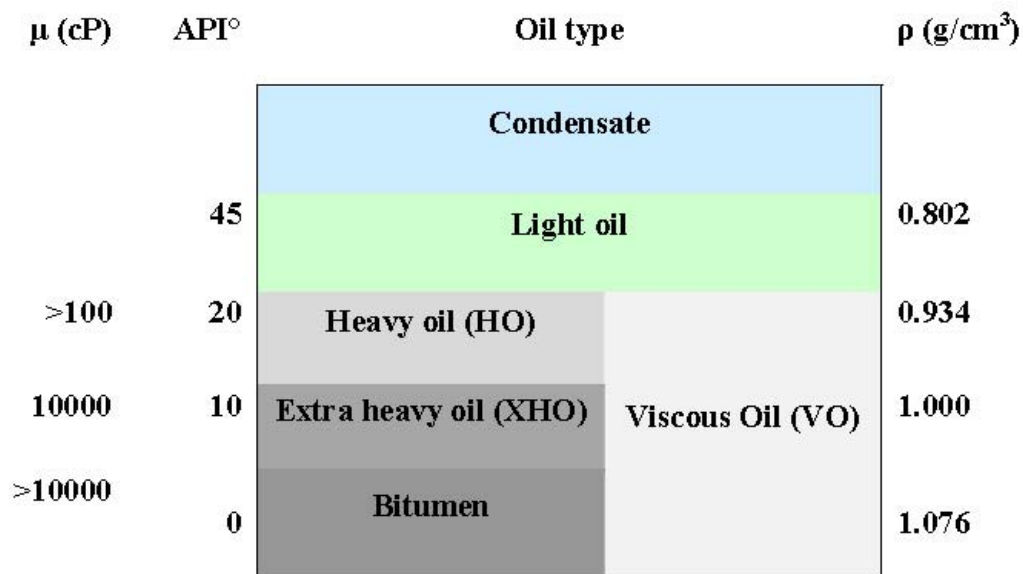


Figure 2-2: A graphical demonstration of the oil definitions used in this dissertation.

A brief list of definitions and recommended usage is given here:

- **Viscous Oil (VO)** refers to all crude oil with $\mu > 100$ cP *in situ*.
- **Heavy Oil (HO)** refers to crude oil with $100 < \mu < 10000$ cP *in situ*.
- **Extra Heavy Oil (XHO)** refers to crude oil with $\mu < 10000$ cP *in situ*, but with $\rho > 1.0$ g/cm³ (as in the Orinoco deposit).
- **Bitumen** refers to crude oil with $\mu > 10000$ cP *in situ*.
- **Conventional oil** refers to crude oil with $\mu < 100$ cP *in situ* that can be produced by conventional methods.
- **Original Oil In Place (OOIP)** refers to the volume of liquid crude oil in a defined resource area, irrespective of producibility.
- **Recovery Factor (RF)** is the percentage of OOIP that can be recovered, used most commonly with reference to a particular technology and specific reservoir conditions.

These terms may imply other information, such as the elemental hydrogen-to-carbon ratio (high for conventional oil, low for bitumen) or the S–N–O and heavy metal content (low for

conventional oil, high for bitumen), but without quantitative limits attached. Importantly, *in situ* viscosity-based definitions, when combined with thickness and permeability data, relate to producibility through a commonly used factor (kh/μ) expressed in units of mD-m per cP, where h is the reservoir thickness, k is the permeability, and μ is the viscosity in centipoises (cP). Bitumen is generally considered immobile *in situ*, HO as ranging from relatively to slightly mobile and conventional oil as being mobile.

2.3 Reservoir Definitions

There are industry guidelines for classification of oil reserves into categories such as ‘proven’, ‘probable’, and ‘possible’. Furthermore, there are additional classifications such as estimates of oil not yet discovered and oil that is not recoverable. It is important to put into place a credible evaluation method, based on known methods and available data, which can lead to reasonable estimates of recoverable reserves in a consistent manner. A reasonable estimate can be arrived at through the systematic application of selection criteria for the set of production technologies that are recommended, plus the choice of a suitable *RF* based on experience or best possible estimates. These two factors, applied over an area, and corrected for reservoir quality, presence of water, and other factors, will allow estimation of recoverable reserves.

Figure 2-3 is the recommended Society of Petroleum Engineers (SPE)/World Petroleum Council (WPC)/American Association of Petroleum Geologists (AAPG) classification scheme for resources. The classification of petroleum reserves into categories such as ‘proven commercial reserves (1P)’ or ‘proven plus probable commercial reserves (2P)’ proved to be a contentious issue in financial markets in the period 2000–2010 because of an archaic classification scheme used by the US Securities and Exchange Commission (SEC). Because most large private oil companies are listed on American or European stock exchanges, they must adhere to the SEC rules.

Increasing degree of economic feasibility	Total Petroleum Originally In Place (All conventional and non-conventional, including shale oil but not coal or gas-to-liquids)	Discovered petroleum originally in place	Production			Increasing maturity
			Commercial	Proved (1P)	Proved + probable (2P)	
			Unrecoverable			
		Sub-commercial	Contingent Resources			
			Low estimate	Best Estimate	High estimate	
			Unrecoverable			
		Undiscovered petroleum originally in place	Prospective Resources			
			Low estimate	Best Estimate	High estimate	
			Unrecoverable			
Increasing uncertainty						

Figure 2-3: A resources classification scheme proposed by the SPE/WPC/AAPG (Modified from: [Ross, 2001](#)).

The common term ‘technically recoverable reserves’ refers to oil that can be produced with currently existing technologies, although not necessarily economically if the oil price is low.

For example, there are approximately 0.177 Tb of oil of proven VO reserves in Canada based on mining, steam injection, and cold production methods. However, the Alberta government has published a figure of 0.315 Tb of implied technically recoverable reserves in Alberta's oil sands deposits (ERCB, 2010).

2.4 Chemistry

VO chemical composition is related to *in situ* rheology (Storm *et al.*, 1994) and upgrading response during coking and hydrogenation (Rahimi and Gentzi, 2006); petrochemistry is well addressed in the literature so limited data are presented and discussed here.

Biodegradation of conventional oil to VO increases the viscosity, density, molecular mass and size, heteroatom content, and aromaticity; it decreases hydrogen-carbon ratios (Evans *et al.*, 1971; Larter *et al.*, 2006). These alterations have obvious negative effects on production, transportation, refining, and price. High aromaticity is associated with bacterial lipid production during VO formation, CH₄ is a major biodegradation byproduct, and biodegradation-related S-fixation into complex organosulfur complexes happens with the presence of high initial S contents in the oil upon exposure to shallow groundwater (Scott *et al.*, 1994; Holba *et al.*, 1996; Head *et al.*, 2003; Larter *et al.*, 2005).

In situ, notable local vertical and lateral gradients in composition and viscosity testify to the variability of the local biodegradation and diffusion processes that led to the virtual disappearance of lower M_r aliphatic molecules (Larter *et al.*, 2003, 2006, 2008). Lloydminster area crude oil is the least viscous and lowest S content VO in Alberta and appears to be less biodegraded than oils from other major deposits (Strausz, 1977). Nevertheless, although viscosity-related differences exist, the overall similarity in Alberta VOs suggests common provenance.

VO separation into compound classes (SARA classification – saturates, aromatics, resins, and asphaltenes, (ASTM, 1995) is based on various solubility and adsorption methods (e.g., (Speight, 1998). VO has a broad molecular mass distribution ranging from 16 (CH₄) to 2000, with more viscous oils having higher M_r fractions (and higher density), but in a continuum of

values with no discrete fractions (Boduszynski, 1987). Large molecules range from complex aliphatics to resins and asphaltenes dominated by cyclic groups (benzene rings, and C₅ and C₆ rings), giving VO a severe hydrogen deficiency. The asphaltene content of the most viscous Alberta bitumen is 16–25% and it also contains far more sulfur (8–9%) and other heteroatoms than non-asphaltene fractions.

VO has a high heteroatom content (e.g., S, N, O, V, Ni, and Fe); S is the third most abundant element after C and H, reaching levels > 4% in VO with $\rho > 1.0 \text{ g/cm}^3$ (Clugston *et al.*, 1977; Grizzle *et al.*, 1982; Sturm *et al.*, 1982). Heteroatom content rises with decreasing H/C ratio and increasing density. Coping with vast S quantities is a major factor in upgrading, heavy metals (contents up to 500–600 ppm) act as catalyst poisons, and other atoms (N, O) present challenges to upgrading processes (Tissot and Welte, 1984; Boduszynski, 1987; Rahimi and Gentzis, 2006).

Steam injection is used for most *in situ* VO production. Steam liberates and generates gases such as CH₄, CO₂, H₂ and H₂S (Hyne *et al.*, 1982). Many organosulphur compounds undergo partial scission or limited hydrolysis at T > 225–250 °C, producing small amounts of H₂S and other compounds, and as with all such reactions, temperature and pH play important roles (Clark *et al.*, 1984). Furthermore, the condensed water co-produced with the VO contains many dissolved molecules and salts that require careful water treatment for purposes of recycling to the steam boilers (Boduszynski, 1987, Altgelt and Boduszynski, 1988; Boduszynski and Altgelt, 1992). Table 2-1 presents data on gross composition of bitumens from Alberta, Canada and in Table 2-2 different properties and SARA fractions for the Athabasca and Cold Lake bitumen are presented.

Table 2-1: Gross composition of bitumen from Alberta, Canada (From: [Strausz, 1977](#)).

% of whole bitumen				
	Cold Lake	Athabasca	Peace River	Wabasca
Asphaltenes	15.3	16.9	19.8	18.6
Deasphalted oil	84	83.1	80	81.2
Saturates	21.3	18.3	15.15	14.6
Monoaromatics	8.3	8.1	8.57	7.61
Diaromatics	3.6	3.8		
Polar compounds	24.35	23.8		

Table 2-2: Properties and SARA fractionation results for Athabasca and Cold Lake bitumen ([Rahimi and Gentzis, 2006](#)).

	Athabasca Mod. ASTM 2007		Athabasca ASTM 2007	Cold Lake Mod. ASTM 2007		Cold Lake ASTM 2007
	MW			MW		
API Gravity			8.05		10.71	
Saturates (wt%)	381	17.27	16.9	378	20.74	21.52
Aromatics (wt%)	408	39.7	18.3	424	39.2	23.17
Resin (wt%)	947	25.75	44.8	825	24.81	39.36
Asphaltene (wt%)	2005	17.28	17.18	1599	15.25	15.95
Carbon (wt%)		83.34			83.62	
Hydrogen (wt%)		10.26			10.5	
Sulfur (wt%)		4.64			4.56	
Oxygen (wt%)		1.08			0.86	
Nitrogen (wt%)		0.53			0.45	
Residue (wt%)		0.15			0.01	

Average chemical and physical properties of some conventional and VOs collected from different sources (Meyer and Attanasi, 2004) are presented in Table 2-3. Inspection of Table 2-3 reveals a substantial increase in most properties from left to right.

Table 2-3: Some chemical and physical properties of viscous oils (averages) (From: Meyer and Attanasi, 2004).

Property	Unit	Heavy oil (127 basins, 11 deposits)	Natural bitumen (50 basins, 305 deposits)
API gravity	degrees	16.3	5.4
Depth	feet	3250	1223.80
Viscosity (77°F)	cP	100947	1290254.10
Viscosity (100°F)	cP	641.7	198061.40
Viscosity (130°F)	cP	278.3	2371.60
Coke	wt%	13	23.7
Asphalt	wt%	38.8	67
Carbon	wt%	85.1	82.1
Hydrogen	wt%	11.4	10.3
Nitrogen	wt%	0.4	0.6
Oxygen	wt%	2.5	
Sulfur	wt%	2.9	4.4
Flash point	°F	70.5	
Acid number	mgKOH/g	2	3
Asphaltenes	wt%	12.7	26.1
Asphaltenes + resins	wt%	35.6	49.2
Nickel	ppm	59.106	89.137
Lead	ppm	1.159	4.758
Titanium	ppm	8.025	493.129
Vanadium	ppm	177.365	334.428

2.5 Viscous Oil Origins, Geological Setting and Resource Base Estimates

2.5.1 Viscous Oil Origins

VO is almost always biodegraded older light oil. Deep oil generation, up-dip migration, and biodegradation concepts (Head *et al.*, 2003; Larter *et al.*, 2003) underpin the standard model (Figure 2-4) used to explain the occurrence of gigantic VO deposits in shallow sands in Canada and Venezuela. Oil that has migrated over long distances from deeply buried source rocks (> 3000 m deep) to shallow depths has been exposed to bacteria (leading to aliphatics consumption, lipids generation), different groundwater chemistry (sulfates, bicarbonates instead of chlorides), more rapid groundwater flux (washing of soluble fractions) and reduced pressure (light ends diffusional losses). The bacteria, combined with washing and diffusive efflux, remove the light aliphatic molecular components, generate complex aromatic compounds, concentrate the sulphur, and thereby generate the VO.

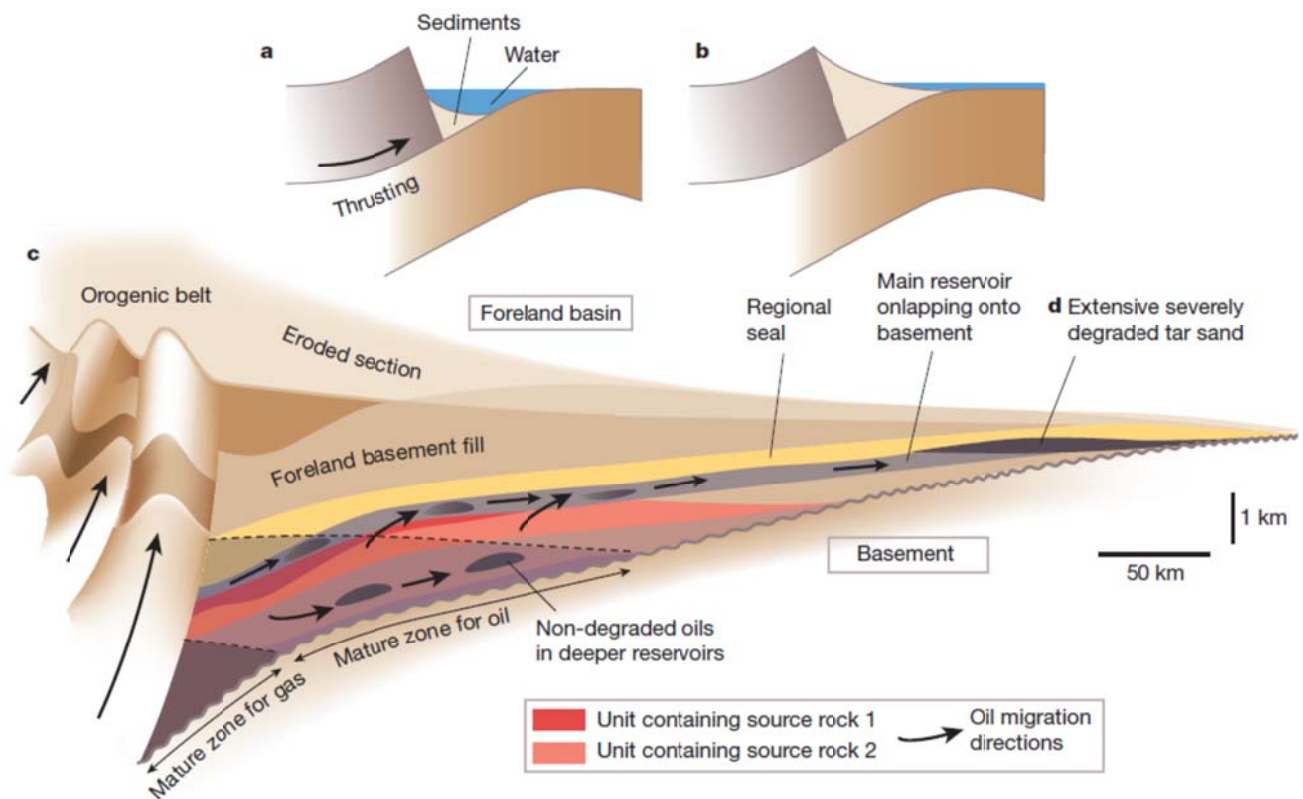


Figure 2-4: A proposed model for VO generation (From: Head *et al.*, 2003).

Oil biodegradation *in situ* is almost exclusively anaerobic in nature (Aitken *et al.*, 2004); the majority of the biodegraded oils contain metabolic markers such as specific reduced naphthoic acids as evidence for anaerobic degradation, (Hollerbach, 1987; Head *et al.*, 2003). Investigations of the hydrocarbon biodegradation process in many VO samples from around the world confirm that generation of the highly viscous, aromatic-rich oil must have been an anaerobic process, leading to liquids with higher density and lower H:C ratio (Hollerbach, 1987). Biodegradation is an enrichment of resin and asphaltene molecules relative to aliphatic molecules. This process in VOs should eventually lead to formation of solid bitumen and asphalts (Curiale, 1983), although some oxidation or other process may be necessary for the final stages.

Biodegradation *in situ* is controlled by temperature, chemical composition of the oil and groundwater, and the relation between the oil volume and the oil–water contact area. Gradients in the composition of the oil and consequent viscosity variations are common at reservoir scales, and are linked with proximity to active water (slow flux) and geochemical factors. As an example, Larter *et al.* (2006) reported a drastic change in viscosity of oil with depth, up to one hundred times, across a 40 m thick reservoir, and they also concluded that viscosity can change laterally by factors of 2–10 times on a length scale of 500–1000 m.

Oils show variation in their organic sulfur content ranging from less than 0.05% to more than 14%, and VOs contain much more sulfur than light oils (Nelson, 1972; Hollerbach, 1987), likely reflecting sources high in sulfur. During biodegradation a combination of lowered volatile content and volumetric diminution increases sulfur abundance as well as molecular mass, increasing the oil density to values that can be greater than that of the pore water. It has been suggested that in high-sulfur oils most of the sulfur was introduced to the system secondarily through a chemical reaction between oil and sulfur, hydrogen sulfide, and resulting polysulfide systems (Orr, 1978). However, loss of other non-sulfur compounds during the biodegradation process may appear as an increase in sulfur content without introduction of additional sulfur.

2.5.2 Geographical Distribution and Resource Base Estimates

The world endowment of VO in both clastic (sandstones, consolidated, or unconsolidated sand deposits) and carbonate rocks is estimated by the United States Geological Survey (USGS) and others to be on the order of 9 Tb [$1430 \times 10^9 \text{ m}^3$], over two times the conventional OOIP resource of about 4.5 Tb (Meyer *et al.*, 2007; Schenk *et al.*, 2009; GEA, 2012).

The majority of VO, mainly XHO and bitumen, is found in shallow high-porosity sandstones ($\phi > 25\%$) (ϕ is the porosity in %) of low cohesive strength, mostly in the western hemisphere (over 65%). Large VO deposits in carbonates are far less common, of lower porosity (usually $\phi < 15\%$), and generally with thinner pay zones; these carbonates host about 1.8 Tb [$286 \times 10^9 \text{ m}^3$] of VO worldwide, mainly HO. The Middle East has about 10% of the world's known VO resource, estimated at 0.8 Tb [$127 \times 10^9 \text{ m}^3$], found mainly in Naturally Fractured Carbonate Reservoirs (NFCRs) in the Arabian and Zagros sedimentary oil provinces off- and on-shore in the Persian Gulf region. Canada has over 0.45 Tb [$71 \times 10^9 \text{ m}^3$] of bitumen trapped in Devonian age carbonates in the Western Canada Sedimentary Basin.

Major occurrences of VO (Figures 2-5, 2-6, and 2-7) are reported in Canada (> 1.85 Tb [$305 \times 10^9 \text{ m}^3$]), Russia (1.8 Tb [$286 \times 10^9 \text{ m}^3$]), Venezuela (> 1.65 Tb [$266 \times 10^9 \text{ m}^3$]), rest of Americas (1.5 Tb [$234 \times 10^9 \text{ m}^3$]), Middle East (0.9 Tb [$127 \times 10^9 \text{ m}^3$]), United States (0.8 Tb [$127 \times 10^9 \text{ m}^3$]), East Asia (0.3 Tb [$48 \times 10^9 \text{ m}^3$]), former Soviet Union excluding Russia (0.2 Tb [$32 \times 10^9 \text{ m}^3$]), and several other countries.

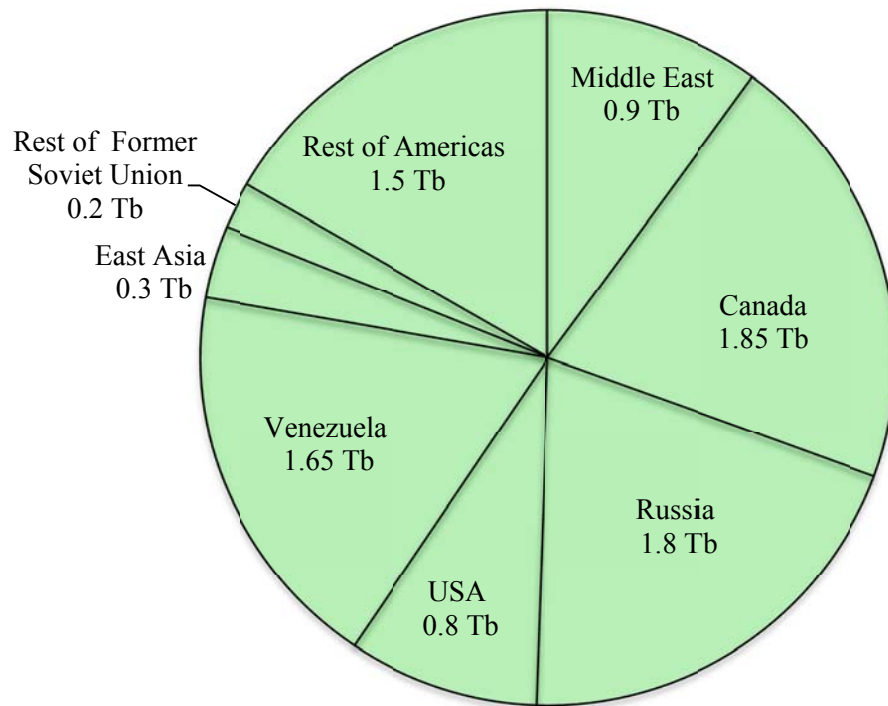


Figure 2-5: Geographical distribution of VO in the world (Dusseault and Shafiei, 2011; GEA, 2012).

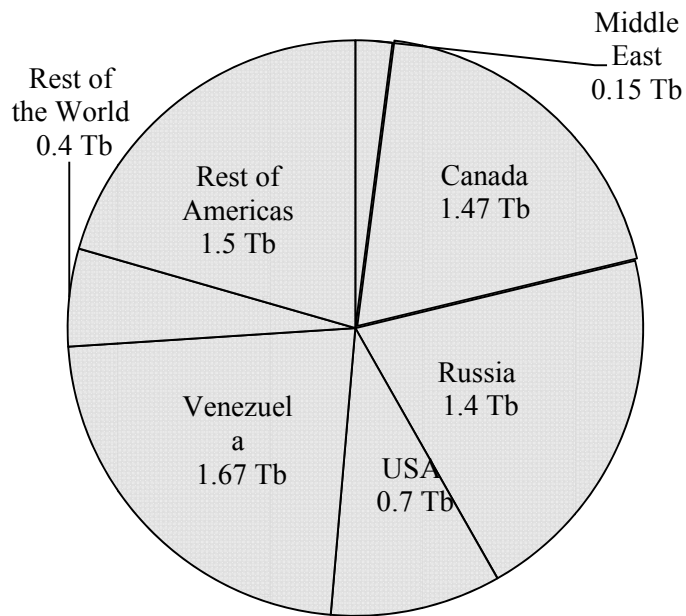


Figure 2-6: Geographical distribution of VO in the world in sandstones and/or oil sands (Dusseault and Shafiei, 2011; GEA, 2012).

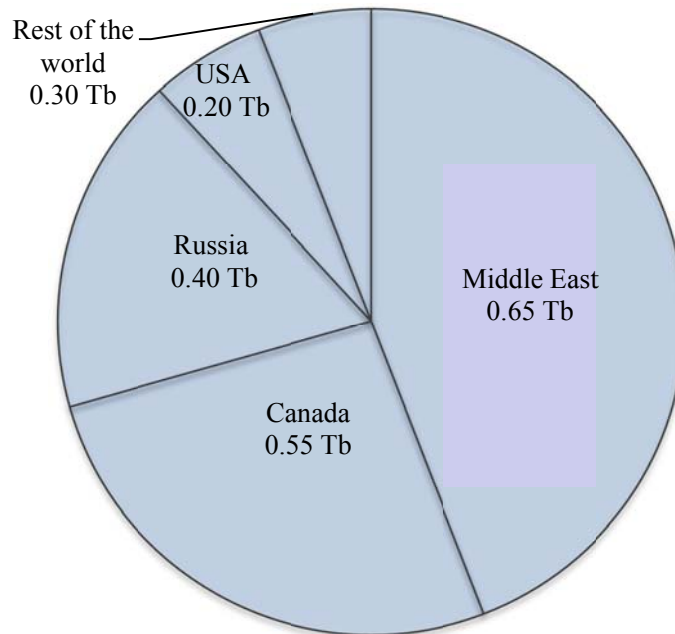


Figure 2-7: Geographical distribution of VO in carbonates (Dusseault and Shafiei, 2011; GEA, 2012).

2.5.3 Canadian Oil Sand Deposits

The VO deposits of Canada (Figure 2-8) are in total the largest bituminous sand deposits in the world with an area over 140000 km² and an estimated initial volume of oil in place ranging from 1.73 Tb [275×10⁹ m³] (ERCB, 2010) to 2.38 Tb [378×10⁹ m³] (Meyer *et al.*, 2007; ERCB, 2010;). In this text, a highly conservative figure of 1.85 Tb [294×10⁹ m³] is used, of which 339 Bb [54×10⁹ m³] is technically recoverable with current technology and oil price (See Table 2-4, Figures 2-9 and 2-10). Figures 2-8 and 2-9 show resource size estimates and technically recoverable reserve estimates for the major Canadian VO deposits. Most of the currently producible VO is hosted in high porosity Lower Cretaceous quartz arenites and arkosic sands in the major Athabasca, Wabiskaw, Cold Lake, and Peace River deposits, as well as in the Heavy Oil Belt (Figure 2-8). Other resources, considered as yet uneconomic, are hosted within fractured Devonian and Mississippian fractured carbonate reservoirs in a region called the Carbonate Triangle, containing over 0.5 Tb of bitumen (Meyer *et al.*, 2007; ERCB, 2010;).

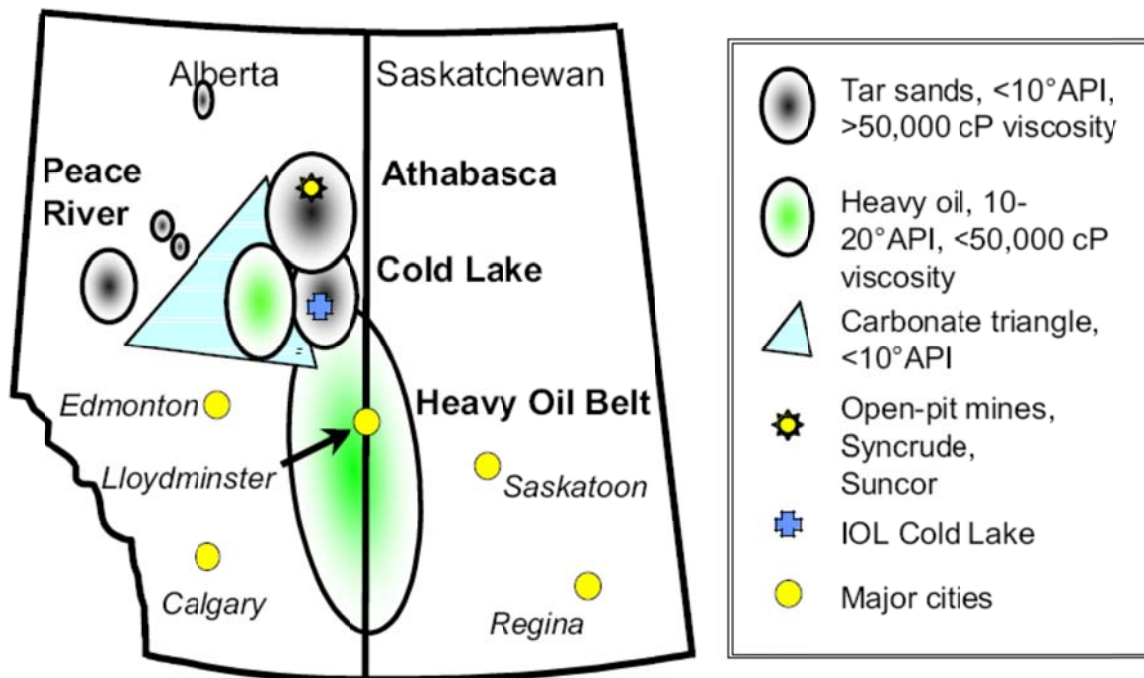


Figure 2-8: Geographical distribution of the major VO deposits in Canada.

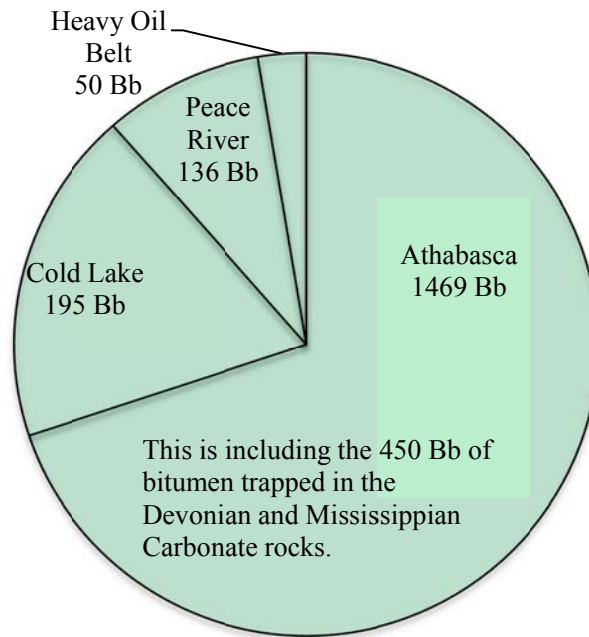


Figure 2-9: Resource based estimates of the major VO deposits in Canada (AERCB, 2010, with minor modifications).

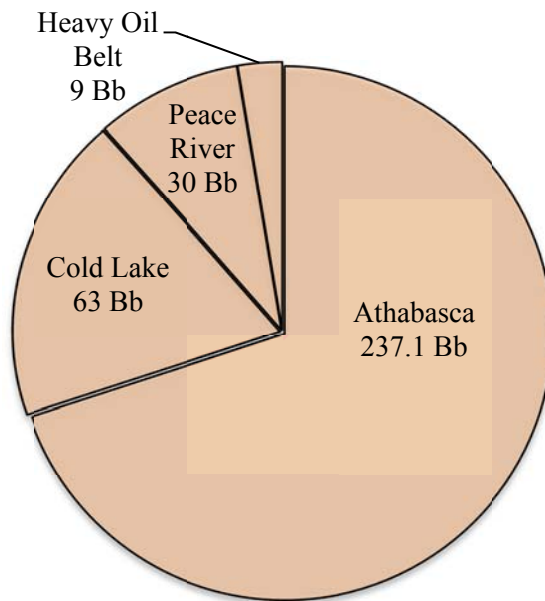


Figure 2-10: Technically recoverable oil with current technology and price in Canada (AERCB, 2010, with minor modifications).

The northern part of the VO region mostly comprises highly viscous bituminous sands of considerable thickness and with great lateral continuity. Toward the central and south-southeast of the region, the viscous oils in the Heavy Oil Belt are classified as HO (usually $\mu = 400\text{--}20000$ cP) and are mainly in small reservoirs of limited lateral extent ranging from channels to bar sands, with some thin deltaic sands. This area has been exploited since the 1930s because the oil is less viscous than in the more northerly deposits.

Geological, reservoir, and fluid properties of the major VO deposits in Canada are presented in Table 2-4. Also, viscosity–temperature relationships for major deposits in Canada and Venezuela are presented in Figure 2-11. The *in situ* viscosity plays a major role in evaluation of VO exploitable reserves and choice of production technology.

Table 2-4: Average geologic, reservoir and fluid properties of the major VO deposits in Canada.

Property	Units	Athabasca, including Grand Rapids, Wabiskaw-McMurray, Nisku (carbonate) and Grosmont (carbonate) Formations	Cold Lake, including Grand Rapids, Clearwater and Wabiskaw-McMurray Formations	Peace River, including Bluesky-Gething, Belloy, Debolt and Shunda Formations	HO Belt
OOIP	Bb	1469	195	136	50
Depth	m	0-600	400-600	450-800	300-900
Avg. ϕ	%	28-30	29-31	18-27	27-30
k	D	0.5-10 D	0.5-2 D	0.5-4 D	0.25 – 6 D
μ @ Pr and Tr	cP	100,000-3,000,000	50,000-300,000	5,000-500,000	400-20,000
Technically recoverable	Bb	237	63	30	9
Reference(s)		AERCB (2010) with minor modifications			NEB (2007)

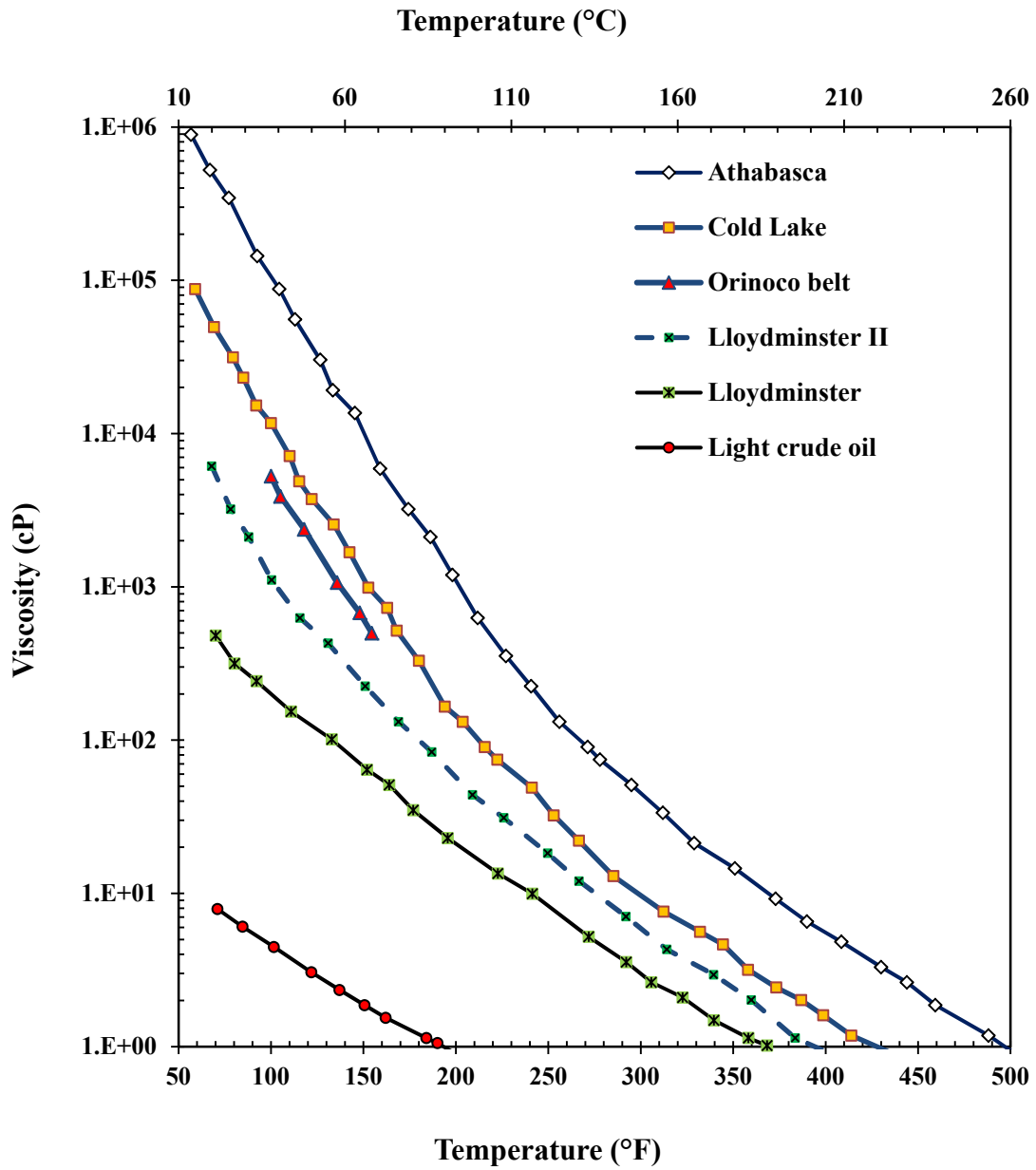


Figure 2-11: Viscosity-Temperature relationships for the major VO deposits in Canada and Venezuela (Modified from Meyer and Attanasi, 2004).

2.5.3.1 The Athabasca Oil Sands

The Athabasca Oil Sands (AOS) is the largest Canadian VO deposit and the second largest single VO deposit in the world, containing in excess of 1 Tb [$162 \times 10^9 \text{ m}^3$] covering an area over 46000 km². This resource estimate excludes bitumen in the carbonate strata (Nisku and Grosmont formations ~ 0.55 Tb) found in and near the Athabasca region. The AOS bitumen is highly viscous, from 100000 to over three million cP, and total producible reserves in this area are estimated at 237 Bb [$37 \times 10^9 \text{ m}^3$]. Over 90% of the VO in the Athabasca deposit is found in the McMurray Formation, the lowermost formation of the lower Cretaceous siliciclastic Mannville Group (ERCB, 2010).

The AOS deposit is formed of arenaceous strata dominantly of estuarine accretion plain origin. The sediment provenance changed from the east (igneous Canadian Shield) to the southwest and south over the Mannville Group time period, and the mineralogy reflects this change, so that the lower-lying McMurray Formation is more quartzose, with no smectite, and overlying strata tend to be less quartzose, with an increasing smectite content in the clay mineral fractions. McMurray Formation sediments, therefore, are quartz arenites with minor amounts of feldspars, chert fragments, and micaceous material (Wightman *et al.*, 1995; Gringas and Rokosh, 2004; Hein and Cotterill, 2006) with minor minerals characteristic of an igneous rock source. The average pay zone thickness of the McMurray Formation is ~ 35 m, but to the northeast it is up to 100 m thick, and in the west it becomes less than 10 m thick as it pinches out against the Grosmont Formation paleotopographic high.

The McMurray Formation was deposited in a N–S trending ridge and valley system that was formed by fluvial surface erosion processes and karstification of underlying carbonate strata acting on units of different lithology, combined with the development of a N–S pre-McMurray dissolution front in the underlying Prairie Evaporites (halite) that created the broad depression that roughly corresponds to the thick axis of the Athabasca deposit.

The McMurray Formation has an estuarine plain stratigraphic structure with many depositional episodes and erosional surfaces with consequent complex facies distributions and variable reservoir quality. The Formation shows lower energy depositional

environments toward its top, having a fining-upward grain size typical of transgressional sedimentation regimes. The complex estuarine accretion plain geology in this deposit leads to a heterogeneous reservoir nature, a challenge for reservoir characterization and optimal deployment and execution of production technologies (Hein, 2006; Hein *et al.*, 2008; Xu and Chopra, 2008).

2.5.3.2 The Cold Lake Oil Sands

The Cold Lake Oil Sands (CLOS) deposit occupies a roughly circular area approximately centred about 20 km north of the town of Bonnyville, Alberta (Figure 2-8). It is estimated to contain 195 Bb [$31 \times 10^9 \text{ m}^3$] of viscous oil in arenaceous deposits classified mainly as deltaic deposits (Vigrass, 1968; Hein and Cotterill, 2006; ERCB, 2010). Total producible reserves in this area are estimated at 63 Bb [$10 \times 10^9 \text{ m}^3$] (ERCB, 2010). The major reservoir is in the deltaic Clearwater Formation, and detrital matter provenance was mainly from the west. The thickness of oil-saturated Clearwater Formation zones averages 15–20 m with strata in excess of 40 m along the delta axis, at a depth of burial of 400–600 m. In the southern part of the CLOS deposit, the overlying Grand Rapids Formation can also be an important reservoir (Scott, 2002; Hein *et al.*, 2008).

The richest part of the CLOS deposits tends to be the central axis of the deltaic sands, where the strata are thick and continuous with few clayey interbeds, of 30% porosity and permeability of 0.5–2 D, and oil saturations in the sands generally about $S_o \sim 0.86\text{--}0.88$ (where S_o is the oil saturation ratio of the pore volume). In all directions from this central oil-rich and high permeability N–S axis, reservoirs tend to be thinner, of lower quality, with lower saturations and a lower net-to-gross pay ratio. In addition, off the central trend, permeabilities are lower because of higher clay content. The CLOS reservoirs in the Clearwater Formation are generally of litharenitic composition with quartz (> 40%), feldspars (~ 10–30%), siliceous volcanic glass shards (~ 5–20%), lithic fragments (~ 5–15%), and a smectitic-illitic clay mineralogy. The interstitial bitumen is generally highly viscous (50000–300000 cP), but in comparison to the AOS it is less viscous, less sulphurous, and with a lower asphaltene content (Scott, 2002).

2.5.3.3 The Peace River Viscous Oil Sands

The Peace River Oil Sands (PROS) area probably contains in excess of 136 Bb [$22 \times 10^9 \text{ m}^3$] of oil in place in sedimentary arenaceous deposits (the Bluesky-Gething Formation reservoir) classified as beach and offshore bar sands laid down against the protruding sediments of the Peace River Arch, a gentle domal feature in the north-east and central part of Alberta. Total producible reserves in this area are estimated at 30 Bb [$4.77 \times 10^9 \text{ m}^3$] (ERCB, 2010). The detrital matter came exclusively from the west, and has an arkosic composition with quartz (> 70%), feldspars (~ 10–30%), volcanic shards (~ 3–10%), lithic fragments and minor smectitic-illitic clay minerals. The bitumen is highly viscous, with some regions similar to the AOS deposit, but with a range of 5000 to 500000 cP. The reservoir is about the same age as the McMurray Formation. The thickness of oil-saturated material varies from 5 m to as much as 30 m in some areas.

2.5.3.4 The Wabiskaw Viscous Oil Sands

The West Athabasca region previously known as the Wabasca (or Wabiskaw) Oil Sands (WOS) contains more than 125 Bb [$20 \times 10^9 \text{ m}^3$] of VO in sandstone deposits classified as barrier bar and glauconitic beach sands (Wightman *et al.*, 1995). Although historically considered as a separate deposit, more recently the deposit has been included as a south-westward extension of the AOS deposit. Much of the WOS deposit lies geographically above the western parts of the AOS and CLOS, and extends westwards, almost to the centre of Alberta (Figure 2-8). In many regions, the Wabasca Formation which overlies the oil-rich McMurray Formation by 10–20 m is oil-rich, forming two stacked reservoirs. Resource estimates for the WOS deposits are included in the estimates for the AOS and CLOS deposits (see Table 2-4). The detrital matter of the WOS arrived mainly from the west instead of the east, but towards the east there is an increasing component of sediments from the Canadian Shield, evidenced by a trace heavy mineral suite diagnostic of igneous rocks. It has a litharenitic composition with quartz (> 50%), feldspars (~ 10–10%), glauconitic pellets, volcanic shards (~ 3–10%), lithic fragments (~ 3–15%), and a clay mineral suite characterized by smectitic-illitic clay minerals.

The bitumen viscosity is variable, from less than 1000 in the southwest to over 500000 cP in north-eastern areas. The reservoir thickness of oil-saturated material varies from a few meters to as much as 8–12 m in some cases. In some more deeply buried regions in the western part of the WOS deposit, the VO is much less viscous (< 1000 cP) than in the eastern area, and has been successfully exploited using long horizontal wells, albeit with low recovery factors ($< 10\%$).

2.5.3.5 The Heavy Oil Belt (HOB)

The heavy oil belt (HOB) straddling the border of Alberta and Saskatchewan in Western Canada (Figure 2-8) contains over 50 Bb [8×10^9 m³] of VO in place with estimated total producible reserves of 9 Bb [1.43×10^9 m³] (NEBC, 2001).

The HOB is not a single largely continuous reservoir with a central thick and oil-rich axis; rather, the HOB is an elongated elliptical region about 600 km long and 200–250 km wide containing literally hundreds of small oil fields. From the northern end where it overlaps the CLOS reservoirs, it stretches southward to the south-west corner of Saskatchewan near the town of Kindersley, about 200 km north of the USA border.

The HOB reserves are found in a series of thin (3–15 m) blanket sands and many sinuous channel sands that can have net oil thicknesses of up to 35 m along the channel axis. Within these blanket sands there are lateral gradational changes in lithology and clay content, as well as variations in thickness. The channel sands can be from 500–2000 m in width, and generally show the best reservoir properties along the central part of the channel where there are also coarse-grained lag gravels. Some of these channels and blanket sands are many kilometers long, incised into low permeability and generally barren shales and silts. In addition to the numerous channels that contain oil, there are many that contain only water or that have thick bottom water zones. Small gas caps are relatively common, as are active bottom-water legs; however, many reservoirs have neither, making exploitation simpler.

Despite different formation names, HOB strata are also part of the Mannville Group, and are the same age as the large oil sand deposits to the north. The individual strata in the HOB

south of Cold Lake vary from highly quartzose and coarse-grained basal Mannville sands to clayey, arkosic sands that are fine-grained. The VO in the HOB is considerably lighter in density (11°–18° API gravity) and of much lower viscosity (as low as 400–500 cP in the western and southern flanks), compared to the bitumen found in the more northerly VO deposits. VO in the HOB is therefore easier to produce, which is why it has been the focus of much *in situ* production activity for many years.

2.5.4 Venezuelan Viscous Oil Deposits

Venezuela has the third largest VO resource in the world after Canada and Russia, estimated at 1.65 Tb [$262 \times 10^9 \text{ m}^3$]. The VO resource in Venezuela occurs in two sedimentary basins, the Maracaibo Basin in the west and the eastern basin – Cuenca Orientale – which contains the large Faja Petrolífera del Orinoco. The Faja Petrolífera del Orinoco (FPO) contains at least 1.4 Tb [$224 \times 10^9 \text{ m}^3$] of VO, mainly HO and XHO rather than bitumen (Dusseault *et al.*, 2008). The FPO VO deposit appears to be the largest single VO deposit on the planet, although some classify the Canadian oil sands as larger, treating all of the eastern Alberta deposits as one ‘mega-deposit’. According to a recent assessment by the USGS at least 500 Bb [$80 \times 10^9 \text{ m}^3$] of this resource are technically and economically recoverable with current technology (Schenk *et al.*, 2009), making Venezuela the country with the world's largest reserve of recoverable VO.

The FPO is located in eastern Venezuela north of the Orinoco River and covers an area of 54000 km². The belt is about 600 km in length and 90–100 km in width, and it lies at the southern extreme of a sedimentary basin where gently northerly dipping strata lap to the south onto igneous basement rock (Dusseault *et al.*, 2008).

The Cuenca Oriental has a synclinal and geometric structure similar to the standard model (Figure 2-4), and general hydrodynamic and oil accumulation conditions may be assumed to be approximately the same as the Western Canadian Sedimentary Basin. The deep E–W synclinal basin lies to the north of the FPO in front of the Sierra Orientale, a mountain belt with a transpressional structure, and the southward distance from the syncline axis to the

FPO is 200–300 km (Dusseault, 2001). Apparently, a number of large estuarine accretion plain and deltaic complexes (at least four) were formed by rivers that drained the Guyana Shield to the south, and the focal area of deposition changed as the sea level changed in response to the sedimentation, the formation of the mountains to the north, and the subsidence of the eastern Venezuelan Basin. The deposit is a unitary sequence of strata with general east–west continuity, although there are topographically high ridges between the four large valleys in which the thickest reservoirs are found. Within the FPO area, the fluvial and marine-margin deposits of the Oficina Formation of early Miocene age form the most important reservoirs in the region.

The FPO is substantially more quartzose and less clayey than the Canadian strata in general, although quite similar to the AOS deposit. This reflects the source rocks to the south in the Guyana Shield, and also suggests that there was a long period of reworking of the sand bodies in the estuarine plain as the strata were gradually laid down (Dusseault *et al.*, 2008). The entire sequence of oil-bearing strata in the FPO can be as thick as 400 m from the basal water zone to the uppermost oil sand. In general, the upper beds are of lower quality than the lower beds (Dusseault *et al.*, 2008) because of increased clay content and lower grain size, reflecting the upward-fining nature (more marine influence) associated with the generally transgressional depositional system, and many of the upper reservoirs are sinuous relatively fine-grained channel sands, but not nearly as high permeability and as low clay content as the lower channel sands that form the reservoirs currently being exploited.

Individual sand channel bodies in the lower channel-dominated part of the FPO range in thickness up to 40–55 m, although the majority of ‘discrete’ oil bearing beds are 8–12 m thick, with sharp lower boundaries from lateral erosional migration of channels, and more gradational upper boundaries, in each case showing a fining-upwards tendency. Some thick coalesced channel sand bodies are of almost uniform properties over many thousands of meters laterally; others are far more heterogeneous and contain multiple laminae of silt and shale, also leading to poor vertical flow properties. Good permeability interconnectivity within the reservoirs is evidenced by a high oil saturation state in the vertical sequence of

strata, along with a total displacement of water (except for the connate water wetting the grains), such that there are few active water zones except in the basal part of the overall oil-bearing FPO sequence where there is a regional oil–water contact.

Porosities of the FPO sands are from 27–28% in the deeper northern and eastern parts of the deposit, to 30–32% in the shallower southern section. The reservoirs range from less than one (upper zones) to as much as 10–15 Darcy in permeability (coarse-grained channel sands in the lowest part of the sequence).

The FPO rock and fluid properties are summarized in Table 2-5. The range of viscosities is from 1000 to over 10000 cP, with 60% of the resource found in the viscosity range 500–3000 cP. In general, the FPO is of substantially higher quality than Canadian VO reservoirs because of higher average permeability values, slightly higher average porosity and oil saturation volumes, higher formation compressibilities, lower clay content, greater thickness with more favorable net-to-gross ratios, and of course a far lower viscosity mainly because of higher formation temperatures (35–55°C instead of 5–25°C). A range of 3000–6000 cP estimated live oil viscosity in the reservoir is typical of the shallower 8–9° API FPO crudes in the upper half of the Oficina Formation, and for the deeper parts, values around 1000–2500 cP and even somewhat lower are found, depending on temperature. The product kh/μ , a measure of reservoir quality, exceeds 10 mDm/cP over vast areas, with values as high as 300 mDm/cP. These are far greater than most Canadian reservoirs where values are typically less than 10, and often less than 1. The most spectacular reservoirs are in the eastern Carabobo region; the thickest areas in this eastern-most paleo-valley axis have about 150 m of almost continuous reservoir rock with a net-to-gross ratio exceeding 90%, a permeability of 2–5 Darcy, and a mean oil saturation exceeding 0.85, giving kh/μ values of 200–600 mDm/cP, the best VO reservoirs in the world.

Table 2-5: Average geologic, reservoir and fluid properties of the VO deposits in FPO and Maracaibo Basin.

Property	Units	Faja (<i>Dusseault et al., 2008</i>)	Maracaibo basin	
			Mene Grande Field (<i>Layrisse, 1999</i>)	Bachaquero-01 Field (<i>Escobar et al., 1997</i>)
OOIP	Bb	1410		6.60
Depth	m	450-1100	168	1000
Avg. ϕ	%	27-31	20-33	33.50
S _o	%	86		80
k	D	1-15	0.50	3
API	degree	8-10	15	11.70
μ @ Pr and Tr	cP	1000-10000	2500-5000	635
Technically recoverable	Bb	500		

The Maracaibo Basin has had oil production since the first commercial oil well was drilled in about 1914 and has long been considered the second most important sedimentary basin for conventional oil after the Persian Gulf Basin. The Maracaibo Basin has an area of 50000 km², is located in western Venezuela, and was thought to contain over 318 Bb [50×10^9 m³] of different quality oils of which over 240 Bb [38×10^9 m³] are classified as VO (*Talukdar and Marciano, 1994*). However, the USGS more recently estimated 491 Tb [78×10^9 m³] OOIP of VO for the Maracaibo Basin, mainly HO 322 Bb [51×10^9 m³] and bitumen 169 Bb [27×10^9 m³] (*Meyer et al., 2007*). The trend of slowly growing VO reserves over time reflects the

increased knowledge of these deposits as the interest levels increase and trigger more exploration.

Interactions between the Pacific, Caribbean, and South American plates have shaped the development of the Maracaibo Basin over geological time and the Basin has undergone many different geological processes, evolving from a passive continental margin during Cretaceous to Eocene times into a foreland basin during the post-Eocene era. Most of the VO in the Maracaibo basin is found in shallow reservoirs of Miocene and Eocene age in the northeastern section of the basin, and it is characterized by the absence of *n*-alkanes in their composition, high sulfur content (> 1.3%), moderate to high vanadium content (200–500 ppm), and a low ratio of saturated to aromatic hydrocarbon (< 2). In addition, some VO deposits can be found in shallow reservoirs of Cretaceous age characterized by high density (11–16° API), high vanadium content (914–1173 ppm), high sulfur content (4.8–5.2%), and high resins and asphaltenes content (34–44%). It should be noted that the reservoir and fluid properties stated here are not for the entire basin, just certain Cretaceous age VO reserves. Geochemical studies have shown that the oil in the Maracaibo basin came mainly from the Upper Cretaceous La Luna source rock; a marine Type II kerogen shale.

Average porosity of the Eocene Miosa Formation and Mirador Sandstone reserves is about 20%, varying between 8–30%, with an average permeability of about 240 mD. Miocene reservoirs are mainly the unconsolidated Lagunillas and La Rosa Formation sandstones with an average porosity of 33% and range from 10–40%, and average permeability of 610 mD (Talukdar and Marcano, 1994). Reported sandstone porosities greater than 33% almost certainly reflect sample damage through expansion during recovery.

2.5.5 Other Major Viscous Oil Deposits

2.5.5.1 Russia

Russia, along with some of the former Soviet Union countries including Kazakhstan, Azerbaijan, Turkmenistan, Georgia, Kyrgyzstan, Uzbekistan, and Tajikistan, have the second largest VO resource in the world, estimated at 2 Tb [$318 \times 10^9 \text{ m}^3$], mainly reported in Russia

(> 1.80 Tb [$286 \times 10^9 \text{ m}^3$]). This number has greatly increased in recent decades because of better delineation of Siberian VO deposits (BGR, 2009).

Most of the VO resource is found in clastic rocks, far less in carbonate rocks (Meyer *et al.*, 2007; BGR, 2009). The VO deposits in Russia consist of a few vast VO deposits along with several hundred smaller deposits in three major oil provinces. In addition, there are a number of shallow or surface deposits of VO where limited mining production is technically feasible (Meyerhoff and Meyer, 1987).

The largest VO deposits in Russia are found in the Eastern European–Siberian platform complex and account for over 70% of the VO resource. The Siberian platform complex with an area of over 2827000 km² is a flat-lying basin covered mainly by Proterozoic and Cambrian shallow-water shelf and lagoonal rocks. The lower sections are made up of mostly marine sandstones and shale of Proterozoic age. Accumulation of the sediments in the Siberian platform started ~ 925 million years ago and continued until the Ordovician Period (~ 448 MMY ago). During this period over 3 km of sediments covered the platform, leading to burial, compaction of the sediments under pressure and temperature, and generation of oil. Reactivation of an old existing fault system generated the structural trapping mechanisms in the Carboniferous period and led to remobilization of the already generated oil and its subsequent biodegradation and alteration after moving up-dip through the fracture systems toward the surface. This process continued for about 200 million years after the generation of oil in the platform, and erosion and uplift led to the destruction of many VO deposits as well as altering the nature of the oils (e.g., changing HO to bitumen) (Meyerhoff and Meyer, 1987). Due to the highly diverse and scattered nature of the VO deposits in Russia the reservoir and fluid properties vary substantially from one deposit to another but in general the VO viscosity *in situ* in the Russian VO deposits is reported from several hundred cP to over 500000 cP, depths range from a few meters to 2800 m in some areas, and there is a wider range of porosities (lower than in Canada and Venezuela) and other rock properties as well. The level of delineation and quantification of the Siberian VO deposits remains far behind

that in Canada and Venezuela, so there are large margins of error associated with VO resource estimates from Russia.

2.5.5.2 Kazakhstan

The wide-spread presence of relatively shallow VO deposits off and on-shore of the Caspian Sea is reported in Kazakhstan (Meyer *et al.*, 2007). A few example VO fields are described in this section. Also, fluid and reservoir properties of some Kazakh VO fields are presented in Table 2-6.

Table 2-6: Average geologic, reservoir and fluid properties of selected VO deposits from Kuwait, Kazakhstan, China, and Iran.

Property	Units	KBM	Kenkiyak	Lower Fars	Soroosh	Kuh-e-Mond (Carbonate VO field in Iran)	Taobao (Dusseault <i>et al.</i> , 2002)	Zaoyuan (Jiayu and Jiyani, 1999)	Guantao (Jiayu and Jiyani, 1999)
OOIP	Bb	0.612		10	10	7	0.15		
Depth	m	350-500	350-400	100-255	2200	1100-1200	272-399		1160-1300
Avg. ϕ	%	28-32		31-33	26-27	16	33-37	24-26	28-32
S_o	%			0.80		46	95		
K	D	0.175-0.50	0.01-4	0.25-6	4-10	< 0.001	5		
API	°	18-20		12 - 18	18				
μ @ Pr and Tr	cP	300-400	150-700	100-1000	500-600	570	1850	525-580	250-5700
Technically recoverable	Bb								

Karazhanbas field (KBM) is located in Western Kazakhstan on the Buzachi Peninsula on the Caspian Sea with estimated OOIP of 0.612 Bb [0.097×10^9 m³]. The onshore part of the KBM covers an area of 180 km², oriented east–west. KBM was discovered in 1974 and is situated in the structurally high portion of the Buzachi uplift, a gentle, anticlinal fold

complicated by western and eastern arches which developed at different geological times. Well data have delineated a geological profile that includes Lower Triassic, Middle Jurassic, and Lower Cretaceous oil-bearing strata. Productive horizons are gently folded, flat-lying beds of sand, river channel sands, and other sand bodies characteristic of clastic cyclic deposition; carbonates are rare, evaporites absent. The reservoir depth ranges from 250–500 m and the average permeability is reported on the order of 0.80 Darcy. The VO in this area is characterized by a density of 0.93–0.95 g/cm³, viscosity of 300–500 cP, a high sulfur content (~ 2 wt%), low asphaltenes content (~ 3 wt %), and a vanadium content of 100–120 µg/g (Meyerhoff and Meyer, 1987; Dorogochinskaya *et al.*, 1989; Zaykinaa *et al.*, 2001; Collins *et al.*, 2003).

Another example of Kazakh VO deposits is the PETEC VO field. The main PETEC reservoirs are unconsolidated sandstone of Jurassic age located in a tectonically active region. The reserves are 410–490 m deep and the oil viscosity is in the range of 300–400 cP under *in situ* conditions. The average permeability in the field is reported as 0.45 D (Darcy) and it varies between 0.19–2 D in different sections of the field (Mosesyan *et al.*, 2009).

2.5.5.3 Kuwait

USGS has reported a large VO resource in Kuwait in naturally fractured carbonate reservoirs similar to the majority of the oil reserves in the Middle East region (Meyer *et al.*, 2007). This is found in the south of Kuwait and in the jointly Kuwait–Saudi Arabia administered zone between the two countries.

The Lower Fars (LF) VO field in a shallow sandstone found over an area of ~ 1000 km² northwest of Kuwait City may be the largest VO accumulation in the country, containing 12–15 Bb. The LF VO deposit is a shallow reservoir with high porosity and permeability, relatively low viscosity, and with a modest variation in fluid properties with depth and with location in the reservoir. The LF deposit appears to have been sourced from near-by deeper strata in the underlying Ratqa-Rumaila fields through vertical and lateral migration, followed by shallow-depth biodegradation upon exposure to suitable conditions.

LF burial depth is approximately 100–225 m, and the reservoir rock is a high-porosity ($\phi \sim 31\text{--}33\%$), high permeability unconsolidated sandstone (0.25–6 D, 3 D being typical). Oil saturation is ~ 0.8 , likely higher in coarser-grained sands, and the *in situ* oil viscosity ranges from as low as 100 cP in the deepest parts of the field (40°C, 270 m) to just over 1000 cP in the shallower parts (25–30°C, 70–100 m deep). The API gravity is reported to be between 12° and 18°. The mean oil-saturated thickness is about 10–11 m, with area of 50 km² having accumulations greater than 15 m thick (Dusseault *et al.*, 2008).

2.5.5.4 China

According to the USGS Meyer *et al.* (2007), the VO resource in East Asian countries is estimated at 178 Bb [$28 \times 10^9 \text{ m}^3$], mainly in China. Based on the latest assessment of the China's conventional and unconventional energy resources known as the 2007 China National Petroleum Assessment conducted by the government of China (Zhu *et al.*, 2008; Liu *et al.*, 2010), over 11% of the Chinese oil resource is classified as HO which is estimated to be on the order of 54 Bb [$8.60 \times 10^9 \text{ m}^3$], mainly distributed in five large basins, Bohai Bay, Songliao, Tarim, Ordos, and Junggar. Furthermore, the oil sands (e.g., bitumen) resource in China is estimated to be on the order of 38 Bb [$6 \times 10^9 \text{ m}^3$], distributed in seven basins including Junggar, Tarim, and in northern Tibet, Qiangtang. Therefore, the total VO resource in China apparently exceeds 92 Bb [$36.6 \times 10^9 \text{ m}^3$].

The VO resource in China is found over a vast country in many basins, so generalizations and averages are difficult to generate, and the space available is limited. The *in situ* viscosity of VO in China ranges from 100–100000 cP in different reservoirs, and it is generally characterized by its high resin and low asphaltene content. Reservoir depth of VO reserves in China vary in different parts of the country. In the southern part of the Songliao Basin (Liaohé, Liaoning Province) the depth is in the range 800–1700 m, whereas on the western flank of this basin, in Jilin and Heilongjiang Provinces, shallower deposits are found in the up-dip part of the sediments, with some zones being near enough to the surface to permit strip mining. In the northwestern part of Xinjiang Province (Karamay Field) the reservoirs

are shallower, from 100–400 m deep, and more heavy oil resources are being regularly delineated in the region. Some deep VO reserves are reported in Xinjiang Province (Tuha region) with depths ranging from 1700–3200 m, as well. Reservoir and fluid properties of a few Chinese VO reserves are presented in Table 6 (Jiayu and Jianyi, 2005; Shouliang *et al.*, 2005).

2.5.5.5 Iran

Viscous oil resources in Iran are estimated to be on the order of 80–100 Bb [(13–16)×10⁹ m³] mainly in NFCRs of the Zagros Mountains foreland basin. About 20–30% of the Iranian VO deposits are found in high porosity, high permeability sandstone reservoirs in the off-shore Persian Gulf. The VO type in this region is mostly HO which is mobile under reservoir conditions, allowing some primary cold production with oil viscosities of 200–600 cP *in situ*. The Soroosh HO field is located in the Persian Gulf with an OOIP of 10 Bb [1.6×10⁹ m³], and an oil viscosity of ~ 600 cP in the “Burgan B” sandstone of Middle Cretaceous age. Soroosh is a high porosity ($\phi \sim 26\text{--}27\%$) and high permeability unconsolidated sandstone (4–10 D) reservoir at a depth of 2200 m below sea level.

Iranian VO deposits are mainly biodegraded light oil originating from different organic rich shale units in the region. After sedimentation, burial and generation of oil in the Persian Gulf oil system (Zagros Foreland Basin), subsequent tectonic activities led to vertical and up-dip migration of oil to a shallower depth, including vertical migration through fracture systems, biodegradation, and eventually formation of VO reserves. Furthermore, ongoing tectonic activities after formation of VO reserves in the Zagros foreland basin has led to more folding and fracturing and in some cases additional burial. This scenario explains the formation of some VO deposits found at depths greater than 3000 m (4000–4300 m in one case). Such a depth is beyond the reach of biological activities which are essential in the formation of most of the VO reserves.

Some data for Irani VO reservoirs are presented in Table 2-6.

2.6 VONFCRs

Despite enormous world VO endowment estimated by the USGS to be on the order of 9 Tb worldwide production is only about 6% of the total oil production of about 87×10^6 b/d. VO resources in NFCRs are estimated to be on the order of 1.5–2.2 Tb, worldwide. The largest accumulations of VO, mainly HO, are reported in the Middle East. At the other hand, Canada has the largest bitumen saturated accumulations in the world estimated to be on the order of 0.45 to 0.55 Tb.

VO resources in NFCRs in the Middle East are estimated to be on the order of $530\text{--}970 \times 10^9$ b, which is equal to 30-35% of the world VO in NFCR resource base (Meyer and Dietzman, 1979; Briggs *et al.*, 1988; Shafiei *et al.*, 2007; GEA, 2012). Contribution to daily production is estimated to be in the range $200\text{--}300 \times 10^3$ b/d, an almost negligible quantity compared to the daily light oil production in the region. VO production in the Middle East was lagged behind the giant light oil producers in except countries like Turkey, Oman, and Egypt who they have very limited light oil reserves and had to attack their VO resource to respond part of their domestic oil consumption demands.

Productive VO bearing NFCRs in the Middle East are characterized by low matrix permeability and high fracture permeability. Large-scale oil flux is through the high permeability fracture system, whereas the matrix-fracture interaction mainly controls recovery efficiency and maintaining production levels. This is the type of production taking place from reservoirs in Oman, Iran, Iraq, Syria, Turkey, and Egypt.

2.6.1 Iran

Iran has the third largest proven oil reserves in the world, according to the EIA in January 2008, which is about 138.4×10^9 b after Saudi Arabia and Canada. It should be noted here that this is not including VO reserves yet. Many believe that the country has passed its peak oil production and some believe oil production in Iran will peak within the next 10-15 years. Oil production in this country is declining 4-6%/yr while domestic consumption is increasing by 6-8%/yr leading to decreasing net oil export. Recently declining conventional oil

production, combined with a desire by Iran to sustain current production level as the major source of national income, is triggering interest in this VO resource.

The first discovery of VO in Iran goes back to early 1931 when wells drilled for gas reservoir evaluation purposes in the southwest of Iran encountered a large VO occurrence. Systematic VO exploration in Iran started in 1982; in 1994 the Petroleum Engineering and Development Company (PEDEC) was established within the National Iranian Oil Company (NIOC) to manage national HO and XHO assets. Significant HO discoveries in the south and southwest of Iran, combined with high oil prices and difficulties in sustaining conventional oil production rates, have led to a greater interest in their development since 2000 (Shafiei et al., 2007).

According to the latest studies, Iran has over $60-90 \times 10^9$ b of VO, mostly occurring in NFCRs (limestone and dolomite) and comprising > 40-65% of Iran's proven oil reserves. Several NFCR VO fields have successfully cold tested oil qualities on the order of 6-18°API, but the VO NFCRs reserves base remains undeveloped mainly because of lack of appropriate technology. PC pumps were successfully field tested and implemented in an Iranian VO NFCR in 2007 and daily production of 3500 bbl/d was recorded. It should be noted here that current VO production rate in Iran is about 250,000 b/d from a VO sandstone reservoir with *in situ* oil viscosity of 600 cP.

Iranian HO reservoirs are found in Upper Jurassic and Cretaceous carbonate formations in the Persian Gulf and surrounding areas. Most reservoirs are composed of pelletal, oolitic, or bioclastic greenstones' and reefal limestone that have high primary porosity and permeability. The reservoirs are sealed either by tight limestone, massive anhydrite, or by impermeable argillaceous rocks, and these seals are effective throughout most of the Persian Gulf and surrounding areas (Bashari, 1988; Moshtaghian *et al.*, 1988; Shafiei *et al.*, 2007).

Most VO reservoir rocks in Iran are structural traps, i.e.: anticlinal structures, found in limestone and dolomite ranging in age from Cretaceous to Eocene. The most important VO fields in the southwest of Iran are Kuh-E Mond, Ferdowsi, Zaqeh and Paydar. Because of

geological variability, production issues, and uncertainty in application of new production technologies in NFCRs, these fields have not been systematically developed, with only a few wells here and there on slow production. The contribution of HO reserves in Iran to total oil production is negligible, and it remains to execute a technically-based assessment of these and other fields to choose optimum production approaches, or modify existing approaches to cope with particular geological circumstances (Bashari, 1988; Moshtaghian *et al.*, 1988; Shafiei *et al.*, 2007).

2.6.2 Turkey

Turkey's proven recoverable light oil reserves estimated to be on the order of 300×10^6 b by the Energy Information Administration (EIA) in January 2008. It should be noted here that this is not including VO reserves of the country yet. Total oil production in Turkey is right now around 40×10^3 b/d which is negligible compared to the total oil consumption of $> 600 \times 10^3$ b/d in the country.

Major VO producing fields in Turkey are Bati Raman, Bati Kozluca, Garzan, Camurlu and Raman. A limited local light oil resource in Turkey was the main driving force for Turkish oil industry toward production of VO during the last half century.

VO resource (OOIP) in Turkey is estimated to be on the order of 6.65×10^9 stbbl. VOs in Turkey are mostly mobile under *in situ* reservoir conditions and can be produced with primary cold production but recovery factor will remain still very low. Turkey has been one of the leading countries in heavy oil production from NFCRs in the region since 1963.

Turkey has five major VO fields, mainly in the southeast of the country: Bati Raman (OOIP of 1.850×10^9 stbbl), Raman (OOIP of 400×10^6 stbbl), Çamurlu (OOIP of 377×10^6 stbbl), Garzan (OOIP of 163×10^6 stbbl) and Bati Kozluca (OOIP of 138×10^6 stbbl) with oils viscosities ranging from 2260 to 64000 cP @ 20 °C and °API ranging from 12-18.

The Bati Raman VO field discovered in 1961 in southeast of Turkey, and it is the largest oilfield in Turkey, a NFCR VO field. It is a low-pressure field containing low-gravity (12° API [0.986-g/cm^3]), high-viscosity (592-cp *in situ*) oil at an average depth of 4300 ft

[1311 m] with a gross thickness of 210 ft [64 meters] and 1.85×10^9 stbbl [294×10^6 stock-tank m^3] OOIP. The producing formation of the field is Cretaceous Garzan limestone, an elongated east/west asymmetric anticline measuring 10.5×2.5 miles [17×4 kilometers]. The Garzan limestone has a reefal origin and a fractured, vuggy character exhibiting areal and vertical heterogeneities. The structure becomes chalky and thus tighter to the east. Average porosity is 18% and is mainly vugular and fissured in type. Average matrix permeability determined from cores is 16 mD. Well tests indicate 200-500 mD effective permeabilities, confirming the contribution of secondary porosity. In the western and central portions of the field, a secondary vugular porosity interconnected by fissures appears to be superimposed over low primary matrix porosity (Karaoguz, 1989; Spivak *et al.*, 1989; Issever *et al.*, 1993).

Turkey is the pioneer of CO₂ VO production in the world. Bati Raman VO field is the only successfully commercialized immiscible CO₂ VO production project in the world despite of complex and heterogeneous geology of the field (Kanta and Topkaya, 1983; Bağcı, 2005). During almost four decades of VO production from Bati Raman VO field, several VO production methods had been implemented such as: carbon dioxide immiscible injection using vertical wells, horizontal wells and pressure maintenance techniques like gel treatment.

The main/primary production mechanism is rock and fluid expansion. Water drive appears to be insignificant except for a very weak aquifer influence at the central north flank wells. The solution Gas Oil Ratio (GOR) is 18 scf/stb resulting in a low bubble point pressure of 1.1 MPa. Before CO₂ immiscible injection, the reservoir pressure did not decrease below the bubble point pressure; therefore, in practice, there was no solution gas drive mechanism. The original reservoir pressure was 12.4 MPa, which dropped to an average pressure of 2.76 MPa after cumulative production of 30×10^6 stbbl prior to CO₂ application. Before the project began, 65 active producers were pumping, with a total production rate of 1600 stbbl/d compared with the year 1969 peak rate of 9000 stbbl/d. Initially, well production rates were up to 400 stbbl/d; this decreased then to an average of 25 stbbl/d before treatment (Karaoguz, 1989; Issever *et al.*, 1993).

Primary recovery prospects were low mainly because of unfavorable oil properties (such as low °API gravity, low solution gas and high viscosity), low reservoir energy, and the type of driving mechanism. It was estimated that ultimate OOIP of 1.5 % could be produced via cold production. The reservoir history and unfavorable properties caused rapid declines in the reservoir pressure and production, which suggested the need for a suitable production technology to increase ultimate recovery from this vast reservoir. Since 1968, several pilot tests have been conducted, including steam huff 'n' puff, steam drive, air injection, and water flooding. The results of extensive laboratory, modeling, and engineering studies; the presence of a CO₂ reservoir 55 miles from Bati Raman; and economic considerations led to apply an immiscible CO₂ huff-'n'-puff-type method. The reservoir gas in Dodan field was almost pure CO₂. The current field production capacity is 60 MMscf/d (Karaoguz, 1989; Issever *et al.*, 1993).

Monitoring of oil production rate, injection pressures, gas/oil ratio (GOR), and gas utilization factor in the reservoir after commencement of the CO₂ injection revealed three different periods in the history of Bati Raman HO filed. From 1986-1993 can be defined as the fill-up period, in which the injected gas filled the fractures and vugs in the reservoir. Because of the high compressibility factor of the CO₂, the injection pressures are stable all over the field. The next period from 1993-1996 is the period of increased oil production rate; in which daily rate of 12000 b/d was reached and remained almost constant. The last period is obviously the decline period. The main cause of this is the high heterogeneity of the filed with combination of adverse factors and very low resistance pathways for recovery fluid. Production rate declined substantially since 2000. Until 2003, cumulative production in the Bati Raman VO field reached 5% of OOIP (Karaoguz *et al.*, 2004; Karaoguz *et al.*, 2007). This is still a very low value. The major reason for low *RF* is the heterogeneous nature of the reservoir reducing efficiency of most of the VO production processes. In 2004 a polymer gel treatment method (a fracture plugging polymer gel system) implemented in the filed in order to impede or reverse the decline to increase CO₂ sweep efficiency. The sweep efficiency was increased by 12%

using this technique. The Bati Raman NFCR VO field is still producing VO using CO₂ immiscible injection and gel treatment techniques. Steamflooding using horizontal wells is being considered as the next technology in order to improve the VO production from this field.

2.6.3 Oman

Oman is one of the pioneer countries in VO production from NFCRs in the Middle East. Because of limited conventional oil reserves in the country compared to other oil rich states in the region and following huge discoveries of VO accumulations mainly in elastic reservoirs and to a lesser extent in NFCRs back in late 1960-70 (Nadyal *et al.*, 1983; Al-Adawy and Nadyal, 1991), Omani authorities became more interested in VO production. Petroleum Development Oman (PDO) supported numerous research projects and pilot tests on VO production from NFCRs. Daily VO production in Oman from NFCRs is about 50×10^3 b/d which is about 6% of daily oil production of 734×10^3 b/d from conventional oil reserves in the country. Oman is the third largest VO producing country after Iraq and Egypt in the Middle East. Proven conventional oil reserves in Oman is about 5.5×10^9 b reported by EIA in January 2008.

Following major VO discoveries in Oman which is estimated to be on the order of $10\text{-}15 \times 10^9$ b, different VO production strategies were investigated, some field tested and implemented such as steam drive, hot water injection, Thermally Assisted Gas-Oil Gravity Drainage (TA-GOGD) utilizing horizontal, multilateral and intelligent well technologies in a number of VO reservoirs.

The Qarn Alam in Oman, a NFCR VO field with OOIP of 1.34×10^9 b [213×10^6 m³] and a 16 °API and 200 cP viscosity oil at reservoir conditions, has been the focus of VO production from a NFCR VO field during the last decade. This field is an intensely fractured carbonate field situated in Northern Oman. The field is an anticline structure of 6×3 kilometres with N-NE by S-SW orientation. The major oil bearing reservoirs, the Shuaiba and Kharaib formations, are separated by a very low permeability oil bearing zone called the Hawar.

Fracturing reported throughout all zones, and it is believed that the fracture networks are in hydraulic communication with a very active aquifer. The initial oil saturation is about 95% and initial water saturation is connate water. The matrix porosity is about 30%, while the matrix permeability ranges between 5-20 mD. Fracture permeabilities of 0.10-1000 D reported using pressure build-up tests in the field (Macaulay *et al.*, 1995; Al-Shizawi *et al.*, 1997).

The Qarn Alam field was discovered in 1968 and was first put on primary cold production back in 1976 and the net oil production peaked in 1978 at 38×10^3 b/d, despite the high oil viscosity. Production from the field started in 1976. Waterflooding was implemented in 1986 following a number of pilot projects. The original development plan was comprised waterflooding using an inverted nine-spot vertical well pattern. Early water breakthrough after initiation of the waterflooding operation has led to change of drilling pattern in 1994-95 to a vertical line drive parallel to the dominant NW/SE trend of faults and fractures in the field. Under primary cold production, the reservoir produces on average about 630 b/d. During the initial cold HO production period, the oil contained in the highly permeable network of fractures was produced with *RF* of about 2% which is very low. By 1979, a small secondary gas cap in the fracture network was formed because of the pressure drop near or slightly below the bubble point in the crest of the field and gas injection into the production wells for of gas lift, purposes. The major oil production mechanisms in the period of 1975 to 1996 are emptying of the fracture system, fluid expansion due to pressure reduction, and isothermal GOGD. Simulation studies based on a history match of this production period indicate that during the initial production peak, half of the oil was supplied by emptying the fracture system, while the other half came from pressure reduction of the matrix hydrocarbon (Macaulay *et al.*, 1995; Al-Shizawi *et al.*, 1997). Shahin *et al.* (2006) investigated application of TA-GOGD in Qarn Alam is to develop additional oil by increasing the *RF* up to 27% of STOOIP. TA-GOGD has been piloted successfully in the Qarn Alam HO field and will be implemented in the field in full scale. Despite of this fact that the Qarn Alam VO field in Oman is a relatively shallow (depth of about 360 meters) and high matrix porosity

and permeability in comparison with other NFCR VO fields, the oil industry is learning a lot from this pioneer project how to develop VO NFCRs.

2.6.4 Egypt

VO resources in Egypt are estimated at 16×10^9 bbl [2.549×10^9 m³] which over 90% is occurred in clastic reservoirs, mainly sandstone and some conglomerate formations. Egypt is the 2nd largest VO producers in the Middle East from VO NFCRs with producing 55×10^3 b/d. Proven conventional oil reserves in the country is reported on the order of 3.7×10^9 b [0.59×10^9 m³] and daily conventional oil production is about 667 Mb/d, according to the EIA as of January 2008.

Issaran and Bakr Amer HO field are amongst VO NFCRs in Egypt. The Issaran field, a Miocene age VO field with OOIP of 0.5×10^9 b [79×10^6 m³], was discovered in 1981. The producing strata were heterogeneous carbonate formations of Miocene with average depth of 330-760 meters. These are the Upper and Lower Dolomite and the Nukhul formation. The reservoir characteristics of the Nukhul formation, consists of a tight limestone matrix with a well-connected leached-fossil mold system with macro-pores. The Nukhul reservoir accounts for 15% of the reserves for the Issaran field. The average reservoir temperature is 85-100 °F; the bottom hole pressure is approximately 650-700 psi. At reservoir temperature, corresponding densities are 0.964 and 0.988 g/cm³, and the viscosities are approximately 3000 and 5000 cp. Porosities ranging from 23-33%, and permeabilities from 1.3-104 mD. The matrix permeability for the Nukhul formation is estimated to be very low, but the fracture permeabilities exceed several Darcies. Before mid-1999, nine wells had been drilled in the field with a very low productivity of 450 b/d. The field has been producing 1800 b/d from five new wells drilled in the area during late-1999 and 2000. CSS pilot test, ten wells, during 2004 to 2006 in the field lead showed a substantial increase in HO production. Three CSS wells produced an average 230 b/d/well. These rates are limited by available pumping equipment. Average production during 2006 in the field was 4474 b/d; from both conventional and CSS wells. 30 additional CSS wells and associated facilities

were planned in 2007 and 50 more CSS wells are planned in 2008. Over than 600 CSS wells and related thermal facilities are planned over a five year period (Waheed *et al.*, 2001).

Due to high reservoir heterogeneity and complex lithology of along with low reservoir pressure in Issaran VO field achieving to higher RF seems to be challenging. A better reservoir characterization with implementation of new production and well completion technologies will help in production of more oil from this complex and challenging reservoir.

2.6.5 Kuwait

Kuwait is the 10th largest oil producing country in the world with producing 2.67×10^6 b/d. Kuwait holds the 5th largest proven oil reserves in the world, according to the EIA as of January 2008, which is about 104×10^9 b. It should be noted here that this is not including VO reserves yet. Kuwait has over $40\text{-}50 \times 10^9$ b of VO in both clastic and NFCRs. Daily VO production in Kuwait is about 28×10^3 b/d which is negligible compared to conventional oil production in the country.

Among the clastic VO reservoirs in Kuwait, the Lower Fars (LF) sandstone reservoir in northern Kuwait is probably the single largest accumulation of heavy oil in Kuwait, containing somewhere in the range of $12\text{-}15 \times 10^9$ bbl distributed over an area of ~ 1000 km² northwest of Kuwait City against the Iraqi border (Al-Qabandi *et al.*, 1995). Although a small resource in comparison to Canadian and Venezuelan VO resources of over $10^{12} \times 10^9$ b each, the LF nonetheless represents a significant fraction of Kuwaiti VO resources.

There are a few number of VO medium fractured carbonate reservoirs in Kuwait with total OOIP of over 30×10^9 b. These reserves are not yet developed and some are situated in partitioned divided zone between Saudi Arabia and Kuwait. Wafra is the largest VO carbonate filed in the divided zone which is consist of two reservoirs with $^{\circ}\text{API}$ ranging from 13-20 degrees, depths ranging from 400–100 meters and good matrix porosity and permeability (Penner, 1982). Cold production seems to be the first rational production option because of its lower CAPEX and OPEX compared with thermal methods followed by

thermal techniques utilizing horizontal well technology such as SAGD and CSS however this has to be investigated carefully and precisely.

2.6.6 Rest of the world

Complete discussion of this VO NFCRs cases is beyond the scope of current research project. Nevertheless, the world's VO resources in NFCRs are estimated to be 1500–2200×10⁹ b which are mainly reported in Canada, the Middle East, and the USA. Geographical distribution of this resource and fluid and reservoir properties are not delineated well, yet, in except for very few cases. It can be said here that there is no clear picture of this immense resource so that the policy makes and technology leaders in this area can predict of the future of development of this resource and its potential contribution to the energy market. Despite this enormous resource size, only a limited production is reported dominantly from lower viscosity reservoirs only, at low rates, thus the ultimate *RF* of the more viscous NFCR resource base will remain close to zero unless for now. Further delineation of this immense energy resource is necessary. A few VO NFCR steamflooding pilot operations are reported in the literature from France, Italy, Congo, Turkey, USA, Kuwait, and Saudi Arabia and Cyclic Steam Stimulation (CSS) also has been used in VO NFCRs, and data are available only from cases in Canada, China, Egypt, and Syria. Some of the field pilots are described in Chapter 3.

2.7 *In situ* Viscous Oil Production Technologies

2.7.1 Historical Development

The earliest systematic use of VO in the form of natural bitumen predates written history. Canadian First Nations people used bitumen (tar) from VO outcrops in Alberta to seal their canoes, and various civilizations have used oil and bitumen from natural seeps for many purposes (Hein, 2000). As Canada has emerged as the leading nation for the VO production industry, home to many new innovations and ideas in developing, testing, and commercializing new production methods, waste disposal techniques, and so on, it will be the focus of historical developments over the last three decades.

Dr. R. Bell identified the AOS in 1882, analyzed many samples, and initiated experiments using hot water to separate the VO. In 1888, R.G. McConnell worked on the geology of the AOS, and later drilled the first oil well in the Athabasca area. However, the acknowledged ‘Father of the Oil Sands’ was Sidney Ells, an engineer who began detailed surveys in the Athabasca River valley in 1913, followed by production experiments on surface-mined specimens (McRory, 1982). D. Diver in 1920 was apparently the first to try producing VO from the AOS by an *in situ* technique based on distillation with a heating unit placed at the bottom of a wellbore near Fort McMurray.

After 1920, efforts to produce VO from the AOS continued at the Alberta Research Council, with Dr. Karl Clark building a hot-water separation unit in Edmonton in 1925. His work became the basis for today’s surface production activity, as all mining projects (>800 000 b/d in 2010) use variations of his hot-water approach. In the 1960s, Sun Oil (now Suncor) built the first commercial oil sands surface mine and upgrading facility with a capacity of 31500 b/d (Hein, 2000) 45 km north of Fort McMurray. Syncrude Canada Ltd., a consortium of several companies, started production in 1978 from their integrated mining and upgrading facility slightly north of the Suncor site, and the Albian Sands Consortium (60% Shell Oil) mine on the east side of the Athabasca River began shipping bitumen to a Shell Oil upgrader 50 km east of Edmonton in 2003, reaching about 155000 b/d by 2006, with expansions planned for the period 2012-2016. The latest operation, the Horizon Project operated by CNRL (Canada Natural Resources Ltd.) began bitumen production in 2009 and reached values in excess of 150000 b/d in 2010. Suncor and Syncrude both have ongoing expansion activities.

Following the 1971–1972 tripling of oil price, the Alberta Oil Sands Technology and Research Authority (AOSTRA) was formed to fund research on VO technologies. A decade later they funded an underground test facility to test horizontal wells using steam assisted gravity drainage (SAGD) technology (O’Rourke *et al.*, 1991), and many other new technology initiatives were initiated through their extensive programs. A dramatic surge in VO development followed the international crude oil price recovery in 1999–2001 (Cunha,

2005) and currently, over 55% of Canada's oil production, which now exceeds 3×10^6 b/d, comes from VO deposits, mostly within 150 km of the Alberta–Saskatchewan border. This is a highest percentage of national production from VO than any other major oil-producing country (CAPP, 2012).

2.7.2 Surface Mining

Canada is the only country with an active and growing surface mining (SM) industry although VO production from shallow deposits is reported in China and Russia. The main factors controlling the feasibility of SM projects are the deposit richness and the burial depth; probably the maximum depth of SM operations is limited to about 75 m of overburden (ERCB, 1979).

A large area of the AOS north of Ft. McMurray, Alberta meets SM feasibility criteria (Hein and Cotterill, 2006). Local richness is a function of saturation times porosity ($S_o \times \phi$), thickness (t), and the net-to-gross ratio, with the latter being defined as the ratio of strata thickness with $S_o > 0.5$ to the total reservoir thickness. Richness can be quantified by summing the product of porosity, saturation (only 1 m thick beds with $S_o > 0.5$) and thickness, giving a 'height of good quality bitumen', then incorporating value adjustments for net-to-gross ratio and burial depth.

Allowing for surface facilities and assuming a combined production Recovery Factor (RF) of 0.82, the in-place minable bitumen reserve is in the order of 42 Bb [6.7×10^9 m³], about 16% of the total technically recoverable VO in Canada. However, improvements in extraction technology suggest that $RF = 0.9-0.92$ is generally feasible with current methods. Production over the period 1967–2012 was over 4 Bb [0.6×10^9 m³] (ERCB, 1979; the author updated this figure) so the SM reserve has been reduced to ~ 38 Bb [6.1×10^9 m³].

The SM VO supply now has a nominal capacity of 993000 b/d with an average contribution of about 850000 b/d in Canada, about a quarter of total Canadian oil production and $\sim 1\%$ of the world's production rate. The actual daily supply from SM activity will likely exceed 1 MM b/d in 2011. Currently, two more mining operations are under construction, others are

being slowly expanded, and 22 new projects and expansions of existing projects are in various pre-construction design stages (Government of Alberta, 2010).

All SM operations use the hot water extraction technique (Clark and Pasternack, 1932); hot water and NaOH are added to the mined oil sand, agitated and then aeration is used to generate a floating bitumen froth that is skimmed and beneficiated through mineral and water separation before being sent for upgrading. Slurried aqueous wastes are pipelined to huge tailings ponds.

Capital expenditures (CAPEX) required in a Canadian integrated SM project are \$95000–105000/b for SCO production and \$85000–90000/b for bitumen production (in 2012), substantially higher than for *in situ* VO production projects (Table 2-7).

Table 2-7: Major *in situ* production technologies for VO (Dusseault and Shafiei, 2011; GEA, 2012).

Abbrev.	Method	Description, Screening Criteria
CP	Cold Production	Non-thermal VO production using long horizontal wells. No free water, $\mu < 5000$ cP, $k > 2 D$, $h > 10$ m, $RF = 0.08-0.2$, solution gas drive
CHOPS	Cold Heavy Oil Production with Sand	Non-thermal production from vertical wells in unconsolidated sands with deliberate massive sand influx. No free water, $\mu < 2 \times 10^4$ cP, $k > 0.5 D$, $h = 2.5-20$ m, $RF = 0.12-0.2$, solution gas drive
IGI (or GOGD)	Inert Gas Injection (Gas over Oil Gravity Drainage)	Non-thermal conventional oil production, long horizontal producers, non-miscible gas injection, gravity-dominated drainage. Good k_v required, $h > 10$ m (or good dip), $RF > 0.5$. A post-steam method for heavy oils when viscosity has been reduced and shale barriers sheared and fractured
PPT	Pressure Pulse Techniques	Sharp pulses applied to a liquid-dominated flowing region to accelerate flow and reduce blockages. Applicable to conventional and VO.
SF, SD	Steam Flood,	Steam injected or circulated using various strategies in vertical &

	Steam Drive	inclined wells. $\mu < 20000$ cP, $k > 1$ D, $h > 10$ m, $RF = 0.25-0.5$, $Z < 1200$ m
CSS	Cyclic Steam Stimulation	Steam injected in vertical or inclined wells, followed by a production phase. $\mu > 20000$ cP, $k > 0.5$ D, $h > 10$ m, $RF = 0.2-0.35$, $Z < 1000$ m
HCS	Horizontal Cyclic Steam injection	Cyclic steam injection in basal horizontal wells 500-1000 m long. No free water, $\mu > 10000$ cP, $k > 0.5$ D, h (net) > 15 m, $RF = 0.3-0.5$, $Z < 1000$ m, a moderate net-to-gross pay ratio is needed (> 0.75)
SAGD	Steam-Assisted Gravity Drainage	Gravity flow at constant pressure to 500-1000 m basal horizontal wells, steam injection into separate vertical or horizontal wells. $k_v > 1$ D, h (net) > 15 m, $RF = 0.60-0.80$, a good net-to-gross pay ratio is needed (> 0.9)
VAPEX	Vapor-Assisted Petr. Production gravity drainage	Diluting condensing gaseous phase, perhaps heated, is used with long horizontal wells. Success to date only when combined with SAGD, HCS, and vertical well cyclic steam. If used cold, good k_v needed, $\mu < 1000$ cP
THAI™	Toe-to-Heel Air Injection	High-T combustion using horizontal producers, vertical air injectors. First field trial began Sept 2006 (Whitesands Project) and now is operating with a nominal production capacity of 1900 b/d. Application criteria as yet undetermined.
H+TC	Heating with Thermal Convection	Electrical and other heating schemes for thick, rich low-k resources (oil shales, low-k sands) involving pyrolysis, thermal and gas fracturing to generate higher k and flow to producing wells. Experimental only.

About 2–4.5 b of water are needed to produce a barrel of SCO in typical SM operations. Production water is extensively recycled, and make-up water is taken mainly from the Athabasca River (NEB, 2006). About 0.9–1 Mcf/b of natural gas are used for energy (heat and power) and to provide hydrogen for upgrading to a SCO product (assuming no local source of synthesis gas).

The number of integrated oil sand SM projects in Canada is growing despite large CAPEX requirements because of excellent resource quality (large oil volumes per hectare, relatively low technical risks (proven technology), Canadian familiarity with large-scale mining, large outputs, less sensitivity to the cost of methane per barrel of SCO produced, low royalties, and the historical stability of large SM and upgrading operations.

2.7.3 Viscous Oil Production Technologies

Technologies required to economically produce VO *in situ*, particularly highly viscous bitumen and XHO, have major differences compared to conventional oil. It is usually necessary to reduce the viscosity; in practice, this can be achieved by heating, diluting, reducing the molecular weight, or a combination of these methods. Economical production rates have become possible because of recent developments in horizontal drilling, new production technologies, better equipment and methods, and improved environmental husbandry. Examples of these advances include shallow horizontal drilling, multilateral well arrays, gravity drainage of hot oil, coiled-tubing use, progressing cavity pumps, pressure pulse workovers, and slurry injection disposal of produced sand and emulsions.

Major *in situ* oil production technologies suitable for production of VO are listed in Table 2-8 and illustrated in Figure 2-12. It is assumed that methods such as high-pressure-gradient gas injection, surfactant or dispersant methods, bacteriological/microbial approaches, polymer displacement approaches, and other techniques suitable for low-viscosity oils are unlikely to see significant application to VO production because of advective, gravitational and capillary instabilities, excessive cost, or marginal production rates. High *RF* values are feasible if high *CSOR* values can be sustained, possible in low-tax, good infrastructure situations. Lowest cost values are associated with better reservoirs and lower viscosities. Cost figures from Canadian experience.

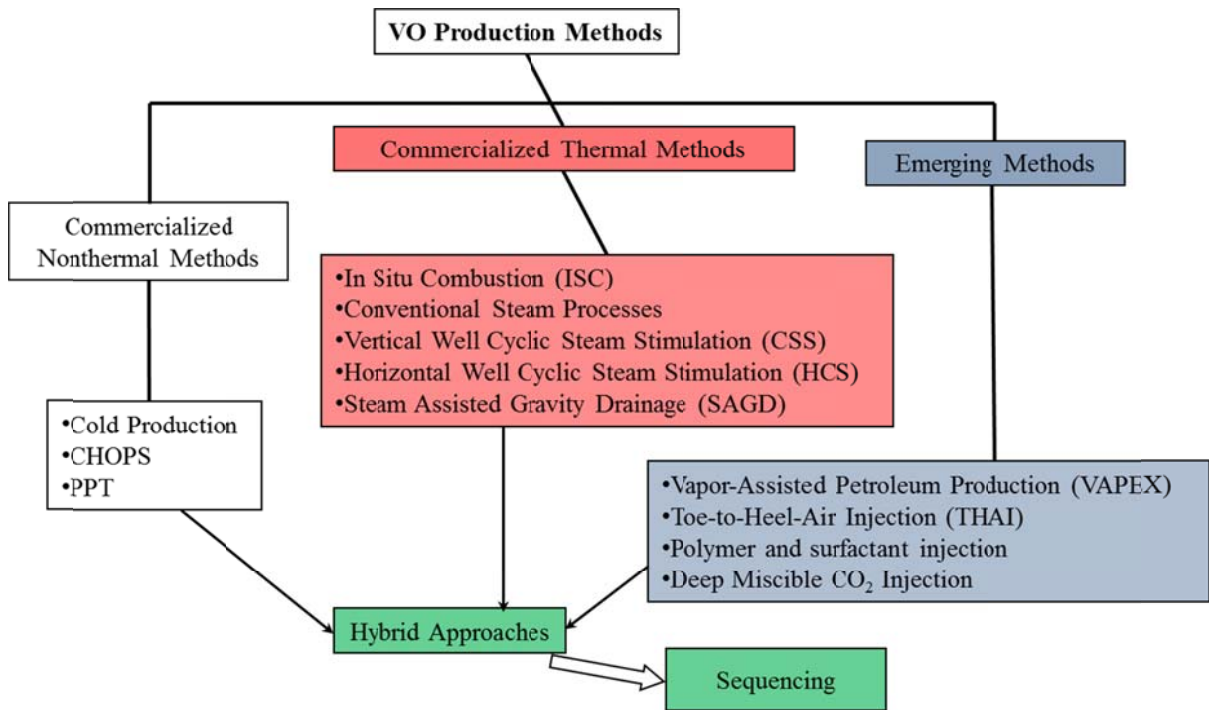


Figure 2-12: VO production methods.

Table 2-8: Estimated production costs for VO production with various methods.

Method	RF	Estimated production costs (US\$/b). Upgrading to Synthetic Crude Oil adds \$10-15/b to production costs	CAPEX per barrel of raw bitumen or VO produced per day (long term)	
			Method	CAPEX
Surface mining	0.80-0.90	\$40-45/b. This is total production cost including CAPEX, hence it is different from the numbers below. Exclusive of upgrading, transportation.	Mining	\$45000 (However, this includes upgrading to make SCO)
CP	0.06-0.15	From \$3-4/b for high permeability thick zones to \$10-12/b for poor zones.	CP (in Venezuela only)	\$5000-10000
CHOPS	0.12-0.20	\$6-18/b, depending on sand cut and rate. Sand separation and disposal \$1-4/b.	CHOPS	\$3000-6000
SF, SD	0.20-0.60*	\$10-\$25/b. High RF leads to higher Cumulative Steam/Oil Ratios (CSOR). For steam processes, costs may be estimated as \$4/b + all steam (and water) costs.		~\$20000
CSS	0.20-0.35	\$15-\$30/b. CSS is generally used in higher viscosity cases that SF & SD.	CSS and HCS	\$18000-22000
HCS	0.25-0.45	\$15-\$30/b. Better reservoir contact than CSS with vertical wells.		
SAGD	0.50-0.70	\$12-\$25/b. Better reservoir conditions needed than HCS, but lower CSOR.	SAGD	\$20000-30000
THAI™	>0.60	No cost figures available. Likely <\$25/b ultimately, without CAPEX.		
H+TC	0.30-0.75	No cost figures known. For oil shales, \$70-90/b w. CAPEX; less for oil sands.		

2.7.4 Technical Screening Criteria for VO Production

Basic issues for VO development are which production technologies are most suitable for which assets, given a large range of properties, depths and conditions, and which assets are the most economically interesting in terms of profits, stable long-term supply, political risk, and so on. It is worth remembering that private companies seek to maximize profits and shareholder value whereas national and provincial regulatory agencies seek to maximize *RF*, minimize environmental impacts, and maximize royalty payments. These different goals lead to various approaches to VO development around the world.

Technical screening criteria are applied when geologists and engineers evaluate a candidate for a particular production technology, and the technical screening is followed by economic screening to identify the best investment opportunity (Taber *et al.*, 1997). Specific screening criteria for new oil production technologies are not yet well documented, therefore some preliminary screening criteria have been developed and are presented here; criteria are listed only for commercialized production technologies (Table 2-8) and are to be taken as approximations and suggestions, not firm limits.

2.7.5 VO Production Cost Estimates

It is estimated that there are a minimum of 1 Tb of VO producible with current commercialized technology (2012) at a pre-tax crude oil price of USD \$75/b. This number is higher than previous estimates because of the impact of new production technologies on recoverable estimates. Table 2-7 contains estimates of production costs for various technologies under reasonable conditions for that technology (see previous table for screening criteria). Expected *RF* values are included because resource recovery is an important aspect, but important externalities such as surface restoration and other environmental costs (e.g., CO₂, particulates, other gases, aquifer impairment, etc.) unfortunately are not included.

Production costs tend to rise with the price of oil mainly because with rising oil price, all equipment and salaries tend to rise and also, energy input costs (e.g., CH₄ for steam

generation and as an H₂ source) usually tend to follow the oil price, as well. Thus, a sharp price rise will not lead to a proportionately large increase in economically recoverable reserves.

2.7.6 Non-Thermal Commercialized Methods

Non-thermal production techniques use natural energy drive mechanisms and, where applicable, are normally the first choice for VO asset development because of lower CAPEX and operational expenditures (OPEX), compared with thermal methods. However, cold methods suffer from low RF , and are limited to lower viscosities ($\mu < 5000$ cP) and cases with good solution gas drive energy. Primary cold production techniques are now responsible for production of over 20% of the daily VO production in the world on- and off-shore (no thermal methods are yet used offshore).

2.7.7 Cold Production

Where $\mu < 5000$ cP and k is sufficient (usually $>1-2$ D), economical cold production (CP) of heavy oil (without sand) can be achieved with long horizontal wells (Figure 2-13). VO recovery using primary methods in ‘average’ sandstone reservoirs normally does not exceed 6–10% of OOIP, but in the Faja del Orinoco XHO deposits at $\mu = 1000-4000$ cP *in situ*, exceptional reservoir conditions (high k , high ϕ , high gas saturation, thick zones), and the use of horizontal wells, Recovery Factors (RF) as high as 12–15% in favorable zones are reported (Dusseault, 2006). These values may be considered an upper boundary for VO production using conventional primary production approaches without sand production. For a given reservoir kh/μ value, the CP rate is constrained by available solution gas energy. Even in excellent reservoirs, $RF \sim 12-15\%$ is all that can be expected because of gas evolution and consequent pore throat blocking, and success is sensitive to the presence of thin clay flow barriers.

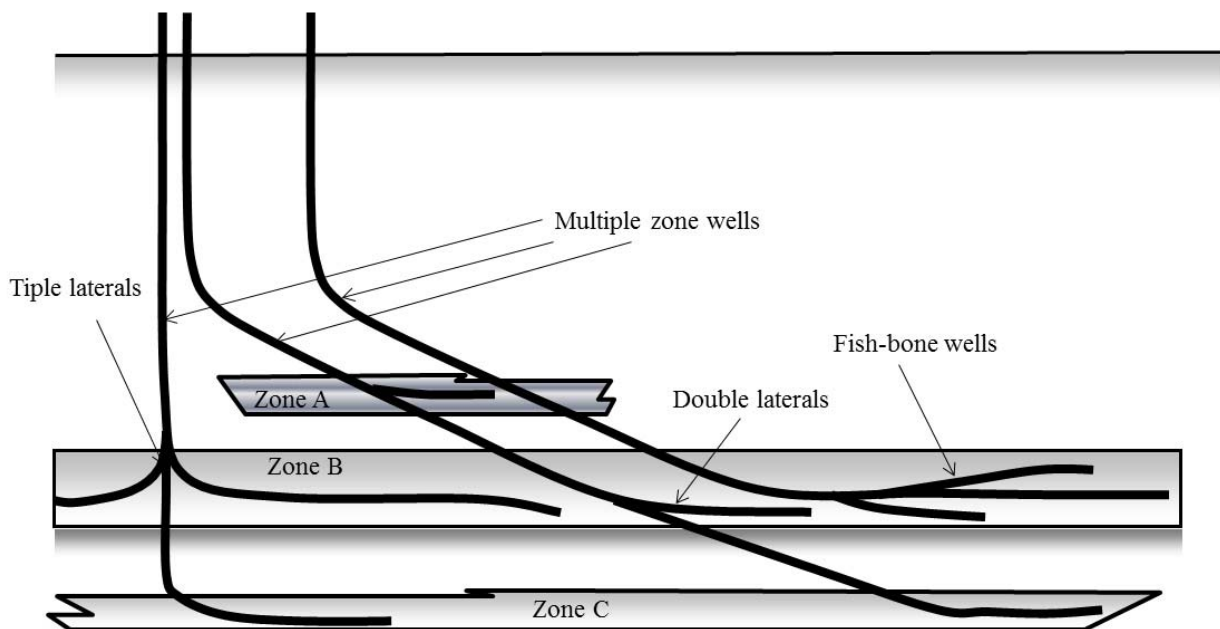


Figure 2-13: Cold Production using long horizontal wells and multilaterals.

CP has been largely abandoned in Canada after its development in the 1990s largely due to lower permeabilities and the viscous nature of the Canadian VO deposits, except in the Heavy Oil Belt. However, CP is used in several on- and off-shore VO fields around the world. For instance, in the off-shore Persian Gulf, the Soroosh VO field is producing over 90000 b/d of 600 cP VO using only vertical wells with no sand encouragement in a high quality sandstone reservoir. CP is now used in off-shore VO fields in Brazil, and has been implemented successfully in Cuba (Yumurí and Puerto Escondido/Canasi fields with 150–200 cP VO), in the HOB in Canada, and in China (particularly in the shallow offshore Bohai fields).

CAPEX per barrel of daily production using onshore CP methods varies between \$5000–10000/b depending on the VO reservoir quality (Table 2-7). This is low compared with other non-thermal and thermal VO production techniques, making CP techniques a more attractive option for VO asset development if low *RF* is deemed acceptable by regulatory authorities.

2.7.7.1 Cold Heavy Oil Production With Sand (CHOPS)

In Canadian VO deposits where $\mu \sim 1000$ to 10000 cP, an ordinary vertical well with no sand production will produce no more than 0.5–15 b/d, usually an uneconomic situation. However, allowing sand ingress enhances oil flux through several processes, and has been shown to be particularly effective for shallow unconsolidated sands with $\mu = 200$ – 15000 cP (Dusseault, 2007) and good solution gas ratios. In typical Canadian VO reservoirs, sand influx is encouraged by aggressive perforation and swabbing strategies and sustained during production by high drawdown. If sand ingress is sustainable, productivity increases of 10–20 times those of sand-free primary production are common and a RF of 10–25% can be achieved, rather than the 2–8% typical of primary production without sand.

CHOPS increases well productivity by improving the basic mobility of the flowing fluid phase, by generating a growing zone of enhanced permeability as a result of sand production, and by generating a non-coalescing but expanding bubble phase that flows with the fluid (and sand), generating an ‘internal’ gas drive mechanism called ‘foamy flow’. Also, as sand is removed, the overburden weight acts to shear, dilate and destabilize sand, helping to drive sand and oil toward the wellbore. Finally, if the sand is moving, asphaltene precipitation and fines plugging of the near-wellbore environment are eliminated. Because massive sand production creates a large disturbed zone of greater porosity and permeability, the reservoir may be improved for later implementation of thermal processes (e.g., CSS or SAGD).

In Canada, in 1000–15000 cP oil, a single CHOPS well may produce 400–2000 m³ of sand in a 6–12 year life span, achieve $RF \sim 0.1$ – 0.25 (depending on kh/μ), and in good zones, reach a cumulative oil production in excess of 250000 b, exceptionally 700000 b. At the peak of CHOPS use in 2004–2006, close to 20% (~ 600000 b/d) of total Canadian oil production was from sand production applied to reservoirs with oil of 11°–18° API.

CHOPS is suitable for unconsolidated sandstones without active water zones and where there is sufficient gas in solution to sustain the foamy flow process. The maximum viscosity in which CHOPS can be applied appears to be 15000–20000 cP; in higher viscosity cases, the sand cut remains too high, and there are more problems associated with overburden

destabilization. The minimum thickness of zones for economic production is ~ 2.5 m, and CHOPS is most suited to reservoirs less than 15 m thick. This is below the thickness requirements for most thermal processes; also, at present, CHOPS is the only economic technology for viscous oil recovery from high porosity sandstones less than 8–10 m thick.

In China, several CHOPS projects (Nanyang, Jilin) have achieved economic success, although in Jilin lateral water invasion was highly detrimental (Dusseault *et al.*, 2002). The KBM in Kazakhstan was converted from steam flood to CHOPS in new zones. There, low viscosities (~ 300 cP) and high porosities give stable sand rates of 0.15–0.25%, a tenth of typical Canadian rates, with well rates increasing to 300–600 b/d, a two to four times productivity increase, and with steam costs reduced to zero (Collins *et al.*, 2008). In the latter case, wells gradually became more gassy with time, something that does not occur in the more viscous CHOPS fields

CAPEX for CHOPS is similar to that for CP, on the order of \$5000–10000 per b/d, depending on reservoir quality. Application in thin VO zones means that some value can be produced from some reservoirs for which there are no other economically viable approaches. For thick zones (> 15 m) thermal methods remain preferable because far higher *RF* values can be achieved.

2.7.7.2 Pressure Pulse Stimulation Technology (PPT)

Pressure pulse stimulation technology (PPT) can be implemented in any liquid-saturated porous medium, and has been developed as a continuous excitation scheme, a workover method, and an approach to placing chemicals (Dusseault *et al.*, 2002). PPT involves applying sharp displacement impulses to liquid at the bottom of an excitation or injection well. A sharp pulse rapidly forces liquid (20–100 liters) through the perforations, creating a displacement wave (called a porosity dilation wave) which propagates through the reservoir. Effects on flow and production response on adjacent wells in CHOPS applications have been shown to be positive, increasing oil flow rates and reducing blockage problems (Dusseault *et al.*, 2002). High-amplitude, low-frequency liquid-phase dynamic excitation reduces some of

the effects of advective and capillary instabilities, as well as unblocking pore throats and accelerating flow, so it should see more applications in various VO applications.

2.7.8 Commercialized Thermal Methods

If VO cannot be economically recovered by SM or primary methods (solution gas drive) due to unfavorable kh/μ , viscosity must be reduced. The three options are to heat the oil, dilute it with solvent, or reduce the molecular mass through pyrolysis. Heating with steam is the only commercialized viscosity reduction approach, and is by far the most successful and widely used production method; > 75% of VO production worldwide involves steaming, and this dominance will continue into the foreseeable future.

Steam processes are limited to reservoirs more than 8–10 m thick because heat losses are a function of surface area (constant), whereas reserves are a function of volume ($V = A \times h$). For all steam technologies, reservoir quality is a paramount issue (h , ϕ , S_o , k , net-to-gross ratio, etc.).

2.7.8.1 *In situ* Combustion

In situ combustion (ISC) is classified as a commercialized VO production technology although it has been applied only in limited conditions (low-viscosity VO, good geological conditions), and has not been commercialized in North America for VO. ISC enhances flow by reservoir heating, pyrolytic molecular scission (thermal cracking and coking), and dissolution of produced low molecular weight products into the VO. The combustion front is sustained by burning the coke deposited from pyrolysis (Figure 2-14) and the driving force is an externally maintained ΔP combined with additional pressure and displacement effects arising from combustion and inert gaseous phases (hydrocarbons (HCs), CO_2 , N_2). If pure O_2 is used, N_2 handling is eliminated, but pure O_2 is expensive and CO_2 and HC gas flows have similar problems of flow instability (channeling, gravity override). Hot produced fluids must be dealt with at the well head through separation, condensation of liquid phases, HC gas separation, and venting or gas re-injection. Water injection with air (wet combustion) seems to improve the process somewhat and, importantly, leads to a lower combustion temperature.

It appears that once the wellhead temperature exceeds 475–500°C, technical difficulties with steel goods and surface facilities are almost insurmountable.

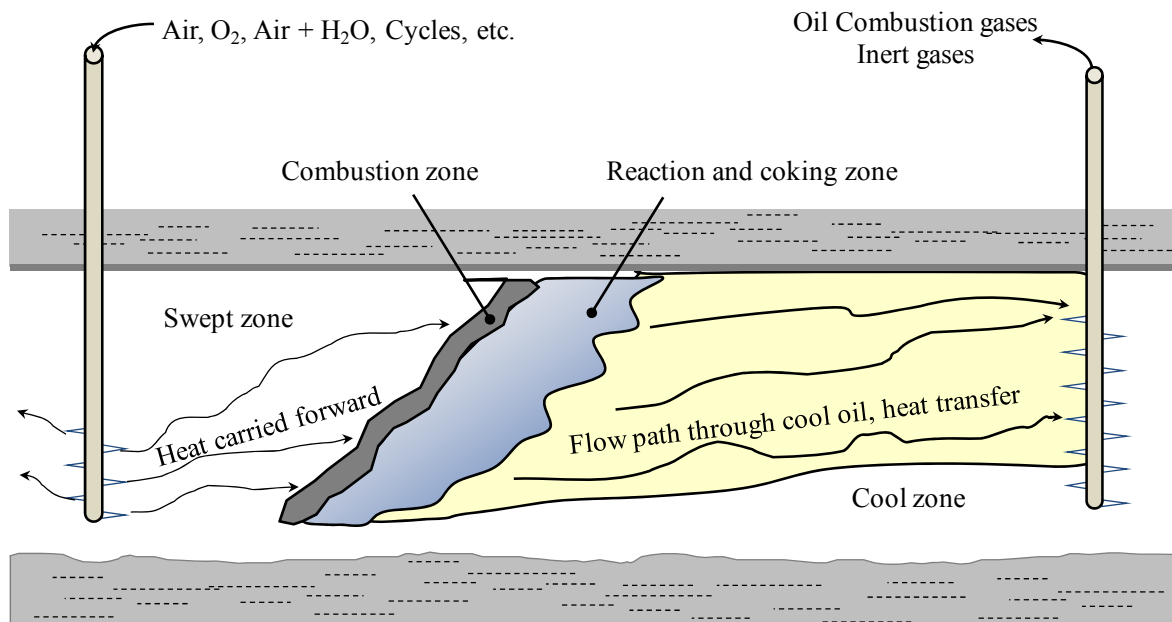


Figure 2-14: The original concept of *In Situ* Combustion process.

ISC appeared first in 1923 in the USA and since 1948 numerous field tests have been conducted (Breston, 1958). It appears suitable for oil recovery from medium viscosity oil reservoirs (up to 2000 cP), but has yet to achieve success in high viscosity cases because of flow instabilities. Apparently, no commercial ISC successes have been reported in VO except in highly unusual conditions such as a reservoir with a high permeability, some oil mobility, and a good dip. Economic successes are reported in the USA for light oil in carbonate strata, in Romania for a dipping reservoir with 2000 cP XHO, and in India for a HO reservoir (Gadelle *et al.*, 1981; Kumar *et al.*, 1995; Chattopadhyay *et al.*, 2004).

ISC in VO is plagued by severe advective and gravity instabilities that arise with fluids of widely differing viscosities and densities. The viscosity contrast is extreme (less than 0.001 cP for hot gases, more than 1000 cP for cold VO), and channeling cannot be ‘blocked’ through the use of special blocking agents which are usually thermally unstable or too costly. Oil cooling during transit and consequent plugging is endemic to conventional ISC methods,

and the cooling oil can also gel *in situ* because of polymerization. Gases that must exit the system cannot flow without fracturing, leading to higher injection pressures, channeling, and loss of control. Where there is active water, ISC is difficult to implement because if the pressure at the production wells drops too low, sudden water coning can develop and quench the hot oil, immobilizing it, and stopping the process.

At the surface, treatment of hot heterogeneous fluids with many noxious and toxic gases is complex, and the combustion oil contains large numbers of double and triple carbon bonds, causing it to gel. This could be mitigated with immediate hydrogenation while fluids are hot, but this requires development of smaller-scale hydrogenation methods than are currently available. Refineries are not equipped to refine streams with significant quantities of ISC oil, creating another difficulty; only a VO upgrader can accept large amounts of ISC product.

ISC methods will remain of great interest because the prize is great: no fuel cost (only air compression), no water requirements, partial upgrading, and reduction of heavy metals content. The advantages of the '*in situ* reactor' are so large that applied ISC research will continue even if interim results continue to disappoint; for example, combustion may eventually be the only viable technology for highly viscous oils (> 10000 cP) in poorer quality zones less than 10–12 m thick where CHOPS cannot be sustained.

2.7.8.2 Conventional Steam Processes

Steam flooding (SF), steam driving (SD) (Figure 2-15), various injection patterns, line drives, and other variants have been used since the 1950s and 1960s, mainly in California, in thicker zones (> 10 m), and almost always for VOs of $\mu < 5000$ cP because initial communication between offset wells is achievable only with lower viscosities. These approaches use vertical wells with continuous steam injection at the base of an interval; this leads to creation of a slowly advancing steam zone, and the increase in temperature reduces the VO viscosity while volumetric sweep mobilizes it and displaces it into the production well. In some California fields, *RF* values > 60 – 70% have been achieved with exceptionally close well spacing (75–125 m), and through the use of high cumulative steam-to-oil ratios (*CSOR*) in a low-tax,

partially subsidized economic environment. High RF from application of SF/SD approaches is reported for the Duri Field, Indonesia, despite steam override problems and substantial heat losses (Farouq Ali and Meldau, 1979; Farouq Ali, 1982), because of highly favorable geological conditions (shallow, high k , etc.).

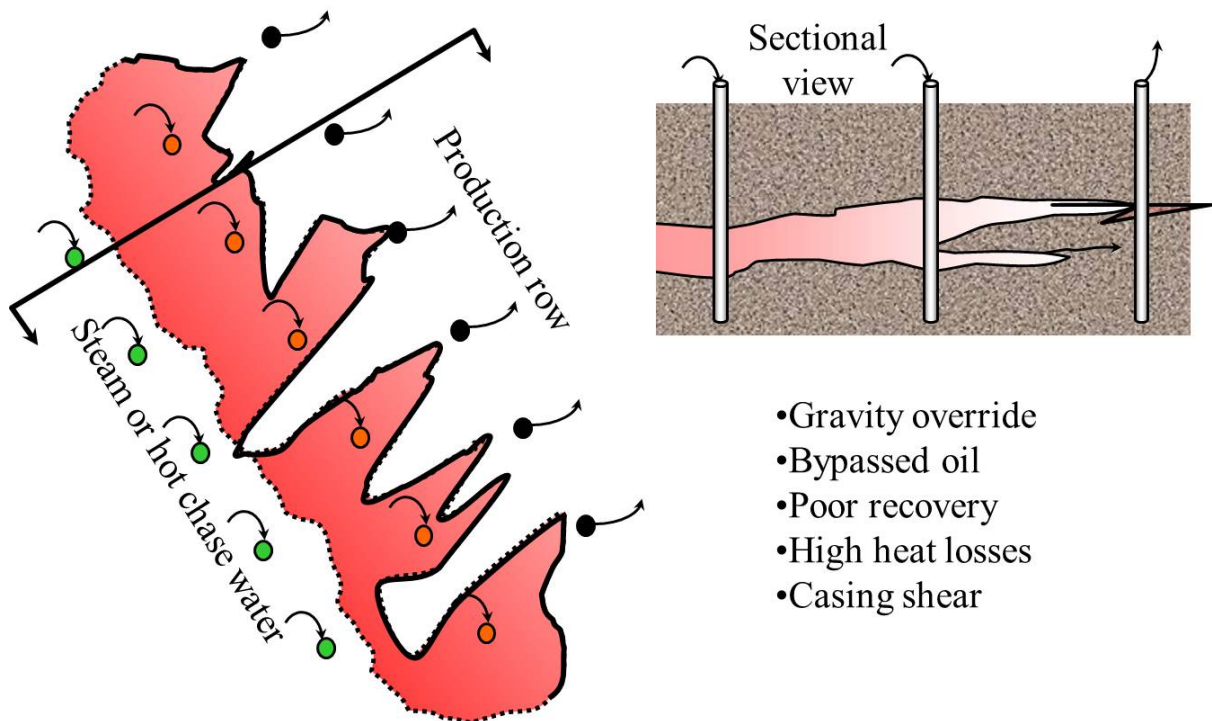


Figure 2-15: Steam Drive concept.

The use of pressure-driven steam injection processes e.g., SF/SD methods, encounter the same problems of advective and gravity instabilities and heat losses as mentioned for ISC.

An important benefit is that steam injection leads to reservoir property enhancement. Thermal expansion leads to elevated shear stresses, causing shearing and dilation (σ increase) of dense oil sands. This enhances the intrinsic permeability, leads to accelerated imbibition of hot fluids, and breaks apart thin shale seams or clay dusting on bedding planes. Reservoir enhancement takes place in all steam injection processes, and can be further enhanced by fracturing (CSS, horizontal well cyclic steam stimulation (HCS)) and high injection pressures which facilitate sand shear and dilation.

SF/SD methods were perfected in California, and continue to be the dominant production method there, although thermal VO production continues to decline from its peak several decades ago because of reduced availability of high quality VO assets. The shallow Duri SF project in Sumatra was for many years the largest thermal steam injection project in the world, with production exceeding 300000 b/d in 1994, but is also now in decline (below 200000 b/d).

As shown in Table 2-7, the CAPEX per barrel of raw bitumen or VO produced per day (long term) using conventional steam processes is about ~ \$20000/b and is similar for different technologies (SF/SD, CSS, HCS, SAGD) because of the relatively consistent costs of steam generation and transmission hardware. Despite a similar CAPEX, other factors such as reservoir quality, OPEX, water requirements and depth are important when selecting processes for development of a particular VO deposit. Steam injection CAPEX is two to three times higher than the CAPEX required to produce a barrel of VO using primary methods (or water flooding if applicable), and this is the reason that initial primary production is almost always used if it is technically feasible, despite low *RF* values.

2.7.8.3 Vertical Well Cyclic Steam Stimulation (CSS)

Vertical well cyclic steam stimulation (CSS), also known as ‘huff-and-puff’, uses vertical or deviated wells to inject high pressure steam into reservoirs where there is little possibility of inter-well communication (e.g., no natural mobility). Injection into a well (or a well row or two parallel rows of wells) is followed by a short soaking period and then a production phase (Figure 2-16) (Owens and Suter, 1965). During production, water rates start off very high, and oil rates first increase, peak, and then decline. This three-stage cycle starts again and is repeated for many years to achieve *RF*s of 0.2–0.4, depending on reservoir quality. Under reasonable conditions, *CSOR* during initial cycles in a high porosity oil sand > 20 m thick is 2:1 and increases with the number of cycles to the range of 3:1–4:1 during the project. Typically, the first cycles are short, and the length of both injection and production phases increases as the project matures. An occasional solvent injection cycle may be implemented,

and inert gas injection after steam cycles are completed to promote some gravity displacement may increase the recovery factor slightly at low additional cost.

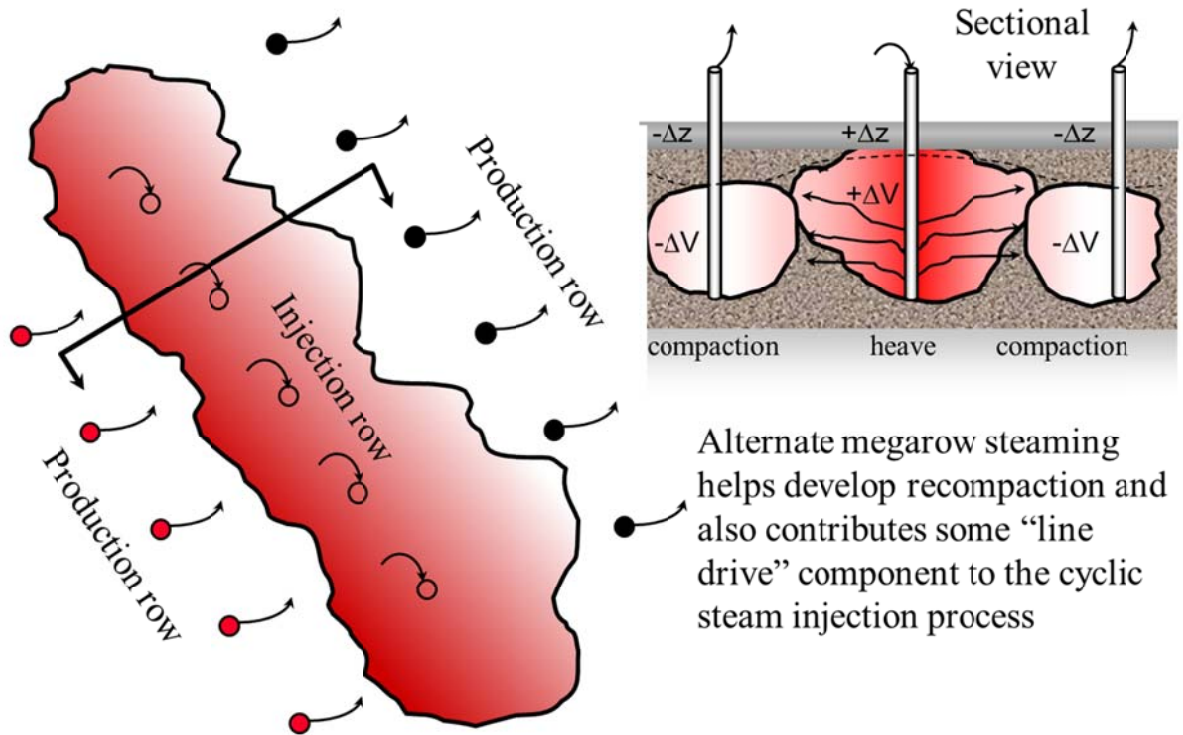


Figure 2-16: Vertical well Cyclic Steam Stimulation process.

CSS uses 25–50 wells/km², placed in an anisotropic pattern depending on the principal fracture injection direction. CSS is appropriate for higher viscosity reservoirs, $\mu > 5000$ cP, where interwell communication is difficult to establish. Even in good reservoirs (thick, high k , low μ) CSS yields only moderate RF (0.2–0.4) because much of the low-lying oil between vertical and inclined wells cannot easily be contacted because of steam override, and because the steam fracturing necessary during early cycles remains somewhat local and affects mainly the upper parts of the formation in the vicinity of the injection well.

Because of high injection pressures and thermally-induced shear dilation, CSS easily breaks through relatively thick shale barriers and enhances reservoir properties, making it applicable in reservoirs of lower k and poorer k_v/k_h (vertical and horizontal permeability) ratios than for

SF and SAGD. CSS (and HCS) can thus be used to ‘condition’ marginal reservoirs for other technologies in a sequenced extraction approach, a powerful concept that promises to lead to substantial increases in technically recoverable VO worldwide.

CSS has been used at a significant scale in Canada in the Imperial Oil Ltd. Cold Lake Project, the largest CSS operation to date. The project is sited in the middle of the thickest and most uniform part of the Cold Lake Oil Sands deposit and currently produces over 140000 b/d with a rated and more usually attained capacity of over 175000 b/d. Major reasons for success at Cold Lake ($RF \sim 0.3\text{--}0.35$, $CSOR \sim 3.5$) include a homogeneous reservoir 35–40 m thick and the contribution of a recompaction drive to production in later cycles. In less favourable reservoirs flanking the rich central zones in the Cold Lake VO deposit, CSS has been unsuccessful or marginally successful. Successful large-scale application of CSS is also reported in Venezuela, China, Trinidad, and USA.

2.7.8.4 Horizontal Well Cyclic Steam Stimulation (HCS)

Horizontal well use for cyclic steam stimulation (HCS) exploits long reservoir well contact, reservoir property enhancement, and more efficient heat placement to achieve RF s of $\sim 0.35\text{--}0.45$ in suitable reservoirs that would yield RF s of $\sim 0.25\text{--}0.35$ for CSS (Figure 2-17). Low oil saturations, thick oil-free interbeds, and low net pay thicknesses are strongly negative factors, as with all steam processes. Well placement near the base of the formation leads to enhanced gravity segregation effects during production periods, and the combination of pressure drive, gravity drainage, and formation recompaction drive leads to the improved RF values. Long horizontal wells also tend to mitigate some negative aspects of gravity override that are common to all steam injection processes, and a larger part of the reservoir is subjected to thermally-induced shear dilation and reservoir property enhancement.

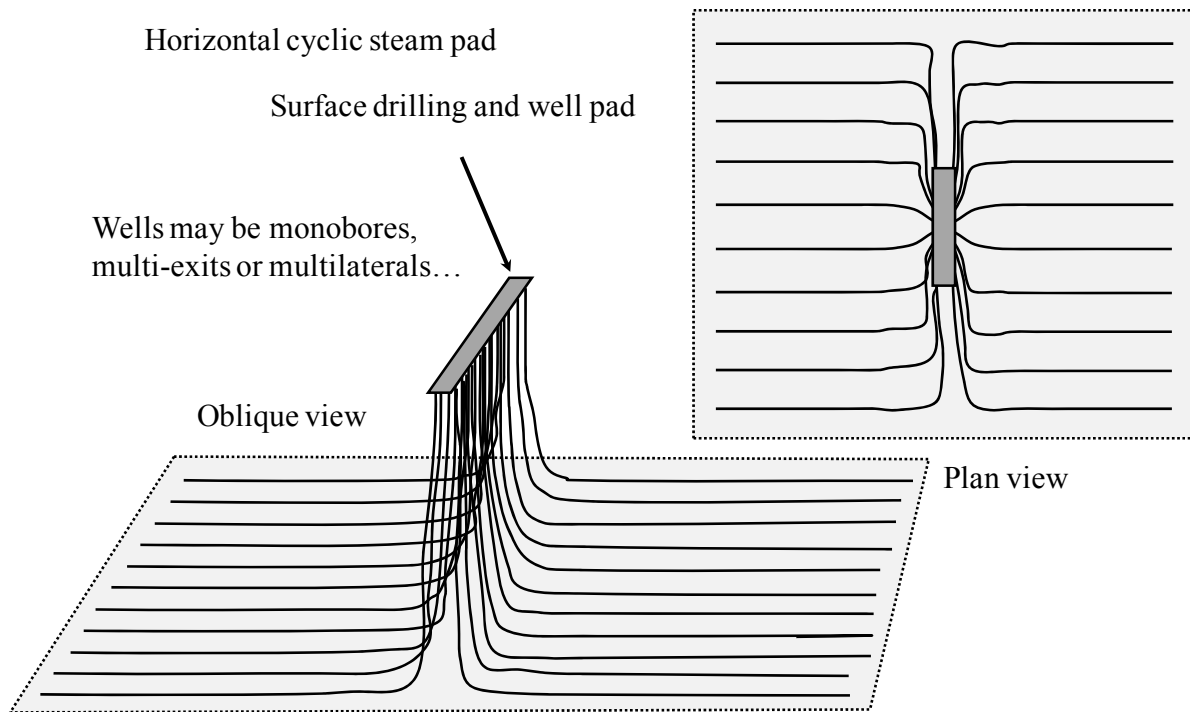


Figure 2-17: Horizontal well cyclic steam stimulation.

During initial cycles in HCS, fracturing moves from the heel of the well to the toe as thermal stresses increase, and continued injection leads to changes in fracture orientation. These effects give a higher reservoir contact area and superior thermal stimulation, compared to vertical wells. Typically, injection and production cycles for HCS are longer than for CCS, but a similar procedure of gradual lengthening of the injection/production periods is followed. However, after several cycles, the horizontal well injectivity is so large that fracturing is usually no longer possible, and if communication then exists with offset horizontal wells, or if vertical wells are available, HCS can be converted to a SD/SF or a SAGD process.

Under identical conditions, HCS is likely to give a *RF* 10% units greater than CSS, with a similar overall *CSOR* (e.g., *RF* of 40% instead of 30%). CAPEX is similar to CSS, but the possibility to switch to SAGD, followed then by inert gas injection, both of which can significantly increase *RF*, is a distinct advantage (although largely untested yet). HCS is

limited to more viscous oils and zones > 15 m in thickness, and can be used in somewhat poorer reservoirs than SAGD because of the high pressure fracturing.

Canadian Natural Resources (CNRL) is currently operating four HCS projects in the Primrose/Wolf Lake area with a total production of 120000 b/d. In total, there are eight CSS/HCS projects operating in Canada with a production of 272500 b/d and six more projects have been planned or are under construction with a nominal daily production of 215000 b ([Government of Alberta, 2010](#)). As shown in Table 2-7 the CAPEX per barrel of raw bitumen or VO produced per day (long term) using HCS is about ~ \$18000–22000/b roughly the same CAPEX as CSS, SAGD, and other steam processes.

2.7.8.5 Steam Assisted Gravity Drainage (SAGD)

[Butler and Stephens \(1980, 1981\)](#) initially proposed and demonstrated the basic mechanism of SAGD processes for VO before it was pilot tested in Canada in the late 1980s using an underground mining and drilling approach. In a typical SAGD project (Figure 2-18) in zero mobility VO, two parallel thermal horizontal wells are drilled about 4-5 m apart vertically. Steaming of both wells is used to establish communication, then 100% quality steam is injected into the upper well, leading to creation and growth of a steam chamber with time. The low density steam and exsolved gases rise, and as heat is transferred at the condensation front, the VO is mobilized and flows to the lower well along with condensed water. The well configuration shown is necessary if there is no initial inter-well communication (zero mobility), but if inter-well communication can be easily established, other configurations are possible such as vertical injector rows (production wells must be horizontal), laterally offset horizontal injectors, or even injector wells in different directions than the producing wells.

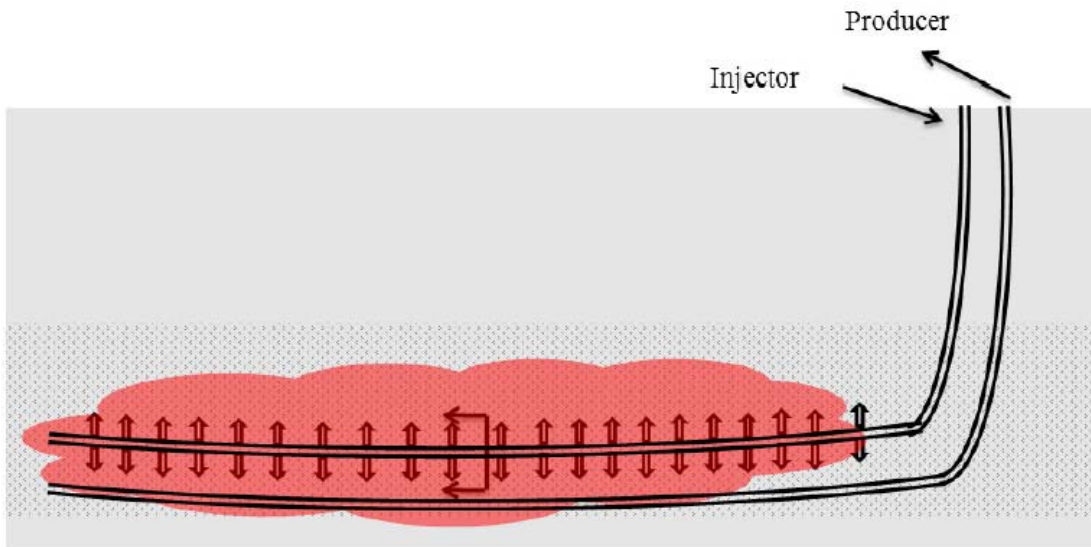
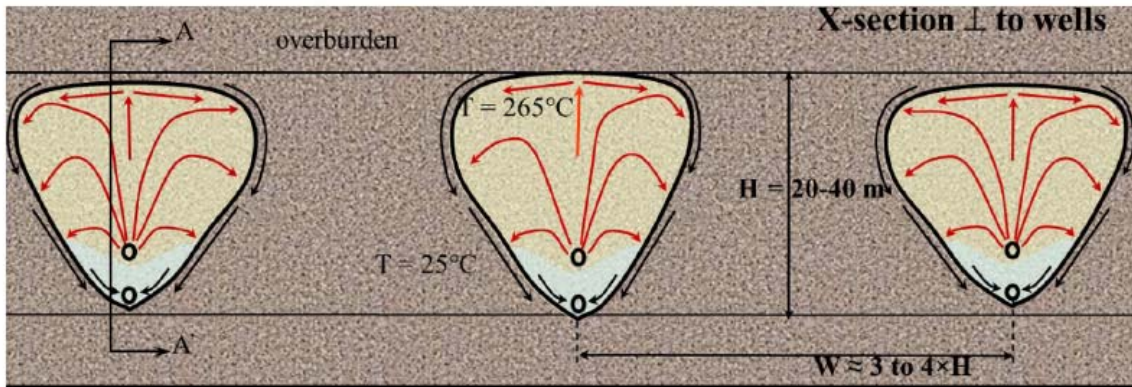


Figure 2-18: Steam Assisted Gravity Drainage (SAGD) concept.

In SAGD, gravity forces arising from density differences must remain dominant over ΔP forces so that vertical immiscible phase segregation dominates flux, eliminating ΔP -induced instabilities such as viscous fingering and channeling. It is necessary to operate injection and production wells at about the same pressure ($\Delta P \sim 20\text{--}40$ kPa) to guarantee that the process is gravity dominated and to avoid all high pressure gradients that could lead to destabilization (coning, viscous fingering, channeling). In principle, SAGD can be used in cases of active

bottom water, provided that production wells are operated at a back-pressure identical to that in the water, and that there is some distance between the horizontal producing well and the active water (e.g., 10 m). If there is no mobile water, there exists a choice of operating pressure, but higher pressures mean more substantial shearing and dilation, as well as a higher T for viscosity reduction, both highly positive factors in this process (Collins, 2002; Thimm, 2004). Conversely, operating at lower pressures means larger latent heat transfer, but dilation and reservoir enhancements are reduced.

In SAGD, 100% quality steam is necessary as any hot water will immediately drop to the producing well and be recirculated without beneficial effect. Steam breakthrough to the producing well is to be avoided, and as much as possible the steam-liquid interface is kept between the two wells. Gravity override now becomes a positive factor because steam rises and moves laterally in the zone while condensed water and hot oil flow through gravity segregation to the horizontal producing well. The steam heats the oil at the walls of a growing chamber, and the melting zone is thin and stable because there are no ΔP -driven advective effects. Evolved or injected non-condensing gases (CO_2 , N_2 , CH_4) tend to stay high in the chamber; they provide some insulation effect which helps reduce overburden conductive heat losses, but too much gas can lead to impairment of the heat transfer at the condensation front.

Despite no hydraulic fracturing taking place, differential thermal expansion and clay dehydration with high temperatures allow substantial shale beds (1–2 m) to be breached, but thick shale beds nonetheless impede flow and stable chamber growth, and the thermal penalty of having to heat the shale is severe (15-25% porosity, filled with water). A more serious impediment to the vertical flow necessary to achieve SAGD is the potential presence of silt-sized strata with low clay content; these can form capillary barriers to vertical steam migration, yet do not experience the beneficial thermally induced shrinkage that clay-rich shale evidences.

As the steam chamber grows laterally, the increasing upper surface area causes heat losses to rise with time. Furthermore, the flow-back angle to the well decreases, so flow rates start to

slowly diminish once chamber width is substantial. Economically, these factors limit the steam chamber width to about four times the reservoir thickness under typical good conditions. Various thermal factors, plus lower OOIP for thin zones, will limit SAGD application as the first technology to cases > 15–20 m thick, and with high S_o values and good net-to-gross pay ratios. However, if the beds are dipping, the additional height component is favorable for SAGD and different well spacings and screening limits may be feasible.

Compared to high ΔP steam injection methods, SAGD advantages reside in greater thermal efficiency and extremely high RF in the swept zone. Higher thermal efficiency arises because of the sharpness of the thermal front moving through the reservoir (no large-scale fingering and channeling) and the reduced heat losses in the vertical direction, compared to high pressure steam processes where the injection pressure and this temperature are higher. When SAGD is close to termination (5–8 yr), steam injection can be replaced by inert gas injection to displace remnant hot liquids and vapors to the production well, where they can be produced and the heat scavenged. SAGD should be about 20–30% more thermally efficient than an equivalent HCS/CSS operation. For example, in Cold Lake, Alberta, $CSOR$ values of 2.5–3.5 have been achieved, but it is likely that SAGD could achieve $CSOR$ values of ~ 2–3, as well as RF values of 60–70% rather than 35%.

SAGD is economically viable in good zones ($k > 1 D$, thickness > 15–20 m) in oils of viscosity as high as 1–2 million cP at depths of 250–1000 m. RF values over a 5–8 yr life span approach 80% in cases with excellent vertical permeability, but values of 65–70% are more reasonable as an overall average.

Although double-well strategies are currently favored, it is possible to achieve stable SAGD in a single well (SW-SAGD) configuration. Steam injection takes place along the well length, with the steam rising out of the well to be replaced by liquids ($\Delta\rho$ effect). ΔP is low, so the process is dominated by $\Delta\rho$ effects. At present, the double-well concept is deemed most appropriate for new, thick VO zones because it keeps the flow path short, thus reducing

heat loss. However, as SAGD is applied to other reservoirs that have already had a production phase using a different technology, different well combinations, such as horizontally alternating injection and production wells, may prove more efficient. Many other potential SAGD variants are reported in the literature.

It is estimated that the CAPEX required to produce a peak barrel of SCO in the SAGD projects of Alberta is \$20000–30000 (see Table 2-7) – the high values are for two poor-reservoir-quality projects). In addition, the amount of natural gas consumed in SAGD projects is estimated to be 0.95–1.05 Mcf/b of SCO.

2.7.9 Emerging Methods

Emerging methods are technologies that have not been commercialized yet, but which have been subjected to at least partial testing at a full field scale, and which appear to have future commercial potential. Discussing all emerging methods for *in situ* production or VO upgrading is beyond the scope of this text; only promising technologies are described.

2.7.9.1 Vapor-Assisted Petroleum Production (VAPEX)

Vapour-assisted petroleum extraction (VAPEX) was proposed initially ([Butler and Stephens, 1980](#)) as the solvent analog of SAGD ([Butler and Mokrys, 1989](#)). It involves dilution with hydrocarbon vapors, e.g., ethane, propane, and butane, depending on reservoir *in situ* conditions (P , T). VAPEX involves injection of gaseous hydrocarbon phases that diffuse and dissolve into the VO to reduce its viscosity. Physical principles are similar to SAGD (Figure 2-18) and a vapor chamber is created that expands vertically and laterally as the diluted (thinned) VO drains by ‘downhill’ flow of the liquid phase.

Compared to SAGD, VAPEX has both advantages and disadvantages. In high viscosity cases ($\mu > 100000$ cP) a great amount of diluent is needed, more than 20–30% by volume; this suggests that VAPEX may be most effective for 10–5000 cP crudes where only 5–15% dilution is needed. In high viscosity crudes, HC liquids cause asphaltene precipitation, which

may block pores and reduce flow rates. Although this has been touted as a means of *in situ* ‘upgrading’, the negative effects of flux impairment are substantial.

Because there are no thermal shear and dilation effects in cold VAPEX, even thin shale beds represent serious flow barriers. To overcome this, propped fractures can be used to create vertical flow paths, but this only partly resolves the problem, as the effective flow angle in such cases can be so flat that recovery rates become too slow.

Nevertheless, VAPEX requires little or no heat, so the severe heat cost penalty (~ 60–70% of OPEX in SAGD and cyclic steam processes) is absent. Other well configurations become feasible and a much longer production time, several decades, could be tolerated in return for the high *RF* values expected (> 70% in appropriate cases). By contrast, SAGD production must be as fast as possible because of heat losses, and well spacing has to be modest.

2.7.9.2 Toe-to-Heel-Air Injection (THAI™)

Toe-to-heel air injection (Greaves and Turta, 1995), THAI™, uses the concept of an enforced short flow path to mitigate advective instabilities, gas override, and oil cooling (Figure 2-19). Vertical wells are used to inject air, O₂-enriched air, O₂ plus water, or other suitable oxidant to propagate a combustion front along a horizontal well array placed low in the formation to form a gravity-enhanced flow sink. Combustion products and thermally cracked or mobilized products are withdrawn after a short, hot flow path to avoid long-flow path instabilities and cooling. A controlled balance between thermal override and fluid down-flow leads to efficient vertical sweep, and high *RF* values can in principle be achieved. The potential advantages of THAI™ are clear: no water or fuel requirements, no solid waste at surface, greatly reduced heavy metal content, somewhat reduced S-content, and partially upgraded oil (higher API gravity).

Implementation in a wide range of reservoir qualities is possible, but complications are being encountered in practice. Sand entry to the producing well has occurred, and plugging of the producers through various geochemical processes is a serious issue. The injected oxidant may short-circuit to the toe of the well, introducing free oxygen to the production well,

leading to steel attrition and coking within the horizontal well section, impeding or stopping flow. Laboratory simulations show a tendency for a coke plug to form within the well upstream of the combustion zone, helping oxidants to follow an overriding flow path through the combustion zone, where they can be totally consumed (Xia and Greaves, 2001).

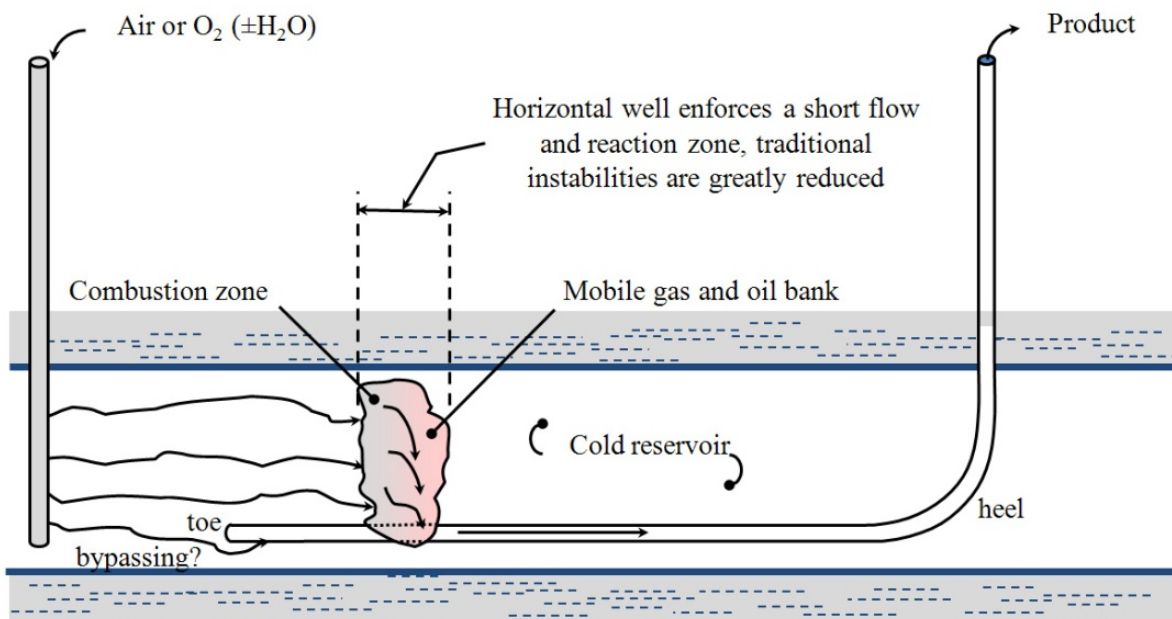


Figure 2-19: Toe-to-Heel Air Injection (THAI™) concept.

Thermal cracking and some hydrogen donation from water and clays lead to partial VO upgrading by up to 8° API (Figure 2-20). Under high temperatures (500–600°C) and pressure of 30–50 bars, the water/steam, oil and gases generated during combustion travel the short distance to the basal production well through a hot mobile oil zone, often referred to as an ‘*in situ* reactor’, and a complex set of reactions occurs to varying degrees of completeness, depending on specie availability and P - T - t conditions. Natural catalysts such as clays aid reactions similar to hydrotreating associated with coke gasification and water dissociation (Hajdo *et al.*, 1985; Greaves *et al.*, 2008).

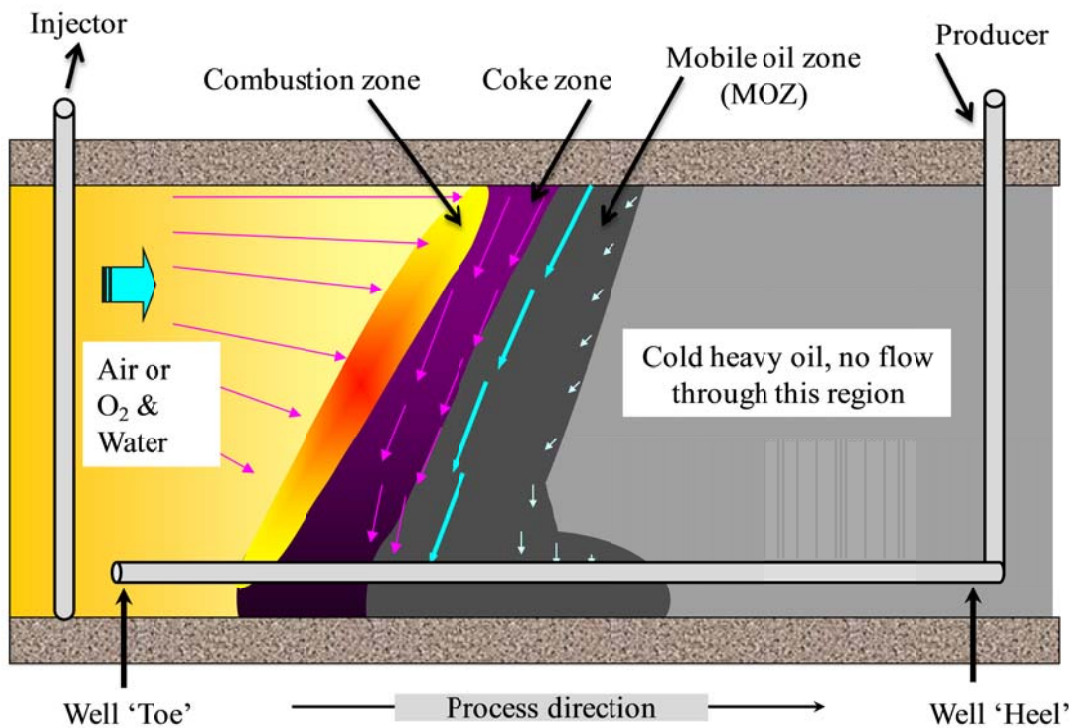


Figure 2-20: Schematic view of process zones in THAI™ (Adopted from [M. Greaves, 2008](#)).

THAI™ has been under trial by Petrobank Energy Resources Ltd. in Canada since 2006 at their Whitesands lease near Conklin, Alberta. The pilot project has three sections each consisting of three injection and three horizontal (500 m long and 100 m apart from each other) production wells with a nominal daily production rate of 1900 b ([Ayasse *et al.*, 2005](#)). Steam injection was used for three months to establish communication between injectors and producers, then air injection commenced leading to ignition, and temperatures up to 700–800°C were recorded during the combustion process. The project announced its first VO production with rates of 300–400 b/d per well under low pressure air injection in 2008, with ~ 4° API upgrading achieved. Condensed water is pure and can be re-used in other thermal projects ([Greaves and Xia, 2008](#)) and partial upgrading means easier transportation and less diluent requirements compared with non-upgraded bitumen products (CSS, HCS, SAGD). Since then, various problems have prevented significant production rates of VO.

If the problems can be overcome, THAI™ sidesteps many of the control problems that plague ISC by avoiding channeling and removing large-volume gaseous products quickly (Xia *et al.*, 2003). Whether THAI™ advantages can be realized systematically in practice over a range of reservoir qualities remains to be seen, and issues such as water ingress, sand production, and product temperatures must be resolved (Turta *et al.*, 2009). Finally, the product does not conform to typical refinery feedstocks, and large-scale production may require dedicated upgrading capabilities. The ideal solution to this would be additional on-site upgrading while the product is hot (450°C).

2.7.9.3 CAPRI™ (*In situ* Catalytic Upgrading)

Processes involving *in situ* upgrading of VO and leaving behind heavy metals which poison refinery catalysts are attractive in principle. The idea of *in situ* upgrading of VO via ISC was initially introduced over a decade ago (Weissman *et al.*, 1996; Weissman and Kessler, 1996; Moore *et al.*, 1999). This idea is based on the flow of VO through a catalyst bed in the reservoir under a favorable pressure and temperature which leads to enhanced upgrading by 4–8°API. Despite positive theoretical and experimental data, field trials have been disappointing for various reasons.

To overcome some obstacles, *in situ* catalytic upgrading of VO via THAI™ was proposed, called CAPRI™ (*in situ* catalytic upgrading) (Ayasse *et al.*, 1998; Greaves *et al.*, 2000). During the THAI™ process, favorable pressure (30–50 bar) and temperature (400–600°C) conditions for catalysis are generated, and use of a catalyst-wrapped production casing means that CAPRI™ is the ‘catalytic extension’ of the THAI™ process. Further thermal cracking of the VO in contact with the catalyst combined with enhanced hydrogen availability are considered the main mechanisms for enhanced *in situ* upgrading (Xia and Greaves, 2002).

Issues in catalyst performance are related to high S and heavy metal content in the VO leading to rapid catalyst poisoning (Bartholomew, 2001). Preliminary evaluations indicate that the CAPEX required for THAI™-CAPRI™ production is about one third of the CAPEX required for a steam processes such as SAGD, but OPEX is highly uncertain, upgrading of large volumes of combustion oil has never been attempted, and it is too soon to judge the

technical and financial viability of these processes at this time (2012). Further investigation at the field scale is needed, and innovative engineering is required to address issues such as sand influx, plugging, casing integrity at high T, co-production of gases and liquids, and the handling and beneficiation of the products at the surface.

2.7.9.4 Deep Miscible CO₂ Injection

Miscible CO₂ injection is based on high pressure gradients (ΔP) to force gaseous, liquid, or supercritical CO₂ into the porous medium where it has effects such as dissolving into the oil, providing a displacement pressure, swelling the oil, reducing viscosity, and replacing voidage (Figure 21). Gaseous CO₂ is of less interest to VO production, comments here are confined to supercritical CO₂ injection. At $p > 7.35$ MPa and $T > 35^\circ\text{C}$, pure CO₂ is a low-viscosity (0.02–0.1 cP) supercritical fluid of density 0.65–0.85 g/cm³ that is at least partially miscible with VO (miscibility increases as pressure increases). As it contacts and mixes with oil it reduces viscosity, so continued circulation eventually leads to a high *RF*. As with HC solvents, asphaltene precipitation may be an issue, and diffusion into cold VO is slow, especially at low temperatures, so deep CO₂ injection (higher T, p) could be attractive in low-viscosity cases, or after a deeper thermal process where substantial amounts of hot oil remain, such as after SAGD or SD (Luo *et al.*, 2005). Also, implementing this technique is attractive in the context of carbon capture and sequestration, and one might even consider injecting hot CO₂ to add the various benefits of thermal stimulation to the dissolution effects.

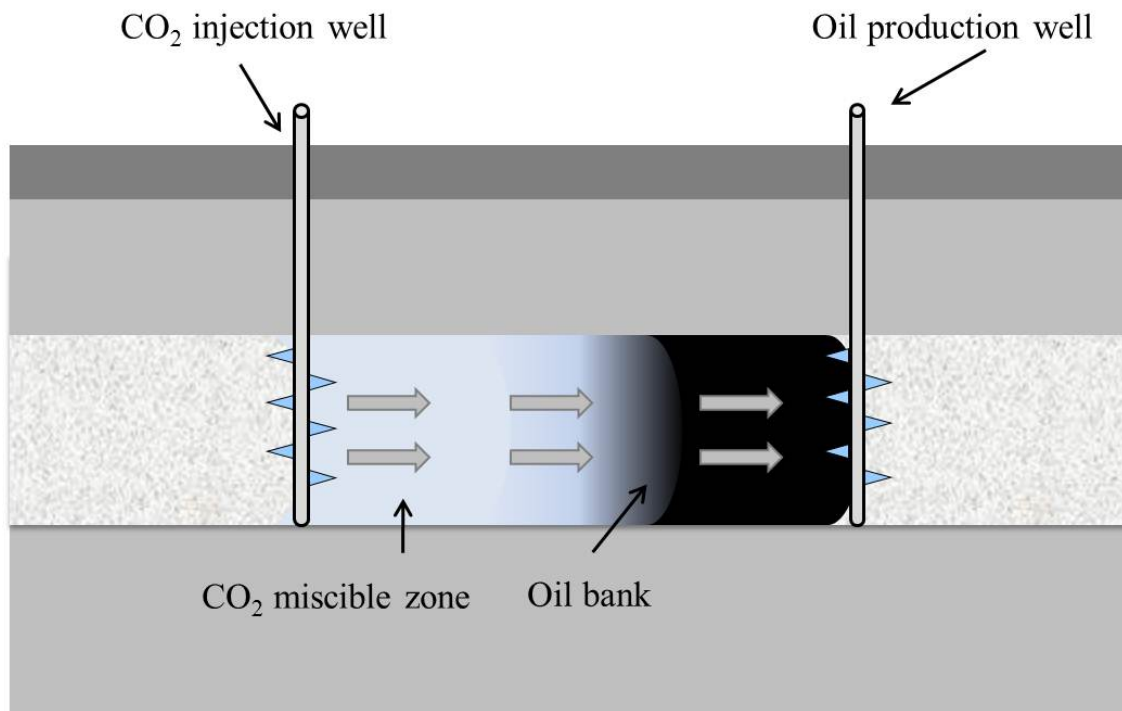


Figure 2-21: CO₂ injection (ideal condition).

Application of CO₂ miscible injection for VO has not been reported yet although limited immiscible CO₂ injection has been tried. However, a few commercialized CO₂ immiscible VO production projects have been reported around the world. In Turkey, the Bati Raman 600 cP VO field, a heterogeneous naturally fractured reservoir at 1300 m depth, is being subjected to CO₂ injection with an expectation of $RF > 6.5\%$. The main production mechanism appears to be dissolution into the oil, causing swelling and reducing viscosity by a factor of 10 (Sahin *et al.*, 2005).

2.7.10 Hybrid Approaches and Sequencing of Technologies

Hybrid approaches involve the simultaneous use of several technologies within the same well or reservoir zone; sequencing involves deliberate advance planning of exploitation to take advantage of changes in reservoir properties, to conserve heat, and to use the cased wellbores in the reservoir for as long as economically possible. These staged approaches hold the promise of significantly increasing recoverable reserves worldwide, not just in VO cases

(Dusseault, 2008). For example, co-injecting steam and a single aliphatic hydrocarbon (e.g., C_5H_{12} to C_8H_{18}) in SAGD will give benefits such as condensing vapors to generate diluted oil, generation of a better partially insulating non-condensing gas at the steam chamber top, and better μ reduction with lower steam-oil ratios (Canbolat *et al.*, 2004), although issues such as retardation of heat exchange efficiency must be balanced with reduced steam cost and the high price of solvents compared to the VO.

As an example, perhaps PPT technology along with SAGD could be beneficial in lower viscosity VO cases. PPT is effective when gas saturation is low, but it may be effective in hybrid configurations where the stimulation waves pass through the liquid-saturated portion of the reservoir to reach the zone where beneficial effects are desired. Figure 2-22 shows one possible configuration where PPT excitation might accelerate steam chamber growth and improve production rates.

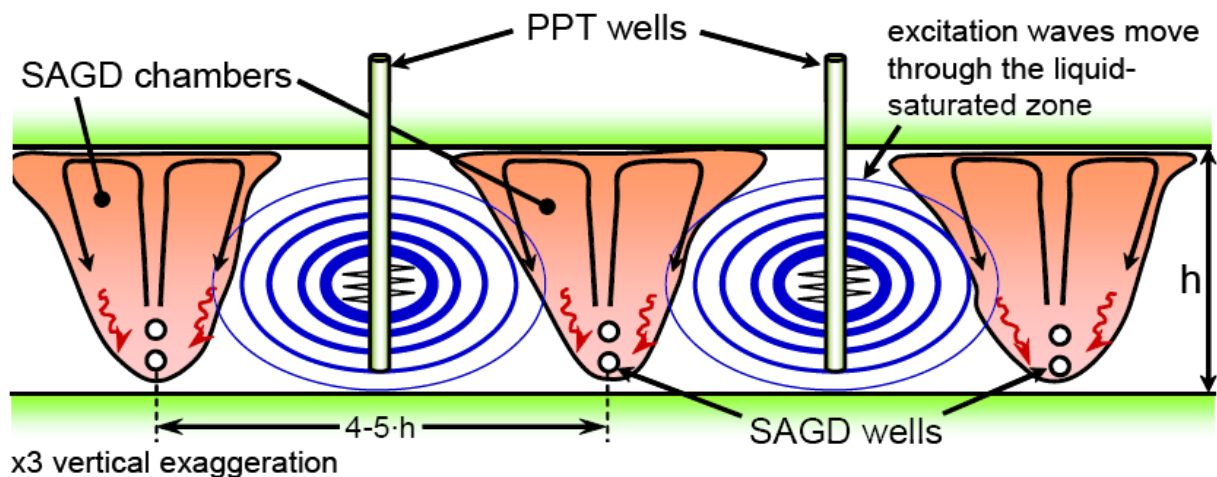


Figure 2-22: Using PPT to accelerate steam chamber growth in SAGD.

As an example for sequencing technologies, implementing a CHOPS-CSS-ISC sequence is discussed here, without making the claim that it is all technologically feasible. Many different sequences can be suggested, but in all cases it appears that if CHOPS is used, it must be the first in a sequence, and if ISC is used, it must be the last in the sequence.

CHOPS generates zones of enhanced porosity, permeability and compressibility in the reservoir because of sand withdrawal and formation shearing; this will result in more efficient and rapid spreading of injected steam during a subsequent CSS exploitation episode. Because of the accelerated time frame, steam injection may be economical in marginal zones where it would not normally be considered.

Various configurations are possible: initial development wells using CHOPS can be initially installed as thermal wells to allow recompletion to CSS wells. CHOPS wells could, on the other hand, be installed on 15 or 20 ha spacing, produced to their economic limit, and then CSS wells installed on a pattern infill basis to halve the spacing. CSS could also be implemented after the CHOPS phase, with new CSS wells drilled as rows and produced as CHOPS wells for the typical initial high-rate production phase (2-3 years). Once a CSS process has been carried out after CHOPS, it may be possible to implement a combustion process because the reservoir now is far more permeable, and since it is already heated, the chances of stable combustion front propagation are greatly increased, provided sufficient fuel remains in the reservoir. If vertical wells are used, it may be necessary to reduce the flow path length in the combustion phase to reduce oil cooling. The well spacing typically used in CHOPS (8-16 ha) or CSS (4-10 ha) is larger than the typical spacing needed for stable high ΔP combustion (2-6 ha), and infill wells would be needed, and then used as injection sites.

2.7.11 Steam Generation

The two major OPEX factors in steam processes for VO production are energy and water requirements for steam generation.

Water issues are particularly severe in remote dry locations (Buzachi Peninsula, Kazakhstan; Iran; Kuwait; Tuha, China...), but maximizing water recycling is implemented also in Alberta. This requires careful planning because of the large volumes of water, ~ 2–5 times the amount of oil produced.

The major OPEX factor is the cost of delivery of high quality steam to the wellbore. This is dominated by the steam generation heat source, although maintenance of steam lines and

maintaining low heat losses are not aspects to be ignored. In particular, the more effective the heat scavenging from the produced fluids, the lower the OPEX, and any rational VO steam process design must focus on minimizing heat losses and implementing heat recovery.

According to the National Energy Board (NEB) of Canada (NEB, 2006) natural gas prices affect substantially the supply costs of VO in SAGD projects in Canada, alone accounting for a substantial fraction of OPEX, and potentially dominating OPEX if prices are high. Natural gas requirements for SAGD are estimated at ~ 1 Mcf/b, so steam processes such as SAGD are intense consumers of natural gas, and more natural gas is used in power generation and upgrading (as a H-source). In Canada, with the sole exception of the OPTI-Nexen Long Lake Project, steam is generated with natural gas; when the cost of natural gas rises, OPEX rises considerably.

Reducing heat needs or changing the fuel for heat generation are interesting options and will become more important in the future, particularly if the price of natural gas increases. Steam cost reduction through steam and electricity cogeneration, combined with heat recovery and solvent co-injection, are characteristic of most new integrated SAGD projects. The separation of asphaltene fractions from the VO has considerable attraction because they can be used to create syngas and heat, which in turn can be used to manufacture steam and electricity, and removing asphaltenes means fewer upgrading problems. The syngas contains hydrogen, which can be used directly in upgrading instead of CH₄. Thus, many needs can be met by asphaltenes fraction (or coal) combustion, and if pure oxygen is used, high purity CO₂ is emitted, and after NO_x and SO_x removal, the CO₂ becomes available for enhanced oil recovery use or direct sequestration. This possibility seems to be about 10 years distant at this time, and because of the increased complexity of such an integrated system, start-up and stable operations will be more challenging, as in the OPTI-Nexen Long Lake project.

In climates such as in Kuwait and Iran, solar heat with linear parabolic collectors can provide a large fraction of the heat needs; technologies that could operate under non-steady steam injection conditions would be favored because of the intermittent nature of solar heat. Alternatively, one might scavenge heat from power plants or geothermal sources, if

economically available. In the more distant future, nuclear power has a singular attraction as a provider of heat because of the more efficient use of the low-level heat that is wasted in nuclear plants; the potential for nuclear to generate high value electricity as well as steam or superheated water for SAGD projects has appeal in a country with a well-integrated energy infrastructure, and advanced electrolysis systems using electricity and heat could be integrated into the nuclear facility to generate hydrogen for upgrading. Under such conditions, having nuclear power sources relatively near to upgrading facilities (100 km) would be desirable, but because of the difficulty of shipping steam long distances, small scale nuclear systems would be needed to service an area probably no greater than 75-100 km². The nuclear heat option is being considered in Alberta, but implementation before 2025 is unlikely.

2.7.12 Further Technical Issues

Advances in drilling, completion, monitoring, production, transportation and upgrading technologies lead to further reduction in OPEX and CAPEX requirements for VO production and pave the road for exploitation of resources currently deemed to be marginal. Processes like SAGD based on novel horizontal well drilling technology are examples of how improvements in technical aspects of VO production lead to better technical (higher *RF*) and economic (lower *CSOR*) performance, which in turn unlocks more VO resources. Some technical issues associated with VO production processes such as horizontal and multilateral wells, slant drilling, cementing and high temperature pumps are briefly discussed.

Long horizontal monobores, often equipped with branches (multilaterals), are used for producing lower viscosity VOs such as the FPO in Venezuela. Better well placement systems along with advances in well positioning systems help ensure maximum reservoir contact and correct placement. SAGD wells, for example, must be placed near the base of the reservoir, or a specified distance above bottom water to reduce steam chamber impairment risk. For instance, in the case of a 20 m thick VO reservoir, if the producer (SAGD well) is placed 4 m off bottom, then 20% of the reservoir will not be produced, and

the SAGD project is likely to be uneconomical; it is necessary to place the well 1 m above the base. Accurate well placement has become a routine matter in the last decade.

Drilling shallow horizontal wells (< 500 m depth) for SAGD using slant rigs is now routine in Canada. This approach avoids sharp bends in producing wells, which reduces wear on the casing and tubing, and makes workovers and repairs easier.

Wells must be designed to survive the high and often cyclic temperatures generated during VO production processes (up to 325°C). This requires thermal/high temperature well completions that function normally and survive periodic expansion–contraction cycles. Slip joints between tubulars are implemented in some thermally completed wells, special high-sealing-capacity thread designs for couplings have been developed, and special high silica cements that do not shrink during thermal cycling all are part of the thermal completion design.

Producing hot fluids (water, VO, solvents) requires approaches such as gas lift, E-Lift (Kisman, 2003), or high-temperature pumps. Progressing cavity pumps (PCP) and electric submersible pumps (ESP) are now available for high temperature applications. Sand resistant pumps for CHOPS are available and new pump designs capable of handling high sand quantities are used in many cases. Injection of diluents in the vicinity of the pump through hollow rods can reduce the viscosity of the VO and ease pumping and transportation problems (Clark *et al.*, 2007).

Many other technological issues associated with VO production technologies, upgrading, reservoir monitoring and management are being addressed by innovative concepts, improved design, or simply better execution and day-to-day engineering.

2.8 Upgrading and Transportation

The need for special upgrading and transportation strategies for VOs will continue to slowly alter these industry sectors in decades to come. VO has a low feedstock value; viscous, high sulfur oil carries a price penalty that, in western Canada, has averaged over \$US15/b since 2000, and was as high as \$US35/b in 2008. This differential price reflects a limited

upgrading capacity as well as the additional costs associated with upgrading, as evidenced by fully integrated mining and upgrading operations that have OPEX values of ~ \$US20–30/b. Likely, true upgrading costs are less than 50% of these costs, that is, ~ \$10–12/b.

High asphaltene and resin percentages in VO mean complex aromatic molecules with many carbon rings (low H:C ratio) which, when broken, generate free carbon, double and triple C bonds, or open bonds that must be satisfied with hydrogen (Figure 2-23). VOs also have high heavy metal contents that rapidly poison process catalysts. A small quantity of VO can be added to conventional refining streams; this increases residual tar production, which is used for asphaltic products, but large-scale treatment of VO requires dedicated upgrading.

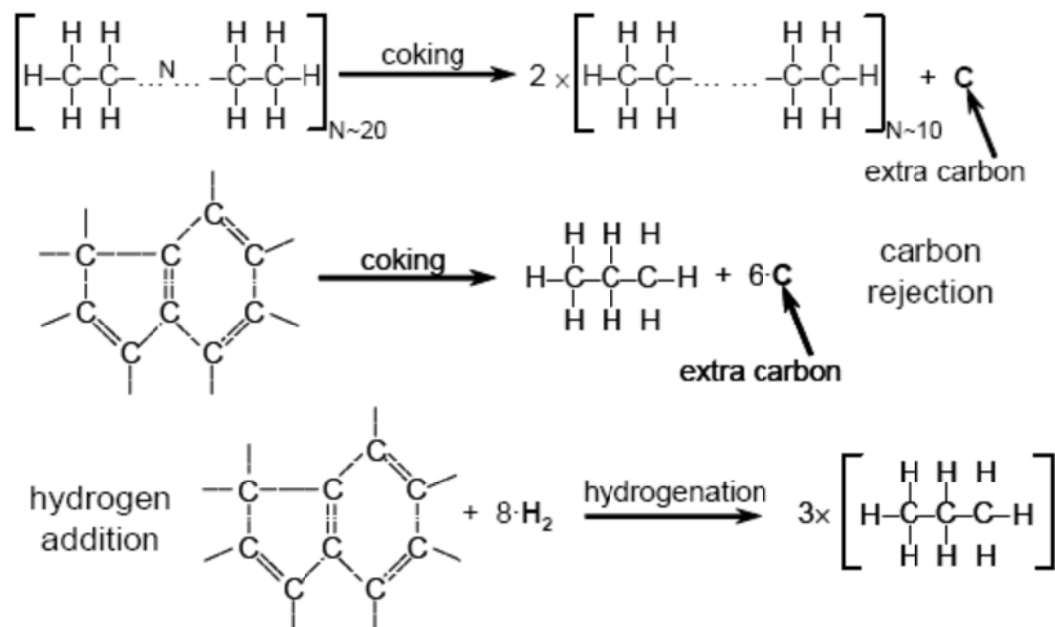


Figure 2-23: Carbon rejection and hydrogen addition for viscous oils.

Direct generation of low-viscosity SCO from VO, called upgrading, usually involves non-catalytic carbon rejection (coking), catalytic hydrogen addition (hydrogenation or hydroprocessing), and sulfur removal to create a product suitable for conventional refineries. Over the years several processes and techniques has been developed for upgrading.

Various types of coking are used, but the basis is always heat to cause molecular scission, accompanied by separation of the coke from the product. Hydrogen addition requires a source of H (usually CH₄), and the process is carried out at high temperature and pressure in the presence of catalysts.

There are many process variants to achieve these goals, depending on whether coking or hydrogenation is favored, what pressures are used, when it happens in the process, and so on. At one extreme, coking may be eliminated altogether. VO is hydrogenated, products are removed by distillation stages, and the ‘residuals’ (e.g., the viscous non-distillable materials) continuously recycled to eventually generate a ‘bottomless’ array of products with no tars or asphalts. This process may generate 1.15 barrels of SCO per barrel of VO, but large amounts of hydrogen are needed, and catalyst poisoning problems are large.

At the other extreme, hydrogenation may be almost eliminated, used only as a minor final step to bring the SCO to a high quality, and the upgrading is then dominated by coking. This may generate only 0.8–0.85 barrels of SCO per barrel of VO, but large amounts of coke will be generated. The coke may have use as a source of heat and syngas to eliminate external sources of heat, power, and hydrogen (CH₄). At the OPTI-Nexen Long Lake Project, instead of coking, asphaltenes are removed and hydrogenation used to generate a 39°API SCO.

2.8.1 Non-Catalytic Processes in VO Upgrading

2.8.1.1 Solvent Deasphalting

Asphaltene in VOs and residual oil can be separated using inexpensive separation processes, and an example is the solvent deasphalting technique (Curtis *et al.*, 1987; Chen *et al.*, 1994). This method exploits molecular weight differences to separate large asphaltene molecules from smaller hydrocarbon molecules, giving a paraffin-enriched higher API gravity product for upgrading. VO is mixed with a light paraffinic solvent (propane, butane, ...), and the high molecular weight and therefore low solubility asphaltenes precipitate from the mixture. Other approaches also exist for asphaltenes removal.

2.8.1.2 Thermal Conversion

Thermal conversion or coking is a direct carbon removal process which transfers hydrogen from heavy to lighter hydrocarbon molecules resulting in production of coke or carbon. Under high temperatures the VO itself is the hydrogen donor and this process increases the H/C ratio of the liquid and gaseous phases, with elemental carbon being withdrawn as coke (petcoke). This can be implemented in various ways: gasification, delayed coking fluid coking and flexicoking, and visbreaking. The amount of carbon removed depends on the oil viscosity and the upgrading technology chosen. Although thermal coking processes give lower product volumes and generate substantial amounts of byproduct coke, because of lower CAPEX and OPEX compared with catalytic processes, thermal coking processes remain widely in use.

2.8.1.3 Gasification

One form of gasification of VO involves complete cracking in the presence of steam under high temperatures ($> 1000^{\circ}\text{C}$) into gaseous phases including CO_2 , CO , H_2 , and SO_x , along with solid phases that include mineral residue and some ash or carbon black (Pindoria, 1997). Because of control issues, gasification has attracted less interest within the industry compared to coking and hydrogenation.

2.8.1.4 Delayed Coking

Delayed coking (Figure 2-24) is a process based on long reaction times in the liquid phase to convert VO into high-value products (naphtha to diesel fractions) and coke. Because of the flexibility of this process for upgrading any type of VO and residual fraction mix, the process has been an attractive choice for the oil industry (Gray, 1994; Tokarska, 1996; Reinoso, 1998).

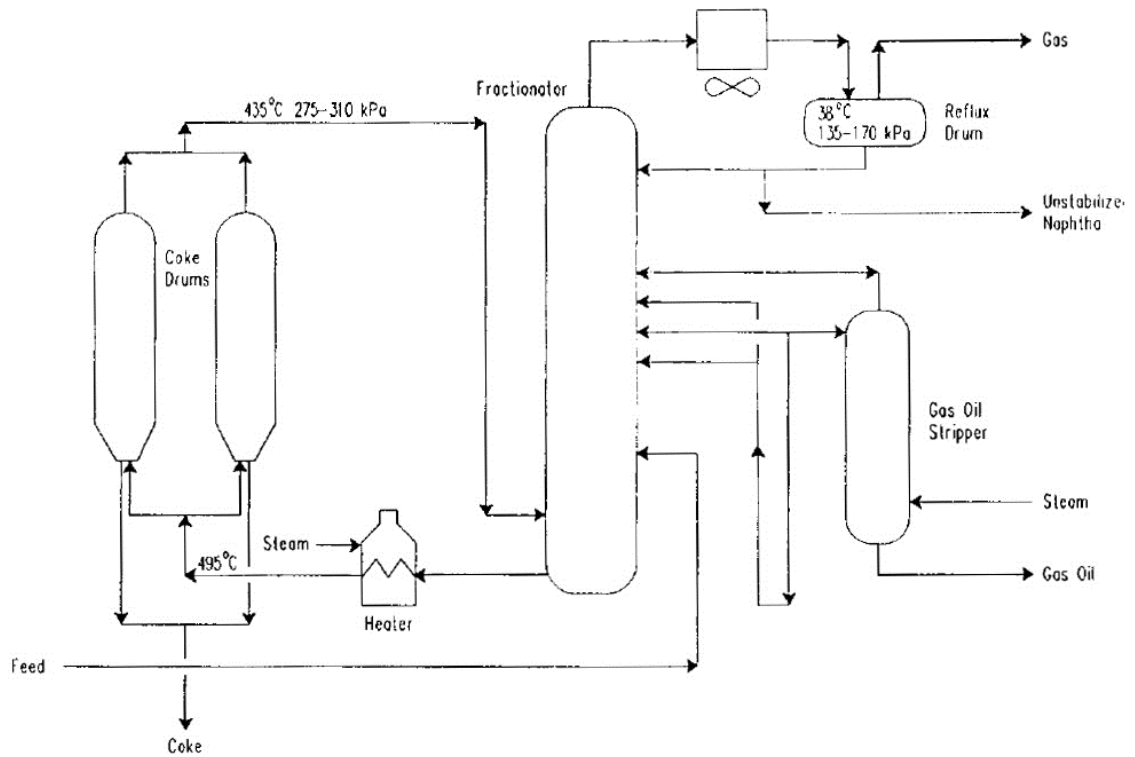


Figure 2-24: Simplified schematic of the delayed coking process (From: [Gray, 1994](#)).

2.8.1.5 Fluid Coking and Flexicoking

Fluid coking (Figure 2-25) processes are based on fluidized catalytic cracking technology. Flexicoking, an extended form of fluid coking, implements a coke gasifier into the process to convert coke to syngas ([Furimsky, 2001](#)).

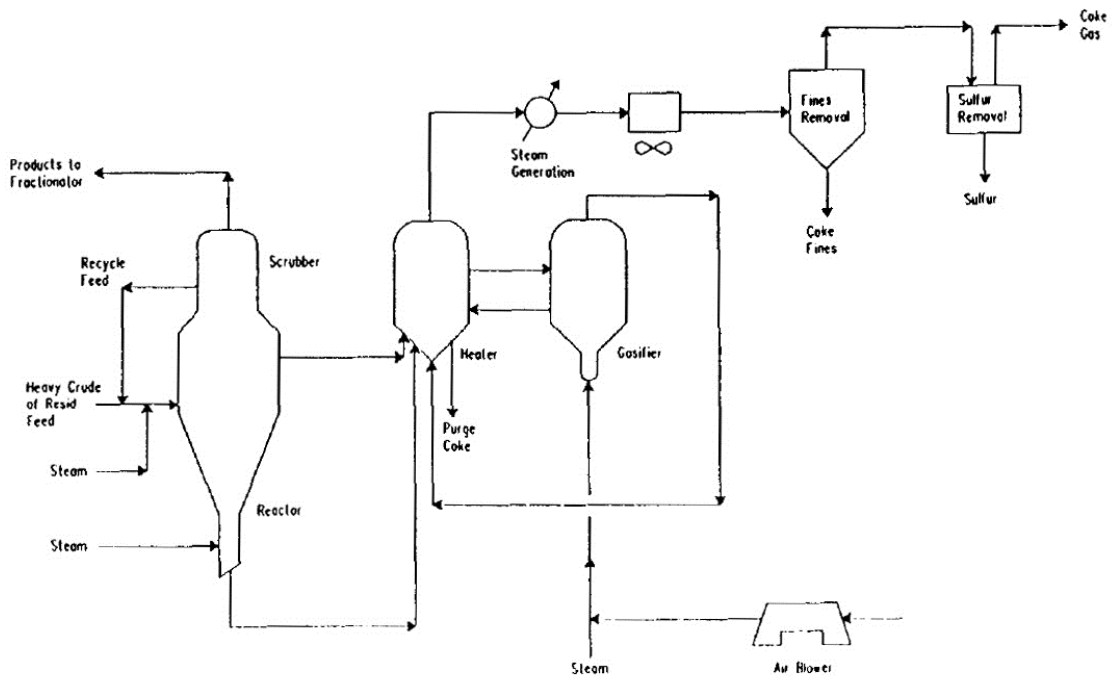


Figure 2-25: Simplified schematics of fluid coking process (From: [Gray, 1994](#)).

2.8.1.6 Visbreaking

The visbreaking (Figure 2-26) or thermal viscosity reduction process involves heating the VO and residue in a furnace under moderate pressures and at temperatures of 450–500°C but with a low residence time to avoid excessive coke production. Normally, this technique is used to increase refinery net distillate yield because this process has a lower CAPEX and OPEX compared with hydrogenation techniques. However, this process suffers from a lower yield of light liquid products, and the heavy metals and sulfur content remain relatively high ([Speight, 2004](#)).

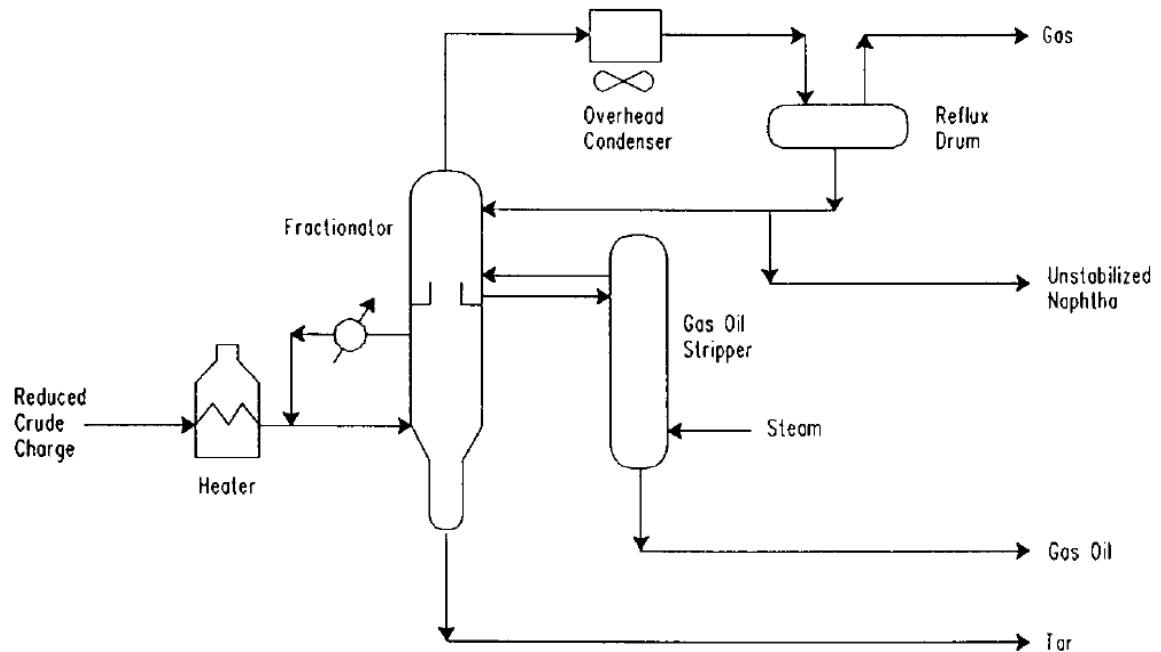


Figure 2-26: Simplified schematics of visbreaking process (From: [Gray, 1994](#)).

2.8.2 Catalytic Processes in VO Upgrading

2.8.2.1 Fluid Catalytic Cracking

Fluid catalytic cracking (FCC) (Figure 2-27) is a process that converts some fraction of VO and residue into gasoline type components with a high octane number. Residue fluid catalytic cracking (RFCC) is an enhanced version of FCC, however, it requires a higher quality feedstock which limits its implementation in terms of VO upgrading. Properties of the catalyst used are important; crystalline zeolite-type aluminosilicates in an organic matrix are common catalysts in the RFCC process ([Andersson and Myrstad, 1998](#)).

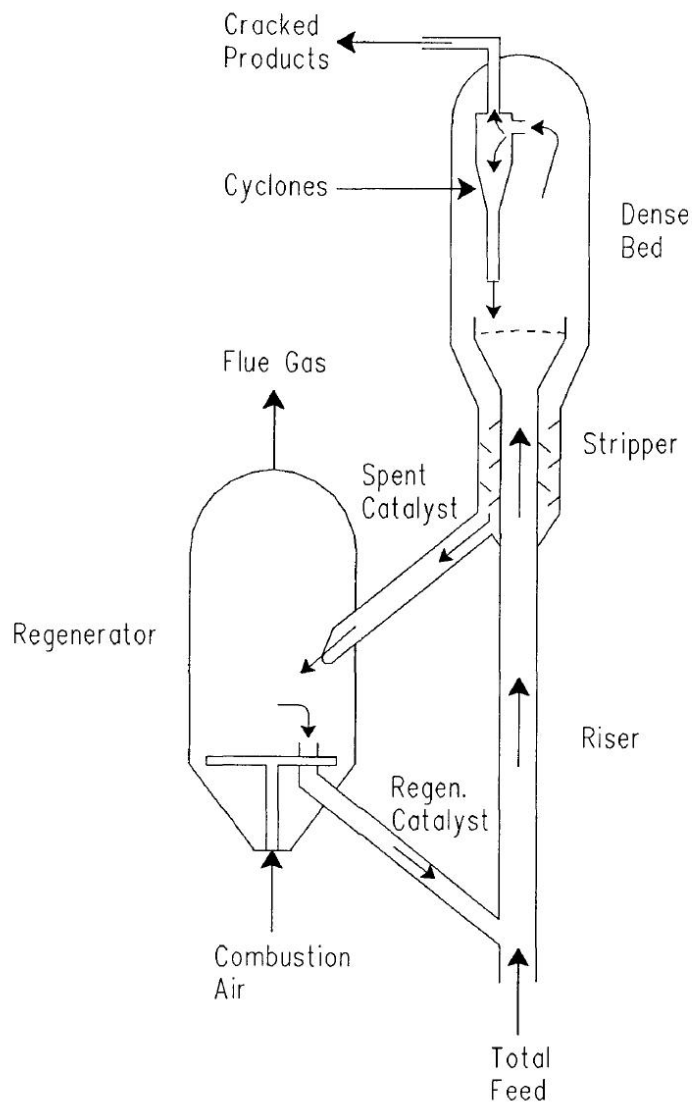


Figure 2-27: Simplified schematics of fluid catalytic cracking (From [Gray, 1994](#)).

2.8.2.2 Hydroprocessing/Hydrogenation

Viscous oils are highly aromatic with a low H:C ratio; as more hydrogen is added, more aliphatic hydrocarbons is produced. Hydroprocessing or hydrogenation techniques require significant amount of hydrogen and compared with thermal upgrading processes have a relatively higher CAPEX and OPEX. However, these processes yield greater volumes of

higher quality products and have better selectivity in liquid yield than other processes (Toulhoat *et al.*, 1990). Continual advancements in catalyst development and better process technology have characterized the various hydrogenation approaches, and upgrading plans involve choosing the optimum process to balance feedstock characteristics with the desired product profile.

2.8.2.2.1 Fixed Bed Residue Catalytic Processes

Use of a fixed bed reactor (Figure 2-28) involves simultaneous or sequential hydrogenation of VO and residue in the presence of catalyst through a direct reaction with hydrogen (Scherzer and Gruia, 1994). These processes suffer from catalyst poisoning with time; however, this can be reduced by process refinements that minimize heavy metal and coke availability for deposition on the catalyst beds.

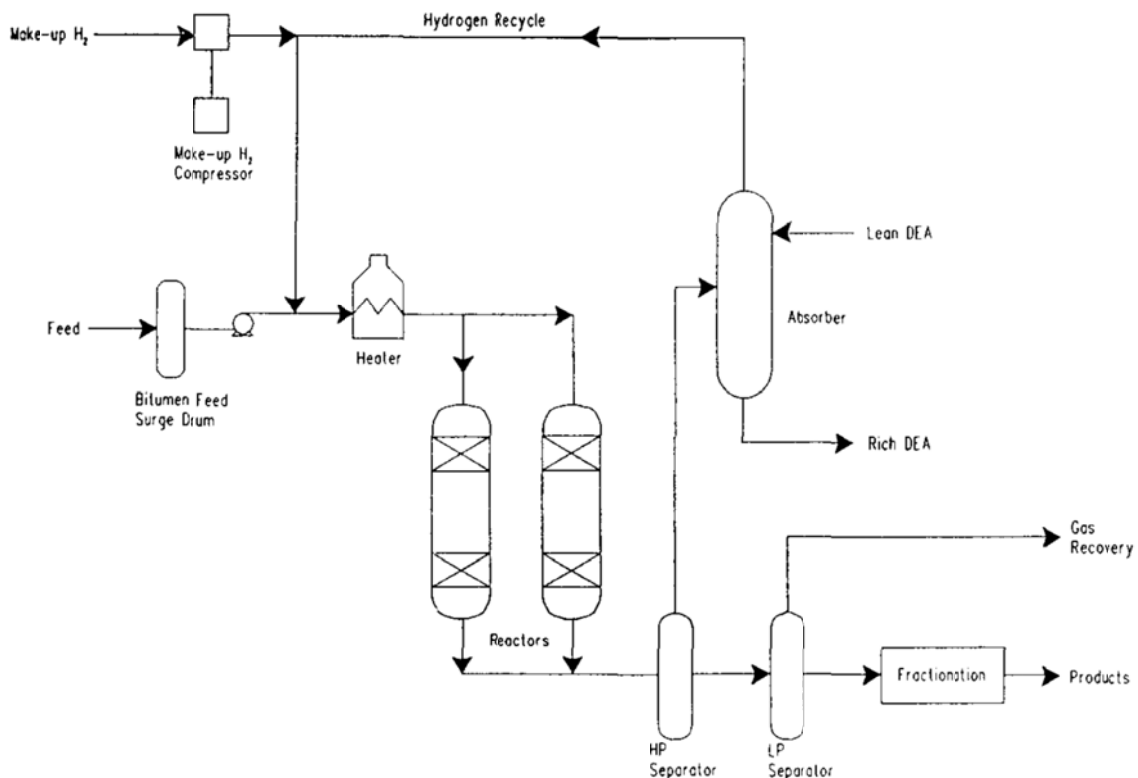


Figure 2-28: Simplified schematics of fixed bed catalytic process (From Gray, 1994).

2.8.2.2.2 Moving Bed Residue Catalytic Process

In the moving (ebullated) bed residue catalytic process (Figure 2-29) the catalyst is kept in suspension because the liquid VO feed enters at the bottom and flows upward through the catalyst. To achieve this, catalysts are made into uniform grains of 1 mm or less, and the moving reaction bed consists of equal-diameter grains (Gray, 1994). The main advantage of moving bed reactors is their ability to hydrogenate the most problematic feedstock that may have high contents of asphaltenes, heavy metals and sulfur.

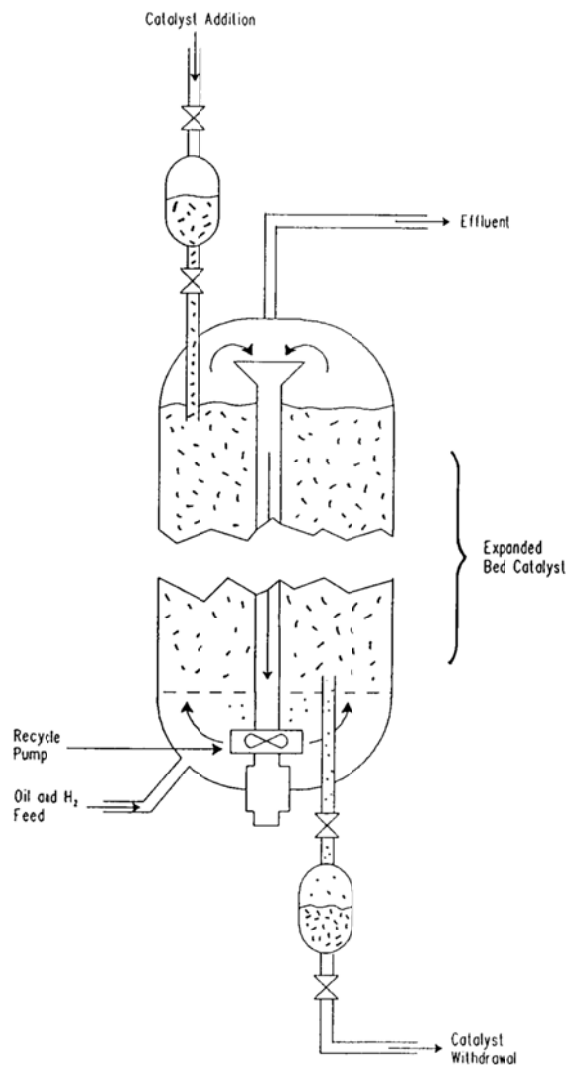


Figure 2-29: Simplified schematics of ebullated bed catalytic process (From Gray, 1994).

2.8.2.3 Hydrogen Sources

There are a number of viable sources for the hydrogen required in hydrogenation processes, although the technologies are not all at the same stage of development. The most widely used process and still the most economical is formation of H₂ directly from CH₄ through the steam methane reforming (SMR) process.

Water can also be used as a hydrogen donor, but high pressures and temperatures are needed to break the strong H–O bonds, as in the syngas manufacture process, and this remains a higher priced option. Gasification (syngas and clean coal technologies) using partial oxygenation in the presence of water can provide a hydrogen source. During gasification, about 10% of the feed VO is needed in order to provide enough H₂ for upgrading the rest of the feedstock.

In hydrogenation processes, continuous recycling loops are incorporated into the upgrading scheme so that the viscous residual hydrocarbons are returned to the hydrogenation facility. It is thereby possible to avoid coking altogether, but coking is considered an aid to upgrading as it greatly reduces sulfur and heavy metals content in the feed to the hydrogen addition units.

2.8.2.4 Coke

Coke is the main by-product of thermal upgrading processes; it can be stockpiled semi-permanently, burned for fuel, used in metallurgical processes, or in the future it may serve as an additive or a feedstock for new processes. Combustion in air results in large flue gas and SO_x generation; the latter is captured during combustion (e.g., fluidized beds with crushed CaCO₃) or stripped from flue gases (flue gas desulfurization), but CO₂ emissions represent a potential future carbon penalty. Future development of O₂-fluidized combustion or economical amine or membrane CO₂ separation methods may provide pure CO₂ for use or sequestration. Elimination of coke altogether using “bottomless” hydrogenation techniques remains an option, though not the cheapest one.

2.8.2.5 Sulfur Removal

The sulfur content of VOs is extremely high, from 0.1–0.2% for the lower viscosities to 4–5% or higher for the most viscous materials. The increasing demand for low-sulfur products means high pressure hydrogenation must be used during upgrading, a process which turns S into a gaseous substance (H₂S) that can be easily separated and turned into elemental sulfur, a relatively inert substance that is easy to store or transport. S-removal is an integral aspect of all upgrading activities.

2.8.3 Future Developments in Upgrading

Recent pilot-plant scale developments in the upgrading of VO indicate that the near future could see a reduction of the differential cost of upgrading VO from ~ US\$10–\$12/b to as low as US\$5–8/b. These processes are based on a better understanding of the issues of asphaltene solubility effects at high temperatures, incorporation of catalysts that are chemically precipitated internally during the upgrading, improving hydrogen addition or carbon rejection efficiency, new nano-dispersed catalysts and so on. The OPTI-Nexen Long Lake Project is the first to attempt full integration of deasphalting and gasification, and is therefore similar to clean coal technologies, but severe start-up problems have occurred (typical for novel technologies). Other alternatives are being considered or tested at small scale to reduce the dependency of the VO industry on natural gas (NEB, 2006).

The ‘heavy oil to light oil’ or HTL process Veith (2006) for upgrading heavy oil through rapid pyrolysis through contact with hot particles holds the promise of being able to be economically developed at a scale of 5000–10000 b/d, and it has been tested at a lesser field scale.

A large increase in upgrading efficiency can be achieved in the area of heat preservation. The ‘hot coupling’ concept, wherein heat is preserved by short flow distances and direct treatment, should allow overall cost efficiencies of 20% over current upgraders, although this leads to control and start-up complexities that are challenging to manage.

2.9 Viscous Oil Transportation

Refineries are designed to provide locally needed products; siting and capital cost issues for existing facilities are not issues, and they can be modified progressively to gradually accept heavier feedstock blends. It is widely thought in the industry that it is better to ship VO directly to these locations with only a small amount of local upgrading (likely by coking), instead of a full upgrading to a light SCO (e.g., 35–39°API). More limited on-site upgrading of VO to create synthetic crude of about 20–30°API gravity generates good refinery feedstock, but with a narrow range of molecular weights, and it is most desirable to blend this with other feedstocks for refining. Thus, massive transportation of VO by pipeline is needed and is now taking place from Western Canada to various centers in the U.S.A.

To pipeline raw or slightly upgraded VO, there are four available options:

- Dilution with 5–20% low molecular mass hydrocarbons;
- Blending high API gravity SCO with raw bitumen;
- Use a heated pipeline; or,
- Generate an emulsion with fresh water as the continuous phase.

The first two are widely used, the third only locally, and the fourth has not been implemented commercially.

Diluent availability in Canada is already a constraint for VO pipelines, and the development of SynBit blends (50% SCO, 50% bitumen) has reduced dependency on the lighter hydrocarbons. Small diameter pipelines to return diluents from remote upgrading facilities to VO shipping points in Alberta and Saskatchewan are also used to provide additional diluent.

Currently, over 95% of VO exports from Canada go to the US, and completion of major pipeline projects in this area during 2010–2012 will increase VO transportation potential by up to 1.3 MMb/d ([ERCB, 2012](#)). The development of a pipeline from Ft McMurray to Prince Rupert on the Pacific Coast will allow about 550000 b/d to be provided to Pacific Rim markets, helping to absorb the predicted increases in raw bitumen and SCO production, mainly coming from Alberta. The major Canadian and U.S.A. oil pipelines are presented in

Figure 2-30, and there are projects planned to extend VO exports to as far south as Texas and Mississippi.

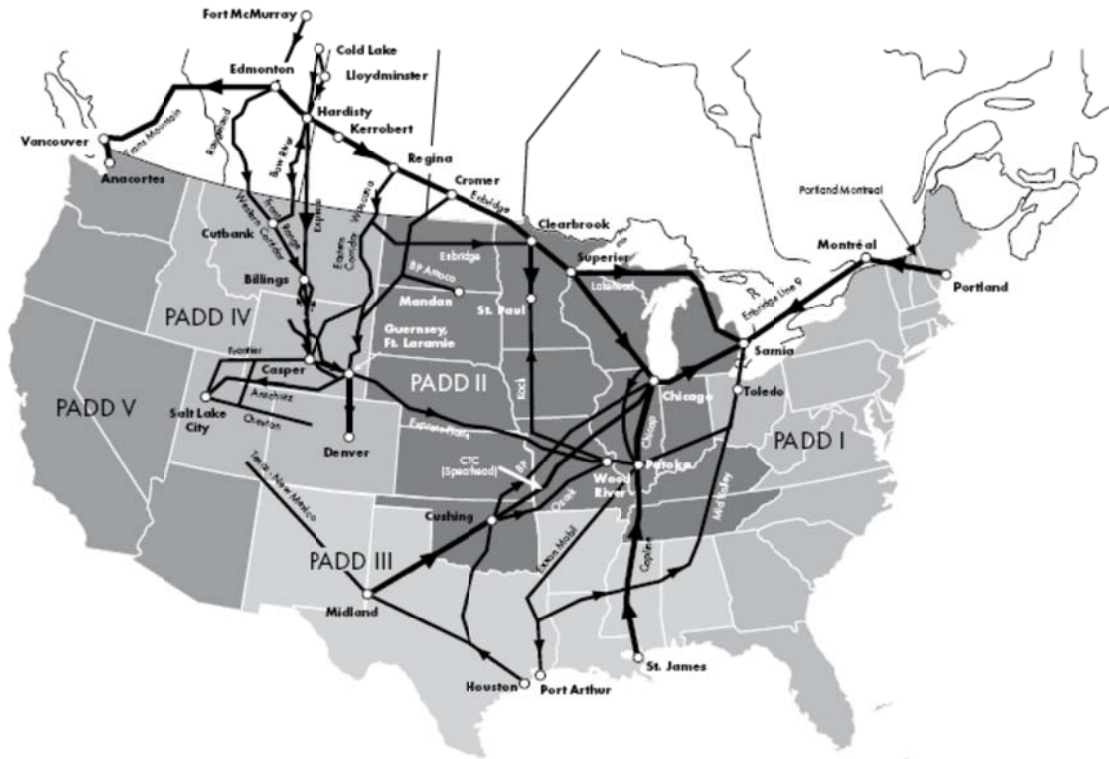


Figure 2-30: The major Canadian and U.S. oil pipelines (From: [ERCB, 2012](#)).

2.10 Environmental Issues

Environmental issues in VO development became more pressing in 2010 because of increased concern over climate change, oil sands mining, a 10% larger carbon footprint for VO, and because of the Deepwater Horizon blowout in the Gulf of Mexico.

Accusations of environmental laxity are common, and often justified. Laxity in the oil and gas industry arises for five reasons:

- Spending on wastes is viewed as direct revenue loss;
- Non-local employees have little commitment to local communities;
- Poor regulatory enforcement and corruption arises in various jurisdictions;

- There remains general ignorance of true environmental impacts; and,
- There remains a culture of ‘fixing it’, rather than proactive avoidance.

VO production generates large waste volumes that must be treated economically and securely. Recent and continued progress suggests that goals of ‘minimal impact – zero emissions’ are economically attainable as well as sociologically desirable, but CO₂ emissions abatement will remain a great challenge for society and the oil industry.

In situ VO development has impacts during exploration, drilling, infrastructure generation, production, transportation (generally pipelines), upgrading, refining and petrochemical facilities, and post-activity clean-up. Mining has even larger impacts; the entire landscape is reformed. More specific issues include atmospheric emissions, water use, solid waste management including long-term coke and sulfur storage, and disposal of large volumes of wastes such as pipe scale, tank bottoms, and emulsions.

2.10.1 Surface Mining Solid Wastes

Huge solid waste volumes are generated in oil sand mining; these must be permanently placed and the landscape rehabilitated to a reasonable quality. Currently, limited successful reclamation is being achieved in Alberta oil sands mining, but reclaimed land appears to be far more ecologically productive than previously existing terrain (mainly bogland and sandy soils).

One cubic metre of ore averages 0.66 m³ of silica sand, 0.23 m³ of oil, 0.07 m³ of water and 0.04 m³ of fine-grained silt and clay. The products are approximately 1.25 b (0.2 m³) of raw bitumen, 1.10 m³ of bulked sand (36–38% porosity) containing water, fine-grained minerals and residual oil in the pores, 1.6 m³ of water, much of which is recycled for further extraction, and 0.15 m³ of oily aqueous sludge containing 40–50% of the clay minerals in the original raw ore. In addition, for each m³ of ore, 0.3 m³ of overburden is removed, organic soil is stored for future reclamation, and 0.01 m³ each of coke and sulfur are produced and stockpiled.

2.10.2 Surface Mining Liquid Wastes and Sludges

After primary water recycle, $\sim 1.25 \text{ m}^3$ of sand and sludge are generated for each m^3 of ore processed; the sludge contains oil, clay, and other fine-grained minerals, and it remains indefinitely as a viscous liquid in the bottom of tailings ponds (Dusseault and Scott, 1984).

Since mining began, sludge volumes per barrel of bitumen have dropped by half, and research continues on anhydrous extraction methods. Process improvements include partial clay flocculation, tertiary oil extraction, and thickened tailings placement; also, various means of accelerating sludge consolidation are being tried to reduce pond volumes and allow reclamation. Anhydrous extraction would eliminate large tailings ponds, but handling 100% solid wastes would also increase transportation costs compared to slurry pipelines, and the long-term groundwater impacts from an anhydrous extraction process are likely to be substantially more severe than from the hot water extraction processes.

Groundwater drainage toward the large local river (Athabasca) from the tailings dams and ponds, and eventually from the rehabilitated landscape, is a long-term concern because of the elevation difference (100-150 m). The seepage water contains dissolved species that are not present in natural groundwater, and the flow paths from the ponds and dams is as low as a kilometer in some cases, so that there is insufficient adsorptive action for groundwater clean up. Whether this has a severe impact on river water quality remains an issue of contention at this time.

Nevertheless, not to minimize the environmental challenges, it is appropriate to recall that the entire oil sands mining area in Alberta comprises but a small fraction of the boreal forest, covering an area far less than the Greater Los Angeles conurbation.

2.10.3 *In situ* Viscous Oil Recovery Processes

Steam for heavy oil recovery requires heat and water sources. CH_4 is by far the main source of heat, but asphaltene and coke combustion for heat and H_2 generation will become more common. On average, VO recovery by steam methods requires about 3 b of steam at 250–300°C per barrel of oil. Steam generation requires water treatment and attendant calcium

sludge disposal needs. VO production also generates emulsions that are challenging to treat and are best disposed through deep injection along with saline boiler sub-feed water and other non-recyclable water streams. CO₂ emissions (extraction and upgrading only) are 125–150 kg/b for SAGD methods (Figure 2-31), 175–200 kg/b for cyclic steam methods, and > 80% of emissions are allocated to steam generation, H₂ generation, and power costs, ranked by size.



Figure 2-31: SAGD Development, eastern Alberta. Courtesy David Dodge, Pembina Institute.

In situ combustion processes, by contrast, are anhydrous, and although CO₂ emissions are on the order of 150 kg/b, this is less than CH₄-based steam projects. Furthermore, lack of significant liquid and solid wastes make *in situ* combustion processes singularly benign in terms of environmental impact. Of course, surface wastes and gaseous emissions must be properly managed.

2.10.4 Sulfur and Coke

Currently in Canada, coke is largely stockpiled, although small amounts are exported. With emerging clean coal technologies, coke may become a fuel for generating power, heat, and hydrogen in an integrated system. Elements of coke combustion could include O_2 as an oxidant, pressurized fluidized bed combustion, heat exchangers, steam generation for viscous oil, and full emissions capture. With pure O_2 , $\sim 97\text{--}99\%$ pure CO_2 is a useable by-product, and hydrogen can also be produced.

Internationally, more and more S-rich natural gas and oil are being exploited, and increasing VO production should sustain the current glut of sulfur for the rest of the century. Thus, sulfur has to be stockpiled indefinitely if it cannot be sold. In SM, storage in the mined-out pit in a local area for easy future access can be implemented. For *in situ* viscous oil production projects, sulfur could be injected at a shallow depth (~ 300 m) leaving it accessible in the future through hot water injection; otherwise, surface sulfur storage will be required.

If fluidized beds with $CaCO_3$ are used to burn sulphur-rich coke fuels, huge volumes of desulfurization sludges, essentially gypsum sludges ($CaSO_4$), will be generated. Because the gypsum contains heavy metals, ash, and other byproducts, it has no industrial use, and will have to be stored permanently at the surface or disposed of in pits or deep underground. Gypsum is quite soluble in groundwater, but the long-term impacts of massive gypsum storage are ill-understood.

2.10.5 General Waste Management Options

Treatment of gaseous emissions to reduce noxious gases (SO_x , NO_x , particulates) is now so efficient that non-conventional oil production and upgrading methods should not significantly impact atmospheric quality. This is merely an issue of regulatory policy and strong enforcement (e.g., [Charpentier *et al.*, 2009](#)).

Large volumes of waste water that cannot be cleaned economically can be injected deep into sedimentary strata with negligible environmental risk. Liquids with oily scum and colloiddally

suspended solids or oil are usually clarified before injection, although this costly step is not necessary if slurry fracture injection is used (Marika *et al.*, 2009). In steam projects, > 90% water recycling is widely practiced, but this water must be treated to remove calcium and other polyvalent cations before steam is generated. Lime sludges generated by water treatment represent solid wastes that must be dealt with, but the clear supernatant liquid can be easily injected.

Solid waste disposal options depend on whether it is dry or in the form of tailings, and whether it is a hazardous or a non-hazardous material. Small amounts of hazardous and non-hazardous solid waste can be treated and disposed of by means such as chemical leaching, thermal decomposition, centrifuging, oil extraction, and landfill placement; except for the latter, these are expensive treatment methods, and the latter is severely constrained in terms of what types of materials can be so disposed.

Non-hazardous slurries can be sent to separators (small volumes), to tailings ponds for gravitational separation (huge volumes), or injected directly at depth under hydraulic fracturing conditions (intermediate volumes). Non-hazardous solid wastes can be disposed of in approved landfills, by deep slurry injection, or through salt cavern placement (Figure 2-32). Attempts to thermally treat or clean and recover oil from large volume oilfield waste streams is invariably more costly than disposal because cleaning creates several additional streams, such as dirty water, poor oil and clean sand, which still must be dealt with.

As an example of a massive waste management issue, huge volumes of oily sand are produced during CHOPS; in Canada, about 1 m³ per 50 m³ of oil is generated, giving over 0.25 × 10⁶ m³ total sand in 2004 alone. The produced sand was once disposed of by land or road spreading, but this is no longer environmentally acceptable. Warm water washing has been tried, but several companies have gone bankrupt trying to do this, and biotreatment and thermal decomposition appear to be technologically risky or costly.

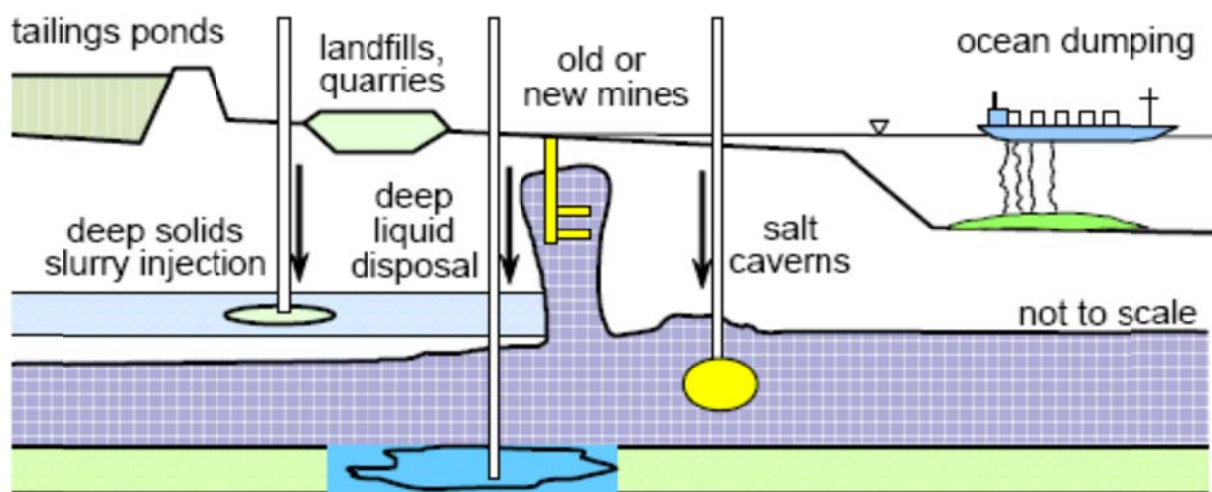


Figure 2-32: Permanent disposal methods for liquid and solid wastes.

Some of the produced sand, along with emulsions, slops, and other wastes, is now placed in local salt caverns where solids settle to the base, displacing brine. Because of its high density (1.2 g/cm), and because it destroys natural ionic surfactants, brine helps separate much of the oil from the wastes, although the recovered oil is of very poor quality.

Produced sand can be slurried with waste water, some emulsion, and slops (all costly to dispose of conventionally), and injected under fracture pressure into appropriate porous and permeable formations. The largest VO operations slurry injection disposal site in the world, in Duri, Indonesia, has averaged over 500000 m³ per year of slurry placement using several injection wells (Marika *et al.*, 2009). Injection costs are lower than for salt cavern creation and placement, and the environmental liability is essentially zero once wastes are injected into an appropriate zone (usually a depleted reservoir).

Most produced sand in Canada is placed in Class II landfills. The wastes must be stackable (no free liquids) with chloride contents less than 3000 mg/L¹. This means that waste sand must be stockpiled on the surface for a year or two to drain and be rain-washed before trucking to disposal. This method is slightly cheaper than the others, but carries a sustained

environmental liability because of near-surface placement of the solids and because of groundwater contamination during the period of rain-washing.

2.10.6 Zero Emissions Targets

Suppressing stack emissions of SO_x , NO_x and particulates to near-zero levels is currently achievable, but CO_2 emissions remain an environmental concern.

Many noxious and even hazardous solid wastes can be injected (Figures 32 and 33) into saline aquifers with adequate seals against upward flow. Already, zero saline water discharge is widely practiced. With deep injection or salt cavern placement methods of solids, it appears that reasonable cost technologies exist to achieve near-zero discharge in VO exploitation. The fossil fuel industry must continue to work toward zero discharge as a goal, or else make sure that discharges are only of materials that have minimal impact; otherwise, a harsher regulatory environment will evolve.



Figure 2-33: Deep Injection Facility for Solid and Liquid Wastes, Duri Oilfield, Indonesia. The black area is a concrete pit for viscous fluids and solids in transit. Duri Oilfield has close to Zero Discharge status.

2.10.7 Greenhouse Gas Emissions

In thermal VO production, greenhouse gas emissions (GHG), particularly CO₂, represent a major environmental concern. [Charpentier et al. \(2009\)](#) reported that, based on review of 13 different studies, CO₂ emission in SM and upgrading and *in situ* and upgrading operations range from 62–164 and 99–176 kgCO₂e/b (kg/b) SCO, respectively, compared with 27–58 kg/b from conventional oil production. Ranges reported in Alberta are 125–150 kg/b SCO for SAGD methods and 175–200 kg/b SCO for CSS methods. *In situ* combustion processes, by contrast, are anhydrous, and although CO₂ emissions are on the order of 150 kg/b SCO, this is probably similar to CH₄-based steam projects overall.

Excluding upgrading, in Canada mining and extraction produces about 80 kg/b and SAGD about 90 kg/b SCO [Donnelly and Pendergast \(1999\)](#), with CSS having 20–30% higher values. Similar studies show CO₂ emissions in the range of 90–160 kg/b from SCO in plants implementing fluid coking and delayed coking processes, respectively ([Furimsky, 2003](#)). If one includes the CO₂ emissions from combustion of the fuels (gasoline, diesel, jet) produced from oil sands, it appears that there are 8–15% greater GHG emissions than for conventional oil, far smaller than many claims.

A report by the Pembina Institute [Bramley et al. \(2005\)](#) suggests that the VO development in Canada is leading to a growing gap between GHG emissions quota under Kyoto Protocol agreements and current GHG emissions. Also, the amount of GHG emissions from oil sands development is projected to be on the range of 113–140 MMtCO₂e (million tonnes CO₂ equivalent)/yr, about 25% of the Canadian CO₂ quota in the original Kyoto Protocol agreement.

The major source of GHG emissions (CO₂) is steam generation; if CH₄ is displaced by coal or asphaltene combustion, GHG emissions per barrel of product will rise unless CO₂ capture is implemented. If heat sources are displaced by nuclear energy, GHG emissions drop substantially.

2.10.8 Water Issues

In addition to extraction uses, during integrated SM operations there are large water requirements for drilling, mining, cooling, hydrotransport of tar sands, dust control, and so on. *In situ* VO production projects, especially processes such as SAGD and CSS, have modest additional water requirements for drilling, cooling of equipment, and other uses (Veil and Quinn, 2008).

Oil sand mining operations consume 12 b of water for each barrel of SCO, but most is recycled, leading to net usage of ~ 4 b of water per b of SCO produced Mikula *et al.* (2008). Water requirements for SAGD are reported to be in the range 2–10 b per barrel of oil produced Gates and Chakrabarty (2006), but > 90% recycling of produced water means make-up water needs are modest (~ 0.2–0.3 b/b), although separation, treatment, and handling costs comprise a significant portion of OPEX.

The other water concern is the potential impact on the water quality of both surface and underground water. Residual organic compounds represent a concern in tar sands formations after application of *in situ* VO processes (Veil and Quinn, 2008). Also, water produced from thermal processes or water consumed to wash the tar sands and separate the bitumen needs to be treated before it can be re-used for steam generation or disposed. As mentioned, groundwater seepage and flux of contaminants remains a concern to mining operations and tailings dam design and operation.

Further technological developments will lead to less and better usage of water in VO production projects, but improved environmental husbandry remains an important regulatory issue.

Nomenclature

Acronyms, Symbols, Units

Acronyms: Production Technologies

CAPRI	=	<i>In situ</i> catalytic upgrading
CHOPS	=	Cold Heavy Oil Production with Sand
CP	=	Cold Production of heavy oil (without sand)
CSS	=	Cyclic Steam Stimulation (vertical wells)
DCI	=	Deep CO ₂ Injection (e.g. supercritical fluid)
GOGD	=	Gas Oil Gravity Drainage
H+TC	=	Heating with Thermal Convection
HCS	=	Horizontal well Cyclic steam Stimulation
IGI	=	Inert Gas Injection
ISC	=	<i>In situ</i> Combustion
PPT	=	Pressure Pulse Flow enhancement
SAGD	=	Steam-Assisted Gravity Drainage
SF, SD	=	Steam Flood, Steam Drive
THAI	=	Toe-to-Heel Air Injection
VAPEx	=	Vapor-Assisted Petroleum Extraction
WAG	=	Water Alternating Gas

Symbols: Latin, then Greek

ϕ	=	porosity in %
AAPG	=	American Association of Petroleum Geologists

AERCB	=	Alberta Energy Resources Conservation Board
AOS	=	Athabasca Oil Sands
AOSTRA	=	Alberta Oil Sands Technology and Research Authority
API	=	American Petroleum Institute gravity scale
ARC	=	Alberta Research Council
b	=	Barrel of oil
Bb	=	Billion barrels of oil
BGR	=	German abbreviation for Federal Institute for the Geosciences and Natural Resources
CAPEX	=	Capital expenditures (pre-production)
CAPP	=	Canadian Association of Petroleum Producer
CLOS	=	Cold Lake Oil Sands
CNRL	=	Canadian Natural Resources Limited
CSOR	=	Cumulative Steam-Oil Ratio
D	=	Darcy
ESP	=	Electric Submersible Pumps
F	=	produceability factor - kh/μ (mD-m/cP)
FPO	=	Faja Petrolifera del Orinoco
GHG	=	Greenhouse Gases
H	=	Reservoir thickness
HC	=	Hydrocarbons
HO	=	Heavy Oil

HOB	=	Heavy Oil Belt
KBM	=	Karazhanbas
k_v, k_h	=	permeability in Darcies, vertical, horizontal
MtCO ₂ e	=	Million tones CO ₂ equivalent
NEB	=	National Energy Board of Canada
OOIP	=	Original Oil In Place
OPEX	=	Operating Expenses
PCP	=	Progressive Cavity Pumps
Pr	=	Reservoir pressure
PROS	=	Peace River Oil Sands
PTRC	=	Petroleum Technology Research Centre
PV	=	Pore Volume
RF	=	Recovery Factor (% OOIP recovered)
RFCC	=	Residue Fluid Catalytic Cracking
SARA	=	Saturates, Aromatics, Resin, Asphaltene
SCO	=	Synthetic Crude Oil
SEC	=	U.S. Securities and Exchange Commission
SM	=	Surface Mining
SMR	=	Steam Methane Reforming
S_o	=	Oil saturation degree (100%)
SPE	=	Society of Petroleum Engineers
S_w	=	Water Saturation (%)

Tb	=	Trillion barrels of oil
Tr	=	Reservoir temperature
USGS	=	Unites States Geological Survey
UTF	=	Underground Test Facility
VO	=	Viscous Oil
WOS	=	Wabiskaw Oil Sands
WPC	=	World Petroleum Council
XHO	=	Extra Heavy Oil
z	=	Depth in meters
Δ	=	difference or change in, as in Δp , $\Delta \rho$
σ	=	Stress (kPa, MPa)

Chapter 3

New Correlations for Prediction of Steam to Oil Ratio and Recovery Factor during Steamflooding in Naturally Fractured Carbonate Heavy Oil Reservoirs

3.1 Abstract

Evaluation of NFCRs for thermal production technologies through pilot tests with numerical and analytical modeling is expensive, difficult, and personnel intensive. Models or correlations have not yet been proposed to predict Cumulative Steam to Oil Ratio (*CSOR*) and Recovery Factor (*RF*) during steamflooding in NFCRs. To address this lacuna, new statistical correlations were developed using multivariable regression analysis for quick estimation of *CSOR* and *RF* in NFCRs in this chapter. The proposed correlations include vital parameters such as *in situ* fluid and reservoir properties. The data used are taken from experimental studies and also field trials of vertical well steamflooding pilots in viscous oil NFCRs reported in the literature. The correlations exhibit an error percentage of < 10% for the worst cases and contain fewer empirical constants compared with existing correlations for oil sands. Investigation of interactions between the parameters indicates that initial oil saturation and oil viscosity are the most important predictive factors. The proposed correlations were successfully predicted steam/oil ratios and recovery factors in two heavy oil NFCRs from Iran. Results of this study can be used for feasibility assessment of steamflooding in NFCRs.

3.2 Introduction

Consumption of fossil fuels will continue as the primary source of energy in the decades to come. According to the U.S. Energy Information Administration (EIA) in their 2011 International Energy Outlook report, global demand for liquid fossil fuels is expected to grow from 85.7×10^6 b/d [13.6×10^6 m³] in 2008 to 97.6×10^6 b/d [15.5×10^6 m³] in 2020 and

112.2×10^6 b/d [17.8×10^6 m³] in 2035 (EIA, 2011). This is mainly because of a growing world population combined with increasing per capita demand in developing economies such as China and India (EIA, 2011). Development of non-conventional energy resources such as shale gas, shale oil, and viscous oil (VO – including heavy oil, extra heavy oil, and bitumen) will fill the growing gap arising from future declining conventional oil production and the steady growth in demand. It is expected that by 2035, VO will comprise about 17% of the daily world oil production, and this includes VO from NFCRs as well (EIA, 2011). The current contribution of the VO to the world daily oil production is about $9\text{--}10 \times 10^6$ b/d [$1.43\text{--}1.59 \times 10^6$ m³/d], approximately 11% of the total oil production, and this represents a doubling of VO production in about 25 years (EIA, 2011).

The temperature sensitivity of VO viscosity controls the flow rate in all thermal production processes; it is far more important in technical and economic assessment than API gravity. Definitions of heavy oils in the literature are inconsistent, but many suggest that heavy oils be defined as having viscosities > 100 cP and < 10000 cP at reservoir conditions; then, “bitumen” refers to oil having a reservoir viscosity > 10000 cP *in situ*. In this dissertation, VO refers to all crude oil with $\mu > 100$ cP *in situ*, Heavy Oil (HO) refers to crude oil with $100 < \mu < 10000$ cP *in situ*, Extra Heavy Oil (XHO) refers to crude oil with $\mu < 10000$ cP *in situ* but with $\rho > 1.0$ g/cm³, and Bitumen refers to crude oil with $\mu > 10000$ cP *in situ*. A list of the various definitions and terms can be found in Dusseault and Shafiei (2011).

The world endowment of VO in both clastic (consolidated or unconsolidated sandstones) and carbonate rocks (mostly limestone and dolomite) is estimated by the United States Geological Survey (USGS) and others to be in the order of 9000×10^9 [1430×10^9 m³], (Meyer and Dietzman, 1981; Meyer and Duford, 1989; Meyer and Attanasi, 2004; Meyer *et al.*, 2007; Schenk *et al.*, 2009, CAPP, 2009; BGR, 2009; IEA, 2009; Dusseault and Shafiei, 2011) over two times the conventional oil resource of about 4500×10^9 b [715×10^9 m³]. Also, the world’s VO resources in NFCRs are estimated to be $1500\text{--}2200 \times 10^9$ b [$238\text{--}35 \times 10^9$ m³] (Briggs *et al.*, 1988; Shafiei *et al.*, 2007; Dusseault and Shafiei, 2011).

The majority of VO, mainly XHO and bitumen, is found in shallow high porosity sandstones ($\phi > 25\%$) of low cohesive strength, with exceptionally large accumulations existing in Canada and Venezuela (Dusseault, 2001; Dusseault *et al.*, 2008; Dusseault and Shafiei, 2011, 2012). Large VO NFCRs are far less common, of lower porosity (usually $\phi < 18\%$), and may have unfavorable wettability conditions in comparison with VO sandstones. Compared with VO sands, which typically have porosities greater than 25% with more than 75% oil saturation, VO NFCRs are considered as poor reservoirs with less oil per cubic meter, which makes thermal operations inherently less efficient (e.g., higher *CSOR*, lower *RF*, less thermal efficiency). In addition, flow instabilities such as viscous fingering, channeling, capillary blockage and gravity override are intensified in VO NFCRs due to the heterogeneous nature and dual porosity systems (fractures and matrix) characterizing most VO NFCRs.

Almost 100% of the VO production from NFCRs comes from cold production operations in Oman, Iran, Iraq, Kuwait, Saudi Arabia, Turkey, and Mexico (Dusseault, 2001; Dusseault *et al.* 2008; IEA, 2009; Shafiei *et al.*, 2007; Dusseault and Shafiei, 2012). The VO in most of these reservoirs is mobile under reservoir conditions. Productive VO NFCRs are characterized by low matrix permeability and high fracture permeability, giving high early production which declines rapidly, leading to *RFs* below 3–5% in most cases. Large-scale, early oil flux takes place through the high permeability, low volume fracture system, whereas the matrix-fracture interaction mainly controls the recovery efficiency and maintenance of longer-term smaller-scale production levels. VO production from NFCRs is in its very early days and is presenting major technical and economic challenges to the oil industry. These reservoirs are not yet widely commercialized and progress remains necessary for them to contribute a notable part of the daily worldwide oil production.

Several researchers have investigated important aspects of steamflooding (e.g., production mechanisms, productivity, wettability effects, process properties, feasibility) in homogeneous and heterogeneous porous media through laboratory, analytical modeling and numerical simulations (Chu and Trimble, 1975; Neuman, 1975; Myhill and Stegemeier, 1978; Farouq Ali, 1982; Gomaa, 1980; Yortsos and Gavalas 1981a and b; Neuman, 1985; Chu, 1990;

Torabzadeh *et al.*, 1990; Jensen *et al.*, 1991; Gajdlca *et al.*, 1993; Jones, 1993; Donaldson and Donaldson, 1997; Edmunds and Peterson, 2007; US-OTA, 1978; Ashrafi *et al.*, 2011; van Heel, 2008; Mollaei and Maini 2007a & b; Souraki *et al.*, 2011; Yortsos, 1995; Tang *et al.*, 2011). Most articles focus on steamflooding in unfractured (single porosity) systems. The interactive flux between the matrix block and fractures, and the consequent impact on the performance of steamflooding, are not well addressed in the literature.

Recovery Factor (*RF*) and Cumulative Steam to Oil Ratio (*CSOR*) are two critical economic parameters when evaluating an asset or designing a steamflood; predicting parameters of paramount interest in assessing viability of a thermal operation. Empirical models or correlations have not been yet developed to estimate *CSOR* and *RF* for steamflooding in VO NFCRs. However, various models and correlations are reported for performance prediction and analysis of various steam injection processes for VO production from oil sands and other unconsolidated sandstone VO reservoirs (Davidson *et al.*, 1967; Coats *et al.*, 1974; Chu and Trimble, 1975; Neuman, 1975; Myhill and Stegemeier, 1978; Farouq Ali, 1982; Gomaa, 1980; Yortsos and Gavalas 1981a and b; Neuman, 1985; Chu, 1990; Torabzadeh *et al.*, 1990; Jensen *et al.*, 1991; Gajdlca *et al.*, 1993; Jones, 1993; Donaldson and Donaldson, 1997; Edmunds and Peterson, 2007; Miura *et al.*, 2010). Without modifications to account for the different production characteristics, such correlations or models cannot be used for VO NFCRs. Overall, it is wise to expect higher *CSOR*, lower *RF*, lower thermal efficiency, and lower ultimate profitability for VO NFCRs steam processes compared with typical oil sands or unconsolidated sandstone VO reservoirs.

Herein, two correlations are developed employing multivariate regression for rapid estimation of *CSOR* and *RF* in VO NFCRs during steamflooding. The relationships involve major parameters such as *in situ* fluid and reservoir properties and process conditions (e.g., steam flow rate and quality). Previous modeling and experimental studies with the aid of a statistical method were used to determine the key variables that most strongly affect the *CSOR* and *RF* in homogeneous and fractured reservoirs experiencing steamflooding. The data used are mainly from field pilots and also some experimental test runs of steaming VO

NFCRs. Employing the required production history, the correlations were then examined by statistical approaches such as ANOVA, residual plots, and correlation coefficient calculations. The correlations were also qualitatively compared with the existing correlations reported for oil sands and unconsolidated sandstones. At the end, the new correlations are applied to predict *CSOR* and *RF* for a real VO NFCR. Our results can be used to estimate the technical and economic feasibility of vertical well steamflooding in VO NFCRs.

3.2.1 Steamflooding

Review of worldwide Enhanced Oil Recovery (EOR) surveys published over the last two decades shows that steam injection, including steamflooding and other processes involving steam placement, is the only commercialized viscosity reduction approach. It has been widely successful and broadly used in VO sandstones. Over 70% of VO production worldwide involves steaming, and this dominance will continue into the foreseeable future (Taber and Martin, 1997; Oil & Gas Journal, 1996, 1998, 2004, 2006, 2008, 2010). It should be noted here that all commercially successful thermal operations are currently in oil sands rather than VO NFCRs. Commercial VO thermal operations began with vertical well steamflooding (SF) or steam drive (SD) (Figure 3-1) and their variants in 1952, mainly in California and then Venezuela (de Haan and van Lookeren, 1969; Farouq Ali, 1974). These were generally implemented in thicker zones (> 10 m), and almost always for VOs with $\mu < 5000$ cP, since initial communication between the offset wells is easily achievable only in cases of sufficient mobility (usually, k/μ is higher than 0.1 mD/cP). Continuous steam injection at the base of an interval leads to creation of a slowly advancing and rising steam zone; the heat lowers the viscosity while volumetric sweep processes (Δp) mobilize the fluids, displacing them to the production well. *CSOR* values < 3 for SD, SF, and CSS might be attained in thicker, high quality reservoirs (kh/μ values greater than ~ 0.25 mD.m/cP); however *RF* is likely to be substantially lower than gravity dominated thermal methods because of reservoir heterogeneity and advective instabilities (e.g., fingering, channeling, coning etc.). Low matrix permeability (< 100 mD), low porosity ($< 20\%$), medium to densely fractured reservoirs with fracture permeability ranging from low to very high are the

most common characteristics of VO NFCRs. These, along with depth, form major constraints for steam technology implementation. As a rough estimate, the VO volume in one cubic meter of oil sand (28–32% porosity) is almost twice that of the typical VO carbonate reservoirs (10–20% porosity). Compared to oil sands, steam processes in NFCRs will necessarily evidence higher *CSOR* and lower ultimate *RF* values, less thermal efficiency, and thus be economically less attractive.

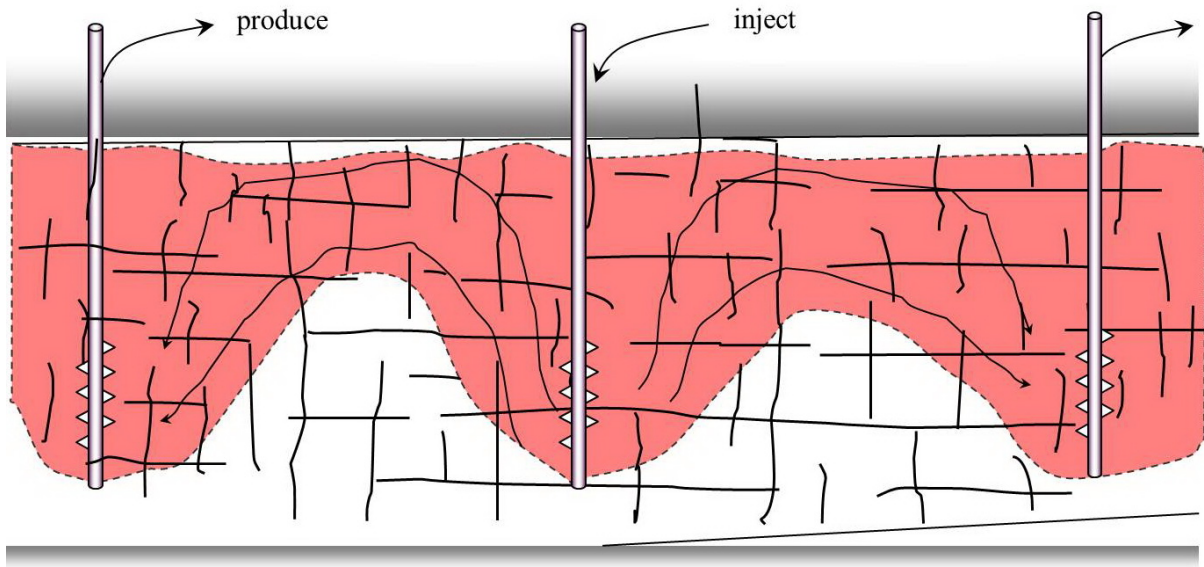


Figure 3-1. Steamflooding in NFCRs (Steamed zone is presented in red).

In several California fields (e.g., Kern River), $RF > 70\%$ and $CSOR = 4.35$ have been reported for steamflooding with remarkably close well spacing (75–125 m) in a low-tax, partially subsidized economic environment (Bursell and Pittman, 1975; Oglesby *et al.*, 1982). Using SF/SD techniques in highly favorable geological conditions (shallow, high k , and high initial oil saturation), high RF was achieved for the Duri Field in Indonesia, despite steam override problems, substantial heat losses, and some steam breakthroughs to surface (Farouq Ali and Meldau, 1979; Farouq Ali, 1982). Of course, all pressure-driven steam injection processes such as SF/SD and CSS experience advective and gravity instabilities (fingering, channelling, override) and therefore suffer from elevated heat losses. Hence, they are

unlikely to be as efficient as gravity-dominated thermal extraction methods, where $\Delta p \sim 0$ conditions leads to diminution of all pressure-viscosity instabilities.

The screening criteria for SF/SD/CSS in oil sands and unconsolidated sandstones are presented in Table 3-1. One may refer to [Dusseault and Shafiei \(2011\)](#), for a brief description and current status of application of steam technologies, and [Boberg \(1988\)](#) and [Butler \(1991\)](#) for production mechanisms involved in steam methods.

Table 3-1: Screening Criteria for SF/SD/CSS in oil sands ([Dusseault, 2012](#)).

Parameter	Steaming Criteria	Comments
Minimum thickness	8–12 m (depending on net pay to gross pay – N/G – ratios)	Continuous net pay (N/G > 0.95) needed for thinner zones
Net pay	8-10 m – > 0.95 15 m – can be 75–80% > 15 m – < 75% (high CSOR)	Shale is expensive to heat. CSS breaks through shales easier than SF/SD because of higher injection pressure
Shale beds	Beds < 2.5 m thick, lateral flow dominated process	CSS has more vertical flow requirement = better k_v needed, comparatively
Porosity	20% (no known cases of commercial success at porosities less than 20%)	At low porosities, there is too much mineral matter to heat, in comparison to oil content
Permeability	> 500–1000 mD	CSS more affected by intact barriers to vertical flow than SD/SF which require lateral flow capacity
Oil viscosity	< 2000–5000 cP for SD/SF 5000 for CSS	SD/SF must have good well-to-well communication, not so for CSS
Steam pressure	< 20 MPa, although in CSS, higher pressures may be needed for	Depth-dependent, CSS in high μ oil uses fracture injection conditions but lower

	fracture injection	pressure during production than SD/SF
<i>CSOR</i> at $k \approx 1$ D (long term)	$> 10000 \text{ cP} > 3$ to 4 $> 500 \text{ cP} > 2$	Dependent on reservoir quality and μ : higher $\mu =$ higher <i>CSOR</i> (slower process)
Recovery Factor (<i>RF</i>)	40–70% (higher <i>CSOR</i> for high <i>RF</i> at the same viscosity)	<i>RF</i> strongly dependent on the full-cycle <i>CSOR</i> that the operator is willing to tolerate, but lower for higher viscosities
Active water	No CSS possible, SF/SD highly unlikely	Active water quenches steam (vacuum created) so significant barriers are needed

3.2.2 Production Mechanisms

Oil production from NFCRs using Δp processes generally occurs in two different stages; first, a pressure gradient within the fracture network acts as a driving force giving early (“flush”) oil production; thereafter, oil is slowly displaced from within the matrix blocks by the pressure gradient from liquid and gas expansion, the pressure gradient enforced between wells, and aided somewhat by gravity drainage forces in the presence of a light (steam) phase. The oil slowly released and displaced from the matrix flows via the fracture network to the production wells. Different driving mechanisms including solution gas liberation and expansion, CO₂ generation, steam distillation, capillary imbibition, and gravity drainage are active during continuous steaming of a VO NFCR [Hernandez and Trevisan \(2007\)](#). The most effective recovery mechanism within the matrix blocks is thermally- and Δp -induced liquid and gas expansion, displacing the oil to the fractures. High temperatures reduce the oil viscosity, permitting these processes, including fracture flow, to take place more quickly.

Two numerical models were developed by [Hernandez and Trevisan \(2007\)](#) to represent the matrix heating process. The first describes the heating of a horizontal cross-section of a matrix block surrounded by a fracture, in which the steam is steadily flowing. The second model is similar to the first, except for the position, which is changed to vertical to incorporate gravity effects arising from phase density differences. Mathematical modeling was conducted for a fractured rock saturated with live oil and the authors noted that steam

distillation is the most effective mechanism due to the fact that it provides complete recovery of methane and also the light and medium components present in the oil phase (these vaporize and therefore are highly mobile and more easily recoverable). Solution gas expansion ($+\Delta T$, $-\Delta p$) sustains the pressure difference between the matrix and the fracture and preferentially displaces the distilled phases. However, the high viscosity of the remnant oil due to the liberation of light compounds restricts the contribution of capillary imbibition mechanisms to the matrix oil recovery.

The solution gases driven off and their expansion, as well as the liquid expansion, dominate the drive energy, and because the matrix block permeability in many NFCRs is less than 100 mD, gravity segregation within the blocks is slow to negligible, although very rapid in the vertical fracture network, maintaining high early Δp between fractures and matrix. Viscosity reduction is not an energy source in itself, although the associated temperature is the dominant agent in gaseous phase exsolution and fluid expansion. Because the gas expansion tends to displace the oil and gravity effects tend to cause the gas to rise, especially in the fractures, oil recovery is somewhat earlier, and gas production somewhat delayed.

CO₂ generation can be responsible for amelioration in the recovery of distilled components from the oil phase and for discrete contributions to the recovery of liquid fractions. More complete discussion of these complex and interacting production mechanisms can be accessed elsewhere, such as [Briggs \(1989\)](#), [Reis \(1990\)](#), [Briggs *et al.* \(1992\)](#), [Prats \(1997\)](#), and [Mollaei and Maini \(2010\)](#).

3.3 CSOR and RF Prediction

Cumulative Steam to Oil Ratio – *CSOR* – is the volume ratio of water injected as steam to oil produced at stock tank conditions. *CSOR* (or its inverse) is used to gauge steamflooding methods' economic success; it is the most common way of expressing thermal efficiency. Recovery Factor (*RF*) is the other important economic parameter, though not in the absence of *CSOR*.

There are various equations available in the literature for performance forecast of a variety of steam processes in oil sands or unconsolidated sandstone VO reservoirs (Davidson *et al.*, 1967; Coats *et al.*, 1974; Chu and Trimble, 1975; Neuman, 1975; Myhill and Stegemeier; 1978; Farouq Ali, 1982; Gomaa, 1980; Yortsos and Gavalas 1981a and b; Neuman, 1985; Chu, 1990; Torabzadeh *et al.*, 1990; Jensen *et al.*, 1991; Gajdlca *et al.*, 1993; Jones, 1993; Donaldson and Donaldson, 1997; Chandra, 2005; Edmunds and Peterson, 2007; Miura et al, 2010).

Chu (1985) proposed the following empirical correlations based on statistical analysis of 28 successful SF/SD operations in oil sands to estimate the *CSOR*:

If $CSOR \leq 5$ (Metric units)

$$CSOR = 18.744 + 0.004767D - 0.16693h - 0.8981K - 0.5915\mu - 14.79S_o - 0.0009767Kh/\mu \quad (3-1)$$

If $CSOR \geq 5$ (Metric units)

$$CSOR = -0.011253 - 0.00009117D + 0.0005180h - 0.07775\phi - 0.007232\mu + 0.00003467Kh/\mu + 0.5120S_o \quad (3-2)$$

In these correlative functions, D is the depth (m), h is the thickness (m), K is the permeability (mD), S_o is the oil saturation, T is the temperature in °C, μ is the viscosity in Pa.s, and ϕ is the porosity as a bulk volume fraction.

The advantage of using such correlations is that they are based on well-known reservoir parameters and do not required simulation or iterative calculations. Chu (1985) recommended using a *CSOR* of 10 as the cut off for economic feasibility of any steaming

operation; of course, this is highly dependent on the price of steam (generally from CH₄ combustion) and the price of oil.

Vogel (1984) developed a model for steamflooding considering the steam over-ride effect (gravity segregation of gases and liquids). He also assumed that the injected steam overlays the formation immediately and then conducts heat upwards (vertically) to the overburden and downward into the reservoir. COSR can be calculated using Vogel's model as follows:

$$\text{COSR} = \frac{62.4h_s \phi S H_t}{\Delta T [h_s (\rho c)_s + 2(K_{h1} \sqrt{t/\pi\alpha_1} + K_{h2} \sqrt{t/\pi\alpha_2})]} \quad (3-3)$$

where h_s is the thickness of steam zone (ft), $(\rho c)_s$ is the volumetric heat capacity of steam zone (Btu/ft³-°F), ΔT is the difference between steam and original reservoir temperature, = $T_s - T_r$ (°F), α_1 and α_2 are the thermal diffusivity values of overburden and oil sand, respectively (ft²/hr), t is the time of steam injection (hr), and K_{h1} and K_{h2} are the thermal conductivity of overburden and oil sand, respectively (Btu/hr-ft-°F). ΔS and H_t are defined as:

$$\Delta S = S_{oi} - S_{ors}, \quad H_t = \bar{X}_t H_{WV} + H_{WS} - H_{Wr} \quad (3-4)$$

Here, S_{oi} is the initial oil saturation prior to steamflood (fraction), S_{ors} is the average steam zone oil saturation at breakthrough (fraction), and H_t is the total energy injected (Btu/lb), H_{WV} is the latent heat of vaporization of water at downhole injection pressure and temperature (Btu/lb), H_{WS} is the enthalpy of liquid water at downhole injection pressure and temperature, Btu/lb, and H_{Wr} is the enthalpy of liquid water at original reservoir conditions, Btu/lb, and \bar{X}_t is the average downhole steam quality during injection (lb/lb).

Boberg (1988) proposed the following equation using Marx-Langenheim's model for estimation of COSR during steamflooding based on thermal efficiency calculations:

$$\text{COSR} = \frac{62.4 \phi h E_h [(\bar{X}_i H_{WV} (S_{oi} - S_{ors}))]}{B_o h_t (T_s - T_r) (\rho c)_{R+F}} \quad (3-5)$$

where T_s and T_r are the steam temperature and reservoir temperature ($^{\circ}\text{F}$), B_o is the oil content of the reservoir, h_t is the reservoir net pay thickness (ft), and E_h is the thermal efficiency,

Butler (1991) introduced the following relationship to predict COSR of steamflooding in oil sands. He employed thermal efficiency computations for constant displacement rate steam drive, relating the cumulative displaced oil ($\phi \Delta S_o h A$) to the cumulative injected heat into the reservoir:

$$\text{COSR} = \frac{H_s \phi (S_o - S_{or})}{\rho_1 C_1 (T_s - T_r)} \left(\frac{1}{1 + \frac{8}{3} \left(\frac{K_2}{\rho_1 C_1 h} \sqrt{t / \pi \alpha_2} \right)} \right) \quad (3-6)$$

Here, H_s is the enthalpy of steam (Btu/lb), α is the thermal diffusivity (ft^2/d), and ρC is the volumetric heat capacity of the steamed reservoir ($\text{Btu}/\text{ft}^3\text{-}^{\circ}\text{F}$).

3.4 Data collection

Only very few steamflooding pilot operations are reported in the literature from France, Italy, Congo, Turkey, USA, Kuwait and Saudi Arabia (Sahuquet and Ferrier; 1982; Nakamura *et al.*, 1995; Ono, 1997; Couderc *et al.*, 1990; Snell and Close, 1999; Snell *et al.*, 2000;

Dehghani and Ehrlich, 2001; Barge *et al.*, 2009; Brown *et al.*, 2011; Hoadley *et al.*, 2011; Meddaugh *et al.*, 2011; Osterloh *et al.*, 2011; Gross *et al.*, 2011; Olsen *et al.*, 2011). Cyclic steam stimulation also has been applied to VO NFCRs, and public data are available only from cases in Canada, China, Egypt, and Syria (Joly *et al.*, 1988; Karaoguz *et al.*, 1989; Issever *et al.*, 1993; Gauchet and Corre, 1998; Smith *et al.*, 2002; Bagci *et al.* 2010; Spadini, 2008; Zhongchun *et al.*, 2012). The first part of the data used in this study is from field trials of steamflooding in VO NFCRs reported in public domain.

In this section, the SF field pilots used in this study is described in a brief way, in chronological order, and the important parameters used for the purpose of this study are summarized in Table 3-2, as well

The Lacq Superieur is a conventional NFCR oil field which is located in the Pyrenees Mountains in SW France. The oil is occurred in heterogeneous and fractured calcareous or dolomitic formations with OOIP of 125×10^6 b [20×10^6 tons] and the production was began since 1950. The oil reservoir is the Lower Senonian limestone of the Upper Cretaceous age. The Lacq Superieur structure is an anticline with a NW/SE. The reservoir depth ranges from 600 to 700 m and its thickness is 120 m. The reservoir is highly heterogeneous. The central part is highly fractured, karstic with a matrix porosity of 0.10 to 0.15 and very low matrix permeability (~ 1 mD). The NW and SE parts of the field are composed of calcareous rocks with porosity of 0.20 and permeability of 1 to 10 mD. The density and viscosity of the oil is 0.893 Kg/m^3 and 17 cP at 60°C or 140°F , respectively. The formation volume factor and the reservoir pressure was 1.04 and 870 psi (6 MPa), respectively (Sahuquet and Ferrier, 1982).

In 1975, after 25 years of production the *RF* reached 17% of the OOIP. Then, to achieve a higher *RF*, the first SD pilot in a VO NFCR was commenced in 1977. However, at the same time, the bitumen saturated Grosmont in Alberta, Canada, was under single well cyclic steam stimulation piloting. The reservoir was carbonated, dolomitized, and highly fractured in the pilot zone. The pilot area is characterized by a fracture permeability of 5 to 10 D, average porosity of 0.5, average matrix permeability of 1 mD, and the water saturation at the start of the pilot for the matrix and the fracture network was 0.6 and 1 PV, respectively. The pilot

pattern was 35 acres or $141 \times 10^3 \text{ m}^2$ with an irregular configuration composed of 6 old producing wells and the injection well was specially drilled for this project, only. A stable steam injection rate of 176 ton/day was maintained since the pilot began in October 1977. VO production increased very early (high early production from the fracture network) and the COSR was about 0.2 or *CSOR* of 5 in 1982. An increase in CO_2 content was observed in several wells during the SD pilot. By the end of June 1980 162000 tons of steam (equivalent water) was injected into the pilot area. Reservoir pressure and temperature and oil production was monitored during the steam drive pilot and the reservoir fluids were sampled and tested, as well. Only 90 days after start of the SD, an increase in oil production was observed in the production wells followed with a peak production ($\sim 150 \text{ b/d}$) in the mid-1979 and then started to decline. No bottom-hole temperature changes were observed during the first 2 years of the steam injection. In mid-1979, a small temperature increase (5°C for 6 month) was recorded in one well. Also, no change in reservoir pressure was observed. By the end of June 1980, the incremental oil production reached 176×10^3 ($28 \times 10^3 \text{ m}^3$) b and the amount of steam injected was 162×10^3 tons. This implies that the incremental COSR was about 0.19 (*CSOR* of ~ 5.2). Considering the highly heterogeneous nature of the reservoir in the pilot area such *CSOR* implies a relatively good thermal efficiency (Sahuquet and Ferrier, 1982). After examining different steam drive patterns in the field, using a horizontal well with high pressure steam injection strategy was adopted in the Lacq Superieur oil field for the relatively heterogeneous parts of the reservoir characterized with very low permeability. After few months of steam injection an increase up to five times was observed in the production wells (Sahuquet and Ferrier, 1982).

The Ikiztepe HO field is one of the world deepest HO fields located in SE Turkey. The Sinan vuggy and fracture limestone formation of tertiary-cretaceous is the reservoir rock at depth 1350 m with an OOIP of 127×10^6 b of HO with viscosity of 936 cP under reservoir condition (120°F and 1841 psi). The average porosity and matrix permeability of the reservoir is 0.15-0.30 and 50-400 mD. The reservoir thickness at the pilot zone is 14-17 m with the start water saturation of 0.12-0.30. Cumulative cold production was led to

production of 88×10^6 STB from 1972 to 1982 when the *RF* of about 1% was reached and then the field was deemed economic and shut down. Steam processes commenced in April 1993 with three cycles of steaming (steam stimulation) and then converted to continuous steam injection (steamflooding) in October 1993 and continued till February 1995 with steam injection rates of 210 to 600 CWEBD with average steam quality of 80% and cumulative HO production of 26180 b. The cumulative steam injection was 81394 CWEB which means a *CSOR* of 3.1 which is a favorable number indicating a successful pilot in terms of thermal efficiency in a very deep HO carbonate reservoir. Despite of this success in terms of *CSOR*, occurrence of several operations issues during the pilot operation was reported. The steam quality was decreased drastically (down to 65%) until it was reached the target zone and maintaining a high steam injection rates was necessary causing conversion of the steamflood to hot water injection by exceeding the critical pressure of steam. The peak BHT was recorded around 500°C (Nakamura *et al.* 1995; and Ono, 1997). This operation remains the deepest steamflood ever tried, to date. Such HO reservoirs are typical deep HO reservoirs reported in the Middle East. Application of steam processes to such deep reservoirs is a challenging issue.

The Emeraude field is a shallow (200-500 m deep) HONFCR located in the offshore Congo on the West African coast. The *in situ* viscosity of the HO is 100 cP. The HO field is composed of two reservoirs of Senonian age (R1 and R2) which contain most of the OOIP of estimated 5×10^9 b with thickness of 50 and 48 m, respectively. The reservoir lithology is a succession of siltstones and highly fractured low matrix permeability limestone. The siltstones range from unconsolidated silts to argillaceous cemented limestones with permeability ranging from 0.1 to 50 mD. Fracture permeability is estimated > 1000 mD. 14 years of cold HO production in the period of 1972 to 1986 has led to a cumulative oil production of 152×10^6 b [24.18×10^6 m³] which is about 3% of the OOIP. After failed attempts for HO recovery through waterflooding, a steamflood pilot was designed and executed in both R1 and R2 HO reservoirs in 1983. Three years of steam injection has led to increase in HO production rate and improved *RF* with a *CSOR* of 3.3 which shows

a reasonable thermal efficiency. In total, 100500 m³ of steam was injected in the R1 from June 1985 through end of April 1988. HO production from R1 and R2 increased from 30 m³/d to 200 m³/d and 10 m³/d to 45 m³/d after steamflooding, respectively. After 5 to 6 month from steam injection, the BHT of 100°C was recorded in one well. Generation of CO₂ was also reported in this field as result of steam injection. The cumulative HO production from the pilot project (2 producers only) reached 264×10³ b [42×10³ m³] which represents a CSOR of 3.3 for the pilot project (Couderc *et al.*, 1990).

The Yates oil field is a light oil highly fractured NFCR in the Permian Basin of West Texas with *in situ* oil viscosity of 6 cP at 82°F and reservoir depth of 457 m. The reservoir rock is the San Andres dolomite with average porosity of 0.15-0.17 and matrix permeability of 100-170 mD. Flow in the reservoir is dominated by fractures originated from tectonic activities. The average fracture porosity is 0.02 with permeability of > 1000 mD. A steam pilot was commenced in this field in December 1998. This project is a sort of TA-GOGD aimed at lowering the oil viscosity rather than displacing it like a steam drive. In this pilot operation, steam is injected into the fractured secondary gas cap to heat the residual oil to reduce its viscosity and accelerate the gravity drainage in the dolomite matrix toward highly conductive fractures. The mobilized oil drains vertically to the oil bank and produced by the offset producers. Injection of steam injection started in December 28, 1998, at an injection rate of ~ 7000 BSPD. Oil production and changes in the reservoir pressure and temperature was heavily monitored during the pilot. Over an injection period of about five month, cumulative steam injection reached 910000 b with a cumulative oil production of 103250 b from three production wells. A CSOR of 8.8 can be calculated for this project. In one of the producers, oil production rate was increased by 100% after steam injection but in the other two producers increase in the oil production rate was not substantial. From the point of view of thermal efficiency, the Yates steam pilot operation seems marginal (Snell and Close, 1999; Snell *et al.*, 2000; Dehghani and Ehrlich, 1998 and 2001).

Wafra HO carbonate field is located in the neutral partitioned zone between the Saudi Arabia and Kuwait off-shore Persian Gulf. 1st and 2nd Eocene age dolomite reservoirs contain the

HO in this field. The 1st Eocene and the 2nd Eocene HO reservoirs are 304-426 m and 580-670 m deep. The average thickness of the 1st Eocene HO reservoir is ~ 228 m with an average porosity of 0.37 and an average core permeability of 250 mD. Core permeability measurements range up to 3000 mD. The *in situ* HO viscosity in the 1st Eocene reservoir is 80 cP and the reservoir temperature is 97°F (36°C). The 1st Eocene had a cumulative production of > 320×10⁶ STBO since the start of cold primary production in March 1956 which is about 3.5% of the OOIP. The daily production in 2009 was about 24700 STBD from over 200 wells. The estimated OOIP in the 1st Eocene HO field is 9×10⁹ b (Barge *et al.*, 2009; Brown *et al.*, 2011; Hoadley *et al.*, 2011; Meddaugh *et al.*, 2011; Osterloh *et al.*, 2011).

The 2nd Wafra Eocene HO dolomite reservoir has also led to a low *RF* from primary cold production due to severe reservoir heterogeneity and HO with viscosities ranging from 30 to 250 cP *in situ*. Two separate zones with oil accumulations were reported in the Wafra 2nd Eocene HO reservoir: the Main Area and the Southeast Area. Primary cold production produced about 8% of the OOIP in this reservoir till 2008. The OOIP is estimated at 7×10⁹ b. A 7 spot steamflooding pattern is currently underway in the Wafra 2nd Eocene dolomite HO reservoir. A comprehensive monitoring program was also designed. The pilot plan described here belongs to the Main Area (Gross *et al.*, 2011). Steamflooding is currently underway and no additional results are reported, to date.

In the Wafra, 1st Eocene dolomite HO reservoir, a single five-spot pattern steamflood (4 injectors, 1 producer, and 1 monitoring well) was designed and conducted in the Wafra 1st Eocene HO reservoir in 2006. Continuous steam injection started in February 2006 at a rate of ~ 500 CWEB per day, pressure of 600 psig, and a temperature of 489°F (250°C). Maximum injection was reached in August 2006 and peaked at over 1200 CWEB with injection pressures averaging 600 psig maintained for 45 days. By November 2006, steam breakthrough was observed in three out of the four producers. Following the steam breakthrough the steam injection rate was reduced to 200 CWEB per day. In September 2006 temperatures around 400°F (200°C) was measured in the monitoring well. Severe

scaling has led to longer downtimes and compromised the increase in oil production rate due to steamflooding. After two years of steam injection, a continuous thermal zone was formed in the 1st Eocene HO reservoir and steam breakthrough occurred at several of the producers. A comprehensive monitoring program was developed for the pilot, as well. Oil production rates increased from 200 b/d to 600 b/d after steamflooding. During this pilot project, cumulative steam injection and oil production was 1×10^6 STB and 180×10^3 STB, respectively. This means a *CSOR* of 5.55 which sounds like a reasonable thermal efficiency for such a reservoir (Barge *et al.*, 2009; Brown *et al.*, 2011; Hoadley *et al.*, 2011; Meddaugh *et al.*, 2011; Osterloh *et al.*, 2011).

The important parameters for SF field tests are summarized in Table 2. To increase the size of the database, some data from pilot plants executed in highly fractured light oil NFCRs and viscous oil highly fractured sandstone reservoirs were included (Chu, 1985; Dehghani and Ehrlich, 2001). In addition, some experimental data were taken from studies conducted on steamflooding in fractured media available in the literature (US-OTA, 1978; Yortsos, 1995; Mollaei and Maini 2007a&b; van Heel, 2008; Ashrafi *et al.*, 2011; Souraki *et al.*, 2011; Tang *et al.*, 2011). The data available covers a range of fluid and reservoir properties under different operational conditions.

Table 3-2: Characteristics of the successful steamfloods conducted in fractured reservoirs.

Field	Lacq Superieur, SW France (Sahuquet et al., 1982)	Ikiztepe, SE Turkey (Nakamura et al., 1995 ; Ono, 1997)	Emeraude, offshore Congo on the West African coast (Couderc et al., 1990)		Yates Field, Permian Basin of West Texas (Snell and Close, 1999 ; Snell et al., 2000 ; Dehghani and Ehrlich, 2001)
Reservoir	Lacq Superieur	Ikiztepe	R1	R2	San Andres dolomite
Geology	Heterogeneous and fractured calcareous or dolomitic formations	The Sinan vuggy and fractured limestone	A succession of siltstones and highly fractured low matrix permeability limestones		Fractured dolomite
OOIP (1×10^6 b)	125	127	5000		-
Depth (m)	600–700 m	1350	186–249	249–297	457
Thickness (m)	120	100–150	50	48	-
μ (cP)	17 (Medium Heavy oil)	936 (Heavy oil)	100		6
P_{ro} (MPa)	6	12.7	3.1		-
T_{ro} ($^{\circ}$ C)	60	49	31		27
ϕ_m (Fraction)	0.12	0.15–0.30	0.2–0.3		0.15–0.17
K_m (mD)	1	50–400	0.1–50	> 50	100–170
K_f (mD)	5000–10000	1000	> 1000		> 1000
Formation volume factor	1.04	1.056	1.01		-
Steam quality (%)	80	60–80	80		80
CSOR	5.5	3.1	1.45	3.98	8.8
Cumulative steam injected (MCWEB)	970	81	480	700	910
Cumulative oil production (b)	176	26	315	176	103

Table 3-2: Continued

Field	Wafra, Neutral Zone (Saudi Arabia and Kuwait) (<i>Barge et al., 2009; Brown et al., 2011; Hoadley et al., 2011; Meddaugh et al., 2011; Osterloh et al., 2011; Gross et al., 2011</i>)	Naval Petroleum Reserve No.3 (NPR-3), Teapot Dome Field, Wyoming (<i>Olsen et al., 1993</i>)			
Reservoir	2 nd Eocene	1B-South	1C-East	3A	4A
Geology	Dolomite	The Shannon, composed of the Upper and Lower Shannon sandstones			
OOIP (1×10 ⁶ b)	7000	0.748	0.748	1.48	1.46
Depth (m)	580–670	134–146	134–146	134–146	134–146
Thickness (m)	-	7–14	7–14	7–14	7–14
μ (cP)	30–250	10	10	10	10
P _{ro} (MPa)	-	2.34	2.34	2.34	2.34
T _{ro} (°C)	-	18	18	18	18
φ _m (Fraction)	-	0.16–0.2	0.16–0.2	0.16–0.2	0.16–0.2
K _m (mD)	-	18–65	18–65	18–65	18–65
CSOR	5.55	9.42	9.5	13.38	10.9
Cumulative steam injected (MCWEB)	1000	2011	1693	3679	1302
Cumulative oil production (1×10 ³ b)	180	213	176	133.7	119

3.5 Methodology

Different experimental and numerical models were studied to understand the main parameters, their interactions, and trends during steamflooding process. The earlier correlations developed for prediction of *CSOR* in oil sands (e.g., [Chu, 1985](#)) do not take into account all the major parameters and their interrelationships during steamflooding. The most important variables for statistical analysis were determined to be *in situ* viscosity, effective porosity, fracture permeability, matrix permeability, reservoir thickness, depth, steam flow rate, steam quality, and initial oil saturation.

Reliable field data and well-documented field trials are the foundation of developing statistical screening tools. However, a limited number of successful case histories (partially or marginally so in some cases) or field trials exist for steamflooding in VO NFCRs. All the field trials of steamflooding in VO NFCRs available in the public domain were studied to assemble a database, and as many of the critical parameters as could be collected or calculated for the purpose of this study. To enhance the value of statistical analysis, the database was extended to include steamflooding trials in highly (naturally) fractured sandstone viscous oil reservoirs, and some experimental data from similar cases was incorporated, as well. Efforts has been made in order to make sure that all the data collected and used in this study are fully compatible with the physics of vertical well steamflooding in naturally fractured reservoirs.

3.5.1 Multivariable Regression Analysis

In order to examine results of multiple linear regression analysis and determine the dependency of a particular response variable on a particular fluid or/and reservoir property, scatter plots are usually generated ([Montgomery and Runger, 2006](#); [Montgomery, 2008](#)). Such plots can illustrate the absolute effect of each independent variable on the response variables. This statistical analysis first assumes no interactions among the identified predictor variables (e.g., no interaction terms). In this case, the correlation equation would have the following form for “k” regressor variables:

$$y = \beta_0 + \beta_1 x_1 + \beta_2 x_2 + \dots + \beta_k x_k + e \quad (3-7)$$

The parameters “ β_0 to β_k ” are the regression coefficients, x_1, x_2, \dots, x_k are the independent variables or dimensionless numbers, and “ y ” is the actual response variable.

Interaction terms should also be considered in order to predict the behavior of the reservoir under steamflooding. The model relating the regressor to the response, y_i , is as follows:

$$y_i = \beta_0 + \beta_1 x_{i1} + \beta_2 x_{i2} + \dots + \beta_k x_{ik} + e_i \quad i = 1, 2, \dots, n \quad (3-8)$$

For “ n ” observations (field data or/and experimental measurements), this represents a system of “ n ” equations and is expressed in the matrix notation as:

$$y = X\beta + e \quad (3-9)$$

where:

$$y = \begin{bmatrix} y_1 \\ y_2 \\ \vdots \\ y_n \end{bmatrix}, \quad X = \begin{bmatrix} 1 & x_{11} & x_{12} & \cdots & x_{1k} \\ 1 & x_{21} & x_{22} & \cdots & x_{2k} \\ \vdots & \vdots & \vdots & & \vdots \\ 1 & x_{n1} & x_{n2} & \cdots & x_{nk} \end{bmatrix}, \quad \beta = \begin{bmatrix} \beta_0 \\ \beta_1 \\ \vdots \\ \beta_k \end{bmatrix}, \quad \text{and} \quad e = \begin{bmatrix} e_1 \\ e_2 \\ \vdots \\ e_n \end{bmatrix} \quad (3-10)$$

The least square estimate of “ β ” parameter can be found as:

$$\hat{\beta} = (X'X)^{-1} X'y \quad (3-11)$$

The physics of steamflooding in VO NFCRs suggests that a combination of the dependent dimensionless groups has a major contribution to the magnitudes of all the objective functions; thus, regression models should also include terms related to the “effect of interaction between the dependent terms”. An interaction between two dependent variables can be represented by a cross product term in the regression model, such as:

$$y = \beta_o + \beta_1x_1 + \beta_2x_2 + \beta_{12}x_1x_2 + e \quad (3-12)$$

After the required parameters such as *CSOR* were collected from the pilot plant and laboratory studies, they were substituted in the corresponding equations to perform a parametric sensitivity analysis to determine the proper relationships between the target function and key independent variable. The procedure to obtain scatter plots and the predictive equation for *CSOR* is given briefly as follows:

In the corresponding equations to perform a parametric sensitivity analysis in order to determine the proper relationships between target function and key independent variable:

- 1) The *CSOR* values are obtained from the data;
- 2) *CSOR* is plotted separately versus all key parameters with other variables kept constant;
- 3) When all figures for *CSOR* are plotted, a general correlation for *CSOR* versus dependent variables with unknown coefficients of contributing terms can be obtained; and,
- 4) Using Equations 3-7 through 3-10, regression coefficients are calculated (for this we used MATLAB™ and Excel™).

This approach was also used for the other major economic assessment metric – Recovery Factor (*RF*).

Three main validity measures are employed when examining the suitability of multivariate linear regression analysis: analysis of variance (ANOVA) tables, residual analysis, and square of residuals’ analysis.

(a) The ANOVA table includes data from a standard sum of the squares of the variance analysis for regression. The ANOVA contains the data for each of two sources of deviation including regression and residuals (e.g., 1st column in Tables 3-5 and 3-6). It should be noted that the total deviation is defined as the sum of regression and residuals, and the source of variation is because of deviation of each predicted data point from its group mean value (e.g., regression) or the deviation of each predicted value from its observed value (e.g., residuals). The sum of these two sources of variance comprises the total variance. For each of these sources of deviations, four measures of variance (e.g., columns 3–5 in Tables 3-5 and 3-6) could be described as follows: Degrees of freedom (e.g., DF, 2nd column of Tables 3-5 and 3-6): For each particular regression analysis, this is the number of correlation coefficients, “N”, with respect to the number of regressor variables used in each particular model. The higher degree of freedom for each particular model exhibits more reliability of the regression model.

(b) Sum of the Squares (e.g., SS; 3rd column of Tables 3-5 and 3-6): Sum of the squared deviations, which are obtained using observed data and predicted results, is a measure of variance for each particular regression analysis. The total SS is the sum of the squares of the residuals plus the sum of the squares of regression as follows.

Total sum of squares = Regression sum of Squares + Error (or Residual) sum of squares

$$\sum_{i=1}^n (y_i - \bar{y})^2 = \sum_{i=1}^n (\hat{y}_i - \bar{y})^2 + \sum_{i=1}^n (y_i - \hat{y}_i)^2 \quad (3-13)$$

where y_i and \hat{y}_i are real (or observed) data and predicted data, respectively. n is the number of observations or data points. \bar{y} refers to the average of all data points of dependent variable that is expressed by the following equation:

$$\bar{y} = \frac{\sum_{i=1}^n y_i}{n} \quad (3-14)$$

(c) Mean squares (e.g., MS; 4th column of Tables 3-5 and 3-6): This column contains the sum of squares corrected for the degrees of freedom.

(d) F test (e.g., F; 5th column of Tables 3-5 and 3-6): This is a variance-related statistical parameter that compares two models that are different from each other by one or more regressor variables to determine if the more complex model would be a better predictor than the less complex model. If the F-test value is greater than a standard tabulated value, the more complex equation would be considered better. Generally, the significance level is set at 0.05.

The reader is encouraged to see these references for further details on the method used here ([Montgomery and Runger, 2006](#); [Montgomery, 2008](#)).

3.6 Results and Discussion

Predictive tools for screening viscous oil reservoirs for a certain production technology would have value in assessing technical feasibility and the potential performance of the process in a candidate reservoir. Two quick predictive models were developed here to estimate *RF* and *CSOR* in NFCRs that undergo steam flooding for heavy oil recovery.

3.6.1 Regression Analysis

Scatter plots showing the dependency of a particular response variable on a particular fluid or/and reservoir property are presented in Figures 3-2 through 3-11 for *CSOR* and 3-12 to 3-21 for *RF*. It should be noted that Figures 2-7 and 12-17 are obtained for the physical models with the same pattern (in shape and number of fractures) and the same dimensions in most cases. Also, it is clear that all properties for steamflooding processes demonstrated on each figure except those on x and y-axes are the same when investigating effect of an independent variable on target functions. It conveys the message that these figures just present a limited volume of data used in this study in order to point out the important trend in the performance of reservoirs during steamflooding processes according to a comprehensive parametric sensitivity analysis. Based on Figures 3-2 to 3-7, *CSOR* increases with an increase in oil viscosity, steam injection rate, fracture to matrix permeability, and gross to net reservoir thickness. However, high steam quality and high initial oil saturation lead to reduction in *CSOR*, indicating better response to steam injection. In addition, Figures 3-2 to 3-11 for *CSOR* indicate acceptable agreement between the field data and the predictions. It is clear that increase in steam injection rate improves the recovery rate but lowers the *RF* before steam breakthrough in fractured reservoirs (particularly highly fractured ones), as shown in Figure 3-12. Also, if the reservoir contains oil with high viscosity, some areas might be bypassed during steamflooding, resulting in early breakthrough and consequently lower *RF*, as demonstrated in Figure 3-13. The same effect may occur when there are many fractures with high permeability in the reservoir (see Figure 3-14). Although the presence of fractures can lead to an increase in oil production rate, a high density of fractures may have undesired effects on the overall performance of steamflooding, as depicted in Figure 3-14. Figure 3-15 shows that the ratio of the reservoir depth to the reservoir thickness does not have a noticeable impact on *RF* during steamflooding. As expected, steam quality and initial oil saturation have direct impacts on the magnitude of *RF* as increases in these two parameters leads to improvements in the performance of the steamflood (see Figures 3-16 and 3-17). Clearly, steam injection with higher quality steam enters more heat into the reservoir leading

to an increase in temperature. Hence, it causes viscosity reduction that enhances the oil recovery. The figures related to RF again confirm the effectiveness of the statistical approach adopted in this study as a good match was observed between the field data and the results obtained from the correlations.

Figures 3-10 and 3-11 are the residual plots for the $CSOR$ with respect to porosity and a combined interaction component (including formation depth and thickness), respectively. In addition, residual plots for RF versus porosity and “steam quality multiplied by steam injection rate” are presented in Figures 3-20 and 3-21, respectively, as two samples of the analysis of residuals. The residual data spread randomly all along the horizontal axis for these four residual plots. In other words, the proposed linear regressions are valid for $CSOR$ and RF in terms of the particular dependent variables shown on x-axis.

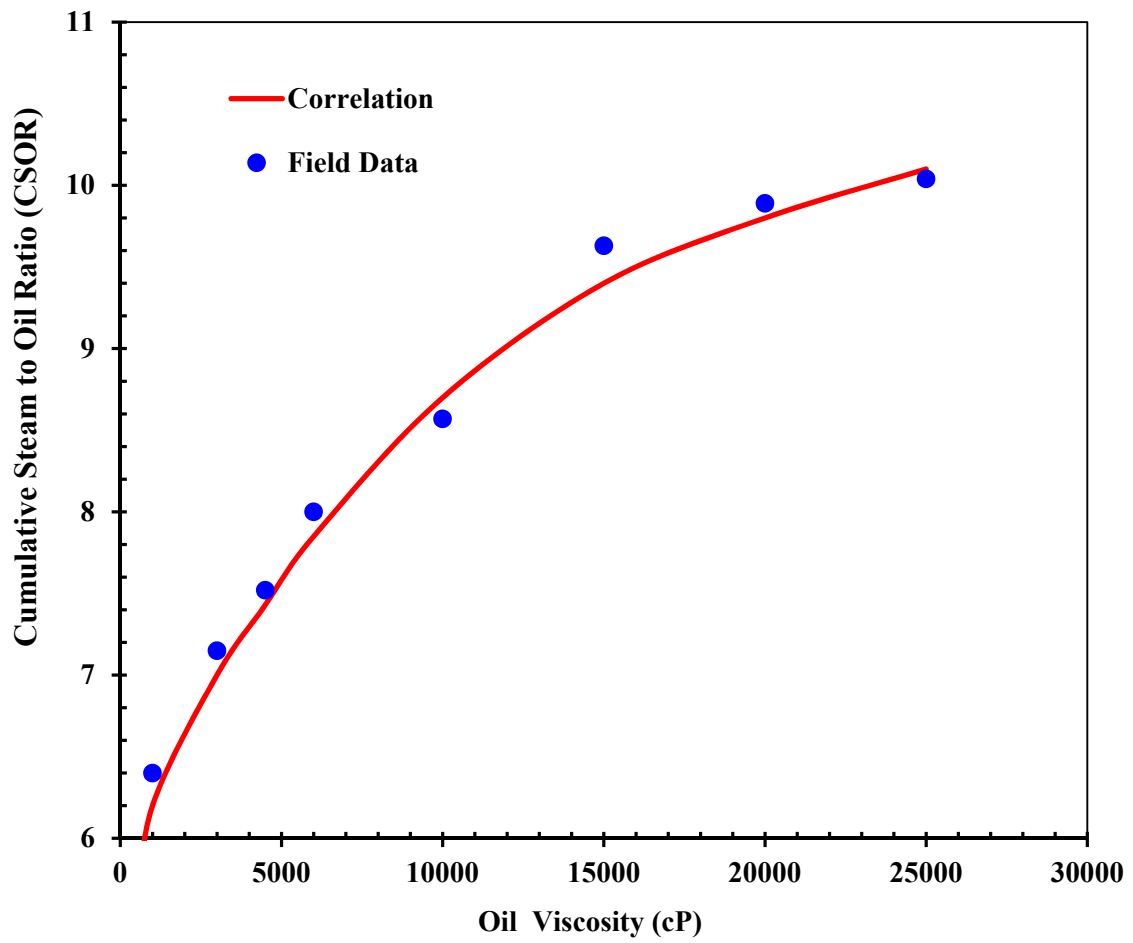


Figure 3-2: CSOR vs. oil viscosity for the database analyzed.

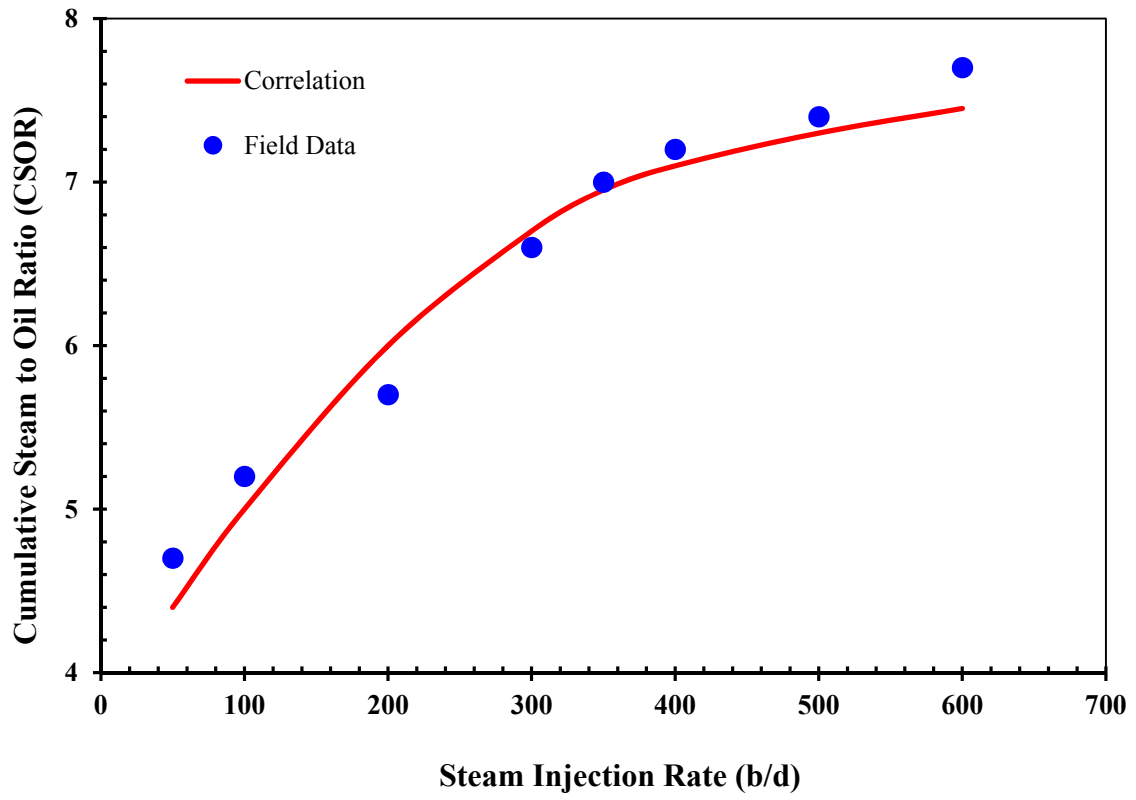


Figure 3-3: *CSOR* vs. steam injection rate for the database analyzed.

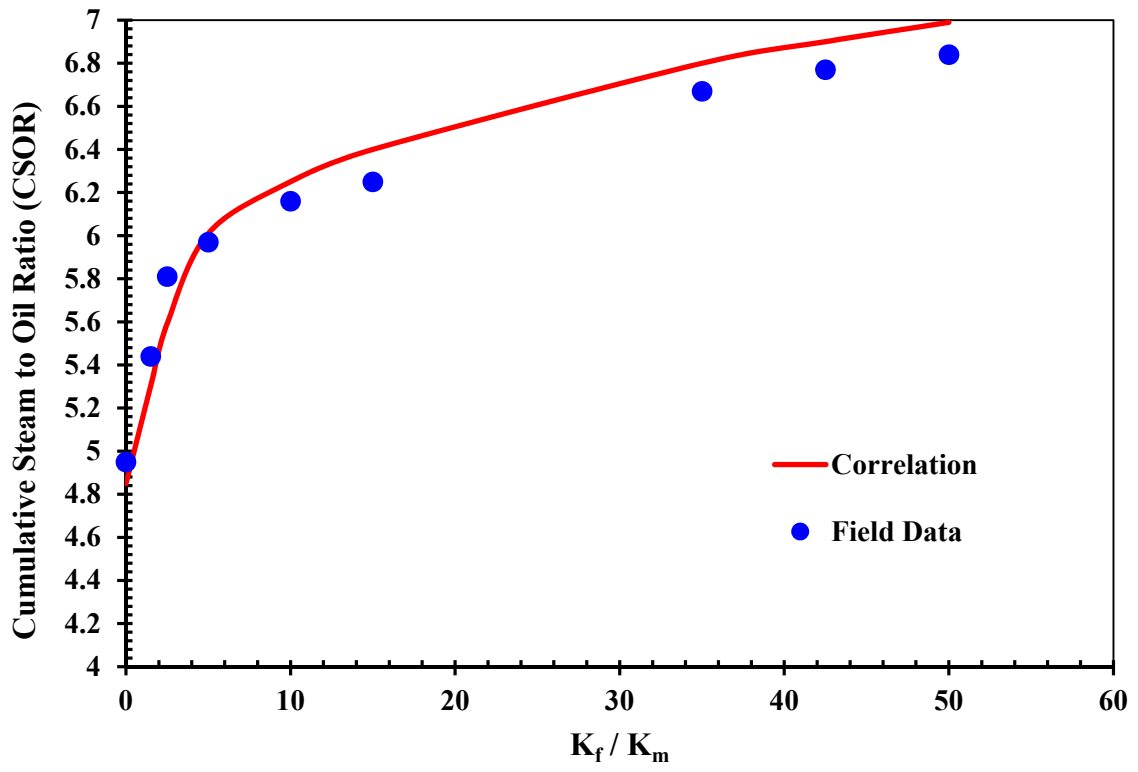


Figure 3-4: CSOR vs. fracture to matrix permeability ratio for the database analyzed.

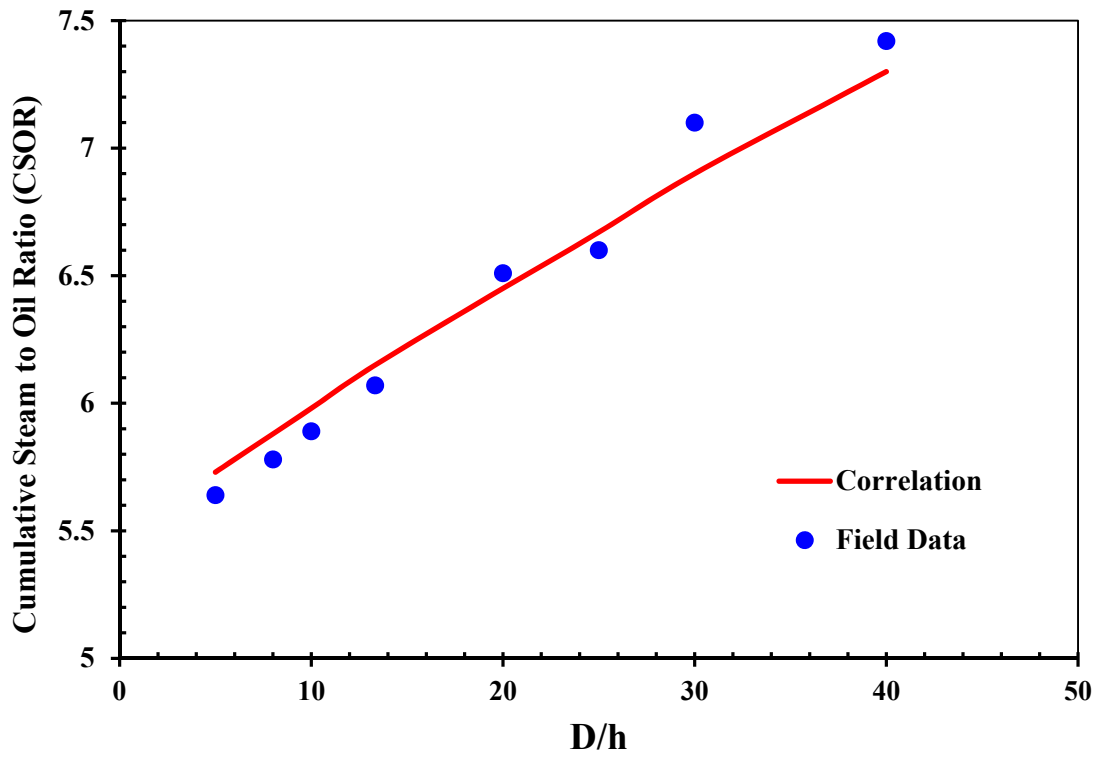


Figure 3-5: *CSOR* vs. gross to net thickness ratio for the database analyzed.

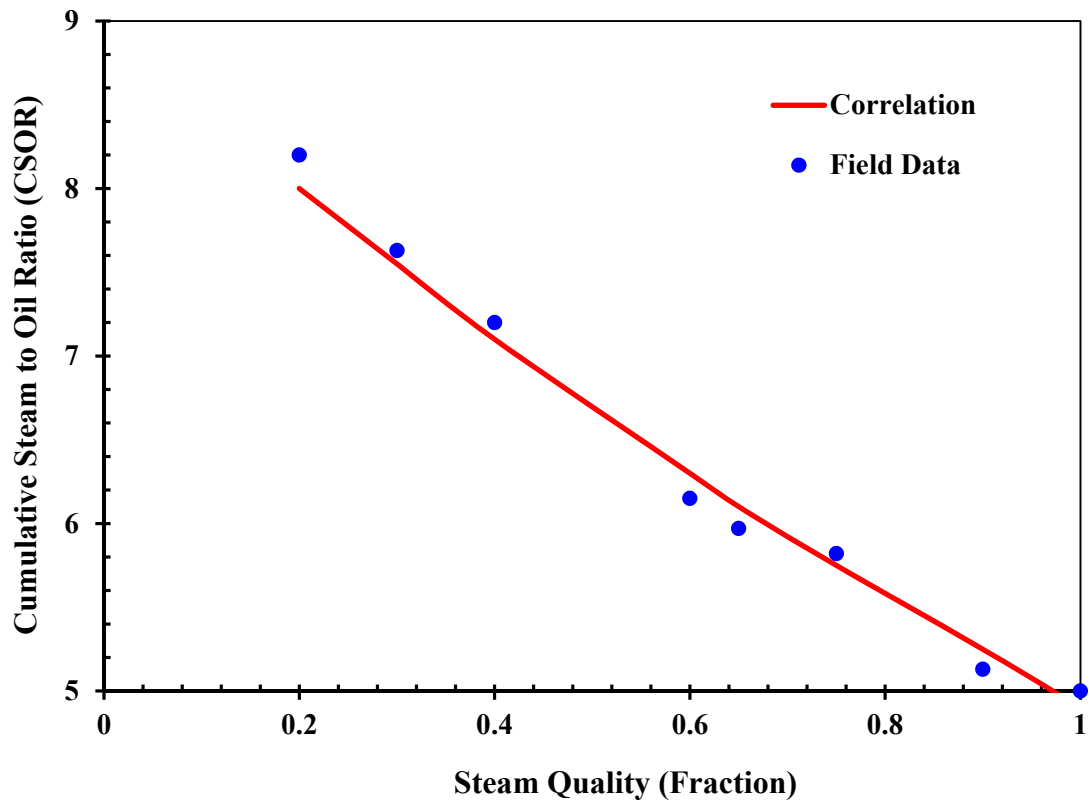


Figure 3-6: CSOR vs. steam quality for the database analyzed.

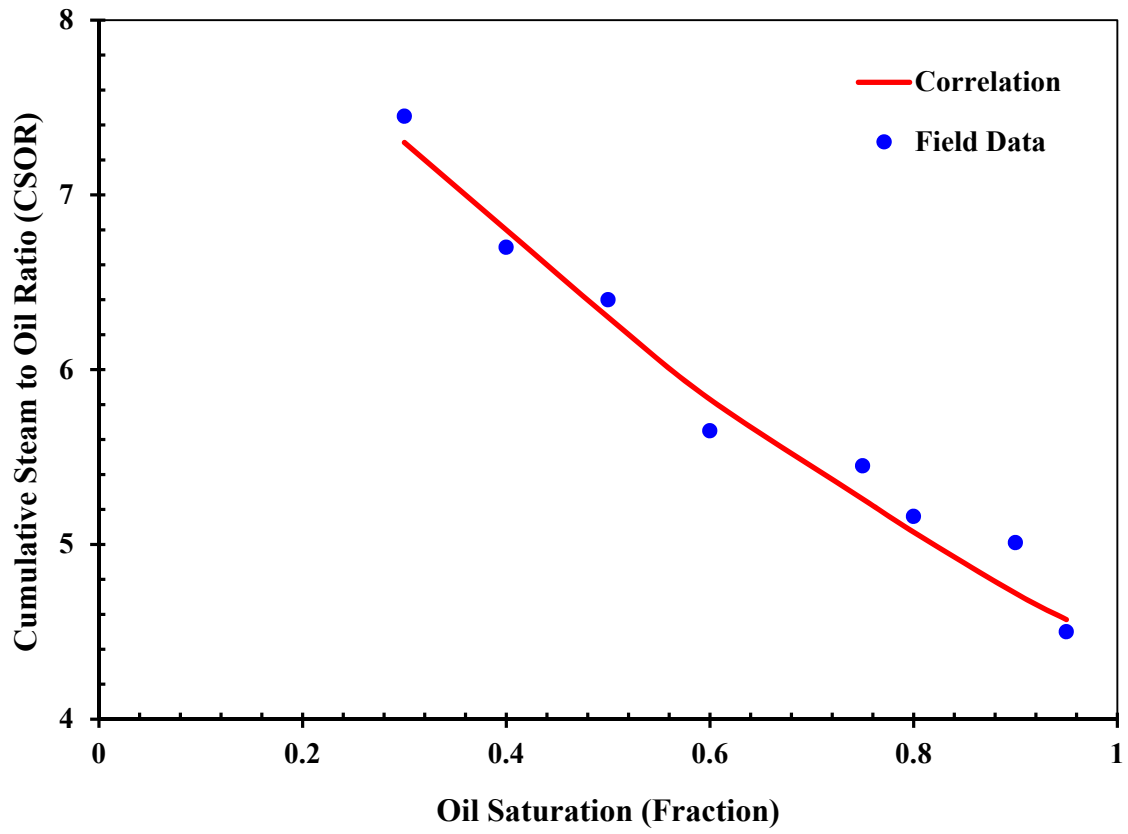


Figure 3-7: *CSOR* vs. oil saturation for the database analyzed.

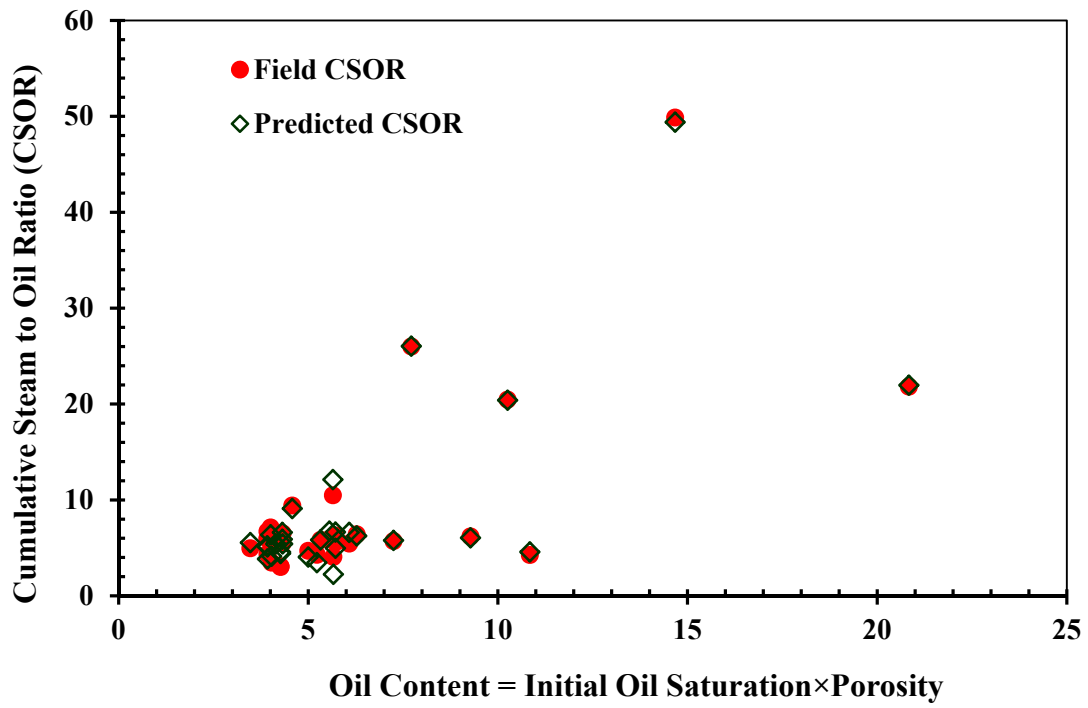


Figure 3-8: CSOR vs. oil content for the database analyzed.

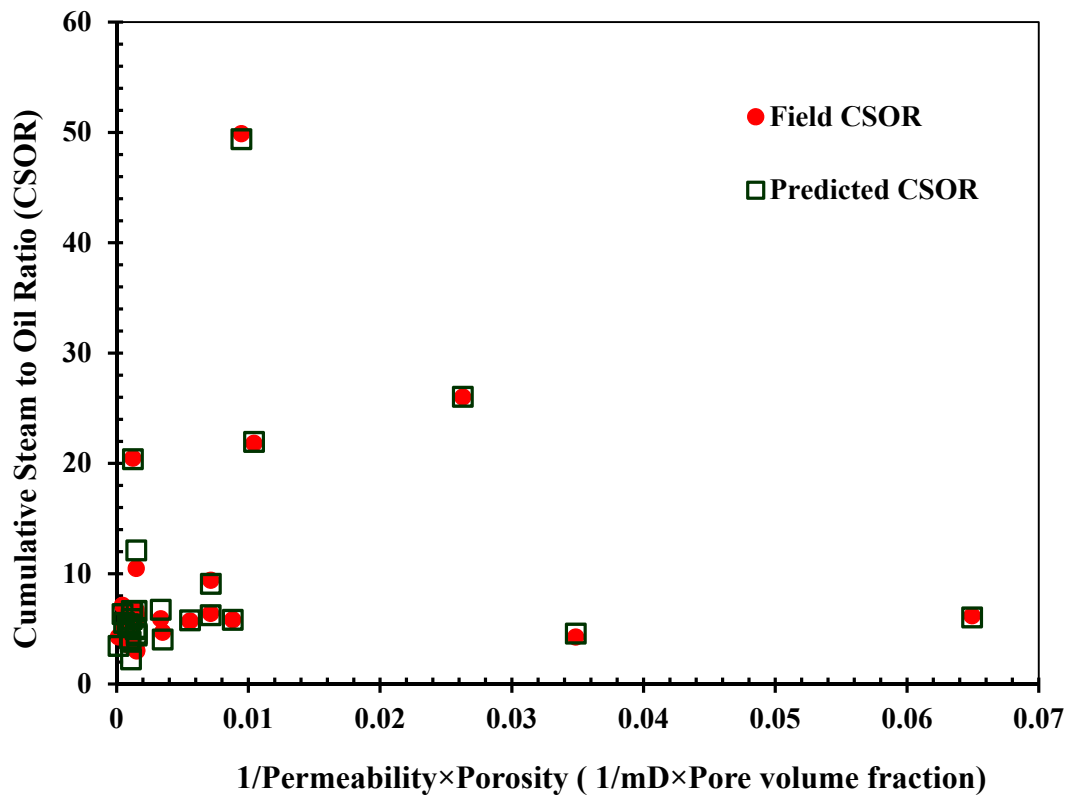


Figure 3-9: CSOR vs. $1/K \times \phi$ for the database analyzed.

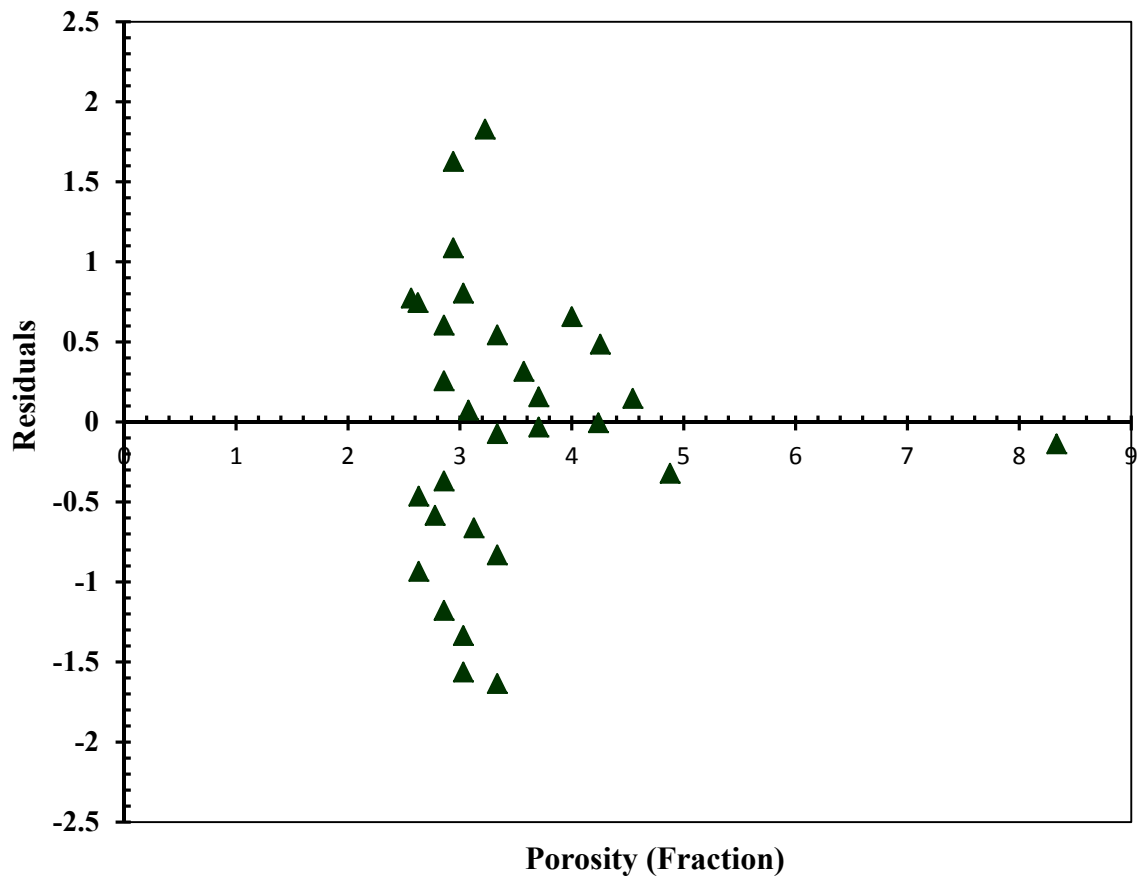


Figure 3-10: Residuals vs. porosity for the database analyzed.

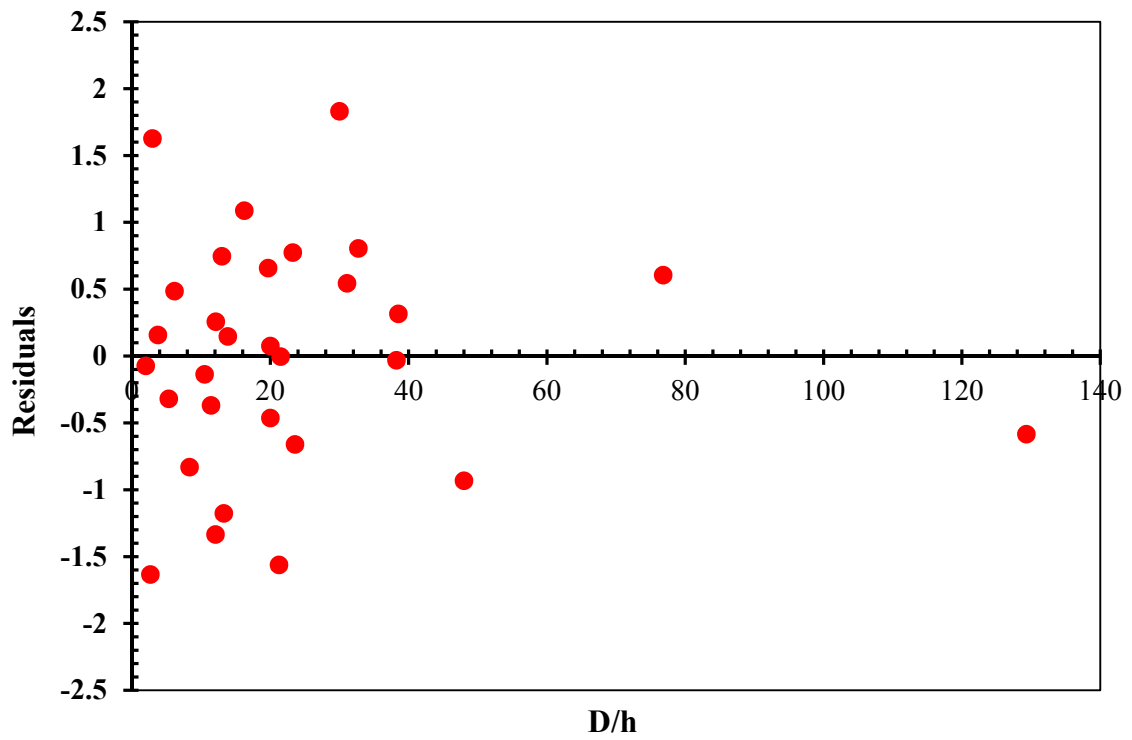


Figure 3-11: Residuals vs. gross to net thickness ratio for the database analyzed.

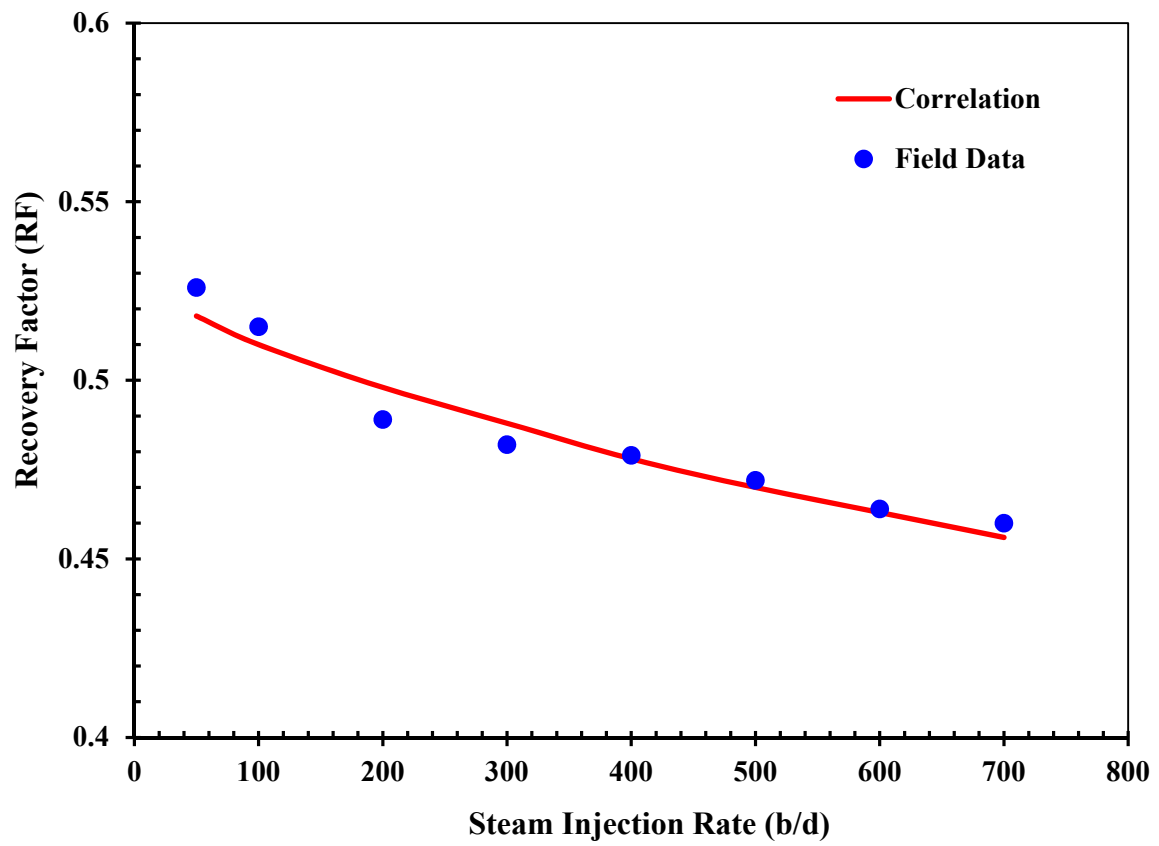


Figure 3-12: *RF* vs. steam flow rate for the database analyzed.

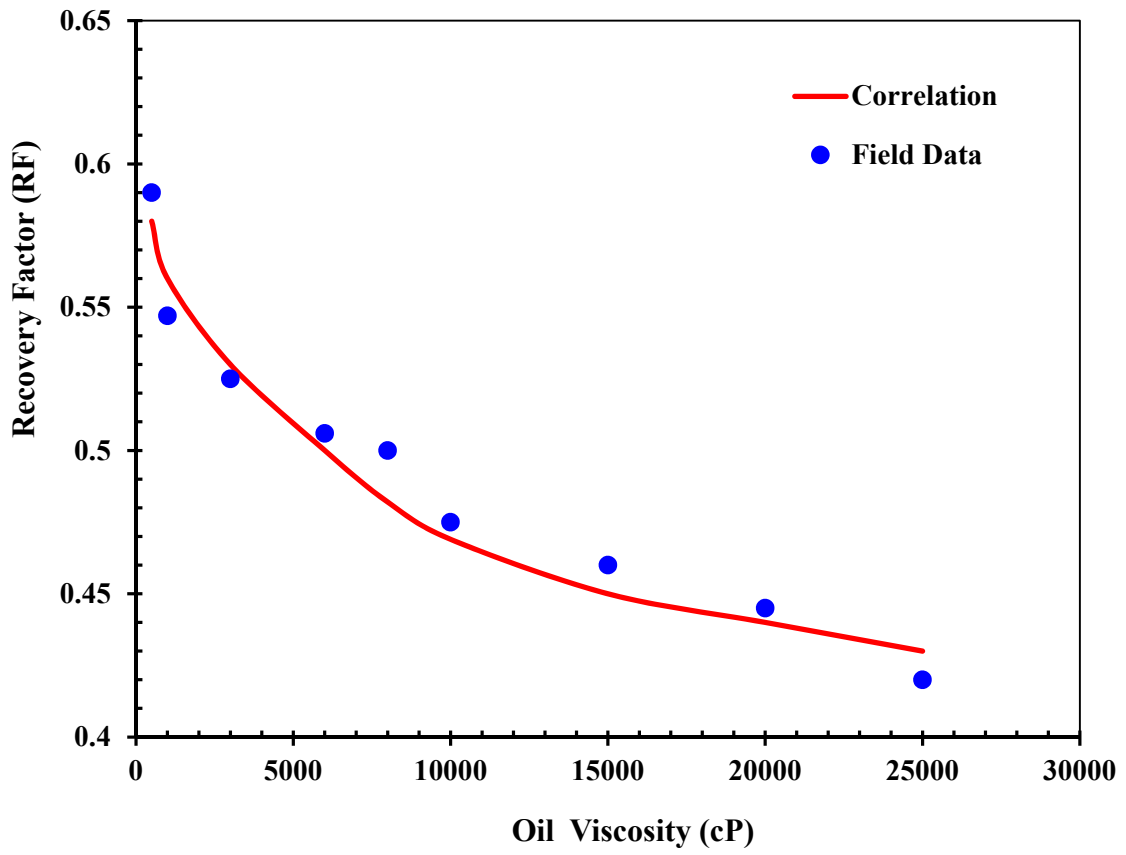


Figure 3-13: *RF* vs. oil viscosity for the database analyzed.

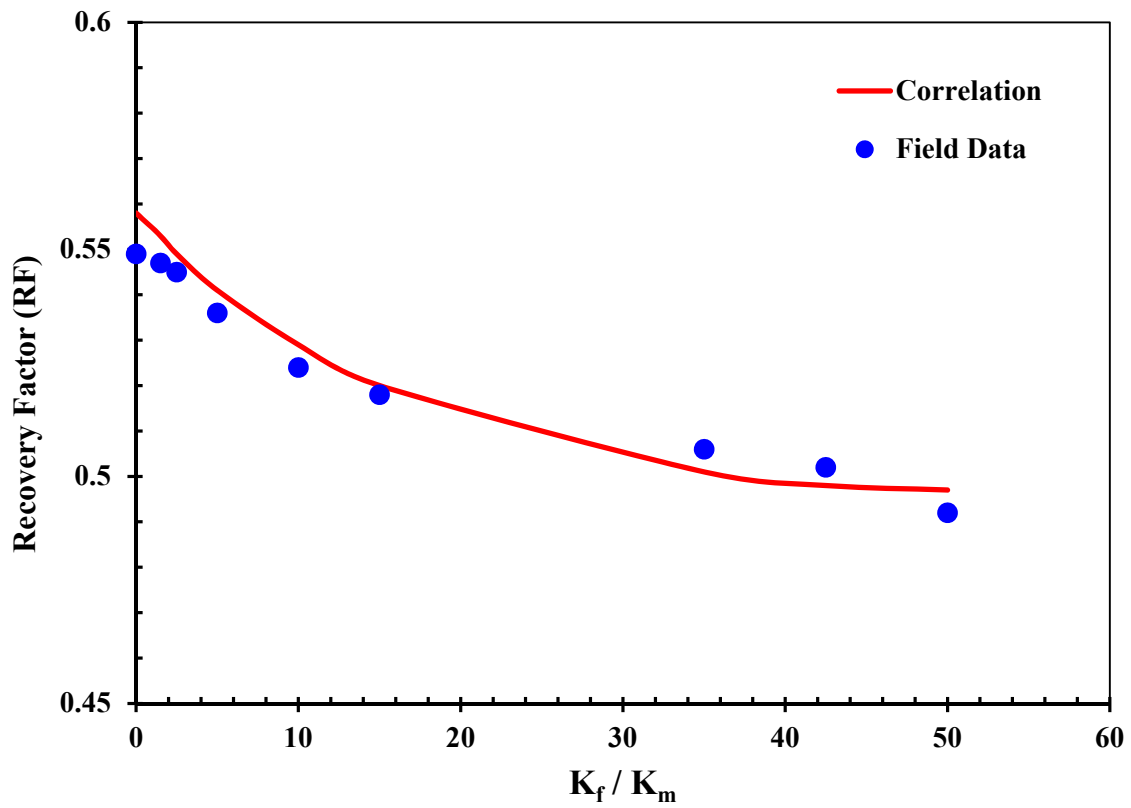


Figure 3-14: RF vs. fracture permeability to matrix permeability ratio for the database analyzed.

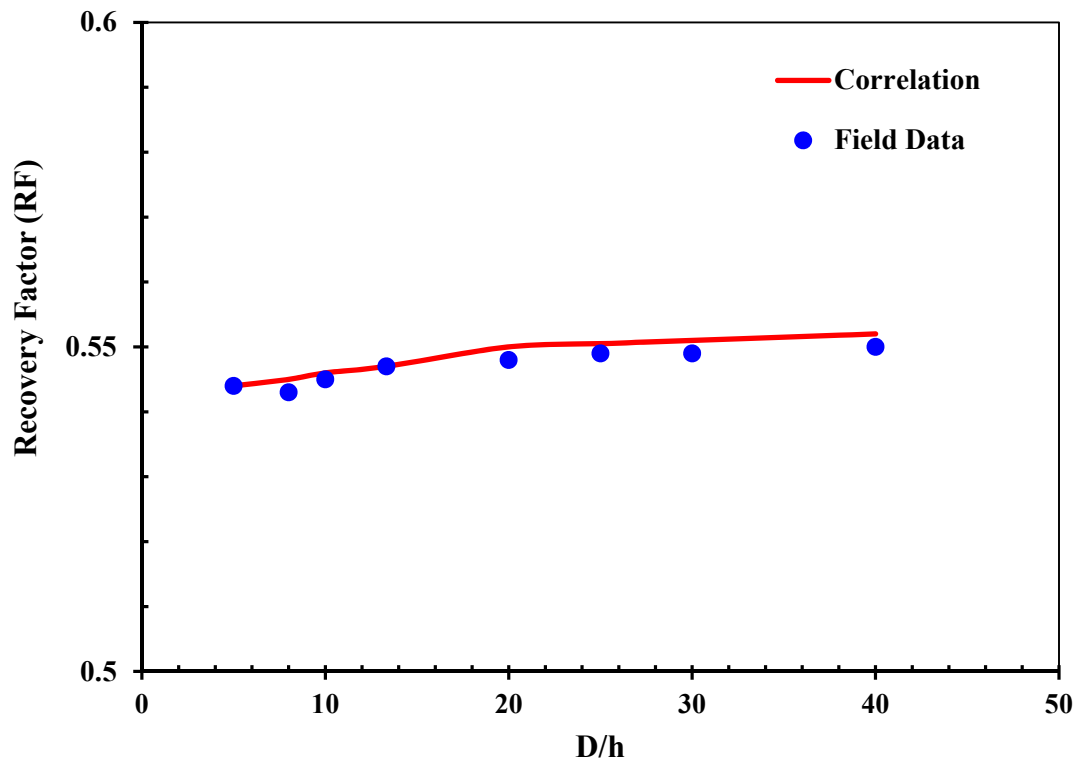


Figure 3-15: RF vs. gross to net thickness ratio for the database analyzed.

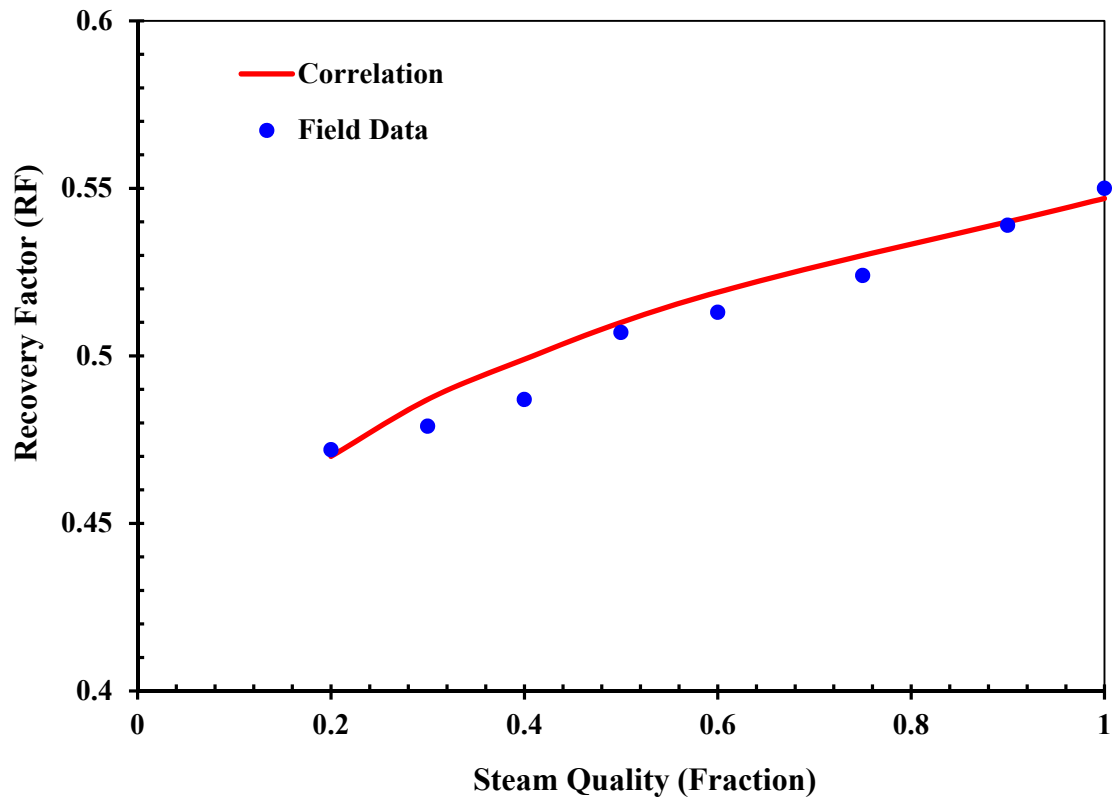


Figure 3-16: RF vs. steam quality for the database analyzed.

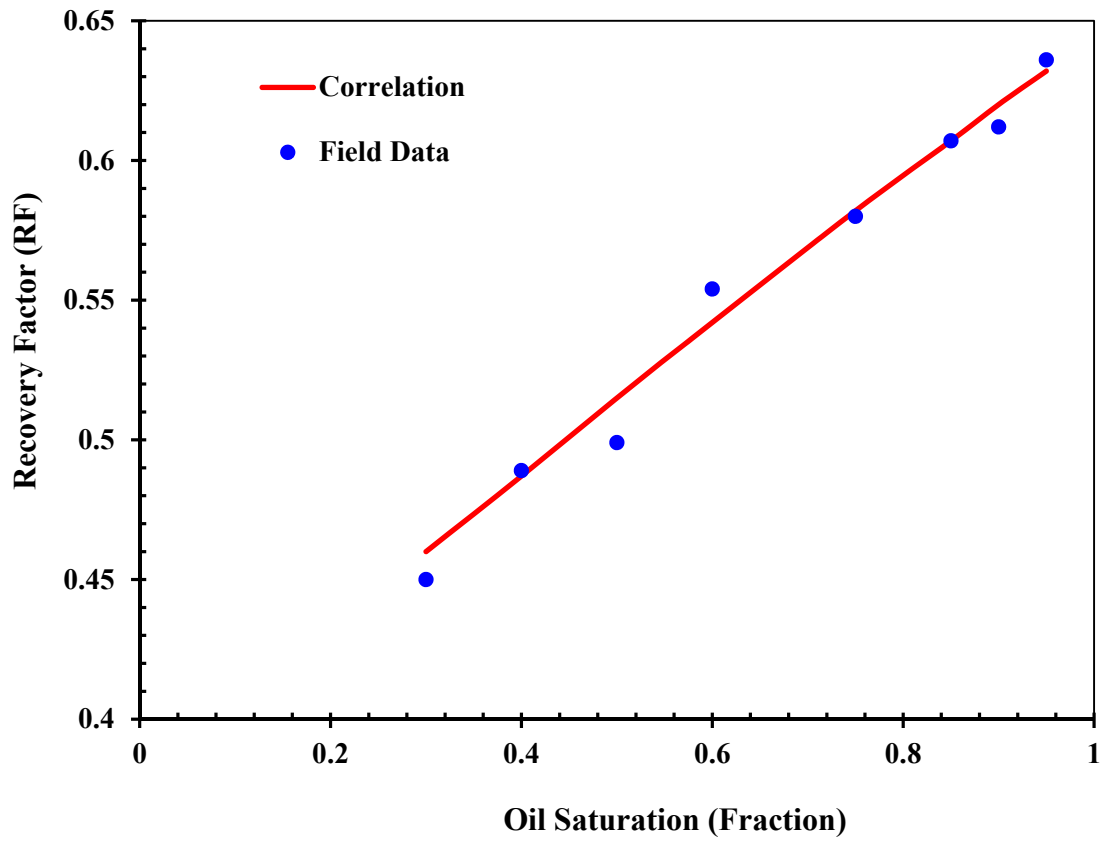
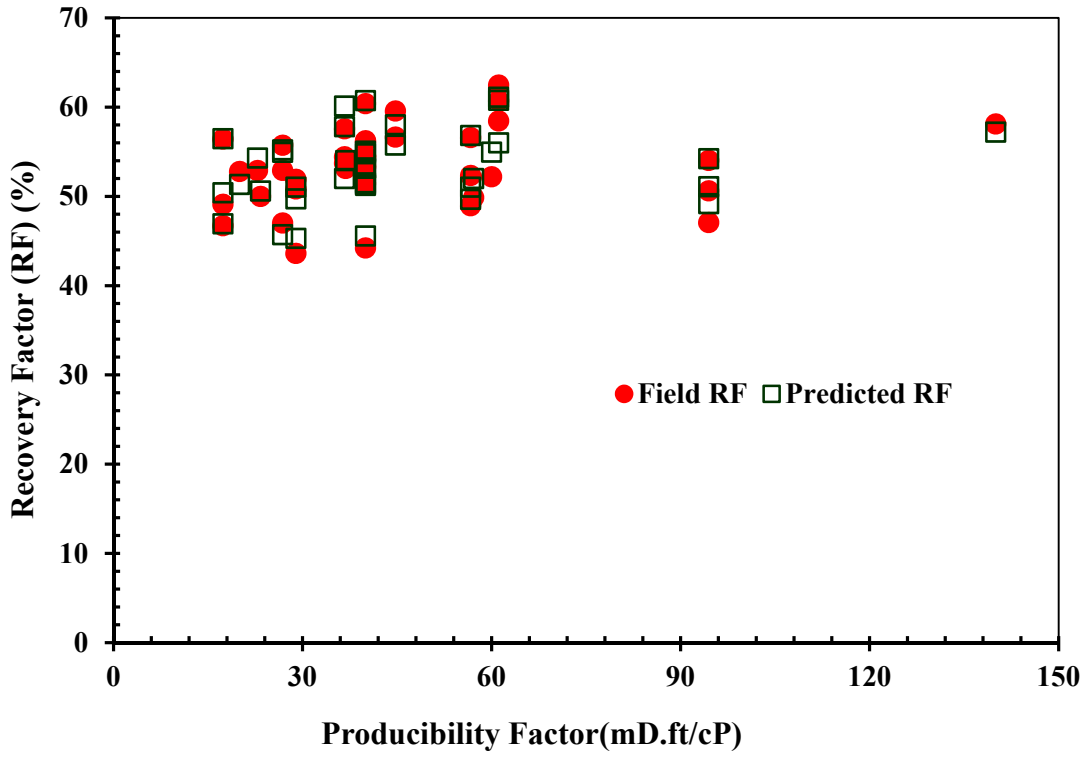


Figure 3-17: *RF* vs. oil saturation for the database analyzed.



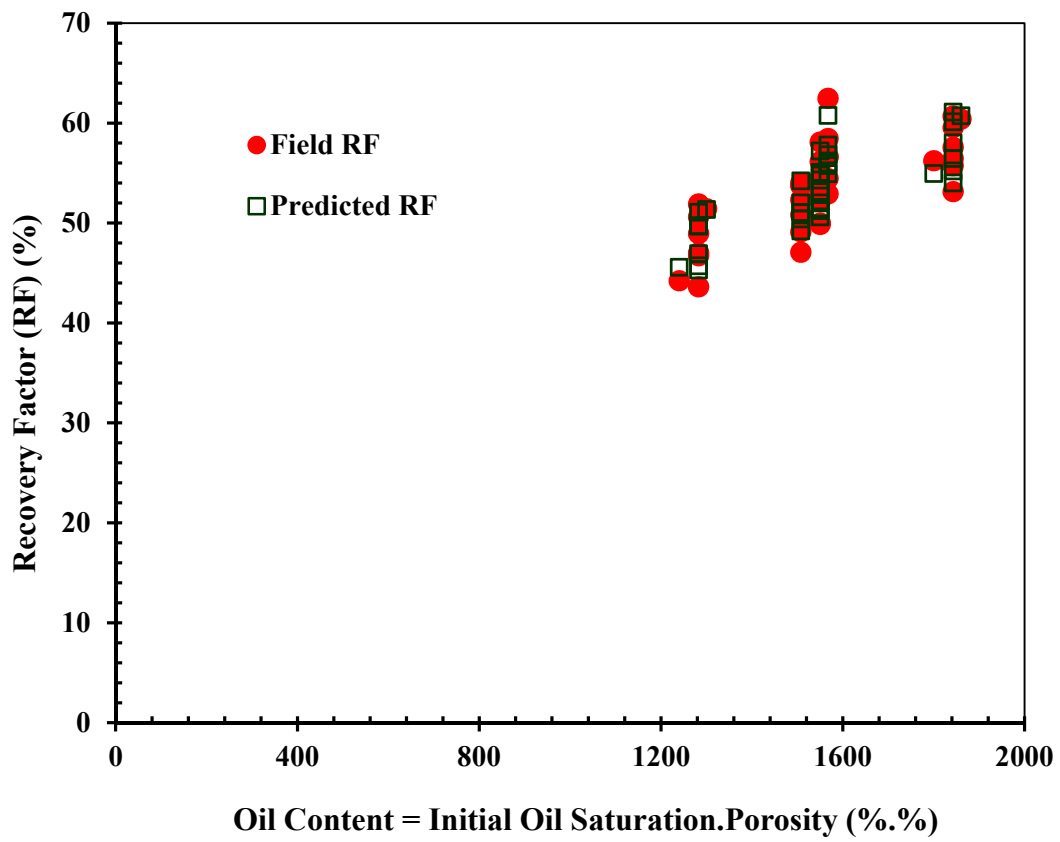


Figure 3-19: *RF* vs. oil content for the database analyzed.

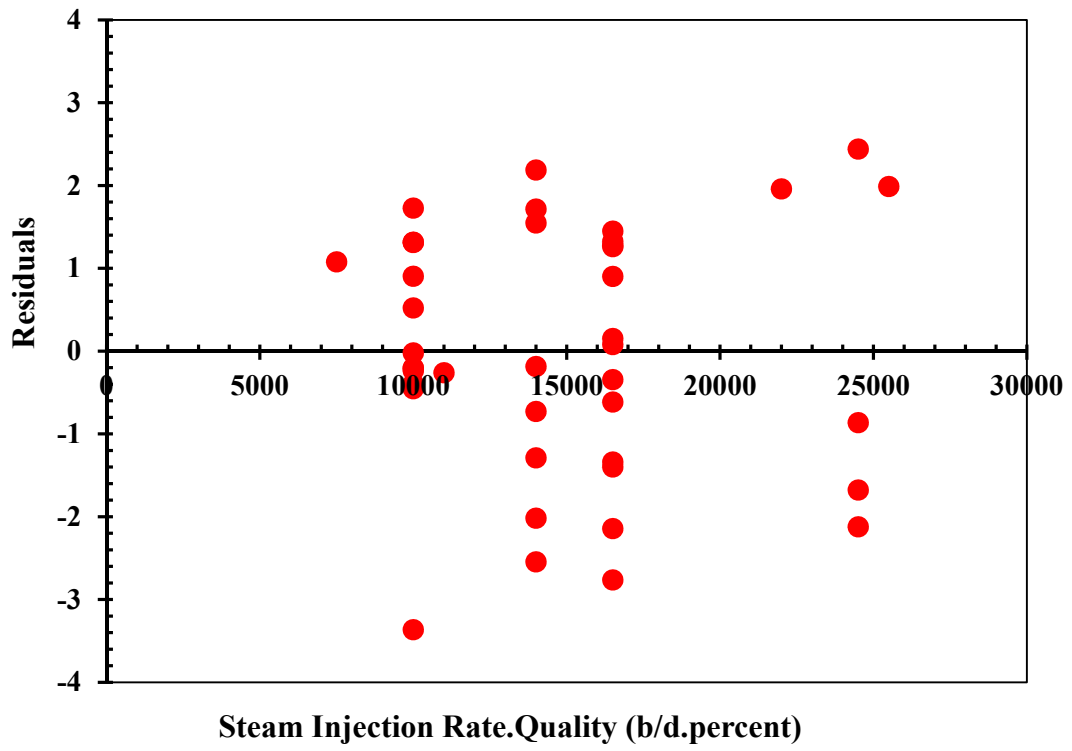


Figure 3-20: Residuals vs. product of steam injection rate and quality for the database analyzed.

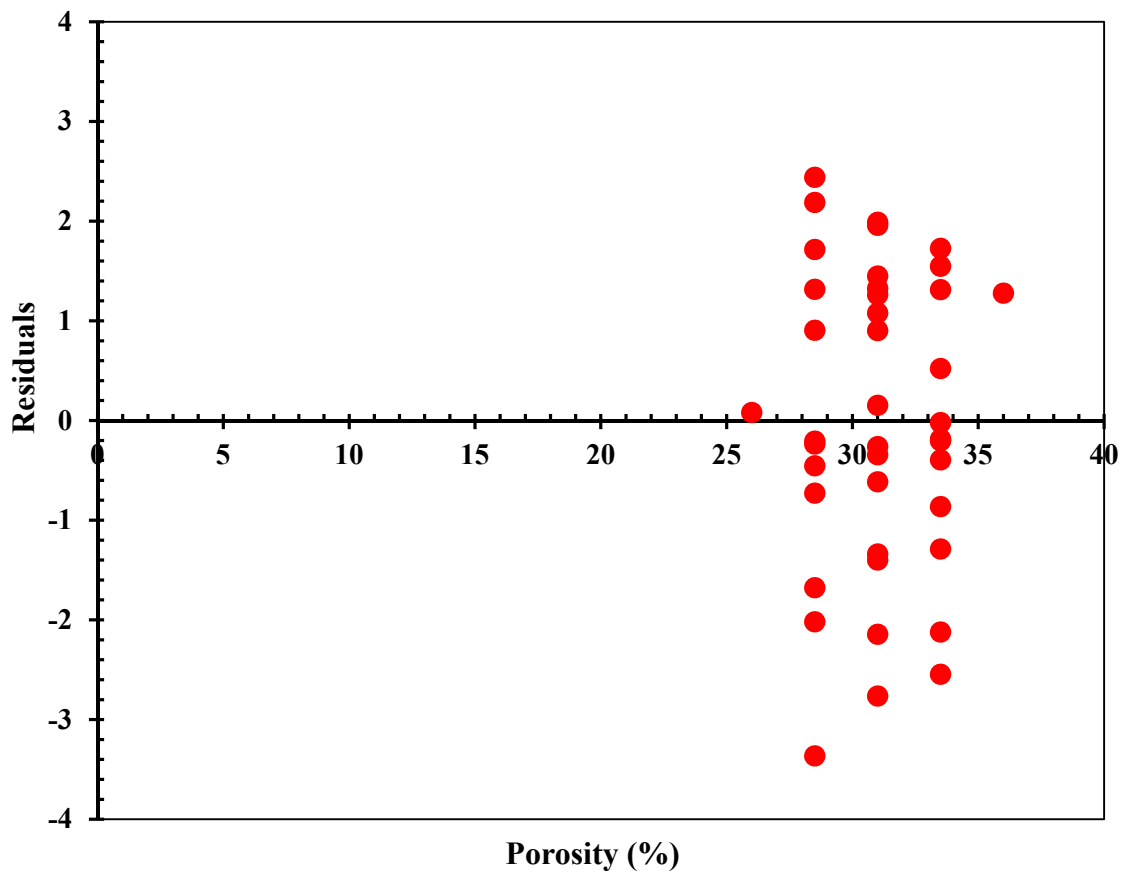


Figure 3-21: Residuals vs. porosity for the database analyzed.

These results show that *CSOR* values for viscous oil extraction from naturally fractured carbonates and some highly naturally fractured sandstone reservoirs can be statistically correlated with reservoir and oil characteristics such as permeability, porosity, thickness, viscosity, and oil saturation. The following empirical relationship predictive function was developed in this study to estimate the *CSOR* during vertical well steamflooding in a naturally fractured carbonate heavy oil reservoir:

$$\begin{aligned}
CSOR = & a_0 + a_1 D + a_2 \frac{1}{\phi_e} + a_3 \frac{1}{K_m} + a_4 K_f + a_5 \frac{1}{\mu_o} + a_6 \frac{1}{S_o} + a_7 \frac{1}{q_s} + a_8 x_s + a_9 \frac{1}{S_o \phi_e} + a_{10} \frac{D}{h} + \\
& a_{11} \frac{D}{h \phi_e K_m \mu_o S_o q_s} + a_{12} \frac{1}{\phi_e q_s} + a_{13} \frac{1}{\phi_e K_m} + a_{14} \frac{K_f}{K_m}
\end{aligned}
\tag{3-15}$$

Table 3-3 presents the values for the correlation coefficients, standard errors, and lower limits and upper limits for the coefficients involved in the equation for the *CSOR*. Since the variables such as K_m (md), K_f (md), porosity (%), S_o (%) have high magnitudes, their coefficients must be 4-6 digits significant while using regression correlations.

Table 3-3: Regression model of the *CSOR* ($R^2 = 0.962$; $F = 196.645$).

Coefficient	Numeric Value	Standard error	Lower 95%	Upper 95%
a ₀	-15.5032	2.8539	-29.6475	-5.0500
a ₁	-0.0010	0.0003	-0.0018	-0.0002
a ₂	6.8709	1.8510	2.9821	10.7597
a ₃	4151.4510	283.5271	404.3983	7898.5014
a ₄	0.000005	0.0000001	0.000002	0.000008
a ₅	-221.2160	18.5879	-260.2673	-182.1637
a ₆	22.4970	3.7313	14.6576	30.3364
a ₇	-46579.0033	4306.2042	-55625.9621	-37531.9634
a ₈	-2.5468	0.1136	-4.6728	-0.9675
a ₉	-7.1402	1.1720	-9.6025	-4.6779
a ₁₀	0.0311	0.0097	0.0105	0.0517
a ₁₁	151755.4003	14188.1505	121947.2318	181563.628
a ₁₂	18115.9311	1348.9456	15281.8993	20949.9586
a ₁₃	-1289.820	146.7237	-2081.2889	-498.3545
a ₁₄	0.0053	0.0002	0.0008	0.0097

Recovery Factor (*RF*) is also an important asset assessment parameter, and a reliable tool to predict *RF*, even if only in a statistical manner, would be valuable for first-order screening. Estimation of production performance is possible with initial and residual oil saturation data, but the magnitude of the irreducible oil saturation is usually unknown until the end of a complete thermal project. Nevertheless, according to the production history of some field pilots and some laboratory scales tests, a correlation was obtained for *RF* prediction in terms

of formation, steam, and oil properties. To derive the following equation, a similar method as that for *CSOR* was employed using statistical regression analysis:

$$RF = a_{15} + a_{16} S_o + a_{17} h + a_{18} q_s + a_{19} \phi_e + a_{20} K_m + a_{21} x_s + a_{22} \mu_o + a_{23} \frac{K_m h}{\mu_o} + a_{24} S_o \phi_e + a_{25} q_s x_s + a_{26} \frac{S_o \phi_e h K_m q_s}{\mu_o x_s} + a_{27} q_s \phi_e + a_{28} \frac{K_f}{K_m}$$

(3-16)

It is worthwhile to note that the product of fracture permeability and matrix permeability and the interaction of all contributing parameters would affect the *RF* parameter in the form of “combinatory effects”. Table 3-4 contains data on the statistical correlation coefficients.

Table 3-4: Information for the Linear Regression Model of the *RF* prediction ($R^2 = 0.964$; $F = 79.317$).

Coefficients	Numeric Value	Standard Error	Lower 95%	Upper 95%
a ₁₅	-85.8301	26.5206	-140.155	-31.505
a ₁₆	137.5069	30.2453	46.8231	228.1906
a ₁₇	0.0235	0.0111	0.0007	0.0463
a ₁₈	0.2158	0.0464	0.1207	0.3108
a ₁₉	282.291	41.5324	111.4806	453.1013
a ₂₀	-0.0009	0.00025	-0.00148	-0.0004
a ₂₁	47.0029	7.076	26.3631	67.6426
a ₂₂	-0.0003	0.0001	-0.0005	-8E-05
a ₂₃	-0.0295	0.0222	-0.0751	0.0159
a ₂₄	-213.1	80.345	-505.3	-2.8975
a ₂₅	-0.159	0.0328	-0.226	-0.092
a ₂₆	6.82E-04	2.44E-04	1.82E-04	1.18E-03
a ₂₇	-0.496	0.0142	-0.788	-0.205
a ₂₈	-.013	0.0034	-.064	-.007

The corresponding ANOVA for *CSOR* is presented in Table 3-5. Because F_{observed} for *CSOR*, which is equal to 196.645, is greater than the critical value (2.31), all of the parameters considered in multivariable linear regression analysis of *CSOR* and their attributed effects are significant and cannot be ignored to simplify the statistical analysis.

Table 3-5: ANOVA table for *CSOR* regression analysis.

Source	DF	SS	MS	F
Regression	14	2598.9799	185.6414	128.7558
Residual	15	21.6271	1.4418	
Total	29	2620.6071		

Table 3-6 indicates a strong dependency of the objective function (*RF*) to the process variables used for statistical analysis based on the high magnitude of the observed “F” function compared with the tabulated critical value. In addition, this table demonstrates a good accuracy of the regression analysis for *RF*.

Table 3-6: ANOVA Table for *RF* during steamflooding.

Source	DF	SS	MS	F
Regression	13	657.685	50.59115	70.60103
Residual	27	19.34763	0.716578	
Total	40	677.0326		

A simple method to check the accuracy of a particular linear regression is to look at the magnitudes of squared residuals. These values for the proposed linear regressions are presented in Table 3-7. Results obtained from the experimental and field data studied here and the linear regression analyses suggest a reasonable compatibility between the measured and the predicted values. The proposed linear regression curves work well for prediction of *CSOR* and *RF* in VO NFCRs under real field operating conditions, given the limitations of the data base available.

Table 3-7: Summary of the Statistical Linear Regressions.

Objective function	Multiple R	R ²	Standard error	Number of observations
<i>CSOR</i>	0.969	0.962	1.097 E-2	30
<i>RF</i>	0.978	0.964	8.384 E-2	41

It is not surprising that this study shows that the initial oil saturation and oil viscosity are the most important factors affecting *CSOR* and *RF* for fractured reservoirs during steamflooding.

It is not surprising that this study shows that the initial oil saturation and oil viscosity are the most important factors affecting *CSOR* and *RF* for fractured reservoirs during steamflooding. According to the statistical information provided in Tables 3-7 and 3-8, an acceptable match is seen between the predicted and measured *RF* and *CSOR* for steamflooding in NFCRs for the statistical investigation conducted in this study. As shown in Table 8, the statistical parameters (e.g., R², minimum percentage error (MIPE), maximum percentage error (MAPE), and mean squared error (MSE)) for the correlations obtained in this study and also the correlations developed by other researches such as [Chu \(1985\)](#), [Vogel \(1984\)](#), [Boberg \(1988\)](#), and [Butler \(1991\)](#) were obtained and compared for various predictive equations. The relationships developed in this paper are more accurate in estimation of *RF* and *CSOR* than other equations as higher R² and lower values for MIPE, MAPE, and MSE are found based on the newly introduced correlations.

Table 3-8: Performances of previous predictive models, and statistical correlations obtained in the current study.

Statistical parameter	Chu (1985)		Vogel (1984)		Boberg (1988)		Butler (1991)		Proposed correlations	
	RF	CSOR	RF	CSOR	RF	CSOR	RF	CSOR	RF	CSOR
R^2	0.9655	0.9463	0.9187	0.9251	0.9143	0.9301	0.9294	0.9134	0.9840	0.976
MSE	0.0934	0.0997	0.1442	0.1572	0.1526	0.1685	0.1523	0.1125	0.0634	0.0892
$MIPE$ (%)	7.6851	9.8759	7.6892	10.5807	9.1132	10.7794	9.1287	10.4162	5.3546	6.0044
$MAPE$ (%)	12.6325	14.5366	13.4765	15.1764	14.5178	16.0059	14.4503	15.5487	10.3218	11.1178

The viscosity of cases analyzed ranges from 6 to 936 cP, thus the reservoirs are heavy oil reservoirs except for one medium heavy and one light oil reservoir in a NFR. The reservoir depth for the studied cases varies from 134 to 1350 meters. This range covers the lower and upper limits of applicability of steamflooding. Matrix porosity and permeability vary from 0.12 to 0.35 and 1 to 4000 mD. Also, the fracture “permeability” is between 1 and 1000 D. Given the few field trials of steamflooding reported in NFCRs, these ranges represent a reasonable coverage of the variation in parameters expected in such heterogeneous reservoirs.

3.6.2 Screening of a HO Field for Steamflooding

Kuh-e-Mond heavy oil field (Figure 3-22), the largest on-shore heavy oil field in Iran, is a giant anticline located in the southwest of the country with a NW-SE trend. The field is 90 km long and 16 km wide with an estimated minimum heavy oil resource base of 6×10^9 b OOIP. The heavy is found in three separate reservoirs with depths ranging from 400–1200 meters and oil viscosities of 550–1120 cP *in situ* (Bashari, 1988; Moshtaghian *et al.*, 1988).

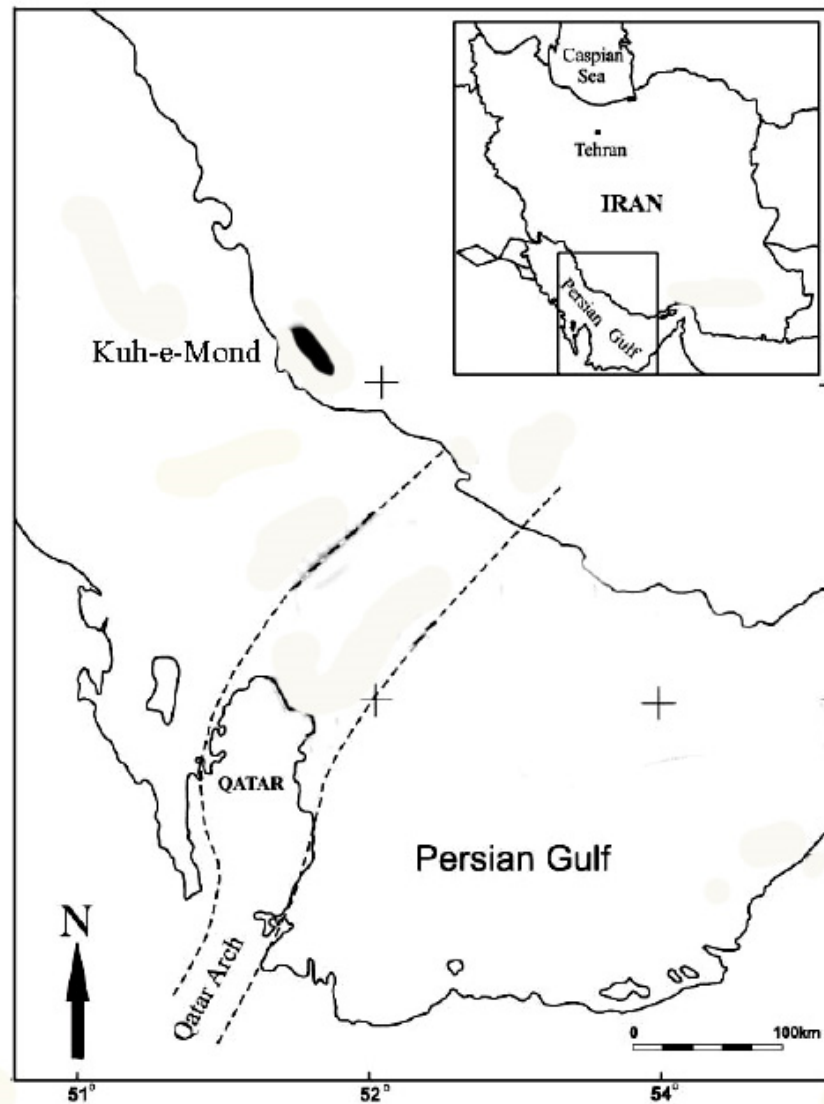


Figure 3-22: Geographical location of the Kuh-e-Mond heavy oil field.

Heavy oil occurrence has been confirmed in three separate intensely fractured carbonate formations, the Jahrum (Eocene) and Sarvak (Cretaceous) Formations. The trap structure formed during the main phase of Zagros folding in the late Miocene and Pliocene, as shown by the relatively constant thickness of the lower Miocene succession (Bashari, 1988; Moshtaghian *et al.*, 1988; Kamali and Rezaee, 2003).

According to petrophysical evaluations, the Jahrum Formation limestone is a poor reservoir; only part of it has good porosity (ϕ) in the range of 0.24–0.31 and water saturation (S_w) around 0.20. The Jahrum Formation, a reservoir of Eocene age, mainly consists of highly fractured light brown medium-grained crystalline dolomite with intercrystalline vuggy and fracture porosity. The lower Jahrum is mainly white detrital dolomitic and partly anhydritic and cherty limestone. This formation contains immobile heavy oil. The OOIP has been estimated at about 3×10^9 b (Bashari, 1988; Moshtaghian *et al.*, 1988; Kamali and Rezaee, 2003).

The Cenomanian Sarvak Formation is mainly composed of highly fractured marly neritic and pelagic limestone with interbedded shale layers. This formation is divided into three main units, upper, middle and lower Sarvak units. The upper unit consists of clean limestone with some slightly argillaceous zones. In the middle Sarvak, shale and marls are dominant, and the lower Sarvak is mainly composed of marly limestone, with some shale bed intercalations. During drilling, heavy mud losses occurred in the Sarvak, indicating a highly-fractured formation. The Sarvak heavy oil reservoir contains an estimated OOIP of 3.6×10^9 b (Moshtaghian *et al.*, 1988).

As the first step in production technology selection, lithostratigraphic information and fluid properties for the HO reservoirs at the Kuh-e-Mond HO field were collected, reviewed and are summarized in Table 3-8. This database was constructed using drilling and geophysical log data, as well as field and laboratory tests conducted in the reservoir (e.g., well tests) or on samples taken from exploration wells. Average reservoir and fluid properties for each selected reservoir was estimated from the available data.

Table 3-9: Reservoir and fluid properties of reservoirs at the Kuh-e-Mond HO field.

Reservoir Abbreviation	Jahrum	Sarvak
Lithology	Dolomite and Dolomitic Limestone	Limestone
Depth (m)	680–900	1100–1200
Thickness (z) (m)	320	100
Net to Gross Ratio (%)	31	47
Net Pay Thickness (m)	99	47
Oil Viscosity (<i>In situ</i>) (cP)	1160	570
Temperature (T) (<i>In situ</i>) °F	70	110
Matrix Permeability (mD)	1	0.2–1.4
Fracture Permeability (mD)	300–500	350–500
Natural Fracturing	Vertical and Sub-vertical Fractures	Vertical and Sub-vertical Fractures
Porosity (ϕ) (Fraction)	0.19	0.16
Oil Saturation (Fraction)	0.66	0.46
Gas Cap	Not Reported	Not Reported
Bottom Water	Not Reported	Not Reported
Wettability	Oil Wet	Oil Wet/Mixed Wet

Based on the predictive regression models, *CSOR* and *RF* are determined in the ranges of 6–7.2 and 41–49%, respectively, for the Jahrum HO reservoir; while, these ranges are 6.3–8 and 37–44% for *CSOR* and *RF*, respectively, in Sarvak HO reservoir number if 200–250 b/d of steam with 80–90% quality is injected into the formation. The quick screening results

suggests that Jahrum HO reservoir is technically recoverable using steamflooding despite a porosity of 0.19 because of other favorable factors such as depth, thick net pay, high oil saturation, and OOIP of 6×10^9 b. The Sarvak HO reservoir also met the screening criteria for steamflooding but the Jahrum HO reservoir is a slightly better candidate. Low porosity (0.16) with very low matrix permeability, despite the presence of vertical and sub-vertical fractures (high fracture permeability), and low oil saturation ($< 50\%$ PV) lead to lower RF and higher $CSOR$ in the Sarvak HO reservoir. Under current economic conditions HO exploitation from these reservoirs remains economically unattractive.

The developed correlations were examined for estimation of $CSOR$ and RF in oil sands and unconsolidated heavy oil sandstone reservoirs and compared the results with the $CSOR$ estimations predicted by a correlation proposed by [Chu \(1985\)](#) [67]. The results suggest that the new correlations also can be used to reliably estimate $CSOR$ and RF in oil sands and unconsolidated heavy oil sandstone reservoirs. The developed correlations can be considered a general form of correlations which can be used for wide ranges of reservoir properties from NFCRs to oil sands and unconsolidated heavy oil sandstone reservoirs.

During field development and implementation of a thermal method like steamflooding for a particular reservoir, laboratory analysis and field intervention assist the operator to avoid or remediate high cumulative steam/oil ratio through choosing a proper production rate and/or steam injection flow rate, since recovery and injection rates affects thermodynamic conditions, steam/oil rate and composition of the liquid phase moving towards the production well. Thus, implementation of experiments and statistical modeling (employing various flow rates in the form of dynamic conditions) would be very beneficial to systematically investigate the behaviour of heavy oil fractured in terms of RF and $CSOR$. Obtaining such information provides valuable guidelines to properly design the thermal operation in terms of flow rate and thermodynamic status of fluids such that very low RF and high $CSOR$ are prevented during production process. In addition, accurate prediction of RF and $CSOR$ for a particular heavy oil reservoir provides process engineers with acceptable rules of thumb for

optimum process conditions to minimize heat transfer loss, leading to huge amount of steam condensation in the reservoir.

3.7 Limitations and assumptions for the correlations of CSOR and RF

Table 3-10 presents the range of variables contributed in the correlations developed for prediction of *RF* and *CSOR* in NFCRs.

Table 3-10: Range of variables to estimate RF and CSOR

	Parameter	Min	Max
Input	Depth (m)	134	1350
	Matrix porosity (Fraction)	0.12	0.35
	Matrix permeability (mD)	1	400
	Fracture permeability (D)	1	1000
	Oil viscosity (cP)	6	936
	Initial oil saturation (Fraction)	0.3	0.9
	Steam quality	0.3	1
Output	Recovery factor, RF, (Fraction)	0.4	0.7
	Cumulative Steam Oil Ratio (CSOR)	3.0	10.0

A number of limitations/restrictions associated with the correlations developed in this study are listed as follows:

- (1) Porous medium is non-deformable; thus, it has a constant porosity.
- (2) No source term except the steam exists for mass.
- (3) The case studies taken from the experimental works are mostly two dimensional (2-D).
- (4) The correlations are valid just in the range of parameters

employed in the current study. Ranges of fluid and porous media properties in oil fields are almost the same as in the experimental studies considered in this statistical investigation. (5) The Darcy law is valid throughout the thermal process. It is proven that flow in porous media is often laminar (e.g., $Re < 1$) during steamflooding cases. (6) Geometry of physical models used in the experimental works (taken from the literature) does not have big effects on RF and CSOR in steamflooding; it just affects residual oil saturation slightly because geometry dictates the shape of the corners and end points and no change is observed for a high capillary threshold and permeability with respect to geometry variations for the porous system. (7) There were certain number of porous media with specific fracture patterns selected for this statistical study, and the correlations are giving very good results with high accuracy for the porous media having these kinds of fracture configurations. Hence, the only main limitation would be the type of fracture configuration for the fractured porous media. It should be also noted here that, if the effective fracture permeability is known for a porous medium with unknown fracture patterns, the obtained regressive relationships can help to predict the *RF* and *CSOR* of the porous system under steamflooding operations with a reasonable precision.

3.8 Concluding Remarks

In developing predictive correlations for steamflooding in VO NFCRs, a number of additional issues may arise. These issues may or may not have a significant impact on the nature and reliability of the predictive equations, but they deserve to be mentioned:

- The data do not extend into the class of bituminous NFCRs ($\mu > 10000$ cP). Vast NFCR resources with such high viscosities exist in Canada and elsewhere, but insufficient project data exist from these reservoirs to allow inclusion in this study.
- The data are for rock masses where the fractures are significantly more transmissive than the matrix. Carbonate reservoirs that are only weakly or locally fractured exist, and in many actual cases, the intensity and fabric of the fractures can vary spatially.

- Only reported data could be incorporated. There is a strong human tendency to not report failures; therefore, we must assume that the cases we found comprise technical successes and commercial successes. It is not feasible to surmise the results of unpublished failures, and data from such cases may alter the relationships or reduce their predictive capacity in general.

Nevertheless, with these caveats, this chapter presents new correlations to predict cumulative steam to oil ratio (*CSOR*) and recovery factor (*RF*) in NFCRs under steamflooding. The *CSOR* and *RF* were statistically correlated in terms of physical properties of the oil, petrophysical properties of the reservoir, and steam properties. The following conclusions seem reasonable, despite a modest database:

- The *CSOR* and *RF* were statistically correlated to physical properties of the oil, petrophysical properties of the reservoir, and steam properties.
- The correlations developed are derived from data obtained from field and laboratory tests. High correlation coefficients (R^2) and low mean squared errors show that the multivariable regression method used is a strong predictor of the economic assessment factors *CSOR* and *RF*.
- The errors involved in even the worst cases were less than 10%, giving confidence that first-order economic decisions can be made with these relationships.
- The parameters considered for regression analysis are not able to forecast the oil production characteristics of steamflooding in NFRs if they are used alone. Combination terms for the main variables were used, leading to better results.
- Initial oil saturation and oil viscosity have the greatest impacts on predictor models for *CSOR* and *RF*. Nevertheless, all of the chosen parameters have a significant influence on the predictions; therefore, none of them should be abandoned in the search for a simpler predictive tool.
- The proposed correlations were applied to predict *CSOR* and *RF* in two fractured heavy oil reservoirs, with apparently good results. This supports the use of these

relationships for initial technical feasibility assessment of VO NFCRs for vertical well steamflooding.

- *CSOR* increases with an increase in oil viscosity, steam injection rate, fracture to matrix permeability, and gross to net reservoir thickness. However, high steam quality and high initial oil saturation lead to reductions in *CSOR*, indicating better response to steam injection.
- Increase in steam injection rate improves the recovery rate but lowers the *RF* before steam breakthrough in fractured reservoirs (particularly highly fractured reservoirs).
- Although the presence of fractures can lead to an increase in oil production rate, a high density of fractures may have undesired effects on the overall performance of steamflooding.
- The ratio of the reservoir depth to the reservoir thickness does not have a noticeable impact on *RF* during steamflooding. As expected, steam quality and initial oil saturation have direct impacts on the magnitude of *RF* as increases in these two parameters leads to improvements in the performance of the steamflood. Clearly, higher quality steam injection brings more heat into the reservoir, leading to an increase in temperature that causes viscosity reduction that enhances the oil recovery.
- *CSOR* values for viscous oil extraction from NFCRs and some highly naturally fractured sandstone reservoirs can be statistically correlated with reservoir and oil characteristics such as permeability, porosity, thickness, viscosity, and oil saturation.
- A reasonable agreement exists between the experimental and field data and the predicted values. The proposed linear regression curves work well for prediction of *CSOR* and *RF* in VO NFCRs under real field operating conditions, given the limitations of the data base available.
- Comparison of statistical correlations developed in this chapter, and the previous correlations shows that the newly defined equations can predict steamflooding

efficiency in heavy oil NFCRs with high accuracy such that the maximum error percentage is lower than 12% for the equations obtained in this study.

Nomenclature

Acronyms or abbreviations

ANOVA	=	Analysis of Variance
CSOR	=	Cumulative Steam to Oil Ratio
CSS	=	Cyclic Steam Stimulation
EIA	=	the U.S. Energy Information Administration
HO	=	Heavy Oil
MCWEB	=	1000 Cold Water Equivalent Barrels
NFCRs	=	Naturally Fractured Carbonates Reservoirs
NFR	=	Naturally Fractured Reservoir
OSR	=	Oil Steam Ratio
<i>RF</i>	=	Recovery Factor
SD	=	Steam Drive
SF	=	Steamflooding
USGS	=	the United States Geological Survey
VO NFCRs	=	Viscous Oil Naturally Fractured Carbonates Reservoirs
VO	=	Viscous Oil
XHO	=	Extra Heavy Oil

Symbols: Latin, then Greek

<i>A</i>	=	planar area of the steam chamber, m ²
\dot{A}	=	rate of change in the planar area of the steam chamber, m ² /t
\bar{y}	=	Average of all data points of dependent variable in Eq. (3–13)

\hat{y}_i	=	Predicted data in Eq. (3–13)
b	=	exponent in Cardwell and Parson's equation for relative permeability (dimensionless)
C_{vo}	=	overburden volumetric heat capacity, MJ/m ³ .K
C_{vr}	=	initial reservoir volumetric heat capacity, MJ/m ³ .K
g	=	gravity acceleration, m/year ²
H	=	enthalpy, MJ/m ³
h	=	height of reservoir above producer, m
H_{lv}	=	latent heat of condensation of steam, MJ/m ³
Hs	=	height of the steam chamber, m
K	=	permeability, m ²
K_t	=	overburden thermal conductivity, MJ/m.K.year
k	=	number of regressor variables
n	=	chamber coalesced factor, dimensionless
N	=	Number of observations or data points in Eq. (3–13)
T	=	time since first steam injection, year
V_{sz}	=	volume of the steam chamber, m ³
y_i	=	Real field or observed data in Eq. (3–13)
Δ	=	Difference operator
ΔS_o	=	initial minus residual oil saturation, dimensionless
ΔT	=	temperature rise above initial condition, °C
μ	=	Dynamic viscosity (kg.m/s or cP)

β	=	effective sweep efficiency factor, dimensionless
β_i	=	Regression coefficients in Eqs. (3–5) to (3–7)
η_s	=	effective sweep efficiency, dimensionless
ν_s	=	kinematic viscosity of the oil at the temperature of the steam, m ² /year
ρ	=	Density of fluid (kg/m ³)
ϕ	=	Total effective porosity of the model

Variables

E	=	Error value in Eqs. (3–6) to (3–7)
g	=	Gravitational acceleration (m/s ²)
K	=	Intrinsic permeability (Darcy or m ²)
K_f	=	Intrinsic permeability of the fracture (Darcy or m ²)
K_m	=	Permeability of matrix in the model (Darcy or m ²)
PV	=	Pore volume (m ³)
RF	=	Recovery Factor
S	=	Liquid saturation
t	=	Time (s)
x_i	=	Regression variables in Eqs. (3–5) to (3–7)
y	=	System response in Eqs. (3–5) to (3–7)

Subscripts

f	=	fracture
i	=	number of test runs
m	=	matrix

max = maximum

min = minimum

Metric Conversion Factors

°F = $(^{\circ}\text{C} \times 1.8) + 32$

1 barrel oil = 0.159 m³

1 psi = 6.8947 kPa

1 psi/ft = 22.62 kPa/m or 22.62 MPa/km

“There are only two ways to live your life. One is as though nothing is a miracle. The other is as if everything is.”

Albert Einstein

Chapter 4

A New Mathematical Model for Steamflooding in Naturally Fractured Carbonate Heavy Oil Reservoirs²

4.1 Abstract

This chapter presents a three dimensional mathematical model for steamflooding in heavy oil saturated naturally fractured carbonate reservoirs where the governing equations are written for the matrix and fracture media, separately. Uncertainties associated with the shape factor for the communication between the matrix and fracture was eliminated through setting a continuity boundary condition at the interface. Using this boundary condition, the solution method employed differs from the most of the modeling simulations reported in the literature. Newton-Raphson approach was also used for solving mass and energy balance equations. The recovery factor and cumulative steam to oil ratio were obtained as a function of steam injection rate, temperature, and also characteristics of the fractured media such as matrix size and permeability. The numerical solution clearly shows that fractures play an important role in improving the conduction of heat into the matrix part. It is also concluded that the matrix size and total permeability are the most important parameters affecting the dependent variables involved in steamflooding in this type of reservoirs. The results obtained from the mathematical modeling were compared with the field data, exhibiting a reasonable agreement.

4.2 Introduction

Naturally Fractured Carbonate Reservoirs (NFCRs) contain around one quarter of the heavy, extra heavy oil, and bitumen resources in the world ([Brigs *et al.* 1988](#); [Shafiei, 2012](#)).

² Materials presented in this chapter are contributed to the following publication:

[Shafiei, A.](#), Zendejboudi, S., Dusseault, M.B. and Chatzis, I. 2013. A New Mathematical Model for Steamflooding in Naturally Fractured Carbonate Heavy Oil Reservoirs. *Industrial & Engineering Chemistry* (In press).

Moreover, NFCRs especially enormous oilfields in the Middle East provide over 40% of current world oil production (Oil & Gas Journal, 1996, 1998, 2004, 2006, 2008, 2010; Xie *et al.* 2005). It is important to note that viscous oil (VO) includes all kinds of oil with viscosity higher than 100 cP, e.g., heavy oil (HO), extra heavy oil (XHO), and bitumen at reservoir conditions, was considered in this dissertation (Dusseault and Shafiei, 2011).

Thermal VO recovery techniques commercially commenced with steamflooding (SF) or/and steam drive (SD) in 1952 in California and after that Venezuela where the reservoir thickness is over 10 m (de Haan and van Lookeren, 1969; Farouq Ali, 1974). Steamflooding is generally appropriate for crude oils of $\mu < 5000$ cP, since communication between offset wells is effectively established at low viscosity. According to worldwide EOR surveys published by Oil & Gas Journal, steam processes are the sole commercialized VO recovery technology that can be successfully used for viscosity reduction. It is reported that over 70 percentage of existing production methods for VO are dealing with steaming, and this domination is expected to proceed in the future (Taber and Martin, 1997; Oil & Gas Journal, 1996, 1998, 2004, 2006, 2008, 2010). Most commercial thermal operations are currently being applied in tar sands and unconsolidated sandstone reservoirs mostly in USA, Canada, and (Dusseault and Shafiei, 2011). Only very few steamflooding pilot operations are reported in the literature from France, Italy, Congo, Turkey, USA, Kuwait and Saudi Arabia. Cyclic steam stimulation also has been applied to VO NFCRs, and public data are available only from cases in Canada, China, Egypt, and Syria (Sahuquet and Ferrier, 1982; Chierici *et al.* 1985; Couderc *et al.* 1990; Sahuquet *et al.* 1990; Nakamura *et al.* 1995; Ono, 1997; Snell and Close, 1999; Snell *et al.* 2000; Dehghani and Ehrlich, 1998 and 2001; Barge *et al.* 2009; Brown *et al.* 2011; Gross *et al.* 2011; Hoadley *et al.* 2011; Meddaugh *et al.* 2011; Osterloh *et al.* 2011).

Several numerical models along with experimental works on steamflooding, mostly in oil sands and unconsolidated sandstones, are reported in the literature. Miller and Leung (1985) combined a numerical model with a simulation approach for steam injection into a reservoir. They obtained cumulative production versus time and compared the results for both methods

employed in their work; however, their model was unable to determine the production rate. In fractured systems, [Dreher *et al.* \(1986\)](#) conducted some steam and hot water injection tests. However, they did not simulate the process. [Jensen *et al.* \(1991\)](#) reported a number of core-flooding tests on fractured systems with some simulations to analyze the experimental results but a complete investigation was impossible as heat losses, temperature, and steam and oil saturation in various parts (e.g., matrix and fracture) were unknown. [Hong \(1994\)](#) studied the effects of rate and quality of steam on production performance for different situations and concluded that there is no single steam quality or injection rate to be considered as optimal conditions based on the technical and economic aspects of steam consumption and oil prices. [Mohammadi *et al.* \(2012\)](#) conducted a study on steam injection in heavy oil reservoirs through a numerical modeling. Although there are some similarities between their approach and the methodology presented in this chapter with respect to derivation of governing equation for the matrix part, they did not take into account the presence of fracture appropriately as their model only has one horizontal fracture which is not representative of a fractured system. In addition, the numerical modeling was solved using a coupling technique; however, no equation or/and method was introduced to calculate the effective porosity and permeability. Apparently, some values for these parameters were estimated based on the physical properties of the matrix part. Their results clearly indicate that their proposed model is proper for homogeneous reservoirs such as unconsolidated sandstone VO reservoirs; however, there are major constrains in terms of boundary conditions, combination of governing equations for the matrix and fracture parts, and determination of properties while applying the method for fractured porous systems. The main focus of these researches was on homogeneous reservoirs or/and single porosity systems such that there is no comprehensive experimental or simulation work to predict process performance, production history, RF , and $CSOR$ in heterogeneous and fractured reservoirs such as VO NFCRs.

A number of experimental and mathematical models also are reported for performance prediction of steamflooding process in VO sandstones. For instance, a 2-D model was

introduced by [Shutler \(1970\)](#) to simulate oil, water, and gas phases in VO sandstones considering both heat conduction and convection terms in 2-D while determining the temperature profile. [Abdalla and Coats \(1971\)](#) solved a governing mathematical equation through a numerical method for steam injection in VO sandstones. They employed an implicit pressure-explicit saturation technique to obtain the pressure and saturation distributions of all three phases, assuming the fluids are compressible. Based on the results of their study, a model was developed to determine the rate of steam condensation. [Coats *et al.* \(1974\)](#) developed a 3-D model to conduct numerical simulations to model steam injection in VO sandstones. This model includes mass and energy balance in both reservoir and the overburden. Their solution does not require the iteration procedure while considering the condensation term. Mass and heat transfer interphase involved in multi-component flow was studied by [Ferrer and Farouq Ali \(1977\)](#) using a numerical model to simulate three phase and 3-D flow during steam injection in VO sandstones. They concluded that compositional constraints approach represents a good procedure for practical simulation purposes. [Coats \(1978\)](#) simulated distillation and solution gas phenomena in steamflooding through an implicit model. All the terms related to solution gas, distillation and capillary pressure were included in the model to investigate the variations of saturation and compositions during steamflooding. Beside the modeling studies, systematic experimental works were performed by a number of researchers such as [Sumnu *et al.* \(1996\)](#), [Mollaei *et al.* \(2007\)](#), and [Souraki *et al.* \(2011\)](#). These laboratory investigations were mostly focused on parametric sensitivity analysis approach to capture main aspects of the steamflooding process. It should be noted here that majority of the above research works have some flaws that are not applicable in the real field conditions; especially for heterogeneous and dual or triple porosity systems such as HO NFCRs. For example, the reservoirs under study were treated as homogeneous in fairly small dimensions. Also, the numerical methods are generally facing divergence issue in the fluid/fluid and medium/medium interfaces. Most of the models proposed to forecast the performance of VO reservoirs under steamflooding are on the basis of reservoir heating model developed by [Marx and Langenheim \(1959\)](#). The injection of hot fluid into a well is assumed to be operating at constant injection rate and temperature according to their

proposed method. The volume control considered in this model is composed of a radial flow system, with a well in the central point. The temperature in the heated zone was assumed to be constant, as well.

In the absence of appropriate models and predictive tools, all of the field pilots rely deeply on experimental work and simulations employing available commercial petroleum engineering softwares like CMGTM and ECLIPSETM. Furthermore, only limited parameters involved in NFCRs over a narrow range of process and reservoir conditions can be examined using commercial softwares.

In this chapter, a 3-D mathematical model for steamflooding in NFCRs is presented considering the matrix part and fracture part in the form of two subdomains, by writing the separate governing equations. A continuity boundary condition was applied at the interface of the matrix and fracture media to remove the uncertainties associated with the shape factor when determining the communication rate between the matrix and fractures. The proposed method uses the fluid flow and heat transfer equations for both the steam and oil phases. A convective heat loss model was employed to calculate the heat transfer from the system to the surrounding environment via an overall convective heat transfer coefficient and temperature difference between two media. In addition, it was assumed that nonlinear relative permeability function is valid for both matrix and fracture but with different coefficients. The results obtained from the proposed numerical model were examined against the production history of field scale pilots and also experimental studies reported in the literature to verify the accuracy and validate the proposed model.

4.2.1 Naturally Fractured Reservoirs

A Naturally Fractured Reservoir (NFR) is defined as a reservoir that contains fractures created by natural processes (e.g., tectonics forces), distributed as a connected or disconnected network throughout the reservoir (Saidi, 1987). Natural fractures have a significant impact on flow rates, anisotropy, storage and recovery (Saidi, 1987; Ershaghi, 1995). The porous system of any reservoir is usually divided into two domains; a) Primary

porosity (matrix) which is typically inter-granular and is controlled by lithification and deposition processes. The matrix medium contributes notably to fluid storage; however, its role to fluid flow is normally low due to low permeability; b) Secondary porosity (fractures) which is generated by post lithification phenomena. Fractures are highly permeable and hence contribute appreciably to the fluid flow. However, they are not very porous and their contribution to fluid storage is not important. The post-lithification processes that generate secondary porosity are generally in the form of solution, recrystallization, dolomitization, and opening the existing fractures, faulting, or jointing. In NFRs, dual porosity formulation was developed by [Warren and Root, 1963](#) (Figure 4-1).

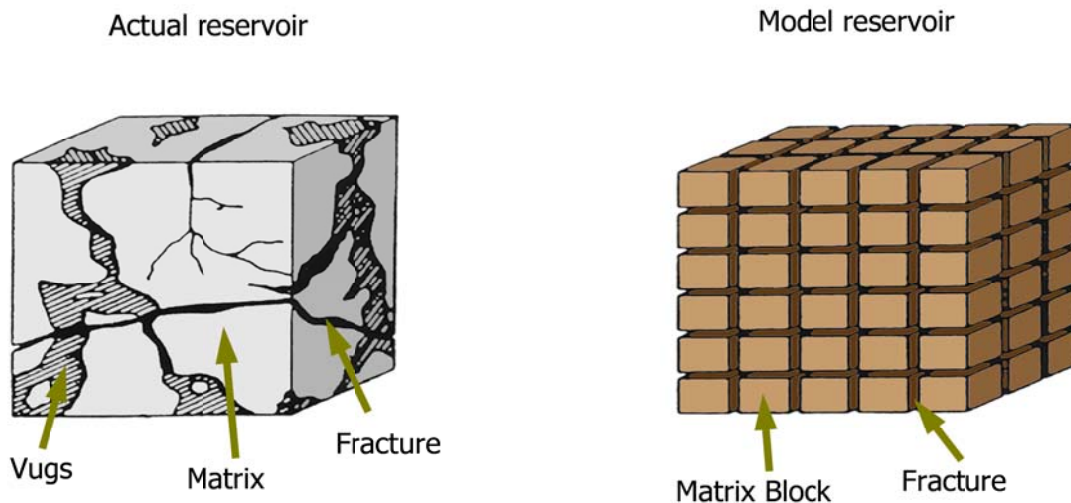


Figure 4-1: Idealized dual porosity reservoir model (Modified from [Warren and Root, 1963](#)).

Most of the oil reservoirs show dichotomy of porous space but with varying degree of matrix and fracture presence. A low fractured reservoir is one in which the fracture part is insignificant. However, most NFRs are highly fractured and consist of a considerable amount of secondary porosity. Hence, this dichotomy for NFRs is justified. Dual porosity formulation superimposes the secondary (or fracture) medium on the primary (or matrix) medium and this superimposition ideally corresponds to the primary porosity coupled with the secondary porosity as depicted in Figure 4-1. It should be noted here that some NFRs

(e.g., bitumen saturated Grosmont formation in Alberta, Canada) contain vuggy and karst related porosity along with the matrix and fracture porosities that make simulation of these types of NFRs much more complicated.

In a NFR, the total porosity (ϕ_t) is the result of the simple addition of the primary and secondary porosities:

$$\phi_t = \phi_1 + \phi_2 \quad (4-1)$$

where ϕ_1 and ϕ_2 are primary porosity and secondary porosity, respectively.

Based on a large number of laboratory measurements on various types of rocks, the fracture porosity was considerably lower than the matrix porosity (Warren and Root, 1963; Saidi, 1987; Nelson, 2001). The two porosities are expressed by conventional definitions:

ϕ_1 = matrix void volume/total bulk volume; ϕ_2 = fracture void volume / total bulk volume

The two porosities are relative to the total bulk volume (matrix + fractures).

Considering matrix porosity (ϕ_m), it refers only to the matrix bulk volume as given below:

$$\phi_m = \frac{\text{Volume of voidspace of the matrix}}{\text{Matrix bulk volume}} \quad (4-2)$$

while the fracture porosity (ϕ_f) is expressed by the following relationship:

$$\phi_2 \approx \phi_f \quad (4-3)$$

The primary porosity (ϕ_I) in terms of matrix porosity is expressed as follow:

$$\phi_1 = (1 - \phi_2)\phi_m \quad (4-4)$$

In addition, the effective primary porosity ($\phi_{1,eff}$) considering the oil saturation is defined as the following:

$$\phi_{1,eff} = (1 - \phi_2)\phi_m(1 - S_{wi}) \quad (4-5)$$

Hence, the equation of double porosity in fractured systems can be written as follow (Saidi, 1987; Ershaghi, 1995):

$$\phi_t = \phi_m + \phi_f - \phi_m\phi_f \quad (4-6)$$

The basics of permeability established for a conventional reservoir remain valid in the case of a NFR. However, permeability should be redefined as a function of matrix permeability, fracture permeability, and system (fracture-matrix) permeability. This definition of permeability may cause some confusion especially for fracture permeability, which can be interpreted either as single fracture permeability or as fracture network permeability, or sometimes as fracture permeability of fracture bulk volume. Therefore, various expressions of permeability will be examined and discussed in this section in more detail (Sahimi, 1995).

The effective fracture permeability ($K_{eff,f}$) can be also correlated with the fracture porosity and aperture through the following two equations (Saidi, 1987; van Golf-Racht, 1996):

$$K_f = \frac{b^2}{12} \quad (4-7)$$

$$K_{eff,f} = K_f \cdot \phi_f \quad (4-8)$$

There are some limitations related to Equations (4-7) and (4-8) as the fracture permeability estimated from Equation (4-7) is based up on solving Stokes equation in a 2-D (e.g., x-y) system, assuming that aperture (b) is small compared with depth (z).

The effective fracture permeability of a liquid phase flowing across a fracture was derived by [Dindoruk and Firoozabadi \(1995\)](#) with more accuracy for simulation purposes. The correlation that gives the effective fracture permeability is:

$$K_{eff,f} = 8.75 * 10^4 R b^2 \sqrt{I} \quad (4-9)$$

In Equation (4-9), R is the aspect ratio of the liquid film flow in fracture, and b is the fracture aperture. ' I ' is the liquid film shape factor through the fracture. ' I ' is approximately 7.5 for $R = 1$, and $1/R$ for large values of R . It should be added here that the units of $K_{eff,f}$ and b are Darcy and centimeter in Equation (4-9), respectively.

If fracture-matrix communication is neglected (the assumption is acceptable when dealing with viscous oil and very low permeable matrix which are typically found in VO NFCRs), the total effective permeability for the whole model with a long vertical fracture would be like two parallel porous media ([Zendehboudi et al., 2011](#)):

$$K_e = K_f \cdot \phi_f + K_m \frac{W_m}{b + W_m} \quad (4-10)$$

In Equation (4-10), K_m is the matrix permeability and W_m represents the width of the matrix.

The intrinsic fracture permeability is associated with the conductivity measured during the fluid flow through a single fracture or through a fracture network, independent of the surrounding rock (matrix). This is the conductivity of a single channel (fracture) or of a group of channels (fracture network). In this case, the flow cross-section is represented only by the fracture void areas excluding the surrounding matrix area. In a simplified case of a block, where the fracture is parallel to the flow direction, K_{ff} is obtained using the flow equation for a conduit and also Darcy's law as follow (van Golf-Racht, 1996):

$$K_{ff} = \frac{b^2}{12} \cos \alpha \quad (4-11)$$

where α is the dip angle.

For a fracture system having n fractures of similar orientation, the intrinsic permeability is expressed by arithmetic average (Saidi, 1987; Ershaghi, 1995; van Golf-Racht, 1996):

$$K_{ff} = \frac{\sum_{i=1}^n b_i^2}{12} \cos \alpha \quad (4-12)$$

For a fractured system with fracture porosity (ϕ_2), the conventional fracture permeability (K_f) is determined as the following (Saidi, 1987; Ershaghi, 1995; van Golf-Racht, 1996):

$$K_f = K_{ff} \cdot \phi_2 \quad (4-13)$$

4.2.2 Steamflooding in NFCRs

Low permeable matrix, low porosity, relatively great depth and fracture permeability ranging from low to medium values are the typical features of VO NFCRs especially in the Middle East. These characteristics are usually the main drawbacks for implementation of thermal methods in NFCRs. The ranges of porosity for VO unconsolidated sandstones and VO NFCRs are 30% to 35% and 10% to 20%, respectively (Dusseault and Shafiei, 2011). Based on this statement, it can be concluded that the Oil Originally In Place (OOIP) in a VO unconsolidated sandstone reservoir is about two times of that in a typical VO NFCR with the same bulk volume. Thus, greater *CSOR*, lower *RF*, and lower thermal efficiency for VO NFCRs are expected in contrast to VO unconsolidated sandstone reservoirs.

Figure 4-2 shows a schematic of steam flooding in a NFCR. This technology employs vertical wells with continuous injection of steam into the reservoir. This makes a steam zone moving slowly to cover further areas of the reservoir, leading to an increase in the temperature of the rock and oil. Consequently, oil phase with lower viscosity is obtained that leads to oil mobilization and oil flow toward the production well.

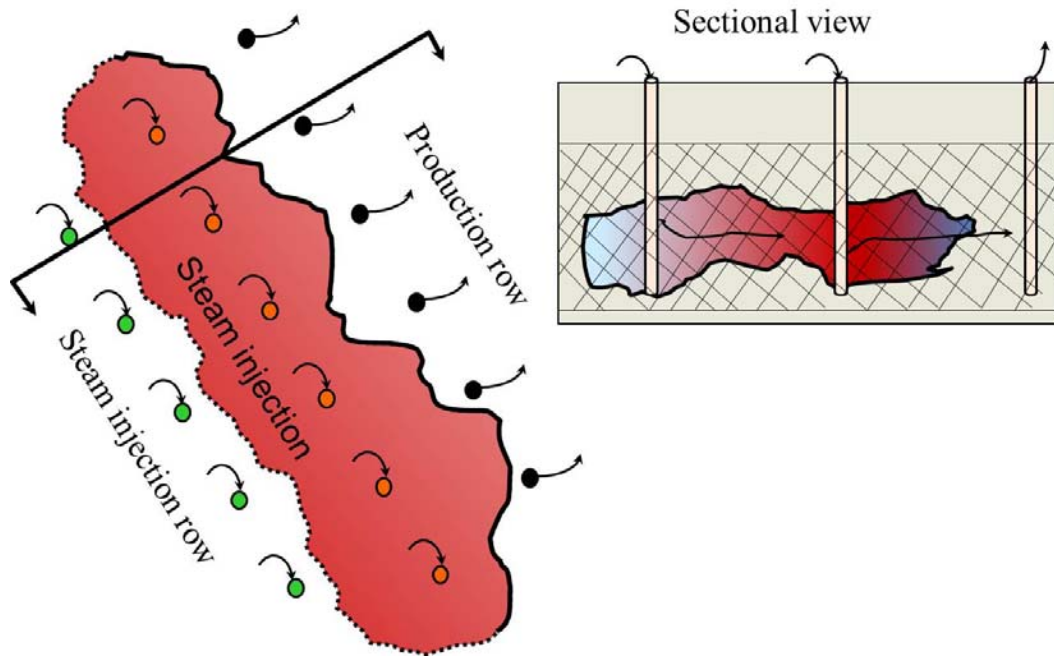


Figure 4-2: Idealistic view of Steamflooding in NFRCs (Steamed zone is presented in red).

4.3 Mathematical Formulation

In this study, the fracture is considered as a separate porous medium and similar governing equations were used for both matrix and fracture parts. The governing equations were simultaneously solved in order to obtain the 3-D dynamic pressure and velocity distributions within the model using the initial and boundary conditions. The two boundaries B-1 and B-2 (see Figure 4-3) impose the no-flow conditions for both phases. The continuity of velocity and pressure as the main variables holds at the boundary of matrix and fracture parts (IB-1 and IB-2). These two boundary conditions vanish for a homogeneous porous system where the model has no fractures. The initial condition at any position (x,y) in the model is attained for each phase by assigning the pressure to be equal to the static pressure applied by the column of the corresponding fluid above it. For the steam phase, however, the initial saturation was assumed to be zero, as initially there is no vapor in the porous medium and the model was fully or partially saturated with oil. If steam is initially present in the model, then this boundary condition changes to the pressure of steam phase at time zero.

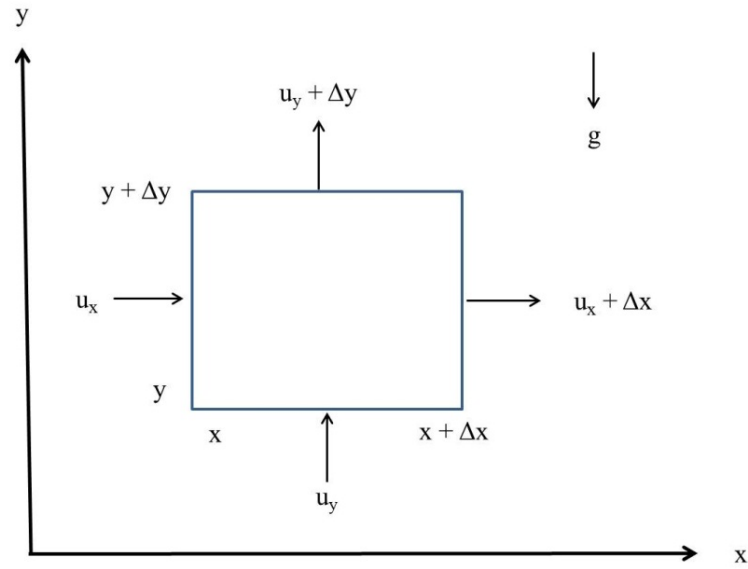
4.3.1 Model Assumptions

The following assumptions were taken into consideration in the modeling approach presented in this modeling work:

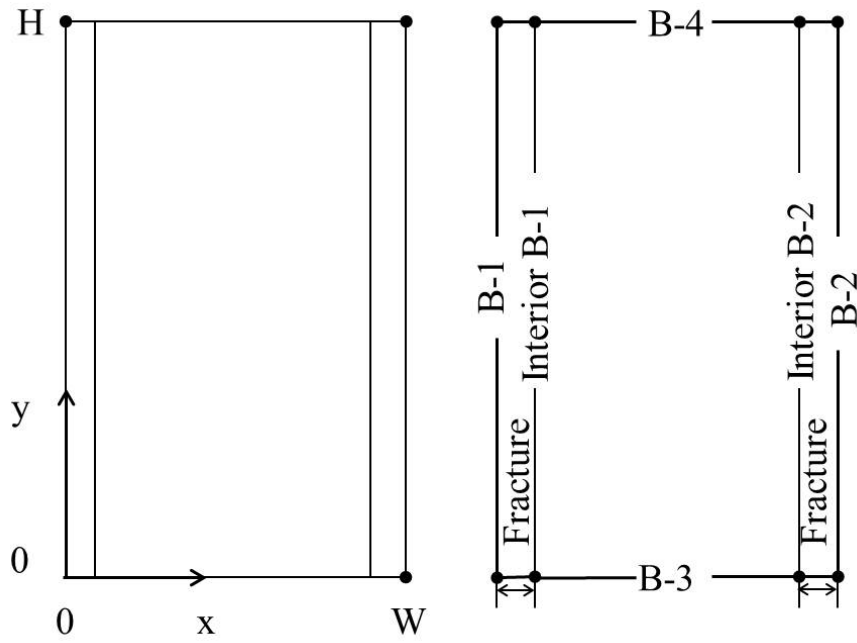
- (1) Three phases such as water, oil, and steam are considered in the proposed model
- (2) Darcy's law is valid for all three phases introduced (e.g., Reynolds number is < 1)
- (3) No hydrocarbon gas is available in the system, indicating total pressure above bubble point pressure and just liquid phase exists in the physical system
- (4) Rock is incompressible throughout the steamflooding process such that porosity is assumed to be constant
- (5) Specific heat of the rock is not pressure dependent but it varies with temperature
- (6) Diffusion mechanism is weak during the mass transfer and convection process is dominant during the steamflooding
- (7) Fourier's law and energy convection relationship are utilized in order to determine the heat loss and the temperature profile

4.3.2 Governing Equations

First, a differential element and macroscopic view of a porous medium is considered as presented in Figure 4-3(a) and 4-3(b), respectively. For the differential element in Figure 4-3(a), the continuity equation for an arbitrary phase, k ($k = \text{water, oil, steam}$) can be written in the form of Equation (14). In this equation, ρ_k , S_k , and u_k are the density, saturation, and velocity of the phase k , respectively. ϕ is porosity of the porous medium and t represents the time. Furthermore, the momentum equation is taken from the generalized Darcy equation as shown in Equation (15). It is also possible to adopt a more general momentum conservation equation such Navier-Stocks. In this equation, k_{rk} , μ_k , and ∇Z_k are relative permeability, viscosity, and the pressure gradient for phase k and g is the gravity acceleration constant. The gravity is in the opposite direction of z axis as shown in Figure 4-3(a).



(a)



(b)

Figure 4-3: A schematic of (a) differential element and (b) A side view of the physical model.

Mass balance for any phase during steamflooding is calculated as follows:

$$\frac{\partial}{\partial t}(\phi \rho_k S_k) - \nabla \cdot (\rho_k u_k) - \rho_k q_k = 0 \quad (4-14)$$

The first term represents accumulation, the second term indicates input or output into/from the control volume, and the third is mass generation or consumption. The sign of terms involved in Equation (4-14) (e.g., input or exit and production or consumption) is negative or positive, depending on the type of stream including output and output. In addition, the last term of the left side of Equation (4-14) shows the impact of mass transfer.

Darcy's law gives the relationship for the velocities of the three phases in the porous system as follows:

$$u_k = -\frac{K k_{rk}}{\mu_k} \cdot [\nabla \cdot p_k - \rho_k g \nabla \cdot Z_k] \quad (4-15)$$

If Darcy's equation is substituted in mass balances for oil, water, and steam phases, then the partial differential equations (PDEs) are obtained as follows:

Oil phase:

$$\phi \frac{\partial(\rho_o S_o)}{\partial t} = \frac{\partial}{\partial x} \left[K k_{ox} \frac{\partial p_o}{\partial x} \right] + \frac{\partial}{\partial y} \left[K k_{oy} \frac{\partial p_o}{\partial y} \right] + \frac{\partial}{\partial z} \left[K k_{oz} \frac{\partial}{\partial z} (p_o - \rho_o g h) \right] + \rho_o q_o \quad (4-16)$$

Water phase:

$$\phi \frac{\partial(\rho_w S_w)}{\partial t} = \frac{\partial}{\partial x} \left[K k_{wx} \frac{\partial p_w}{\partial x} \right] + \frac{\partial}{\partial y} \left[K k_{wy} \frac{\partial p_w}{\partial y} \right] + \frac{\partial}{\partial z} \left[K k_{wz} \frac{\partial}{\partial z} (p_w - \rho_w g h) \right] + \rho_w q_w + \rho_w q_c \quad (4-17)$$

Steam phase:

$$\phi \frac{\partial(\rho_s S_s)}{\partial t} = \frac{\partial}{\partial x} \left[K k_{sx} \frac{\partial p_s}{\partial x} \right] + \frac{\partial}{\partial y} \left[K k_{sy} \frac{\partial p_s}{\partial y} \right] + \frac{\partial}{\partial z} \left[K k_{sz} \frac{\partial}{\partial z} (p_s - \rho_s g h) \right] + \rho_s q_s - \rho_w q_c \quad (4-18)$$

where q_c is the steam condensation rate. q_k is the flow rate of fluid 'k'.

The energy balance, considering both convection and conduction terms, can be written as follows:

$$\nabla \cdot K_T \nabla T - \nabla \cdot \left[\sum \rho_k u_k H_k \right] + Q = \frac{\partial}{\partial t} \left[\phi \left(\sum \rho_k S_k U_k \right) + (1 - \phi) \rho_R U_R \right] \quad (4-19)$$

where K_T , H_k , and u_k are the rock thermal conductivity, fluid enthalpy, and fluid internal energy, respectively.

The right side of Equation (4-15) represents the accumulation term which includes two parts. The first part is related to the substances that are in pores block and their internal energy changes by heat transfer. The second term indicates the energy accumulated in the reservoir rock. R subscript in the energy equation refers to the rock reservoir. In the left side of Equation (4-15), the first and second terms are conductive heat transfer in solid rock and

convective heat transfer due to fluid flow, respectively. Also, the last part of the left side represents heat losses to the surrounding area of the reservoir.

By simplifying Equation (4-19), the following expression for heat balance can be attained:

$$\phi \sum_k \frac{\partial(\rho_k S_k U_k)}{\partial t} + (1 - \phi) \frac{\partial(C_{pR} \rho_R T)}{\partial t} = \frac{\partial}{\partial x} \left[K k_{rx} \frac{\partial}{\partial x} (\bar{p} - \bar{\rho} g H) \right] + \frac{\partial}{\partial x} \left[K_{Tx} \frac{\partial T}{\partial x} \right] + \frac{\partial}{\partial y} \left[K_{Ty} \frac{\partial T}{\partial y} \right] + \sum_k \rho_k H_k q_k \quad (4-20)$$

where k = o (oil), w (water), and s (steam). \bar{p} and $\bar{\rho}$ indicate the average pressure and density, respectively.

The last governing equation is an equilibrium relationship which presents the temperature of the saturated steam (T^{sat}) as a function of saturation pressure (p^{sat}):

$$T^{sat} = f(p^{sat}) \quad (4-21)$$

This relationship can be easily found in the steam table which is available in Perry's Handbook and/or books introducing proper correlations to determine properties of gases and liquids (Firoozabadi, 1999; Perry and Green, 2001; Poling *et al.*, 2001).

4.3.3 Auxiliary Equations

Additional equations are related to saturation of the existing phase and two capillary pressure functions as the following:

$$S_w + S_o + S_s = 1 \quad (4-22)$$

$$p_o - p_w = p_{cwo}(S_w) \quad (4-23)$$

$$p_s - p_o = p_{cso}(S_s) \quad (4-24)$$

According to [Brooks and Corey \(1964\)](#), the relative permeability functions for the wetting and non-wetting phases are presented in Equation (4-25) and Equation (4-26), respectively ([Brooks and Corey, 1964](#)).

$$k_{rw} = S_{we}^{\left(\frac{2}{\lambda}+3\right)} \quad (4-25)$$

$$k_{rnw} = (1 - S_{we})^2 (1 - S_{we}^{\left(\frac{2}{\lambda}+1\right)}) \quad (4-26)$$

The capillary curve is defined as the following ([US-COTA, 1978](#)):

$$S_{we} = \left(\frac{p_c^o}{P_c} \right)^\lambda \quad (4-27)$$

where p_c^o stands for the threshold capillary pressure, S_{we} is the effective wetting saturation obtained from equation below, and the parameter λ was estimated at 0.37 as reported by [Briggs \(1989\)](#).

$$S_{we} = \frac{S_w - S_{wr}}{S_{wi} - S_{wr}} \quad (4-28)$$

The effective wetting phase saturation was correlated to the wetting phase saturation at any time (S_w), residual wetting phase saturation (S_{wr}), and the initial wetting phase saturation (S_{wi}) as observed from Equation (4-28). It is important to note that oil and steam are the wetting and non-wetting phases for oil/steam mixture in this study, respectively. However, oil acts as non-wetting phase in the oil/water system.

4.3.4 Fluid and Rock: Physical, Thermal, and Thermodynamic Properties

The following equations relating saturation temperature-pressure for steam are derived employing the data from the steam table (Firoozabadi, 1999; Perry and Green, 2001; Poling *et al.*, 2001):

$$T = 185.5 + 2.7p - 0.02p^2 + 8 \times 10^{-5} p^3 - 1 \times 10^{-7} p^4 \quad 20 \leq p \leq 200 \quad (4-29)$$

$$T = 94.5 \ln(p) - 120.16 \quad 200 < p < 600 \quad (4-30)$$

$$T = 404.44 + 0.1562p - 2 \times 10^{-5} p^2 \quad 600 \leq p \quad (4-31)$$

Pressure (p) and temperature (T) are in psig and °F, respectively.

In order to estimate oil viscosity (μ_o) in the numerical model, the following equation can be employed based on PVT studies (Poling *et al.*, 2001):

$$\ln(\mu_o) = a_1 + a_2 \ln(T) \quad (4-32)$$

where a_1 and a_2 are the constant parameters that are different for various oils. These two constants are generally obtained based on the experimental data within a wide range of temperature.

The following relationship is also used to determine the viscosity of water (μ_w) (Firoozabadi, 1999):

$$\mu_w = \exp[0.484045 - 3.1115 \times 10^{-2} T^{0.95} + 1.3192 \times 10^{-4} T^{1.9} - 2.2934 \times 10^{-7} T^{2.85}] \quad (4-33)$$

Also, the steam viscosity (μ_s) was obtained as follow (Firoozabadi, 1999):

$$\mu_s = 0.0085 + \exp[-7.00661 + 2.1106 \times 10^{-2} T - 7.2058 \times 10^{-5} T^2 + 1.0111 \times 10^{-7} T^3] \quad (4-34)$$

In the above relationships, the units of temperature and viscosity are °C and cP, respectively.

It should be noted here that the dependency of steam viscosity to the pressure is very weak. Thus, it is usually neglected.

The following equations can be used to compute the oil density (ρ_o) (Firoozabadi, 1999; Perry and Green, 2001):

$$\frac{\rho_o}{\rho_{o,REF}} = 1 + \alpha_o(p - p_{REF}) - \beta_o(T - T_{REF}) \quad (4-35)$$

where $\rho_{o,REF}$ is the reference oil density and T_{REF} is the reference temperature. α_o and β_o are the isothermal compressibility and thermal expansion coefficient of the oil, respectively.

α_o and β_o for the oil phase are calculated using the following equations (Firoozabadi, 1999; Perry and Green, 2001; Poling *et al.*, 2001):

$$\alpha_o = -\frac{1}{V} \frac{\partial V}{\partial p} \quad (4-36)$$

$$\beta_o = \frac{1}{V} \frac{\partial V}{\partial T} \quad (4-37)$$

According to the steam table, the following equations are obtained to calculate the saturated densities of steam (ρ_s) and water (ρ_w) (Firoozabadi, 1999):

$$\rho_s = \exp[-5.6294 + 0.14564T^{0.8} - 2.1242 \times 10^{-4} T^{1.6} - 7.4288 \times 10^{-6} T^{2.4} + 4.7323 \times 10^{-8} T^{3.2}] \quad (4-38)$$

$$\rho_w = 398.942 + 8.288558 \sqrt{5335.9562 - T^{1.45}} \quad (4-39)$$

Temperature is in °C and density is kg/m³ for the above relationships.

Thermal conductivity of rock (K_T) is a function of temperature, pressure, fluid saturations (S_f), and porosity (ϕ). This parameter is generally determined using correlations as given below (Dullien, 1992; Wu, 2004):

$$K_T = \frac{6.36 \exp(0.6(2.65(1 - \phi) + S_f))}{(0.566T + 255.3)^{0.55}} \quad (4-40)$$

In Equation (4-40), the units of thermal conductivity and temperature are Btu/hr.ft. °F and °F, respectively.

Steam enthalpy (H_s) and water enthalpy (H_w) as functions of temperature are expressed as (Firoozabadi, 1999):

$$H_s = 178.758 + 5.14455T + 119.8224\sqrt{374.094 - T} \quad (4-41)$$

$$H_w = 2751 - 212.23333\sqrt{170.86 - T^{0.85}} \quad (4-42)$$

Enthalpy (H) and Temperature (T) are in kJ/kg and °C, respectively. The following relationship gives the internal energy (U):

$$\rho_s U_s = \rho_s H_s - p_s \quad (4-43)$$

Dependency of porosity to pressure is expressed according to the formula given below (Firoozabadi, 1999; Perry and Green, 2001; Poling *et al.*, 2001):

$$\phi = \phi_0 [1 + C_R (p - p_0)] \quad (4-44)$$

where C_R is the compressibility of the reservoir rock. ϕ_o and p_o are the initial porosity and pressure, respectively.

4.3.5 Boundary and Initial Conditions

No flow boundary conditions were applied as pressure and temperature around the external boundary of the porous system were set on a certain amount. Heat transfer through any cross section normal to the direction of heat remains constant when Fourier's law is valid. Also, all physical and thermodynamic properties of matrix and fractures on the interface are assumed to be identical. The initial and boundary conditions for whole physical model are presented as follow:

Initial conditions:

Continuous phase (oil),

$$p_o(x, y, z, 0) = p_{o0} \quad (4-45)$$

Where p_{o0} is the initial pressure of the oil phase.

Water phase,

$$p_w(x, y, z, 0) = p_{o0} - p_{cwo}(S_w(x, y, z, 0)) \quad (4-46)$$

Discontinuous phase (steam),

$$p_s(x, y, z, 0) = p_{cso}(S_s(x, y, z, 0)) + p_{o0} \quad (4-47)$$

The boundary conditions along the model width (at $x = 0$ and $x = W$) and length (at $y = 0$ and $y = L$) can be easily obtained by imposing no-flow conditions for all three phases, as confined boundaries are considered in x and y directions:

$$\frac{\partial}{\partial x}(p_k(0, y, z, t)) = 0 \quad k = w, s, o \quad (4-48)$$

$$\frac{\partial}{\partial x}(p_k(W, y, z, t)) = 0 \quad k = w, s, o \quad (4-49)$$

$$\frac{\partial}{\partial x}(p_k(x, 0, z, t)) = 0 \quad k = w, s, o \quad (4-50)$$

$$\frac{\partial}{\partial x}(p_k(x, L, z, t)) = 0 \quad k = w, s, o \quad (4-51)$$

The boundary condition at zero height ($z = 0$) can be written by applying no flow condition to the oil phase, as there is no inflow of oil phase and only steam enters the porous system. This is shown in Equation (4-52). From mass conservation ($q_t = q_s$) and Darcy equations for momentum, the gradient of pressure of the steam phase at $z = 0$ can be obtained in the form of Equations (4-53) and (4-54).

$$\frac{\partial}{\partial y}(p_o(x, y, 0, t)) = 0 \quad (4-52)$$

$$q_t = q_w + q_s + q_o = q_s = - \left[\frac{Kk_{rs}A}{\mu_s} \frac{\partial p_s}{\partial z} \right]_{z=0} \quad (4-53)$$

$$\frac{\partial}{\partial z} (p_s(x, y, 0, t)) = - \frac{q_t \mu_s}{Ak_{rs}(S_s(x, y, 0, t))} \quad (4-54)$$

The boundary condition at $z = H$ is tricky. This is one of the reasons why defining the set of governing equations in the form of pressure results in rationale boundary conditions. The dilemma here is that before steam breakthrough, the oil is the continuous phase, but after breakthrough, now the steam also becomes a continuous phase, and after some time, the oil becomes discontinuous. The other challenge is that steam can move to the other side of the medium; however, it does not mean that it can breakthrough, because of the capillary discontinuity at outflow exit face. In other words, the water or/and steam cannot breakthrough unless the gradient of hydrodynamic pressure at exit face overcomes the capillary pressure gradient (there is zero capillary pressure at downstream). This well-acknowledged phenomenon is called “capillary retention” and makes the boundary conditions even more complex. These boundary conditions before and after breakthrough are formulated in Equations (4-55) through (4-59), respectively. Before steam breakthrough, oil is the continuous phase; therefore, the pressure of oil is same as that applied by the back pressure p_{BP} , which is zero if the outflow is drained to the atmosphere. The pressure of steam phase before breakthrough is obtained from capillary pressure of steam at corresponding saturation at exit face. As steam accumulates at the exit face, the capillary pressure reduces accordingly to a value which is finally compensated by hydrodynamic pressure at exit pore spaces. After breakthrough, the situation is reversed. The pressure of steam phase cannot be assumed as that of the back pressure (or, zero if the outflow is drained to the atmosphere) and the capillary pressure of oil is dictated by capillary pressure at that saturation level.

Boundary conditions at $z = H$ before breakthrough using the definition for the capillary pressure:

$$p_w(x, y, H, t) = p_{BP} - p_{cwo}(S_w(x, y, H, t)) \quad (4-55)$$

$$p_o(x, y, H, t) = p_{BP} \quad (4-56)$$

$$p_s(x, y, H, t) = p_{cso}(S_s(x, y, H, t)) + p_{BP} \quad (4-57)$$

Boundary conditions at $z = H$ after breakthrough:

$$p_o(x, y, H, t) = p_{cow}(S_w(x, H, t)) - p_w(x, y, H, t) \quad (4-58)$$

$$p_s(x, y, H, t) = p_{BP} \quad (4-59)$$

4.4 Solution Method

The sets of relationships are reduced using the auxiliary equations. Then, the system of Partial Differential Equations (PDEs) is solved using Finite Difference Method (FDM). The solution method employed in this study is different from the most of modeling works conducted on steamflooding. In this numerical modeling, gravity force and capillary pressure have been considered. Also, thermal conductivity of the rock is assumed not to be constant. In order to solve the governing equations, condensation term is eliminated by adding the balance equations of steam and water. The FDM has the flexibility of Finite

Element Method (FEM) and there is no pre-determined limit on the number of neighbors that a grid block can have. The time interval is determined using a backward, first-order FDM technique. Finally, the discretized equations of mass and energy balance are solved iteratively by Newton-Raphson approach. The developed numerical model is presented in Figure 4-4.

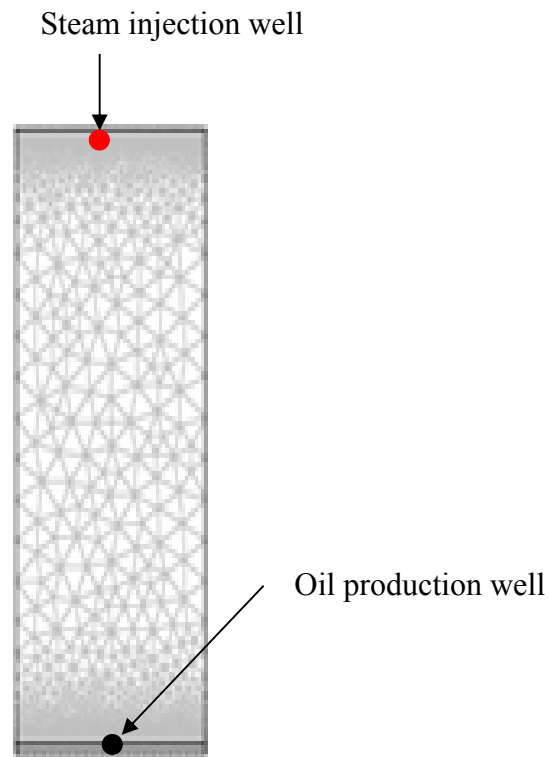


Figure 4-4: The developed numerical model with two vertical wells as injector and producer (This is an aerial view)

Depending on pressure and temperature of the different components, the fluids might have various thermodynamic statuses that are related to the type of phase. Each phase perhaps appears and disappears in a grid block during the modeling run. The phases of each grid

block are tested for the thermodynamic compatibility with new extents of the initial variables at the end of each Newton-Raphson iteration. The numerical algorithm for treatment of the phase appearance and disappearance is taken into account such that the primary parameters in the grid block are switched when a phase appears or disappears. In addition, the mesh configuration was considered to be rectangular with an exponential distribution as the meshes were a lot finer at the boundaries B-3, B-4, IB-1, and IB-2, coarser away from these boundaries. As a rule of thumb accepted in FEM, the mesh sizes in the horizontal and vertical directions were set to be about 10% of the model in that direction (W and H). The time interval used in this dynamic simulation was chosen based on the following scaling equation (Chen, 2005):

$$\Delta t \leq \frac{0.5(\frac{\mu}{\rho})}{\frac{1}{\Delta x^2}} \quad (4-60)$$

where Δt is the time interval and Δx is the mesh size in the horizontal direction.

Considering the solution procedure described above, the numerical modeling method contains the following parts, in brief (see Figure 4-5):

- 1- Specify the model dimensions and the process conditions
- 2- Do gridding of the physical model and choose appropriate size for the meshes
- 3- Define two subdomains, namely matrix and the fracture parts
- 4- Set initial and boundary conditions for each subdomain, separately
- 5- Enter the input data such as flow rates, temperatures, and pressures
- 6- Introduce the functions for physical, and thermal properties of the fluids and the reservoir rock in terms of temperature and pressure

- 7- Enter the functions and/or values for petrophysical properties of the medium such as various characteristics are assigned to the matrix and the fracture parts
- 8- Set assumptions (e.g., Darcy's law is valid)
- 9- Apply mass balance for each phase placing within each single subdomain
- 10- Write the energy balance considering both conduction and convection terms for each separate subdomain
- 11- Enter auxiliary relationships for the saturation degree and pressure
- 12- Enter functions for thermodynamic properties and variables contributing to the energy balance equation
- 13- Solve the PDEs (e.g., mass and energy equations) simultaneously for both subdomains using Finite Difference Method (FDM)
- 14- Use the Newton-Raphson technique iteratively to meet the stopping condition. The stopping condition is met when the difference between the estimated temperature and pressures for each trial and the calculated values approaches to zero (e.g., 10^{-6})

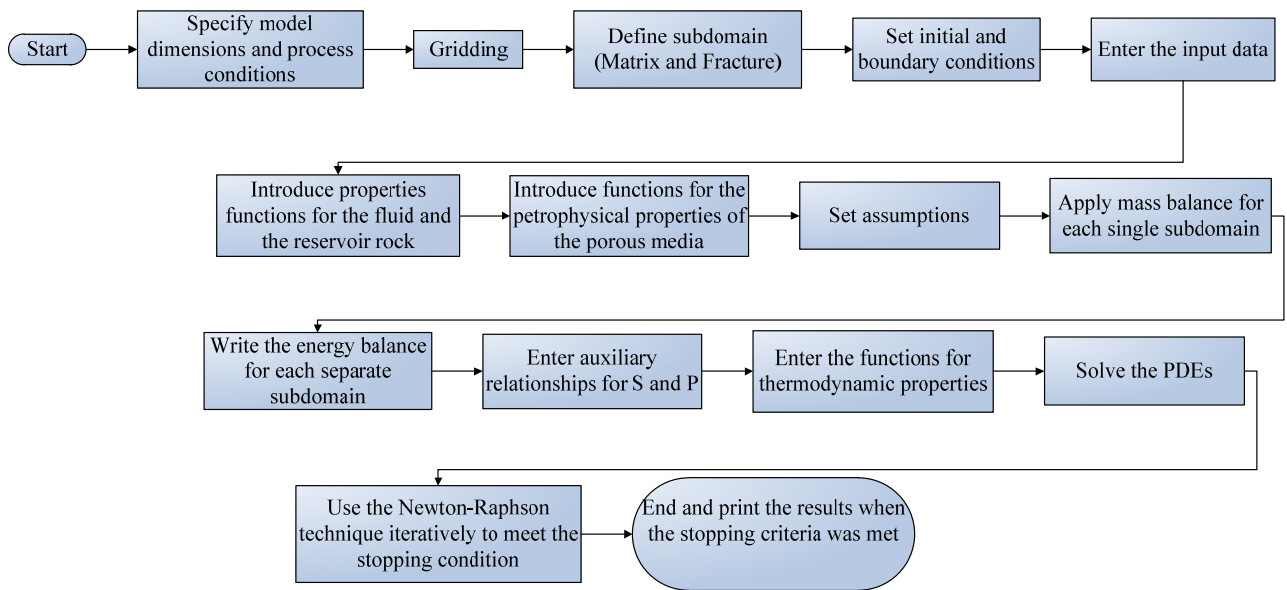


Figure 4-5: Flowchart of the numerical modeling study for VO NFRs.

4.4.1 Mesh Size and Configuration

Once all variables are entered into the system and the matrix and fracture subdomains are discretized into small elements. Typically, smaller mesh size produces more accurate numerical simulation; however, there is a limit to the mesh size used in numerical models due to the fact that the smaller mesh size in the subdomain increases the number of elements in the numerical simulation. This will in turn increase the computational efforts and time required for the simulation runs. To further understand the effect of mesh size on the numerical simulation result, various simulations were run with different mesh sizes in order to study the effect of the mesh size on the precision and accuracy of the numerical simulation.

The mesh configuration was considered to be rectangular with an exponential distribution as the meshes were a lot finer at the boundaries, coarser away from these boundaries. As a rule

of thumb accepted in finite element methods, the mesh sizes in the horizontal and vertical directions were set to be about 10% of the model in that direction.

4.4.2 Equations Discretization

The bulk volume is expressed as follow:

$$V_b = \Delta x . \Delta y . \Delta z = A_x . \Delta x = A_y . \Delta y = A_z . \Delta z \quad (4-61)$$

Here, the mass balance equations for all three phases (e.g., oil, water and steam) are written as follow, respectively:

$$\begin{aligned} & \frac{\partial}{\partial x} (\beta_c A_x K_x \frac{k_{ro} \rho_o}{\mu_o} \frac{\partial p}{\partial x}) \Delta x + \frac{\partial}{\partial y} (\beta_c A_y K_y \frac{k_{ro} \rho_o}{\mu_o} \frac{\partial p}{\partial y}) \Delta y + \frac{\partial}{\partial z} (\beta A_z K_z \frac{k_{ro} \rho_o}{\mu_o} (\frac{\partial p}{\partial z} - \rho_o g \frac{\partial h}{\partial z})) \Delta Z \\ & = \frac{V_b}{a_c} \left[\frac{\partial}{\partial t} (\phi \rho_o S_o) - \rho_o q_o \right] \end{aligned} \quad (4-62)$$

$$\begin{aligned} & \frac{\partial}{\partial x} (\beta_c A_x K_x \frac{k_{rw} \rho_w}{\mu_w} \frac{\partial p}{\partial x}) \Delta x + \frac{\partial}{\partial y} (\beta_c A_y K_y \frac{k_{rw} \rho_w}{\mu_w} \frac{\partial p}{\partial y}) \Delta y + \frac{\partial}{\partial z} (\beta A_z K_z \frac{k_{rw} \rho_w}{\mu_w} (\frac{\partial p}{\partial z} - \rho_w g \frac{\partial h}{\partial z})) \Delta Z \\ & = \frac{V_b}{a_c} \left[\frac{\partial}{\partial t} (\phi \rho_w S_w) + \rho_w q_{con} \right] \end{aligned} \quad (4-63)$$

$$\begin{aligned}
& \frac{\partial}{\partial x} (\beta_c A_x K_x \frac{k_{rs} \rho_s}{\mu_s} \frac{\partial p}{\partial x}) \Delta x + \frac{\partial}{\partial y} (\beta_c A_y K_y \frac{k_{rs} \rho_s}{\mu_s} \frac{\partial p}{\partial y}) \Delta y + \frac{\partial}{\partial z} (\beta A_z K_z \frac{k_{rs} \rho_s}{\mu_s} (\frac{\partial p}{\partial z} - \rho_s g \frac{\partial h}{\partial z})) \Delta z \\
& = \frac{V_b}{a_c} \left[\frac{\partial}{\partial t} (\phi \rho_s S_s) - \rho_s q_{con} \right]
\end{aligned} \tag{4-64}$$

The energy balance equation is discretized as follow:

$$\begin{aligned}
& \frac{\partial}{\partial x} (K_T A_x \frac{\partial T}{\partial x}) \Delta x + \frac{\partial}{\partial y} (K_T A_y \frac{\partial T}{\partial y}) \Delta y + \frac{\partial}{\partial z} (K_T A_z \frac{\partial T}{\partial z}) \Delta z + \frac{\partial}{\partial x} (\frac{A_x K_x k_{rw} \rho_w H_w}{\mu_w} \frac{\partial \theta_w}{\partial x} + \frac{A_x K_x k_{ro} \rho_o H_o}{\mu_o} \frac{\partial \theta_o}{\partial x} + \\
& \frac{A_x K_x k_{rs} \rho_s H_s}{\mu_s} \frac{\partial \theta_s}{\partial x}) \Delta x + \frac{\partial}{\partial y} (\frac{A_y K_y k_{rw} \rho_w H_w}{\mu_w} \frac{\partial \theta_w}{\partial y} + \frac{A_y K_y k_{ro} \rho_o H_o}{\mu_o} \frac{\partial \theta_o}{\partial y} + \frac{A_y K_y k_{rs} \rho_s H_s}{\mu_s} \frac{\partial \theta_s}{\partial y}) \Delta y + \\
& \frac{\partial}{\partial z} (\frac{A_z K_z k_{rw} \rho_w H_w}{\mu_w} \frac{\partial \theta_w}{\partial z} + \frac{A_z K_z k_{ro} \rho_o H_o}{\mu_o} \frac{\partial \theta_o}{\partial z} + \frac{A_z K_z k_{rs} \rho_s H_s}{\mu_s} \frac{\partial \theta_s}{\partial z}) \Delta z + q_H + q_L \\
& - V_b \frac{\partial}{\partial t} [(1-\phi) \rho_R U_R + \phi (\rho_w S_w U_w + \rho_o S_o U_o + \rho_s S_s U_s)] = 0
\end{aligned} \tag{4-65}$$

q_H and q_L in the above equation are defined as the following:

$$q_H = \Sigma \rho_k q_k H_k \tag{4-66}$$

$$q_L = - K_T A_z \frac{\partial T}{\partial z} \tag{4-67}$$

q_L and K_T represent the heat losses to the surrounding environment and the thermal conductivity of the surrounding area.

The following first and second order spatial differential equations are employed to discretize the governing equations:

$$\frac{\partial f}{\partial x} \approx \frac{f_{i+1} - f_{i-1}}{2\Delta x} \quad (4-68)$$

$$\frac{\partial}{\partial x} \left(g \frac{\partial f}{\partial x} \right) \approx \frac{g_{i+1/2}(f_{i+1} - f_i) + g_{i-1/2}(f_{i-1} - f_i)}{\Delta x^2} = \Delta x(g\Delta x(f)) \quad (4-69)$$

The forward finite difference equation for the time function is written as below:

$$\frac{\partial f}{\partial t} \approx \frac{f^{n+1} - f^n}{\Delta t} = \frac{\delta f}{\Delta t} \quad (4-70)$$

After applying FDM method for mass and energy balances of oil, water, and steam phases, the following relationships are obtained as given:

$$\begin{aligned} \frac{V_b}{\Delta t} \left[\phi^{n+1} \left[\rho_w^{n+1} \delta S_w + S_w^n \rho_{wk} \alpha_w \delta p - S_w^n \rho_{wk} \beta_w \delta T + \rho_s^{n+1} \delta S_s + S_s^n \frac{d\rho_g}{dT} \delta T \right] + (\rho_w^n S_w^n + \rho_s^n S_s^n) \phi_0 C_R \delta p \right] = \\ \Delta(T_H \Delta(\delta p)) + \Delta(T_H \Delta p^n) - \Delta(T_{hw} \Delta p_{cw}) + \Delta(T_{hs} \Delta p_{cs}) - \Delta(T_{ho} \rho_o g \Delta z) - \Delta(T_{hw} \rho_w g \Delta z) - \Delta(T_{hs} \rho_s g \Delta z) \end{aligned} \quad (4-71)$$

$$\frac{V_b}{\Delta t} \left[\phi^{n+1} \left[\rho_o^{n+1} (-\delta S_w - \delta S_g) + (1 - S_w^n - S_s^n) \rho_{ok} \alpha_o \delta p - (1 - S_w^n - S_s^n) \rho_{ok} \beta_o \delta T \right] + \rho_o^n (1 - S_w^n - S_s^n) \phi_0 C_R \delta p \right] = \Delta(T_o \Delta(\delta p)) + \Delta(T_o (\Delta p^n - \rho_o g \Delta z)) \quad (4-72)$$

$$\frac{V_b}{\Delta t} (A_1 + A_2 + A_3 + A_4) = \Delta(T_H \Delta(\delta p)) + \Delta(T_H \Delta p^n) - \Delta(T_{hw} \Delta p_{cw}) + \Delta(T_{hs} \Delta p_{cs}) - \Delta(T_{ho} \rho_o g \Delta z) - \Delta(T_{hw} \rho_w g \Delta z) - \Delta(T_{hs} \rho_s g \Delta z) \quad (4-73)$$

where A_1 , A_2 , A_3 and A_4 are defined as:

$$A_1 = U_w^{n+1} \left[\phi^{n+1} \left[\rho_w^{n+1} \delta S_w + S_w^n \rho_{wk} \alpha_w \delta p - S_w^n \rho_{wk} \beta_w \delta T \right] + \rho_w^n S_w^n \phi_0 C_R \delta p \right] + (\phi \rho_w S_w)^n C_{pw} \delta T \quad (4-74)$$

$$A_2 = U_o^{n+1} \left[\phi^{n+1} \left[\rho_o^{n+1} (-\delta S_w - \delta S_s) + (1 - S_w^n - S_s^n) \rho_{ok} \alpha_o \delta p - (1 - S_w^n - S_s^n) \rho_{ok} \beta_o \delta T \right] + \rho_o^n (1 - S_w^n - S_s^n) \phi_0 C_R \delta p \right] + (\phi \rho_o (1 - S_w - S_s))^n C_{po} \delta T \quad (4-75)$$

$$A_3 = U_s^{n+1} \left[\phi^{n+1} \left[\rho_s^{n+1} \delta S_s + S_s^n \frac{dp_s}{dT} \delta T \right] + \rho_s^n S_s^n \phi_0 C_R \delta p \right] + (\phi \rho_s S_s)^n \delta U_s \quad (4-76)$$

$$A_4 = (1 - \phi^{n+1}) (\rho C_p)_R \delta T - ((\rho C_p)_R T^n \phi C_R \delta p) \quad (4-77)$$

A_1 represents the thermal energy of the water phase, A_2 is the representative of input, output, and cumulative energy terms (e.g., internal and enthalpy) for the oil phase, A_3 indicates the thermal energy of the steam phase, and A_4 shows the variations in the value of energy of the rock and pore space during a time element.

In addition, the equilibrium equation for the temperature is turned to the following form:

$$\delta T - \frac{dT_s}{dp} \delta p = T_s^n - T^n \quad (4-78)$$

All of the above equations are written for the matrix part in a fractured system. Thus, similar equations (Three mass balance equations and one energy balance equation) should be written for the fracture domain. Following this statement, there are 8 main relationships and 8 unknown variables such as T and P in matrix, T and P in fracture, and fluid saturations in both matrix and fracture. The matrix equations for matrix or fracture part can be given as:

$$C_{11} \cdot \delta S_s + C_{12} \cdot \delta S_w + C_{13} \cdot \delta T + C_{14} \cdot \delta p = \Delta((T_w + T_s)\Delta(\delta p)) + R_1 \quad (4-79)$$

$$C_{21} \cdot \delta S_s + C_{22} \cdot \delta S_w + C_{23} \cdot \delta T + C_{24} \cdot \delta p = \Delta(T_o \Delta(\delta p)) + R_2 \quad (4-80)$$

$$C_{31} \cdot \delta S_s + C_{32} \cdot \delta S_w + C_{33} \cdot \delta T + C_{34} \cdot \delta p = \Delta(T_H \Delta(\delta p)) + R_3 \quad (4-81)$$

$$C_{41} \cdot \delta S_s + C_{42} \cdot \delta S_w + C_{43} \cdot \delta T + C_{44} \cdot \delta p = R_4 \quad (4-82)$$

The coefficients of the above equations are determined as follows:

$$C_{11} = \frac{V_b}{\Delta t} (\phi^{n+1} \rho_s^{n+1}) \quad (4-83)$$

$$C_{12} = \frac{V_b}{\Delta t} (\phi^{n+1} \rho_w^{n+1}) \quad (4-84)$$

$$C_{13} = \frac{V_b}{\Delta t} (\phi^{n+1} (-S_w^n \rho_{wk} \beta_w + S_s^n \frac{d\rho_s}{dT})) \quad (4-85)$$

$$C_{41} = 0 \quad (4-86)$$

The matrix of the coefficients and variables is written as given below:

$$\begin{bmatrix} C_{11} & C_{12} & C_{13} & C_{14} \\ C_{21} & C_{22} & C_{23} & C_{24} \\ C_{31} & C_{32} & C_{33} & C_{34} \\ C_{41} & C_{42} & C_{43} & C_{44} \end{bmatrix} \begin{bmatrix} \delta S_s \\ \delta S_w \\ \delta T \\ \delta p \end{bmatrix} = \begin{bmatrix} 1 & 0 & 0 & 0 \\ 0 & 1 & 0 & 0 \\ 0 & 0 & 1 & 0 \\ 0 & 0 & 0 & 1 \end{bmatrix} \begin{bmatrix} Y_1 \\ Y_2 \\ Y_3 \\ 0 \end{bmatrix} + \begin{bmatrix} R_1 \\ R_2 \\ R_3 \\ R_4 \end{bmatrix} \quad (4-87)$$

Thus, the matrix is simplified as follows:

$$CX = IY + R \quad (4-88)$$

In this stage, the numerical method through the Gaussian Elimination Algorithm (GEA) is utilized to solve the final equation. This technique lowers the error percentage and probability of divergence. After employing the GEA, the last equation changes to the following equation:

$$\begin{bmatrix} 1 & C'_{12} & C'_{13} & C'_{14} \\ 0 & 1 & C'_{23} & C'_{24} \\ 0 & 0 & 0 & C'_{34} \\ 0 & 0 & 0 & C'_{44} \end{bmatrix} \begin{bmatrix} \delta S_s \\ \delta S_w \\ \delta T \\ \delta p \end{bmatrix} = \begin{bmatrix} B_{11} & 0 & 0 & 0 \\ B_{21} & B_{22} & 0 & 0 \\ B_{31} & B_{32} & B_{33} & 0 \\ B_{41} & B_{42} & B_{43} & 1 \end{bmatrix} \begin{bmatrix} Y_1 \\ Y_2 \\ Y_3 \\ 0 \end{bmatrix} + \begin{bmatrix} R'_1 \\ R'_2 \\ R'_3 \\ R'_4 \end{bmatrix} \quad (4-89)$$

$$C'X = IY + R' \quad (4-90)$$

δp is determined from the last row of the equations' matrix:

$$C'_{44}\delta p = B_{41}Y_1 + B_{42}Y_2 + B_{43}Y_3 + R'_4 \quad (4-91)$$

Back substitution technique is employed to calculate δT , δS_s and δS_w :

$$\delta T + C'_{34}\delta p = B_{31}Y_1 + B_{32}Y_2 + B_{33}Y_3 + R'_3 \quad (4-92)$$

$$\delta S_s + C'_{12}\delta S_w + C'_{13}\delta T + C'_{14}\delta p = B_{11}Y_1 + R'_1 \quad (4-93)$$

$$\delta S_w + C'_{23} \delta T + C'_{24} \delta p = B_{21} Y_1 + B_{22} Y_2 + R'_2 \quad (4-94)$$

The solution procedure followed can be summarized as the following: First, one particular pressure and one temperature are estimated for the first node; then, the fluid and rock characteristics are computed by using the auxiliary equations and the coefficients of equations' matrix are determined. The matrix is solved via Gaussian elimination technique. If the calculated pressure and temperature satisfy the pressure and temperature conditions then, they will be admitted as pressure and temperature of the first node and this procedure repeats for the all nodes in the control volume. Otherwise, that pressure and temperature will be the base for the next guess for the first node, and this iteration is repeated until the pressure and temperature conditions are satisfied. Computation will continue until the certain time specified for modeling.

4.4.3 Validation of of the Results

As for each grid block, the output temperature is guessed in the simulation runs, it is necessary to check the accuracy of the computations using components' enthalpies in the energy balance equation. The mass conservation law for all components contributed in steamflooding is also employed in order to examine the appropriateness of the numerical modeling runs in terms of mass balance equation. It is important to note here that the outputs attained from the modeling phase are required to be compared with the real field data available in the literature in order to assess the precision of the model developed.

4.5 Results and Discussion

Numerical modeling of steamflooding in NFCRs was investigated in this study in order to examine performance of the process for VO recovery. The physical model considered in this simulation study is Cartesian. The governing equations in terms of pressure, temperature, and oil saturation for matrix and fracture parts were solved using the MATLABTM software. Several simulation runs were conducted here. In the numerical modeling program, reservoir

properties (e.g., porosities of matrix and fracture, effective permeabilities and dimensions) and fluid properties such as viscosity, density, and surface tension are the input data. Employing single porosity-single permeability fractured model, important parameters such as *RF*, oil saturation, and *CSOR* were determined for various reservoirs and process conditions. The results obtained from the numerical simulation are depicted in Figures 4-5 to 4-13. In addition, the experimental and field pilot data are taken from the literature in order to test the validity of the numerical modeling carried out in this chapter (US-OTA, 1978; Sahuquet and Ferrier, 1982; Chierici *et al.* 1985; Chu, 1985; Couderc *et al.* 1990; Sahuquet *et al.* 1990; Nakamura *et al.* 1995; Yortsos, 1995; Ono, 1997; Snell and Close, 1999; Snell *et al.* 2000; Dehghani and Ehrlich, 1998 and 2001; Mollaei and Maini 2007a & b; van Heel, 2008; Barge *et al.* 2009; Ashrafi *et al.* 2011; Souraki *et al.* 2011; Brown *et al.* 2011; Gross *et al.* 2011; Hoadley *et al.* 2011; Meddaugh *et al.* 2011; Olsen *et al.* 2011; Osterloh *et al.* 2011; Tang *et al.* 2011).

4.5.1 Effect of Matrix Permeability

The change in average oil saturation with the amount of steam injected per pore volume is presented in Figure 4-6 for matrix permeability ranging from 4 to 90 mD when fracture permeability is equal to 5 D. According to Figure 4-6, the average oil saturation during steamflooding lowers as the steam injection rate or pore volume injected increases. It also implies that the higher the matrix permeability in VO NFCRs the higher the oil recovery (lower residual oil saturation) for the same amount of steam injected into the reservoir. It is known based on the Darcy's law that high permeable matrix part maintain better fluid flow and communication between the injection and production wells. In fact, VO NFCRs with higher matrix permeabilities are considered as better candidates for steamflooding.

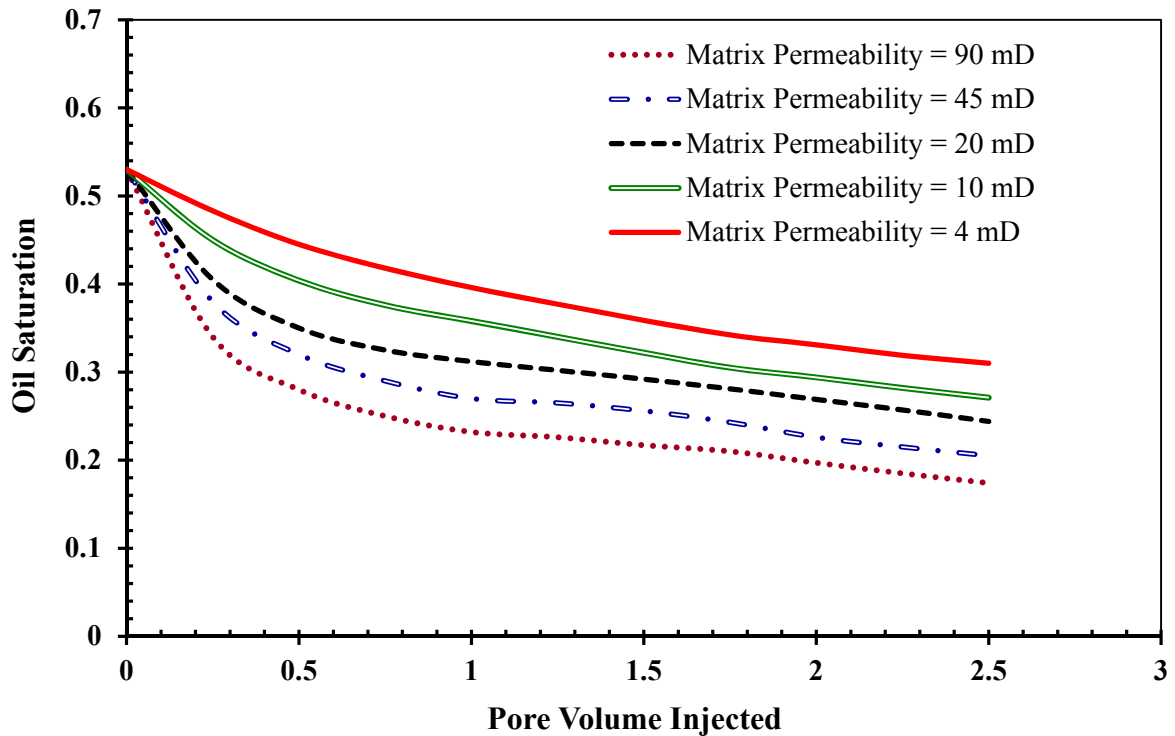


Figure 4-6: Average oil saturation during steamflooding vs. PV in fractured reservoirs for different matrix permeabilities; fracture permeability (K_f) = 5 D.

4.5.2 Effect of Fracture Aperture

Figure 4-7 shows oil recovery prior to breakthrough versus pore volume of steam injected in the reservoir at various fracture apertures (0.5 to 2.0 mm). The production histories were obtained for a reservoir that has a matrix with permeability of 20 mD. As shown in Figure 4-7, oil recovery rate decreases slightly with increase in the fracture aperture (e.g., higher fracture permeability). The oil recovery here is not significantly decreased confirming the fact that the fracture systems in the reservoir do not contain significant amount of the oil and the main role of fractures is acting as conduits to pass the oil from the matrix, which holds most of the oil (normally > 97%), into the production well. Clearly, the presence of fracture or/and higher fracture permeability leads to a higher production rate if the area containing

fractures is invaded by the steam flow. For the case studied here, a decrease of about 18% in recovery rate was observed when the fracture aperture changed from 0.5–2 mm.

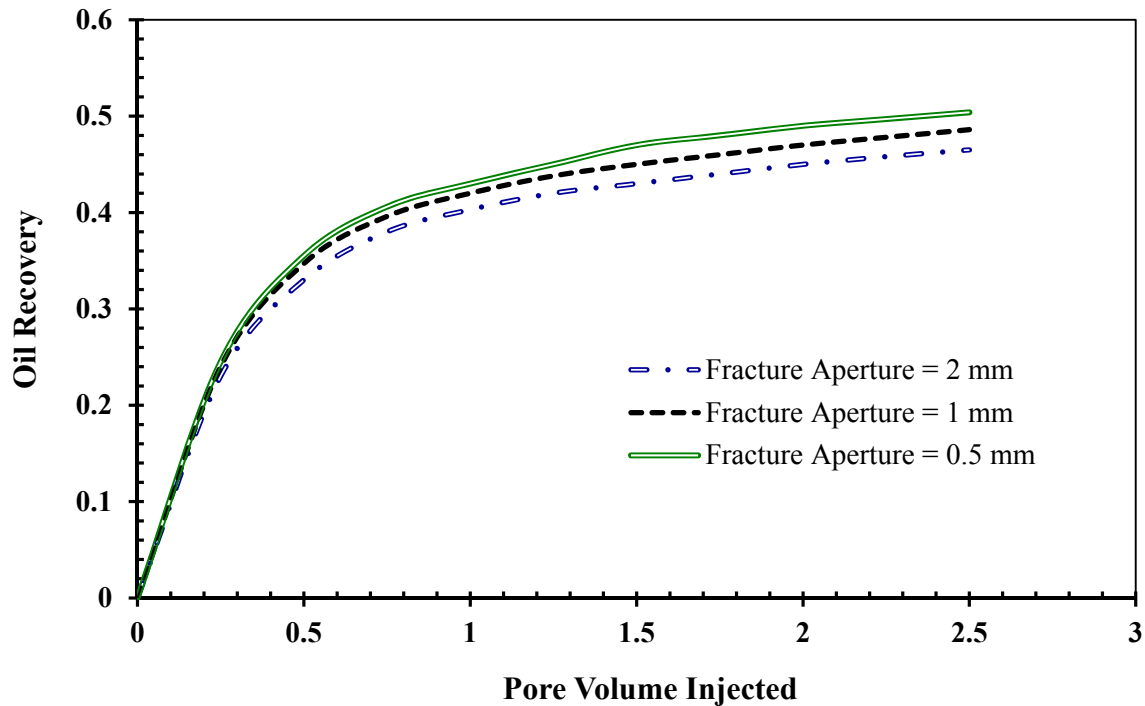


Figure 4-7: Effect of fracture aperture on oil recovery before breakthrough during steamflooding; Matrix permeability (K_m) = 20 mD.

4.5.3 Effect of Matrix Size

Effect of matrix block size on RF in NFCRs is shown in Figure 4-8. To investigate the impact of matrix dimensions, square matrix blocks with different sizes varying between 1 to 20 ft were chosen in the MATLABTM code of the numerical modeling. For the same amount of steam injected into the reservoir, the larger the matrix block size the greater the oil recovery as larger matrix blocks contain more oil. Having matrix blocks with large size indicates the high density of fractures in the form of connected or disconnected networks that cause early breakthrough, resulting in lower steamflooding performance. This statement clearly conveys the message that intensely fractured systems generally experience a lower RF at breakthrough time during the injection process. Based on the interaction of important

independent variables involved in the steamflooding technique, a maximum RF for a given steam injected stream is attainable at a certain combination of fracture density, matrix block size, and matrix permeability. Well understanding of steamflooding physics can help to determine this maximum point through an optimization technique with technical considerations.

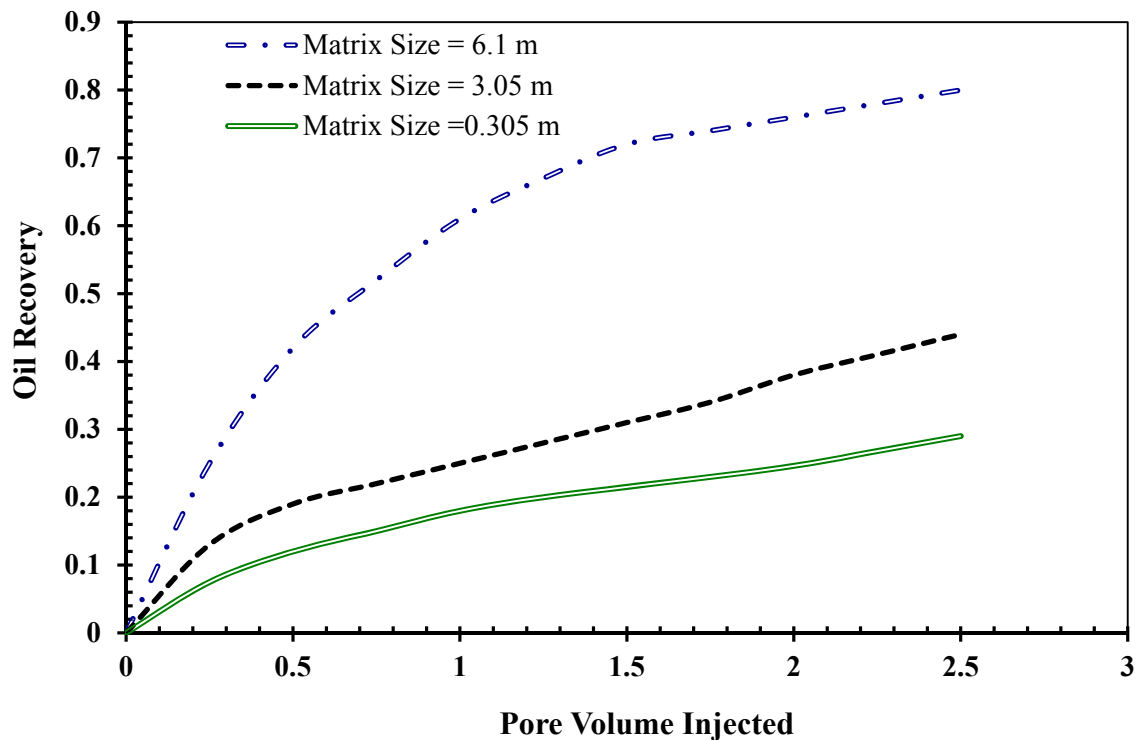


Figure 4-8: Effect of matrix size on oil production during steamflooding.

4.5.4 Effect of Injection Rate

The oil recovery in terms of the amount of steam injected (PV) into the reservoir for different injection rates ranging from 100 to 1000 b/d is given in Figure 4-9. The highest oil recovery was attained when the steam injection rate has the lowest value. This is due to the fact that, the higher steam injection rate provides higher chance of steam early breakthrough that leads to larger area not swept by the steam phase. Hence, higher amounts of oil would be left in the reservoir due to occurrence of flow instabilities under higher steam rates with greater

extents of pressures. It can be simply concluded that more contribution of gravity drainage, lower system pressures, weaker effects of advective flow instabilities, and better volumetric sweep efficiency at lower steam injection rates enhance the heat, momentum, and mass transfer during steamflooding process and consequently higher RF s are obtained. However, at low rate condition it may take a longer time (higher operational expenses) to reach that high amount of oil recovery. Thus, there is a trade-off between achieving higher ultimate RF or higher the production rate over a reasonable time period. In this case, it is beneficial to optimize the process parameters such as pressure and rate of steam injection in order to minimize the duration of the operation in the form of lower operational expenses and also to maximize the profit.

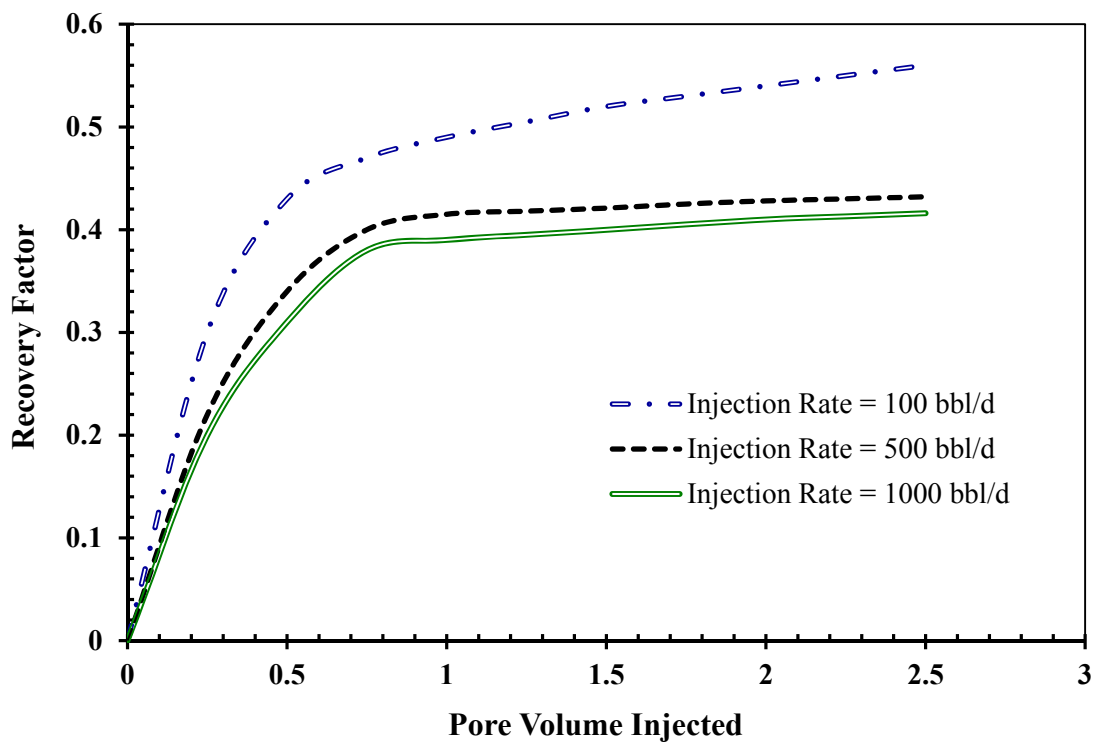


Figure 4-9: Recovery factor vs. PV of injected steam for different injection rates.

4.5.5 Effect of Formation Thickness

The effect of pay zone thickness on incremental *SOR* for fractured and non-fracture reservoirs is shown in Figure 4-10; while, the steam injection rate is set on 2000 b/d. In addition, well spacing and fracture permeability are 8 acers and 20 D in these simulation runs, respectively. Based on Figure 4-10, as the pay zone thickness increases up to a certain value, a sharp decline in the amount of *SOR* occurs. However, the curves for *SOR* become flat after that specific thickness. For the same pay zone thickness, NFCRs are less thermal efficient than homogenous reservoirs, meaning higher incremental *SORs* for the fractured reservoirs are achieved due to early breakthrough. It should be noted here that the variation trend of *SOR* with respect to the formation thickness is the same for both types of VO reservoir systems investigated in this study. Figures 4-10 also indicates that the VO reservoirs with thickness greater than 10 m are appropriate for the steamflooding technology as an acceptable *SOR* of less than 4 is obtained during the production process.

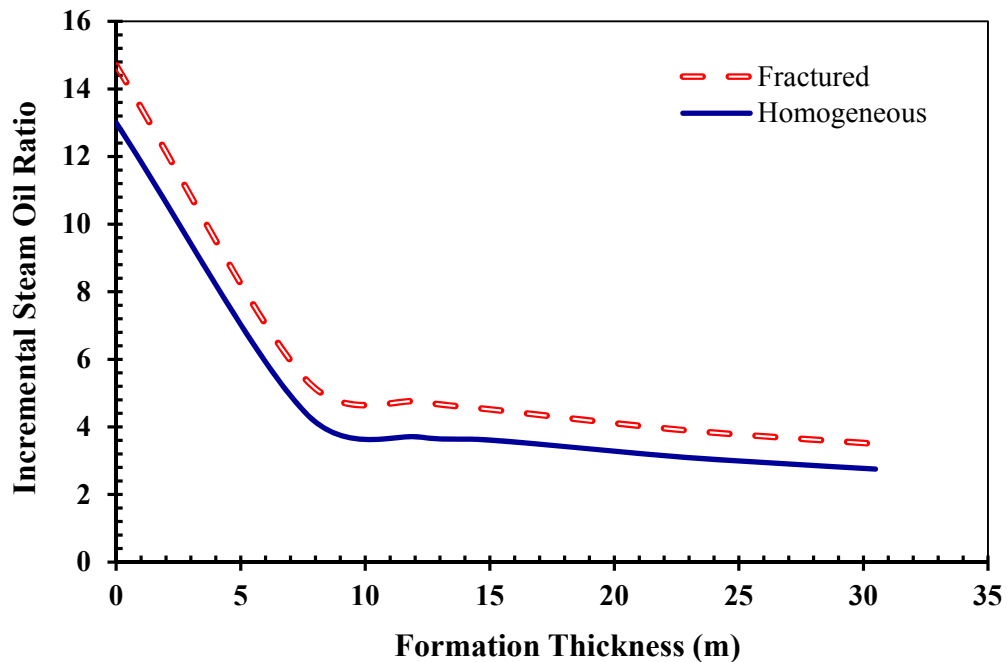


Figure 4-10: Effect of formation thickness on *SOR* for fractured and homogeneous systems [Injection rate = 2000b/d, area = 8 acers, and fracture permeability = 20 D].

4.5.6 Effect of Reservoir Porosity

Figure 4-11 presents the influence of initial oil saturation on cumulative oil production. To perform such an investigation, a porosity range of 20 to 40% was used in the simulation runs. As expected, if the matrix porosity increases, the *RF* improves, as well. The main reason for this increase in oil production is that higher matrix porosity is a good indicator of greater value of oil saturation that exhibits the presence of a richer formation. The similar effects of formation porosity on steamflooding performance in terms of qualitative findings are expected to be observed for oil sands and unconsolidated sandstone oil reservoirs and VO fractured reservoirs as *RF* during steamflooding increases with an increase in pore space for all types of oil reservoirs.

In order to validate the numerical modeling outputs, physical properties of fluids and petrophysical characteristics of real field cases such as Lacq Superieur (France), Ikiztepe (Turkey), Emeraude (Congo) and Yates (USA) oil fields, and experimental systems (e.g., [Mollaei and Maini \(2007\)](#) and [Souraki et al. \(2011\)](#)) are considered as input data for the simulation runs. Having the same conditions for the real projects and this mathematical modeling study, the comparison of the results obtained from the numerical modeling and the real field data is also depicted in Figure 4-11. As it is clear from Figure 4-11, an acceptable match is observed between the predicted and real field results as the maximum absolute error percentage is lower than 6%. More information about the real field data can be found in [Shafiei \(2013\)](#) and [Shafie et al. \(2013\)](#).

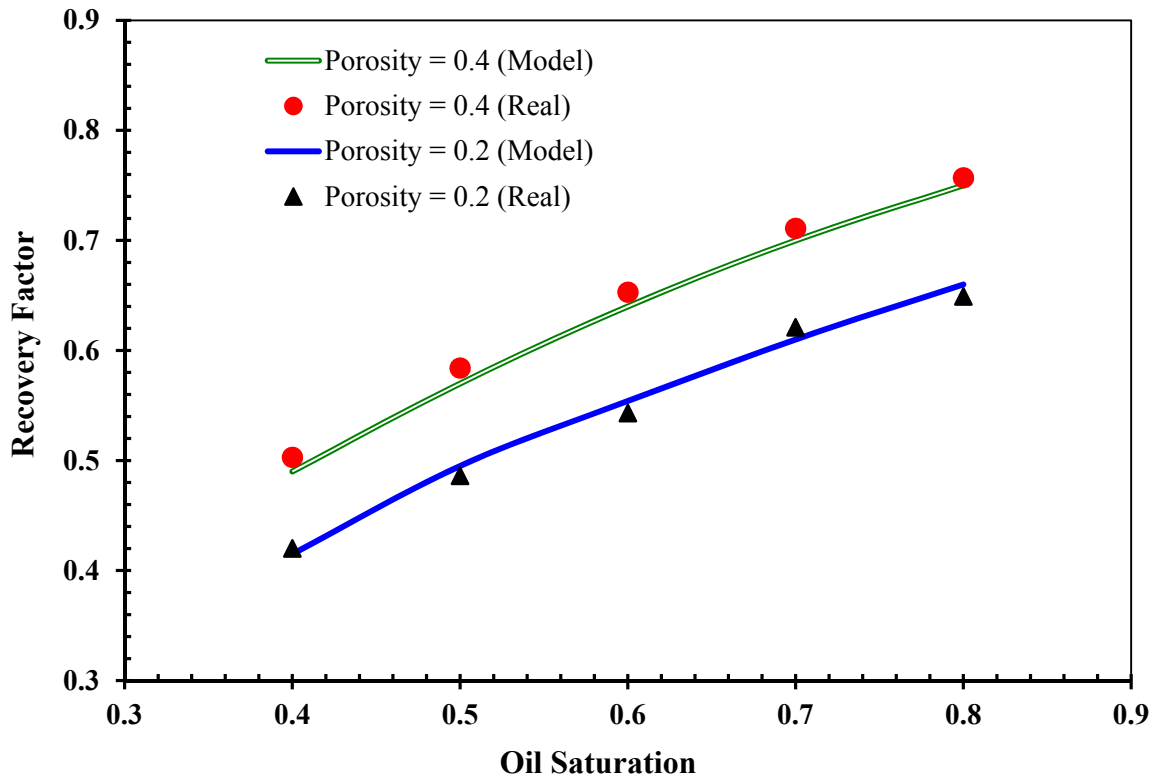
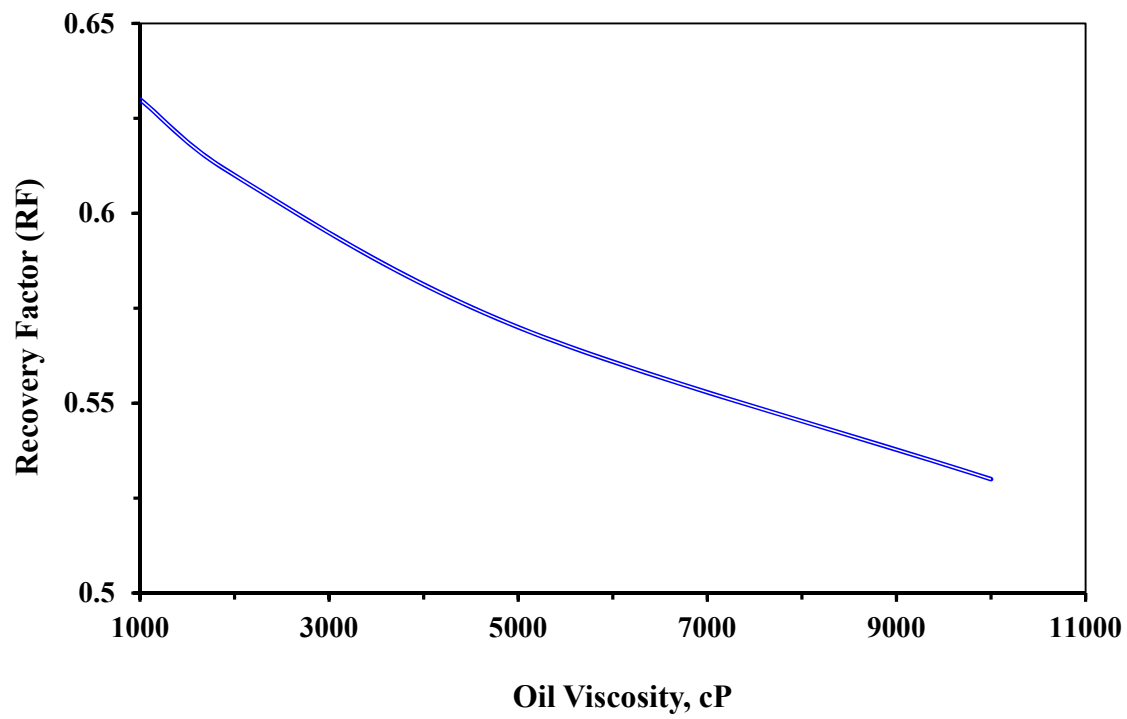


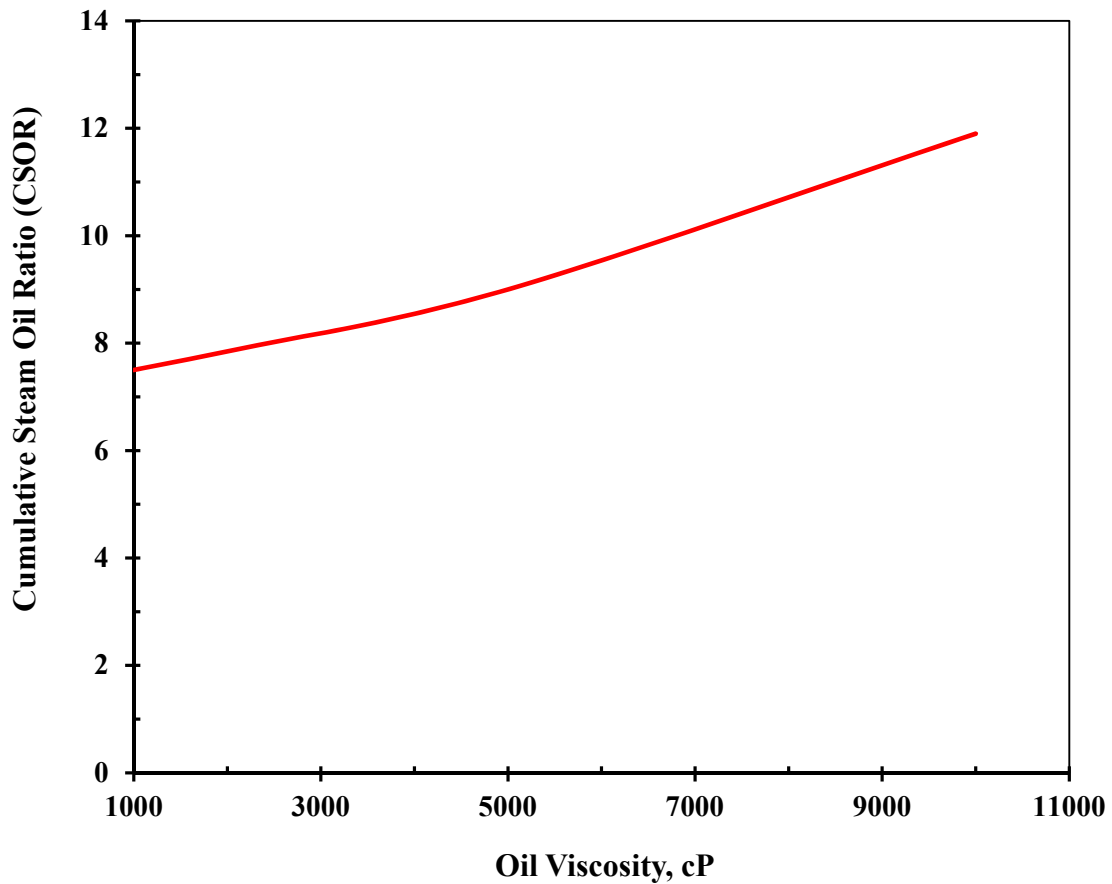
Figure 4-11: Effect of oil saturation on recovery factor for different porosity values.

4.5.7 Effect of Oil Viscosity

A parametric sensitivity analysis in terms of oil viscosity was conducted in order to investigate the effect of oil viscosity on steamflooding performance such as *CSOR* and *RF*. The oil samples with viscosities of 1000, 2000, and 5000 cP were examined in this numerical modeling. The steam injection rate, matrix permeability, fracture permeability, porosity, oil saturation are: 2000 bbl/d, 20 mD, 20 D, 0.25, 0.75, respectively. Figure 4-12 demonstrates this impact for three different viscosities. As expected, higher viscosity lowers the efficiency of steamflooding as greater magnitudes of *CSOR* and lower *RF* values are attained. On the other hand, a lower amount of steam is required when the reservoir contains less viscous oil. Thus, lower magnitude of steam or *CSOR* is observed in the production stream.



(a)



(b)

Figure 4-12: Steamflooding performance versus oil viscosity; a) Recovery Factor, b) Cumulative Steam Oil Ratio

4.5.8 Fractured Versus Unfractured Systems

Cumulative steam injected into the reservoir versus time for homogeneous and fractured systems is depicted in Figure 4-13; where steam injection rate of 2000 b/d, well spacing of 8 Acers, and fracture permeability of 20 D was used in the simulation run. As one can see from Figure 4-13, cumulative steam injected into a fractured reservoir is about 10% higher than that into a homogeneous reservoir if other parameters remain unchanged. This means

that the thermal efficiency of VO NFCRs is lower than homogeneous reservoirs as expected and their steam requirement would be higher, as well.

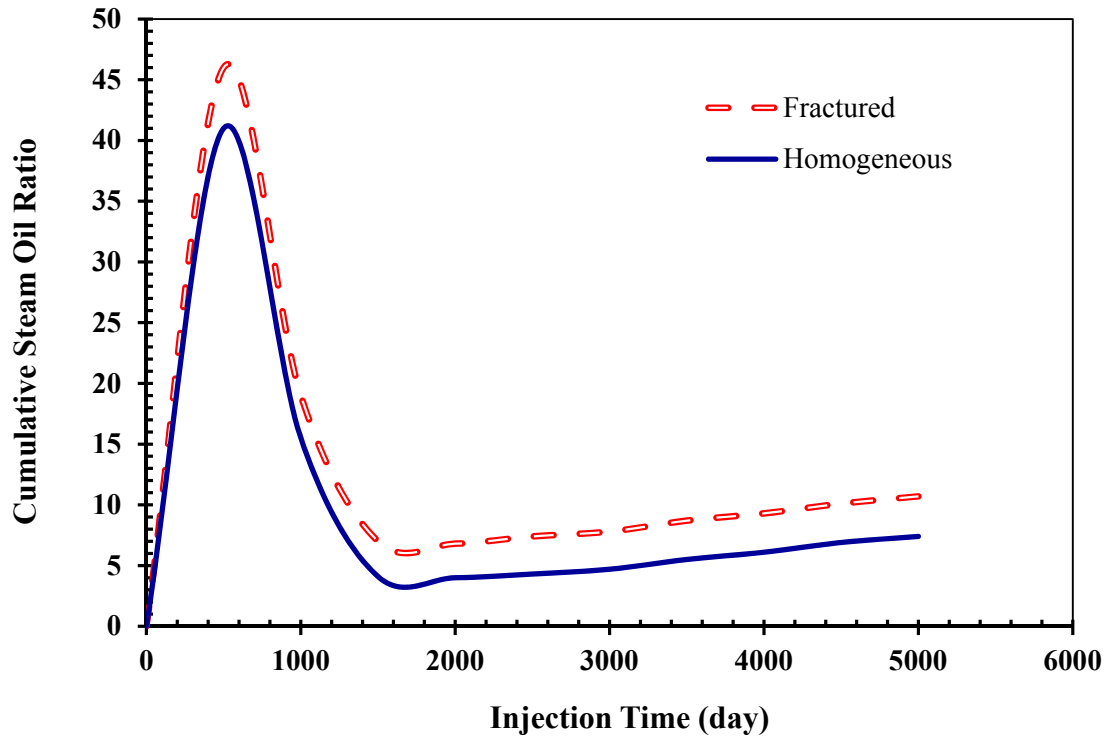


Figure 4-13: CSOR vs. time for homogeneous and fractured reservoirs; Injection rate = 2000 b/d, area = 8 acers, fracture permeability = 20 D.

Figure 4-14 shows oil production rate versus the time for fractured and non-fractured reservoirs under steamflooding with steam injection rate of 2000 b/d, well spacing of 8 Acers, and fracture permeability of 20 D. For the same period of steam injection, the oil production rate in the fractured reservoir is about 10% higher than that in non-fractured reservoir, reflecting the fracture part plays an important role in maintaining an effective interaction between the matrix and itself. In this case, presence of fracture enhances the vertical permeability, resulting in acceleration of the oil production rate. In addition, communication of matrix and fracture media created a pressure difference that acts as a

driving force for oil to flow toward the producing well as long as oil with reduced viscosity exist in the fracture.

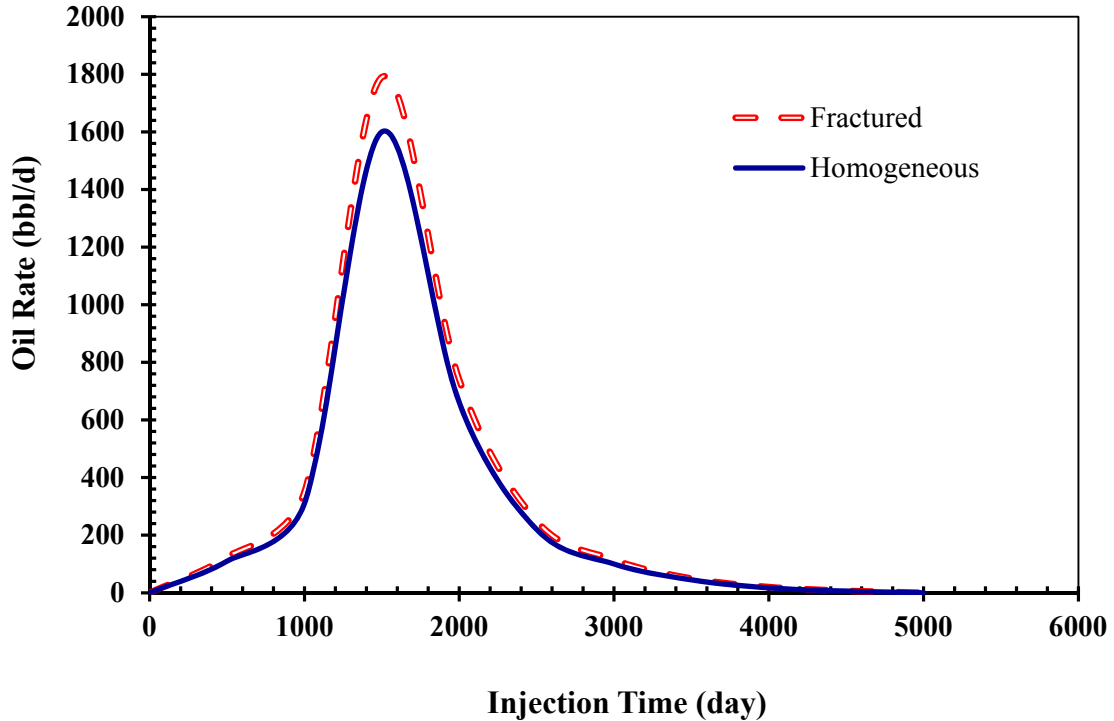


Figure 4-14: Variation of production rate for fractured and unfractured systems under steamflooding; Injection rate = 2000 b/d, area = 8 Acres, and fracture permeability = 20 D.

Based on the parametric sensitivity analysis presented in Figures 4-6 through 4-14 and results from Analysis of Variance (ANOVA) technique, matrix size and overall permeability that considers both matrix and fracture parts affect mostly the target variables such as *CSOR* and *RF* in this study.

According to Figures 4-6 to 4-14 and match between experimental and predicted results, it is proved that independently gridding of the matrix and fracture media is an appropriate way to solve energy and mass conservation equations. In this numerical modeling, matrix block size is directly related to the thermal swelling and capillary imbibitions. The solution technique proposed here assumes steam injection in both fractures and oil production from fractures and matrix. It can be concluded here that the most important recovery mechanisms involved

in the steamflooding of VO NFCRs are thermal swelling and capillary imbibition. These mechanisms strongly depend on the properties of fluids (oil/steam) within the matrix blocks and fracture part, and also characteristics of the matrix medium. Thus, the solution methodology is able to predict the fluids transfer from the matrix into the fracture and vice versa in an accurate manner. For such a numerical modeling scheme, careful calculation of petrophysical properties of the reservoir along with capillary pressure is required.

As mentioned earlier, production behaviour of VO fractured reservoirs in terms of *RF* and *CSOR* during steamflooding process was simulated using a mathematical method. The results were validated based on the experience from field steamflooding projects and also experimental physical-model tests. The developed model appears to be a fairly precise tool to evaluate steamflooding projects. In other words, the proposed numerical model is a proper technique for assessment of important parameters such as *CSOR*, instantaneous heat losses, temperature profile, and saturation distribution during the injection process. It is expected that engineers find the mathematical model developed in this study as an acceptable, quick, and useful technique when performance forecast of steamflooding in fractured reservoirs is targeted, provided that the physical properties of fluids and characteristics of the reservoir rocks are available.

4.6 Limitations

The numerical modeling study suffers from some limitations as listed in the text below:

In the model, fractures with constant size along the length are considered, while variable fracture aperture seems to be more realistic. In addition, apertures with various size distributions should be taken into account to simulate real field cases

To obtain more accurate simulation results, the relative permeability should be obtained through experimental work, while the current study employs functions that are based on theory.

Thermal properties are strongly dependent on the type of formation rocks and need to be determined for each particular case based on some experimental data, while these parameters were taken from other studies for this numerical mathematical investigation.

Further efforts should be made to obtain petrophysical characteristics of the fracture part. Also, fluid flow regimes and transport phenomena in fractures require more comprehensive studies to capture the profiles of temperature and saturation with higher accuracy.

4.7 Concluding Remarks

Steamflooding in VO NFCRs was investigated in a comprehensive manner using a 3-D numerical modeling which led to the following main conclusions:

The following conclusions resulted from conducting comprehensive numerical modeling and simulations on vertical well steamflooding in VO NFCRs:

- A new numerical model for steamflooding in NFCRs was developed using a single-porosity/single-permeability modeling technique through solving separate governing mass, momentum and energy equations for the matrix and fractures, simultaneously. Production rate and cumulative steam to oil ratio in fractured systems were successfully simulated with an acceptable accuracy.
- The proposed numerical model considers complex mechanisms such as imbibitions, interaction between matrix and fracture, heat transfer between various phases contributed in steamflooding, and time dependence of production rate and heat transfer.
- The matrix blocks with smaller size lead to improved (more rapid) heat transfer between oil and steam, resulting in higher oil production rate and lower cumulative steam to oil ratio.
- Increase in matrix permeability enhances the imbibition process that results in a higher oil production rate and recovery factor.

- Heat capacity of the fracture is directly proportional to fracture porosity such that fractures with higher porosity increase the heat transfer into the matrix, leading to lower oil viscosity and consequently higher production rates.
- An increase in steam injection rate causes a higher volume of reservoir exposed to the heat in a shorter time period, leading to greater oil mobilization and improved oil recovery (Not higher ultimate *RF*).
- The most effective parameters in steam injection include matrix block dimensions and overall permeability.
- The average oil saturation during steamflooding decreases as the steam injection rate or pore volume injected increases. This means that higher the matrix permeability in VO NFCRs, the higher the oil recovery (lower residual oil saturation) for the same amount of steam injected into the reservoir. It is known based on Darcy's law that a high permeability matrix maintains better fluid flow and communication between the injection and production wells. In fact, VO NFCRs with higher matrix permeabilities are considered as better candidates for steamflooding.
- Oil recovery increases only slightly with increase in the fracture aperture (e.g., higher fracture permeability). The oil recovery here is not significantly increased, confirming the fact that the fracture systems in the reservoir do not contain significant amount of the oil. The main role of fractures is acting as conduits to pass the oil from the matrix, which holds most of the oil (normally > 97%), into the production well. Clearly, the presence of fractures or/and higher fracture permeability leads to a higher production rate if the area containing fractures is effectively invaded by the steam flow.
- For the same amount of steam injected into the reservoir, the larger the matrix block size the greater the oil recovery as larger matrix blocks contain more oil. Having matrix blocks with small size indicates the high density of fractures in the form of connected or disconnected networks that cause early breakthrough, resulting in lower

- steamflooding performance. This means that the intensely fractured systems generally experience a lower RF at breakthrough time during the injection process. Based on the interaction of important independent variables involved in the steamflooding technique, a maximum RF for a given quality steam injection stream is attainable at a certain combination of fracture density, matrix block size, and matrix permeability. Better understanding of steamflooding physics can help to determine this maximum point through an optimization technique with technical and economic considerations.
- The highest oil recovery was attained when the steam injection rate had the lowest value. A higher steam injection rate provides higher potential of early breakthrough that leads to larger area not swept by the steam phase. Hence, higher amounts of oil would be left in the reservoir due to occurrence of flow instabilities under higher steam rates with greater pressures. The higher the contribution of gravity drainage, the lower the system pressures, the weaker the effects of advective flow instabilities, and the better the volumetric sweep efficiency at lower steam injection rates due to the enhancement of the heat, momentum, and mass transfer during steamflooding process which leads to a higher RF . However, at low rate conditions it may take a longer time (higher OPEX) to reach that high amount of oil recovery. Thus, there is a trade-off between achieving higher ultimate RF or higher the production rate over a reasonable time period. In this case, it is beneficial to optimize the process parameters such as pressure and rate of steam injection in order to minimize the duration of the operation in the form of lower operational expenses and also to maximize the profit. Also, shorter time means lower heat losses to unproductive surrounding strata.
 - As the pay zone thickness increases up to a certain value, a sharp decline in the amount of SOR occurs. However, the curves for SOR become almost flat after that specific thickness. For the same pay zone thickness, NFCRs are less thermally efficient than homogenous reservoirs, meaning higher incremental $SORs$ for the

- fractured reservoirs are achieved due to early breakthrough. The VO reservoirs with thickness greater than 10 m are found to be more appropriate for steamflooding as an acceptable SOR of less than 4 is obtained during the production process.
- As the matrix porosity increases, the *RF* improves as well. The main reason for this increase in oil production is that higher matrix porosity is a good indicator of a greater value of oil saturation that exhibits the presence of a richer formation. This finding is also valid for other types of VO such as oil sands and unconsolidated sandstone VO reservoirs.
 - Cumulative steam injected into a fractured reservoir is about 10% higher than that into a homogeneous reservoir if other parameters remain unchanged. This means that the thermal efficiency of VO NFCRs is lower than homogeneous reservoirs, as expected, and their steam requirements would be higher, as well.
 - For the same period of steam injection, the oil production rate in the fractured reservoir is about 10% higher than that in non-fractured reservoir, showing that the fracture part plays an important role in maintaining an effective interaction between the matrix and itself as well as other fractures in a network. In this case, the presence of a fracture enhances the vertical permeability, resulting in acceleration of the oil production rate. In addition, communication of matrix and fracture media create a pressure difference that acts as a driving force for oil to flow toward the producing well as long as oil with reduced viscosity exists in the fracture.
 - Based on the parametric sensitivity analysis from Analysis of Variance (ANOVA) technique, matrix block size and overall permeability that considers both matrix and fracture parts most affect target variables such as *CSOR* and *RF* in this study.
 - Experimental and predicted results matched very well indicating that independently gridding of the matrix and fracture media is an appropriate method to solve the momentum, energy and mass conservation equations.

- The most important recovery mechanisms involved in the steamflooding of VO NFCRs are thermal swelling and capillary imbibition. These mechanisms strongly depend on the properties of fluids (oil/steam) within the matrix blocks and fracture part, and also characteristics of the matrix.

Nomenclature

Acronyms and Abbreviations

2-D/3-D	=	Two or Three Dimensional
ANOVA	=	Analysis of Variance
<i>CSOR</i>	=	Cumulative Steam to Oil Ratio
FDM	=	Finite Difference Method
GEA	=	Gaussian Elimination Algorithm
NFCR	=	Naturally Fractured Carbonate Reservoir
NFR	=	Naturally Fractured Reservoir
OOIP	=	Oil Originally In Place
PDE	=	Partial Differential Equation
<i>RF</i>	=	Recovery Factor
SD	=	Steam Drive
SF	=	Steam Flooding
VO	=	Viscous Oil

Symbols

<i>A</i>	=	Block area, (ft ²) or (m ²)
<i>b</i>	=	Fracture aperture, (mm)
<i>c_k</i>	=	Heat capacity of phase k, (J/g.mol.K)
<i>C_R</i>	=	Compressibility of reservoir rock, (psi ⁻¹) or (Pa ⁻¹)
<i>dx</i>	=	Differential in x direction, (ft) or (m)
<i>dy</i>	=	Differential in y direction, (ft) or (m)

dz	=	Differential in z direction , (ft) or (m)
g	=	gravitational force, (ft/s ²) or (m/s ²)
H	=	Height, (ft) or (m)
H_o	=	Oil enthalpy, (Btu/lb) or (J/kg)
H_s	=	Steam enthalpy, (Btu/lb) or (J/kg)
H_w	=	Water enthalpy, (Btu/lb) or (J/kg)
I	=	Liquid film shape factor through the fracture
K	=	Absolute permeability, (Darcy) or (m ²)
K_{eff}	=	Effective fracture permeability, (% or fraction)
k_H	=	Heat capacity of rock reservoir, (Btu/°F.ft.day) or (J/°C.m.s)
k_{Hover}	=	Heat capacity of the overburden, (Btu/°F.ft.day) or (J/°C.m.s)
K_m	=	Matrix permeability, (mD) or (D)
k_{ro}	=	Relative permeability of oil
k_{rs}	=	Relative permeability of steam
k_{rw}	=	Relative permeability of water
K_T	=	Thermal conductivity, (Btu/°F.ft.day) or (J/°C.m.s)
P	=	Pressure, (psi) or (Pa)
\bar{p}	=	Average pressure, (psi) or (Pa)
p_c	=	Capillary pressure, (psi) or (Pa)
p_k	=	Pressure of phase k, (psi) or (Pa)
p_o	=	Oil pressure, (psi) or (Pa)
p_s	=	Gas pressure , (psi) or (Pa)

p_{wf}	=	Well pressure, (psi) or (Pa)
q	=	Volumetric flow, (ft ³ /day) or (m ³ /s)
q_c	=	Steam condensation rate, (bbl/day) or (m ³ /s)
q_H	=	Heat flow rate, (Btu/day) or (J/s)
q_k	=	Flow rate of fluid of k , (bbl/day) or (m ³ /s)
q_L	=	Heat loss, (Btu/day) or (J/s)
R	=	Aspect ratio of the liquid film flow in fracture
S_k	=	Saturation of the phase k
S_o	=	Oil saturation
S_s	=	Steam saturation
S_w	=	Water saturation
S_{we}	=	Effective wetting saturation
S_{wi}	=	Initial wetting phase saturation
S_{wr}	=	Residual wetting phase saturation
T	=	Temperature, (°F) or (°C)
t	=	Time, (s) or (day)
T_R	=	Temperature of rock reservoir, (°F) or (°C)
T_{REF}	=	Reference Temperature, (°F) or (°C)
T_s	=	Steam temperature, (°F) or (°C)
u_k	=	Velocity of the phase k , (ft/s) or (m/s)
U	=	Internal energy, (Btu/lb) or (J/kg)
U_o	=	Internal energy of oil, (Btu/lb) or (J/kg)

U_R	=	Internal energy of rock reservoir, (Btu/lb) or (J/kg)
U_S	=	Internal energy of steam, (Btu/lb) or (J/kg)
U_W	=	Internal energy of water, (Btu/lb) or (J/kg)
V_b	=	Block volume, (ft ³) or (m ³)
W_m	=	Width of the matrix, (ft) or (m)

Greek Letters

ϕ	=	Porosity (% or fraction)
ϕ_1	=	Primary porosity (% or fraction)
$\phi_{1,eff}$	=	Effective primary porosity (% or fraction)
ϕ_2	=	Secondary porosity (% or fraction)
ϕ_f	=	Fracture porosity (% or fraction)
ϕ_m	=	Matrix porosity (% or fraction)
ϕ_o	=	Initial porosity (% or fraction)
Δ	=	Difference operator
Δt	=	Time interval
Δx	=	Mesh size in the horizontal direction
∇Z_k	=	Pressure gradient of phase k
α	=	Dip angle
α_o	=	Isothermal compressibility of oil, (psi) or (Pa)
β_o	=	Thermal expansion coefficient of oil, (°F ⁻¹) or (°C ⁻¹)
δ	=	Time difference operator ($\delta T = T^{n+1} - T^n$)
μ_g	=	Gas viscosity, (cP) or (Pa.s)

μ_o	=	Oil viscosity,(cP) or (Pa.s)
μ_w	=	Water viscosity ,(cP) or (Pa.s)
ρ_k	=	Density of phase k, (lbm/ft ³) or (kg/m ³)
$\bar{\rho}$	=	Average density, (lbm/ft ³) or (kg/m ³)
ρ_g	=	Gas density, (lbm/ft ³) or (kg/m ³)
ρ_o	=	Oil density, (lbm/ft ³) or (kg/m ³)
ρ_R	=	Rock density, (lbm/ft ³) or (kg/m ³)
ρ_{REF}	=	Reference density, (lbm/ft ³) or (kg/m ³)
ρ_w	=	Water density, (lbm/ft ³) or (kg/m ³)

Metric Conversion Factors

$^{\circ}\text{F}$	=	$(^{\circ}\text{C}\times 1.8) + 32$
1 barrel oil	=	0.159 m ³
1 psi	=	6.8947 kPa
1 psi/ft	=	22.62 kPa/m or 22.62 MPa/km
1cP	=	0.001 Pa.s
1 Btu	=	950.500 J
1 ft	=	0.3048 m
1 ft ³	=	0.0283 m ³
1 lb	=	0.45359 kg
1 Darcy	=	9.869 E-13 m ²

Chapter 5

A New Smart Screening Tool for Evaluation of Steamflooding Performance in Naturally Fractured Carbonate Heavy Oil Reservoirs³

5.1 Abstract

Appropriate production method selection for Viscous Oil (e.g., Heavy Oil, Extra Heavy Oil, and Bitumen) Naturally Fractured Carbonate Reservoirs (VO NFCRs) mostly depends on the quality of the fluid and reservoir properties. Selection of a particular production method for a reservoir is generally evaluated through an exhaustive experimental, field pilot, and mathematical modeling approach. In absence of robust and quick predictive tools, using connectionist techniques for performance prediction of a certain production method can be a valuable asset. In this study, a new screening tool is developed based on Artificial Neural Networks (ANN) optimized with Particle Swarm Optimization (PSO) to assess the performance of steamflooding in VO NFCRs. As expected, Recovery Factor (*RF*) and Cumulative Steam to Oil Ratio (*CSOR*) during steamflooding are highly affected by the magnitudes of oil saturation and viscosity. The developed PSO-ANN model, conventional ANN and statistical correlations were examined by using real field data. Comparison of the predictions and real field data implies the superiority of the proposed PSO-ANN model with an absolute average error percentage $< 6.5\%$, a determination coefficient (R^2) > 0.98 , and Mean Squared Error (MSE) < 0.06 in contrast with conventional ANN model and also correlations for prediction of *RF* and *CSOR*. This indicates a great potential for application of hybrid PSO-ANN models to screen viscous oil carbonate reservoirs for steamflooding.

³ Materials presented in this chapter are contributed to the following publication:

Shafiei, A., Zendejboudi, S. and Dusseault, M.B. and Chatzis, I. 2013. A New Screening Tool for Evaluation of Steamflooding Performance in Naturally Fractured Carbonate Heavy Oil Reservoirs, *Fuel*, Vol. **108**, pp. 502–514.

5.2 Introduction

Different types of carbonate rocks, mostly naturally fractured (NFCRs), make up about 30% of the sedimentary rocks on the earth's surface. Also, they contain around 40–45% of the world's present proven conventional oil reservoirs (Roehl and Choquette, 1985) and above 20% of the world's Viscous Oil (VO) endowment (including Heavy Oil, Extra Heavy Oil, and Bitumen) (Briggs *et al.*, 1988; Meyer *et al.*, 2007; Dusseault and Shafiei, 2011; GEA, 2012). The presence of VO in NFCRs is reported in many countries such as Iran, Canada, the USA, Brazil, Congo, Turkey, Egypt, Russia, Oman, Kuwait, Saudi Arabia, China, India, Cuba, Italy, France, Algeria, Libya, Congo, and Mexico.

According to the U.S. Energy Information Administration (EIA) in their 2011 International Energy Outlook report, the global demand for liquid fossil fuels will increase from 85.7×10^6 b/d in 2008 to 112.2×10^6 b/d in 2035 mainly due to the growing world population and development of industrial sectors. This increase in global energy demand will be led especially by rapidly developing economies such as China and India (EIA, 2011). It is also expected that by 2035, VO will make up for about 17% of the daily world oil production and this includes VO from NFCRs, as well. The current contribution of VO to the world daily oil production is about $9\text{--}10 \times 10^6$ b/d almost all from sandstones (EIA, 2011). Large VO deposits in carbonates (Figure 5-1) are far less common and of lower porosity (usually $\phi < 20\%$) than VO sandstones; nevertheless, carbonates host about 2×10^9 b VO worldwide.

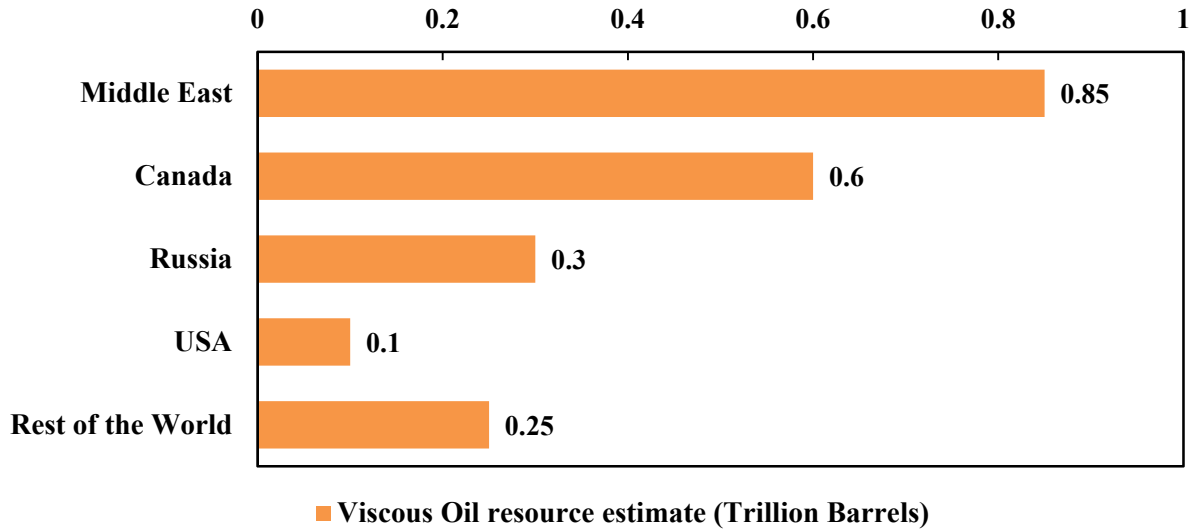


Figure 5-1: Resource estimates and worldwide distribution.

A quick look at the worldwide Enhanced Oil Recovery (EOR) surveys published in the Oil & Gas Journal during the last two decades shows that steam injection is the only commercialized viscosity reduction approach. Over 70% of the current VO production worldwide involves steam injection, and this dominance will continue into the foreseeable future (Taber and Martin, 1997; Oil & Gas Journal, 1996, 1998, 2004, 2006, 2008, 2010).

Technologies required for economical VO production in NFCRs, particularly XHO and bitumen, have major differences compared to conventional oil recovery methods. It is usually necessary to reduce the viscosity; in practice, this can be achieved by heating, diluting, reducing the molecular weight (usually pyrolytically), or a combination of these methods. Despite the immense resource size, a full-field commercial thermal production operation in VO NFCRs has not yet been reported. The application of thermal processes to VO NFCRs remains limited to very few vertical well steamflooding and cyclic steam stimulation field pilots in Canada, France, Italy, Turkey, China, the USA, Egypt, Syria, Congo, Kuwait, and Saudi Arabia. To date, only primary cold production (e.g., Oman, Iran, Iraq, Kuwait, Saudi Arabia, Turkey, France, Italy, Cuba, Brazil, China, Russia, Congo, and

Mexico) and CO₂ flooding (e.g., Turkey) have achieved some commercial success in accessing this immense energy resource.

Several experimental and mathematical models are reported for performance prediction of steamflooding process in VO sandstones, and some of these are briefly mentioned here. For instance, a 2-D model was introduced by [Shutler \(1970\)](#) to simulate oil, water, and gas phases in VO sandstones considering both heat conduction and convection terms while determining the temperature profile. [Abdalla and Coats \(1971\)](#) were among the very first to solve a set of governing differential equations through a numerical method for steam injection into VO sandstones. They employed an implicit pressure-explicit saturation technique to obtain the pressure and saturation distributions of all three phases, assuming the fluids are compressible. Based on the results of their study, a model was developed to determine the rate of steam condensation to allow heat transfer calculations to be made. A few years later, [Coats *et al.* \(1974\)](#) developed a 3-D model to conduct numerical simulations to model steam injection in VO sandstones, including mass and energy balance in both the reservoir and the overburden. Their solution did not require an iterative procedure while considering the condensation term, reducing computational effort in an era when execution time was a critically limiting factor.

Mass and heat transfer amongst phases involved in multi-component flow was studied by [Ferrer and Farouq Ali \(1977\)](#) using a numerical model to simulate three phases and 3-D flow during steam injection into VO sandstones. They concluded that compositional constraints approach represents a good procedure for practical simulation purposes, and this formed the initial efforts toward development of what are now known as compositional models, using an assumption that thermodynamic equilibrium exists throughout the domain. This assumption allows ignoring kinetic processes such as time-dependent phase evolution, and if the time constant of the local process is small compared to the execution time for the model, a compositional assumption is a reasonable approximation. [Coats \(1978\)](#) simulated distillation and solution gas phenomena in steamflooding through an implicit model. All the terms related to solution gas, distillation and capillary pressure were included in the model to

investigate the variations of saturation and compositions during steamflooding, again assuming thermodynamic equilibrium.

Most of the models proposed for steam injection to date rely on similar assumptions but differ in solution methods they offer, computational effort they require, and the degrees of freedom that they can handle. Besides modeling studies, systematic experimental work has been performed by a number of researchers such as [Sumnu *et al.* \(1996\)](#), [Mollaei *et al.* \(2007\)](#), and [Souraki *et al.* \(2011\)](#). These laboratory investigations mostly focus on parametric sensitivity analysis approaches to capture the major aspects of the steamflooding process. Of course, given the complexity of steamflooding, most experimental research has limitations in terms of applicability to real field conditions, and this is particularly so for heterogeneous and dual or triple porosity systems such as VO NFCRs. For example, the laboratory simulations were generally based on relatively homogeneous specimens of fairly small dimensions, with no possibility of a reasonable representation of a naturally fractured reservoir case. This is not a criticism; it is a noting of the great difficulty in being faithful to scale issues in the case of fractured reservoirs, to the mixed boundary conditions that exist in the field, to different scales of heterogeneity, and so on. In contrast to high-porosity sandstones, where laboratory tests at reasonable scale can be carried out and scaled to the field, experimentation on naturally fractured limestone cannot be easily scaled, nor is modeling straight-forward (especially in geomechanics), and the integration of laboratory data with modeling to predict full-field behavior for steam injection projects remains a challenge to all of us.

Another difficulty is that numerical methods generally face divergence issues with respect to fluid-fluid and fluid-medium interfaces. Sharp fronts (shock waves such as a sharp condensation front or a sharp jump in saturation) are notoriously difficult to stabilize numerically, and mixed convective-conductive solutions may suffer from oscillations and other types of instabilities, especially in coupled problems ([Yin *et al.*, 2009](#)). In any case, mathematical solutions to differential equations are of themselves insufficient for screening of assets with respect to production methods. During the last two decades, advances in

computer technology have improved the application of screening criteria via application of artificial intelligence (AI) techniques in the oil industry. The value of these programs of course depends on the accuracy of the input data used (Parkinson *et al.*, 1990; Parkinson *et al.*, 1991; Elemo and Elmahtab, 1993; Alvarado *et al.*, 2002; EL-M Shokir *et al.*, 2002; Ibatulin *et al.*, 2002). Neural networks concepts have been used extensively in geosciences and geophysics as well as in reservoir engineering for prediction of reservoir properties (Aminzadeh and De Groot, 2006). This method is capable of modeling complex inputs and outputs relationships from a process with high uncertainty and to identify reasonable patterns in the data.

This chapter introduces a predictive “screening tool” based on Artificial Neural Networks (ANN) combined with Particle Swarm Optimization (PSO) for performance prediction of steamflooding in VO NFCRs. PSO is applied to obtain the initial weights of the parameters involved in the ANN model. To avoid early convergence and permutation issues, the parameters required for construction of a network model are selected carefully. Training and testing phases are conducted based on statistical analyses to estimate *RF* and *CSOR*, and the accuracy of the proposed PSO-ANN model is also assessed using experimental and field data. The PSO-ANN model’s outputs are compared with the results obtained from the Back Propagation-Artificial Neural Network (BP-ANN) and regression correlations for *RF* and *CSOR*. The developed model has the capability to be used for analysis of reservoir performance and also for technical feasibility assessments before field implementation of steamflooding in VO NFCRs.

5.3 Steamflooding

Steamflooding (SF) is a process in which steam is injected continuously and a zone (chamber) around the injection well is heated to the saturation temperature of the steam. This chamber expands toward the production well, thermally reducing the oil viscosity, and displacing it in a manner referred to as volumetric sweep (Figure 5-2). Almost all of the commercial thermal projects are based on oil production from VO sandstones rather than VO NFCRs. Commercialized thermal HO production methods using vertical well steamflooding

(SF) or steam drive (SD) with several different well patterns have been practiced since 1952 in California in thicker zones (> 10 m), and almost always for HOs with $\mu < 5000$ cP, since rapid initial communication between the offset wells is achievable only with lower viscosities (unless very tight well spacing is used) (de Haan and van Lookeren, 1969; Farouq Ali, 1974).

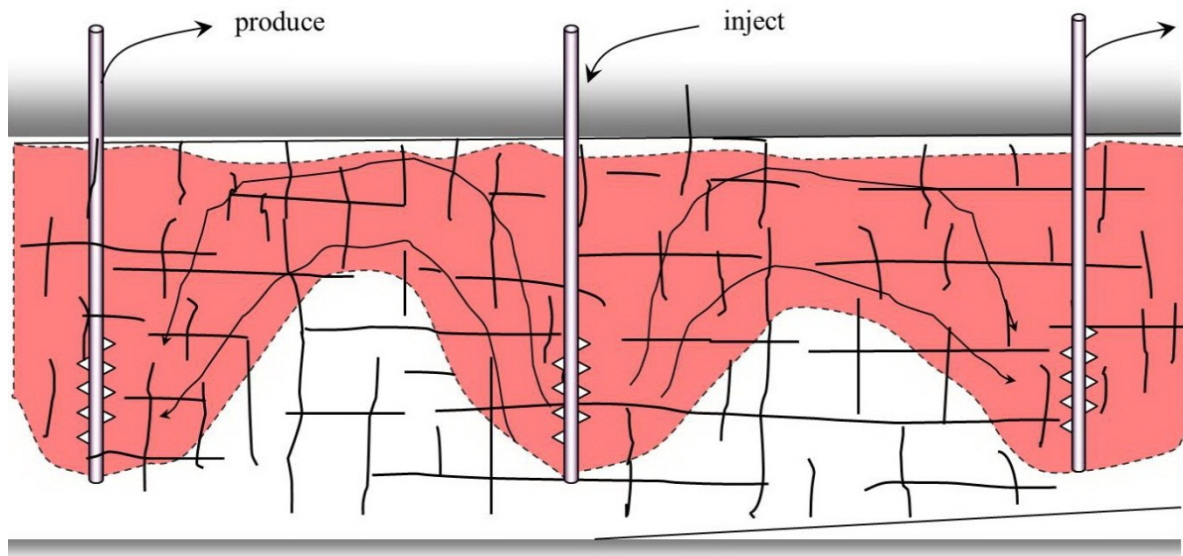


Figure 5-2: Steamflooding in NFCRs (Steam zone is presented in red).

In general, NFCRs are dual or triple porosity systems⁴ with moderate porosity, low permeability matrix, and fractures with low overall porosity but moderate to high fluid transmissivity properties. Limited porosity, low matrix permeability, great depth, and complicated patterns of multiphase flow in vugs and fractures are considered as key barriers to the application of thermal methods in NFCRs. The amount of oil in place in VO sandstones is roughly double of that for VO NFCRs as the porosity ranges are 30% and 10–20% for VO sandstones and VO NFCRs, respectively. Based on this estimate, greater *CSOR*, lower *RF*, and consequently lower profitability, are expected for VO NFCRs.

⁴ Triple porosity here means that void space that exists contiguously at three different characteristic length scales in a rock mass: fractures at the scale of meters, vugular porosity at the scale of cm, and matrix porosity at the scale of mm or less.

5.4 Artificial Neural Network

The mathematical tool known as Artificial Neural Networks or ANNs, has been around for nearly six decades. ANNs were implemented extensively in various fields such as process control, behavior prediction, model recognition, system classification, communication and vision aspects. More recently, ANNs were introduced in geosciences and reservoir engineering to forecast the spatial distribution of parameters where there is a substantial uncertainty typical of spatially irregular geological data (McCulloch and Pitts, 1943; Hagan *et al.*, 1966; Brown and Harris, 1994; Ahmadi *et al.*, 2012; Zendehboudi *et al.*, 2012).

ANNs are “trained” with real field data to address nonlinear and complex problems where mathematical modeling may be too complicated or inappropriate. ANNs use inputs and outputs of a complex system to generate a reliable system model even though the data may be incomplete and less than straightforward in nature. A large number of simple computational components known as neurons are activated to find empirical correlations between the inputs and outputs for the desired process, leading to a correlative model based on real field data (McCulloch and Pitts, 1943; Hagan *et al.*, 1966; Brown and Harris, 1994). Defining the input for a new case then allows the ANN to compute a set of output patterns, providing of course that it has been previously trained with suitable examples.

A typical interconnected ANN may be viewed as a multiple-layer structure. Figure 5-3 shows an input layer, one hidden layer, and one output layer, all appropriately linked, but with a unidirectional flow. The weighting factors for the links must be determined, and this constitutes the ANN training through iterative adjustment of the connection weights until the appropriate precision of the desired output parameters can be estimated with an acceptable precision level. The precision of the ANN model depends on the topology of the input-output representation, as more than one hidden layer can be introduced to generate different calculation patterns and conditional weights. The training seeks to identify the optimum internal patterns for the ANNs, and the analogy to a neuron-axon model of a brain for pattern identification is the origin of the name artificial neural network (McCulloch and Pitts, 1943; Hornik *et al.*, 1990; Garcia-Pedrajas *et al.*, 2003; Vallés, 2006).

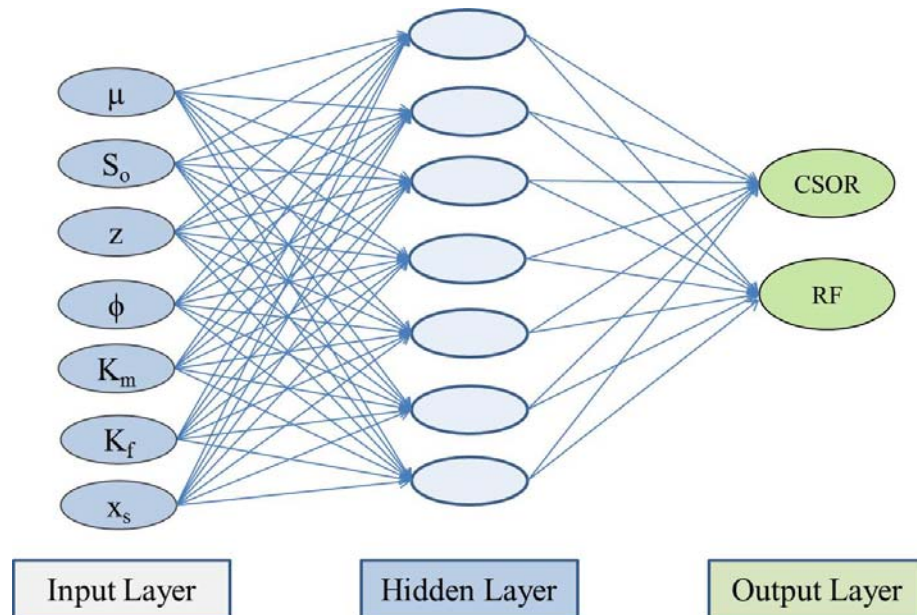


Figure 5-3: A three layer ANN structure used for the purpose of this study.

The numbers of neurons and hidden layers depend on the degree of complexity and nonlinearity of the problem attacked. The input connection to each neuron has a weight, the value of which may be uniform, assigned randomly, or partially pre-determined. These weights are modified throughout the training process using cases where the inputs and outputs are known until the error between the actual outputs and the predicted outputs is minimized (McCulloch and Pitts, 1943; Hagan *et al.*, 1966).

There are a number of different neural network structures, and learning algorithms (e.g., back propagation (BP) and multiple layer perceptron (MLP)) for the ANN technique. The BP method is recognized as one of the most general learning algorithms. The BP technique is employed in the feed-forward ANN. It implies that the neurons are arranged in layers, and convey their signals “forward”, and then the errors are propagated backwards. The BP algorithm includes a training process in which a series of inputs and outputs is provided and the network predicts the outputs based on the randomly assigned initial weights. Then the error (mean squared error) between real field and predicted results is computed. The weights are modified through the training process until the error between the actual output and the

predicted output is minimized. The BP algorithm adjusts the weights using the gradient descent principle where the change in the weight is proportional to the error gradient with a negative sign (Hornick *et al.* 1989; Souto *et al.* 2002; Garcia-Pedrajas *et al.* 2003). The validation set prevents over-fitting of the network by stopping training once MSE in the validation set begins to increase. The performance of the ANN model is finally checked by introducing new and independent datasets to the trained model (Hornick *et al.* 1989; Souto *et al.* 2002; Garcia-Pedrajas *et al.* 2003). Optimizing the weights for the interconnections to each single node to achieve the best architecture for the neural network usually is based on the mean squared error (*MSE*) of the network, defined as:

$$MSE = \frac{1}{2} \sum_{k=1}^G \sum_{j=1}^m [Y_j(k) - T_j(k)]^2 \quad (5-1)$$

where m is the number of output nodes, and G is the number of training examples. $Y_j(k)$ and $T_j(k)$ are the expected output and the actual output, respectively. There are other error norms that may be used such as the sum of linear deviations – unsquared – or even norms with non-integral exponents, but MSE is the most widely used, although it weights outliers very heavily. To obtain a certain number of weights for the connections to give a reasonable ANN model, there must be sufficient data and cases available for the number of neurons chosen, and the problem may be under-determined (not good) or over-determined (not an issue, it just means more training and refinement of weights). In general, some cases are reserved for ANN model verification, although eventually all known cases can be incorporated into the ANN model, and new cases added as they become available, so that the ANN can continue to “learn” in an experiential probabilistic sense.

5.5 Particle Swarm Optimization

Particle Swarm Optimization (PSO) is a population-based optimization method introduced by Eberhard and Kennedy (1995). The PSO technique is currently being employed to solve numerous optimization problems in which a point or a surface in a multi-dimensional parameter space corresponds to the best solution and must be sought. One may view this method as an iterative calculation of the optimum location of a group (swarm) of particles that have a current, a velocity and direction of movement, and can be acted upon by acceleration forces applied to each particle.

The magnitude and direction of the accelerations are the subject of the calculations, and the locations of the particles in the swarm are updated iteratively using the following equations:

$$v^{k+1} = w^k v^k + c_1 r_1 (x_1^k - x^k) + c_2 r_2 (x_g^k - x^k) \quad (5-2)$$

$$x^{k+1} = x^k + \lambda v^{k+1} \quad (5-3)$$

$$w^k = w_{\max} - (w_{\max} - w_{\min}) \left(\frac{k}{\text{Maximum Iterations}} \right) \quad (5-3)$$

where k represents the current iteration, and λ is defined as the limiting factor to express the particles diversity and to assure convergence. c_1 and c_2 are the acceleration coefficients, considering individual experience of particles and interaction between them. v^k and x^k indicate the vectors of real velocity and position, respectively, and r_1 and r_2 are two random variables varying between 0 and 1. w_k is the inertial weight that controls the effect of the earlier velocity on the new velocity vector (a momentum calculation). x_l and x_g are the local best position and global best particle position in the swarm, respectively.

The movement of particles in the multiple parameter space is dictated by their previous individual experiences and the interaction between particles and their neighbors to seek the defined optimal condition. Furthermore, there are defined constraints that must be properly introduced, and this is usually based on a penalty function that “pushes” the particles back into an acceptable solution space, and to do this, a fitness function is defined:

$$F(x) = D(x) + \theta(x) \quad (5-5)$$

Here, $\theta(x)$ is the penalty function that is used to enforce the constraint, and $D(x)$ is the distance value, which is defined mathematically as

$$D(x) = \begin{cases} \varepsilon(x) \\ \sqrt{fn(x)^2 + \varepsilon(x)^2} \end{cases} \quad \text{If } r_f = 0 \quad (5-$$

6)

In the above equation, r_f is defined as the number of feasible solutions divided by the swarm size, where $fn(x)$ and $\varepsilon(x)$ represent the normalized objective cost function and the summation of the average normalized violation in each constraint, respectively. Any number of constraints can be introduced by employing this technique such that unacceptable positions (x) are iteratively corrected and a minimum error value reached. The PSO algorithm is superior to some other minimization techniques such as simulated annealing in that it does not converge on a local minimum in the multiple parameter space, but tends to find the global minimum in most cases that have local and global optima. Clearly, it differs in the convergence rate and structure properties such as number of particles, upon the nature of problems in which the PSO is applied. The work flow of the PSO is presented in Figure 5-4.

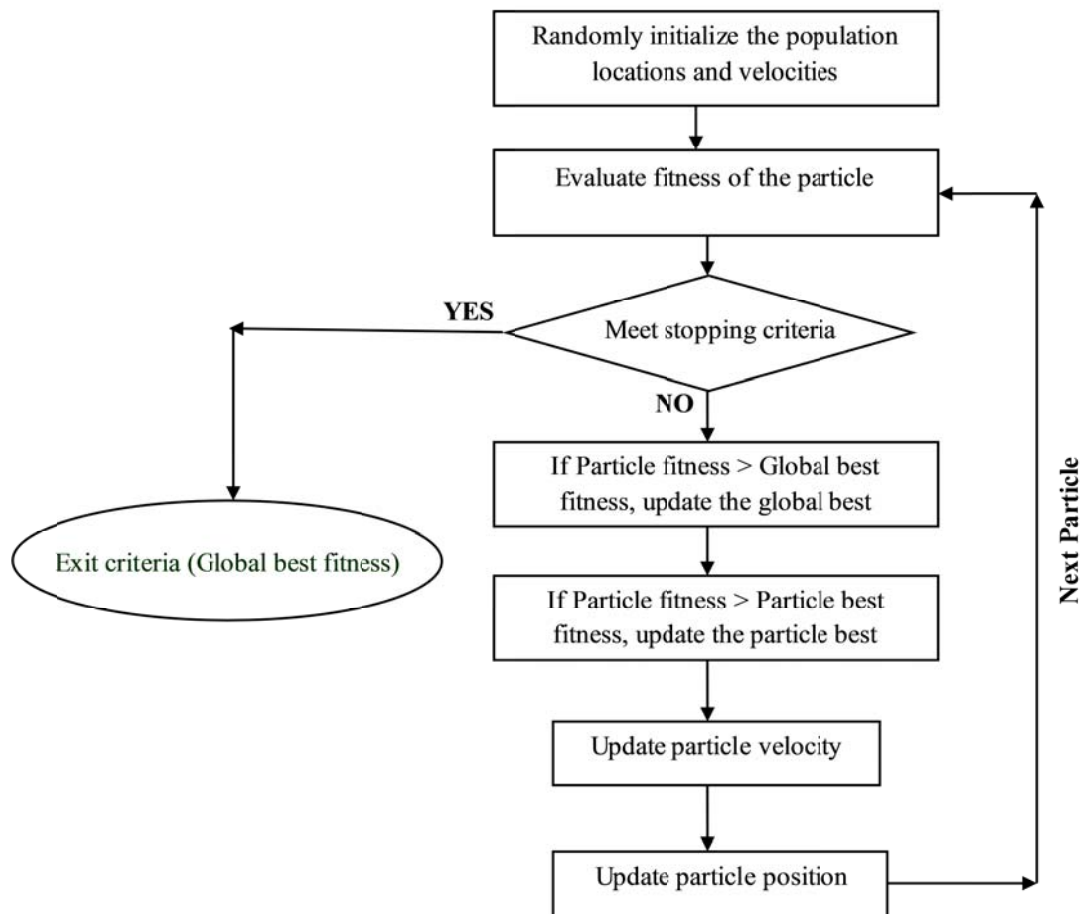


Figure 5-4: Particle Swarm Optimization method work flow.

5.6 ANN Model Development

5.6.1 Selection of Input Variables

Some parameters are so critical to a screening process that without them the task would be impossible (or inadequate). These parameters are defined as “first order” (or “critical”) screening criteria. A “first-order” parameter potentially has a great effect (> 10%) on which technology is chosen and will directly affect the suitability ranking of feasible technologies

during a general screening process or when making performance forecasts for a certain method. For example, initial oil saturation has > 10% “impact” on all thermal processes. Thus, oil saturation, as well as other parameters, is deemed critical and must be taken into account as a first-order screening parameter in any asset evaluation (see [Dusseault, 2012](#)).

First-order parameters may vary from one technology to another. For instance, reservoir depth, *in situ* oil viscosity, net pay thickness, and water/oil saturations are among first-order screening criteria for most VO production methods. However, design and operation of a certain production technique for specific conditions will require assessment of many other factors. For example, thermal conductivity of the overburden will affect decisions, although it is not a first-order screening parameter because although there are differences in thermal conductivity among cases, the range of values is not so large as to make it a “make-or-break” parameter. In early screening phases, only first-order parameters that are related to the geological and lithostratigraphical disposition, fluid and petrophysical properties, and *in situ* conditions are important enough to be considered. Based on steamflooding physics and the statistical investigation carried out by the authors, the crucial variables of VO NFCRs to conduct ANN modeling for *RF* and *CSOR* include *in situ* viscosity, effective porosity, fracture permeability, matrix permeability, reservoir thickness, depth, steam injection rate, steam quality, and initial oil saturation.

5.6.2 Data Collection and Model Evaluation

Most of the data used in construction of the ANN model to estimate *RF* and *CSOR* are collected from field data reported in the literature for steamflooding in VO NFCRs ([Sahuquet and Ferrier, 1982](#); [Nakamura *et al.*, 1995](#); [Ono, 1997](#); [Couderc *et al.*, 1990](#); [Snell and Close, 1999](#); [Snell *et al.*, 2000](#); [Dehghani and Ehrlich, 2001](#); [Barge *et al.*, 2009](#); [Brown *et al.*, 2011](#); [Hoadley *et al.*, 2011](#); [Meddaugh *et al.*, 2011](#); [Osterloh *et al.*, 2011](#); [Gross *et al.*, 2011](#); [Olsen *et al.*, 2011](#)). The important characteristics of SF projects are given in Table 3-2, as well. To examine the validity of the PSO-ANN model and also generalize the results obtained, the database also includes some highly fractured carbonate reservoirs containing light oil and fractured VO sandstones ([Chu, 1985](#); [Dehghani and Ehrlich, 2001](#)). Well-described

experimental studies available in the literature provide the second part of the input data for the ANN system (US-OTA, 1978; Yortsos, 1995; Mollaei and Maini 2007a&b; van Heel, 2008; Ashrafi *et al.*, 2011; Souraki *et al.*, 2011; Tang *et al.*, 2011). It should be noted here that the data employed in this study cover wide ranges of reservoir characteristics and operational conditions.

5.6.3 Range of Parameters

Table 5-1 lists the range of the parameters that are employed to construct the PSO-ANN model.

Table 5-1: Range of parameters to predict *RF* and *CSOR*.

	Property	Min	Max
Input	Depth, z (m)	134	1350
	Matrix porosity, ϕ (Fraction)	0.12	0.35
	Matrix permeability, K_m (mD)	1	400
	Fracture permeability, K_f (D)	10	1000
	Oil viscosity, μ (cP)	6	936
	Initial oil saturation, S_o (Fraction)	0.3	0.9
	Steam quality, x_s (Fraction)	0.3	1
Output	Recovery Factor (<i>RF</i>) (Fraction)	0.4	0.7
	Cumulative steam oil ratio (<i>CSOR</i>)	3.0	10.0

Based on data from field trials of steamflooding in NFCRs available in the public domain, Table 5-1 contains wide ranges of important variables involving in the PSO-ANN, which are relevant to the most of VO NFCRs reported. If a data point is out of the above intervals, the method to run the PSO-ANN modeling remains the same; however, some important factors

(e.g., number of hidden neurons and acceleration coefficients) must be altered in a way that an acceptable agreement is observed.

5.7 Results and Discussion

Accurate estimation of *CSOR* and *RF* is vital in design of an efficient steamflood for heavy oil recovery from NFCRs. Development of a smart technique called PSO-ANN is explained here to predict *CSOR* and *RF* in NFCRs during steamflooding. The hybrid ANN model consisting of three layers (e.g., one input layer, one hidden layer, and one output layer) was trained with a back-propagation network using the Levenberg-Marquardt algorithm (Levenberg, 1944; Marquardt, 1963). Sigmoid and linear transfer functions were also employed in the hidden and output layers, respectively. Particle Swarm Optimization was implemented by minimizing a cost function based on the mean square error (*MSE*). Each initial weight in the network was between -1.0 and 1.0 and every initial particle was set in the range of $[-1, 1]$. For example, the initial and last values of the inertia (ω_{min} and ω_{max}) were 0.4 and 0.5, respectively.

A common question in neural networks is what the sample size of data (or ratio of total data) required to train the network? No simple procedures have been proposed to answer this question. Certainly, it requires adequately large and representative data for the neural network to learn. However, the number of samples (or ratio of samples) for training depends on several parameters such as factor selection and the structure of the neural network model. Once the factor selection and neural network architecture are determined, different sampling sizes are employed to train while the testing phase of the PSO-ANN was being conducted using the rest of the real field data. In general, the percentage of training data to total data is selected between 70 and 80 %. Therefore, about 75% of the data population (38 testing data +105 training data) was chosen for the purpose of network training in this study. The remaining 25% (e.g., 38 data points) was put aside to be used for testing and validating the network's integrity and robustness.

The developed PSO-ANN model was tested with 3, 5, 7, 8, and 10 neurons in the hidden layer. Evaluation of the effectiveness of the ANN model was based on the performance coefficient (R^2), mean square error (MSE), minimum absolute percentage error ($MIPE$), and maximum absolute percentage error ($MAPE$). Table 5-2 shows the results obtained using various numbers of hidden neurons. The precision of the modeling runs was increased by increasing the number of hidden neurons from 3 to 7, but the performance of the PSO-ANN model decreased when the number of hidden neurons exceeded 8. Thus, the optimum number of hidden neurons is taken as 7 to avoid problems of under- or over-determinacy and to reduce computational training time. The model may be updated frequently or adjusted as better input parameters become available for the data in the table, so an efficient training time is a valuable model asset.

Table 5-2: Performance of the PSO-ANN model based on the number of hidden neurons.

Number of hidden neurons	Training				Testing			
	R^2	MSE	$MIPE$ (%)	$MAPE$ (%)	R^2	MSE	$MIPE$ (%)	$MAPE$ (%)
3	0.8652	0.0943	9.2467	14.1567	0.8120	0.1465	10.8441	16.1356
5	0.9127	0.0675	8.9479	11.3829	0.9078	0.0972	10.0012	12.9572
7	0.9799	0.0241	5.3564	7.9546	0.9551	0.0406	6.0352	9.1628
8	0.9275	0.0372	6.1423	9.0024	0.9101	0.0745	6.9408	10.4709
10	0.9478	0.0498	7.9457	11.3471	0.8931	0.0916	8.9876	12.9356

The acceleration constants (c_1 and c_2) in the PSO methodology are related to the stochastic acceleration that forces each particle toward particle best and global best positions. The c_1 constant shows the influence of the global best solution over the particle, while the c_2 constant illustrates how much the particle best solution affects the particle status. Good results were attained when the PSO-ANN model was trained with acceleration constants

between 1.6 and 2.6, and values of 2.2 were found to give the most rapid convergence to an optimum solution. A tendency to divergence above values of 2.2 indicates that the PSO-ANN algorithm becomes unequivocally divergent for elevated acceleration constant values. At the best c_1 and c_2 values of 2.2, R^2 was 0.9789 for the training phase and 0.9087 for the testing phase. Furthermore, the minimum values of MSE , $MIPE$, and $MAPE$ were found for both training and testing phases when c_1 and c_2 were set at 2.2 (Table 5-3).

Table 5-3: Performance of the PSO-ANN model for different values of c_1 and c_2 .

c_1 and c_2	Training				Testing			
	R^2	MSE	$MIPE$ (%)	$MAPE$ (%)	R^2	MSE	$MIPE$ (%)	$MAPE$ (%)
1.6	0.9247	0.0859	9.3069	13.2738	0.8456	0.0968	10.5259	14.7859
1.8	0.9415	0.0798	8.3651	12.4514	0.8681	0.0855	9.6742	13.5475
2.0	0.9523	0.0597	7.4232	11.3517	0.9043	0.0649	8.5342	12.4406
2.2	0.9775	0.0371	5.8768	9.5687	0.9301	0.0451	6.9659	9.4592
2.4	0.9637	0.0414	6.1878	10.0065	0.9015	0.0523	7.4968	11.1221
2.6	0.9552	0.0501	8.0013	11.8577	0.8925	0.0637	9.1761	12.3437

The number of particles in the PSO-ANN model dictates the size of the parameter space covered; Table 5-4 illustrates the impact of number of particles on the performance of the model. The performance of the PSO-ANN algorithm increases with an increase in the number of particles from 15 to 21, although the neural network component did not perform well at particle numbers from 15 to 18 because the small number of particles could not accommodate all the data behavior. At values larger than 21, a decrease in the PSO-ANN performance as a predictor was evident (Table 5-4). The main reason behind this decline is that the space covered in the problem appears to be too wide. Although the decline in

performance after 21 particles is small, as the number of particles rises, the optimization process becomes appreciably slower.

Table 5-4: Effect of number of particles on performance of the PSO-ANN model.

Number of particles	Training				Testing			
	R^2	MSE	$MEAE$ (%)	$MAAE$ (%)	R^2	MSE	$MEAE$ (%)	$MAAE$ (%)
15	0.9532	0.0968	8.9575	13.5858	0.8937	0.0996	10.6581	15.5869
18	0.9685	0.123	10.4672	14.4586	0.8655	0.0972	12.6871	16.4356
20	0.9731	0.0982	7.5422	11.3906	0.9285	0.0873	10.5263	13.4958
21	0.9844	0.0857	5.8651	9.1459	0.9346	0.0828	7.6063	10.4252
22	0.9786	0.0999	7.6735	10.2924	0.9172	0.0996	9.0069	12.2560
25	0.9782	0.1048	7.2888	10.7521	0.9178	0.0998	9.5384	12.1863

The same approach was followed for other variables of the network and the optimal structure for the PSO-ANN algorithm was determined to be:

- a) Number of the layers= 3 including 1 input layer, 1 hidden layer, and 1 output layer
- b) Number of maximum iterations = 450
- c) c_1 and $c_2 = 2.2$
- d) Time interval = 0.0100
- e) Number of particles = 21

Hence, the best ANN architecture is: 7-7-2 (7 input units in one layer, 7 neurons in the hidden layer, and 2 output neurons in one layer).

To evaluate the performance of the PSO-ANN algorithm, predicted and measured $CSOR$ and RF values at training and testing phases for BP-ANN and PSO-ANN models were compared, shown in Figures 5-5 and 5-6 for RF and Figures 5-8 and 5-9 for $CSOR$.

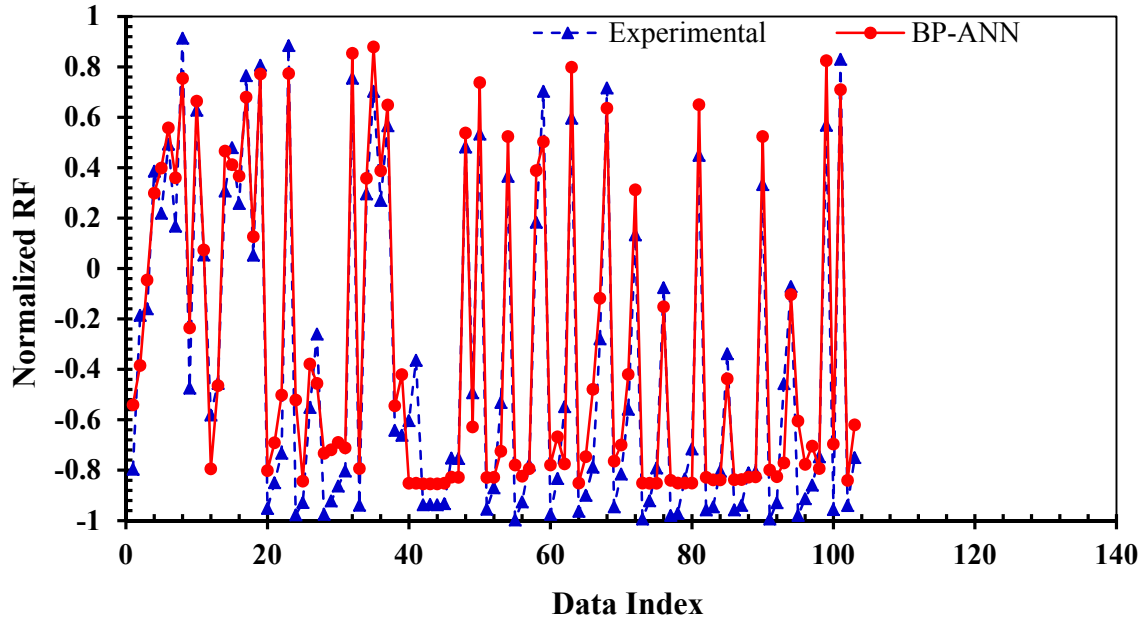
As input and output variables are commonly of various types with different orders of magnitudes, such as initial oil saturation (S_o from 0.3 to 0.9), fracture permeability (K_f from 10 to 1000 mD) and $CSOR$, arithmetic normalization of input and output parameters is used. For example, -1 and 1 are assigned to the minimum and maximum data points and the rest lie within the interval $[-1, 1]$, such that, for example, the following equation is used to normalize the data used for RF in the ANN model:

$$\text{Normalized } RF = \frac{2(RF - RF_{\min})}{(RF_{\max} - RF_{\min})} - 1 \quad (5-7)$$

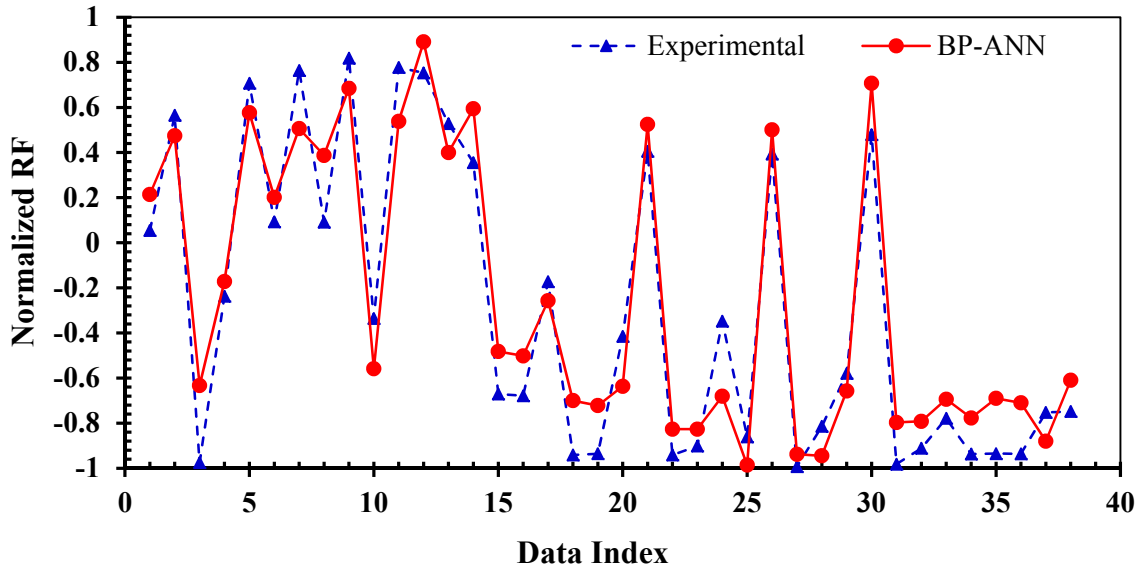
where RF_{\min} and RF_{\max} are the minimum and maximum RF of the data points.

50 generations followed by a BP training procedure was employed to train the PSO-ANN model. The BP training algorithm was run with a learning coefficient and momentum correction factor of 0.75 and 0.0001, respectively.

According to Figures 5-6 and 5-8, a good match is observed between the predicted and measured RF and $CSOR$ for steamflooding in NFCRs for the testing phase conducted in this study. The parameters for RF [$MSE = 0.0623$; $R^2 = 0.9850$] and for $CSOR$ [$MSE = 0.0516$; $R^2 = 0.9877$] obtained using the PSO-ANN approach were compared to RF [$MSE = 0.0941$; $R^2 = 0.9244$] and $CSOR$ [$MSE = 0.1030$; $R^2 = 0.9430$] using the BP-ANN approach. The PSO-ANN model is more accurate in estimation of RF and $CSOR$ than either regression equations or the BP-ANN model (Figures 5-5 and 5-6, Table 5-5).

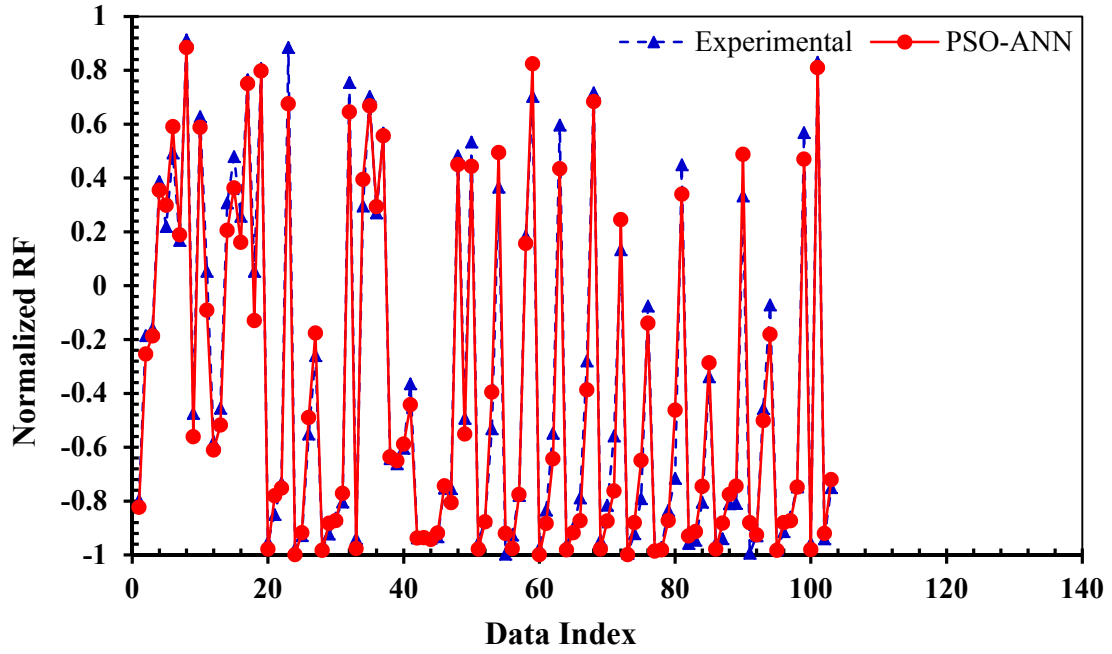


(a) Training

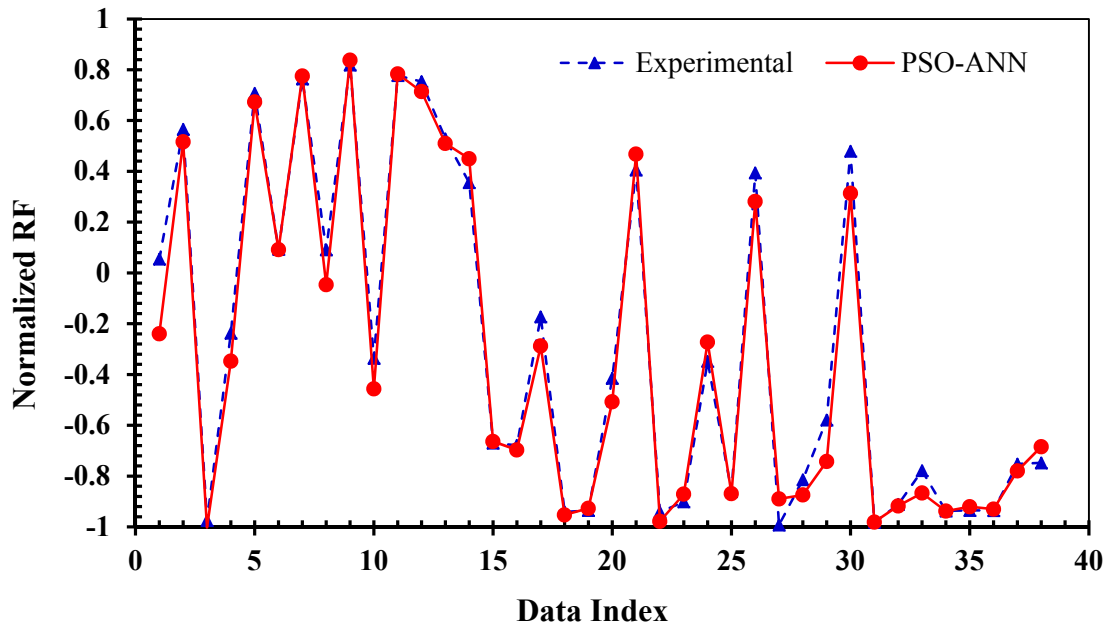


(b) Testing

Figure 5-5: Real field vs. predicted RF based on BP-ANN; a) Training, b) Testing.

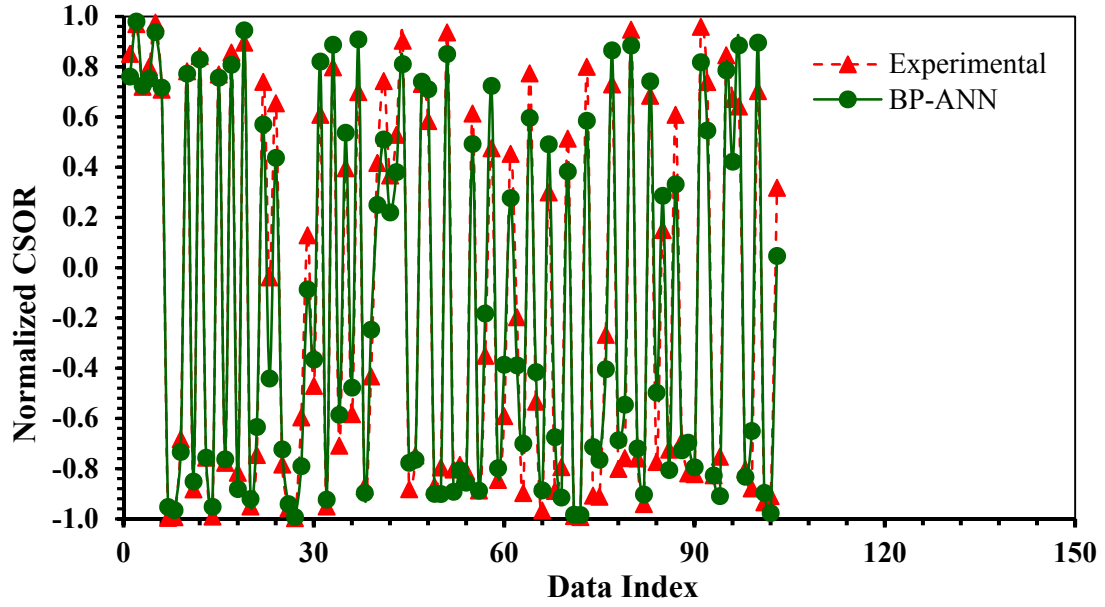


(a) Training

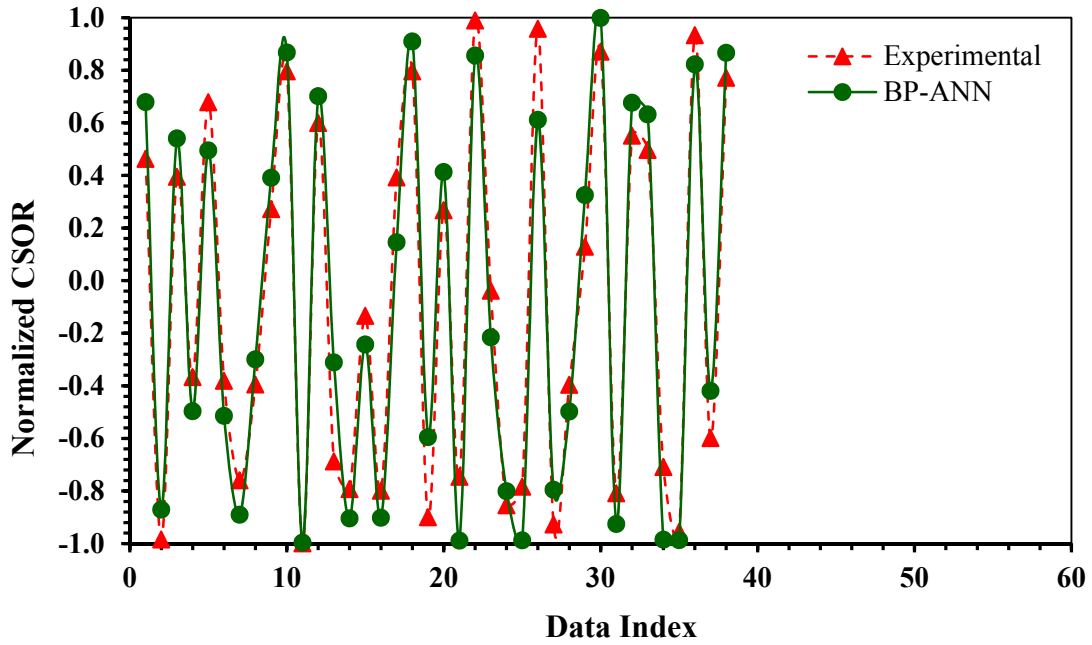


(b) Testing

Figure 5-6: Real field vs. predicted RF based on PSO-ANN; a) Training, b) Testing.

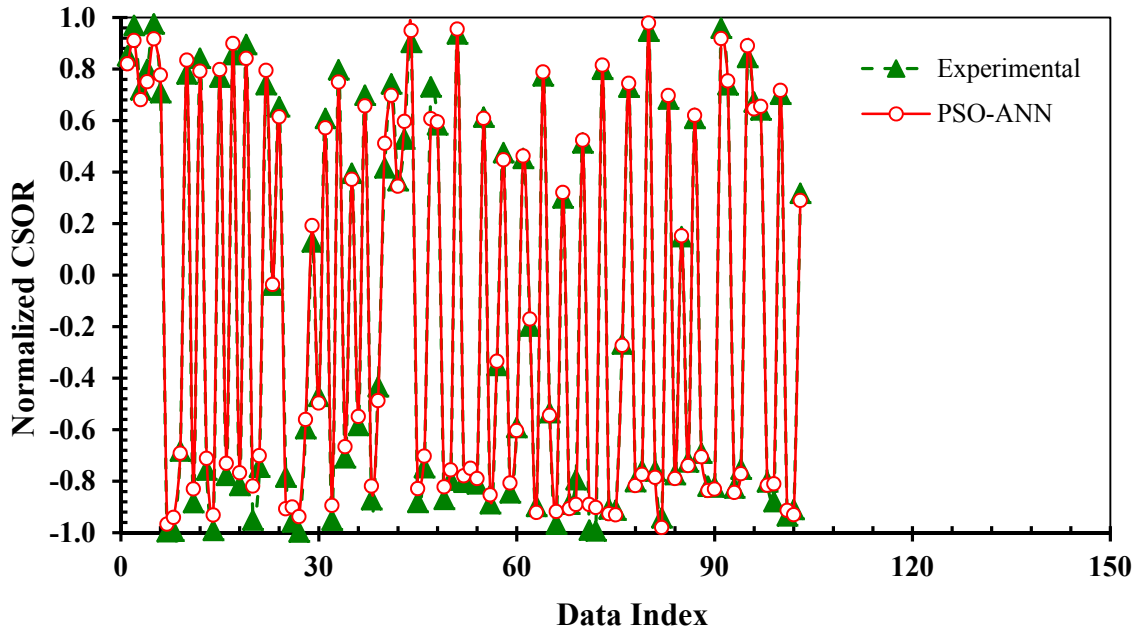


(a) Training

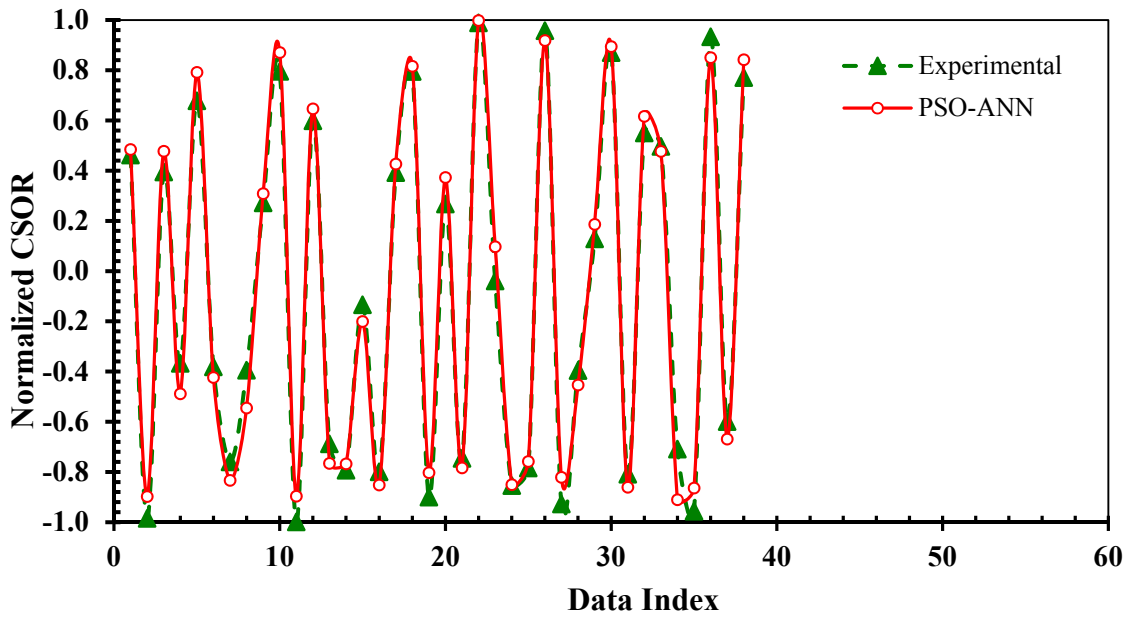


b) Testing

Figure 5-7: Measured vs. predicted *CSOR* based on BP-ANN; a) Training, b) Testing.



(a) Training

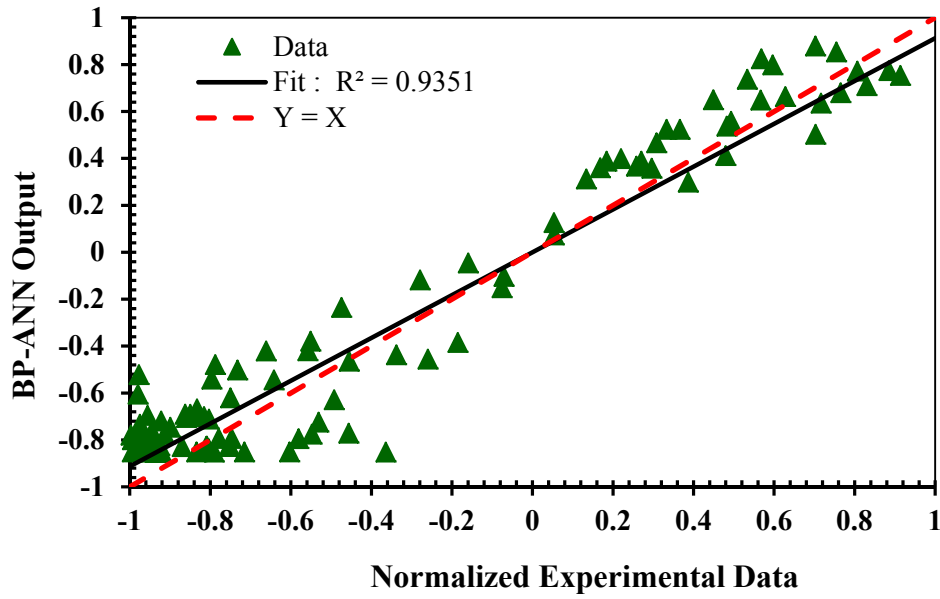


(b) Testing

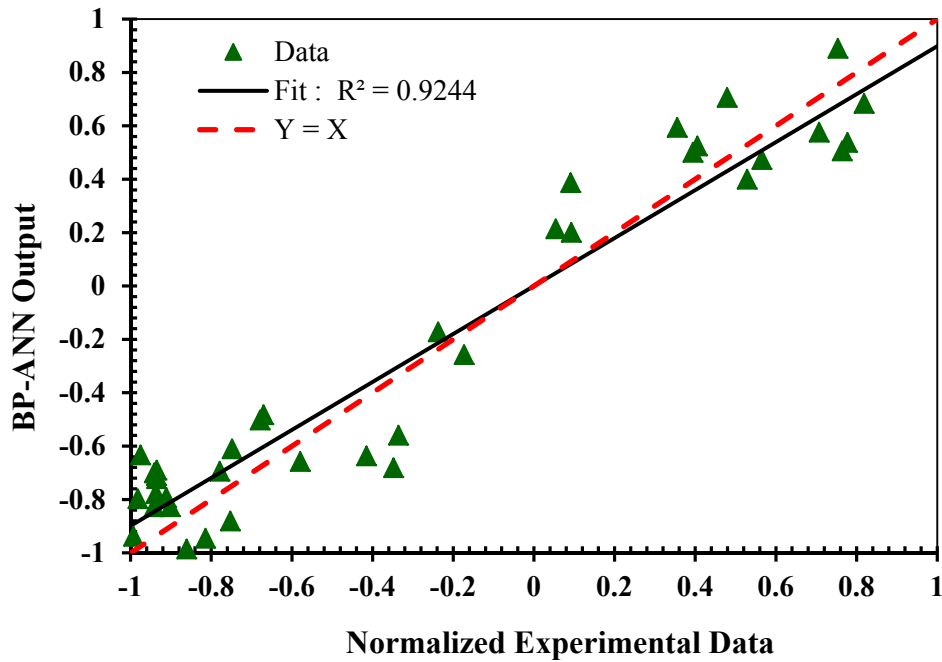
Figure 5-8: Measured vs. predicted *CSOR* based on PSO-ANN; a) Training, b) Testing.

The level of agreement between the real field field and simulated values by the BP-ANN and PSO-ANN models are depicted in Figures 5-9 and 5-10 for *RF* and Figures 5-11 and 5-12 for *CSOR* in the form of scatter diagrams. Because the PSO-ANN has the potential to recognize local optima and avoid becoming trapped in them, a higher performance for PSO-ANN is seen in the estimation of the outputs *RF* and *CSOR*, which are the critical measures of value of steamflooding for these VO NFCRs.

Comparison of *RF* values attained from the regression equation and the PSO-ANN and BP-ANN models is carried out here to assess the performance of the PSO-ANN model. The values of *MSE*, *MEAE*, *MAAE*, and R^2 for the testing phase of these three different predictive methodologies are listed in Table 5-5. The PSO-ANN approach exhibits better performance compared to the conventional ANN model and also to the multivariate regressive correlation in forecasting steamflooding performance in VO NFCRs.

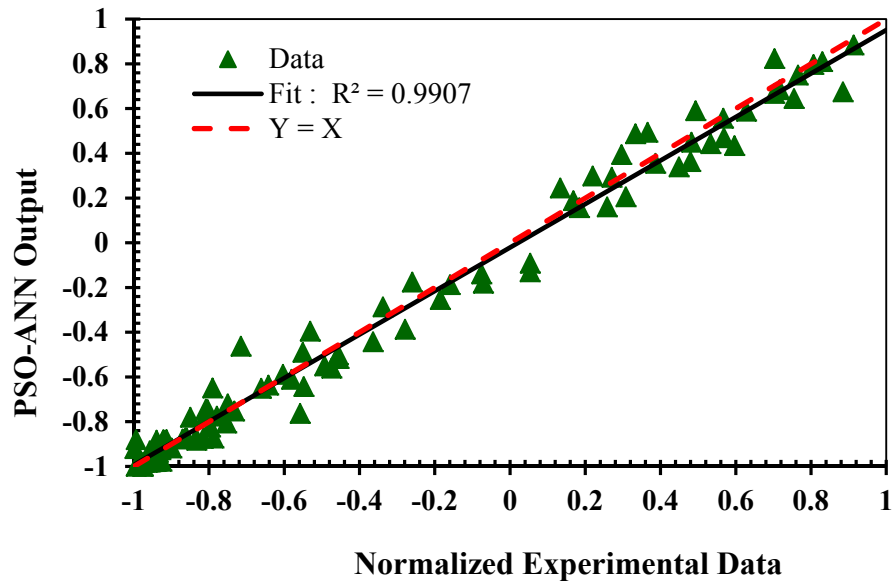


(a) Training

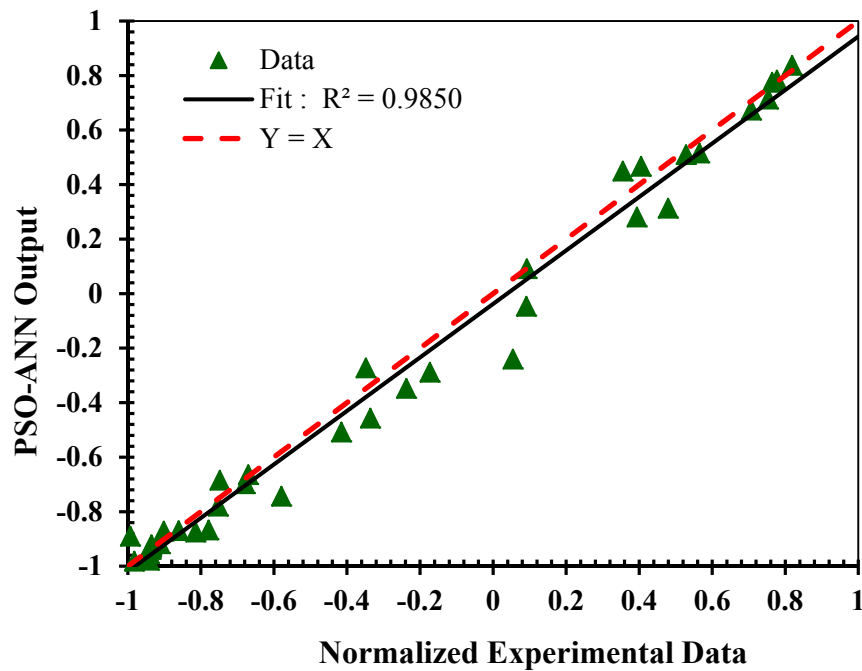


(b) Testing

Figure 5-9: Scatter diagrams for steamflooding - *RF* based on BP-ANN in terms of R^2 ; a) Training, b) Testing.

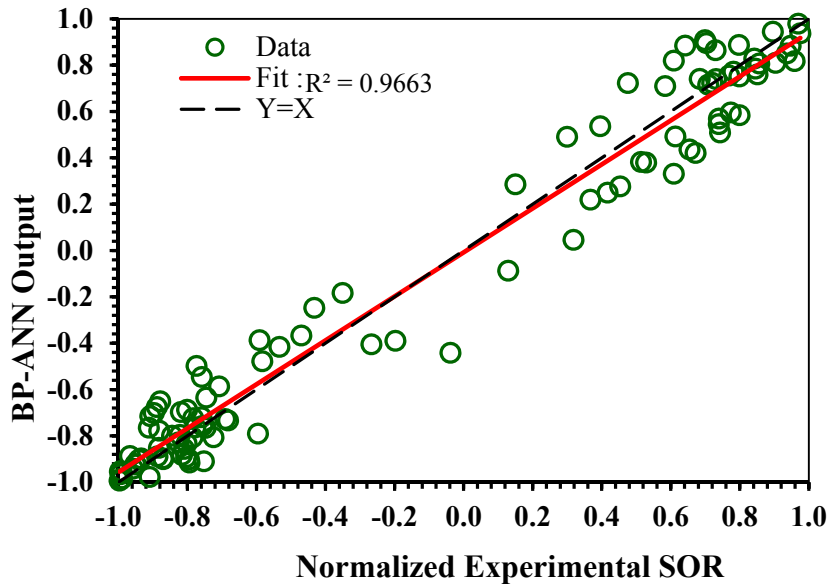


(a) Training

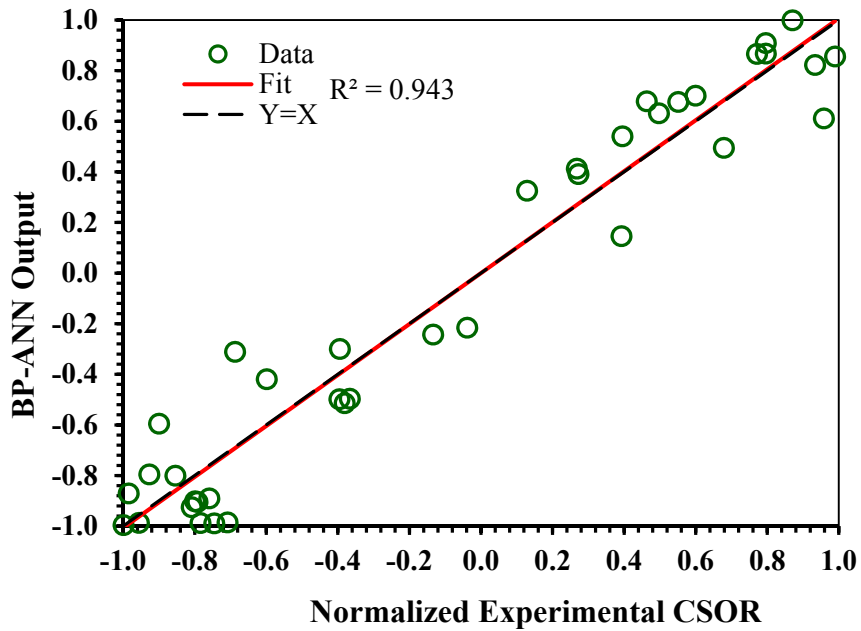


(b) Testing

Figure 5-10: Scatter diagrams for steamflooding - *RF* based on PSO-ANN in terms of R^2 ; a) Training, b) Testing.

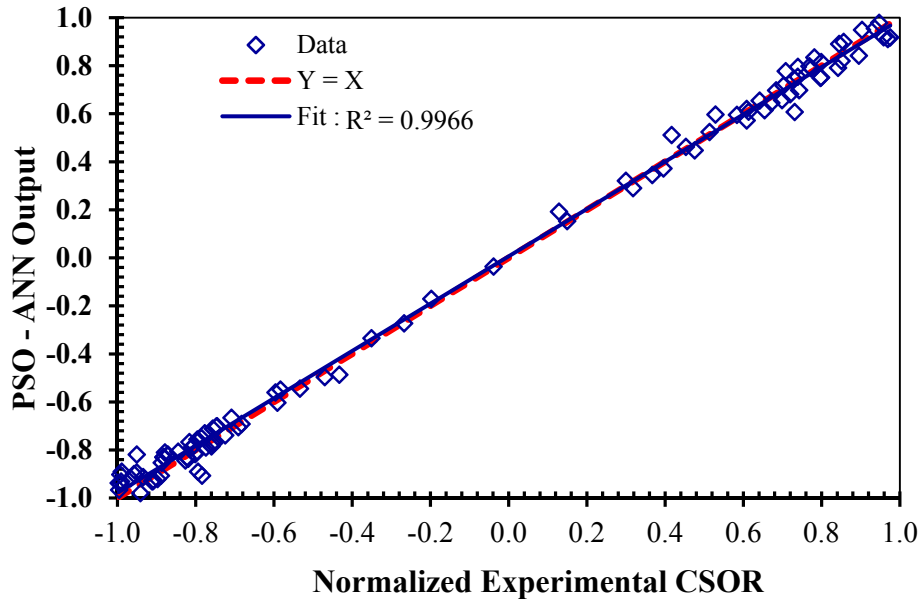


(a) Training

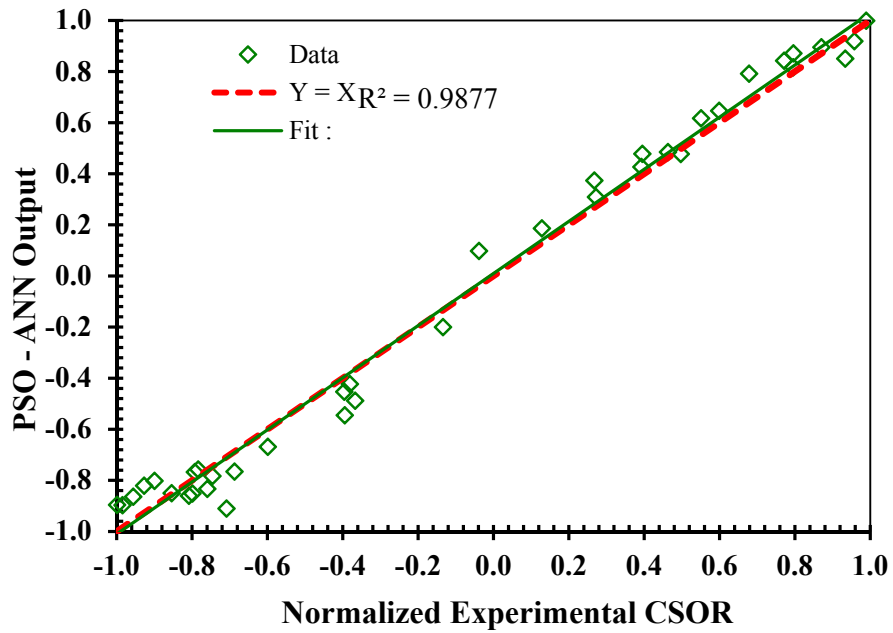


(b) Testing

Figure 5-11: Scatter diagrams for steamflooding - CSOR based on BP-ANN in terms of R^2 ; a) Training, b) Testing.



(a) Training



(b) Testing

Figure 5-12: Scatter diagrams for steamflooding - $CSOR$ based on PSO-ANN in terms of R^2 ; a) Training, b) Testing.

Table 5-5: Performances of the PSO-ANN model, BP-ANN model, and statistical correlations.

Statistical parameter	PSO-ANN		BP-ANN		The proposed regression correlations	
	<i>RF</i>	<i>CSOR</i>	<i>RF</i>	<i>CSOR</i>	<i>RF</i>	<i>CSOR</i>
R^2	0.9850	0.9877	0.9244	0.9433	0.9840	0.976
<i>MSE</i>	0.0623	0.0516	0.0941	0.1030	0.0634	0.0892
<i>MIPE</i> (%)	4.4156	3.9785	7.5978	6.9085	5.3546	6.0044
<i>MAPE</i> (%)	9.4127	8.7746	11.4765	11.1102	10.3218	11.1178

For completeness, here the correlations equations for *RF* and *CSOR* obtained in Chapter 4 using direct regression methods, in contrast to the neural networks approaches used in this chapter:

$$\begin{aligned}
 RF = & a_{15} + a_{16} S_o + a_{17} h + a_{18} q_s + a_{19} \phi_e + a_{20} K_m + a_{21} x_s + a_{22} \mu_o + a_{23} \frac{K_m h}{\mu_o} + \\
 & a_{24} S_o \phi_e + a_{25} q_s x_s + a_{26} \frac{S_o \phi_e h K_m q_s}{\mu_o x_s} + a_{27} q_s \phi_e + a_{28} \frac{K_f}{K_m}
 \end{aligned}
 \tag{5-8}$$

$$\begin{aligned}
CSOR = & a_0 + a_1 D + a_2 \frac{1}{\phi_e} + a_3 \frac{1}{K_m} + a_4 K_f + a_5 \frac{1}{\mu_o} + a_6 \frac{1}{S_o} + a_7 \frac{1}{q_s} + a_8 x_s + a_9 \frac{1}{S_o \phi_e} + a_{10} \frac{D}{h} + \\
& a_{11} \frac{D}{h \phi_e K_m \mu_o S_o q_s} + a_{12} \frac{1}{\phi_e q_s} + a_{13} \frac{1}{\phi_e K_m} + a_{14} \frac{K_f}{K_m}
\end{aligned}
\tag{5-9}$$

Although regression using parameter groups is a widely recognized method, we must conclude that neural networks models give better predictive results.

5.7.1 Sensitivity Analysis

Using the analysis of variance (ANOVA) technique, a sensitivity analysis was conducted for the PSO-ANN model. The contribution of each input variable to the predictions of *RF* and *CSOR* was determined by this methodology. Figure 13 presents the results of the sensitivity analysis, and a greater correlation between any independent variable and the dependent variable is indicative of the importance of the variable on the value of the target function. According to Figure 13, the oil viscosity and initial oil saturation have the greatest contribution to both dependent variables, *CSOR* and *RF*. An increase in initial oil saturation leads to an increase in *RF* and a decrease in *CSOR*, a result in agreement with the studies available in the literature and also the regression correlation developed in Chapter 4. In addition, the effect of other parameters on *RF* and *CSOR* supports the validity of the prediction correlations previously developed by the authors, although the neural network methods give better predictive capabilities.

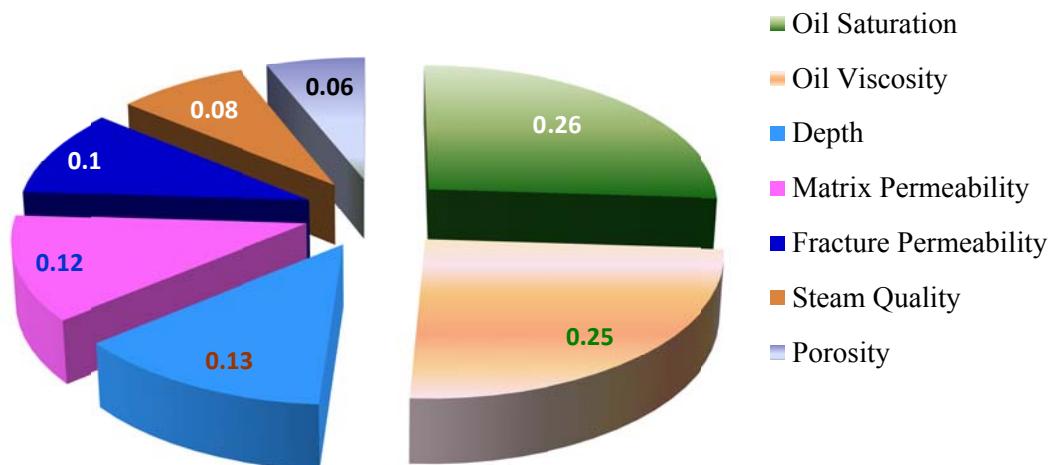


Figure 5-13: Relative impacts of main independent variables on RF and $CSOR$ during SF.

To investigate the impact of fractures, the production performance of a particular case (e.g., $K_m = 0.3 D$, $K_f = 5 D$, $\phi = 0.24$) was obtained in terms of $RF = 0.56$, $CSOR = 4.9$ for the model having fractures and $RF = 0.61$, $CSOR = 4.2$ for the porous medium without fractures, based on the developed PSO-ANN model. Based on this case, the presence of fracture would seem to lead to an increase in the magnitude of $CSOR$ and a lower RF , likely because fractures increase the effective vertical permeability, resulting in early steam breakthrough. This is consistent with the field observations of steamflooding in NFCRs. Also, a small difference between the experimental and modeling results is observed for this case such that the absolute error percentage is lower than 7%, again showing the capability and high accuracy of the PSO-ANN model in prediction of the RF and $CSOR$ during steamflooding in NFCRs.

Black oil softwares are common tools to anticipate production history of heavy oil reservoirs under various technologies. The computation process in the softwares is often a complicated job due to the flow behavior complexity and uncertainties present in the important input factors such as relative permeability functions. However, using ANN techniques leads to reduction of costs associated with production performance estimation as the most promising conditions can be validated. Consider implementation of a "blind test" in the ANN model in which 20-30% of the field data is available. Then, utilization of the smart technique enables to forecast the *CSOR* and *RF* with high precision if the magnitudes of input variables (e.g., oil viscosity, and porosity) and also production history are known somehow. Clearly, the error due to presence of some uncertainties is lowered and it would also allow an independent check on the value of absolute error percentage. In general, ANNs are very strong techniques with respect to underlying data distributions (e.g., non-parametric), and no assumptions are made about relationships between variables contributing in oil production process in spite of the non-linear mathematical models and/or empirical equations. Therefore, ANNs are more suitable and faster to model complex and nonlinear phenomena such as heavy oil production through steamflooding.

5.7.2 Case Study

Kuh-e-Mond heavy oil field is the largest on-shore heavy oil field in Iran (Figure 5-14); OOIP is estimated at 10×10^9 b for the worst case. The depth of the reservoirs varies from 400–1200 meters at various points in the structures, and the oil viscosity is in the range of 550–1120 cP at reservoir conditions, making this a heavy oil, and suitable for application of the model derived above.

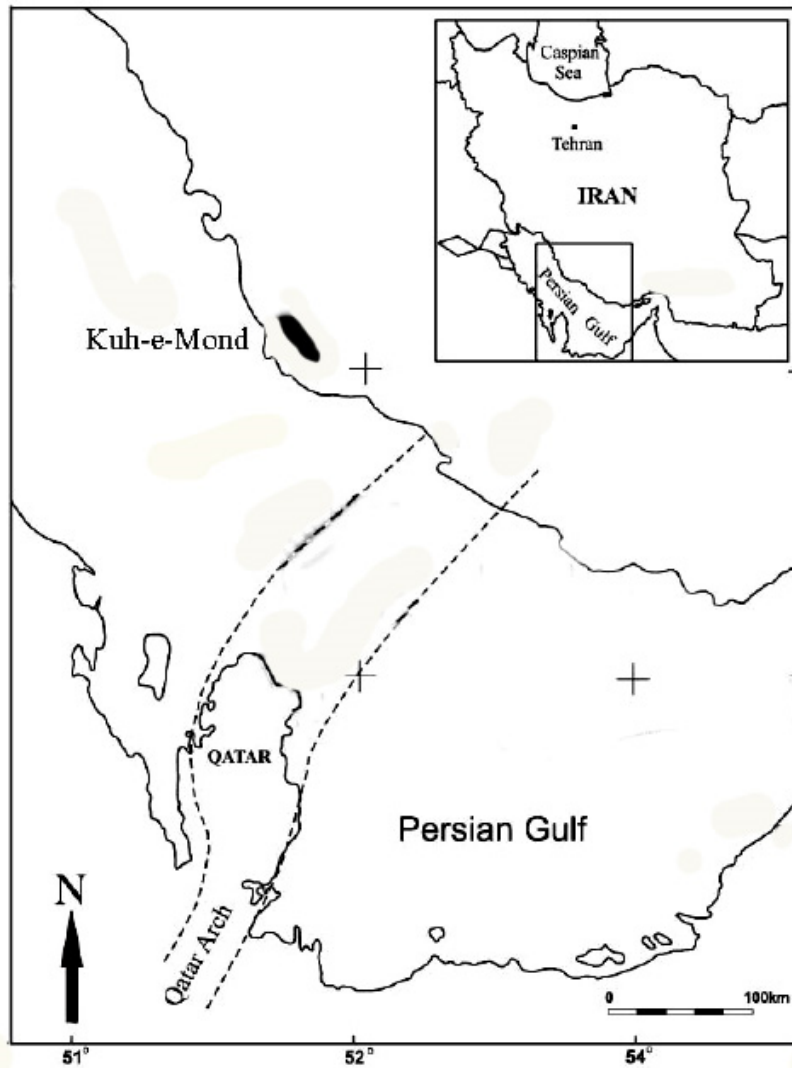


Figure 5-14: Geographical location of the Kuh-e-Mond heavy oil field.

The heavy oil is trapped in separate fractured carbonate formations, the Jahrum (Eocene) and Sarvak (Cretaceous) Formations. The Jahrum Formation is composed mostly of highly fractured fine-grained crystalline dolomite that includes heterogeneities such as vugs and fractures (Bashari, 1988; Moshtaghian et al., 1988). The Cenomanian Sarvak Formation is a highly fractured limestone with interbedded shale layers. This formation has three major parts; the upper unit is made of clean limestone with some slightly argillaceous zones; the

middle Sarvak mostly contains shale and marls; and, the lower Sarvak is essentially marly limestone, with some shale bed intercalations (Bashari, 1988).

Table 5-6 lists the average reservoir and fluid characteristics of the Kuh-e-Mond HO field. This database was prepared from drilling and geophysical log data with the support of field and laboratory tests performed on samples taken from exploration wells.

Table 5-6: Reservoir and fluid properties of the Kuh-e-Mond HO reservoirs.

Reservoir Abbreviation	Jahrum	Sarvak
Lithology	Dolomite and Dolomitic Limestone	Limestone
Depth (m)	680–900	1100–1200
Thickness (z) (m)	320	100
Net to Gross Ratio (%)	31	47
Net Pay Thickness (m)	99	47
Oil Viscosity (<i>In situ</i>) (cP)	1160	570
Temperature (T) (<i>In situ</i>) °F	70	110
Matrix Permeability (mD)	1	0.2–1.4
Fracture Permeability (mD)	300–500	350–500
Porosity (ϕ) (Fraction)	0.19	0.16
Oil Saturation (Fraction)	0.66	0.46
Wettability	Oil Wet	Oil Wet/Mixed Wet

Employing the developed PSO-ANN model, *CSOR* and *RF* for the Jahrum HO reservoir are found to be in the ranges of 6.2–7.3 and 42–50%, respectively. In the Sarvak Formation HO

reservoir, a *CSOR* of 6.45–8.1 and *RF* between 37–43% are predicted with steam injection at 80–90% quality. This quick screening analysis implies that it is technically feasible to employ steamflooding for HO production from both reservoirs but the Jahrum reservoir is a better candidate due to more favorable reservoir parameters (a combination of depth, fracture permeability, and higher initial oil saturation) though the reservoir contains a lower permeability matrix than the Sarvak reservoir. The Sarvak HO reservoir passes the screening criteria for steamflooding but remains a poor candidate compared with the Jahrum reservoir. With such high *CSOR* predictions, economical oil production from this heavy oil field is still questionable at the moment, unless a more economic heat source for steam is developed.

5.8 Limitations

In general, there are some constraints when employing ANN to predict important parameters in petroleum production processes such as steamflooding. A number of these issues are as the following:

- ANN modeling usually requires a fairly large amount of production history data to predict production performance of steamflooding.
- ANN systems are like a “black box” and have limited capability to clearly identify possible important relationships in terms of production mechanism and heterogeneity in reservoir properties. In fact, it is highly likely that application of ANN models to predict *RF* and *CSOR* for the heterogeneous reservoirs is not viable when enough data is not available.
- ANN modeling requires higher computational efforts compared with conventional methods such as regressive correlations.
- Over-fitting is a major problem in ANN models particularly conventional systems. Therefore, developing optimization algorithms is inevitable to resolve this problem. Such a development requires extensive mathematical resources and knowledge.

- Being stuck in local optima for conventional ANN may cause considerable errors in estimation of RF and $CSOR$. Employing evolutionary techniques appears to be important in tackling this issue.
- ANN may not be able to capture physical concepts and main aspects (e.g., diffusion and heat transfer convection term) related to transport phenomena in porous media involved in steamflooding.
- Developing ANN modeling is usually empirical, and many issues in terms of methodology and structure remain unsolved.

5.9 Concluding Remarks

The use of an Artificial Neural Network (ANN) approach optimized by co-implementation of a Particle Swarm Optimization (PSO) algorithm was applied to predict Recovery Factor (RF) and Cumulative Steam to Oil Ratio ($CSOR$) during steamflooding as a measure of process performance in Heavy Oil Naturally Fractured Carbonate Reservoirs (VO NFCRs). Field and experimental data from the literature were used to build the proposed new predictive tool.

Based on the results obtained from this study, the following main conclusions can be drawn:

- Comparison of statistical correlations, BP-ANN and PSO-ANN shows that the PSO-ANN model is best able to forecast steamflooding performance in VO NFCRs with high precision such that the maximum error percentage is less than 8% for this hybrid ANN.
- The neural network structure for the PSO-ANN model was determined manually. A supplementary technique in the form of evolutionary algorithms (e.g., [Atashpaz-Gargari and Lucas \(2007\)](#)) is recommended to optimize an appropriate ANN structure for the case under study (e.g., RF and $CSOR$ for steamflooding in NFCRs).

- Using experimental and field data, the developed PSO-ANN model shows that the presence of fractures increases the value of $CSOR$, leading to a lower RF at the time of breakthrough.
- Determining an optimum structure for the PSO-ANN model is a key feature in estimation of $CSOR$ and RF . The optimum configuration in our case contains seven neurons in one hidden layer.
- Trial and error procedures yielded optimum acceleration constants for the PSO algorithm equal to 2.1, with a number of particles equal to 21.
- The predictive PSO-ANN model and statistical correlations have strong potentials to be merged with heavy oil recovery modeling software available for thermal methods. This combination is expected to speed up their performance, reduce their uncertainty, and enhance their prediction and modeling capabilities. Further studies are required to develop a hybrid method (e.g., smart technique-finite difference modeling simulation) for determining recovery performance of VO NFCRs during steamflooding with acceptable accuracy.
- The hybrid ANN model consisting of three layers (e.g., one input layer, one hidden layer, and one output layer) was trained with a back-propagation network using the Levenberg-Marquardt algorithm (Levenberg, 1944; Marquardt, 1963). Sigmoid and linear transfer functions were also employed in the hidden and output layers, respectively. Particle Swarm Optimization was implemented by minimizing a cost function based on the mean squared error (MSE). Each initial weight in the network was between -1.0 and 1.0 and every initial particle was set in the range of $[-1, 1]$. For example, the initial and last values of the inertia (ω_{min} and ω_{max}) were 0.4 and 0.5 , respectively.
- About 75% of the data population (38 testing data +105 training data) was chosen for the purpose of network training in this study. The remaining 25% (i.e., 38 data

- points) was put aside to be used for testing and validating the network's integrity and robustness.
- The precision of the modeling runs was increased by increasing the number of hidden neurons from 3 to 7, but the performance of the PSO-ANN model decreased when the number of hidden neurons exceeded 8. Thus, the optimum number of hidden neurons is taken as 7 to avoid problems of under- or over-determinacy and to reduce computational training time. The model may be updated frequently or adjusted as better input parameters become available for the data in the table, so an efficient training time is a valuable model asset.
 - The performance of the PSO-ANN algorithm increases with an increase in the number of particles from 15 to 21, although the neural network component did not perform well at particle numbers from 15 to 18 because the small number of particles could not accommodate the behavior of all the data. At values larger than 21, a decrease in the PSO-ANN performance as a predictor was evident (Table 5-5). The main reason behind this decline is that the space covered in the problem appears to be too wide. Although the decline in performance after 21 particles is small, as the number of particles rises, the optimization process becomes appreciably slower.
 - The following optimal structure for the PSO-ANN algorithm was determined: Number of the layers= 3 including 1 input layer, 1 hidden layer, and 1 output layer; Number of maximum iterations = 450; c_1 and $c_2 = 2.2$; Time interval = 0.0100; and Number of particles = 21. Hence, the best ANN architecture is: 7-7-2 (7 input units in one layer, 7 neurons in the hidden layer, and 2 output neurons in one layer).
 - To investigate the impact of fractures, the production performance of a particular case (e.g., $K_m = 0.3$ D, $K_f = 5$ D, $\phi = 0.24$) was obtained in terms of $RF = 0.56$, $CSOR = 4.9$ for the model having fractures and $RF = 0.61$, $CSOR = 4.2$ for the porous medium without fractures, based on the developed PSO-ANN model. Based on this case, the presence of fracture would seem to lead to an increase in the magnitude of $CSOR$ and

- a lower RF , likely because fractures increase the effective vertical permeability, resulting in early steam breakthrough. This is consistent with the field observations of steamflooding in NFCRs. Also, a small difference between the experimental and modeling results is observed for this case such that the absolute error percentage is lower than 7%, again showing the capability and high accuracy of the PSO-ANN model in prediction of the RF and $CSOR$ during steamflooding in NFCRs.
- The use of an ANN technique optimized by co-implementation of a Particle Swarm Optimization (PSO) algorithm was applied to predict RF and $CSOR$ during steamflooding as a measure of process performance in VO NFCRs. Field and experimental data from the literature were used to build the new predictive tool proposed in this study.

Nomenclature

Acronyms and abbreviations

2-D, 3-D	=	Two or Three Dimensional
AI	=	Artificial Intelligence
ANN	=	Artificial Neural Network
ANOVA	=	Analysis of variance
BP	=	Back Propagation
<i>CSOR</i>	=	Cumulative Steam to Oil Ratio
EIA	=	Energy Information Administration
EOR	=	Enhanced Oil Recovery
HO NFCR	=	Heavy Oil Naturally Fractured Carbonate Reservoir
HO	=	Heavy Oil
MAPE	=	Minimum Absolute Percentage Error
MEAE	=	Mean Absolute Error
MIPE	=	Minimum absolute percentage error
MSE	=	Mean Squared Error
NFCR	=	Naturally Fractured Carbonate Reservoir
NN	=	Neural Network
OOIP	=	Oil Originally In Place
PSO	=	Particle Swarm Optimization
<i>RF</i>	=	Recovery Factor
SD	=	Steam Drive

SF	=	Steamflooding
VO	=	Viscous Oil
XHO	=	Extra Heavy Oil

Variables

P_g^t	=	Best ever particle position of particle i
P_i^t	=	Global best position in the swarm until iteration t
$\theta(x)$	=	Penalty function (Eq. 2–5)
V_i^t	=	Velocity vector at iteration t
°C	=	Degrees Celsius
°F	=	Degrees Fahrenheit
b	=	Barrel of oil
c_1, c_2	=	Acceleration coefficients (Eqs. 2–4)
D	=	Darcy
$D(x)$	=	Distance value (Eq. 2–5)
F	=	Produceability factor - kh/μ [mD-m/cP]
$fn(x)$	=	Normalized objective cost function (Eq. 2–6)
G	=	Number of training samples
H	=	Reservoir thickness
k	=	Current iteration (Eqs. 2–4)
k	=	Permeability (milliDarcy or Darcy)
K_f	=	Fracture permeability (mD or D)

k_v, k_h	=	Permeability in Darcies, vertical, horizontal
m	=	Meters
m	=	Number of output nodes
mD	=	Millidarcy
MPa	=	Mega Pascal
n	=	Number of samples
r_1, r_2	=	Two random variables varying between 0 and 1 (Eqs. 2–4)
R^2	=	Coefficient of determination
r_f	=	Number of feasible solutions divided by the swarm size (Eq. 2–6)
S_o	=	Oil Saturation (% or fraction)
S_w	=	Water Saturation (% or fraction)
T	=	Temperature in °F or °C
$T_j(k)$	=	Actual output
w_k	=	Inertia weight (Eqs. 2–4)
X_i	=	Position of the i-th particle
x_l, x_g	=	Local best position and global best particle position (Eqs. 2–4)
x_s	=	Steam quality (% or fraction)
$Y_j(k)$	=	Expected output
z	=	Depth in meters
z_i	=	Overall composition of component i
$\varepsilon(x)$	=	Summation of the average normalized violation in each constraint (Eq. 2–6)

λ	=	Limiting factor (Eqs. 2–4)
v^k, x^k	=	Vectors of real velocity and position, respectively (Eqs. 2–4)

Greek Letter

ω	=	Inertia weight
ϕ	=	Porosity
μ	=	Dynamic viscosity (kg.m/s or cP)
Δ	=	Difference operator

Subscripts

i	=	Particle i
max	=	Maximum
min	=	Minimum

Superscripts

M	=	Measured
net	=	Network
P	=	Predicted

Metric Conversion Factors

$^{\circ}\text{F}$	=	$(^{\circ}\text{C} \times 1.8) + 32$
1 barrel oil	=	0.159 m ³
1 psi	=	6.8947 kPa
1 psi/ft	=	22.62 kPa/m or 22.62 MPa/km

“Real integrity is doing the right thing, knowing that nobody's going to know whether you did it or not.”

Oprah Winfrey

Chapter 6

Geomechanics of Thermal Oil Production in Sandstones⁵

6.1 Abstract

Over 7 trillion barrels of viscous oil (heavy oil, extra heavy oil, and bitumen) are trapped in sandstones or unconsolidated sand formations around the world, mainly in Canada, Venezuela, and Russia. To date, only cold flow methods and steam injection processes have achieved commercial success in accessing this immense resource. This chapter highlights approaches to calculating thermally-induced stresses are presented, as well as discussions of thermo-mechanical issues associated with commercial thermal processes. Then, thermal, physical, and geomechanical properties of sandstone under high temperature and pressure are investigated, based on field and laboratory data. An important factor is the change in rock properties that takes place because of the large thermally-induced stresses. Finally, a practical example of thermal geomechanics effects during thermal oil production operations (example of Steam Assisted Gravity Drainage) is demonstrated, emphasizing that thermal oil production methods change reservoir rock behavior. Under elevated temperature and pressure, large changes in porosity, permeability, and compressibility occur; hence, the reservoir response evolves in time, a factor generally ignored in simulation. Whereas these geomechanical changes are largely beneficial as they tend to accelerate recovery rates, some difficult operational issues may arise, including casing shear, breach of reservoir seal, and excessive heat loss.

6.2 Introduction

Thermal geomechanics is a vital aspect of viscous oil recovery because of massive stress-induced effects. These include positive effects such as rock dilation, leading to

⁵ Materials presented in this chapter are contributed to the following publication:

Shafiei, A. and Dusseault, M.B. 2013. Geomechanics of Thermal Viscous Oil Production in Sandstones, *Journal of Petroleum Science and Engineering*, (In press).

improvements in permeability, porosity and compressibility. The economic impact of these effects is huge; without the massive increases in vertical permeability that are caused by high temperature stress effects and shear dilation, gravity drainage processes would likely be uneconomical. There are also potentially negative aspects associated with thermally induced stresses and volume changes including casing shearing, casing seal deterioration, and impairment of caprock integrity because of stress redistribution, high steam pressures, and shale shrinkage.

There are $\sim 1.54 \times 10^{12} \text{ m}^3$ [$\sim 9.7 \text{ Tb}$ (Tb = trillion barrels of oil)] of viscous oil (VO) known to exist in the world. By comparison, originally there were $\sim 0.75 \times 10^{12} \text{ m}^3$ [$\sim 4.7 \text{ Tb}$] of conventional oil, of which almost $0.19 \times 10^{12} \text{ m}^3$ [$\sim 1.195 \text{ Tb}$] have been produced to date (Meyer *et al.*, 2007; Dusseault and Shafiei, 2011; GEA, 2012). VO resources are not evenly distributed: Canada and Venezuela alone possess over 30% of the world endowment. Sandstone and unconsolidated sand formations contain over 7 Tb of the world VO endowment, and furthermore, the physical properties of these resources are highly variable, leading to large differences in producibility from place to place. The ultimate world VO reserves are estimated to be about $0.41 \times 10^{12} \text{ m}^3$ [$\sim 2.6 \text{ Tb}$], or 27% of the total OOIP (Original Oil In Place) (Meyer *et al.*, 2007; Dusseault and Shafiei, 2011; GEA, 2012). Only in Alberta, Canada, can significant amounts of VO be open-pit mined, but proven mineable oil reserves are relatively small in the global context, constituting 1 to 1.5% of the total reserve.

The importance of high temperature geomechanics ($T > 180^\circ\text{C}$) has long been acknowledged in areas such as volcanology and structural geology (folding, magmatism, volcanism, plate tectonics) (Shimamoto and Hara, 1976; Parrish *et al.*, 1976; Anderson and Bridwell, 1980; Kirchoff and McKinnon, 2009), geothermal energy development (Anderson, 1979; Anderson and Bridwell, 1981; Cho *et al.*, 2009; Trautwein-Bruns *et al.*, 2010) and high-level nuclear waste disposal (Lee and Nichols, 1972; Logan, 1973; Klett, 1974; Bertram, 1976; Hueze, 1981; Bergman, 1980, Hodgkinson *et al.*, 1983). It is also important in thermal oil extraction methods.

The importance of rock mechanics to petroleum engineering is not a new concept (e.g., Somerton and Boozer, 1960a, 1960b, 1961; Somerton and Selim; 1961; Gray, 1967; Komar, 1971; Lauriello, 1974; Heard, 1982; Li *et al.*, 1999; Dusseault *et al.*, 2001; Zhang *et al.*, 2009; Yavuz *et al.*, 2010), but the development of better computational, field, and laboratory tools, combined with an increase in the number and magnitude of rock mechanics-driven issues, have led to rapid adoption of rock mechanics in petroleum engineering as a basic science input to reservoir analysis, along with the geological, thermodynamic, and transport sciences. Production from deeper and hotter reservoirs as well as steam injection into shallow VO reservoirs has triggered interest in rock mechanics concepts and calculations and their inclusion in planning and reservoir management.

The impact of thermal stimulation on reservoir properties has attracted interest; for instance, thermal alteration of reservoir rock wettability at elevated temperatures dramatically affects flow rates and Recovery Factors (*RF*), impacting project economics, modeling and simulation, and production prediction efforts (Rao and Karyampudi, 1995; Rao, 1999; Al-Hadhrami, and Blunt, 2000; Civan, 2004; Schembre *et al.*, 2006; Kumar and Verma, 2010; Al-Aulaqi *et al.*, 2011). Thermal alteration of capillary pressure (Sanyal *et al.*, 1973), changes in relative and absolute permeabilities in oil sands subjected to high temperatures (Waldorf, 1965; Heath and Jones, 1971; Closmann *et al.*, 1988; Elsworth, 1989; Davies and Davies, 1999; Rutqvist *et al.*, 2008), and thermal stress changes in VO operations have been discussed (Butler, 1986; Dusseault, 1993; Scott *et al.*, 1994; Pooladi-Darvish *et al.*, 1994a, 1994b; Hettema *et al.*, 1998; Ito *et al.*, 2002). Covering all thermal aspects is beyond the scope of this chapter, but references are provided on several aspects of thermal oil production.

The two major VO reservoir lithotypes are unconsolidated sandstones (UCSS) and Naturally Fractured Carbonate Reservoirs (NFCRs). Other lithotypes containing limited VO volumes in some locations in the world are North Sea Chalk, California Diatomite, fractured shale oil reservoirs, and oil shales (usually high-porosity kerogenous marls). High T and p production

processes (steam injection, hydraulic fracturing) have a profound impact on the geomechanical behavior of both UCSS and NFCR VO reservoirs.

Heating rock around an injection point to 200 to 300°C causes large thermoelastic expansion which acts against the surrounding cool rock. This gives rise to zones of increased and reduced compressive stresses in advance of the front; for example, $+\Delta T$ leads to increased σ_r' and reduced σ_θ' , where the “r” direction is normal to the thermal front, and “ θ ” is tangential and 90° to the “r” direction. If the reservoir is a UCSS, these stress changes lead to general shearing in advance of the thermal front. Because of the kinematic constraints in the reservoir configuration, the dense sand undergoes generalized shear, not single-plane shear, and because σ_3' is low (< 1000 m depth), the sand dilates irreversibly as it shears ([Dusseault and Rothenburg, 1988](#)). Dilation shows up as vertical heave (Δz) at the surface, as much as 500 to 800 mm in shallow, thick reservoirs experiencing steaming. The σ_3' value is particularly low in cyclic steam stimulation (CSS) injection cycles which employ high injection pressures (p_{inj}) and hydraulic fracturing to achieve reasonable steam injectivity. More dilation is expected in CSS processes compared to steam-assisted gravity drainage (SAGD) methods ([Chalaturnyk, 1996](#)), which generally are operated at the formation pore pressure or lower, and do not employ high p_{inj} fracturing strategies.

Induced dilation occurs throughout the sand, albeit not uniformly because of perturbations in the thermal front shape, and it leads to porosity increases from 28 to 30% to as high as 34 to 36% locally, with concomitant permeability increases. Shear dilation also breaks apart thin clay layers on bedding planes and disrupts 10 to 20 mm thick clayey streaks (even thicker), so the effect on bulk reservoir permeability is profound: average permeability can easily be increased from 1–2 D to 5–10 D ([Touhidi-Baghini, 1998](#)), but most importantly, the small horizontal clayey beds impeding vertical flow are breached. This allows the macroscopic vertical permeability (k_v) of cross-bedded and laminated sandstone to go from low values to several Darcies. Since k_v is the major constraint on vertical phase segregation, the dilation and k_v enhancement allow one to reap the beneficial impact of vertical segregation of immiscible phases of different density, the basic physical process involved in gravity

drainage. Because of experimental difficulties in replication of the boundary conditions *in situ*, the quantification of shear dilation vs. permeability relationships, especially in laminated strata, remains almost non-existent. Therefore, the numbers in this paragraph and elsewhere in this chapter must be regarded as semi-quantitative estimates. Evaluation of the performance of *in situ* thermal processes indicates that these changes are realistic (Collins *et al.*, 2002), and deformation measurements at the surface (Stancliffe and van der Kooij, 2001) show that shear dilation is a much larger component of volume change than the thermal expansion effect alone (Yin *et al.*, 2010).

Figure 6-1 shows surface uplift above a SAGD project in Canada. Estimates of Δz from thermal expansion give surface uplift values in the range of 50 to 60 mm. Clearly, the remainder of the uplift (310 mm maximum) can only be attributed to shear dilation, discussed in greater detail later.

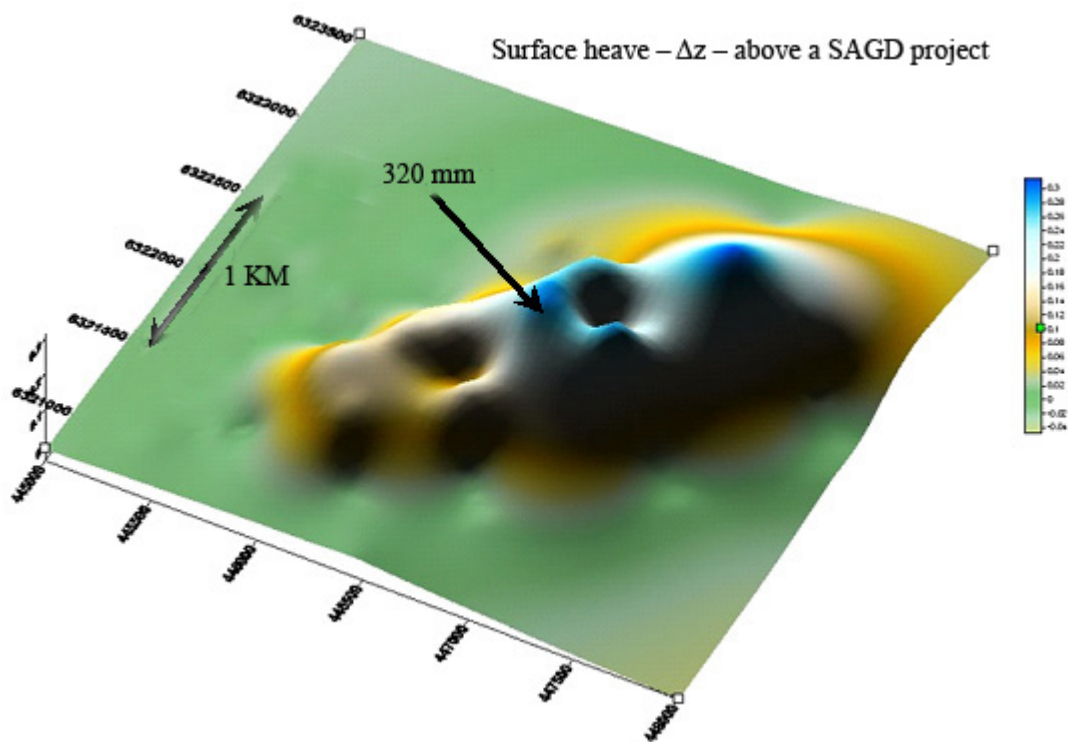


Figure 6-1: Surface uplift ($+\Delta z$) above a SAGD project in Canada.

Other major thermal effects that must be considered in thermal project planning include:

- Casing shear from large thermally induced displacements at interfaces between rock layers with different transport and geomechanical properties.
- The possibility of breaching of larger shale barriers (0.2 to 3 m) through direct fracturing ($p > \sigma_{hmin}$) - CSS, HCS), differential thermal expansion, or shale shrinkage (loss of σ_{hmin}) from dehydration (these can be positive or negative: shale breaching can access more resource but may also lead to greater heat losses).
- Risk of blowout to surface because of stress changes and shale shrinkage, especially with shallow steam projects ($z < 200$ m depth).
- Accelerated well corrosion leading to internal blowouts of hot fluids into shallow aquifers, or loss of well sealing capacity through changes in mechanical properties of the wellbore cement and surrounding strata subjected to many thermal cycles ($\Delta T, \Delta V$).
- In the exceptional case of the high-porosity ($\phi > 50\%$) Diatomite in California, steam injection leads to porosity collapse, massive compaction and surface subsidence ([Diabira et al., 2001](#); [Hoffman and Kovsky, 2005](#); [Kumar and Beatty, 1995](#)).

Despite the impact of geomechanics on VO thermal development, such issues are often addressed only once severe problems emerge, rather than as part of a proactive design process that seeks to exploit the benefits and manage the negative impacts.

In this chapter, definitions, geology and origins, and geographical distribution of the VO resources in the world are presented. The world VO endowment is huge and thermal production will dominate their development. Methods and physical mechanisms of the major commercialized viscous oil production methods being practiced around the world are described. Geomechanics is important; some methods of calculating thermally induced stresses are described and some temperature effects on reservoir rock properties are discussed. Finally, a practical example of reservoir rock behavior during SAGD thermal oil production is described, emphasizing that thermal methods change reservoir behavior,

leading to production enhancement (deterioration is less common), although thermal stimulation can generate operational issues such as thermally induced casing shear and cap rock breaching.

6.3 Thermally Induced Stresses in Reservoir Rocks

Few attempts have been made to define and formulate stress change issues during thermal VO production methods. Despite its long history, thermal oil production is fairly new in terms of significant contribution to daily world oil production. As long as easy conventional oil reserves are available, little investment tends to be made in thermal VO production methods. Currently, ~ 8% of the total daily oil production worldwide comes from thermal VO production.

Mathematical simulation of thermal effects has suffered from inadequate tools and few opportunities to verify or calibrate model results with adequate field measurements. Reservoir simulators generally ignore rock mechanics issues such as dilation and stress redistribution, and executing fully-coupled thermal-flow-stress simulations remains a complex process for which there exist few adequate commercial software options. An overview of related literature shows that thermal effects modeling in simulating carbonate reservoir behavior is in an embryonic state, and there is a dearth of suitable deformation monitoring data for geomechanics model verification.

Some efforts in thermal reservoir modeling and simulation for different reservoir rock types are presented here, focusing on changes in petrophysical, geomechanical, and to a lesser extent chemical properties of reservoir rocks for steam processes limited to temperatures up to ~ 325°C.

6.4 Thermal Reservoir Simulation and Numerical Modeling

Temperature changes induce thermal strains that lead to thermoelastic stresses (e.g., [Hojka *et al.*, 1993](#)) which can result in rupture or shear ([Dusseault *et al.*, 1988](#)), accompanied by dilation ([Dusseault and Rothenburg, 1988](#)). Stresses in the elastic range can be computed by incorporating thermoelastic rock volume changes using the equations of fluid-saturated,

poroelastic solids developed originally by Biot (1941, 1955, and 1956). Analytical or numerical solutions may be used to calculate thermal stress changes for various media with different properties and geometries (Stavsky, 1963; Aktan and Ali, 1978; Chen, 1988; Hojka, 1993; Dusseault, 1993; Wu, 1997; Pooladi-Darvish *et al.*, 1994a, 1994b). Depending on reservoir lithotype, the needs are different: in UCSS reservoirs, shear dilation is general and the rock matrix changes properties; in NFCRs, the strong rock matrix is less affected, but joint dilation and shear generate massive changes in local flow capacity and therefore pressures and temperatures (e.g., Dusseault *et al.*, 2011). Hence, different methodologies and approaches are required, depending on lithology.

Analytical solutions are based on work of Boley and Weiner 1960, Florence and Goodier (1959, 1960), Chen (1967), and many others, generally using homogenous assumptions and simple geometries, and usually based on complex variable techniques such as proposed by Green (1954), but which in turn mean that they are limited to linear problems with simple boundary conditions. As an example, Wang and Dusseault (1997) analyzed a circular opening in a friable low permeability medium subjected to temperature and pore pressure changes; they used an incremental elastic-perfectly-plastic constitutive stress-strain relationship under non-isothermal conditions to attempt to understand the propagation of yielded zones around injection wellbores.

Dusseault (1993) proposed a simple first-order approximation based on a uniform homogeneous flat-lying and extensive reservoir (Figure 6-2) subjected to uniform heating, where an assumption of no-lateral-strain can be justified. According to Hooke's law and Terzaghi's effective stress principle:

$$\varepsilon_i = \frac{1}{E} [\Delta\sigma'_i - \nu(\Delta\sigma'_j - \Delta\sigma'_k)] + \beta\Delta T; \Delta\sigma'_i = \Delta\sigma_i - \Delta p \quad (6-1)$$

where ε_i is the strain component in direction i , and E , ν , and β are Young's modulus, Poisson's ratio, and the coefficient of linear thermoelastic expansion, respectively, $\Delta\sigma'$, Δp and ΔT are the changes in effective stress, pressure and temperature respectively. This leads to:

$$\Delta\sigma'_h = \left(\frac{\beta E}{1-\nu}\right)\Delta T - \left(\frac{\nu}{1-\nu}\right)\Delta p \quad (6-2)$$

$$\Delta\sigma_h = \left(\frac{\beta E}{1-\nu}\right)\Delta T - \left(\frac{1-2\nu}{1-\nu}\right)\Delta p \quad (6-3)$$

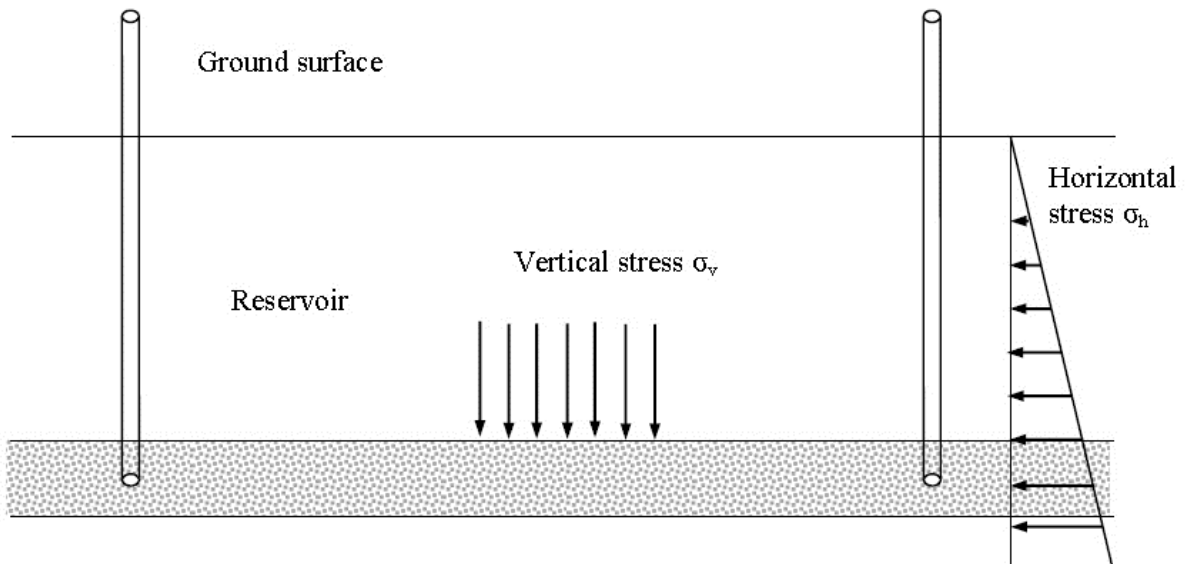


Figure 6-2: A schematic model of stresses in a laterally extensive reservoir (Dusseault, 1993).

Assume $\Delta T = +100^\circ\text{C}$ (e.g., hot water injection), Young's modulus (E) of 50 GPa (for a carbonate), Poisson's ratio (ν) of 0.25, and a thermal expansion coefficient (β) of $10 \times 10^{-6}/^\circ\text{C}$.

Assuming no pore pressure change (e.g., $\Delta p = 0$ so that $\Delta \sigma = \Delta \sigma'$), the horizontal stress will increase by ~ 66 MPa, large enough to lead to shearing and even cracking of the matrix rock if there are sharp thermal fronts with steep gradients of thermal strain (differential local differential expansion). Rock joints dilate and shear in response to non-uniform stress changes arising from non-uniform temperature changes, and the resulting changes in macroscopic permeability certainly exceed an order of magnitude. Similar calculations for steam injection into shallow oil sands (< 800 m) show that shearing and dilation are unavoidable, and massive non-linear property changes take place at ΔT values as low as 60 to 80°C.

Early work on thermoelasticity in reservoirs include [Aktan and Farouq Ali \(1978\)](#) who used a Finite Element (FE) method in a 2-D porous media model subjected to single-phase hot water injection. They concluded that thermally induced stresses dominate the stress state, and as temperature rises, they are far larger than pressure effects and even gravitational stresses. This important conclusion has withstood the test of time.

In an attempt to reduce the number of degrees of freedom in complex reservoir modeling, [Yin *et al.* \(2009a\)](#) developed a fully coupled THM approach using a FE solution to model the reservoir and the surrounding thermally affected zone, combined with a displacement discontinuity method to model the surrounding elastic, non-thermal zone. The method can be implemented for simulation of thermal viscous oil production and unconsolidated sandstone reservoir development involving large volume changes associated with dilation, but the specification of the constitutive behavior of the changing rock mass remains a challenge.

6.5 Geomechanical Behavior of Reservoir Rocks at Elevated Temperatures

Geomechanics is central to modeling and simulation of processes involved in VO production because of massive thermal alteration of the reservoir rock mechanics and transport properties.

6.5.1 Thermal Characteristics of Rocks at Elevated Temperatures

6.5.1.1 Thermal Conductivity and Thermal Diffusivity

[Somerton and Boozer \(1960a, 1960b, 1961\)](#) measured thermal diffusivity and conductivity of some typical sedimentary rocks using an unsteady-state conductivity method for $T = 90$ to 800°C , reporting that thermal diffusivity and conductivity decreased drastically at elevated temperatures. As an example, changes in thermal diffusivity at elevated temperatures are presented for Bandera Sandstone, a very fine-grained consolidated sandstone with 20% porosity, and a medium-coarse grained vuggy limestone with 18% porosity in Figure 6-3, up to 400°C only.

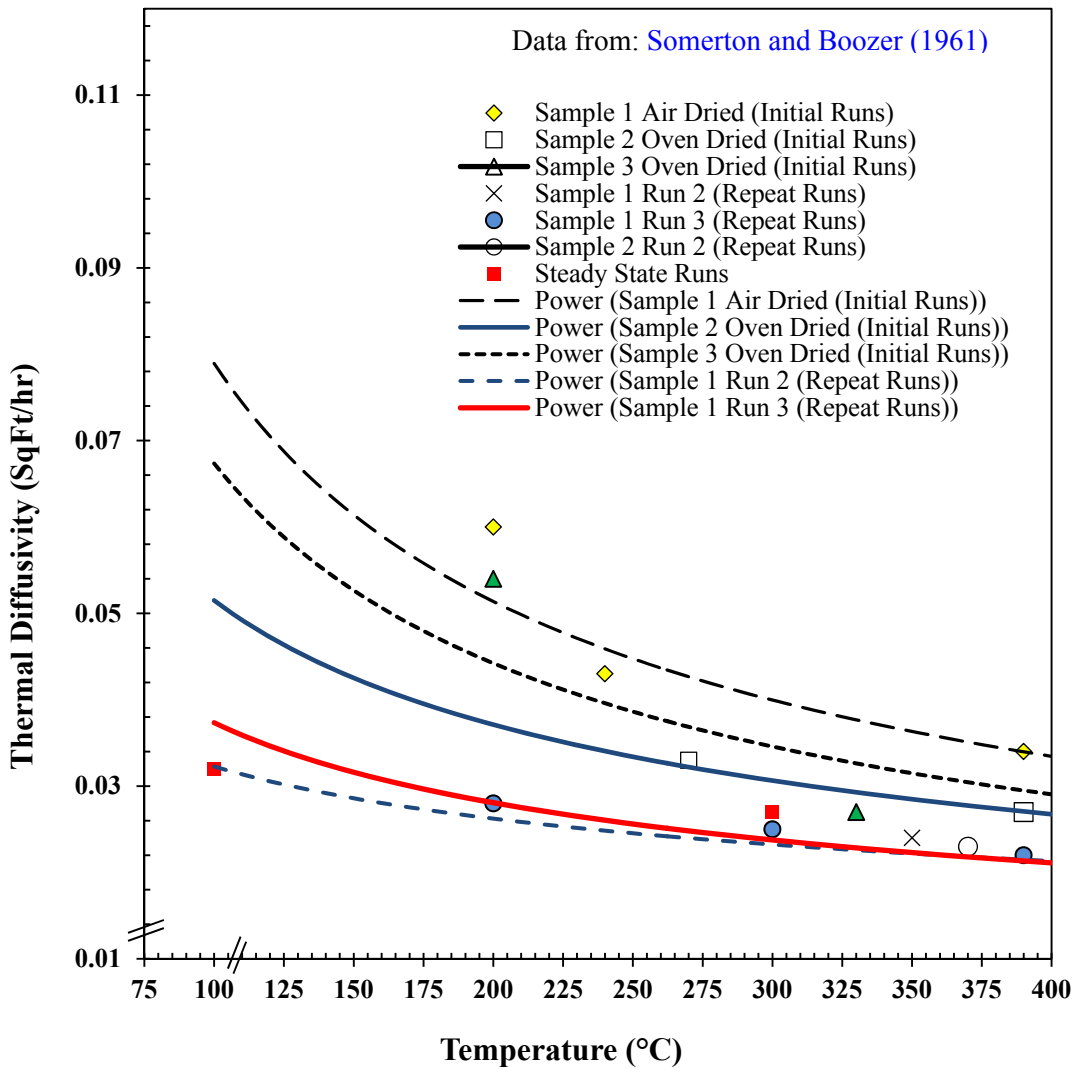


Figure 6-3: Thermal diffusivity of Bandera Sandstone.

Thermal diffusivity decreases with increased temperature: an unsteady-state thermal diffusivity of 0.034 Ft²/hr @ 200°F and 0.032 Ft²/hr @ 200°F and an unsteady state thermal conductivity of 0.898 Btu/hr ft°F @ 200°F and 0.903 0.898 Btu/hr ft°F @ 200°F were reported for the Bandera Sandstone and the Limestone, respectively.

6.5.1.2 Thermal Volume Expansion and Heats of Reactions

[Somerton and Selim \(1961\)](#) measured and reported thermal volume expansions and heats of reactions of three typical sandstones (Bandera, Berea, and Boise) for 25 to 1000°C. They concluded that sandstone expansion is controlled by the expansion characteristics of the quartz content. Also, they reported permanent deformation or structural damage to the tested samples after heating, leading to a change in thermal conductivity of the heated sandstone samples. The volume thermal expansion of the three tested sandstones is presented in Figure 6-4.

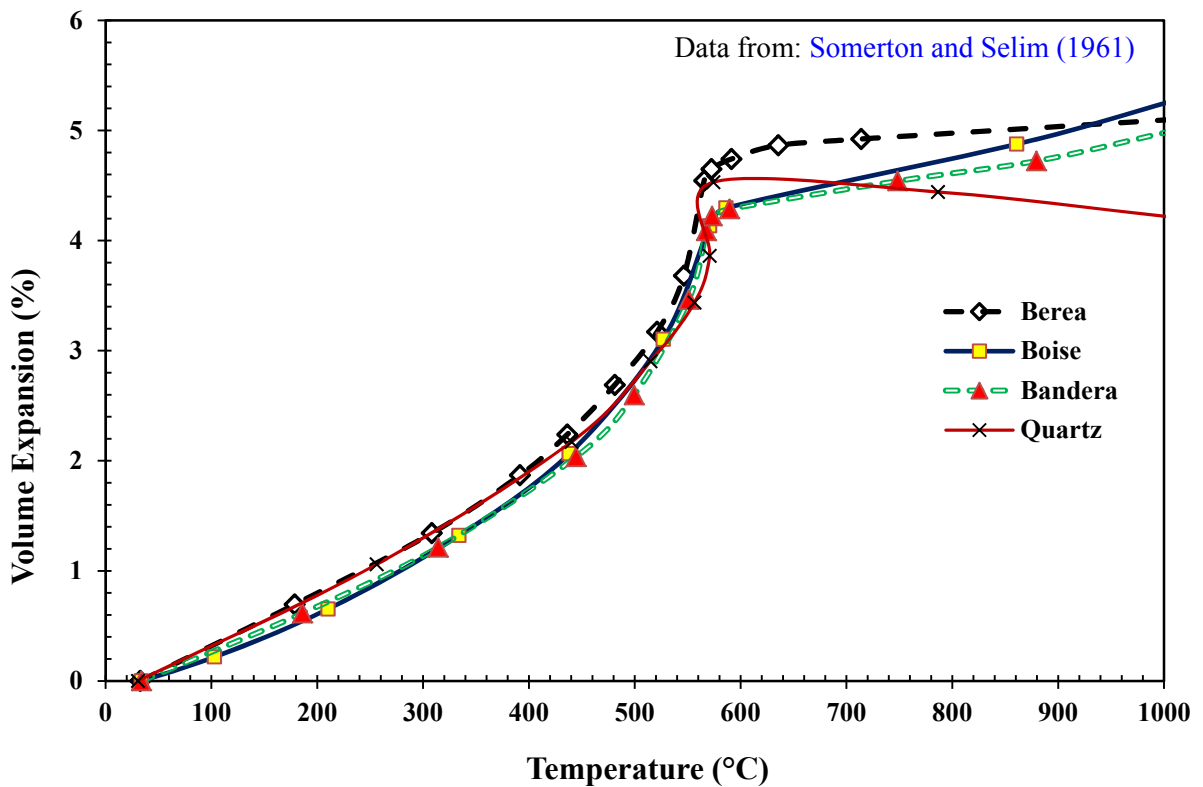


Figure 6-4: Volume thermal expansion of three tested sandstones.

[Somerton and Selim \(1961\)](#) reported that based on their laboratory observations and measurements, the linear thermal expansions of the three sandstones were nearly the same despite the fact that the quartz contents of the three sandstones ranged from about 50% for Boise to 90% for Berea. This finding implies that there is an irreversible internal damage

due to heating of the crystalline rocks due to internal differential grain expansion; such damage has important effects on permeability and fluid flow properties. However, Figure 6-4 also shows something very important with respect to steam injection: at the temperatures that can be achieved by steam injection (325°C), there is no “special” behavior of the SiO₂ grains, they behave thermoelastically as individual grains without crushing or deforming.

6.5.2 Chemical Reactions

[Nadeau \(1990\)](#) reported that the formation of a small amount of smectite (< 5%) can lead to a significant permanent reduction (1 to 2 orders of magnitude) in the reservoir rock permeability. [Kirk *et al.* \(1987\)](#) concluded that newly formed smectite during laboratory steam flood experiments using rock samples from the Clearwater Formation (Alberta) was the main cause of permeability reduction. [Keith *et al.* \(1998\)](#) experimentally investigated the rock fluid interactions in siliciclastic carbonate-cemented reservoirs during steam processes. They concluded that smectite is the dominant authigenic phase affecting permeability in the experiments conducted. The literature on chemical reactions during thermal viscous oil processes is vast, but such reactions may play a role in understanding reservoir properties alterations especially in carbonate reservoirs. In sandstones undergoing shear dilation, it is easily argued that these reactions have far less consequence on the transport properties in practice because newly-formed clays can be flushed out of the system more easily.

6.5.3 Ultrasonic Velocities of Unconsolidated Sandstones

[Doan *et al.* \(2010\)](#) investigated T effects on ultrasonic velocities of natural and reconstituted unconsolidated sandstones from the Fontainebleau sand to the McMurray Formation in Canada (porosity up to 37 to 40%, permeability of 10⁻¹² m²). The samples were tested at -30°C to 80°C and at effective stresses from 1.2 to 8 MPa. They concluded that the elastic wave velocities measured are strongly temperature dependent, mainly because of viscosity effects, whereas little effect of effective stress was observed. Velocities decrease with increasing temperature and increase with increasing effective pressure. This is an indication of how stress and temperature changes during thermal VO production operations impose

complex changes in the elastic properties of the reservoir rock (not even accounting for elastoplastic shear dilation). Figure 6-5 shows the changes in compressional (V_p) and shear velocities (V_s) in a VO saturated reconstituted sample. Seismic techniques have merit in delineating reservoir changes in VO thermal methods, but a great deal needs to be done before factors such as dilation can be quantified separately from effects of stress, saturation and viscosity changes. In the laboratory, control over variable is feasible, but in the field, all changes act simultaneously, making deconvolution challenging.

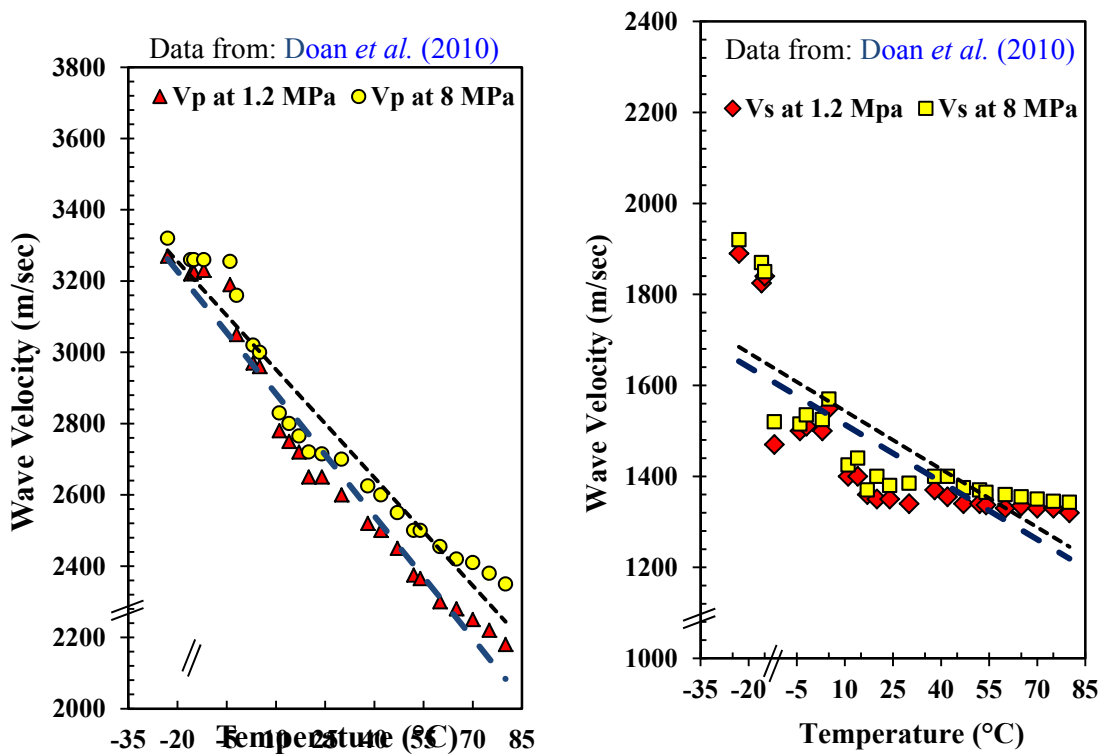


Figure 6-5: Compressional (V_p) and shear velocities (V_s) in VO saturated reconstituted sample.

6.5.4 Geomechanical Properties of Rocks at Elevated Temperatures

Meibner *et al.* (1999) investigated the stress-strain behavior and temperature dependence of a quartz-bonded sandstone from Queiderzbach/Pfalz in Germany up to 250°C and 60 MPa. They also developed a constitutive relation allowing approximation of rock strength under

any 3-D tensile stress states. They reported a significant decrease in Young's modulus of the sandstone with temperature (Figure 6-6), but again, in the context of thermally induced shear dilation, these results have limited application, only suited to the pre-plastic phase of deformation.

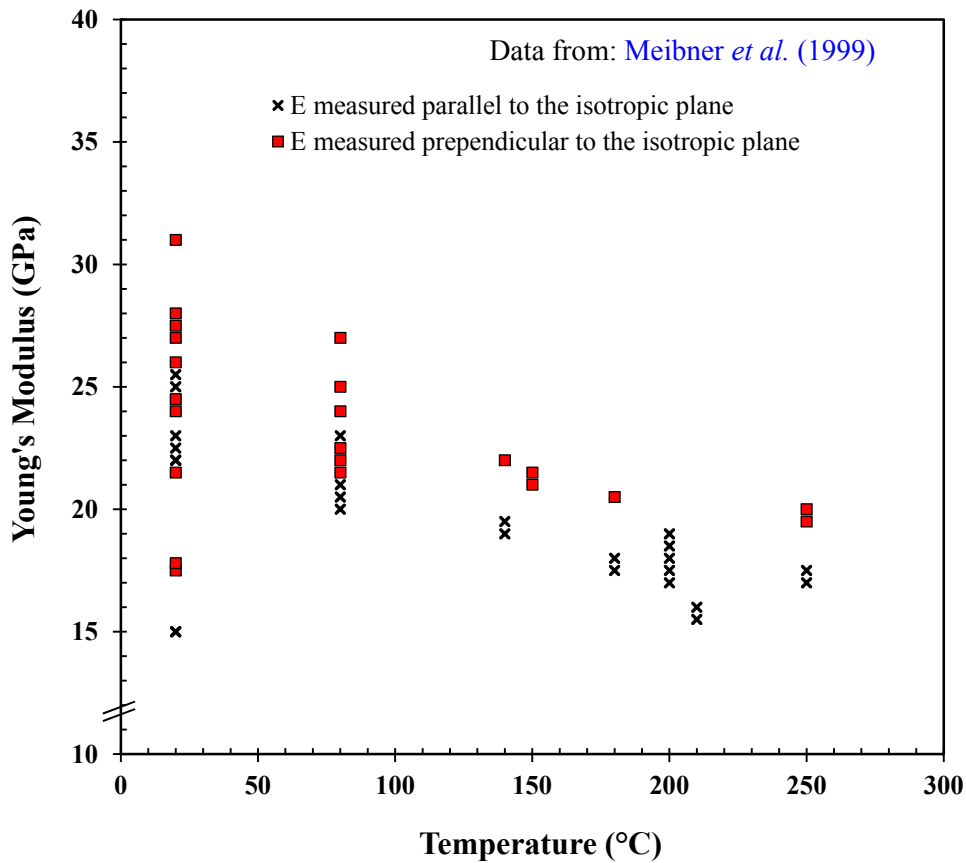


Figure 6-6: Sandstone (compression); Young's modulus parallel and perpendicularly to the isotropic plane.

Zhang *et al.* (2009) examined the geomechanical properties of some rock types including sandstone subjected to temperatures of 25 to 800°C (Figure 6-17). The peak strength and elastic modulus change in the range up to 300°C, but as stated before, the magnitude of the changes are in the range of 20 to 30%, and this is small in proportion to the changes arising from shear dilation. Data above 300°C are not considered relevant for steam processes.

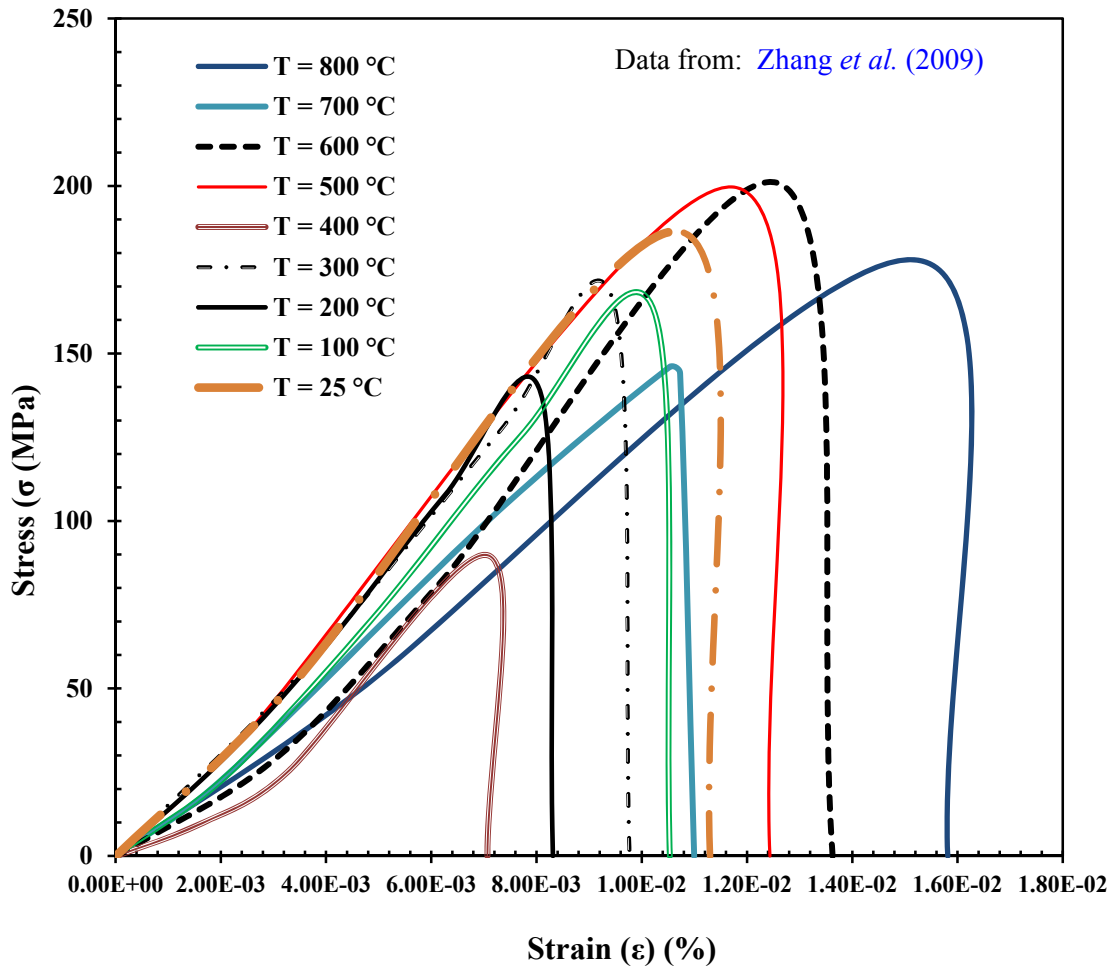


Figure 6-7: Stress-Strain curve obtained for the tested sandstone samples at elevated temperature.

Hettema *et al.* (1991) performed triaxial tests on Felser sandstone (Germany) to investigate the effects of temperature (150 to 250°C) and pore pressure on geomechanical behavior. The Felser is a moderately poorly sorted immature homogeneous sandstone in a clayey matrix with $\phi \sim 20\%$, $k \sim 5$ mD, and at 29 MPa, $\nu \sim 0.25$, and $E \sim 50$ GPa. Some typical strain-time curves obtained for the Felser sandstone under different differential stresses at 150°C and 250°C are presented in Figure 6-8. These researchers concluded that the temperature dependence of the strain rate is also stress dependent, and proposed that under higher stress levels thermally activated creep is active, leading to additional time-dependent deformation.

The relevance of these results to thermal VO processes using steam in UCS reservoirs remains undefined, and a deficiency of all the literature identified to date is that the effects of shear dilation in sandstones and massive thermally-induced microcracking from differential thermal expansion in limestones are simply not understood, and are apparently very difficult to study in the laboratory.

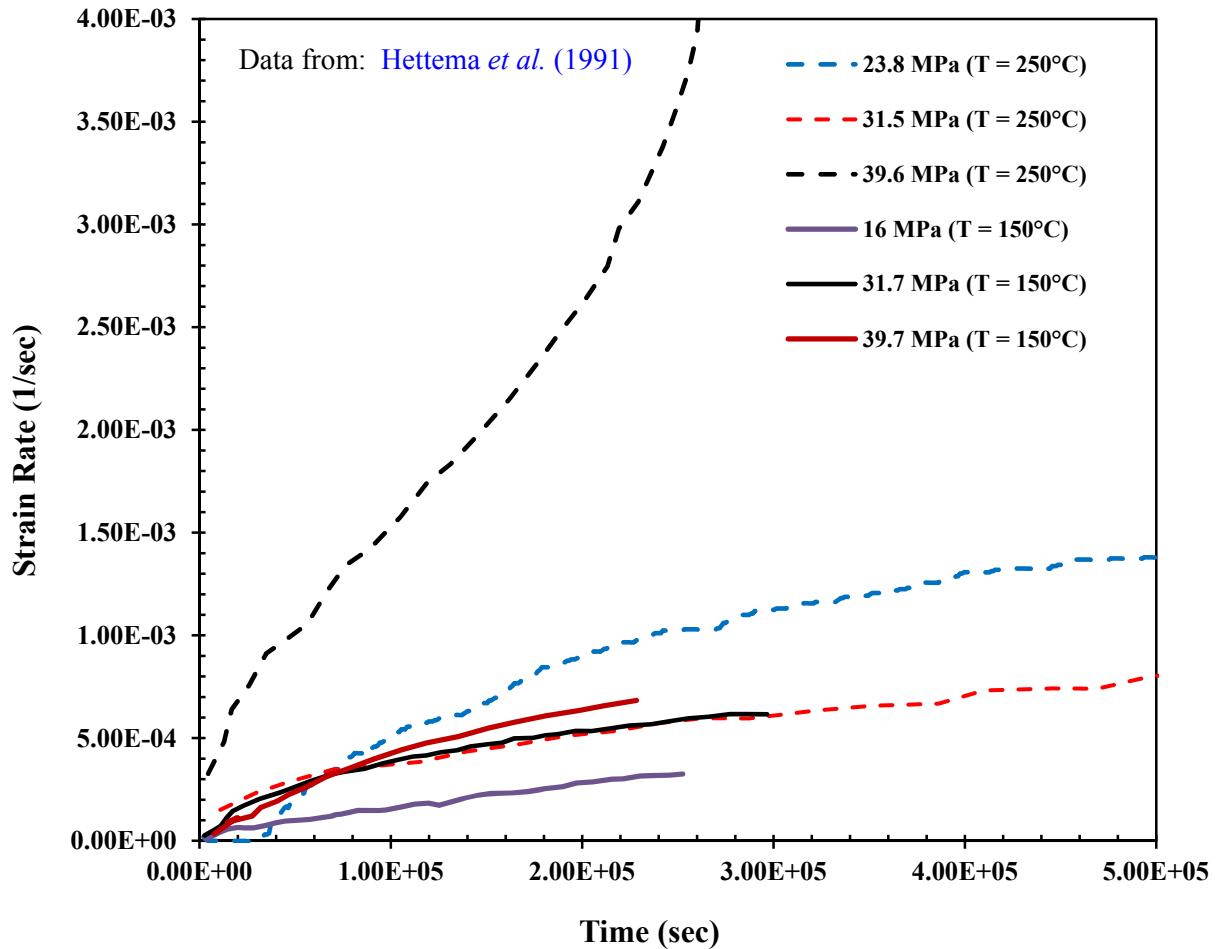


Figure 6-8: Strain-time curves for the Felser sandstone under different differential stresses at 150°C to 250°C.

Almost all of the literature relating to thermal behavior reported in the literature is of little practical value to steam injection process simulation in VO extraction projects, whether in limestones or in UCSS. Some points can be made, not all of them fully backed up by laboratory data, but considered to be correct nonetheless.

General shear and dilation are very important processes in UCSS because they affect transport properties. Shear dilation will be suppressed if the effective confining stresses remain high during the thermal process. For example, at a depth of 300 to 400 m, a quartzose UCSS may dilate substantially, but the same sand may dilate only minimally at a depth of 1 to 1.5 km, as long as the pore pressure remains approximately hydrostatic. However, if a thermal process is accompanied by a very high pore pressure (hot fluid injection close to fracture pressure), or if it is shallow (< 200 m) dilation will be proportionately greater and therefore more important to the success of the project.

In general, thermal diffusivity and conductivity of sedimentary rocks decreases drastically at elevated temperatures, but in a range beyond that encountered in steam injection. Thermal conductivity is altered, more so with dilation, but because the heat transfer processes are advectively driven, the consequences on processes may be minimal.

In the range of temperature less than about 325°C, properties such as Young's modulus and Poisson's ratio, strength, permeability, and so on, may be altered by as much as 20 to 40%, but these changes are in the absence of dilation, or in the case of carbonates containing VO, in the absence of microcracking from differential thermal expansion. Again, the question arises as to the relevance of laboratory data in the context of the overwhelming evidence of massive shear dilation *in situ* (see Figure 6-1). It is possible in the laboratory, without shear and dilation, to generate permeability impairment, but in field, such impairment is not evident.

Chemical reactions may play a role in controlling reservoir permeability during thermal oil extraction production operations, more so in carbonates than in dilating UCSS strata.

Elastic wave velocities measured in thermal experiments are strongly temperature dependent, mainly because of viscosity effects rather than because of effective stress or fracture aperture changes. Velocities decrease with increase in temperature and increase with increase in effective stress (a weak dependence). Clearly, changes in stress and temperature during thermal VO production operations impose complex changes on the elastic and seismic properties of the reservoir rock. Seismic methods (including passive microseismic tomography) can be implemented for reservoir monitoring with some degree of success, despite the fact that a great deal of research needs to be done in this area because of the complexity of coupled processes (stress, pressure, heat, and porosity changes).

Rocks under high temperatures are weakened and softened; laboratory work indicates that at high temperatures ($T = 500$ to 600°C) there is a significant reduction in Young's modulus, peak strength, and tensile strength. These temperatures are never reached in steam injection, but are easily encountered in any combustion or *in situ* gasification process.

Laboratory studies support that heating carbonate rocks sufficiently leads to the point of internal dilation of the rock (e.g., dilation of calcite crystals and initiation of thermal cracking within the rock material), leading to decreases in V_p , and increases in ϕ . This dilation must be important with respect to permeability and hence the rate of a thermal process; it should be investigated more thoroughly in the context of transport property changes for VO NFCRs.

In higher porosity rocks (high porosity carbonates and dolomites), thermal shock can cause shrinkage as the internal structure is weakened and contracts under the ambient effective stresses, constricting channels connecting the pores and reducing the rock permeability. It is unlikely that these processes would be dominant in steam processes, but they would arise at higher temperatures associated with a combustion process, or in rocks with exceptionally high porosity (e.g., high porosity chalk or diatomite).

We conclude that reservoir properties of UCSS will be enhanced during thermal oil production operations, helping make them a promising energy resource in the future, but for

carbonates, there is less clarity at the present time as to how much damage occurs in the matrix blocks and what is its effect on transport behavior).

6.6 Thermal Geomechanics Effects in Sandstones/Oil Sands (SAGD Case)

Researchers have addressed thermal geomechanics aspects of VO production in the past two decades, trying to understand the impact of geomechanics processes on reservoir simulations, SOR values, production mechanisms, and predictions (Butler, 1986; Dusseault and Rothenburg, 1988; Scott *et al.*, 1994; Chalaturnyk, *et al.*, 1991; Chalaturnyk and Scott, 1995; Chalaturnyk, 1996; Singhal *et al.*, 1998; Shen, 2000; Collins *et al.*, 2002; Chalaturnyk and Lee, 2004; Collins, 2005; Li and Chalaturnyk, 2006; Yin *et al.*, 2010). Major driving factors have been the obvious large vertical surface deformations, extensive microseismic activity (largely stick-slip shear), and the failure of conventional reservoir simulators in making predictions based on constant virgin permeability and compressibility values.

In an early attempt to address reservoir properties alteration during thermal oil production processes, Butler (1986) investigated thermal expansion of pore liquids and resultant pore pressure increase during steam injection (CSS). He proposed a model to explain the effects of steam injection into a permeable stratum on the adjacent reservoir (e.g., surface heave, permeability improvement) assuming that heat flows only by thermal conduction and the major effects are pore volume and bitumen expansion. Without invoking geomechanics, he concluded that during CSS high pore pressures may extend several meters into the reservoir, mainly in zones where heating has caused notable thermal expansion, but where bitumen viscosity is still too high to permit rapid pressure relief. These views are no longer widely held.

Chalaturnyk *et al.* (1991) developed a geomechanical model which used temperatures from a classical reservoir simulator to compute an equivalent single-phase hydraulic conductivity, concluding that dilation zones (induced through generalized shear failure) within the cold reservoir might occur between wells, as well as near the thermal fronts. Scott *et al.* (1994) also concluded that the volume and permeability changes are controlled by changes in mean

principal effective stress, shear stress, and temperature. In a similar vein, [Singhal *et al.* \(1998\)](#) noted partially irreversible shear dilation if some threshold pressure was exceeded in the formation; also, effective permeabilities were increased, enabling larger-than-expected injectivity and productivity, and confirming the vital role of geomechanics in viscous oil development.

[Shen \(2000\)](#) carried out a numerical investigation of SAGD and shear dilation zones with attendant reduced capillary pressure and enhanced permeability; oil rates were predicted to be five times greater than for the base case without dilation. [Collins *et al.* \(2002\)](#) concluded that shear dilation in and in advance of SAGD chambers developed through differential thermal expansion, especially for shallow reservoirs (“thermal jacking” in the vertical direction in advance of the growing steam chamber).

Figure 6-19 shows conceptual shear and dilation behavior for sands; dense quartzose sands under moderate confining stress expand during shear, leading to increases in porosity and permeability. In a lithostratigraphic sequence with thin shale seams and clay dustings on bedding planes, massive permeability increases would be expected, especially in k_v as horizontal clay barriers are broken.

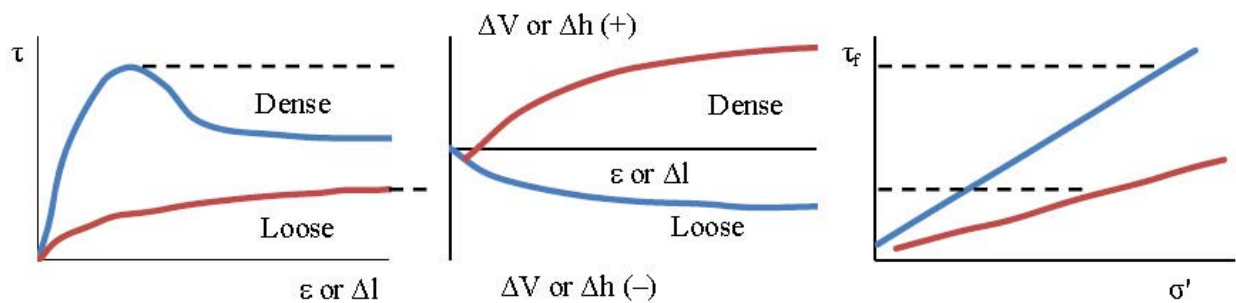


Figure 6-9: Shear test results for dense and loose sand: From left to right: Shear stress – lateral displacement, shear stress – normal effective stress (Mohr-Coulomb shear yield diagram), and volumetric strain – lateral strain.

Heating dense sand to 200 to 300°C causes large thermoelastic expansion (Figure 6-10), which acts against the surrounding cool rock. This gives rise to zones of increased and reduced compressive stresses, which in turn leads to shearing and dilation of dense intact reservoir sand in advance of the thermal front. This dilation is volumetrically widespread and occurs throughout the sand, giving porosity increases from 28 to 30% to as high as 32 to 34% locally, with concomitant increases in permeability. As the shear dilation also breaks apart thin clay layers on bedding planes and 10 to 20 mm thick clayey streaks, the effect on bulk permeability of the bulk reservoir is profound: average permeability can easily be increased from 1 to 2 D to 5 to 8 D, but most important, barriers to vertical flow are breached, allowing the macroscopic vertical permeability to reach values of 2 to 5 D, thereby reaping the full beneficial impact of gravity segregation of immiscible phases of different density (Collins *et al.*, 2002).

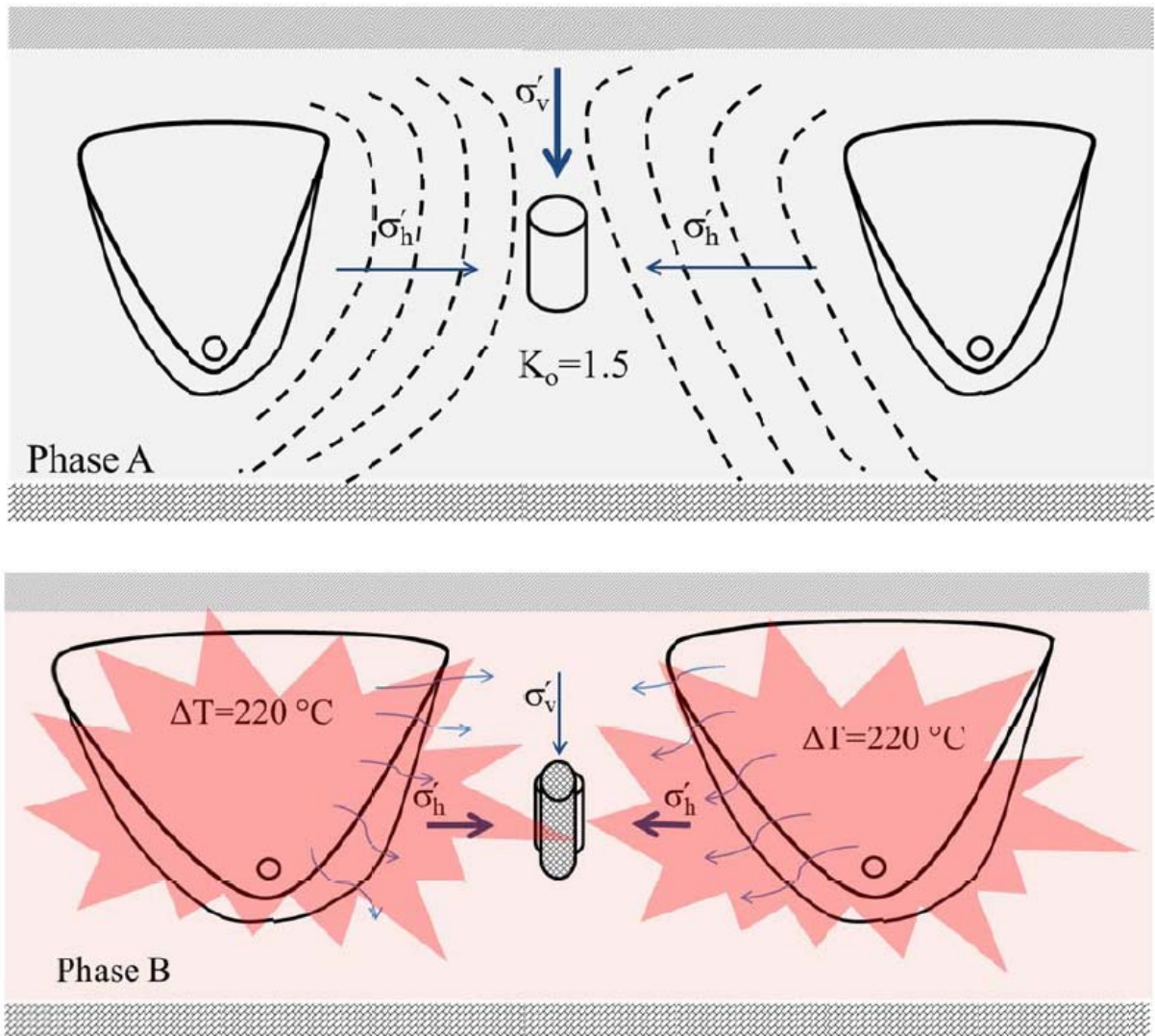


Figure 6-10: Thermally induced shear dilation in SAGD. Phase A: Initial stage of a SAGD operation. Phase B: A mature SAGD operation. These sketches show how horizontal stresses increase during a thermal operation.

Figure 6-11 demonstrates a perpendicular slice of a group of SAGD chambers, as well as an axial cross-section of one SAGD well pair. Gravity drainage is implemented at about the virgin p_o , so there is no significant regional flux arising from induced pressure gradients. Steam rises under gravitational thermal segregation, moves laterally, condenses into water,

and flows along with hot oil toward the producing well. The phase density difference ($\Delta\rho$) dominates flow because of the difference in head ($\Delta\rho \times g \times z$), and the flow rate is of course proportional to the vertical permeability, which is greatly improved by shear dilation.

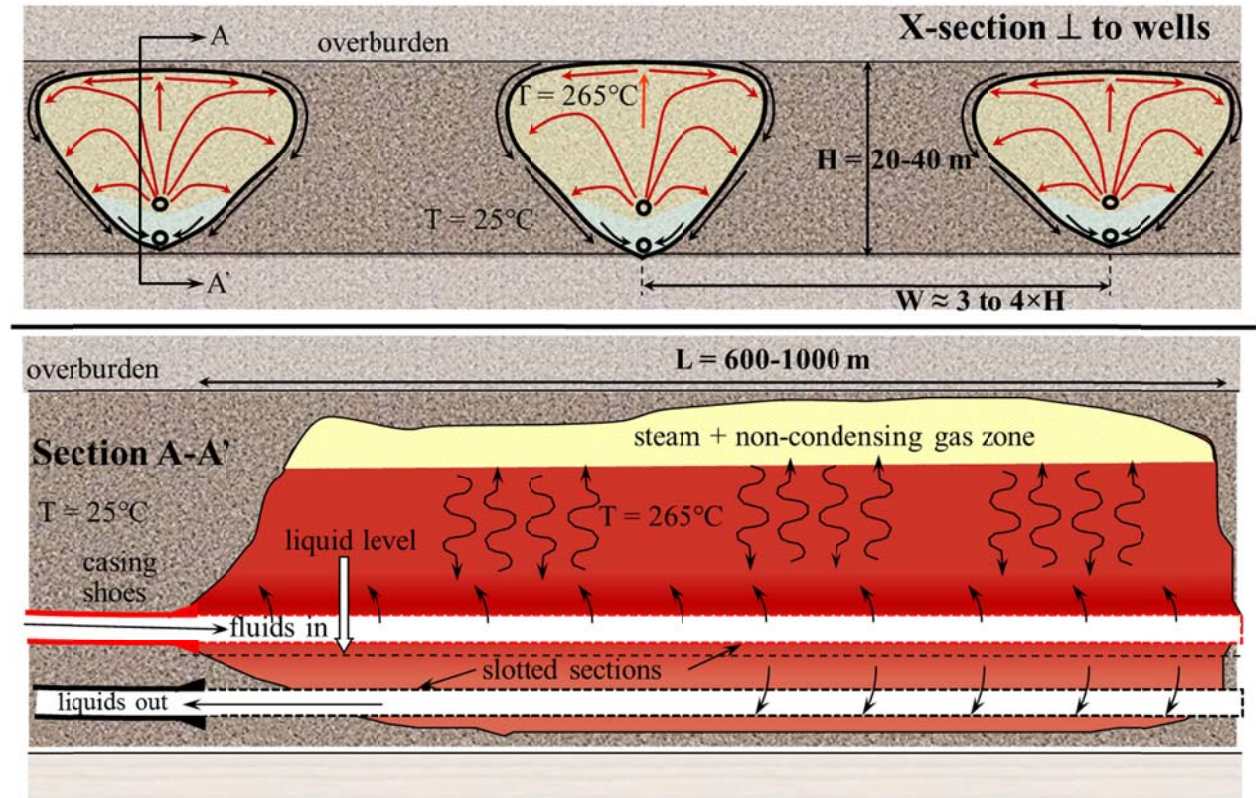


Figure 6-11: The geometry of the SAGD and thermally induced stresses. Typically, $H = 20$ to 35 m , $W/H \approx 3.5$ to 4 and $L = 750$ to 1000 m .

Assuming $H = 30\text{ m}$, $Z = 500\text{ m}$ with initial conditions $T \sim 25^\circ\text{C}$, $\sigma_v = \sigma_h \sim 12\text{ MPa}$ and $p_o \sim 5\text{ MPa}$, the equilibrium T of the steam at 5 MPa is 265°C , thus $\Delta T \sim 240^\circ\text{C}$. A typical thermal expansion coefficient of $\phi = 0.28$ to 0.3 quartz sand is 8 to $10 \times 10^{-6}/^\circ\text{C}$, and the elastic parameters are on the order of $E \sim 3\text{ GPa}$, and $\nu = 0.25$.

When a group of SAGD steam chambers under these conditions is ‘grown’, the surface of the ground rises by about 300 to 400 mm (Figure 6-1). However, a thermoelastic calculation, even assuming 100% of the volume of the reservoir is heated to 265°C , gives

$(0.000010 \times 240 \times 30) \sim 70$ mm, about 20% of the Δz_{\max} measured. Because pore pressures are approximately constant, there is little confining-stress-related dilation, which would be small in any case (the compressibility effect). Therefore, the rest of the vertical heave must be the result of fabric dilation, which can only happen if high shear stresses are generated, under either hot or cold conditions.

Consider the limiting case where the entire stratum is homogeneously heated to 265°C , assuming no lateral strain, $\epsilon_x = \epsilon_y = 0$. For the parameters above, this approximation gives $\Delta\sigma'_x \sim 10$ MPa, or $\sigma'_v \sim 7$ MPa, $\sigma'_h \sim 17$ MPa. However, this is insufficient for shearing and dilation to develop (a higher *in situ* value for E is also reasonable). Another analysis that accounts for the non-uniform distribution of strain leads to a different conclusion. The key observation is that in advance of the thermal front (Figure 6-11), stress changes are compressive in horizontal directions, but the vertical stress is diminished substantially, taking the deviatoric stress sharply into a condition of shear failure at low confining stresses (Yin *et al.*, 2009b). This is a relatively local effect that is focused in the region of 0 to 20 m in advance of the steam front, and one can perform calculations that show that even at ΔT as low as 100°C , the vertical effective stress in advance of the thermal front drops below the pore pressure value for any reasonable set of mechanical parameters, leading to dilation and changes of properties.

The mechanisms are more fully detailed here:

- Injection of steam leads to thermal expansion in all directions.
- In advance of the chamber wall, the sand is subjected to strong compression in the horizontal (radial) direction and extension in the vertical (tangential) direction.
- Changes in deviatoric stress ($\sigma_1 - \sigma_3$) can easily exceed 20 MPa, likely much larger.
- Shearing takes place once the local shear yield criterion is satisfied.
- Because of moderate σ'_3 , a large amount of dilation accompanies the shearing process.
- Shear occurs throughout the reservoir, not on just a few planes; general dilation ensues.

- As the chamber grows, previously dilated material is progressively incorporated into it.
- Within the steam chamber compressive stresses are higher; some dilation is lost by compression – or “re-compaction”, but most shear dilation is irreversible.
- Strong dilation in front of the chamber increases permeability by ~ 2 to 5 times.
- Clay dustings on bedding planes and shale layers a few cm thick are sheared and breached, strongly enhancing k_v , which in turn governs gravity drainage rate.
- A strong porosity increase (probably 4 to 5% locally) causes water influx (imbibition, as the oil is far less mobile), so k_w increases by at least an order of magnitude, allowing thermal convection to develop in advance of the zone where the oil is starting to be “melted” by the high T.
- Increased pore throat size and dislodging of clay particles in pore throats greatly reduces capillary entry pressure, allowing better displacement and easier heat flux.
- The chances of pore throat blockage in sand once it has undergone general shear dilation is reduced.

These permeability increases and accelerated heat transfer mechanisms make gravity drainage more efficient, allowing heat flux to become dominated by convection in the dilated zone in front of the steam chamber. The mechanism of dilation-induced improvements in properties is a major reason why SAGD has proven far more successful in practice than initial simulation results suggested (Collins *et al.*, 2002; Collins, 2007), and SAGD can thus be used in many cases where the intrinsic vertical permeability might seem too low to allow success. Higher pressure SAGD increases the dilation potential of the quartz sands if this is deemed desirable.

6.7 Caprock Integrity and Thermally Induced Casing Shear Mechanisms

The beneficial effects of thermal stimulation have been highlighted above, but there are several concerns. Here, three geomechanical effects that are generally negative in consequence are briefly described.

In Figure 6-10, increased horizontal compressive stress in the heated zone from thermal expansion is shown. However, above the steam chambers, especially if heating is not spatially homogeneous along the axis of the steam chambers, the horizontal stress in the caprock drops. If a high-pressure process is used and the amount of drop is such that P_{inj} becomes greater than σ_h , an upward propagating vertical fracture can develop. This can breach the flow integrity of the chamber, leading to loss of heat, but in an extreme case, such as took place in northern Alberta in 2006, a gas and steam blow-out can develop (stopping development of a project in which half a billion dollars had been invested). These processes are currently the focus of intense study because of the high value of shallow heavy oil resources in Canada and elsewhere (Collins, 2005; Uwiera-Gartner *et al.*, 2011; Carlson, 2012; Ibatullin *et al.*, 2012; Walters *et al.*, 2012).

Another geomechanical effect arising from thermal stimulation that can impact caprock integrity is shrinkage of clay-rich overlying shale barriers. Once the temperature exceeds $\sim 125^\circ\text{C}$, adsorbed water is stripped off clay minerals, leading to a drying and shrinkage of the shale bed if it has an initially high porosity ($> 15\%$). As a small amount of shrinkage occurs, the horizontal stress is reduced, and eventually drops below the pressure of the pore fluid (steam-oil-water-gas) in the reservoir, so that vertical hydraulic fractures are generated. This can lead to loss of fluid and heat, as well as creating conditions leading to a blowout if the project is shallow.

Shrinkage of shale or clay-rich sediments can lead to a loss of seal around casings in the strata overlying the thermal zone. The high temperature in the cased wellbore diffuses into the rock around the casing, and the shales undergo thermal shrinkage, opening a gap between the casing and the rock, allowing vertical migration of fluids behind the casing. A related problem in cyclic steam methods is that the cyclic thermal effects lead to expansion/contraction of the casing, leading to deterioration of the cement sheath and loss of seal (Taoutaou *et al.*, 2010).

Differential thermal expansion between a convectively heated reservoir (rapid) and a conductively heated overburden (slow) leads to concentration of shear stress (Figure 6-12).

The shear stresses generated by even 40 to 60°C differential temperature are enough to cause shear slip, and the casing cemented through the interface is first distorted, then ruptured or collapsed (Dusseault *et al.*, 2002). Because the area experiencing shear is large, no cemented casing can resist the shear loads, therefore avoidance and mitigation are needed to reduce the incidence of casing shear. As an example, in the IOL Cold Lake Project, at least 40 to 50 wells must be repaired annually because of casing shear.

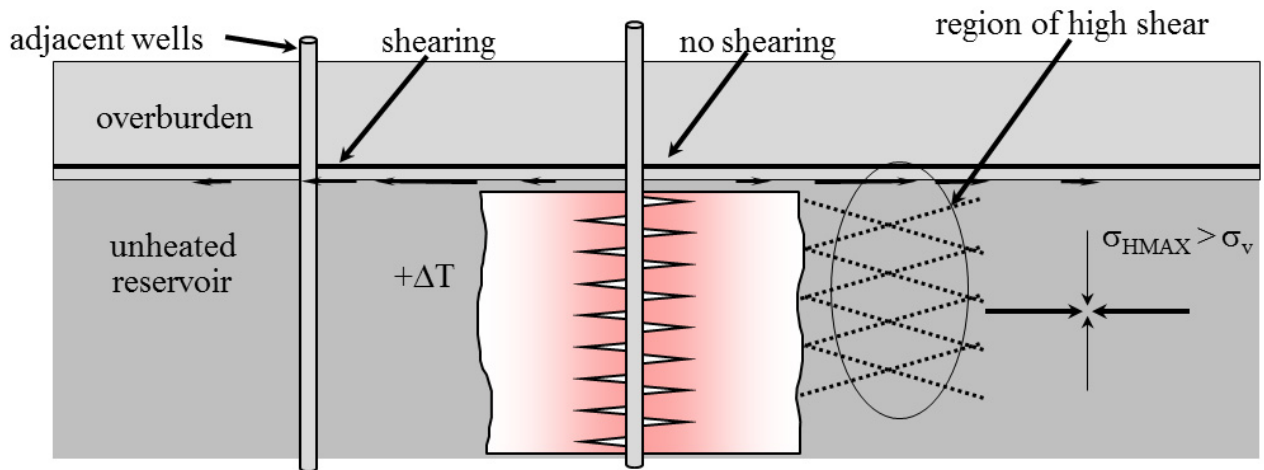


Figure 6-12: Schematic view of thermally induced shearing in unconsolidated sandstones.

6.8 Concluding Remarks

About 70% of the world's liquid petroleum is in the form of viscous oil in unconsolidated sandstones (55%) and fractured carbonates (15%). Each lithotype presents unique technical challenges for analysis and production predictions, and understanding the geomechanical behavior of these strata at temperatures up to 325°C is becoming central to any thermal VO production scheme.

Steam injection processes have achieved commercial success in accessing this immense resource, and a major contributing factor to economical production is the beneficial change in permeability, porosity and compressibility that takes place because of large thermally-induced stresses. Shear dilation in sandstones enhances flow properties and greatly

accelerates oil extraction, particularly by breaching thin clay layers and thereby increasing vertical permeability by as much as an order of magnitude; this permits gravity drainage processes to take place at economical rates. Similarly, fractured carbonates will evidence improvements in flow behavior as fractures shear and dilate. Some difficult operational issues may arise from thermal effects, including casing shear and breach of overlying reservoir seal.

To improve mathematical modeling capabilities in thermal VO exploitation, coupled models that include changes in rock mechanics properties should be developed. This also means that deformation monitoring of field projects should be improved and more widely used so that these coupled geomechanics models can be calibrated, and thereby give better predictions on which to found economic decisions. Microseismic emissions monitoring or active seismic surveys to quantify changes in seismic attributes are promising but hampered by a weak understanding of the effects of temperature and dilation on rock response in the presence of saturation, pressure, effective stress and fluid properties changes.

Thermal petroleum geomechanics is and will continue to be an exciting and highly useful area as VO production continues to slowly increase. The area is ripe for new ideas in monitoring, modeling, and production methods.

Nomenclature

Acronyms, Symbols, Units

Acronyms: Production Technologies

CSS	=	Cyclic Steam Stimulation (vertical wells)
HCS	=	Horizontal well Cyclic steam Stimulation
SAGD	=	Steam-Assisted Gravity Drainage
SF, SD	=	Steam Flood, Steam Drive

Acronyms: Others

2-D	=	Two Dimensional
API	=	American Petroleum Institute gravity scale
b	=	Barrel of oil
b/d	=	barrel per day
Bb	=	Billion barrels of oil
D, mD	=	Darcy, millidarcy
DDM	=	Displacement Discontinuity Method
FEM	=	Finite Element Method
HO	=	Heavy Oil
HPHT	=	High-Temperature/High-Pressure
IOL	=	Imperial Oil
NFCR	=	Naturally Fractured Carbonate Reservoir
OOIP	=	Original Oil In Place
SOR	=	Steam-to-Oil Ratio

Tb	=	Trillion barrels of oil
THM	=	Thermal Hydro Mechanical
THMC	=	Thermal Hydro Mechanical Chemical
UCSS	=	unconsolidated sandstones
UTF	=	Underground Test Facility in Alberta, Canada
VO	=	Viscous Oil
XHO	=	Extra Heavy Oil

Symbols: Latin first and then Greek

$^{\circ}\text{K}$	=	Degrees Kelvin
E	=	Young's modulus (GPa)
H	=	Reservoir thickness
k_v, k_h	=	permeability in Darcies, vertical, horizontal
n	=	Corresponds to heat transfer in crystalline substances
p	=	Pressure
<i>RF</i>	=	Recovery Factor (% OOIP recovered)
S_o	=	Oil saturation degree (100%)
S_w	=	Water Saturation (%)
S_{wr}	=	Residual water saturation
T	=	Temperature ($^{\circ}\text{K}$, $^{\circ}\text{C}$, $^{\circ}\text{F}$)
V_p	=	Compressional wave velocity
V_s	=	Shear wave velocity
z	=	Depth in meters

α	=	Thermal diffusivity (Ft ² /hr or m ² /sec)
B	=	Coefficient of thermal expansion ($10 \times 10^{-6}/^{\circ}\text{C}$)
β	=	Thermal volume expansion
Δ	=	Difference or change in, as in Δp , $\Delta \rho$
δ_c	=	Uniaxial Compressive Strength (MPa)
Δp	=	Changes in pressure
ΔT	=	Changes in temperature
ΔV	=	Changes in volume
Δz , Δz_{\max}	=	Surface heave or uplift
$\Delta \rho$	=	Changes in density
$\Delta \sigma'$	=	Changes in effective stress
ε	=	Deformation
ε_i	=	Strain component in direction i
ε_x , ε_y	=	Deformation in the direction of x or y
μ	=	Viscosity (cP)
ν	=	Poisson's ratio
σ	=	Stress (kPa, MPa)
σ_1'	=	Effective maximum principal stress (MPa)
σ_3'	=	Effective minimum principal stress (MPa)
σ_r'	=	Effective radial stress (MPa)
σ_{θ}'	=	Effective tangential stress (MPa)
ϕ	=	Porosity (%)

Unit conversions

1 barrel	=	0.159 m ³
1°F	=	5/9°C=5/9°K
MPa	=	145 psi

“We must all suffer from one of two pains: the pain of discipline or the pain of regret. The difference is discipline weighs ounces while regret weighs tons.” Jim Rohn

Chapter 7

Geomechanics of Thermal Oil Production from Naturally Fractured Carbonate Reservoirs

7.1 Abstract

Over two trillion barrels of viscous oil (heavy oil, extra heavy oil, and bitumen) are reported in naturally fractured carbonate rocks, worldwide. At present, only primary cold production and CO₂ flooding with very low recovery factors have achieved some commercial success in unlocking this immense energy resource. Steam injection in viscous oil carbonates is being piloted in the Middle East and soon in Canada. This chapter presents the definitions, geology and origins, geographical distribution and the world endowment of viscous oil in fractured carbonates to emphasize its size, then some approaches and physical mechanisms involved in thermal viscous oil production processes are described. High T and p production processes have a profound impact on geomechanical behavior of viscous oil carbonate reservoirs. Thermal-stress-pressure effects on natural fractures can generate changes in flow capacity of several orders of magnitude from wedging or shear dilation around the thermally stimulated zone. Approaches to calculating thermally-induced stresses are described. Available experimental data and field evidence of the thermal, physical and geomechanical behavior of carbonate rocks under elevated temperature and pressure are reviewed, and some of the practical consequences discussed. Most importantly, thermal production changes reservoir behavior, generally leading to production enhancement, although thermal stimulation can generate operational issues such as CO₂ production, induced casing shear, and seal breaching.

7.2 Introduction

The U.S. Energy Information Administration (EIA) in their 2011 International Energy Outlook reported that the world demand for liquid fossil fuels will grow from 85.7×10^6 b/d in 2008 to 112.2×10^6 b/d in 2035. This is mostly because of growing world population and the consequent increase in energy demand, especially in developing economies such as China and India (EIA, 2011). It is expected that by 2035, VO (Viscous Oil – viscosity $\mu > 100$ cP) will make up for about 17% of the daily world oil production and this includes VO from NFCRs (Naturally Fractured Carbonate Reservoirs). The current contribution of VO to world daily oil production is about $9\text{--}10 \times 10^6$ b/d of which about 2×10^6 b/d comes from primary cold production from VO NFCRs (EIA, 2011).

Technologies that can economically produce VO from NFCRs, particularly XHO and bitumen, have major differences compared to conventional oil production technologies. It is usually necessary to reduce the viscosity; in practice, this is achieved by heating, diluting, reducing the molecular weight, or a combination of these. Only very few steamflooding pilot operations are reported in the literature from France, Italy, Congo, Turkey, USA, Kuwait, and Saudi Arabia (Sahuquet and Ferrier, 1982; Chierici *et al.*, 1985; Couderc *et al.*, 1990; Sahuquet *et al.*, 1990; Nakamura *et al.*, 1995; Ono, 1997; Snell and Close, 1999; Snell *et al.*, 2000; Dehghani and Ehrlich, 1998 and 2001; Barge *et al.*, 2009; Brown *et al.* 2011; Gross *et al.*, 2011; Hoadley *et al.*, 2011; Meddaugh *et al.*, 2011; Osterloh *et al.*, 2011). Cyclic steam stimulation also has been applied to VO NFCRs, and public data are available only from cases in Canada, China, Egypt, and Syria (Union Oil Company, 1982; Zhou *et al.*, 1998; Waheed *et al.*, 2001; Li *et al.*, 2010; Samir, 2010a, 2010b). Contribution to the world daily production from VO NFCRs is estimated to be $\sim 2 \times 10^6$ b/d (Shafiei, 2012) which is about 2% of the current world daily oil production of 91.1×10^6 b/d in June 2012 (IEA, 2011), with a minuscule amount coming from the higher viscosity deposits. This suggests that with current rates of exploitation, the ultimate *RF* (Recovery Factor) of the more viscous NFCR VO resource base will remain close to zero unless new technically and economically viable production processes are implemented.

The importance of rock mechanics to petroleum engineering is not new (e.g., Somerton and Boozer, 1960a, 1960b; Somerton and Selim; 1961; Gray, 1967; Komar, 1971; Lauriello, 1974; Heard, 1982; Li *et al.*, 1999; Dusseault *et al.*, 2001; Zhang *et al.*, 2009; Yavuz *et al.*, 2010), but the development of better computational, field, and laboratory tools, combined with an increase in the number and magnitude of rock mechanics-driven issues, have led to a rapid adoption of rock mechanics in petroleum engineering as a basic science input to reservoir analysis, along with the geological, thermodynamic, and transport sciences. Production from deeper and hotter reservoirs as well as steam injection into shallower VO reservoirs have triggered large interest in and more rapid adoption of rock mechanics concepts and calculations into planning and reservoir management. For example, the bottom-hole temperature range for known steam pilots in VO NFCRs is typically about 180–225°C, although bottom-hole temperatures of up to 500°C were reported for a deep (1350 m deep) steamflooding case (Nakamura *et al.*, 1995). Such high temperatures must lead to thermally-induced stresses that are large, compared to the virgin stresses, leading to fracture aperture changes, shearing and dilation.

The impact of thermal stimulation on reservoir properties has attracted interest; for instance, thermal alteration of reservoir rock wettability at elevated temperatures dramatically affects flow rates and recovery factors, impacting project economics, modeling and simulation, and production prediction efforts (Rao and Karyampudi, 1995; Rao, 1999; Civan, 2004; Schembre *et al.*, 2006; Al-Hadhrami, and Blunt, 2010; Kumar and Verma, 2010; Al-Aulaqi *et al.*, 2011). Thermal alteration of capillary pressure (Sanyal *et al.*, 1973), changes in relative and absolute permeabilities in oil sands subjected to high temperatures (Waldorf, 1965; Larman and Jones, 1971; Closmann *et al.*, 1988; Elsworth, 1989; Davies and Davies, 1999; Rutqvist *et al.*, 2008), and thermal stress changes in VO operations have been highlighted as important aspects of VO recovery processes (Butler, 1986; Dusseault, 1993; Scott *et al.*, 1994; Pooladi-Darvish *et al.*, 1994; Pooladi-Darvish and Farouq Ali, 1994; Hettematz *et al.*, 1998; Ito *et al.*, 2002).

High T and p production processes (steam injection, hydraulic fracturing) affect the geomechanical behavior of VO reservoirs. Heating rock around an injection point to 200–250°C causes large thermoelastic expansion which acts against the surrounding cool rock. This gives rise to zones of increased and reduced compressive stresses in advance of the front. More specifically, considering a roughly spherical heated zone, $+\Delta T$ leads to increased radial effective stress (σ_r') and reduced tangential stress (σ_θ') in front of the heated zone, which in turn leads to fracture aperture changes in NFCRs because of changed effective normal stresses across the fracture, or shearing induced by the increase in shear stress (also called deviatoric stress).

A Naturally Fractured Reservoir (NFR) is a reservoir that contains a significant number of fractures (e.g., planar discontinuities) created by natural processes (e.g., diagenesis, dissolution, tectonic forces), distributed as a consistent connected network throughout the reservoir (Saidi, 1987). A more operationally oriented definition would say that a NFR is any reservoir in which naturally occurring fractures have, or are predicted to have, a significant effect on flow rates, anisotropy, recovery or storage (Ershaghi, 1995), either before stimulation (open inter-connected network) or after stimulation (opening of natural fractures through hydraulic fracturing or thermal fluid injection, for example).

Massive geomechanical effects occur in NFCRs when subjected to thermal stimulation. Compressing or opening of natural fractures by effective normal stress changes may alter flow capacity by up to an order of magnitude; wedging open of fractures or the generation of permanent flow paths along natural fractures by shear displacement and permanent dilation (Figure 7-1) around the thermally stimulated zone may alter flow capacity by several orders of magnitude.

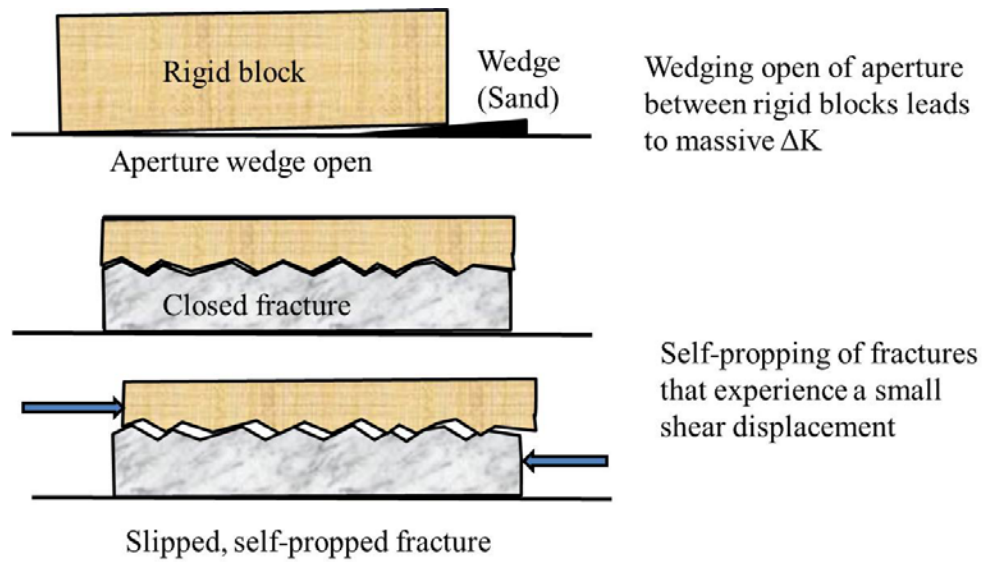


Figure 7-1: Wedging, or crack opening strain from rotational displacements, increases fracture aperture (top) and flow capacity; shear of natural fractures leads to self-propping and permanent increases in flow capacity

Natural fractures that lie approximately normal to the thermal (or expanding) zone in a NFCR, whether the expansion process is thermal (ΔT), hydromechanical (Δp , $\Delta \sigma'$), or because of direct solids injection as in Figure 7-2, will be wedged open.

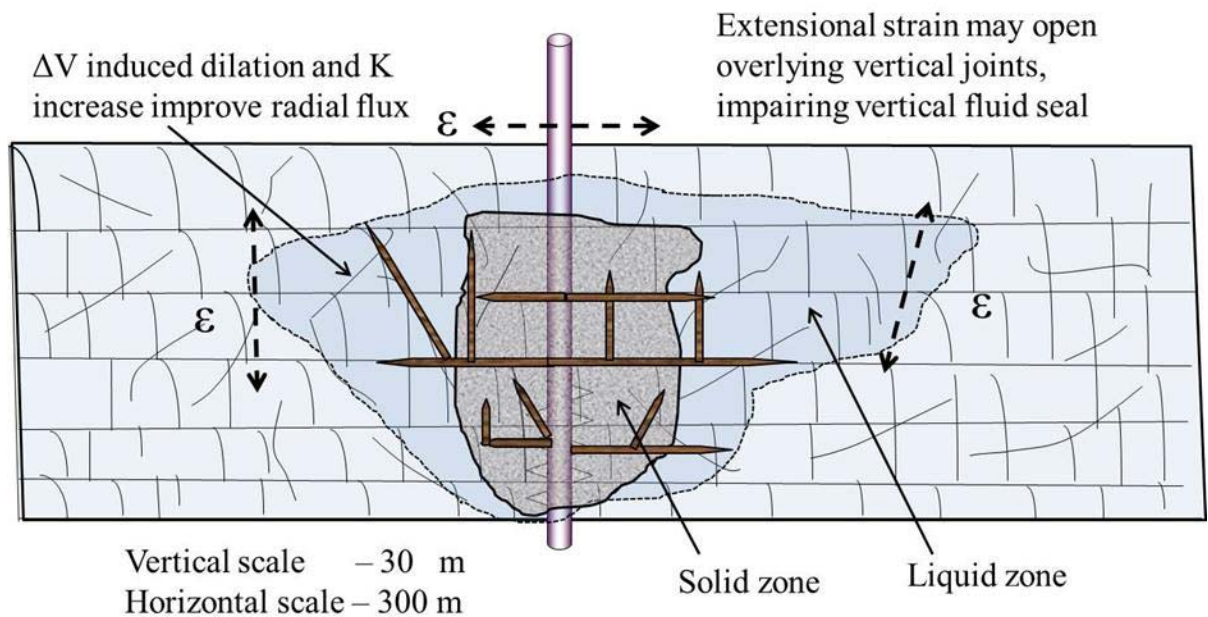


Figure 7-2: Volume change effects during slurried solids injection into a NFR.

The figure shows the direction of extensional strain around the zone of $+\Delta V$. Fractures lying at an angle to the front are subjected to high shear stresses, and as the temperature goes up and the size of the heated zone grows, shear dilation will occur. Although fractures that are approximately parallel to the thermal front will tend to be stressed and closed, the reduction in flow capacity is far less than the increase in flow capacity in directions normal to the front. This leads to a number of effects, but first it should be restated that high temperature steam injection leads to large thermoelastic volume changes, which in turn lead to large differential stresses, far larger than the ability of the rock to resist tensile parting or shear. The anisotropic changes in stresses lead to wedging (direct opening and extensional fracture opening associated with rigid block rotation) and shear displacement (and permanent dilation). Dominantly, fractures near to normal to the front experience the greatest extensional effects, leading to preferential outward flow paths from the heated volume. Less resistance to flow in directions away from the injection zone develops as the volume change increases because of ΔT , Δp , or direct ΔV (solids injection or fracture self-propping). Issues

such as casing shear, potential breaching of the cap rock, steel corrosion, and so on, will occur and should be planned for.

Despite the impact of geomechanics on VO thermal development, such issues are often addressed only once severe problems emerge, rather than as part of a proactive design process that seeks to exploit the benefits and manage the negative impacts. Other major thermal effects that must be considered in thermal project planning include:

- Casing shear from large thermally induced displacements at interfaces between rock layers with different thermal and geomechanical properties
- The possibility of breaching of larger shale barriers (0.2–3 m) through direct fracturing (CSS, HCS), differential thermal expansion, or shale shrinkage from dehydration. These can be positive or negative: shale breaching can access more resource or lead to greater heat losses.
- Risk of blowout to surface because of stress changes and shale shrinkage, especially with shallow steam projects ($z < 200$ m depth)
- Accelerated well corrosion leading to internal blowouts of hot fluids into shallow aquifers
- Loss of well sealing capacity through changes in mechanical properties of the wellbore cement and surrounding strata subjected to high temperatures, especially if there are many thermal cycles

It will eventually be possible to calculate stresses, displacements, and their effects on flow for a jointed rock mass subjected to thermal stimulation through steam injection, although this is currently beyond coupled mathematical modeling capability. Some simple calculations are shown here, merely to allow estimation of the potential magnitude of thermally induced stress changes. Some modeling and simulation efforts to model and simulate thermal VO production methods are also discussed. Finally, a practical example of reservoir rock behavior during thermal oil production operations is described, emphasizing that thermal oil production methods changes reservoir behavior, generally leading to

production enhancement (deterioration is less common), although thermal stimulation can generate operational issues such as thermally induced casing shear and seal breaching.

7.3 Viscous Oil in NFCRs

There is at least 9.7×10^9 b of VO in the world (Meyer *et al.*, 2007; Schenk *et al.*, 2009; Dusseault and Shafiei, 2011; GEA, 2012) (Figure 7-3). Large VO deposits in carbonates (Figure 7-4) are far less common and of lower porosity (usually $\phi < 15\%$); carbonates host about 2×10^9 b VO worldwide. The occurrence of VO in NFCRs is reported in many countries including Iran, Canada, the USA, Brazil, Congo, Turkey, Egypt, Russia, Oman, Kuwait, Saudi Arabia, Algeria, Libya, China, India, Cuba, Italy, France, and Mexico (Meyer and Dietzman, 1981; Sahuquet and Ferrier, 1982; Chierici *et al.*, 1985; Hoffmann and Strausz, 1986; Harrison 1987; Meyerhoff and Meyer, 1987; Joly *et al.*, 1988; Moshtaghian *et al.*, 1988; Bashari, 1988; Meyer and Duford, 1989; Couderc *et al.*, 1990; Al-Adawy and Nandyal, 1991; Briggs *et al.*, 1992; Gauchet and Corre, 1998; Padhy and Singh, 1998; Zhou *et al.*, 1998; Snell *et al.*, 2000; Waheed *et al.*, 2001; Smith *et al.*, 2002; Meyer and Attanasi, 2004; Penny *et al.*, 2005; Castiñeira *et al.*, 2006; Meyer *et al.*, 2007; Penny *et al.*, 2007; Alvarez *et al.*, 2008; Bağcı *et al.*, 2008; Shandrygin and Lutfullin, 2008; Spadini, 2008; Barge *et al.*, 2009; BGR, 2009; Sayd *et al.*, 2009; Li *et al.*, 2010; Samir, 2010a, 2010b; Brown *et al.*, 2011; Faizov *et al.*, 2011; Aguilar *et al.*, 2012; Zhongchun *et al.*, 2012). Over 900×10^9 b of VO, mostly HO and a small portion of XHO, is reported in the Middle East, mainly in NFCRs in the Arabian and Zagros sedimentary oil provinces off- and on-shore in the Persian Gulf region. As a region, the Middle East has the largest HO resource in NFCRs in the world. Over 550×10^9 b of VO, mostly XHO and bitumen, is reported in Canada trapped in Devonian age carbonates in the Western Canadian Sedimentary Basin (WCSB) (e.g., Grosmont Formation) which makes Canada host to the largest natural bitumen and XHO resource occurred in NFCRs in the world (Dusseault and Shafiei, 2011; Shafiei, 2012). Almost 100% of the VO production from NFCRs comes from cold production operations in Oman, Iran, Iraq, Kuwait, Saudi Arabia, Turkey, and Mexico (Bağcı *et al.*, 2008; EIA, 2010; Shafiei, 2012). The VO in most of these reservoirs is mobile under reservoir conditions and

either is not stimulated by steam injection, or is subjected to modest amounts of steam stimulation.

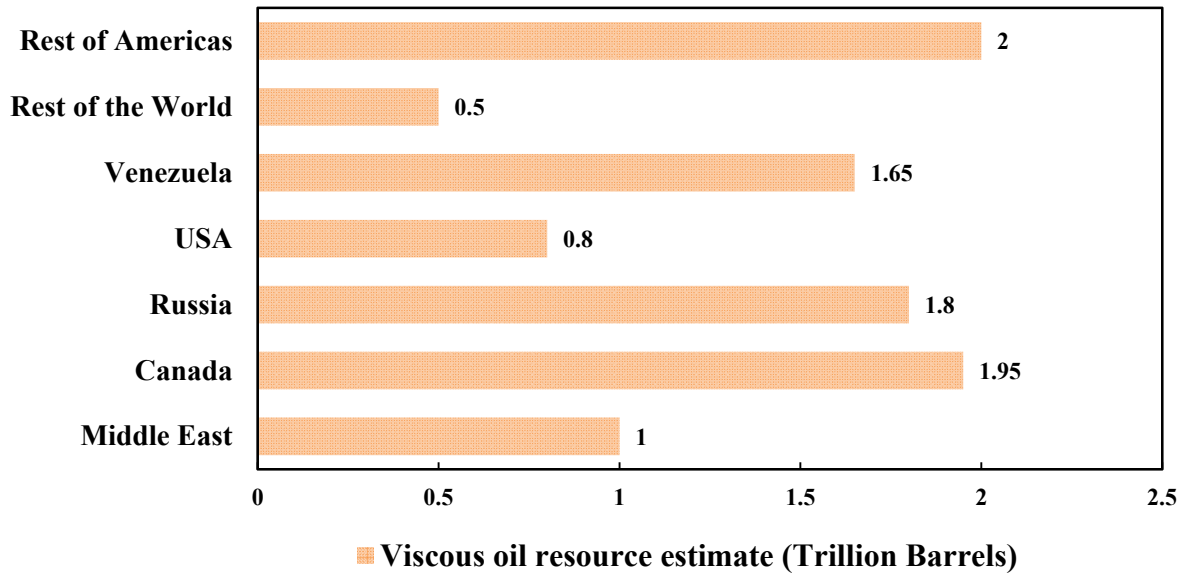


Figure 7-3: World resource estimates and distribution of VO in both clastics and carbonates.

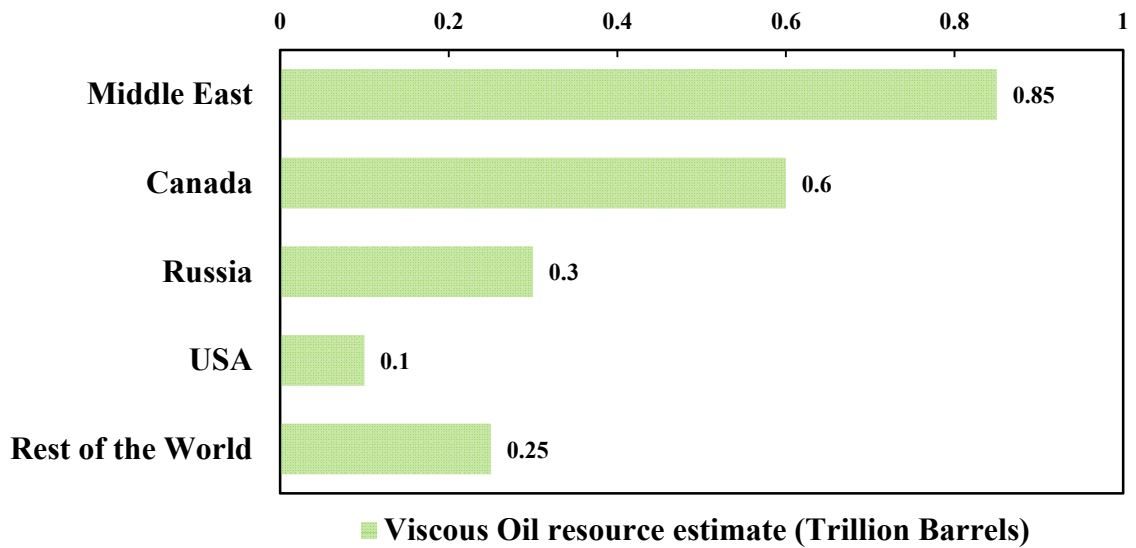


Figure 7-4: World resource estimates and distribution of VO NFCRs.

VO is almost always biodegraded older conventional oil. Deep oil generation, up-dip migration, and biodegradation (Head *et al.*, 2003; Larter *et al.*, 2006; Eschard and Huc, 2008) shape the standard model (Figure 7-5) proposed to explain the occurrence of immense VO deposits in both NFCRs and oil sands around the world. Conventional oil that has migrated over long distances from deeply buried source rocks (> 3000 m deep) to shallower horizons has been exposed to bacteria (leading to aliphatics consumption, lipids generation), different groundwater chemistry (sulfates, bicarbonates instead of chlorides), more rapid groundwater flux (washing out of H₂O-soluble fractions) and reduced pressure (diffusional losses of light molecules). Bacterial activity removes most light aliphatic molecular components, generates complex aromatic compounds, concentrates sulphur, and thereby generates VO.

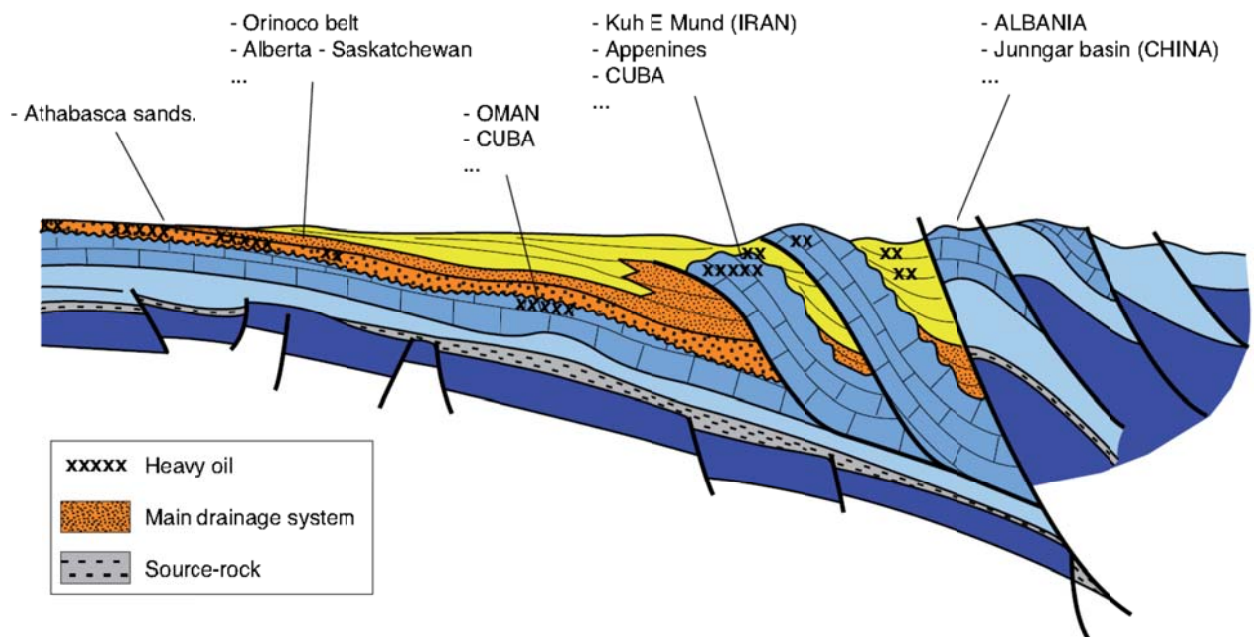


Figure 7-5: A basin-tectonic context for VO deposits (Eschard and Huc, 2008).

Study of metabolic markers suggests that oil biodegradation *in situ* is almost exclusively anaerobic (Head *et al.*, 2003; Aitken *et al.*, 2004). Other investigations also confirm that biodegradation enriches resin and asphaltene molecules content relative to aliphatic molecules, generating highly viscous, aromatic-rich oil with increased density and lowered

H:C ratio (Hollerbach, 1987). Biodegradation is controlled by temperature, chemical composition of the oil and groundwater, and the relation between the oil volume and the oil–water contact area. Gradients in oil composition and consequent viscosity variations are common at reservoir scales, and are linked with proximity to active water (slow flux) and geochemical factors (Larter *et al.*, 2006).

7.4 Thermal Methods in VO NFCRs

The reviews of worldwide enhanced oil production surveys published by Oil & Gas Journal and some individual articles published during the last two decades showed that heating with steam is the only commercialized viscosity reduction approach, and is by far the most successful and widely used production method. Over 60% of the current VO production worldwide involves steaming, and this dominance will continue into the foreseeable future (Taber and Martin, 1997; Oil & Gas Journal, 1996, 1998, 2004, 2006, 2008, 2010). Note that all of the commercial thermal operations are happening now in oil sands and unconsolidated VO-saturated sandstones rather than in VO NFCRs. The application of thermal processes to VO NFCRs remains limited to a few vertical well steamflooding and cyclic steam stimulation field pilots that took place in Canada, France, Italy, Congo, Turkey, China, the USA, Kuwait, and Saudi Arabia (Joly *et al.*, 1988; Karaoguz *et al.*, 1989; Issever *et al.*, 1993; Gauchet and Corre, 1998; Smith *et al.*, 2002; Bagci *et al.*, 2008; Spadini, 2008; Zhongchun *et al.*, 2012).

NFRs are characterized by an interconnected fracture system that provides the main flow paths (high permeability, low storage volume), and a reservoir rock or matrix that acts as the main location for the hydrocarbons (low permeability, high storage volume). The matrix system contains almost all the oil, but flow of oil to wells is through the high permeability fracture system, implying that the matrix-fracture flow interaction controls the production process and the recovery factor. Production from the matrix-fracture system can be associated with various physical mechanisms including oil expansion or pressure diffusion, imbibition or saturation diffusion, gravity imbibition or drainage, mass diffusion and viscous displacement or convection. (Nolan *et al.*, 1980; Saidi, 1987; Quettier and Corre, 1988;

Briggs, 1989; Reis, 1990; Briggs *et al.*, 1992; Pooladi-Darvish *et al.* 1994a and 1994b; Sumnu *et al.*, 1996; Donmez, 1997; Prats, 1998; Shahin *et al.*, 2006; Hernandez and Trevisan, 2007; Mollaei and Maini 2007; Mollaei *et al.*, 2007; van Heel *et al.*, 2008; Ashrafi *et al.*, 2011; Souraki *et al.*, 2011; Tang *et al.*, 2011).

Technology progress in oil production technologies during the last 2–3 decades, especially in Canada, has played a major role in implementation of different concepts of oil production from VO reserves. Major *in situ* VO oil production technologies are listed in Figure 8. Technologies for highly viscous bitumen and XHO have major differences compared to conventional oil; it is necessary to reduce the viscosity, and in practice this involves heating, dilution, or reducing the molecular weight. Recent developments in horizontal drilling (including multiply-branched wells), production technologies (including gravity drainage methods, non-thermal production of VO with or without sand co-production, pressure pulse flow enhancement), and better equipment and methods (progressing cavity pumps, efficient separation, slurry injection disposal of produced sand) have helped achieve economic production rates (Towson, 1997; Cunha, 2005; Dusseault and Shafiei, 2011). Description of other steam processes is out of the scope of this chapter; refer to Dusseault and Shafiei (2011) for a brief description and current status of application of steam technologies, and Boberg (1988) and Butler (1991) for production mechanisms involved in steam methods.

7.5 Commercialized Thermal VO Production Techniques in NFCRs

Development of new oil production technologies in Canada during the two last decades has played a major role in implementation of different concepts of oil production from VO reserves. Canada, the only major producing country to produce more than 50% of total production from VO, has become the world leader in the development of VO production technologies. Canada now holds the world's third-largest proved oil reserves after Saudi Arabia and Venezuela, ahead of Iran (Oil & Gas Journal, December 2003; USGS, 2009), based on commercialization of new VO production technologies.

Major *in situ* VO oil production technologies are listed in Figure 7-6. Technologies for highly viscous bitumen and XHO have major differences compared to conventional oil; it is necessary to reduce the viscosity, and in practice this involves heating, dilution, or reducing the molecular weight. Recent developments in horizontal drilling (including multiply-branched wells), production technologies (including gravity drainage methods, non-thermal production of VO with or without sand co-production, pressure pulse flow enhancement), and better equipment and methods (progressing cavity pumps, efficient separation, slurry injection disposal of produced sand) have helped achieve economical production rates. A dramatic surge in VO development in Alberta and Saskatchewan developed following the international crude oil price recovery in 1999-2001 (Towson, 1997; Cunha, 2005; Dusseault and Shafiei, 2011). Currently, over 50% of Canada's oil production, which should exceed 3×10^6 b/d by 2013, comes from oil sands and heavy oil deposits along the Alberta-Saskatchewan border. This is a higher percentage of national production from VO than any other country, and it will increase (CAPP, 2012).

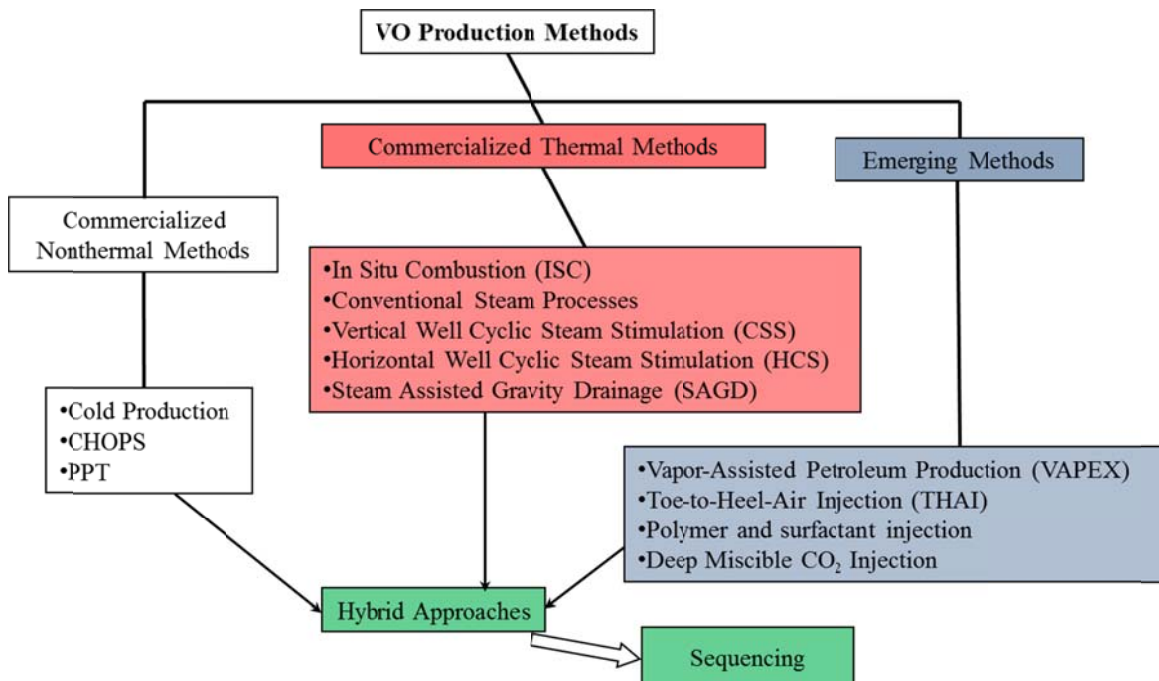


Figure 7-6: Viscous oil production methods.

In this section, only commercialized VO production techniques in NFCRs are described. In contrast to conventional oil production it is usually necessary to reduce the viscosity; in practice, this can be achieved by heating, diluting, or reducing the molecular weight through pyrolysis. Heating with steam is the only commercialized approach and is by far the most successful and widely used production approach; reviews of worldwide EOR activity during the last two decades show that steam flooding and its variations are responsible for > 75% of VO production worldwide (Taber and Martin, 1997; Oil & Gas Journal, 1996, 1998, 2004, 2006, 2008, 2010a, 2010b), the remainder being almost exclusively cold production methods applied to lower viscosity VO.

7.5.1 *In Situ* Combustion

In-situ combustion is a technique suitable for recovery of oil from medium to VO reservoirs. In this technique, crude oil is ignited at the wellbore and a heat front is generated by continuous injection of air into the reservoir. The combustion front is sustained as long as enough coke is produced by cracking of crude oil to be consumed as fuel.

Sixteen experiments were conducted to study the combustion reaction kinetics of Turkish heavy oils (12-32 °API) in carbonate medium. A mixture of the carbonate rock and VO was subjected to a controlled heating program under a constant flow rate of air. The produced gas was analysed for its oxygen and carbon oxides contents. Although the molar CO₂/CO ratios vary during low-temperature oxidation (LTO), for fuel deposition (FD) and high-temperature oxidation (HTO), these values can be indicated at different temperatures. A decrease in the atomic H/C ratio with an increase in temperature was observed for all runs. The activation energies of Çamurlu (12 °API), Bati Raman (12 °API), and Raman (18 °API) heavy oils for both fuel deposition and high-temperature oxidation reactions were observed similar. For medium-gravity oils (Adiyaman, 26 °API and Garzan, 28 °API), the activation energies for the high-temperature oxidation reaction is higher than that for the fuel deposition reaction. For the LTO in carbonate rocks, the activation energies are almost twice those of FD and HTO reactions for each crude oil. The activation energies are almost independent of the gravity of the oil used. The Arrhenius constant is not affected by the API gravity of the

oils (Bağcı and Kok, 2004). During fuel deposition reaction, the crude oil is coked and deposited on the solid matrix as fuel during the in-situ combustion process. At low temperatures, some oxygen is consumed to produce carbon oxides as CO₂ and CO, which is a smaller amount than the oxygen consumed, indicating that some oxygen is consumed in other reactions. At high temperatures, almost all of the oxygen is consumed to produce CO₂ and CO, which indicates complete combustion. At higher temperatures, the oxygen consumed is stoichiometrically equivalent to the carbon oxides produced. However, at lower temperatures, the oxygen consumption is greater than that accounted for in carbon oxides. This suggests that LTO and/or the cracking reaction are occurring in this lower-temperature region. The increased oxygen consumption and greater production of CO₂ and CO at lower temperatures for the heavier oil indicate a higher reactivity of these oils with oxygen at lower temperatures in carbonate rocks. Another feature of the combustion of the VO NCFRs is that the concentration of CO₂ is now much greater than that of CO in LTO and HTO regions. Thus, although in this case, the total fuel deposited and/or burnt is low, compared to that for the VO, almost all of the oxygen consumed is accounted for, particularly in the HTO region. This suggests that less cracking has occurred during fuel deposition and combustion than with the VO.

Sweep efficiency during in-situ combustion is one of the most important process parameters, but which has not been extensively evaluated and is least understood. Most laboratory investigations are conducted in combustion tubes, which essentially use a vertical well arrangement and which, of course, because of their basically one-dimensional geometry, can not provide information on either areal or vertical sweep. Information on the combustion sweep efficiency is very important for comparing process variations and also for predicting performance. 3-D scaled physical models can provide much valuable insight into the areal and vertical sweep processes and stability of the combustion front over a range of operating conditions. Results from such experiments may be used to predict performance in the field, and also to validate numerical simulator models. Experimental study was conducted with various injection-production well couples (vertical injector-horizontal side producer, vertical

injector-diagonal horizontal producer, and vertical injector-vertical producer) in a 3-D model using two different heavy oils (Akin *et al.*, 2000a, 2000b). For 12 and 18 °API oils, centre plane of the model was observed to be much warmer than top and bottom planes. This is because the igniter was located near the centre plane. The occurrence of HTO at the vicinity of injection end in both runs can be verified by looking into reaction kinetics of Raman (18 °API) and Bati Kozluca (12 °API) oils. The heat front propagation in Raman oil was faster at the beginning and slowed down in later time steps. The peak temperatures observed in Raman oil were lower than those in Bati Kozluca oil. Stabilized combustion front was observed in Raman oil whereas, no period of stabilization was apparent in Bati Kozluca oil due to severe bypassing. In Raman oil, with a lower air rate, the channelling occurrence was severe. It can be concluded that superficial burning of sand pack is usual in vertical injector-vertical producer configuration, which leads to a poor vertical sweep in this configuration. With vertical injector-horizontal producer configuration, at the start of air injection, a uniform temperature distribution throughout the centre plane in both oils was observed. The front stabilized in both runs and proceeded in the direction of the producer. The creation of isotherms was parallel to the side horizontal producer in both runs which is suggestive of distributed flow filed at the centre plane. Early production of hot fluids that transport heat as a result of convection was noted. Heat was removed from burned-out sand pack by vaporization of water behind the combustion front. The heat was deposited ahead of the burning zone by condensation in cooler regions of the reservoir. The horizontal production well conveyed heat downstream into the colder regions. No indication of flow channel or bypass was noted. Since horizontal producers cause a larger areal contact, they can drain fluid without creating a by passing flow path. With the same burned volume it was observed that horizontal producers recovered more oil than vertical producers. Although, dual horizontal producers recovered the highest amount of oil, the net recovery per producer was lower than that of a single producer placed alone at the boundary. The main reason for this is presumably the flow interference between the twin producers due to the restricted drainage area.

A 1-D simulation model was built using CMG-STARs and was tuned with experimental data (Bağcı, 2007). Parameters such as temperature profiles, cumulative oil and water produced, pressure profiles, amount of heavy and light oil produced were investigated and compared with results. In this model six components and pseudo components such as water, heavy oil, light oil, oxygen, inert gas and coke were considered. Simulated oil and water production lag behind actual oil and water production, respectively, during nitrogen injection. However, once air injection starts and combustion occurs, simulated oil production increases rapidly. Toward the end of the experiment, simulated oil production is about the same as the actual oil production. Combustion tube test results were also simulated using a model representing oil as two components “heavy” and “light” oil fractions. Also, coke was described as a solid phase. Four chemical reactions were used to describe cracking of heavy oil to light oil and coke, VO burning, light oil burning, and coke burning. In summary, combustion tube test results can be adequately matched using 4-reaction model. Matching combustion tube test results yields some confidence in fluid model as well as chemical reaction descriptions, which would then be used in a field scale model. To study the impact of complicating situations for a typical field case for VO, one may wish to tune results from a numerical simulation model. Having obtained a reasonable history match of laboratory combustion tube data, same fluid description along with chemical reaction was used to simulate production performance for a field situation using a 1/8th element of symmetry model for a 5 acre inverted, five spot pattern. Homogeneous reservoir properties chosen for this simulation are similar to the characteristics of a Bati Kozluca VO reservoir. Homogeneous reservoir model has been used in this study because of numerous modelling and process description uncertainties inherent in combustion simulation. The simulation model is a Cartesian, three-dimensional model with $12 \times 12 \times 5$ grid blocks of $\Delta X = \Delta Y = \Delta Z = 19.4$ ft. Six components (water, heavy oil, light oil, nitrogen, oxygen and coke) are used in the model. VO has been represented as a two-component model oil of 12 °API and molecular weight of 675. VO burning is represented by two-chemical reactions corresponding to the air-fuel ratio requirement calculated from the laboratory observations. Chemical reaction uses activation energy and frequency 85600 and 2×10^{10} , respectively. The model represents a homogeneous

reservoir with $k_x = k_y = 700$ mD, $k_z/k_x = 1.0$, $\phi = 0.25$, formation thickness = 100 ft, initial reservoir temperature = 77 °F, initial oil saturation = 0.75, initial water saturation = 0.25, and initial reservoir pressure = 1000 psia at the formation top depth of 4000 ft. Constant air injection rate of 10×10^6 CF/d is maintained throughout the simulation period of 5 years. Producer operates under a constant flowing bottom hole pressure constraint of 14.7 psia. The numerical model incorporated external heater option to raise the temperature of the injector in the beginning. In order to simulate adiabatic conditions, no external heat losses or gains were allowed. Several locations for the producers have been tried while keeping the length of the wells constant: vertical injector - vertical producer, vertical injector - horizontal producer (right side) and vertical injector - horizontal producer (left side). The centre plane of the reservoir is observed to be much better than the top and bottom planes in combustion process. The occurrence of HTO at the vicinity of injection well can be verified by looking into reaction kinetics of Bati Kozluca oil. A uniform temperature distribution throughout the centre plane was observed shortly after sustaining of the combustion front. The front stabilizes and proceeds in the direction of the producer VI-HP well configuration. The breeding of isotherms are parallel to the producer, which is suggestive of distributed flow field at the centre plane. Early production of hot fluids, which transport heat as a result of convection, was notified. No indication of flow channel or bypass was observed. The upward channelling is not severely apparent as it can be seen in vertical cross-sectional plane of reservoir. The temperature levels at the top and bottom planes are comparable, which implies a uniform combustion of the reservoir. Contours with higher temperature levels are prevalent at the top of the reservoir model than at the bottom. This is an implication of the upward movement of the hot fluid, which means a superficial burning of the reservoir model is inescapable in the assigned well configuration in the reservoir. As it propagates, the front leaves behind clean burned sand wherein, the temperature decreases gradually. The upper portion of the reservoir was efficiently burned in vertical injection-vertical production well configuration, whereas almost each portion of the reservoir equally burned in vertical injection-horizontal production well configurations. With the same burned volume, more oil was recovered by horizontal producers than that of vertical production wells. This was due

to the fact that the horizontal wells remove oil without the creation of any extensive mobile flow path in the colder region, whereas, because of their flow geometry, more volume should be burned to create a flow path between a vertical injector and a vertical producer with in which the fluid can flow readily.

7.5.2 Steam Processes

The most widely used thermal technique to extract residual oil from VO fields is steam injection. There is an interest in using CO₂ gas as immiscible phase for recovering VO.

Research into the application of a simultaneous steam-CO₂ drive process and the examination of vertical and horizontal injection-production well configurations was conducted in a physical model of 1/12th of an inverted regular seven-spot pattern to determine the recovery performance of Bati Kozluca (12 °API) VO (Gumrah and Bağcı, 2007). Three groups of well configurations were mainly investigated: a vertical injection and production wells scheme, a vertical injection and horizontal production wells scheme and a horizontal injection and production wells scheme. In steam alone tests, the vertical injector and horizontal producer scheme supplied a higher recovery than that of the others. The lowest ultimate recovery was obtained from the horizontal injector-horizontal producer well configuration. The co-injection of CO₂ with steam increased the ultimate oil recovery and the production rate over steam alone. The recovery efficiency of horizontal injector-horizontal producer was also the lowest one, but vertical injector-horizontal producer gave the best performance when compared to other tests. When steam alone and steam-CO₂ tests were compared, the oil recovery increased with increasing CO₂/steam ratio till an optimum value was reached, after which a diminishing effect was observed. The other factor which influenced the oil recovery was the well type of injector and/or producer whether it is horizontal or vertical. The distance between the wells also affected the efficiency of the process.

Traditionally, the addition of non-condensable gas to steam is known to have a beneficial effect on heavy oil production when conventional vertical wells are used. 1-D and 3-D

physical models were used to examine the effects of simultaneous injection of CO₂ and CH₄ together with steam on the recovery of Bati Kozluca (12 °API) heavy oil mixed with unconsolidated carbonate rock (Bağcı and Gumrah, 2004). Gas/steam ratio was found to be a significant factor among the studied variables in heavy oil recovery. The higher CO₂/steam ratio over optimum value diminished oil recoveries. This was attributed to the increase in gas saturation along the model causing steam channelling through a production well and the increase in gas volume reducing the amount of steam injected. The steam injectivity was also less at higher CO₂ concentrations. The lower residual oil saturations were obtained in gas-steam injection tests, compared to the values obtained with steam alone. The injected non-condensable gas created a permanent gas phase across the top of the model therefore heat arrived to the producing well earlier than steam alone test. The depression of steam temperature was also observed due to the presence of non-condensable gases, CO₂ and CH₄. The higher temperature distribution indicated the steam overriding at the top of the model. For steam-gas tests, temperatures increased and then decreased following the injection pressure behaviour. However, for the steam alone tests, the injection pressure stayed at the increased level during tests. Bottom of the model was warmed with conductive heating resulting from the steam staying at the top of the model.

The SOR is indicative of the success of a steam drive. The SOR increases as the thickness of the bottom water zone increases for a horizontal producer. Because the bottom water is more mobile than oil and steamed rapidly, it is displaced more rapidly by horizontal producers with larger areal contact, and as a result, more steam invades inside the models to pass into the bottom water zone. This demonstrates the improved injectivity of steam in the presence of bottom water. In the absence of a bottom water zone, the highest SOR was noticed in the vertical injection-vertical production configuration in the model. The SOR decreased toward the end of the experiment and became almost similar to the ratio that was observed in the vertical injection-horizontal production configurations. The well configurations were changed during the course of experiments to determine their effects on oil recovery. Bottom water thicknesses were changed to see the effects on oil recovery. The maximum oil

recoveries were obtained by placing the horizontal producers along the hypotenuse of the triangular model. This well configuration provided better oil recovery than any other well configuration, even in the presence of a bottom water zone. Oil recoveries decreased with an increase in the thickness of the bottom water zone. There are two important cases with the application of steam injection in the presence of bottom water zone. In the first case, the oil above the bottom water zone invades the bottom water zone and remains as residual oil, clarifying the reason for the lower recovery in the presence of a bottom water zone. The second case leads to the increased tendency for coning of condensate into the vertical well.

7.5.3 Thermally Assisted Gas Oil Gravity Drainage

(TA-GOGD) of the Qarn Alam (Figure 7-8) fractured low permeability carbonate reservoir is being enhanced by steam injection in the world's first full field carbonates thermal development. Gravity drainage is typically used to drain heavily fractured low permeability reservoirs, particularly carbonates. The process relies on the density difference between either oil in the matrix and water in fractures (WOGD) or gas in fractures and oil in the matrix (GOGD). Cold Gas Oil Gravity Drainage (GOGD) occurs when gas is introduced into the oil filled fracture system of a highly fractured oil reservoir resulting in the formation of a fracture gas-cap at the top of the structure. The rate of GOGD drainage through the matrix is very low due to high oil viscosity and low matrix vertical permeability. In order to remedy this problem, the oil viscosity can be reduced by heating the oil. As such, steam injection in Qarn Alam only enhances the ongoing GOGD process to what is known as TA-GOGD. In TA-GOGD, the injected steam heats up the oil at the top of the matrix block by conduction of heat from the fracture into the matrix. Further steam injection heats oil progressively deeper in the matrix block. The hot, less viscous oil starts draining down the matrix at an accelerated rate until it encounter cold, more viscous oil. The cold oil "mobility barrier" acts as a flow restriction in a similar way to a vertical permeability barrier, forcing the oil out of the matrix into the gas filled fracture system. Once in the fracture system, the oil will flow downward into the oil rim under gravity. Unusually for a thermal process, the oil cools as it drains vertically to the oil rim. The Qarn Alam pilot, one of a small number of

steam projects in carbonates had the specific aims of demonstrating sustainable steam injection and retention of matrix and cap rock integrity during exposure to heat and condensed steam, as well as providing evidence that oil expulsion from the matrix justifies full field development. The pilot project had proven that the recovery process worked, but only the heavily fractured crestal area had been tested. The TA-GOGD process relies heavily on fractures to provide a conduit for steam and hence heating of the matrix blocks by conduction, as well as providing the means for gravity differences and drainage of oil via the fracture oil rim (Shahin *et al.*, 2006; Penney *et al.*, 2007).

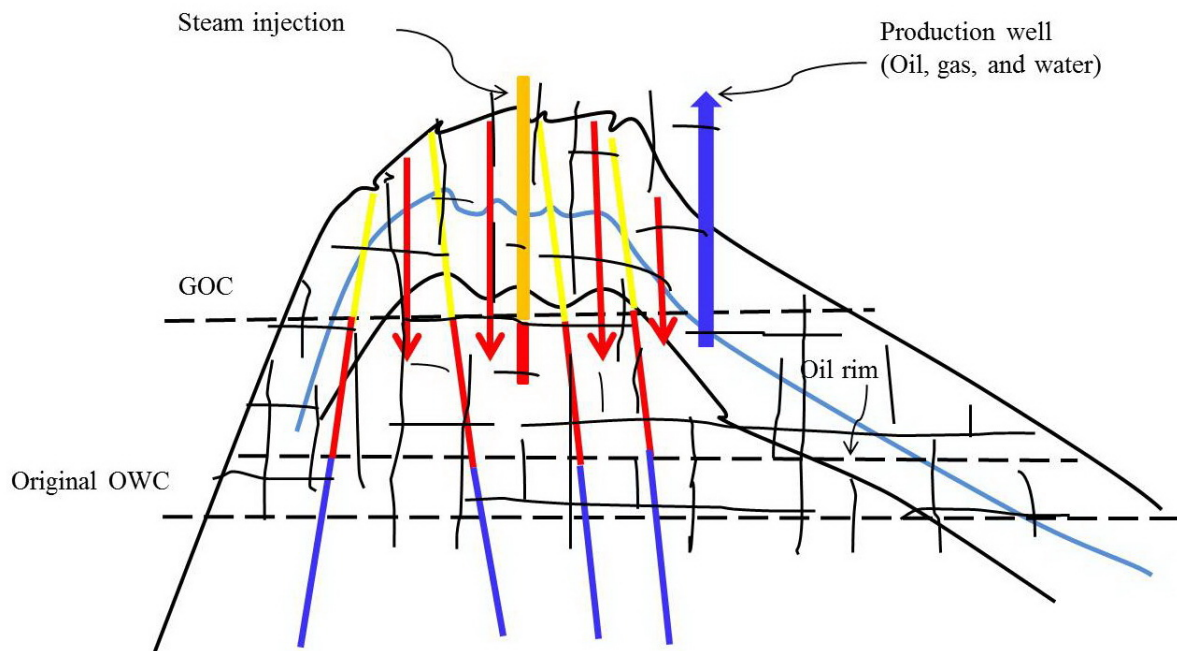


Figure 7-7: TA-GOGD in the Qarn Alam VO NFCR (From: Shahin *et al.*, 2006).

Hernandez and Trevisan (2007) studied on the driving mechanisms, namely, solution gas, CO₂ generation, steam distillation, capillary imbibition and gravitational drainage for the recovery of oil and gas during the continuous steamflooding of a naturally fractured reservoir containing VO. Two numerical models were used to represent the matrix heating process. The first describes the heating of a horizontal cross-section of a matrix block surrounded by a fracture, in which the steam is steadily flooding. The second model is similar to the first,

except for the position, which is changed to vertical to incorporate gravity effects. The studies were performed for a fractured rock saturated with live oil. In this study, steam distillation is the most effective mechanism, since it provides complete recovery of methane and of the light and medium pseudo-components present in the oil phase. The mechanism of solution gas is responsible for a significant increase of the pressure difference between the matrix and the fracture. The high viscosity of the oil due to the release of methane; and of the light and medium pseudo-components; and the magnitude of the capillary pressure; makes the contribution of the capillary imbibition mechanism insignificant for the matrix oil recovery. Because of better conditions for oil flow, the mechanism of thermal expansion associated to the reduction of viscosity presents better matrix oil recovery than the solution gas mechanism associated to the reduction of the viscosity. The reduction of viscosity is not exactly a mechanism because it is not an energy source, but it has a definite role in helping oil recovery from the matrix, when a pressure gradient between the matrix and the fracture is generated. The overall effect is to anticipate oil recovery and delay gas production. The CO₂ generation mechanism is responsible for the anticipation in the recovery of distilled components from the oil phase and for discreet contributions in the recovery of the heavy pseudo-components. The mechanism of gravitational drainage has no relevant influence on oil recovery from the matrix. Its effect is minor and only in the recovery of the heavy pseudo-component.

7.5.4 SAGD

Steam Assisted Gravity Drainage (SAGD) is a promising recovery process for producing VO and bitumen. The method ensures both a stable displacement of steam in economical rates by using gravity as the driving force and a pair of horizontal wells for injection/production. This is achieved by drilling a pair of horizontal wells located at a short distance one above the other. Steam is injected into the upper well and hot fluids are produced from the lower well. This progressively creates a steam chamber, which develops by condensing steam at the chamber boundary and gives latent energy to the surrounding reservoir. Heated oil and

water are drained by gravity along the chamber walls of the production well (Butler and Stephens, 1981; Joshi and Threlkeld, 1985; Joshi, 1987; Butler, 1987).

SAGD process can be an attractive recovery process for many fractured heavy oil reservoirs (Joshi, 1986). In VO NFCRs, thermal conduction allows heat to sweep areas of the reservoir, which has no contact with steam. In this case, thermal expansion is an important recovery mechanism. After steam injection, viscosity reduction increases significantly as the heat migrates to the upswept regions. When compared to homogeneous systems without fractures, vaporization in fractured systems takes a longer time. This is mainly due to the fact that the injected steam flows at a high speed through the fractures without heating the reservoir matrix (Hoffman, 2003). The previous experimental studies were performed for homogeneous, isotropic VO reservoirs and tar sand reservoirs, thus the effect of heterogeneity and anisotropy on the performance of the SAGD process has not been focused. Recent field activities indicate that steam injection in fractured reservoirs may have economic potential. Even though injected steam moves rapidly through fractures, the heat front moves uniformly. These studies have shown that the rate of oil recovery is enhanced. Results show that heat was efficiently transferred from injected steam to the reservoir matrix.

Bağcı (2006) presented an experimental investigation of the effect of fractures and well configurations on the steam-assisted gravity drainage (SAGD) process in a 3-D model, using Bati Kozulca VO (12 °API) in carbonate rocks. Three different well configurations were investigated: a horizontal injection and production well pair, a vertical injection-vertical production well pair, and a vertical injection-horizontal production well pair, with and without fractures that provided a vertical path through the horizontal producer. The influence of fracture distribution on the steam-oil ratio (SOR) and oil recovery was analyzed using the horizontal well pair scheme, a vertical injection-horizontal production well pair, and a vertical injection and vertical production well scheme. The experimental results indicated that vertical fractures improved SAGD. Maximum oil recovery was observed during the horizontal injection-horizontal production well scheme with a fractured model, because of the favourable steam-chamber geometry. Runs showed that the location of the fractures

affects the performance of the process. The very high permeability path (fractures) above the injection well aids the natural convection of steam resulting in efficient oil drainage. During the early stages of the runs, the fractured model gave significantly higher SOR's than those observed in the uniform permeability reservoir. Whether heat communication between the wells is formed before SAGD is an important factor in VO reservoirs with fractures. Heat communication directly influences the development, growth and the geometry of the steam chamber. If heat communication is established, better lateral growth behaviour is observed, and because this restricts the vertical growth rate, it reduces the heat requirements and the rate of temperature increase in the physical model. If heat communication does not form, steam chamber grows rapidly in the vertical direction, increasing the rate of temperature increase in the model, and undoubtedly leading to increased heat losses at the top (higher SOR values).

The SW-SAGD technique for the extraction of VO and bitumen has attracted considerable interest in recent years. A number of oil companies are applying, developing or evaluating SW-SAGD because worldwide, there are numerous VO reservoirs that are thin and/or underlain by water. If the process can be effectively applied, a large amount of resource that is currently considered uneconomical to produce could be amenable to economic exploitation. Although this approach and its variations are being field tested by several operators, a systematic evaluation of the process and its performance is not available. Some suggest that the SW-SAGD process is essentially a near-wellbore heating process effective for a finite (150 m) length of the horizontal section, whereas others are more optimistic. [Akin and Bagci \(2003\)](#) investigated the optimization of start-up procedure for single-well steam-assisted gravity drainage (SW-SAGD) in Bati Kozluca VO field in Turkey. They performed experimental study of two early-time processes namely cyclic steam injection and steam circulation to improve reservoir heating and to compare with other well configurations like vertical injector-horizontal producer and horizontal injector-horizontal producer. The effectiveness of the methods is compared within themselves and to conventional SAGD by

measuring the size of the steam chamber as a function of time. The steam chamber area for cyclic steam injection is slightly greater than that of steam circulation case.

7.6 Thermally Induced Stresses in Reservoir Rocks

Thermal oil production is fairly new in terms of significant contribution to daily world oil production and as long as easy conventional oil reserves were available, little investment was made into more costly thermal VO production methods. Thus, thermally-induced stress changes and their consequences, especially in NFCRs, are not well treated in the literature. Conventional reservoir simulators cannot accommodate rock mechanics issues such as dilation and stress redistribution, and mathematical simulation of coupled thermal-flow-stress processes is complex. Coupled simulations are even more complex in NFCR VO cases where the effects of chemical reactions cannot be neglected and where the properties change massively because of shear and dilation of natural fractures (joints). Literature overview shows that thermal effects modeling in NFCRs is in an embryonic state, and there is almost a complete lack of suitable deformation monitoring data for model verification. Some efforts in thermal reservoir modeling and simulation for different reservoir rock types are presented here, focusing on changes in petrophysical, geomechanical, and to a lesser extent chemical properties of reservoir rocks for steam processes at temperatures up to $\sim 325^{\circ}\text{C}$. However, there have been few opportunities to verify or calibrate models with field measurements because distributed deformation measurements are needed.

7.7 Thermal Reservoir Simulation and Numerical Modeling

Temperature changes induce thermal strains that lead to thermoelastic stresses (e.g., [Hojka *et al.*, 1993](#)) which can result in rupture or shear ([Dusseault *et al.*, 1988](#)), accompanied by dilation ([Dusseault and Rothenburg 1988](#)). Stresses in the elastic range can be computed by incorporating thermoelastic rock volume changes using the equations of fluid-saturated, poroelastic solids developed originally by [Biot \(1941, 1955, and 1956\)](#). Analytical or numerical solutions may be used to calculate thermal stress changes for various media with different properties and geometries ([Stavsky, 1963](#); [Aktan and Ali, 1978](#); [Chen, 1988](#); [Hojka,](#)

1993; Dusseault, 1993; Wu, 1997; Pooladi-Darvish *et al.*, 1994a and 1994b). Depending on reservoir lithotype, the needs are different: in unconsolidated sandstone reservoirs, shear dilation is general (pervasive rather than localized) and the rock matrix changes properties; in NFCRs, the strong rock matrix is less affected, but localized dilation and shear displacement of natural fractures (joints) generate massive changes in local flow capacity and therefore pressure and temperature distribution over time. Hence, different methodologies and approaches are required, depending on lithology and fabric.

Analytical solutions based on work of Boley and Weiner 1960, Florence and Goodier (1959, 1960), Chen (1967), and many others, generally using homogenous assumptions and simple geometries, sometimes based on complex variable techniques such as proposed by Green (1954). Wang and Dusseault (1997) analyzed a circular opening in a friable low permeability medium subjected to temperature and pore pressure changes; they used an incremental elastic-perfectly-plastic constitutive stress-strain relationship under non-isothermal conditions to attempt to understand the propagation of yielded zones around injection wellbores (a high-symmetry, homogeneous model).

For a tabular geometry, Dusseault (1993) proposed a simple first-order model of a uniform homogeneous flat-lying and extensive reservoir (Figure 7-9) subjected to uniform heating, where an assumption of no-lateral-strain can be justified. According to Hooke's law and Terzaghi's effective stress principle:

$$\varepsilon_i = \frac{1}{E} [\Delta\sigma'_i - \nu(\Delta\sigma'_j - \Delta\sigma'_k)] + \beta\Delta T; \text{ and } \Delta\sigma'_i = \Delta\sigma_i - \Delta p \quad (7-1)$$

where ε_i is the strain component in direction i , and E , ν , and β are Young's modulus, Poisson's ratio, and the coefficient of linear thermoelastic expansion, and $\Delta\sigma'$, Δp and ΔT are the changes in effective stress, pressure and temperature. Applying the no-lateral-strain condition leads to:

$$\Delta\sigma'_h = \frac{\beta E}{1-\nu} \Delta T - \frac{\nu}{1-\nu} \Delta p \quad (7-2)$$

$$\Delta\sigma_h = \frac{\beta E}{1-\nu} \Delta T + \frac{1-2\nu}{1-\nu} \Delta p \quad (7-3)$$

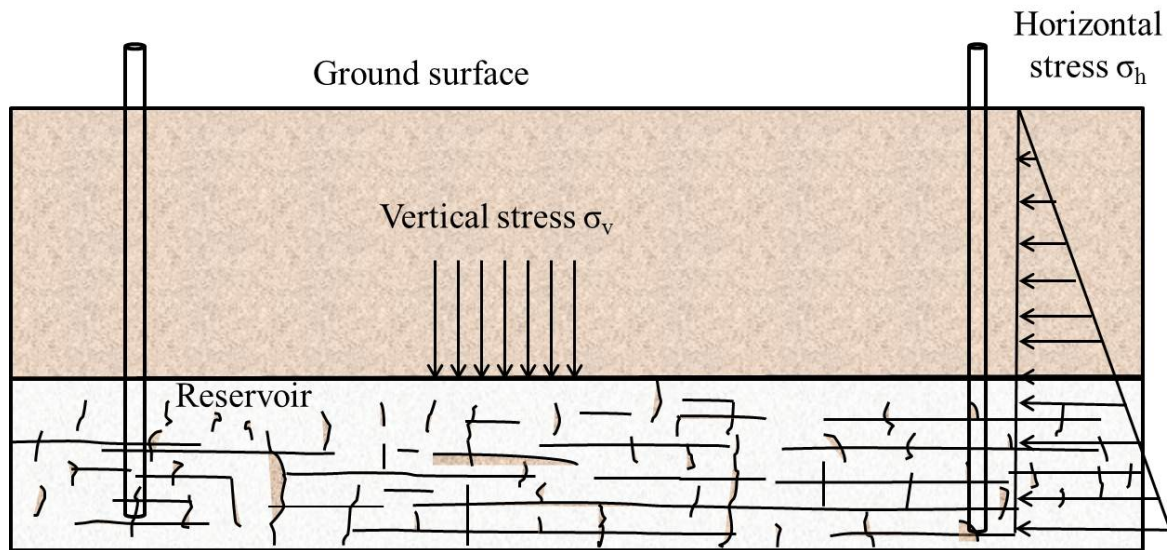


Figure 7-8: A schematic model of stresses in a laterally extensive reservoir (Dusseault, 1993).

Assume $\Delta T = +100^\circ\text{C}$ (e.g., hot water injection), Young's modulus (E) of 50 GPa (for a 10% porosity limestone), Poisson's ratio (ν) of 0.25, and a thermal expansion coefficient (β) of $10 \times 10^{-6}/^\circ\text{C}$. Assuming no pore pressure change (e.g., $\Delta p = 0$ so that $\Delta\sigma = \Delta\sigma'$), the horizontal stress will increase by ~ 66 MPa, large enough to lead to shearing and even cracking of the matrix rock if there are sharp thermal fronts with steep gradients of thermal strain (local differential expansion). Rock joints dilate and shear in response to non-uniform stress changes arising from non-uniform temperature changes, and the resulting changes in

macroscopic permeability certainly exceed an order of magnitude because the flow capacity of a fracture is approximately a cubic function of aperture. Similar calculations for steam injection into shallow oil sands (< 800 m) show that shearing and dilation are unavoidable, and massive non-linear property changes take place at ΔT values as low as 60–100°C.

Early work on thermoelasticity in reservoirs include [Aktan and Farouq Ali \(1978\)](#) who used a Finite Element (FE) method in a 2-D porous media model subjected to single-phase hot water injection. They concluded that thermally induced stresses dominate the stress state, and as temperature rises, they are far larger than pressure effects and even gravitational stresses. This important conclusion has withstood the test of time. More rigorous coupling and modeling based on FE methods have been developed, and [Bai and Roegiers \(1994\)](#) developed an early model for a dual-porosity fractured medium (e.g., a typical NFCR). [Barton *et al.* \(1985\)](#) developed a coupled joint model based on empirical data to simulate the stress and size dependent coupling of shear stress, displacement, dilation, and conductivity, and of normal stress, closure and conductivity in jointed rock masses, but such models have seen limited applications in realistic reservoir cases. Complications in all approaches include numerical instability problems when joint surfaces separate, strongly non-linear compressibility of the natural fractures, uncertainty as to the distribution of natural fractures in the reservoir, uncertainty as to the temperature distribution because of the massive accompanying permeability changes, and limited (unverified) models for permeability changes associated with shear displacement along joint surfaces.

[Kocabas \(2006\)](#) and [Ghassemi *et al.* \(2008\)](#) investigated porothermoelastic (THM) effects of cold water injection into hot rock assuming that flow occurs only in a single pre-existing fracture. They showed that high rock stiffness (E) and low fluid diffusivity (k) lead to poroelastic contraction, allowing fractures to dilate (open), causing a reduction in fluid injection pressure at constant injection rate. Empirically, fracturing during cold water injection in sandstones has been well-known since the 1990's because of unexpected hydraulic fracturing arising during seawater injection ($\Delta T \sim 60^\circ\text{C}$) for flooding reservoirs: induced thermoelastic shrinkage led to a drop of the fracture pressure below the injection

pressure, fractures propagated, and well injectivity was dramatically increased. Conversion to warm produced water re-injection reverses the process, and well performance is thence badly degraded in comparison. [Ghassemi and Tarasovs \(2004\)](#) explored similar issues in NFCRs, showing development of tensile stresses that undoubtedly are associated with shear fracture propagation or the separation of fracture surfaces, and of course this would result in huge permeability changes. All these authors also noted high local shear stresses, sufficient to shear and dilate weak rocks, or cause slip along joints and bedding planes.

In an attempt to reduce the number of degrees of freedom in complex reservoir modeling, [Yin *et al.* \(2009a\)](#) developed a fully coupled THM approach using a finite element solution to model the reservoir and the surrounding thermally affected zone, combined with a displacement discontinuity method to model the surrounding elastic, non-thermal zone. The method can be implemented for simulation of thermal VO production and unconsolidated sandstone reservoir development involving large volume changes associated with dilation, but the specification of the thermo-mechanical constitutive behavior of the naturally fractured rock mass remains a challenge, and likely always will.

[Briggs *et al.* \(1992\)](#) conducted a high-temperature/high-pressure (HPHT) mechanistic study with modeling to investigate the contributions of different proposed recovery mechanisms (e.g., viscosity reduction, oil swelling, gravity drainage, and solution gas drive) for VO production from NFCRs using CSS (cyclic steam stimulation) processes. They reported that very small changes in the residual water saturation (S_{wr}) changed the production rate drastically because it generated large changes in k_{rw} . This is what happens during shear dilation and micro-fissuring of matrix blocks stimulated with high temperatures: any volume change is filled with the most mobile phase (water imbibition) so that the permeability increases disproportionately ([Dusseault and Rothenburg, 1988](#)). They also concluded that internal gas exsolution is effective at driving oil from the rock matrix into the fracture network; indeed, gas effects are vital to many VO production technologies, including non-thermal approaches ([Dusseault, 2007](#)). Additionally, in the case of carbonates, CO₂ generation increases significantly at temperatures over 200°C, contributing to the drive

process. A recovery factor of more than 50% was measured by [Briggs *et al.* \(1992\)](#) when these two mechanisms were studied under controlled conditions through a two-stage process, suggesting that reasonable *RF* values may be attained in NFCRs in some conditions.

[Pooladi-Darvish *et al.* \(1994a, 1994b\)](#) proposed an analytical solution to compute heat flow and gravity drainage from a single NFCR block under steam injection. They suggested that heat transfer via convection within a block can be disregarded in heat transfer analysis and a linear but unsteady-state conduction approach can be implemented to address this issue. Based on analytical solutions, the rate of thermal gravity drainage is proportional to the oil mobility at steam temperature. Clearly, block size, thermal diffusivity, and the μ -*T* relationship for the VO must dominate the results, but there is no capacity in such solutions to explicitly introduce changes in rock properties arising from temperature-induced internal damage. In real NFCR cases, it is the change in aperture of the natural fractures surrounding the matrix blocks, arising from thermal and pore pressure effects, which governs large-scale fluid flux, although it is the behavior of the matrix blocks that governs recovery factors and rates. THM coupling in such cases remains a serious challenge.

7.8 Carbonate Rocks at High Temperature

Geomechanics is central to modeling and simulation of processes involved in VO production because of massive thermal alteration of reservoir properties. In this section, thermal, chemical, physical, and geomechanical behavior of some carbonate reservoir rocks at elevated temperature is discussed.

7.8.1 Thermal Conductivity and Diffusivity

[Somerton and Boozer \(1960a, 1960b, 1961\)](#) measured thermal diffusivity and conductivity of some typical sedimentary rocks using an unsteady-state conductivity method for $T = 90$ – 800°C , reporting that thermal diffusivity and conductivity decreased drastically at elevated temperatures. As an example, changes in thermal diffusivity at elevated temperatures are presented for a medium-coarse grained vuggy limestone with 18% porosity in Figure 7-10, up to 400°C .

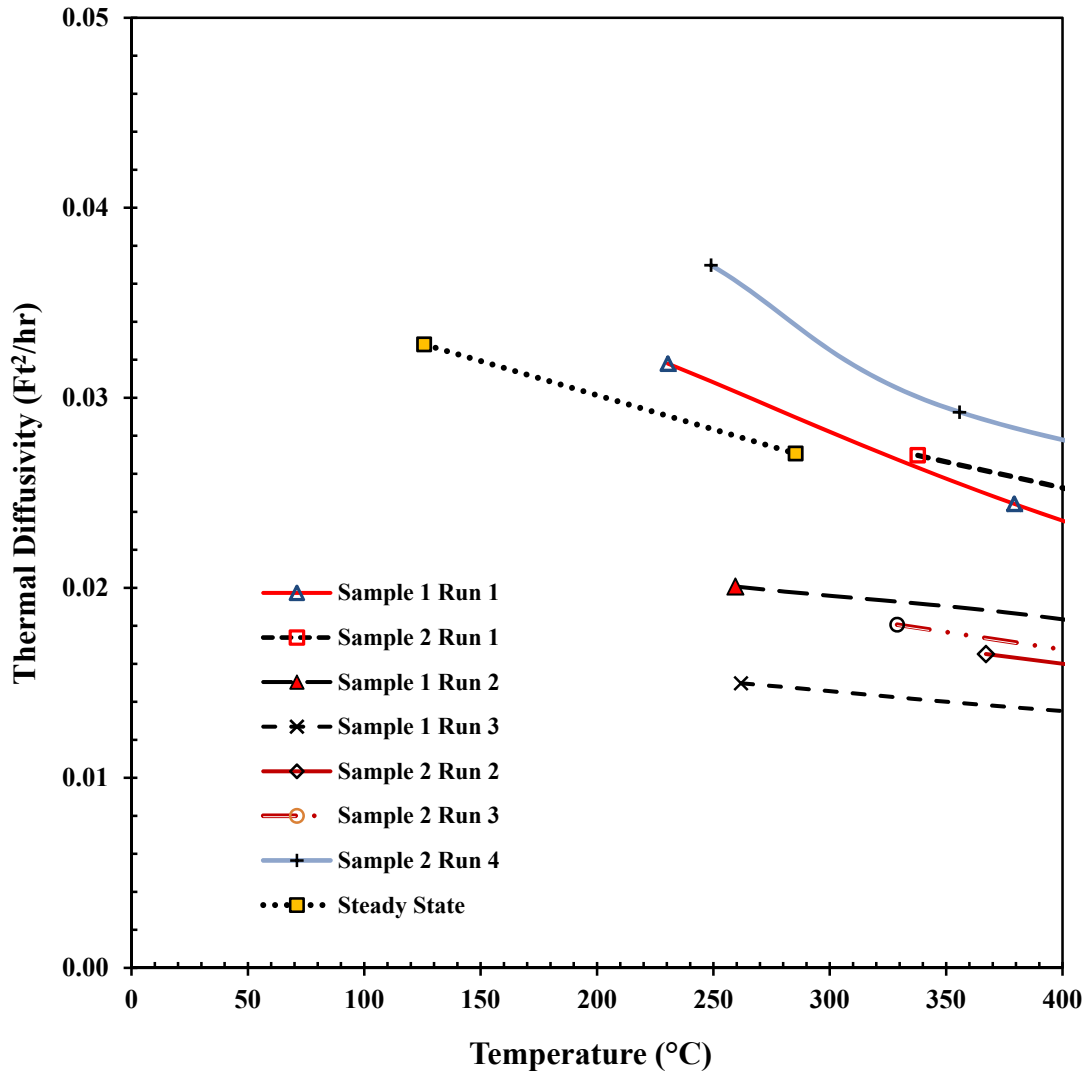


Figure 7-9: Thermal diffusivity of a limestone (Data from: [Somerton and Boozer, 1961](#)).

Thermal diffusivity decreases with increased temperature: an unsteady-state thermal diffusivity of 0.032 ft²/hr @200°F (2.97×10⁻³ m²/hr @ 93.4°C) and an unsteady-state thermal conductivity of 0.898 to 0.903 Btu/hr ft °F @200°F (0.263 to 0.264 watts @ 93.4°C) were reported for the limestone.

7.8.2 Physical Properties

Yavuz *et al.* (2010) studied elevated temperature (100–500°C) effects on physical properties (e.g., bulk density, effective porosity, V_p) of some carbonate rocks including three limestones: Finike Lymra (FL), Denizli Travertine (DT), and Burdur Beige (BB). They reported that heating limestone cubes led to dilation of the samples (e.g., differential thermal dilation of calcite crystals leading to thermal cracking in the rock material), decrease in the compressional acoustic wave velocity (v_p), and of course an increase in porosity.

Physical properties of the tested limestones are presented in Table 7-1.

Table 7-1: Physical properties of limestone (Yavuz *et al.*, 2010).

Name	Bulk density (g/cm ³)	Total porosity (%)	Effective porosity (%)	P-wave velocity (m/s)
FL	2.375	11.513	7.855	4301
DT	2.490	5.323	3.427	5126
BB	2.678	1.108	0.658	5941

At 100°C, no remarkable changes in v_p were observed. At 200°C, low porosity limestone (BB) retained 88% of its initial value, and the highly porous limestones (FL and DT) showed insignificant reduction. However, at 400°C, significant damage in all rock samples was observed within 24 hours of heating time. Low porosity limestone (BB) was less damaged and kept 64% of its initial v_p . At 500°C, v_p continued to decrease slightly after 24 hour of heating time compared with the lower temperatures. Final v_p values were 48%, 51%, and 57% of their initial values for BB, DT, and FL samples, respectively. This constitutes clear evidence of massive internal damage.

They concluded that the porosity of the thermally damaged less porous limestone (BB) increased with increase in temperature. However, the porosity of the travertine (DT)

decreased until 150°C and reached its original value again at 300°C and increased thereafter. The porosity of the Finike Lymra (FL) did not change notably until 300°C but increased at higher temperatures. Damage to highly porous rocks (DT and FL) was strong between 300–500°C, impeding water flow channels connecting the pores, causing a reduction in effective porosity of these rocks.

Even though experimental geomechanical data remain sparse for limestones in the steam temperature range, it is clear that dilation and microstructural cracking are important, and the consequences on production rate and RF are of first-order importance. In a field situation, NFCR matrix block heating is likely to be strongly non-uniform because of convective heat flux along the fractures, especially at the beginning, and it is likely that internal differential thermal expansion within blocks will further enhance shear cracking with attendant positive flow effects.

7.8.3 Geomechanical Behavior

[Zhang *et al.* \(2009\)](#) examined the geomechanical properties of some rock types including limestone subjected to temperatures of 20–800°C (Figure 7-10). The peak strength and elastic modulus of limestone decreased with T up to 200°C, little significant change occurred between 200–600°C, and a dramatic decrease occurred above 600°C. The peak strain to failure showed little or no change for the range 20–600°C, but it increases drastically for $T > 600^\circ\text{C}$. This study suggests that, in view of the range of bottom-hole temperatures recorded during steamflooding pilots in NFCRs (175–225°C) or expected in future projects (up to 325°C), one may expect some changes in the elastic and strength properties, but these changes are not severe. However, these conclusions do not pertain to differential thermal straining in a blocky rock mass, only to homogeneously heated small-scale specimens, therefore the results are of limited value in the large-scale context of NFCR VO extraction rate predictions.

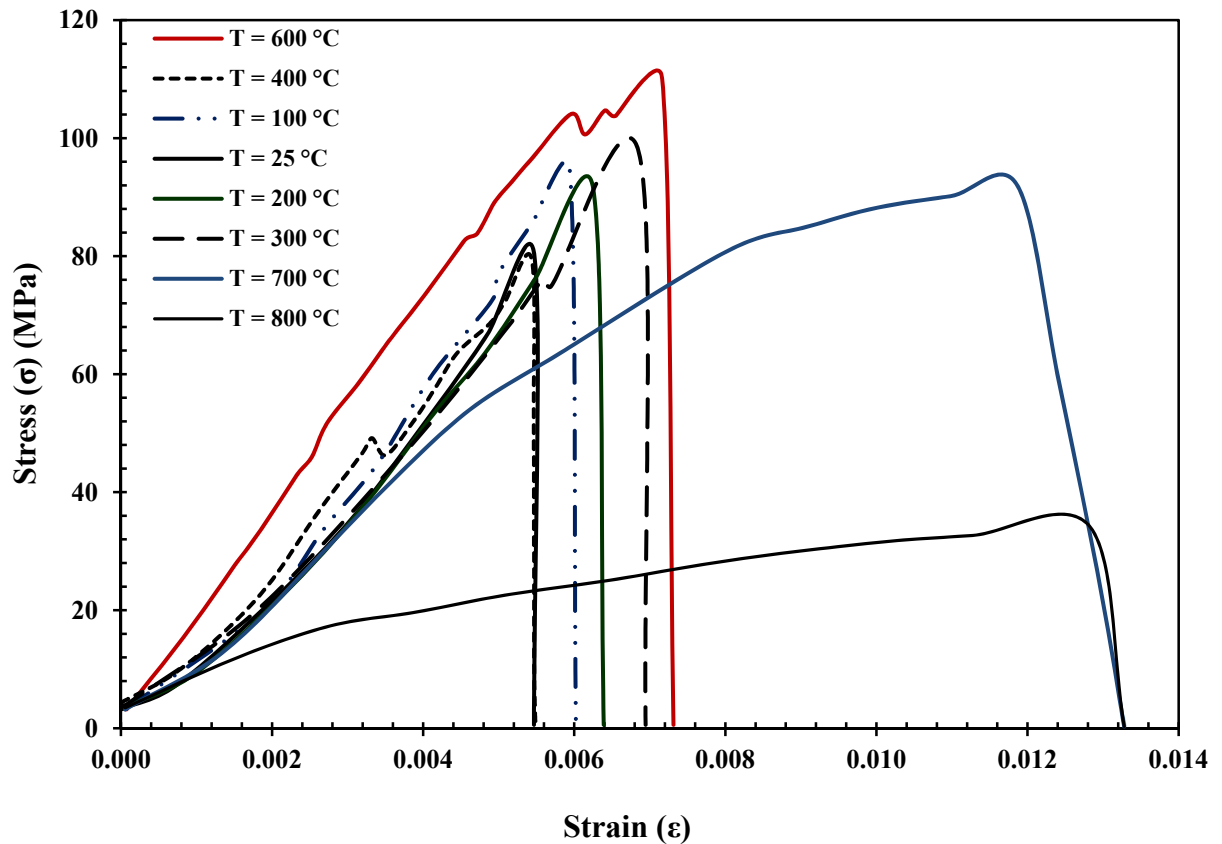


Figure 7-10: Stress-strain curve for limestones at elevated temperature (Data from: [Zhang et al., 2009](#)).

[Zekri and Chaalal \(2001\)](#) experimentally studied fracture development and propagation in carbonate formations under thermal and mechanical stresses. The effect of thermal shock (heating the samples at a specific temperature (e.g., 100°C, 150°C) for 24 hours and then immersing them immediately into water at 25°C to simulate the thermal shock) on non-fractured core permeabilities is presented in Figure 7-11. A reduction in core permeability by 50% was observed for core 1MIS under a thermal shock of 150°C. Thermal shock causes shrinkage, constricting channels connecting the pores and reducing core permeability, but less so in cases of low permeability (0.11 mD - Figure 7-12). For the second set of experiments the fractured core samples were tested and a thermal shock of 150–200°C was applied. As shown in Figure 7-12, the applied thermal shock enhanced the core permeability,

apparently through extending existing micro-fissures in the core sample, leading to an increase in core permeability. They concluded that thermal shock leads to a decrease in the permeability of non-fractured cores, in general, but as for previous studies, these conclusions (somewhat different from others') may have limited relevance in the context of a naturally fractured rock mass subjected to large thermoelastically-induced stress gradients. Furthermore, what happens to the matrix blocks can be very different than what happens to the jointed rock mass.

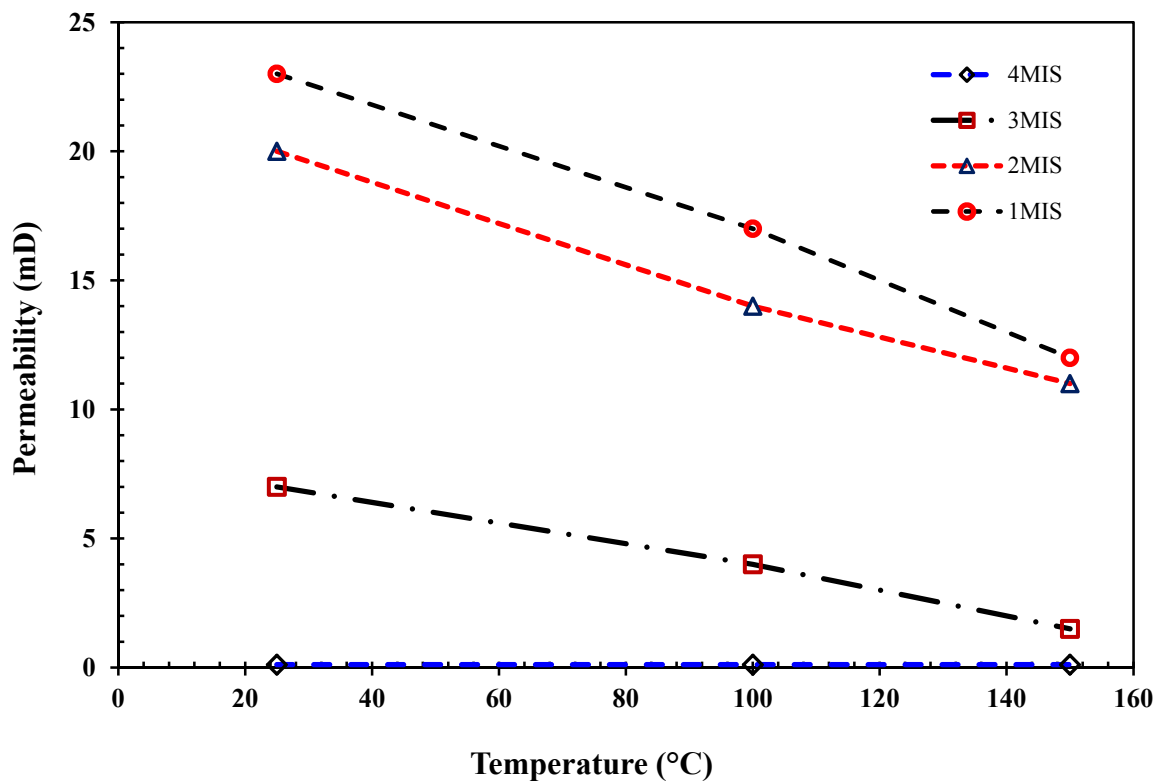


Figure 7-11: Effect of thermal shock on non-fractured carbonate core permeability (Data from: [Zekri and Chaalal, 2001](#)).

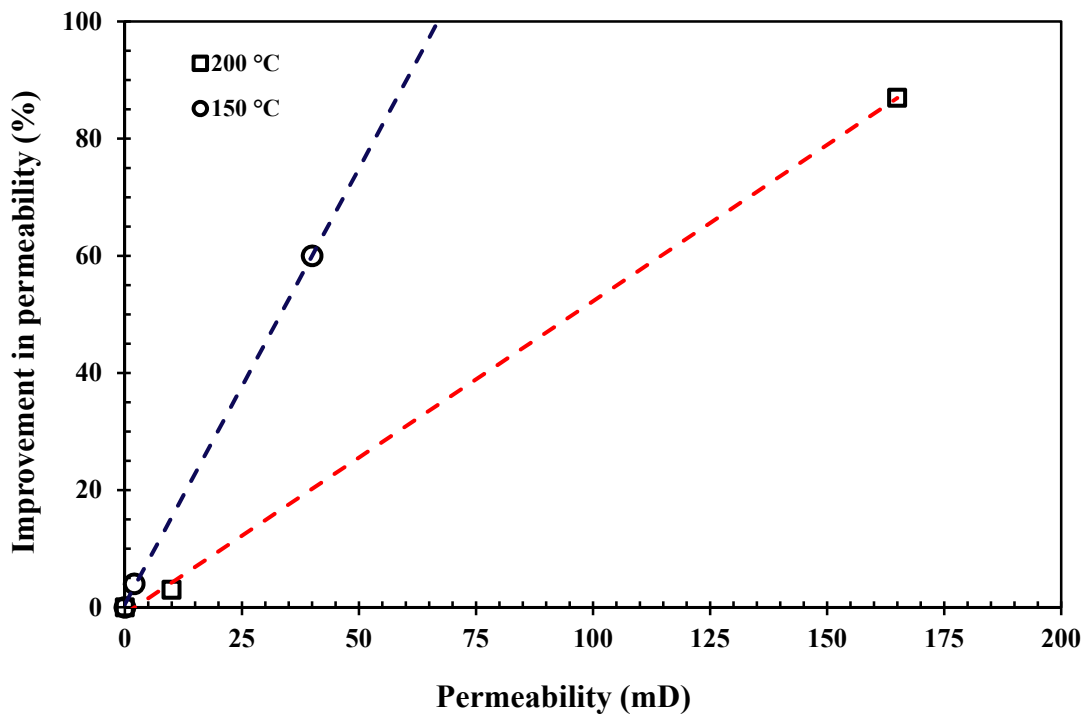


Figure 7-12: Effect of thermal shocks on fracture carbonates core permeability (Data from: [Zekri and Chaalal, 2001](#)).

Tensile strength tests were also carried out on the same samples which underwent thermal shock and a stress-strain curve is presented in Figure 7-13. The thermal shock reduced the tensile strength of all tested samples compared with the base case stress-strain curve (no thermal shock). Also, the stiffness of the specimens was reduced considerably, further reinforcing the idea of extensive internal damage as the result of differential thermal expansion.

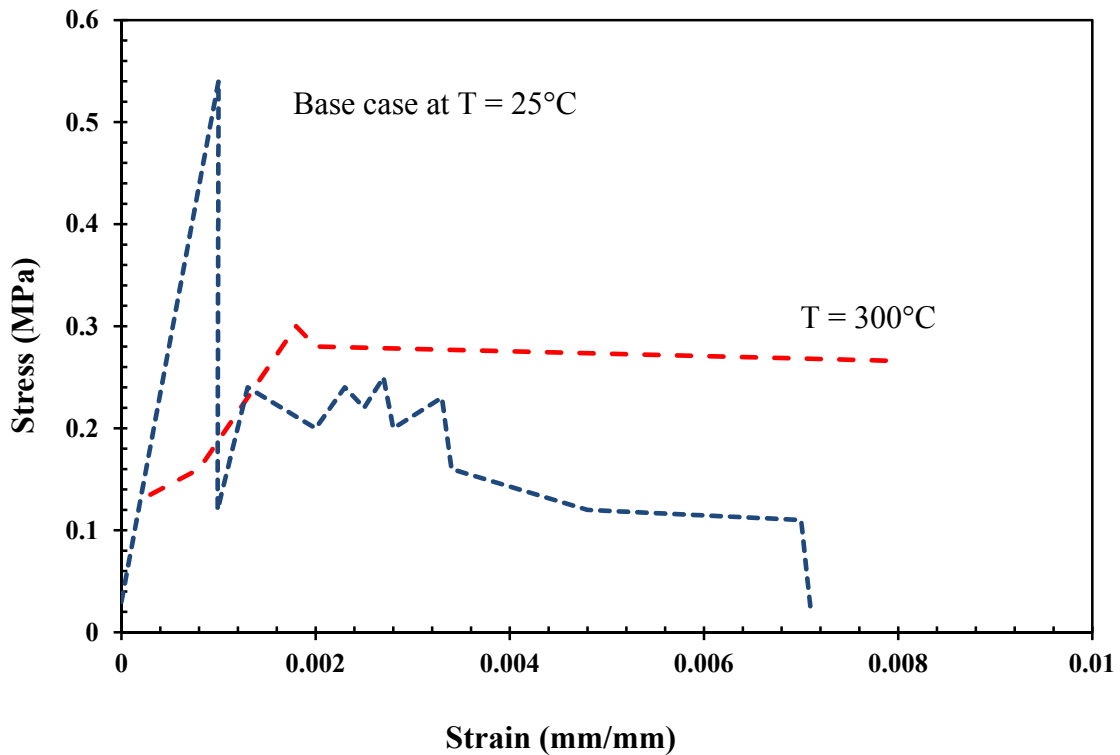


Figure 7-13: Stress-Strain relationship before and after thermal shocks for different temperatures (Base case: TZ2 Specimen # 1 tested at 25°C. TZ6 Specimen # 2 tested at 300°C) (Data from: [Zekri and Chaalal, 2001](#)).

7.9 Discussion

Some important points can be summarized based on the limited geomechanics results available and on the literature found on this subject.

7.9.1 Temperature, Stress, Shear, Dilation

Strongly differential thermally-induced stress fields arise during steam injection into fractured carbonates. Steep thermal gradients exist at two scales: at the scale of the stimulated volume (10's of meters) throughout the process until the entire reservoir is heated, and at the scale of the blocks (meters or less) as they are heated conductively by the hot fluids. Because the block temperatures achieve equilibrium with the steam temperature more

quickly than the entire reservoir does, there are also different time scales associated with the length scales. At the large scale, shear and dilation (or contraction) occur along appropriately oriented existing fractures, and this affects fluid transmission capacity because of aperture changes, and massive anisotropy in the macroscopic transmissivity of the rock mass may be generated at the same scale (tens of meters). Incipient or closed fractures are opened by rotational strains and increased shear stresses, and partially penetrating fractures that are appropriately oriented can be propagated under the stress and pressure conditions arising during large changes of temperature.

Within matrix blocks, as steep thermal gradients and large temperature differences are generated because of diffusive heat flux from the hot steam flowing in the surrounding natural fractures, large local stresses develop, and this can lead to of new sets of smaller internal fractures (micro- or meso-cracking from differential thermal strains), and this will likely improve rock matrix flow properties. This is an important point because it is the drainage rate of the matrix blocks that has the greatest impact on the economics of a thermal process in a VO NCFR. However, the strength of the matrix blocks is generally so high that generating new macro-fractures is unlikely because of the existence of the weak macrofracture network.

7.9.2 Comparison to Unconsolidated Sandstone Behavior

The response of a fractured medium with strong matrix blocks is unlike the response of oil sands or unconsolidated sandstone where general shear and dilation take place within the reservoir during thermal oil production operations ([Stancliffe and van der Kooij; 2001](#) [Collins *et al.*, 2002](#)). This is important; steam injection responses in unconsolidated sandstones cannot be extrapolated to VO NCFR responses without great care. Carbonate rock blocks are strong (high cohesion) but the natural or incipient fractures are weak (no or low cohesion); unconsolidated sands are inherently of low cohesion at all relevant scales, without joints that are conductive to fluids and are massively weaker in tension and shear. From a geomechanical point of view, carbonate rocks are a strong and stiff rock class, even

though fractured, whereas unconsolidated sandstones such as oil sands are far weaker in shear and more compressible.

General shear and dilation in unconsolidated sandstones is suppressed if the effective confining stresses remain high during the thermal process. For example, at a depth of 300–400 m, a quartzose unconsolidated sand (e.g., Athabasca Oil Sand) may dilate substantially (Dusseault and Rothenburg, 1988), but the same sand may dilate only minimally at a depth of 1–1.5 km, as long as the pore pressure remains approximately hydrostatic, because of the elevated effective confining stress. However, if steam injection is also accompanied by a very high pore pressure, close to the fracture pressure so that effective stresses are small, dilation of the unconsolidated sandstone will be proportionately greater. This is shown in Figure 7-14 below, where the effect of a higher confining stress is seen to suppress dilation.

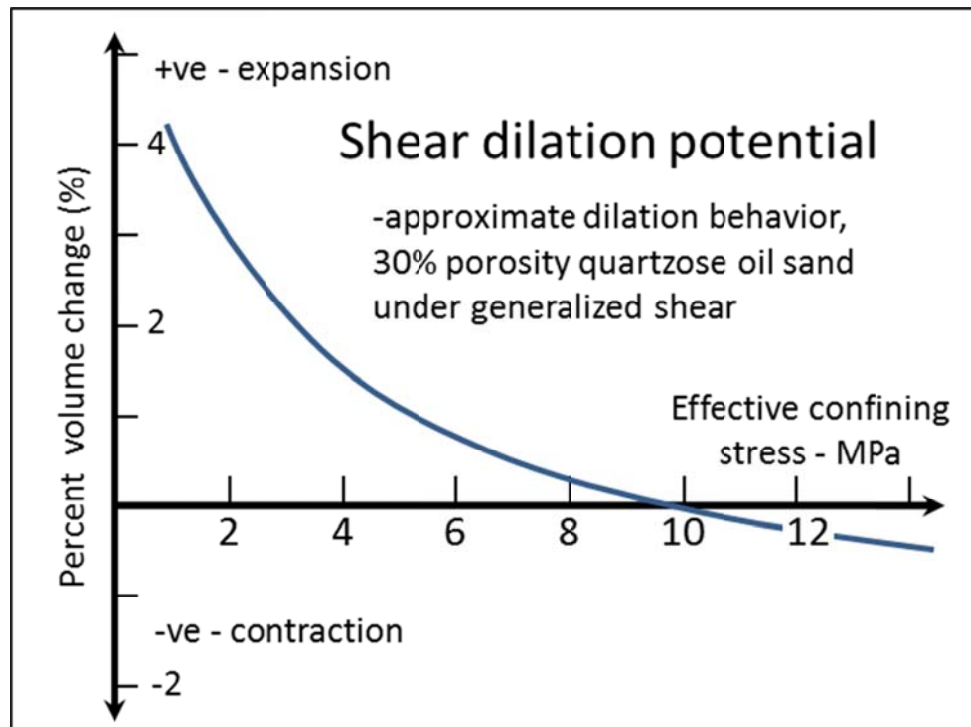


Figure 7-14: Typical dilation potential (maximum) for a quartzose 30% porosity oil sand.

In NFCRs, however, the shear stresses generated by differential thermal straining cannot be dissipated homogeneously in the rock mass by general shearing and dilation. These high

shear stresses are dissipated by macroscopic slip (likely on the scale of mm to a cm or two) along optimally oriented natural fractures. The fractures themselves will almost certainly show permanent dilation, but the matrix itself will not evidence shear dilation. This is a key issue in understanding the geomechanical behavior of NFCRs at elevated temperatures: they will shear only along pre-existing natural fractures, these shear planes will dilate, the dilation will be largely irreversible, and the effect on fluid transmissivity will be large and likely anisotropic because shear will occur mainly on optimally oriented fractures.

However, NFCRs may undergo internal micro-fissuring because of differential heating of blocks. Based on laboratory evidence (see above), irreversible thermally-induced internal damage takes place in rocks because of internal differential grain expansion. Such permanent deformation and microstructural damage leads to a change (reduction) in the thermal conductivity of heated geomaterials, but the effect is very small if the rock remains liquid-saturated. More important are potential effects on matrix permeability which should lead to more effective matrix block drainage. Laboratory studies support that heating carbonate rocks leads to the point of internal dilation of the rock (e.g., dilation of calcite crystals and initiation of thermal cracking within the rock material) leads to decreases in V_p , and increases in ϕ (Yavuz *et al.*, 2010). This dilation must be important with respect to permeability and hence the rate of a thermal process.

In higher porosity rocks (high porosity carbonates and dolomites), thermal shock can cause shrinkage but the porosity of less porous limestones during thermal loading probably always increases with temperature over the depth ranges of interest (up to 2 km, as for the Middle East and Alberta carbonates). In any case, even in higher porosity carbonates, there will be an interplay among local thermal stresses, expansion, internal micro-fissuring, and the externally imposed temperature, pressure and stress fields, so that a sharp thermal shock (steam injection) will likely lead to some increase in permeability of the matrix blocks. In some cases these changes are of the order of a factor of 10 or more on the macroscopic rock mass transmissivity (Zekri and Chaalal, 2001), the effects are potentially huge, but remain poorly understood and are not properly incorporated into simulations.

It seems reasonable to assume that high internal (block scale) thermal gradients associated with early-time steam flow through bounding fractures could be an important effect in VO NFCRs if there is internal thermal dilation from micro-fissuring. This is an important area for further work.

Chemical reactions may affect reservoir permeability during thermal oil extraction production operations. Reactions leading to accelerated precipitation of minerals in fractures lead to reduction in reservoir permeability in some areas, whereas in other regions of the reservoir, minerals are being dissolved. H_2CO_3 generated from dissolving of CO_2 in condensed water from steam processes can further dissolve the carbonate minerals, increasing flow path aperture, and increasing reservoir permeability. These effects remain ill-understood in practical situations, but some experimental work and simulations conducted by Briggs *et al.* (1988) suggest that certain reactions lead to improvement in fracture permeability during steam injection in NFCRs.

Changes in stress and temperature during thermal VO production operations impose complex changes on elastic and seismic properties of the reservoir rock because of changes in fluid viscosity, saturation, effective stress and rock microstructure (Somerton and Boozer, 1960a, 1960b, 1961; Zekri and Chaalal, 2001; Zhang *et al.*, 2009; Yavuz *et al.*, 2010). Geophysical wave techniques (3-D seismic surveys and passive microseismic tomography) have been used for reservoir monitoring with some degree of success, but much research needs to be done before changes in seismic attributes can be linked explicitly to specific changes in the rock mass because of the complexity of coupled processes (stress, pressure, heat, and porosity changes).

Laboratory work indicates that at high temperatures ($T = 500\text{--}600^\circ\text{C}$) there are significant reductions in Young's modulus, peak strength and tensile strength (Somerton and Boozer, 1960a, 1960b, 1961; Zekri and Chaalal, 2001; Zhang *et al.*, 2009; Yavuz *et al.*, 2010). These temperatures are not reached in steam injection, but do occur in combustion or *in situ* gasification processes.

VO production from NFCRs is in its infancy and most of the processes involved and their interactions are more complex than in sandstones because of the dual-porosity nature of the NFCRs. Nevertheless, we conclude that reservoir properties of NFCRs will be improved substantially during thermal oil production operations because of dilation and micro-fissuring.

7.9.3 Thermally Induced Casing Shear Mechanisms

Differential thermal expansion between a convectively heated reservoir (rapid) and a conductively heated overburden (slow) leads to a concentration of shear stress (Figure 7-15). The shear stresses generated by even 40–60°C differential temperature are enough to cause shear slip, and the casing cemented through the interface is first distorted, then ruptured or collapsed as the shear displacement increases (Dusseault *et al.*, 2001). Because the area experiencing shear is large, no cemented casing can resist the shear loads, therefore avoidance and mitigation are needed to reduce the incidence of casing shear. As an example, in the IOL Cold Lake Project, at least 40–50 wells must be repaired annually because of casing shear. The use of horizontal production and injection wellbores greatly reduces the incidence of casing shear.

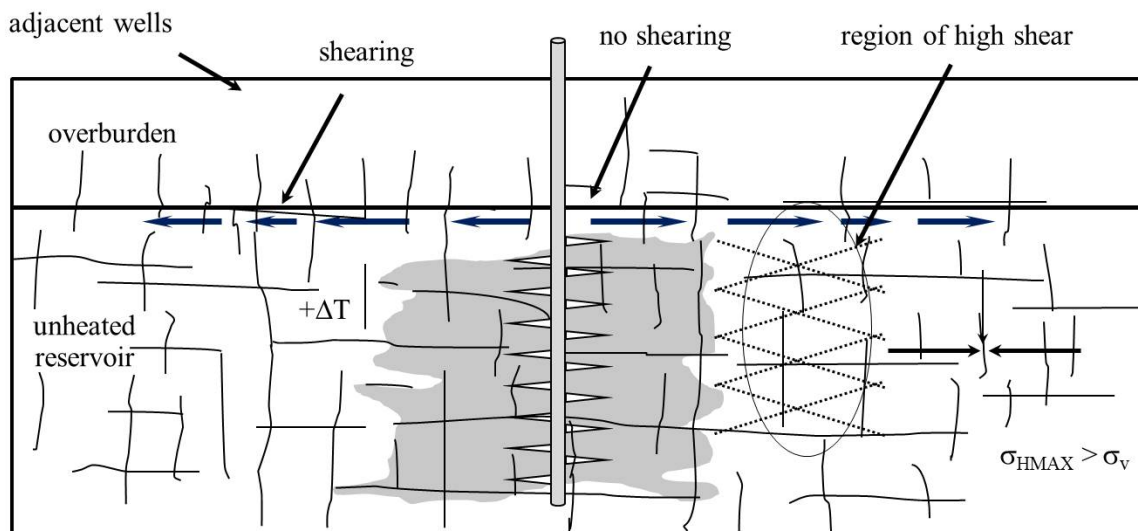


Figure 7-15: Schematic view of thermally induced shearing in unconsolidated sandstones.

Another geomechanical effect arising from thermal stimulation is shrinkage of clay-rich shale barriers. Once the temperature exceeds $\sim 125^{\circ}\text{C}$, adsorbed water is stripped off clay minerals, leading to a drying and shrinkage of the shale bed if it has an initially high porosity ($> 15\text{-}20\%$). As a small amount of shrinkage occurs, the horizontal stress is reduced, and eventually drops below the pressure of the pore fluid (steam-oil-water-gas) in the reservoir, so that vertical hydraulic fracture propagation is more likely. This can help access overlying resources in the case of thick reservoirs, in which case it is beneficial, but it can also lead to a breach of a cap rock, leading to loss of fluid and heat. Careful study of lithologies and their response to heating is clearly needed in individual cases, and data are lacking in this area.

7.9.4 Geomechanics Effects in NFCRs (Steamflooding Case)

NFCRs are jointed rock masses with fracture-delineated blocks of porous limestone (or dolomite, marl, or mixed carbonates) containing oil in the pores. Because there is 2×10^{12} b of VO in such reservoirs worldwide (Dusseault and Shafiei, 2011), production will take place eventually, likely based on some form of steam injection in the gravity-dominated domain (e.g., low Δp to minimize advective instabilities). The impact of geomechanics on VO NCFR thermal development remains poorly understood; there are no good data on the intrinsic response of the matrix blocks to differential thermal expansion, much less the response of the entire fractured rock mass.

Thermal VO recovery in NFCRs is economically more challenging than in sands because of the lower oil content (generally 6–10% by weight rather than 10–14%), adverse wettability, low matrix permeability, and ill-understood alterations in natural fracture permeability upon introducing steam or heat. However, massive geomechanics effects occur in NFCRs when subjected to thermal stimulation, so much so that the nature of the flow regimes is totally changed (for shear dilation effects in fractured rock see: Barton *et al.*, 1985; Hossain *et al.*, 2002; Dusseault *et al.*, 2011).

NFCRs have pronounced property contrasts between intact matrix blocks and fractures, so scale issues arise with natural fracture networks; only at very large volumes may one speak

of a characteristic system transmissivity ('macro-permeability'), but the drainage from intact matrix blocks will remain governed by the local and generally low 'micro-permeability'. In pressure-driven advective transport, high fracture permeability leads to severe advective instabilities (viscous fingering, coning and channeling). Hence, some variant of steam-assisted gravity drainage involving long horizontal wells and gravity stabilization of flow seems to be favored for VO production from NFCRs. The rate of heating of the limestone blocks will be slow, even dominantly through conductive heat transfer, because the permeability of the matrix block is generally in the range of 5–100 mD. This value is also too low to allow for rapid drainage of oil from the matrix, where over 95% of the oil is found.

Field trials of VO production from NFCRs are limited. Qarn Alam in Oman is the only significant project from relatively shallow VO NFCRs, and there is no information in the literature addressing the thermal geomechanical effects in this type of reservoir. Nevertheless, it is possible to speculate about the important geomechanics issues. They are similar to some degree to those arising in high-porosity sandstone reservoirs in that the resultant reservoir alteration at the macroscopic scale is expected to be similar. However, there will be differences between the response of oil sands and NFCRs to heat due to their different physical, mechanical, and reservoir properties, and because the NFCR matrix blocks almost certainly will not experience the general dilation observed in oil sands.

Figure 7-16 shows a blocky NFR and a heated zone generated by steam circulation in a sealed horizontal heater well, with a configuration of offset production wells placed at the base of the zone. This figure is not intended to suggest that this is likely to be a preferred method of production, merely to serve as a point of discussion without addressing the issues of massive active steam injection (a more likely technology).

permeability and reducing capillarity, which will allow heat to enter the blocks more rapidly (convectively), and allow hot oil to seep out more quickly.

Macroscopic heated zone expansion leads to radial stress increase and tangential stress reductions, in a manner similar to Figure 7-4. The tangential strains in advance of the thermal zone are extensional, so fracture apertures increase, and this has a sharp effect on permeability, allowing radially outward flux to be improved. Although the strength of the limestones is such that shearing and massive dilation within intact rock blocks are unlikely, the reservoir blocks are displaced by aperture wedging and by small amounts of slip along existing fractures (Hossian *et al.*, 2002; Dusseault *et al.*, 2011). Slip must take place because the elastic stiffness of intact limestone blocks is far greater than for high-porosity sandstones; values of $E \sim 20\text{--}30$ GPa (and $\nu \sim 0.20$) are probably reasonable for a porosity of 15–20%. The thermal expansion coefficient is similar, $\sim 10^{-5}\text{C}^{-1}$, so the high stiffness means that thermally-induced stress changes for a given ΔT will be far higher than in high-porosity sandstones, enough to cause some slip along favorably oriented joints (those joints lying at angles of 15–35° from the maximum induced stress direction generated by the heating).

The concept of favored slip directions is shown in Figure 7-17 for a regular orthogonal array of fractures, and a heating process in a strongly differential stress field. The pairs of arrows show the relative slip direction of the joint set that is favorably oriented. In this figure, the opening of the fractures in front of the heated zone is not indicated (see Figure 7-4 or 7-16 for the directions of extensional strain leading to fracture opening, but not shear). Predicting which orientations will slip and by how much in real situations remains an exceedingly challenging task because it is a fully coupled thermal – hydraulic – mechanical coupled system.

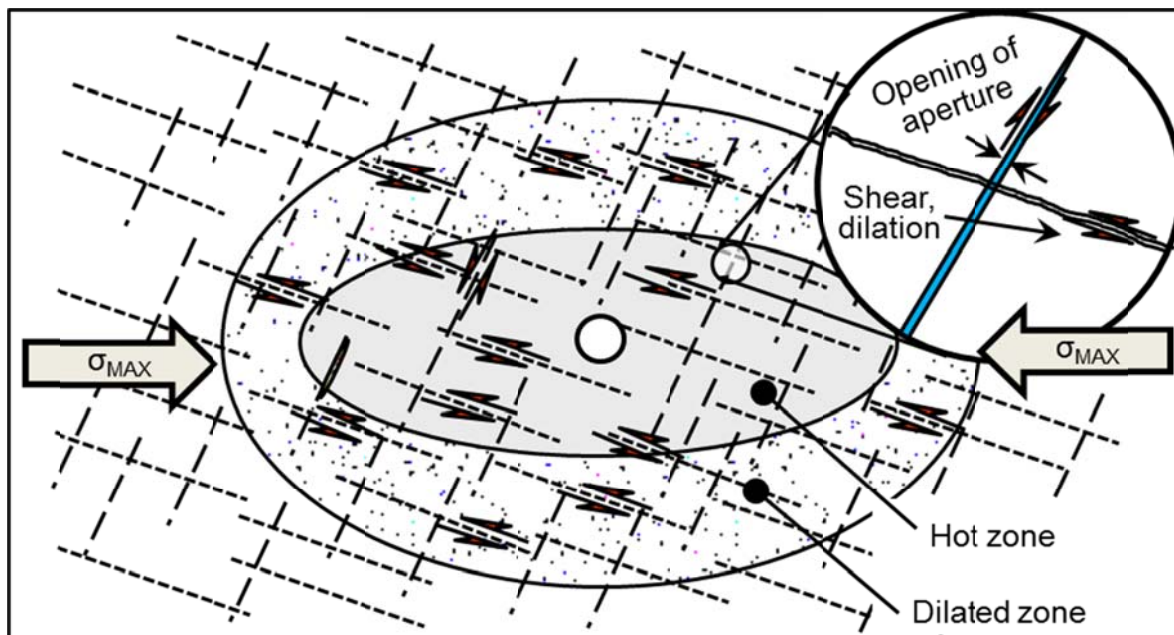


Figure 7-17: Favored slip directions for a regular orthogonal array of fractures subjected to a heating process in a strongly differential stress field.

Off the lateral flanks of the heated zone, horizontally oriented natural fractures will open as the blocks undergo small rotations; above the zone, vertically oriented natural fractures are opened because of the horizontal strain above the heated zone. Conversely, off the flanks of the heated zone, vertical fractures will experience compression and a reduction in permeability (likely explaining the results reported by [Macaulay et al., 1995](#)). In general, permeability increases from fracture opening are far greater than permeability impairments by fracture compression, and shearing processes make such changes in part irreversible. Hence, processes in general open the natural fractures, which greatly enhances the macro-permeability, but which also raises issues of seal maintenance above the heated zone.

Now, consider a heating process at temperatures above 400°C designed to generate pyrolysis; more gaseous phases are generated by the heat, and strong thermal convection aided by density differences and condensation take place and dominate the flux (in the absence of injection). The gaseous phases initially are solution gas driven out of the oil by the high temperature, then steam, and then hydrocarbon gases from pyrolysis and CO₂ from partial

decomposition of some less stable carbonate minerals. Water and other liquids will condense in the cooler zones, flowing downward because of gravity. As gases are generated, effective stresses are reduced, promoting opening of joints and shearing.

At this stage, something similar to the heat transfer process in SAGD will become dominant. Steam and vaporized hydrocarbon gases rise, condense, and flow back to the lower part of the reservoir as liquids where they can be produced. Depending on the matrix permeability and the rate of heating, high pore pressures are generated inside the individual matrix blocks, and because gases are generated, their strong expansion potential can help propagate internal micro-fissuring. The production wells are operated at back pressures commensurate with gravity-dominated flux, in other words, at about the same pressure as the heating well. This means production of liquids low in the zone, with the non-condensing gases replacing the liquids high in the zone, with the possibility of control of the process by injection of solvents or gases in additional injection wells.

A more common configuration would likely be an active steam injection well instead of a heating well, more in line with conventional approaches to steam-assisted gravity drainage. However, similar processes would take place, and the geomechanics effects will be equally important.

7.10 Concluding Remarks

High T and p production processes (steam injection, hydraulic fracturing) have a profound impact on the geomechanical behavior of VO reservoirs. To date, only cold flow methods and steam injection processes have achieved commercial success in accessing this immense resource, and almost exclusively in sandstones. An important factor in thermal VO production is the change in rock properties that takes place because of the large thermally-induced stresses. Hence, understanding the geomechanical behavior of these materials at elevated temperature is central to any thermal VO production scheme. Production from deeper and hotter reservoirs as well as steam injection into shallower VO reservoirs has triggered a large interest in and adoption of rock mechanics concepts and calculations into

planning and reservoir management. Large changes in porosity, permeability, and compressibility occur, so the reservoir response evolves in time. Whereas these geomechanical changes are largely beneficial as they tend to accelerate recovery rates, some difficult operational issues may arise, including casing shear and breach of reservoir seal.

These conclusions have been expressed generally, but are no less important for naturally fractured carbonate reservoirs containing VO. However, the mechanical response of a NFCR to heating or steam injection will be different than for sandstone. We make the following conclusions for VO NFCRs:

- Exploitation will have to be dominantly a thermal gravity-dominated method such as closed-well conductive heating, SAGD, or related process, to reduce advective instabilities.
- The rock matrix (within blocks) during early-time heating is likely to undergo some micro-fissuring as the result of differential thermal expansion, leading to increases in permeability, and reduction in capillary blockage.
- It is unlikely that rock blocks will experience macroscopic fracturing or shear that reduces the block size because carbonates are strong.
- Thermal expansion in stiff NFCRs will lead to large changes in compressive and shear stresses, with the following effects:
 - Increased compression in the heated zone will tend to reduce fracture aperture.
 - Appropriately oriented fractures will open in directions of extensional strain in advance of the thermal front; this fracture opening will be accompanied by shear displacement, making the aperture increases partly irreversible.
 - Along appropriately oriented natural fractures in advance or even within the heated zone, shear will be induced. This is a dilatant process, and largely irreversible, enhancing the macroscopic transmissivity of the rock mass.

- The state of understanding the geomechanical aspects of thermal processes in NFCRs is in its infancy, and there remain many issues to be resolved. For the jointed rock mass, these aspects can best be studied by monitoring field sites because the scale effects mean that laboratory tests will always remain unrepresentative of the mechanical response of the NFCR at the reservoir scale.
- Nevertheless, further detailed geomechanical study of the response of matrix rock to thermal shock and sharp thermal gradients under confined conditions are needed to help understand field behavior.
- Because of geomechanics effects, the transport and mechanical properties of NFCR reservoirs change during heating. This should be explicitly included in the interpretation of field data and in the results obtained from mathematical modeling of processes.

Nomenclature

Acronyms, Symbols, Units

Acronyms: Production Technologies

CSS	=	Cyclic Steam Stimulation (vertical wells)
GOGD	=	Gas Oil Gravity Drainage
HCS	=	Horizontal well Cyclic steam Stimulation
ISC	=	<i>In situ</i> Combustion
SAGD	=	Steam-Assisted Gravity Drainage
SF, SD	=	Steam Flood, Steam Drive

Acronyms: Others

2-D	=	Two Dimensional
API	=	American Petroleum Institute gravity scale
b	=	Barrel of oil
b/d	=	barrel per day
Bb	=	Billion barrels of oil
BB	=	Burdur Beige
D, mD	=	Darcy, millidarcy
DDM	=	Displacement Discontinuity Method
DT	=	Denizli Travertine
FEM	=	Finite Element Method
FL	=	Finike Lymra
HO	=	Heavy Oil

HPHT	=	High-Temperature/High-Pressure
IOL	=	Imperial Oil
NFCR	=	Naturally Fractured Carbonate Reservoir
OOIP	=	Original Oil In Place
SOR	=	Steam-to-Oil Ratio
TA-GOGD	=	Thermal Assisted Gas Oil Gravity Drainage
Tb	=	Trillion barrels of oil
THM	=	Thermal Hydro Mechanical
THMC	=	Thermal Hydro Mechanical Chemical
UCS	=	unconsolidated sandstones
UTF	=	Underground Test Facility in Alberta, Canada
VO	=	Viscous Oil
XHO	=	Extra Heavy Oil

Symbols: Latin first and then Greek

°K	=	degrees Kelvin
E	=	Young's modulus (GPa)
H	=	Reservoir thickness
k_v, k_h	=	permeability in Darcies, vertical, horizontal
n	=	Corresponds to heat transfer in crystalline substances
p	=	Pressure
P*	=	irreversibility
P _c	=	Crack-closing pressure

P_{inj}	=	injection pressures (MPa, psi)
RF	=	Recovery Factor (% OOIP recovered)
S_o	=	Oil saturation degree (100%)
S_w	=	Water Saturation [%]
S_{wr}	=	residual water saturation
T	=	Temperature ($^{\circ}K$, $^{\circ}C$, $^{\circ}F$)
V_p	=	Compressional wave velocity
V_s	=	Shear wave velocity
Z	=	depth
z	=	Depth in meters
α	=	Thermal diffusivity (Ft^2/hr or m^2/sec)
B	=	Coefficient of thermal expansion ($10 \times 10^{-6}/^{\circ}C$)
β	=	Thermal volume expansion
Δ	=	difference or change in, as in Δp , $\Delta \rho$
δ_c	=	Uniaxial Compressive Strength (MPa)
Δp	=	Changes in pressure
ΔT	=	Changes in temperature
ΔV	=	Changes in volume
$\Delta z, \Delta z_{max}$	=	Surface heave or uplift
$\Delta \rho$	=	Changes in density
$\Delta \sigma'$	=	Changes in effective stress
ϵ	=	Deformation

ε_i	=	Strain component in direction i
$\varepsilon_x, \varepsilon_y$	=	Deformation in the direction of x or y
μ	=	Viscosity (cP)
ν	=	Poisson's ratio
σ	=	Stress [kPa, MPa]
σ_1'	=	Effective maximum principal stress (MPa)
σ_3'	=	Effective minimum principal stress (MPa)
σ_r'	=	Effective radial stress (MPa)
σ_θ'	=	Effective tangential stress (MPa)
ϕ	=	Porosity (%)

Unit conversions

1 barrel	=	0.159 m ³
MPa	=	145 psi
°F	=	(°C×1.8) + 32

Chapter 8

Fracture Characterization and *In situ* Stresses Inference in a Naturally Fractured Carbonated Heavy Oil Reservoir – An Integrated Geophysical-Geological Approach

8.1 Abstract

Fracture system characterization along with *in situ* stress field determination in naturally fractured reservoirs have several applications in the petroleum industry including better drilling management, horizontal well placement, and planning for hydraulic fracture stimulation. Relative magnitudes and orientations of the *in situ* principal stresses in a naturally fractured carbonate heavy oil field in the Middle East were estimated with a combination of available data (World Stress Map, geological and geotectonic evidence) and techniques (core analysis, borehole image logs). In addition, magnitudes of the *in situ* principal stresses and pore pressure were estimated. A combination of outcrop studies, core studies, seismic data, and borehole image logs were also used to characterize natural fractures. Estimates made in this study using multiple sources such as core analysis and image logs are in good agreement with estimates suggested by the World Stress Map and geological and geotectonic evidence. The orientations of maximum and minimum horizontal stresses are NE-SW and NW-SE. Three general orientations of mainly vertical and sub-vertical fractures were identified and characterized over the crestal area of the anticlinal structure. Borehole image logs proved useful in identification and characterization of natural fractures.

8.2 Introduction

In the first part of this chapter, the fracture generation, classification, and characterization techniques applied in characterization of Naturally Fractured Carbonate Reservoirs (NFCRs)

are briefly described. Then, natural fractures are studied in a heavy oil field in Iran using different geological, geomechanical, and geophysical data. Different seismic methods available for the purpose of fracture orientation estimation and porosity estimation in NFCRs are also reviewed and discussed. A field study of fractures at the surface and in the sub-surface was conducted and regional tectonic fracture systems characterized. In the second part of this chapter, first some of the techniques for *in situ* stress state determination are described; then, a combination of geological, geomechanical, and log data is used to infer magnitude and orientation of the *in situ* stresses. Results obtained from this study can be used in field development, well placement, hydraulic fracture design, and reservoir simulation practices. Also, the methodology is generally applicable.

8.2.1 Naturally Fractured Reservoirs

The great majority of carbonate reservoirs are highly fractured; these are referred to as Naturally Fractured Reservoirs (NFRs), and defined as oil or natural gas reservoirs that contain fractures (planar discontinuities) created by natural processes (e.g., tectonic forces, diagenesis) distributed as a consistent connected network throughout the reservoir (Saidi, 1987). In NFRs, an interconnected fracture system provides the main flow paths (high permeability, low storage volume) and the reservoir rock or matrix acts as the main source of the hydrocarbons (low permeability, high storage volume). The matrix (usually over 97% of the reservoir volume) contains almost all the oil but the production into the wells is through the high permeability fracture system (less than 3% of the reservoir volume), hence matrix-fracture interactions must be quantified for reservoir evaluation.

More than 40% of current world conventional oil production comes from Naturally Fractured Carbonate Reservoirs (NFCRs), dominantly in the Persian Gulf Basin. As much as 50% of the world's present proven conventional petroleum reserves are in NFCRs (Roehl and Choquette, 1985). Moreover, over 20% of the heavy oil, extra heavy oil, and bitumen endowment of the world are found in NFCRs, located mainly in the Middle East and Canada (Briggs *et al.*, 1988; Dusseault and Shafiei, 2011).

8.2.2 Natural Fractures Impacts on Field Development

In this section the impact of natural fractures on hydrocarbon reservoirs during planning and reservoir development is examined. Investigation of natural fractures should start during the exploration stage. Surface outcrops of the reservoir section or reservoir analogs can form the basis of a lithological, structural and stratigraphic foundation from which geologists develop conceptual models. These models should include knowledge of the regional stresses (Figure 8-1) because of the well-known stress effects on fracture permeability in NFCRs, and in order to assess whether the fractures are open to conduct reservoir fluids. In addition, the magnitude and direction of horizontal stresses play critical roles in hydraulic fracture design, as hydraulic fracturing is the primary stimulation method for NFCRs. Different seismic surveys acquired early in field development yield important data for determination of azimuthal anisotropy, which is essential to characterize natural fractures and to place wells effectively (Kristiansen *et al.*, 2005). For instance, knowing the general orientation of fracture systems during well planning dramatically improves the chance that wells will be placed so as to intersect fractures.

Information about natural fractures is also useful during the well-construction stage. During overbalanced drilling and cementing operations (e.g., when $p_w > p_o$), open natural fractures can cause lost circulation problems, loss of expensive drilling fluids and the potential loss of wells. A less obvious cost may be associated with the reduced productivity that results when drilling fluids and cement seal fractures that were once open and potentially productive. Employing underbalanced drilling techniques and using less damaging drilling or cementing fluids are possible ways to reduce lost circulation and its associated damage. However, in many cases, drillers' options are more limited. When drilling weakened and depleted NFCRs surrounded by low-permeability shales or zones of higher pressure, drillers must maintain a certain mud weight to support the shale or to prevent a blowout from the higher pressure zone.

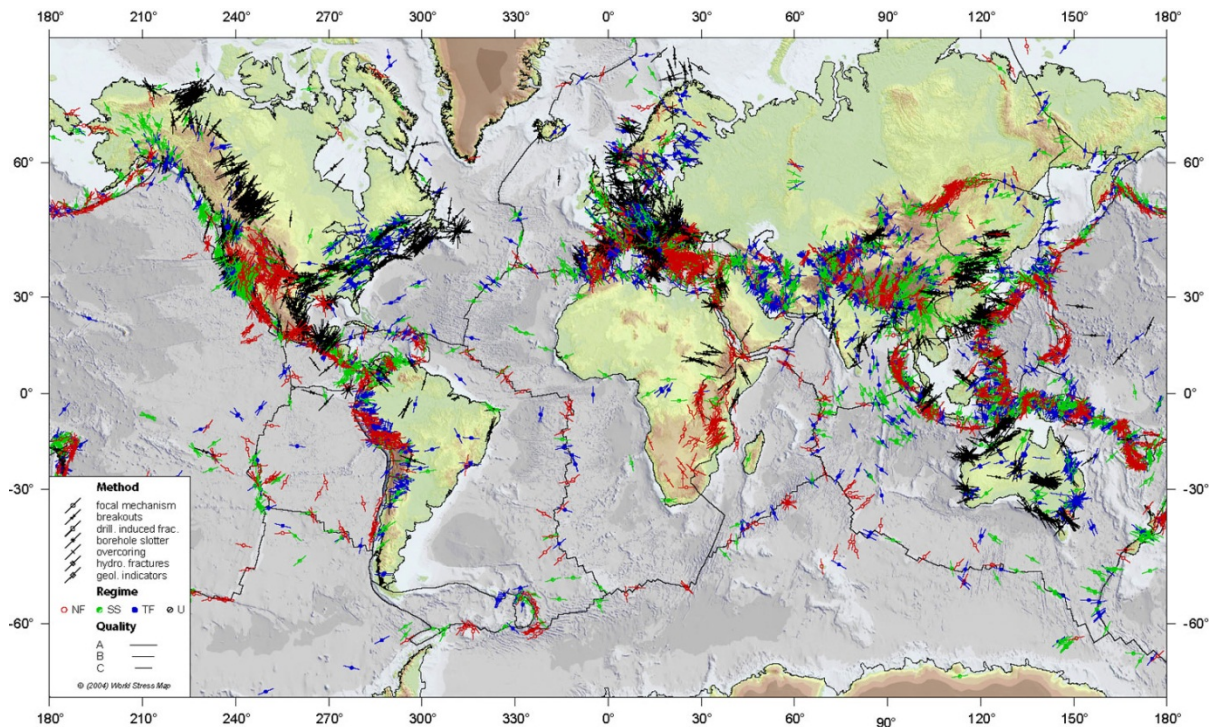


Figure 8-1: World stress map showing stress data compiled from various sources. In oil and gas regions, borehole measurements are an important source of present-day *in situ* stress information. This basic information is used in modeling to help understand fracture networks in fields worldwide (From: the [World Stress Map Project](http://www-wsm.physik.uni-karlsruhe.de), <http://www-wsm.physik.uni-karlsruhe.de>).

It is not surprising that one of the greatest challenges facing reservoir experts is how to precisely simulate the effects of fractures on reservoir behavior. Understanding these reservoirs requires the acquisition and analysis of vast amounts of data, and usually begins with detailed, foot-by-foot characterization of the fracture and matrix systems in extensive core samples and geophysical log traces. It is the interaction between the fractures and matrix that must be understood because the reservoir flow properties change with continued production or injection. As field development continues, other information (e.g., well-test data, production data, passive and time-lapse seismic data, deformation measurements and p & T data in thermal processes) helps validate and improve reservoir models.

During the primary-production stage, changes in reservoir pressure, and consequently effective stress, alter the fluid flow capacity of fracture networks (Lorenz, 1999). Water or gas breakthrough is the most common negative implication of conductive fractures during the primary-production stage. Besides adding water production and disposal costs, producing large volumes of high-mobility water tends to isolate substantial volumes of low-mobility oil because of the generation of capillary barriers. Enhanced oil recovery techniques using fluid injection methods also change the field pressure and effective stress distribution, and therefore change fracture conductivity to fluids. Ideally, primary production and secondary-recovery strategies (well patterns and spacings, and selection of injection and production zones and sequences) should reflect the level of influence that natural fractures have on hydrocarbon sweep, as determined by simulations based on highly realistic and representative data bases.

8.2.3 Origin and Classification of Natural Fractures

When developing and modeling fractured reservoirs, the ability to understand and predict the characteristics of fracture and fault systems takes on a crucial importance (Lacazette, 2007). The complexity of natural-fracture systems is captured in the descriptive, genetic and geometric methods that geoscientists employ to classify natural fractures. Knowing fracture types enhances the ability to simulate fluid flow through fracture networks because various types of fractures conduct fluid differently. To appreciate common classification schemes, a basic understanding of how natural fractures develop is needed. However, achieving this understanding requires more than extensive field observation of natural fractures; it requires linking those observations with data from controlled laboratory experiments (Stearns and Friedman, 1972). In geomechanics, fracture types are divided into two groups related to their mode of formation: shear fractures (Figure 8-2) that form with shearing parallel to the created fracture, and tension fractures (Figure 8-3) that form with tension perpendicular to the created fracture plane.

In the laboratory, shear and tension fractures form in consistent orientation with respect to the three principal stress directions, namely the maximum compressive principal stress, σ_1 ,

the minimum compressive principal stress, σ_3 , and the intermediate stress, σ_2 (Figure 8-5). Shear fractures are created under high differential stress and in conjugate pairs, forming an acute angle with σ_1 . Tension fractures, a term sometimes used interchangeably with the term “extension (or extnsional) fractures”, form perpendicular to σ_3 and at relatively low differential stresses, when the value of σ_3 , after adjustment for pore pressure (the local effective stress) has become tensile. In the laboratory, it is common to observe the creation of tension fractures during compression experiments at low confining pressures and in association with shear fracturing (Engelder, 1993).



Figure 8-2: Shear fracture on a shear joint surface in limestone from Iran.



Figure 8-3: Tensile fracture on a tensile joint surface in cordierite hornfels from Iran.

Shear and tension fractures described from laboratory experiments have clear counterparts that occur naturally; shear fractures correspond to faults, whereas tension fractures correspond to joints (Pollard and Aydin, 1988). This mechanically based distinction provides a useful way to classify fractures. Most faulting occurs during significant tectonic events when the differential stress is high. Tectonic faults typically occur over a broad range of scales, with displacements that range from millimeters to kilometers. Seismic images generally allow the detection of the larger faults, while borehole data are required to identify and characterize smaller faults. Tectonic faults typically cut unimpeded through stratigraphy and are therefore termed “non-stratabound”. Joints, or fractures having no visible

displacement, usually form approximately perpendicular to bedding, especially in flat-lying conditions. Joints can be either stratabound or non-stratabound. Stratabound joints stop at bedding surfaces and often develop a regular spacing and form systematic connected networks in plan view. Commonly, there is a long and continuous set of joints, termed systematic joints, which are joined by a perpendicular array of cross joints that abut the systematic joints (Gross, 1993).

The diagram presented in Figure 8-4, shows the directions of the principal stresses (maximum compressive principal stress, σ_1 and the minimum compressive principal stress, σ_3). The resultant fracturing is also indicated.

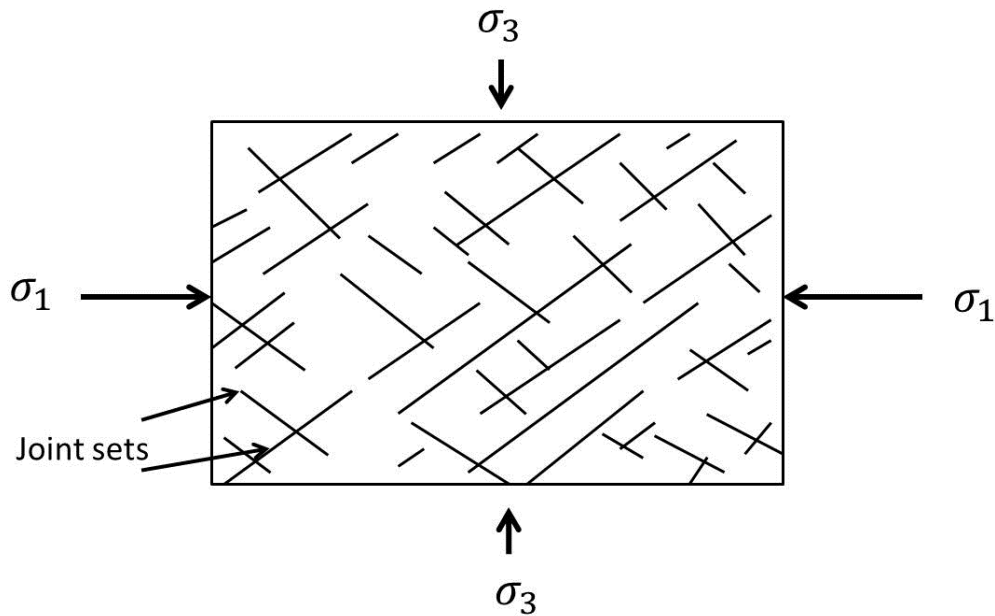


Figure 8-4: Principal stresses and the creation of low angle conjugate fractures.

The origin of joints is often difficult to determine, but it is known from rock mechanics that they occur at low effective σ_3 . Truly tensile stress occurs at shallow depths, so some joints form close to the surface. However, at reservoir depths, joints can probably form only under high fluid pressure or under conditions of rock shrinkage. Increasing fluid pressure can arise from compaction without drainage, hydrocarbon generation, and other processes, and it leads

to a process of internal hydraulic fracture. Shrinkage is associated with diagenesis such as carbonate dissolution, or through mineral changes such as the alteration of smectite to illite (with liberation of H₂O and SiO₂). In conditions of rock shrinkage, the vertical strains are accommodated by downward movement, but the horizontal strains cannot be relieved, so the lateral stresses in the rock decline as shrinkage continues, until the condition $\sigma_3 < p_0$ occurs, at which point a vertical tensile fracture should develop (neglecting any cohesion effects). In the shrinkage process, analogous to thermal cooling joints in basalt, the joints should be roughly equally spaced, and more closely spaced and persistent in the direction normal to the far-field σ_3 direction (e.g., [Pollard and Aydin, 1988](#)).

It is relatively simple for a geologist to distinguish faults and joints at an outcrop, but the distinction is often less clear using subsurface data, as stratigraphic offsets may not be resolvable. Geologists may therefore have to rely on a number of criteria, such as fracture fill, orientation and spatial distribution, to determine whether fractures of a given set are likely to be faults or joints. It may be necessary in such cases to develop a pragmatic classification system based on observed properties of the fractures.

Because carbonates dissolve relatively easily under pressure, they have a tendency to form stylolites that form perpendicular to σ_1 . Stylolites may cause local permeability reduction, or alternatively they may facilitate subsequent dissolution and permeability increase. Tension gashes, or fracturing associated with stylolites, are common ([Nelson, 2001](#)). While tension gashes may contribute to permeability measured in core, their subsurface impact on reservoir producibility is thought to be minimal. A genetic classification system examines how fractures relate to the formation and the structure in which they are located. The creation of endogenetic fractures relates to the stresses during sedimentation. Exogenetic fractures are formed after sedimentation and lithification, usually from tectonic stresses caused by folding and faulting.

8.2.4 Classification of Naturally Fractured Reservoirs

As mentioned earlier, most, if not all, reservoirs contain fractures. It is the degree to which fractures influence fluid flow through a reservoir that should dictate the level of resources needed to identify, characterize and model fractures. The effects of fractures can change through the productive life of the reservoir as pressures and fluid types change during primary- and enhanced oil-recovery stages. Moreover, fractures do not always conduct fluid; they can act as barriers to flow under some circumstances (e.g., a gas-filled fracture that forms a capillary barrier to liquid flux). Fractured reservoirs are classified based on the interaction between the relative porosity and permeability contributions from both the fracture and matrix systems (Figure 8-5) (Nelson, 2001):

- Type 1 reservoirs, fractures provide both the porosity and permeability elements.
- Type 2 reservoirs have low porosity and low permeability in the matrix, and fractures provide the essential permeability for productivity.
- Type 3 reservoirs have high porosity and may produce without fractures, so fractures in these reservoirs provide added permeability.
- Type 4 reservoirs have high matrix porosity and permeability, so open fractures can enhance permeability, but natural fractures often complicate fluid flow in these reservoirs. Another reservoir class, Type G, has been created for unconventional fractured gas reservoirs, such as coal-bed methane reservoirs, and fractured gas condensate reservoirs. Most Type G reservoirs fall within or near the Type 2 reservoir classification.

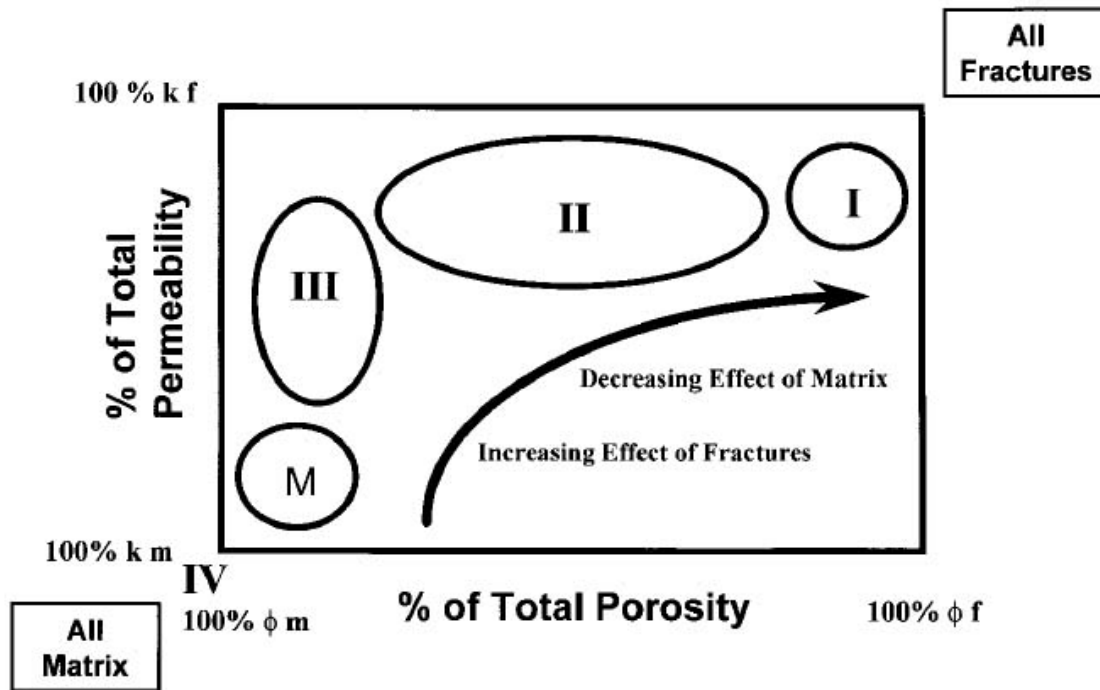


Figure 8-5: Naturally fractured reservoir classification system (From: Nelson, 2001).

Before NFR classification can be done in any meaningful way, both natural-fracture and matrix systems within a reservoir must be understood, along with the complex flow interaction between those systems. Many factors affect fluid flow within a NFR, including present-day stress orientation, natural fracture directions, whether the fractures are mineral filled or open, reservoir fluid properties and phases, and the production and injection history of the field. While many of these factors cannot be controlled, some of the problems that they pose can be mitigated. Field-development strategies can generally be tailored to the natural-fracture systems to optimize production and recovery.

8.2.5 Evaluation of Fractures and Fields

There are many different ways to characterize natural fractures and to evaluate their role in reservoir exploitation. Geometric methods measure specific attributes to identify and characterize natural fractures and assess their potential impact on production or injection. While traditional logging measurements, such as caliper and micro-resistivity logs, can

identify the presence of natural fractures, they are generally not quantitative in terms of fracture parameters such as aperture, flow capacity, and so on. Recently, various technologies have been developed to address the properties of NFCR's. Most of the common small-scale, log-based fracture-evaluation techniques use ultrasonic and resistivity borehole imaging methods that can be deployed by wireline or (Logging While Drilling) LWD methods. While the resolution of wireline-conveyed electrical borehole imaging tools is exceptional, the most detailed way to assess NFCR's is by acquiring full-bore cores across intervals of interest (Lorenz and Hill, 1994). Having access to full-bore core allows geologists and petrophysicists to examine specific properties that influence a fracture's ability to conduct fluids. Full-bore coring can be expensive and poor core recovery can be a problem in highly fractured rock; in addition, coring induced fractures can be difficult to distinguish from unmineralized natural fractures (Lorenz *et al.*, 1996). Finally, it should be noted that the flow behavior of a fracture is difficult to determine from a core sample because of the perturbation of the core, the difficulty in reconstituting the *in situ* conditions, and so on.

8.2.6 Fluid Flow and Stress Coupling in NFRs

Fluid flow in NFRs and the interaction between matrix and fracture flow is controlled by the fracture system characteristics (azimuth, dip, spacing, aperture, persistence and continuity, filling materials, water saturation and transmissivity), geomechanical parameters (magnitude and direction of principal stresses, rock stiffness, anisotropy), and intact rock petrophysical properties (matrix porosity, permeability, saturation, wettability). Large-scale flow is almost exclusively through the interconnected fracture network (Rutqvist *et al.*, 2002; Rutqvist and Stephansson, 2003); a particle of fluid typically travels a short distance within a matrix block to a fracture, then a long distance along the fracture network to the wellbore. As depletion occurs, small volume changes take place (the compressibility effect) and the *in situ* stress state is perturbed; the resulting effective stress changes ($\Delta\sigma'_{ij}$) lead to fracture aperture changes, and thus to alteration of the fracture transmissivity. This is a strongly coupled

stress-flow process which can lead to large changes in rock mass permeability and thus injection or depletion rate (Rutqvist *et al.*, 2002; Rutqvist and Stephansson, 2003).

8.2.7 The Need to Characterize NFRs

The greatest risk in not characterizing natural fractures early in a reservoir evaluation process is that oversight can severely limit future field development options, or can result in an inefficient geometrical pattern of wells. For example, a lack of natural fracture evaluation in an early development stage may sterilize a greater volume of resources through early water breakthrough, or lead to inappropriate infill drilling strategies. Incomplete data may result in inefficient well spacings and patterns that reduce not only the recovery factor, but may affect the rate of recovery.

Information about natural fractures is also used during the well construction stage. During overbalanced drilling and cementing operations, open natural fractures can cause lost circulation problems, loss of drilling fluids and the potential loss of wells. A less obvious cost may be associated with the reduced productivity that results when drilling fluids and cement seal fractures that were once open and potentially productive. The natural fractures can be severely impaired far beyond the perforation depth and then require additional costly stimulation (hydraulic fracturing, acidizing). Employing underbalanced drilling techniques and using less damaging drilling or cementing fluids are possible ways to reduce lost circulation and its associated damage. However, in many cases, drillers' options are more limited. When drilling weakened and depleted NFRs surrounded by low-permeability shales or zones of higher pressure, drillers must maintain a certain mud weight to support the shale or to prevent a blowout from the higher pressure zone.

Oil production techniques involving fluid injection (e.g., hot water, steam, chemical solutions) change the pressure field and effective stress distribution, and therefore change the fracture network conductivity and induce significant local anisotropy in flow properties as fractures in particular orientations are more affected than others. Ideally, primary and secondary recovery strategies should be based on the level of influence that natural fractures

have on hydrocarbon sweep efficiency and production rate. These strategies include well patterns and spacings, selection of injection and production zones, and stimulation sequences such as design of hydraulic fractures or acid injection for redevelopment. These factors should be studied by mathematical simulations based on realistic and representative data, and using formulations based as much as possible on the actual physics of multi-phase flow in a fracture network, in contrast to empirical correlation functions and “pseudo-” factors. The work flow from characterization to flow prediction is far more challenging than in unfractured sandstone reservoirs and monitoring plays a vital role as well to validate work flow conclusions and verify assumptions.

An ability to understand and predict the characteristics of the natural fracture system is a fundamental aspect of developing and modeling NFRs. Natural fracture systems are studied and categorized with descriptive, genetic, and geometric methods, generating data of a qualitative to highly quantitative nature. Knowing fracture types enhances the engineer’s ability to simulate fluid flow through fracture networks because various types of fractures conduct fluid differently (Nelson, 2001). To appreciate common classification schemes, a basic understanding of how natural fractures develop is needed.

8.2.8 Stresses

Sedimentary basin stress delineation (magnitude and direction as functions of depth and location) has broad engineering applications in NFR development, the most important being (Morgenstern, 1962; Kashnikov *et al.*, 2000; Nolen-Hoeksema and Rabaa, 1994; Tingay *et al.*, 1995; Banks *et al.*, 1996; Bell, 1996a and 1996b; Heffer, 2002; Henk, 2005; Araújo *et al.*, 2009; Han *et al.*, 2009; Yang *et al.*, 2009):

- Understanding the structural fabric of the sedimentary basins and rock densification,
- Evaluation of stress and pressure controlled hydrocarbon migration episodes in exploration activities (paleo-stresses),
- Calculation of mud-weight windows for safe drilling (blow-out prevention),

- Determination of optimum drilling trajectories to reduce borehole instability in shales,
- Evaluation of horizontal well placement in reservoirs with horizontal permeability anisotropy arising from stressed natural fracture fabric,
- Casing shoe depth choice in mildly and strongly over-pressured regimes,
- Casing design including casing-rock interaction potential during production leading to shear or parting,
- Design of cementing operations to avoid fracture losses (in both natural and induced fractures),
- Well completion design to manage or exclude sand,
- Design of hydraulic fracture installations,
- Assessment of compaction potential and magnitude,
- Evaluation of potential fault reactivation,
- Thermal stress calculations in thermal methods or cold water flooding,
- Microseismic monitoring data interpretation,
- Interpretation of acoustical wave velocity and quality changes in 4-D seismic surveys or tomographic surveys,
- Design and evaluation of liquid and solid deep well waste disposal,
- Autopsies and post-analysis of unexpected problems in drilling and production

Because naturally occurring fractures are the dominant flow paths, NFRs are deemed to be stress-sensitive reservoirs, where transport properties are sensitive to $\Delta\sigma'_{ij}$. Strong stress effects on fracture transmissivity in NFRs means the geological model should include regional stress data to help assess whether fractures are open in specific orientations, and how depletion-induced stress changes may affect fracture flow behavior. Furthermore, horizontal stress magnitudes and directions play critical roles in hydraulic fracture design for stimulation or field redevelopment.

In situ stresses can be estimated through field measurements (e.g., image logs, hydraulic fracture tests, step-rate injection tests, calibrated dipole sonic logs) or inferred through

geological indicators (e.g., tectonic fabric and history, faults, fractures, borehole breakouts). A combination of methods for each study region is necessary in order to integrate data between wells, in order to reduce uncertainty (each method has particular limitations in NFRs), and in order to build the 3-D geomechanics model that will serve as the basis for reservoir simulations and predictions.

8.3 Fracture Characterization Techniques

Because the nature and geomechanical behavior of a fractured geomedium at depth under *in situ* stress fields is different than at the surface, *in situ* fracture network characterization inevitably uses mostly indirect techniques rather than direct fracture characteristics' measurements. Most of the common small-scale, geophysical borehole log-based fracture evaluation techniques use ultrasonic and resistivity borehole imaging methods that can be deployed by wireline or Logging While Drilling (LWD) methods. While the resolution of wireline-conveyed electrical borehole imaging tools is exceptional, the most detailed way to assess NFRs is by acquiring full-bore cores across intervals of interest (Lorenz, 1999) and combining the core data with the logging information.

8.3.1 Outcrop Studies and Core Analysis

Structural geology and field description of fractures in outcrops is the first routine step in understanding fracture genesis and properties. Having access to full-bore core allows examination of specific properties that influence a fracture's transmissivity, though coring-induced fractures must be distinguished from unmineralized natural fractures (Lorenz, 1999). Large-diameter coring is expensive and poor recovery is a problem in highly fractured rock. Fracture flow behavior is difficult to determine from core specimens because of the perturbation (fracture surface displacement), difficulty in reconstituting *in situ* conditions, and the small surface area available (several hundred cm² at best for a fracture surface in a core specimen).

8.3.2 Seismic Techniques

Application of geophysical methods in NFCRs is less common compared to clastic reservoirs mainly because carbonate reservoirs are more heterogeneous and difficult to characterize. Seismic velocities of carbonate rocks are functions of porosity, pore type, mineralogy, and grain size, with the porosity and pore type being the most important parameters (Palaz and Marfur, 1997; Guadagno and Nunziata, 2007).

Fracture characterization usually uses relatively high-resolution techniques as compared to conventional seismic methods which use wavelengths up to 100 meters to detect the presence of natural fractures using azimuthal anisotropy analysis (Caldwell *et al.*, 1999; Barkved *et al.* 2004). These long-wavelength seismic techniques do not detect individual faults or fractures, but rather exploit the average response across a large volume of rock. For example, measuring travel-time differences between the fast and slow shear waves, together with the polarization direction of the fast shear wave, helps to infer the fracture intensity and fracture orientation, respectively.

The Side View Seismic Location method (SVSL – Figure 8-6) was introduced and implemented in Russia (~ 1990) to investigate open fractures via seismic wave scatter (Kouznetsov *et al.*, 2001).

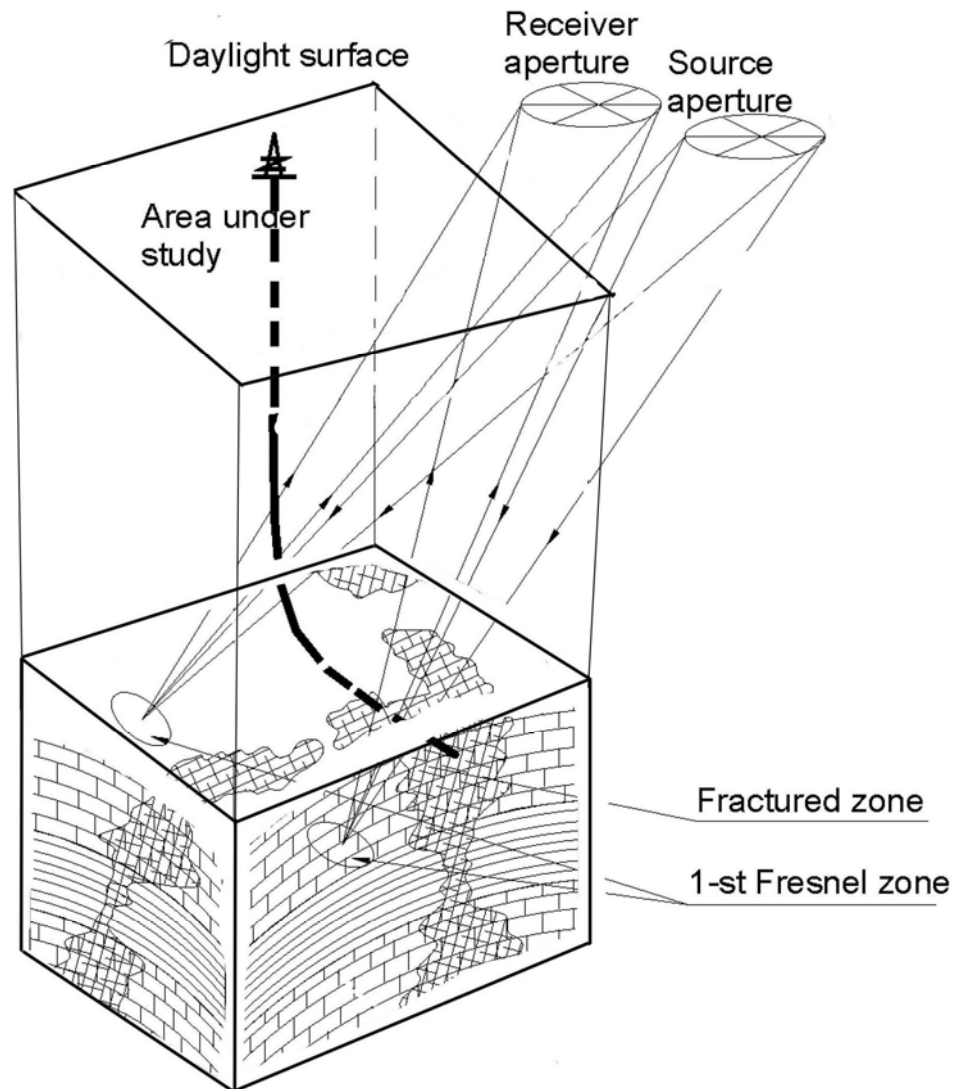


Figure 8-6: Side View Seismic Location technique (SVSL) (From: [Kouznnetsov *et al.*, 2001](#)).

The SVSL approach is founded on identifying back-scattered waves (SW) and determining their loci – the SW generation loci. The most intense SW's are generated by fully open fractures with maximum reflectivity contrast and the back-scattered energy depends on the density or intensity of fracturing in the zone (labeled 1st Fresnel zone in the figure because of the analogy to a Fresnel mirror or lens). Therefore, from the 3-D distribution of back-scattered energy one can estimate the spatial intensity of fracturing. The energy of SW's is

less by a factor of 10 to 100 than the energy of reflected P-waves which are used to characterize the structure of the layered sedimentary series, so to identify low-energy SW's it is necessary to apply special-designed field observation and data-processing systems based on SVSL principles.

As usual, many factors enter into the interpretation including mechanical properties, fracture void space and degree of partial fracture filling, overburden seismic properties (especially high frequency attenuation behavior), and stresses. Brittle rocks (dense, low-porosity) more readily form zones of intense fracturing whereas more ductile rocks such as higher porosity shales rarely form fractured zones, and in salt rocks fractures generally do not exist. Fractures in carbonates are far more pronounced than in sandstones, except for very low porosity sandstones that have been tectonically deformed. Zones with open fractures can be captured on vertical and horizontal sections of a SVSL survey as fracturing anomalies with different signs (Kouznetsov *et al.*, 2001). Effects of overburden load can also be identified in form of a predominant subvertical fracturing orientation and growth of fracturing intensity with depth, as well. In carbonates, their high solubility leads to porosity loss, and in the direction normal to the vertical stress, stylolites form because of the loads that do not allow the fractures to open. In contrast, in the horizontal directions, fractures form readily because of lateral stress diminution as intense diagenesis takes place through dissolution and precipitation, diminishing the porosity. Also, earth stresses affect the fracture fabric during fracture formation: a more random distribution for vertical fractures develops if the horizontal stresses are the same, but if fracture formation took place in an anisotropic stress field (e.g., tectonically loaded), the fractures are strongly and consistently oriented with the most persistent and closely spaced fracture set developing normal to the least principal horizontal stress direction. Certain types of fractures are associated with each tectonic structure which makes their identification feasible using SVSL techniques and tectonic models of the region.

8.3.3 FMI and UBI

Image logs are resistivity or acoustic devices that measure certain physical properties of the rock on the borehole wall or near the well that can be displayed as images to be interpreted visually or with computer-aided analysis. Formation Micro-Imager logs (FMI) provide a resistivity image of the borehole wall in water-based mud drilling with a resolution on the order of a millimeter. Introduced by Schlumberger in 1991 (Prensky, 1999), they are now applied widely to study geological features in boreholes such as fractures, bedding plane orientation and shape, borehole breakouts and washouts, and drilling-induced axial extensional fractures.

The Ultrasonic Borehole Imager or UBI was introduced by Schlumberger in 1993 (Prensky, 1999) and works independent of mud type. In a manner similar to the FMI log, the UBI imager can be used to analyze fractures and the stress regime and conduct borehole stability studies in any type of rock. An amplitude image is used for interpretation of geological features including bedding patterns (planar, non-planar, lenticular), stylolites or dissolution seams, natural fractures (open and closed), drilling induced fractures, and fine sedimentary structures such as flaser bedding and burrow casts. The radial UBI image gives a precise borehole geometry view, used to understand wellbore stability issues.

Both FMI and UBI logs were used to identify and characterize fractures as part of the sub-surface fracture characterization in this study.

8.4 Earth Stresses – Geological Inference

Natural stresses can neither be computed nor precisely measured; they can only be estimated at some level of reliability. Stresses are different for each point in the earth, and a "stress state" can only be defined at a single point.

8.4.1 Stresses and Effective Stresses

The three principal (and orthogonal) compressive total stresses (major/intermediate/minor - $\sigma_1/\sigma_2/\sigma_3$) and their orientations comprise six independent measures (a 2nd-order tensor) as

well as the pore pressure (P_o). If all seven values are known, the normal stress and two orthogonal principal shear stresses can be calculated for any plane.

Full stress state data are rarely available; usually four or five of the seven values can be estimated. In reasonably flat-lying sedimentary basins, it is assumed that σ_v is a principal stress (either σ_1 , σ_2 , or σ_3); thus, the other two are orthogonal and parallel to the earth's surface, referred to as the maximum (σ_{HMAX}) and minimum (σ_{hmin}) principal total horizontal stresses.

Porous strata stresses are carried by both fluid (water, oil, gas) pressure and solid phase (mineral "skeleton") stress, the pore pressure and the effective stress, respectively. Tectonic stresses are referred to in total stress terms, the sum of the effective stress and pressure. However, only stresses carried by the mineral skeleton contribute significantly to deformation, yield, or tensile fracture; hence, stress-strain analysis is in terms of the solid skeleton stresses - the effective stresses - sometimes called the "matrix stresses": $\sigma'_1 = \sigma_1 - P_o$, $\sigma'_2 = \sigma_2 - P_o$, $\sigma'_3 = \sigma_3 - P_o$. Importantly, shear stress is independent of the magnitude of pore pressure; it depends only on the differences between the principal compressive stresses.

8.4.2 Stress Orientation Determination

Stresses are controlled primarily by lithostatic loads and present-day tectonic loading (Becker *et al.*, 1987; Bell, 1996b). Surface indicators (contemporary stress orientations) such as "pop ups" (small stress-relief anticlines), may reveal mean stress orientations, the axis of the anticline will be roughly perpendicular to σ_{HMAX} (Adams, 1982; Wallach *et al.*, 1995). Brittle fractures parallel to σ_{HMAX} can form at the surface. Wellbore features indicators such as breakouts are useful stress indicators in vertical oil wells, as these are aligned with σ_{hmin} . Borehole images help in distinguishing genuine breakouts from other features (Bell, 1996a and 1996b). In most cases where breakouts occur the rock was subject to a high stress anisotropy. Core features, stress relief (center line / petal / fracturing, coring induced fractures, core diskings) can be used, and orientations of principal stresses can be estimated from the orientation of recovered strains using stress relief techniques on cores.

In the laboratory, shear and tension fractures form in consistent orientations with respect to the principal stress directions (Figure 8-4). Shear fractures are created under high differential stress in conjugate pairs, forming an acute angle with σ_1 . Tension fractures, a term sometimes used interchangeably with the term “extension (or extensional) fractures”, may form perpendicular to σ_3 and at relatively low differential stresses when effective stresses become temporarily tensile (a version of hydraulic fracturing). In the laboratory one may observe tension fracture development during compression experiments at low confining pressures and in association with shear fracturing (Engelder, 1993).

Laboratory fractures have clear natural counterparts; shear fractures correspond to faults, tension fractures correspond to joints (Pollard and Aydin, 1988). This mechanically-based distinction provides a useful way to classify fractures. Most faulting occurs during significant tectonic events when the differential stress is high. Tectonic faults typically occur over a broad range of scales, with displacements that range from millimeters to kilometers. Seismic images generally allow the detection of the larger faults, while borehole data are required to identify and characterize smaller faults. Tectonic faults typically cut unimpeded through stratigraphy and are therefore termed “non-stratabound”. Joints or fractures having no visible shear displacement usually form approximately perpendicular to bedding, especially in flat-lying strata. Joints can be either stratabound or non-stratabound. Stratabound joints stop at bedding surfaces and often develop a regular spacing and form systematic connected networks in plan view. Commonly, there is a long and continuous set of joints, termed systematic joints, which are joined by a perpendicular array of cross joints that abut the systematic joints (Gross, 1993).

Geological inference is a powerful aid to assessing stress directions. Generally, near faults, mountain chains, grabens (rifts), and so on, stress directions mirror the geological structures. For example, $\sigma_3 = \sigma_{\text{hmin}}$ points in the direction of the strike of an active, planar, high-angle fault (a normal fault), but at 90° to the fault strike if the fault is a compressive thrust fault, and then it is also σ_v . If the fault is a strike-slip fault, the direction of motion must be determined, and then $\sigma_3 = \sigma_{\text{hmin}}$ directions can be estimated; usually, σ_{hmin} lies in an

orientation about 60 to 70° from the strike of the fault. Great care must be taken to assure that the present-day stresses are measured, and that there has not been rotation of the stress field since the time the fault was last active.

The orientation of large hydraulically induced fractures will be at 90° to the orientation of σ_3 , as this is the most energetically favorable orientation for fractures to open. Providing that $\sigma_{\text{hmin}} = \sigma_3$, the fracture will propagate vertically in the natural stress field. To be used as an indicator of stress directions, the fracture must be large enough to be beyond the effects of the borehole region, and also of a length much larger than any joint spacing in the rock (joints affect local propagation direction, but not the large-scale direction).

Finally, seismic shear wave velocity anisotropy can reflect stress anisotropy, but caution is advised: wave transmission is highly sensitive to the fabric, and if the rocks now have a different stress orientation than at the time that the fabric developed through diagenesis, the seismic anisotropy may not reflect the present day stress orientations.

It is the most recent geological/tectonic events that govern the stress state. Thus, a new stress state can be superimposed on a tectonic fabric that was generated by an older phase of tectonic activity. The new tectonic loading may not yet be fully affecting the faulting structure, and it is possible to be misled by older, inactive geological features. Care should be taken in applying geological inference to determine stresses. Interpretation should be constrained by actual measurements, whenever possible.

8.4.3 Stress Magnitude Estimation

Vertical stress magnitudes (σ_v) can be estimated by establishing depth-density relationships within about 2 to 4% reliability. Hydraulic Fracturing (HF) including leak-off tests is the most common technique for measuring σ_{hmin} magnitudes while drilling (Daneshy *et al.*, 1986) if σ_{hmin} is vertical, but no method alone can reliably measure the σ_{HMAX} . σ_{HMAX} can be estimated using a formula proposed by Hubert and Willis (1957) or can be estimated from the extended leak-off test (XLOT) with fracture reopening methods (Bredehoeft *et al.*, 1976),

on the condition that the rock behaves elastically and that there are no severe thermal, poroelastic, or plasticity effects.

Cornet and Valette (1984) developed a method of measuring both σ_{hmin} and σ_{HMAX} at the same time by conducting hydraulic fracturing tests on pre-existing fractures through opening and closing two or more natural fractures which cut the wall of the well at different angles. This method is applicable for special circumstances and it is not very common, but may have particular applications in NFRs if the fracture density is not too high.

The relative magnitude of the principal stresses can often be gauged by geological inference, using the tectonic history of the basin, relatively recent faults that are sufficiently close. For example, salt at depth sometimes forms distinct elongated ridges (almost "waves"). These structures are oriented at 90° from σ_{hmin} ($= \sigma_3$), and thus a relative magnitude compared to the other two principal stresses can be obtained.

Stress measurements using hydraulic fracturing and extended leak-off tests data are widely employed and commercial services are available (e.g., Minifrac™) based on precision pumps, downhole gauges, and a refined methodology. Minimum stress magnitudes from these data are highly reliable. Because of various effects, σ_{HMAX} values may be interpreted often as a lower-bound estimate: the actual σ_{HMAX} stress is likely to be larger than the calculated.

In contrast to $\sigma_v(z)$, lateral stresses do not increase monotonically with depth at the scale of lithological units. Strata of different stiffnesses will display deviations from a regular increase in lateral stress magnitude, and the amount and nature of the difference depends on the lithology and the stress history (tectonic loading and erosion unloading). In general, lateral stresses in ductile shales are closer to the vertical stress than the lateral stresses in adjacent dolomites and sandstones, and in salt an isotropic stress state can be assumed.

8.4.4 Pore Pressure

To complete the stress state, knowledge of pore pressure is required. In general, P_o cannot be estimated reliably and with precision with any known means although seismic methods and

extrapolation from offset wells can be quite useful in specific basin settings. During hydraulic fracturing with precision tools and packers to isolate the fracture zone, it is often possible to also obtain a good P_o value.

After application of various approaches, it is usually possible to have good data on orientations, and reasonable values for P_o , σ_v , and σ_{hmin} , with a rough estimate of σ_{HMAX} from geological inference.

8.4.5 Geomechanical Implications

Optimum horizontal well placement and design of hydraulic fractures for redevelopment of NFCRs require *in situ* stress state information. Flow anisotropy can be determined, and preferred flow directions are usually related to stresses (Heifer and Lean, 1991). Because preferred flow directions often seem to be independent of geological fabric or fracture geometry (Bell, 1996a and 1996b), the great potential value *in situ* stress knowledge in well design seems apparent.

8.4.6 Anomalous Horizontal Stress Orientations

Anomalous stress directions are believed to be mainly related to local structures such as salt domes, shale diapirs, reef structures, and channels which affect the stress orientations locally (Bell, 1996a and 1996b).

8.5 Kuh-e-Mond Heavy Oil Field

Kuh-e-Mond is the largest on-shore heavy oil field in Iran, found in a giant anticline with a NW-SE trend. This relatively symmetrical anticline is 90 km long and 16 km wide with an estimated minimum heavy oil resource base of 6×10^9 b, found in three separate reservoirs with depths ranging from 680 to 1200 meters and oil viscosities of 550 to 1120 cP *in situ*. Many faults cut the axial plane of the structure causing some relative strata displacements around the central and plunging parts of the structure. The average dip of the southwest and northeast flanks of the anticline is 17° and 15° , respectively (Heffer *et al.*, 1995; Heffer, 2002).

Heavy oil occurrence has been confirmed in two separate intensely fractured carbonate formations, the Jahrum (Eocene) and Sarvak (Cretaceous) Formations (Figures 8-7 and 8-8) (Moshtaghian *et al.*, 1988; Kamali and Rezaee, 2003).

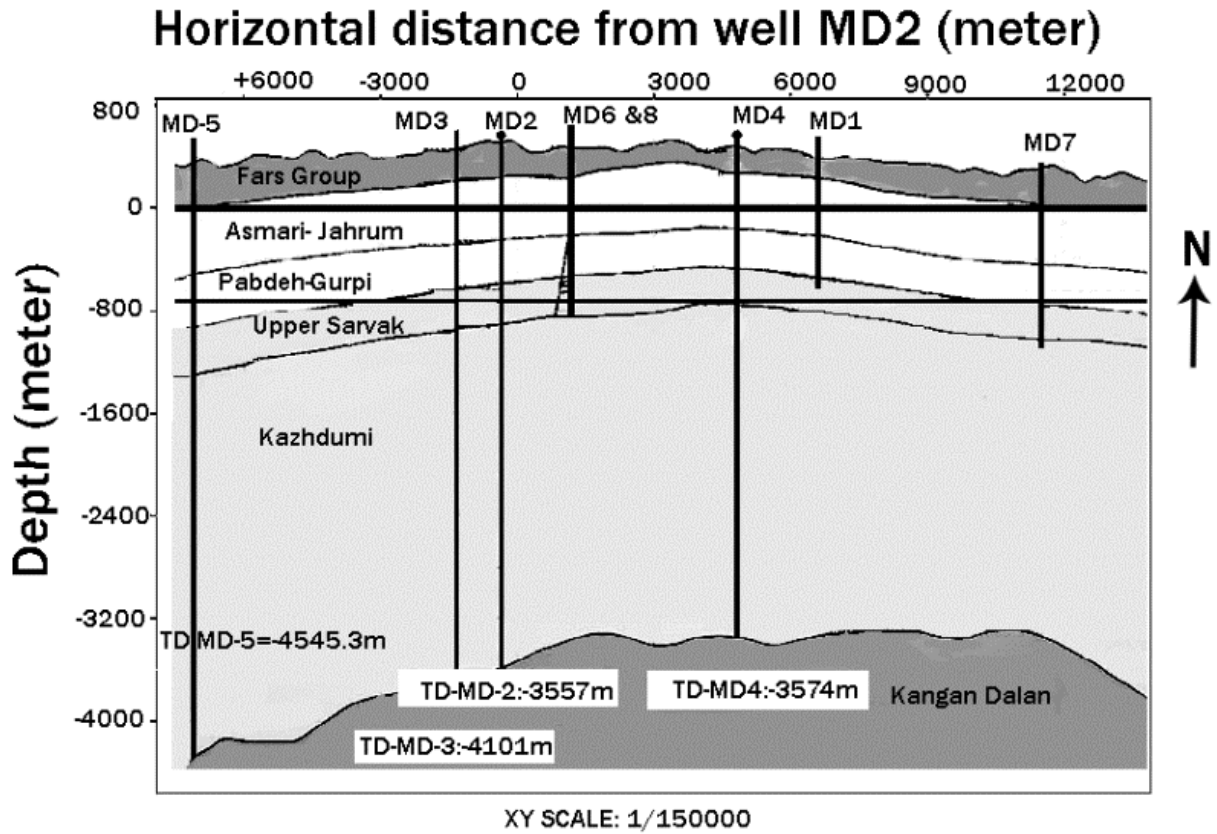


Figure 8-7: Geological cross-section of the Kuh-e-Mond anticline (x-section courtesy of PEDEC).

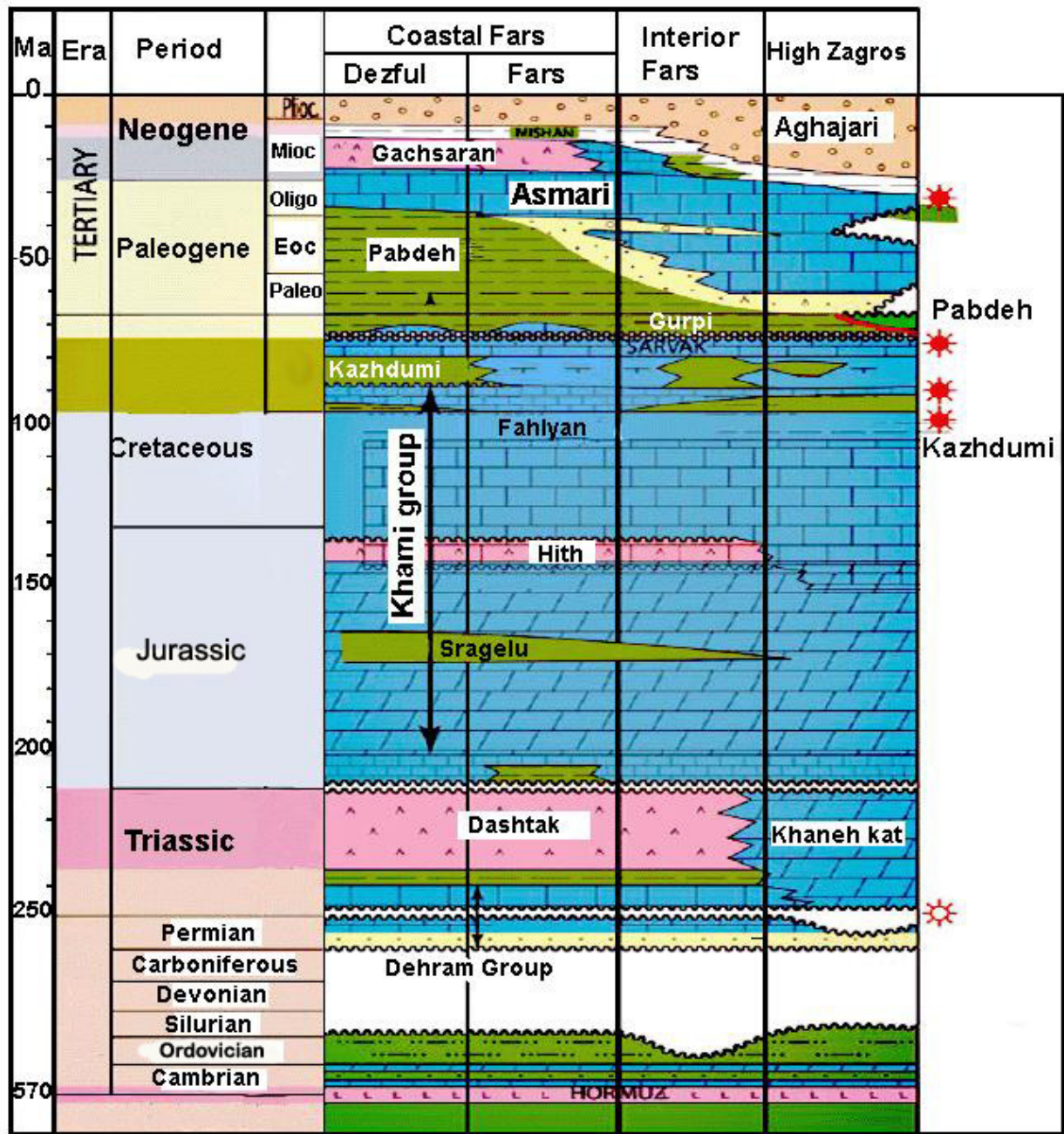


Figure 8-8: Lithostratigraphic column of the reservoirs at the Kuh-e-Mond field (Modified from Bordenave and Burwood, 1990).

8.6 Results and Discussion

8.6.1 Field Geological and Core Studies

Comprehensive field study of fractures at the surface and the regional tectonic fracture systems at Kuh-e-Mond has been undertaken. Surface fracture studies show that normal faults dominate along the structural axis of the anticline and are more frequent at the crestal positions along the structure. Three general orientations of mainly vertical and sub-vertical fractures were identified and characterized over the crestal area, in north, northeast and, east orientations. Two main fracture sets, one shear conjugated and the other clearly a tensile fracture set, were observed and characterized on the ground surface.

The many shear fractures resulted from the compressional tectonic regime of the Zagros orogeny. This type of fracture is normally tight (e.g., low permeability), but in this field they have largely been opened as the stress regime changed to a tensile tectonic regime, accompanied by uplift, bending or drag folding, and thus creating high-permeability fractures. The presence of such fracture systems improves reservoir quality but may impair reservoir seal, an important factor if steam injection technologies are used because of the buoyancy of steam and exsolved gases.

It was concluded that all the reservoirs, including the zones in the Jahrum and Sarvak Formations, are intensely fractured. Tensional fracture sets in rectangular patterns are well recognized in core samples; these fractures are usually open and contain heavy oil stains (Figure 8-9). Shear fractures are also visible in core samples; slickensides are noted on the surface of the shear fractures. Random or second-order fractures are also distinguishable in some of the cores.



Figure 8-9: Vertical fractures and vugs infilled with heavy oil in a core sample from Kuh-e-Mond field (Photo courtesy of PEDEC).

8.6.2 Seismic Surveys

A 3-D seismic survey was conducted over the Kuh-e-Mond field to generate a series of time structure, isochrones, depth structure, and isopach maps to be used in a second phase of reservoir assessment, increasing detail in the geological and reservoir characterization (Figure 8-10).

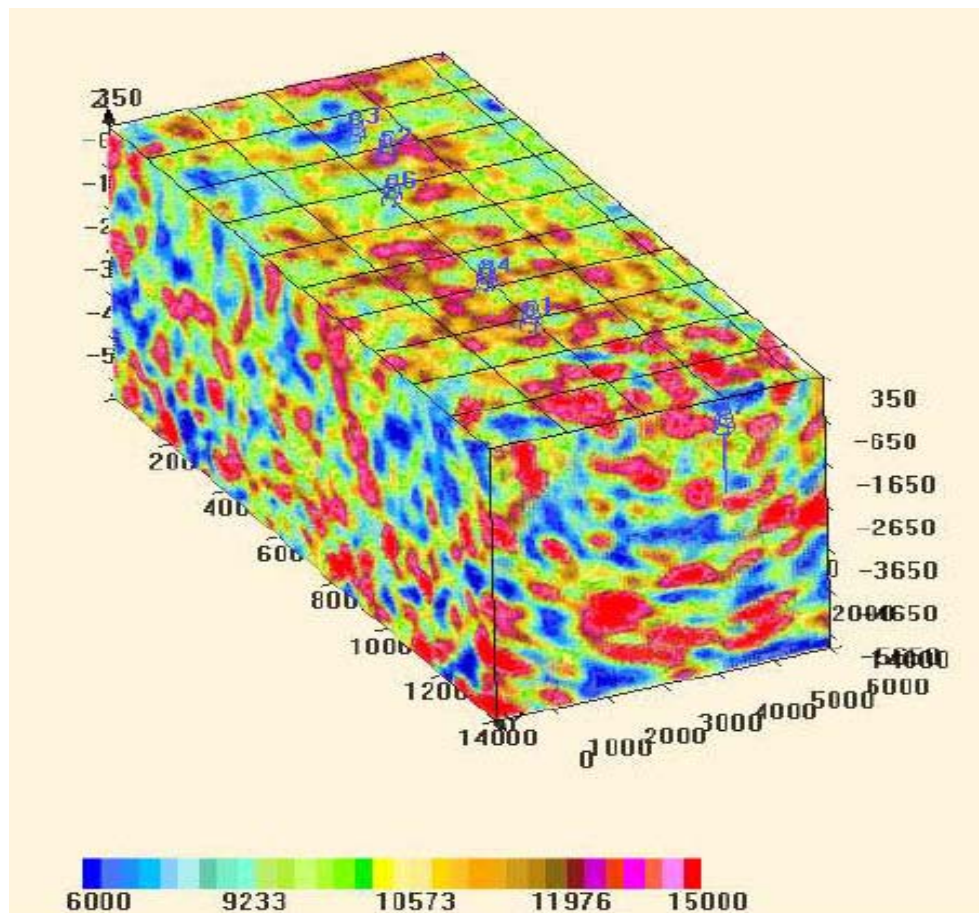


Figure 8-10: 3-D view of open fracture distribution throughout the Kuh-e-Mond field (intensity) (Photo courtesy of PEDEC).

The study area was investigated with the SVSL technique. Analysis and interpretation of the distribution of open fractures in the oil-saturated Sarvak formation zone indicated a transversely oriented zone of minimum open fracturing in the north-west part of Kuh-e-Mond, which separates the field into two isolated blocks. The south-east part is characterized by a high concentration of abnormally fractured zones and is considered to be the most promising area for further technology evaluation and field development (Figure 8-11).

Open fracture analysis in this heavy oil field using the SVSL technique showed that the distribution of open fracture zones follows the systematic jointing along with some randomly distributed fractures.

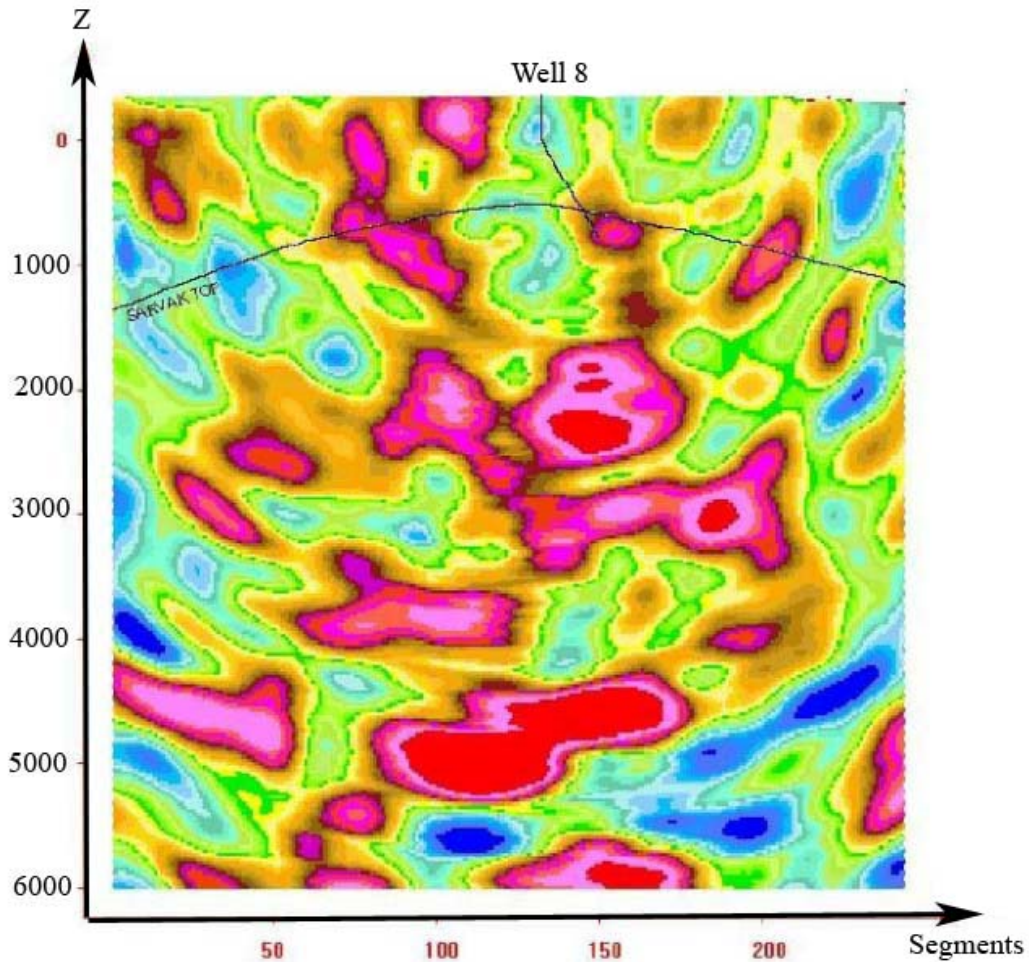


Figure 8-11: Cross-line of open fractures distribution at azimuth 277 in Kuh-e-Mond field (Photo courtesy of PEDEC).

As mentioned earlier, factors such as differential rock strength, formation dilation factor, overburden and *in situ* stresses control the open fracture distribution in the geomedium so that each factor can be distinguished based on its contribution to the presence of open fractures. Evaluation of effects of a particular factor on the presence of open fractures is possible through excluding or accounting for the effects of other factors in the analysis.

Results from this study suggest that there is no difference between variation of mean fracturing in horizontal and lateral planes with depth (Figure 8-12). However, some

anomalies were observed which are associated with the nonconformance of averaging surfaces. Also, there is a clear trend of growth of subvertical fracturing and therefore growth of formation dilation with depth. The highest fracturing intensity is located in the depth interval of 2.4 to 4.2 km (for horizontal slices) or 1.5 to 3 km (for lateral slices).

Below and above these intervals, more ductile strata with less fracturing are found. Hence, this finding implies subdividing the studied section based on the geomechanical properties of the rock units:

- The upper part of the section (up to ~ 0 m) is characterized by high fracture intensity (from 0 to 1500 m);
- Below is a zone with a low fracture intensity;
- Next, to a depth of ~ 4000 m, is the zone characterized by the most intensive fracturing;
- And, in the deepest interval, fracturing intensity decreases sharply.

A comparison of diagrams of fracturing mean values and fracturing variance in the interval of intense fracturing (Figure 8-12) suggests a cophased variation of these two parameters. This suggests a layered structure and a higher ductility as compared to underlying series. The fracturing variance increases with decreasing mean value of fracturing starting at a depth of about 4000 m. This antiphase variation of the mean fracturing and variance indicates that this depth interval consists of more dense and consolidated rocks with a blocky structure.

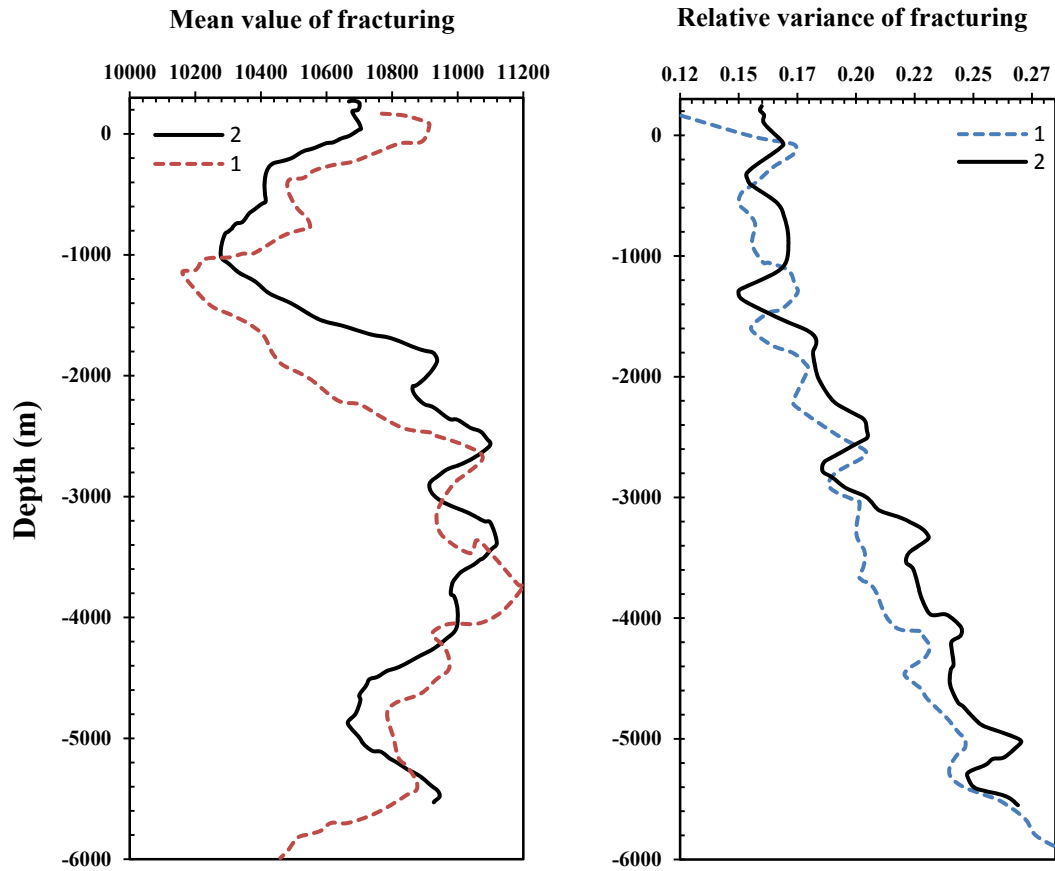


Figure 8-12: Variation of the mean value (a) and relative variance (b) of fracturing within horizontal (1) and lateral slices (2).

Results from SVSL survey are presented in Figure 8-13. In Figure 8-13a, the fracturing sections are averaged over horizontal planes of the source cube of fracturing, and Figure 8-13b presents fracturing sections averaged over the lateral surfaces. Figure 8-13c presents a difference of these two matrices $a) - b)$. Such subtraction allows elimination of the effects of lithological, gravity, and vertical dilation factors on the resulting distribution of fracturing. In fact, the accuracy of accounting for these factors depends on the accuracy of structural maps of the target horizons and the lithofacies persistence in the stratigraphic complexes throughout the area under study.

Comparison of source (a) and resulting (c) sections shows that distribution of the fracturing has changed only insignificantly, an indication that the tectonic factor is dominant, leading to an irregular distribution of fracturing within the vertical section of the study area. Varying intensity and locations are the major reason for a random distribution of fracturing anomalies. However, major systems of fracturing caused by the deformation are pronounced against this random background. Analyzing the averaged vertical cross-line sections (Figs 8-13a and 8-13b) showed that a major fracturing system was formed during formation of the anticlinal fold. This system of fractures is characterized by a V-shaped complex of linear zones orthogonal to the fold flanks and a local anomaly of fracturing in the fold arch.

The local fracturing anomalies confined to the arch of inherited folds form a line tracing the displacement of the arch of the formation series which are varying in lithology. These local anomalies can be positive or negative. In the first case a decompaction is present in the arch, whereas in the second case rocks in the arch are more compacted than expected, attributed to a “welding” of fractures that is characteristic of shallow carbonate series. In addition to the system of fracturing considered above, another major system is identified here and is shown in (Figure 8-13c). This system is characterized by the presence of a series of linear zones with a common north-east dipping direction. Dip angles of different zones are somewhat different and grow with depth, suggesting these zones belong to a radial fracturing system formed by a deep local displacement center. Thus, based on the analysis of the distribution of fracturing averaged over the cross-sections, two major fracturing systems interfering with each other were identified.

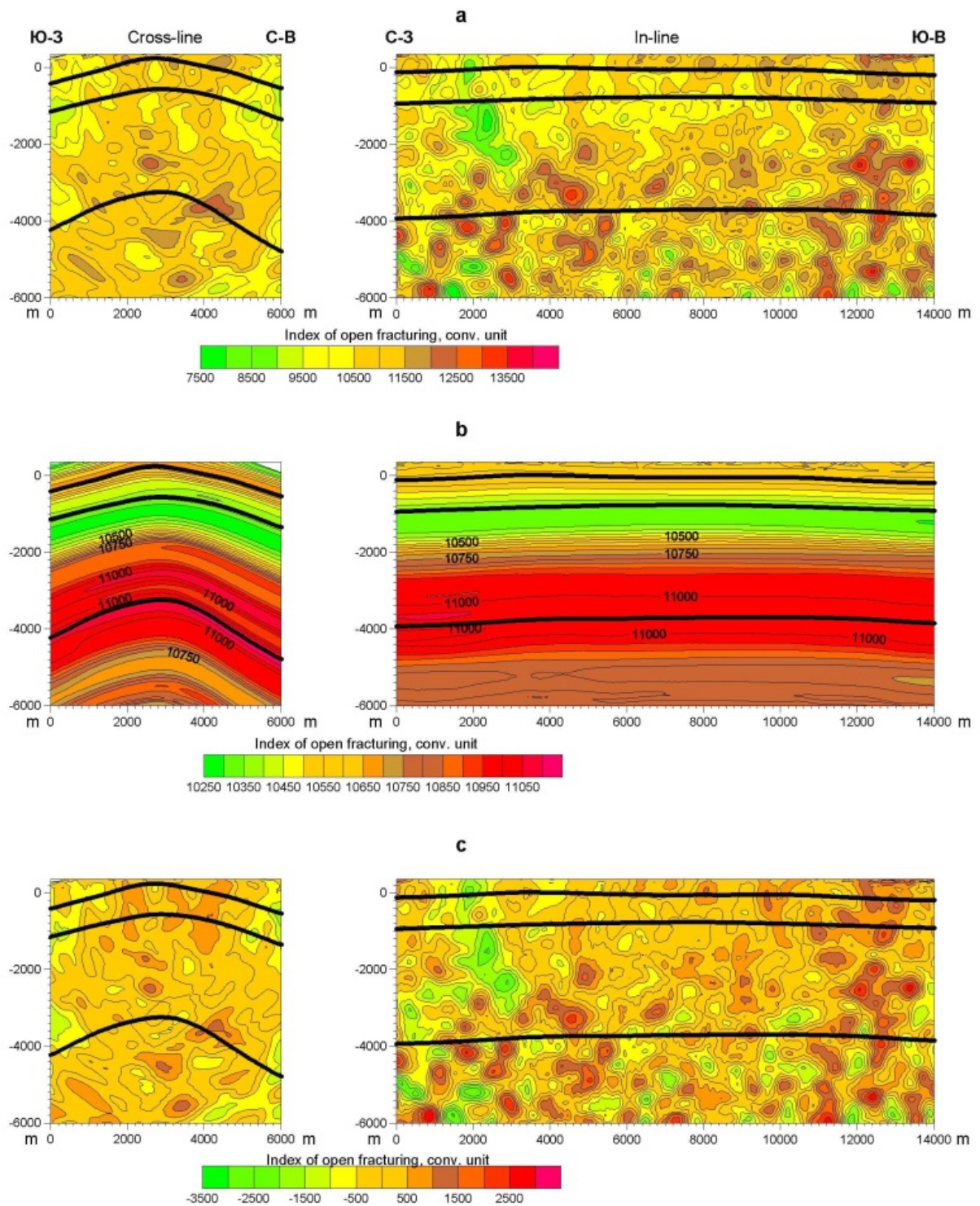


Figure 8-13: SVSL results (Photo courtesy of PEDEC).

The analysis of vertical and horizontal variations of fracturing and geological interpretation of features of fracturing distribution indicates that distribution of open fractures in the study area depends on factors such as tectonic deformation, lithology, overburden depth, and rock mass dilation. Tectonic factors are the major controls on the fracturing.

Based on the additional processing of SVSL data aimed at identification of the tectonic factor and elimination of other factors, a major center of tectonic strain was identified which formed the major system of fracturing distribution in the Kuh-e-Mond. This center is located under the anticlinal structure, generating a system of fractures during formation of the anticlinal fold in the layered media owing to the upward movement of the underlying strata. This system of fracturing is clearly shown in the generalized vertical cross-line section (Figure 8-13c).

An abnormal zone of low fracture intensity (a compacted zone) was also identified in the north-west part of the study area which separates the central and north-west regions of the Kuh-e-Mond heavy oil field.

Study of fracturing distribution in the oil-saturated formation of Sarvak revealed three major centers of strain identified from the analysis of generalized horizontal and vertical variation of fracturing in the study area.

As for the distribution of open fracturing in the potentially heavy oil productive stratum of the Sarvak Formation, it can be concluded that the south-east section of the reservoir (within the limits of the study area) where the largest number of abnormally high open fractured zones is enclosed in the pool outline is the most promising. Most of these zones are extended sub-vertically. A zone characterized by a minimum of open fractures, located in the north-west part of the study area, is the least promising section; this zone also has the minimum permeability. A subvertical zone of abnormally highly fractured rock extends from a large depth up to the productive series and is considered as a potentially productive zone. Recommendations were made based on this study in order to select optimum locations for the purpose of well drilling.

Based on SVSL interpretation, it is concluded that the resulting spatial distribution of fracturing in the depth interval of + 350 m down to – 6000 m in the Kuh-e-Mond field will be useful in developing a drilling program and implementing operations for heavy oil production. Some points for drilling productive deposits of the Sarvak Formation are proposed as top-priority actions to produce high oil flow rates. As shown in Figure 8-7, placements of wells are presented in the structural slice located 175 m below the top of the Sarvak Formation. As far as the south-west part of the studied area, linear fractured zones are common and oriented across the strike of the dip, and it is recommended to drill those strata with horizontal wells along the strike of the south-west slope of the structure.

The SVSL technique proved useful in characterizing fracture opening in the study area. However, this method reaches its maximum utility only when implemented in parallel with other direct techniques of reservoir characterization (core analysis, borehole wall geophysical surveys, well test data, and surface expressions). In 2007 a vertical well (MD-8) was drilled into a highly fractured zone located using the results from this study. Cold production tests using PC pumps in this well reached a daily production of 1000 m³/d, a promising rate for a heavy oil well. However, field experience shows that such high initial productions will drop drastically with no notable cumulative oil production and thereafter consideration of thermal stimulation methods would be necessary to obtain oil production from the matrix blocks.

8.6.3 FMI and UBI

Borehole image logs, FMI and UBI, were used to identify and characterize natural fractures in the boreholes. In addition, the data were used for structural dip evaluation in the Sarvak I interval. FMI and UBI image logs from well MD-8 drilled close to the crest of the Kuh-e-Mond anticline were used; the deviation of the well in the logged interval reaches 36.5°. The mud system used for drilling was oil-based with a resistivity of 200 Ω-m. Summary plots of the features identified and picked out from FMI and UBI images in the Well MD-8 are presented in Figure 8-14. Track 6 shows the Combinable Magnetic Resonance or CMR bin porosity.

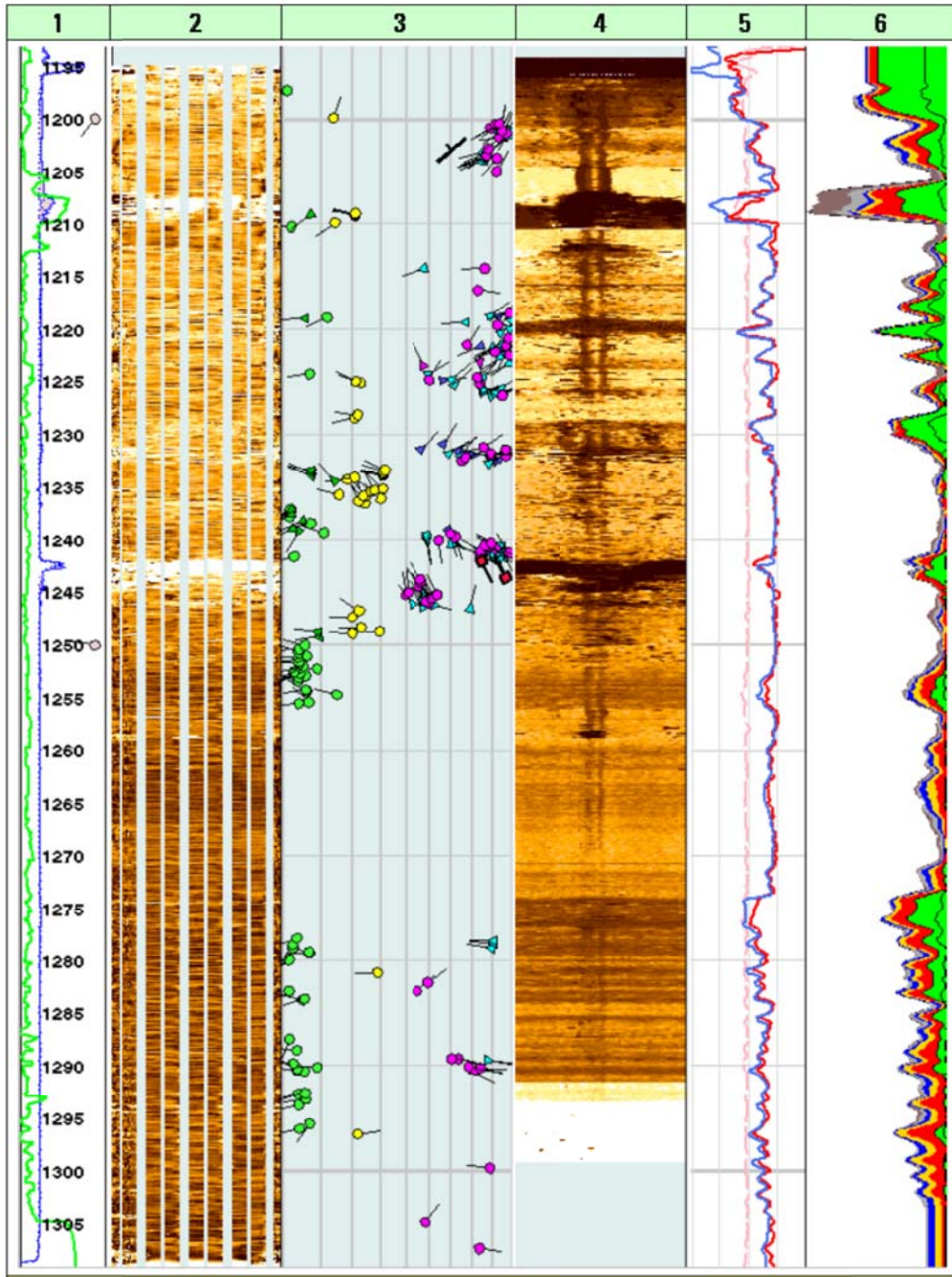


Figure 8-14: Summary plot of the features identified and picked out from FMI (track 2) and UBI (track 4) images in the Well MD-8 (Photo courtesy of PEDEC).

Resistive fractures on the FMI image are indicated by magenta arrows (Figure 8-15). Minor open fractures on the UBI image are shown with cyan arrows, below. In some cases, one feature appears on both images but open on the UBI image and closed on the FMI image. This may indicate that the open fractures are filled with oil-based mud which is detected by the FMI tool as resistive fractures.

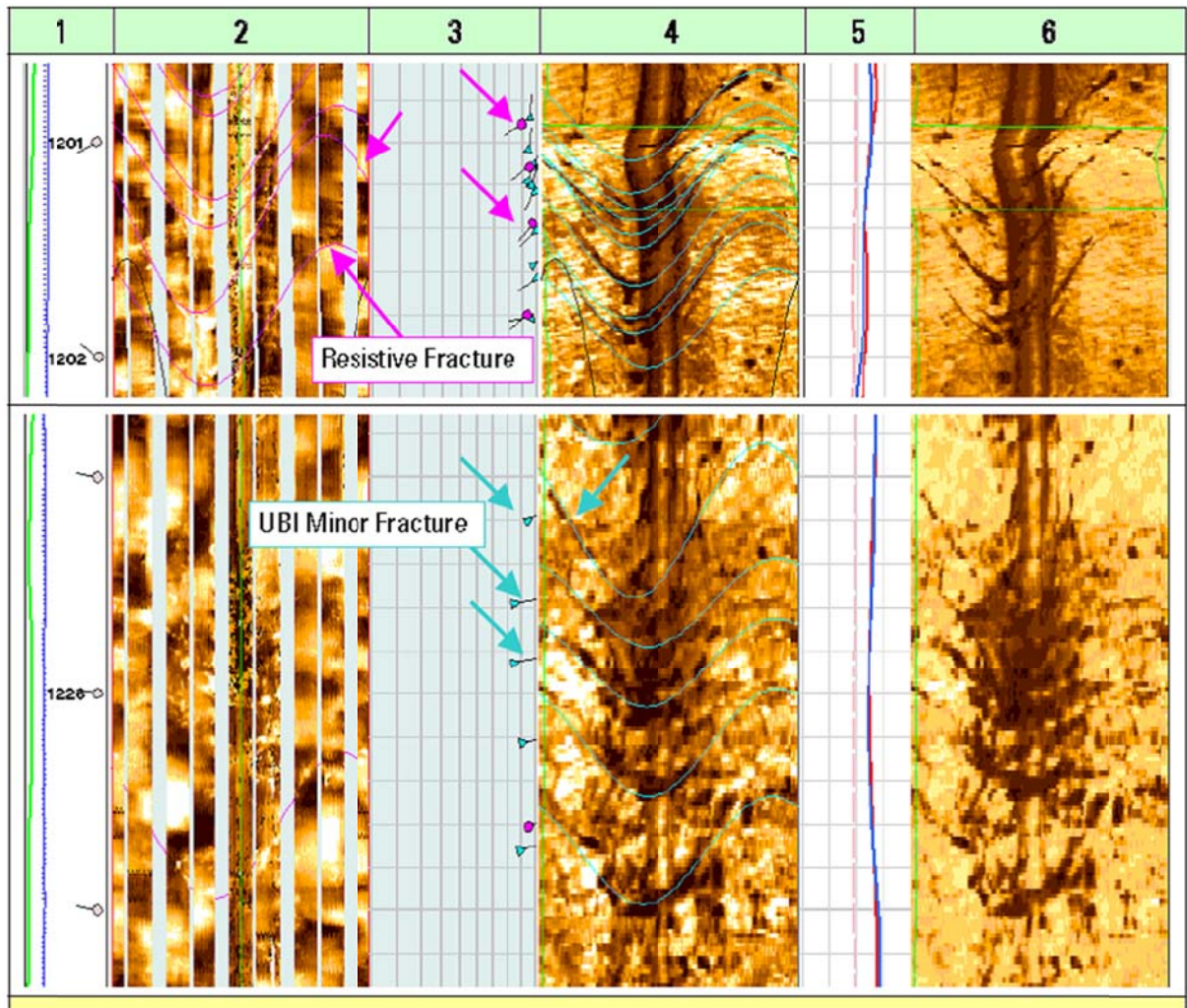


Figure 8-15: Resistive fractures on the FMI (track 2) image indicated by magenta arrows (Figure 10). Minor open fractures on the UBI (tracks 4 and 6) image (cyan arrows, below) (Photo courtesy of PEDEC).

Two highly fractured zones in the Sarvak I interval are shown in Figure 8-16. Blue arrows indicate major open fractures picked from the UBI. On the FMI image (track two), some resistive fractures can be seen (magenta arrows), some of which coincide with open fractures visible on the UBI, but filled with resistive mud. There also are red arrows to indicate two UBI high amplitude minor fractures in the upper image. These minor fractures are interpreted as filled or healed.

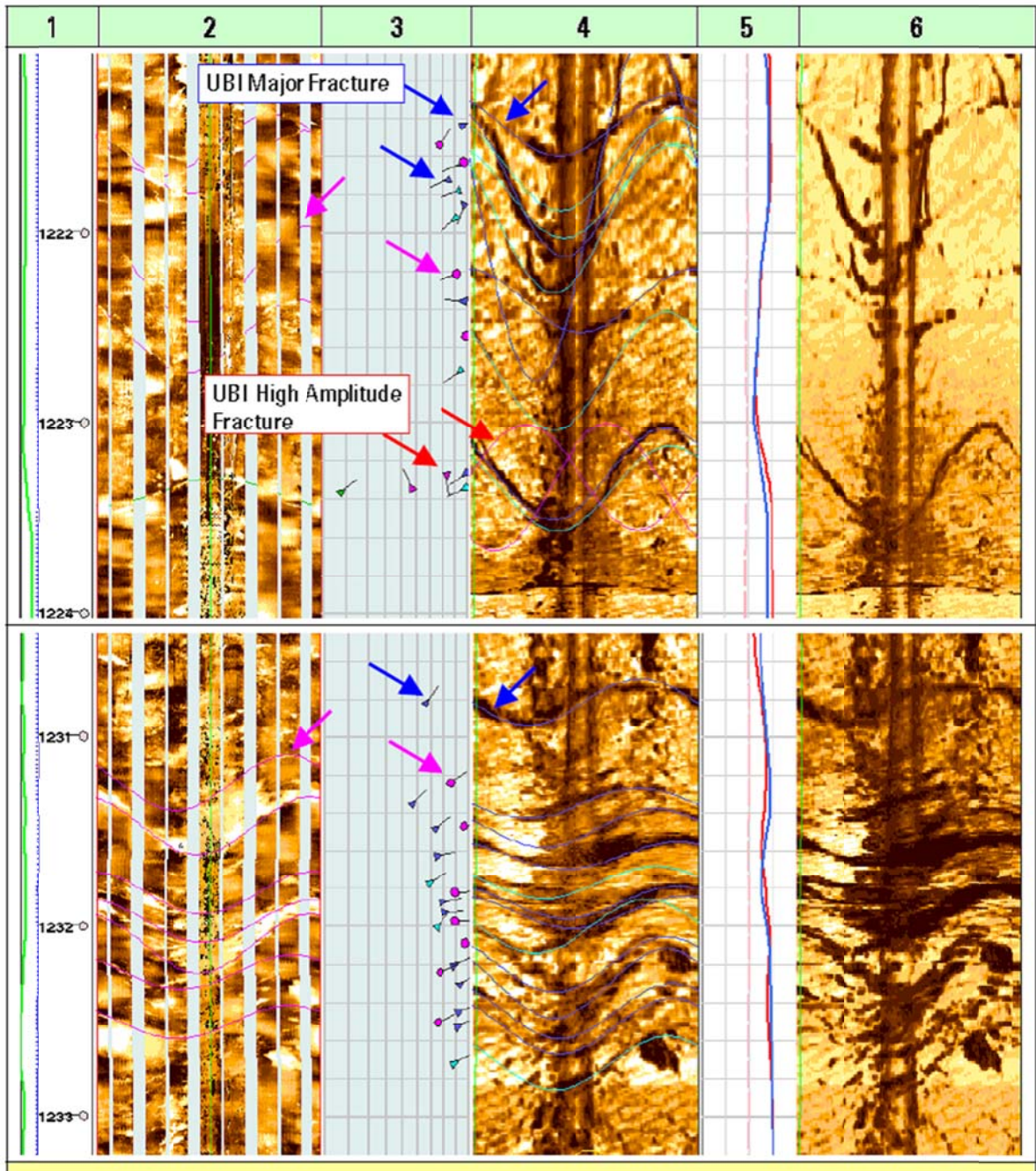


Figure 8-16: Two highly fractured zones in Sarvak I interval on FMI (track 2) and UBI (tracks 4 and 6) logs (Photo courtesy of PEDEC).

A good example of fractures that are seen both on UBI and FMI images is presented in Figure 8-17. On the second track, the fractures (magenta arrows), which are filled with resistive mud, appear resistive on the FMI image. However, on the UBI image, the same fractures, which are about 15 cm off depth, seem open (cyan arrows).

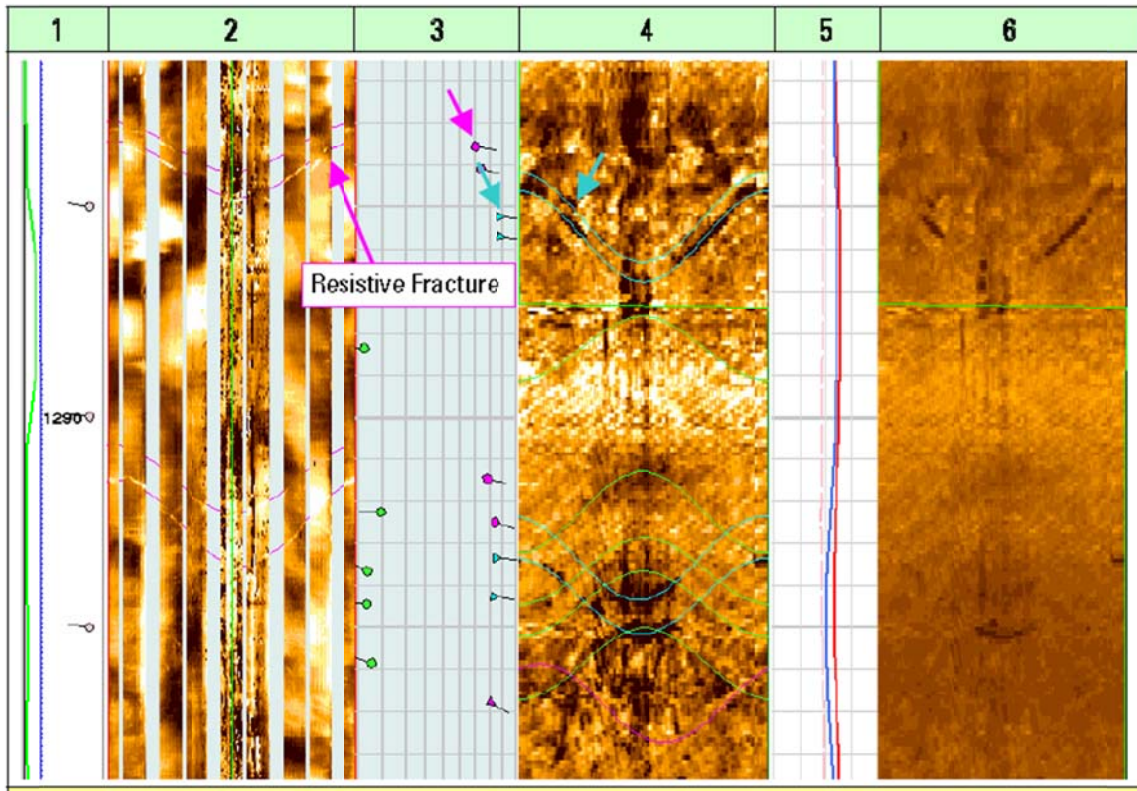


Figure 8-17: A good example of fractures that are seen both on UBI (tracks 4 and 6) and FMI (track 2) images (Photo courtesy of PEDEC).

A UBI snapshot from a section containing a number of bedding features and minor open fractures is presented in Figure 8-18 (upper section). A 3-D view of the same section showing the orthogonal relationship between fractures and beddings is also presented (lower right section). Azimuth rosette and dip histogram of beddings and open fractures showing the orthogonal relationship between beddings and open fractures (lower left section).

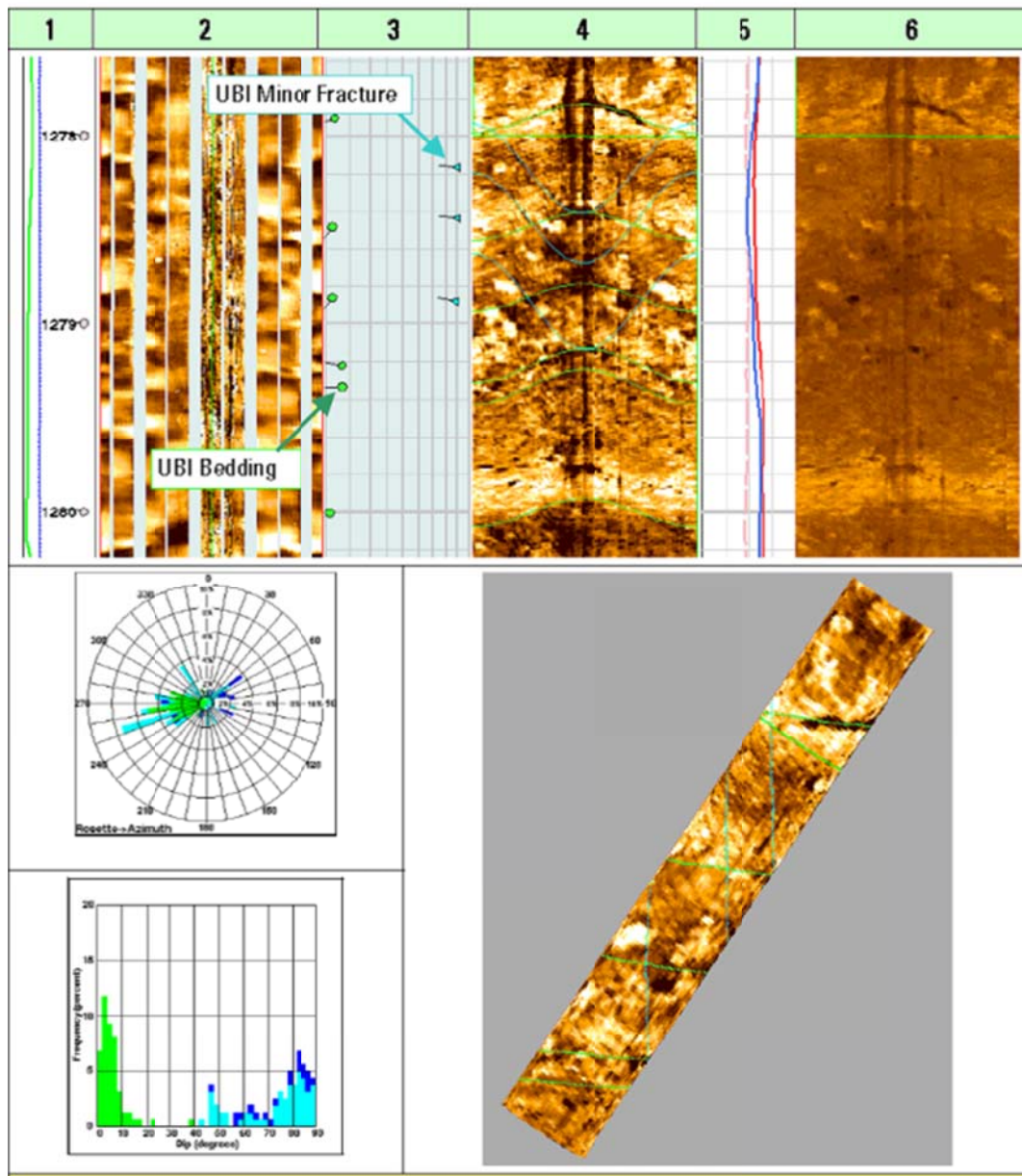


Figure 8-18: Upper section: a snapshot from a section containing a number of bedding features and a minor open fracture (tracks 4 and 6). Below right is a 3-D view of the same section showing the orthogonal relationship between fractures and beddings. Below left is an azimuth rosette and dip histogram of bedding and open fractures showing an orthogonal relationship (Photo courtesy of PEDEC).

Based on the observations and interpretation of the images from 1194.2 to 1310 m (Well MD-8), the highlights of the study are summarized. The structural dip in the logged interval (Sarvak I), based on 52 UBI bedding dips and 13 FMI bedding dips, is 5° towards $S84^\circ W$. This structural dip is consistent throughout the logged interval with no evidence of any major structural boundary such as a major fault or angular unconformity. Fracturing is observed at a number of places. There are 91 UBI open fractures in total, of which 20 are major features and 71 of them are UBI minor open fractures. In addition to open fractures in UBI images, three high amplitude fractures have been identified. FMI images also show fracturing in a number of places: 58 resistive fractures have been picked out, some of which are clearly the same feature as in the UBI images. Both dip magnitude and dip direction of the UBI major open fractures show high variation. However, the dip magnitude varies between 45 to 90° with dominant values of 83 to 88° . The same condition is true for the dip direction that has a dominant direction towards $N67^\circ W$, varying almost in all directions. UBI minor open fractures dip mainly towards the SW, NW, and NE with dip varying from 45 to 90° with a dominant 84° dip. For FMI resistive fractures, the dip ranges between 38 to 90° toward mainly the SW with a similar dominant dip. Some minor dip directions towards NW, NE, and SE are also significant. The highly fractured zones in the logged interval are from 1201 to 1205.5 m, 1218 to 1227 m, 1230 to 1233.5 m, 1239 to 1243 m, 1244 to 1247.5 m, 1277 to 1279 m, and from 1289 to 1293 m.

8.6.4 Origins of Natural Fractures in the Study Area

In geomechanics, fracture types are divided into two groups related to their mode of formation: shear fractures that form with shearing parallel to the created fracture, and tension fractures that form with extensional strain perpendicular to the created fracture plane. In NFCRs, there are at least three sources of these tension fractures. One is the high solubility of the carbonate rock that leads to porosity loss through internal mass transfer, causing a general shrinkage in the horizontal plane and leading to some fracturing when $P_o > \sigma_{hmin}$. Similarly, volume diminution during dolomitization leads to opening of fractures in a similar manner. Finally, there is the flexure aspect of a stiff rock which opens fractures at 90° to the

extensional strain direction. Non-fractured carbonates, invariably not too deeply buried, are far more rare than fractured carbonates because of these processes.

Geological interpretation of the fracturing system in the study area based on the tectono-physical models (Figure 8-19) showed that formation of the anticlinal fold is due to the vertical tectonic displacement (uplift) of a deep-seated feature which could be a basement block or a salt ridge. Another major system of fracturing identified as a radial system was formed by a deep seated local center of tectonic uplift.

The averaged vertical in-line sections (Figure 8-13) show a more complicated image of a random distribution of fracturing as compared to the previous cross-section. The random character of fracturing distribution is growing at the depth below 4 km where the distribution of anomalies of maximum and minimum fracturing has a mosaic character.

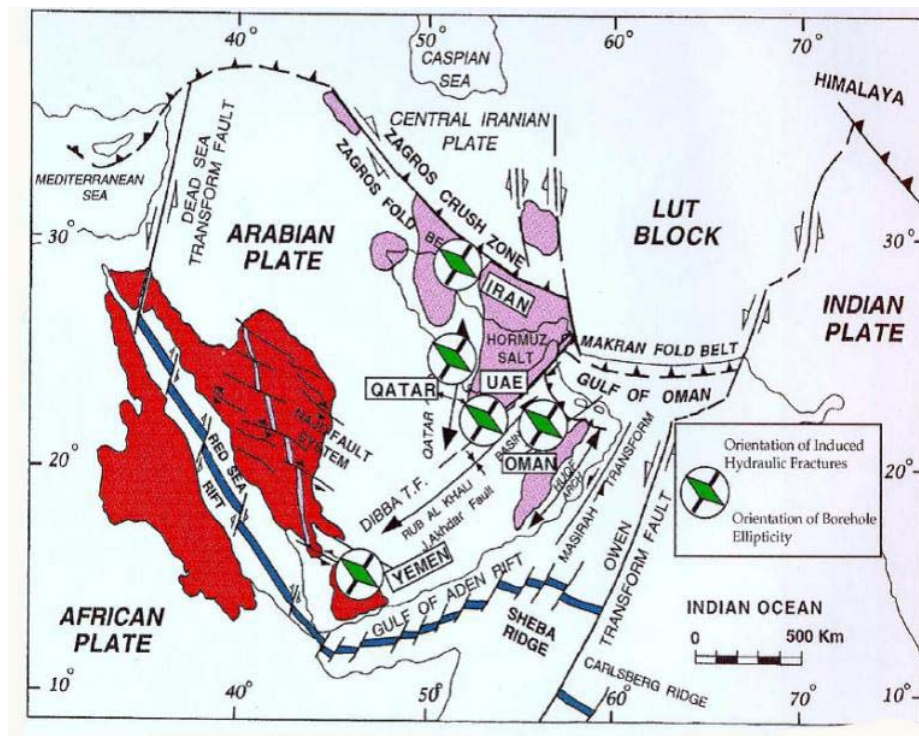


Figure 8-19: Orientation of regional stresses in the Arabian Peninsula based on borehole breakouts and drilling induced fracture data (Modified from Akbar and Sapru, 1994) (Photo courtesy of PEDEC).

Fracturing in the Jahrum Formation occurred as a consequence of tectonic events within a Neo-Tethys basin which included the present Zagros foreland basin. By the Late Cretaceous, basin convergence occurred as a consequence of subduction of the Arabian plate (Berberian and King, 1981). Continuing collision movements up to the late Miocene exerted buckling and neutral-surface forces on the sediment package in the form of combined flexural slip and neutral-surface mechanisms and led to the shortening of the mountain range of the Zagros fold-and-thrust belt.

The shortening normal to the Zagros range has been confirmed by using magnetic fabric data from the Kuh-e-Mond anticline. The record of layer-parallel shortening during early to middle Miocene caused detachment folding in the Kuh-e-Mond area which developed in front of the Kazerun Fault (Al-Laboun, 1986; Alsharhan and Nairn, 1997; Al-Husseini, 2000; Alavi, 2004; Aubourg *et al.*, 2010).

This tectonic event created interconnected fractures over large distances, which significantly increased porosity and permeability and influenced draining and accumulation of petroleum fluids in the carbonate reservoirs (Colman-Saad, 1978; Ge and Garven, 1992; Hansom and Lee, 2005; Vaziri-Moghaddam *et al.*, 2010).

8.7 Geological Inference of Stress State at the Kuh-e-Mond

8.7.1 Core Analysis

In order to conduct a comprehensive assessment of natural fractures in the reservoir, all fractures were measured on whole and slabbed cores reoriented to their original status in the reservoir using geological criteria and image log data. Results obtained from core analysis are presented in Figure 8-20. Orientation of the detected fractures in cores is highly variable; however, most fractures are steep, N-S to NNE trending structures with dip azimuth towards the E to EES. This suggests that the Persian Gulf Sedimentary Basin seems to be detached from its basement.

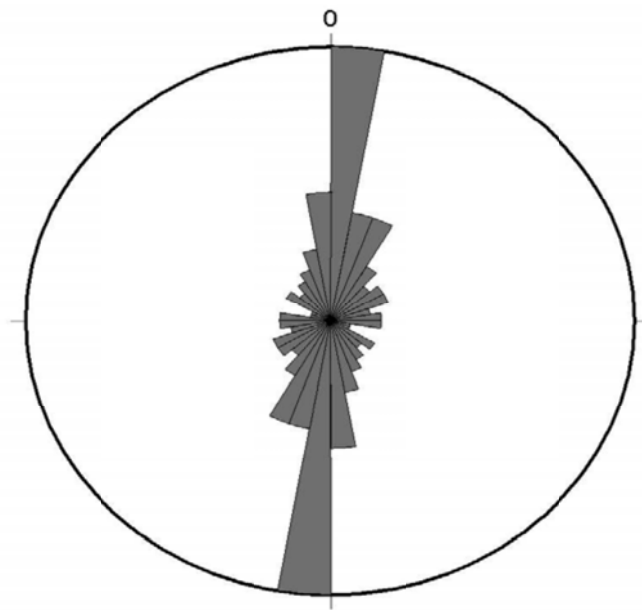


Figure 8-20: Rose diagram of trends of natural fractures from core analysis.

8.7.2 Borehole Images

Results obtained from fracture study by using image logs are presented in Figure 8-21. The results of core analysis are more or less consistent with image log analysis, but there are some differences between the results obtained from these two methods.

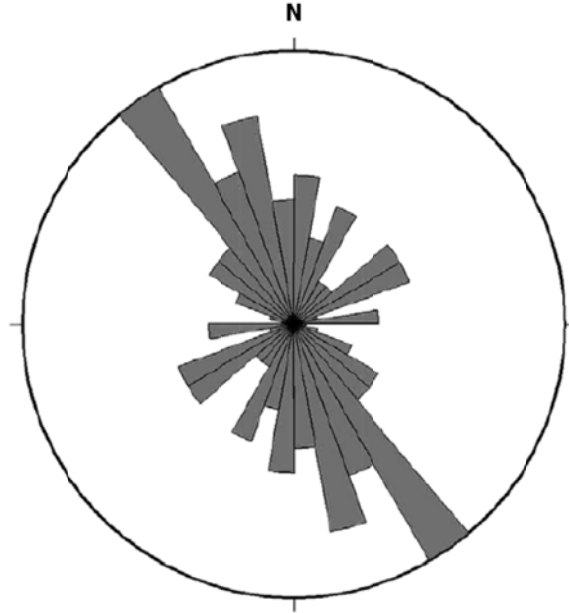


Figure 8-21: Rose diagram of trends of natural fractures measured in image logs.

8.7.3 Magnitude of the *In Situ* Principal Stresses

Magnitudes of *in situ* principal stresses and pore pressure were estimated at a depth of 1200 meters in well MD-8; a hydrostatic stress regime is assumed here for pore pressure.

$$P_o = h \times \gamma_w = 1200 \times 9.81 = 11.8 \text{ MPa}$$

$$\sigma_2 = \sigma_v = h \times \gamma = 1200 \times 25 = 30 \text{ MPa}$$

$$\sigma_3 = \sigma_{hmin} = K \times \sigma_v = K \times \sigma_2 = 13.5 \text{ MPa}$$

K was obtained as 0.45 based on Sheorey's model (Sheorey, 1994):

$$\sigma_1 = \sigma_{HMAX} = > \sigma_2 = \sigma_v = 30 \text{ MPa} > \sigma_3 = \sigma_{hmin} = 13.5 \text{ MPa}$$

$$\sigma_h = [(v/1-v) \times (\sigma_v - P_o)] + P_o = (\sigma_{HMAX} + \sigma_{hmin})/2 = 16.6 \text{ MPa}$$

$v = 0.21$ was assumed for the Jahrum limestone strata

Better estimates can be obtained for the σ_{hmin} and fracturing pressure using hydraulic fracturing data.

8.7.4 Orientations of the *In Situ* Stresses

From core analysis, and image logs, it can be concluded that the orientation of maximum horizontal stress ($\sigma_{HMAX} = \sigma_1$) around the well MD-8 is NE-SW as shown in Figure 8-22. Hence, the orientation of σ_{hmin} ($= \sigma_3$) is NW-SE and σ_2 is vertical, as well.

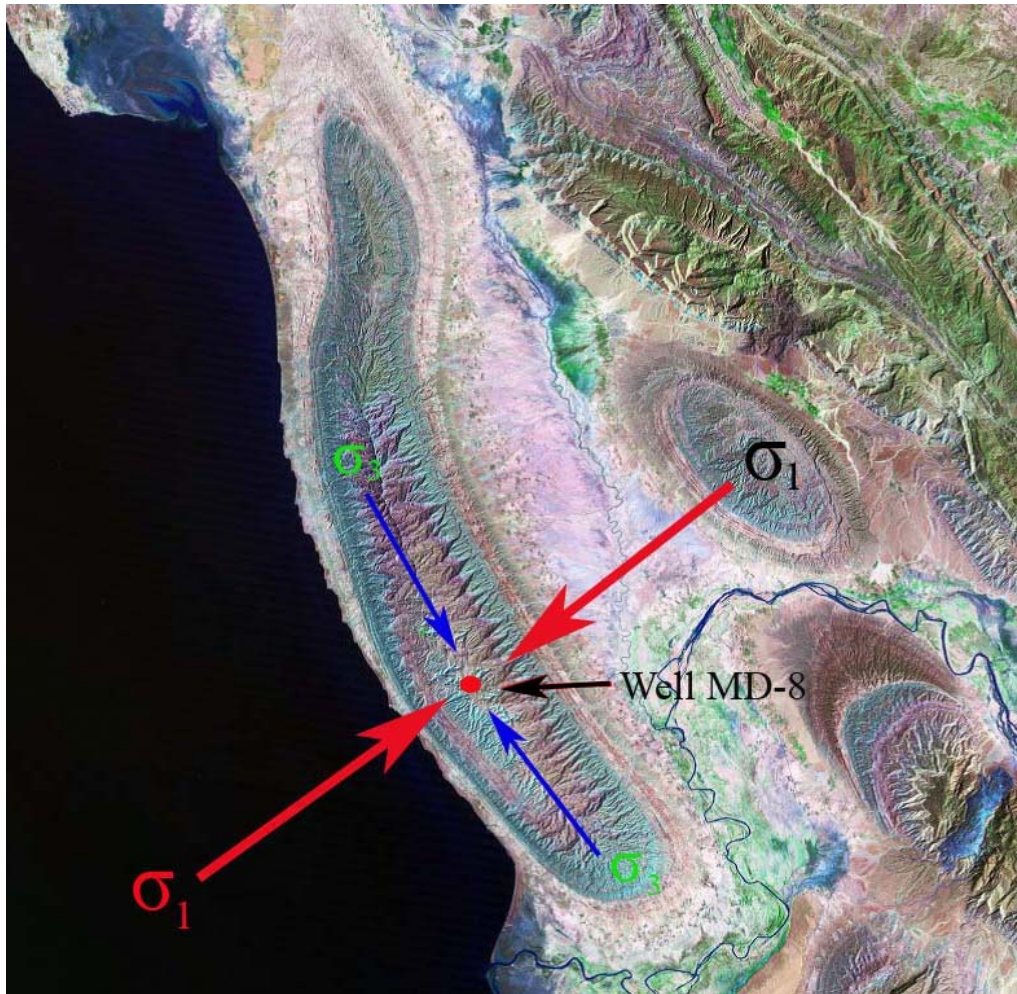


Figure 8-22: The orientation of the *in situ* principal stresses in the study area.

Present day tectonic stress state in the Middle East, the most prolific hydrocarbon basin in the world where vast amounts of hydrocarbons exploration and production are taking place, remains poorly understood in detail because of accessibility to data. Nevertheless, present day stress field orientation in the study area is shown in Figures 8-19 and 8-23.

These maps show that the azimuth of σ_1 and σ_3 in the study area is approximately 030° to 035° and 120° to 125°, respectively and σ_2 is vertical which is equal to the overburden weight. This orientation of *in situ* stress field is consistent with the geotectonics (passive plate tectonics margins), structural geology, image logs, and fracture study used.

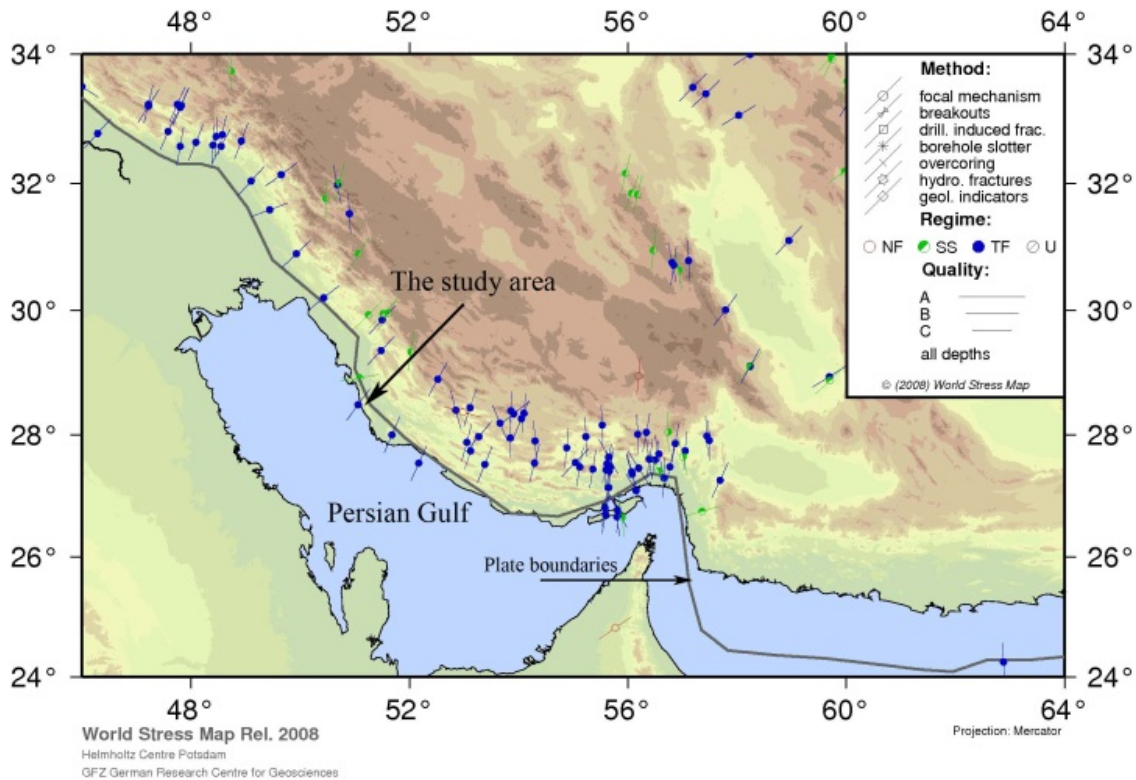


Figure 8-23: World Stress Map generated for the study area to infer the orientation of the *in situ* stress field (Courtesy of the World Stress Map Project) (Heidbach *et al.*, 2008).

Estimates made in this study using multiple sources such as core analysis, and image logs are in a good agreement with estimates suggested by the World Stress Map Project data, as well as geological and geotectonic evidence.

8.8 Concluding Remarks

A combination of outcrop studies, core studies, 3-D and SVSL seismic and borehole image logs were used to characterize natural fractures in a fractured carbonate heavy oil field in Iran. Various available data and techniques including core analysis, image logs (FMI and UBI logs), World Stress Map data, and geological and geotectonic evidence were used to infer the *in situ* stress state in the study area. The following major conclusions can be drawn:

- All the potentially exploitable reservoirs, including the zones in the Jahrum and Sarvak Formations, are intensely fractured.
- Three general orientations of mainly vertical, horizontal and sub-vertical fractures were identified and characterized over the crestal area, in north, northeast and east orientations.
- The surface and subsurface fractures of the same origin and type are nearly in the same directions, and are both controlled by tectonic factors.
- Distribution of open fracturing in the study area depends on tectonic, lithology, overburden, and rock dilation. Tectonics is the major factor.
- Borehole image logs, FMI and UBI have been proved to be useful tools in identifying and characterizing natural fractures in the study area.
- Most fractures are steep, N-S to NNE trending structures with dip azimuth towards the E to EES. This suggests that the Persian Gulf Sedimentary Basin seems to be detached.
- From image logs, the strike azimuth of drilling induced fractures is N45°W, which indicates that the orientation of $\sigma_{HMAX} = \sigma_1$ around the well MD-8 is NE-SW; the orientation of $\sigma_{hmin} = \sigma_3$ is NW-SE, and σ_2 is vertical.
- Estimated magnitudes of the situ principal stresses and pore pressure at depth of 1200 m in well MD-8 are: $P_o = 11.8$ MPa, $\sigma_2 = \sigma_v = 30$ MPa, $\sigma_3 = \sigma_{hmin} = 13.5$ MPa, and $\sigma_1 = \sigma_{HMAX} = > \sigma_2 = \sigma_v = 30$ MPa $> \sigma_3 = \sigma_{hmin} = 13.5$ MPa

- Azimuths of σ_1 and σ_3 in the study area are 030° to 035° and 120° to 125° ; respectively.
- All the reservoirs studied at the Kuh-e-Mond, including the zones in the Jahrum and Sarvak Formations, are found to be intensely fractured. Tensional fracture sets in rectangular patterns are well recognized in core samples; these fractures are usually open and contain heavy oil stains. Shear fractures are also visible in core samples; slickensides are noted on the surface of the shear fractures. Random or second-order fractures are also distinguishable in some of the cores.
- Analysis and interpretation of the distribution of open fractures in the oil-saturated Sarvak formation zone indicated a transversely oriented zone of minimum open fracturing in the north-west part of Kuh-e-Mond, which separates the field into two isolated blocks. The south-east part is characterized by a high concentration of abnormally fractured zones. This region is considered to be the most promising area for further technology evaluation and field development.
- Open fracture analysis in this heavy oil field using the SVSL technique showed that the distribution of open fracture zones follows the systematic jointing along with some randomly distributed fractures.
- There was no difference between variation of mean fracturing in horizontal and lateral planes with depth in the study area. However, some anomalies were observed which are associated with the nonconformance of averaging surfaces. Also, a clear trend of growth of subvertical fracturing and therefore growth of formation dilation with depth was observed. The highest fracturing intensity is located in the depth interval of 2.4 to 4.2 km (for horizontal slices) or 1.5 to 3 km (for lateral slices).
- Below and above these intervals, more ductile strata with less fracturing are found. Hence, this finding implies subdividing the studied section based on the geomechanical properties of the rock units: The upper part of the section (up to ~ 0 m) is characterized by high fracture intensity (from 0 to 1500 m); Below is a zone

with a low fracture intensity; Next, to a depth of ~ 4000 m, is the zone characterized by the most intensive fracturing; And, in the deepest interval, fracturing intensity decreases sharply. As for the distribution of open fracturing in the potentially heavy oil productive stratum of the Sarvak Formation, it can be concluded that the south-east section of the reservoir (within the limits of the study area) where the largest number of abnormally high open fractured zones is enclosed in the pool outline is the most promising. Most of these zones are extended sub-vertically. A zone characterized by a minimum of open fractures, located in the north-west part of the study area, is the least promising section; this zone also has the minimum permeability. A subvertical zone of abnormally highly fractured rock extends from a large depth up to the productive series and is considered as a potentially productive zone. Recommendations were made based on this study in order to select optimum locations for the purpose of well drilling.

- Based on SVSL interpretation, it is concluded that the resultant spatial distribution of fracturing in the depth interval of + 350 m down to – 6000 m in the Kuh-e-Mond field will be useful in developing a drilling strategy and implementing operations for heavy oil production.
- Geological interpretation of the fracturing system in the study area based on the tectono-physical models showed that formation of the anticlinal fold is due to the vertical tectonic displacement (uplift) of a deep-seated feature which could be a basement block or a salt ridge. Another major system of fracturing identified as a radial system was formed by a deep seated local center of tectonic uplift.
- Fracturing in the Jahrum Formation occurred as a consequence of tectonic events within a Neo-Tethys basin which included the present Zagros foreland basin. By the Late Cretaceous, basin convergence occurred as a consequence of subduction of the Arabian plate (Berberian and King, 1981). Continuing collision movements up to the late Miocene exerted buckling and neutral-surface forces on the sediment package in

the form of combined flexural slip and neutral-surface mechanisms and led to the shortening of the mountain range of the Zagros fold-and-thrust belt.

- Orientation of the detected fractures in cores is highly variable; however, most fractures are steep, N-S to NNE trending structures with dip azimuth towards the E to EES. This suggests that the Persian Gulf Sedimentary Basin seems to be detached from its basement.

Nomenclature

Acronyms, Symbols, Units

Acronyms

3-D	=	Three Dimensional
4-D	=	Four Dimensional
CMR	=	Combinable Magnetic Resonance
EOR	=	Enhanced Oil Recovery
FMI	=	Formation Micro Imager logs
HF	=	Hydraulic Fracturing
LWD	=	Logging While Drilling
NFCR	=	Naturally Fractured Carbonate Reservoir
NFR	=	Naturally Fractured Reservoir
OOIP	=	Original Oil In Place
SVSL	=	Side View Seismic Location method
SW	=	Scattered waves
UBI	=	Ultrasonic Borehole Imager
XLOT	=	extended leak-off test

Symbols: Latin first and then Greek

b	=	Barrel of oil
b/d	=	Barrel per day
K	=	Permeability (mD)
p_o	=	Pore pressure (MPa)
Z	=	Depth (m)

γ_w	=	Unit weight of water (KN/M ³)
Δ	=	Difference or change in, as in Δp , $\Delta \rho$
$\Delta \sigma'$	=	Changes in effective stress
μ	=	Viscosity (cP)
ν	=	Poission's ratio
σ	=	Stress (kPa, MPa)
σ_{HMAX}	=	Maximum principal total horizontal stress
σ_{hmin}	=	Minimum principal total horizontal stress
σ_v	=	Vertical stress (kPa, MPa)
ϕ	=	Porosity (%)

Unit conversions

1 barrel	=	0.159 m ³
1 MPa	=	145 psi
°F	=	(°C×1.8) + 32

Chapter 9

Major Contributions, Conclusions, and Recommendations

9.1 Major Contributions

This dissertation makes the following five major contributions to the literature as well as to the oil industry:

1. Two statistical correlations were developed and examined which can be utilized for the purpose of estimation of *CSOR* and *RF* as measures of process performance and technical viability during vertical well steamflooding in VO NFCRs. Such correlations are reported for the first time in the literature for this type of VO reservoirs:

$$\begin{aligned}
 CSOR = & a_0 + a_1 D + a_2 \frac{1}{\phi_e} + a_3 \frac{1}{K_m} + a_4 K_f + a_5 \frac{1}{\mu_o} + a_6 \frac{1}{S_o} + a_7 \frac{1}{q_s} + a_8 x_s + a_9 \frac{1}{S_o \phi_e} + a_{10} \frac{D}{h} + \\
 & a_{11} \frac{D}{h \phi_e K_m \mu_o S_o q_s} + a_{12} \frac{1}{\phi_e q_s} + a_{13} \frac{1}{\phi_e K_m} + a_{14} \frac{K_f}{K_m}
 \end{aligned}
 \tag{9-1}$$

$$\begin{aligned}
 RF = & a_{15} + a_{16} S_o + a_{17} h + a_{18} q_s + a_{19} \phi_e + a_{20} K_m + a_{21} x_s + a_{22} \mu_o + a_{23} \frac{K_m h}{\mu_o} + \\
 & a_{24} S_o \phi_e + a_{25} q_s x_s + a_{26} \frac{S_o \phi_e h K_m q_s}{\mu_o x_s} + a_{27} q_s \phi_e + a_{28} \frac{K_f}{K_m}
 \end{aligned}
 \tag{9-2}$$

The parameters $a_1 - a_{28}$ are determined by statistical methods using pilot project and laboratory data (Chapter 3).

2. A 3-D mathematical model was developed, tested, and presented in this research work to investigate various parameters and mechanisms affecting VO recovery from VO NFCRs using vertical well steamflooding.
3. A hybrid ANN-PSO model was developed and tested in this research work for the purpose of estimation of the *CSOR* and *RF* during vertical well steamflooding in VO NFCRs. It seems that such a “smart technique” has not been reported previously for the purpose of performance prediction of steamflooding in VO NFCRs. It is also apparently the first time that the ANN technique is applied for forecasting these two important parameters.
4. An integrated geological-geophysical-geomechanical approach was designed, presented, and applied in the case of a VO NFCR for the purpose of fracture and *in situ* stresses characterization in VO NFCRs. The proposed methodology can be applied for fracture and *in situ* stresses characterization in general, which is beneficial to various development aspects such as well placement, drilling, production, thermal reservoir modeling incorporating geomechanics effects, technology assessment and so on, in conventional and viscous oil reservoirs.
5. A conceptual study was conducted on geomechanics effects in VO NFCRs during steamflooding which is not well understood yet and still requires further field, laboratory, and theoretical studies. This can be considered as a small step forward in this area identifying positive potentials and/or pitfalls of such effects during large scale thermal operations in VO NFCRs.

9.2 Conclusions

As mentioned in Chapter 1, this dissertation is intended to be a paper-based thesis with integrity of a book-like thesis at the same time. In fact, the chapters are independent research works on various aspects of a single subject: Thermal HO Recovery in NFCRs). Hence, conclusions with further details are made at the end of each chapter.

9.3 Recommendations

The following recommendations are made for the purpose of future research works in the areas investigated over this research project in order to enhance our understanding of more complex and potentially more beneficial approaches (e.g., cyclic steam processes with utilization of long horizontal well and hydraulic fracturing) for the purpose of VO recovery from NFCRs. In addition, some new questions generated during this research studies or questions raised here but still unaddressed are mentioned here to be investigated and addressed in the future by researchers:

9.3.1 Assemble a Database for World Disposition of VO in NFCRs

The world's VO resources in NFCRs are estimated to be $1500\text{--}2200 \times 10^9$ b [$238\text{--}35 \times 10^9$ m³] mainly reported in Canada, the Middle East, and the USA. Geographical distribution of this resource and fluid and reservoir properties are not yet well delineated, with a few exceptions. There is no clear picture of this immense resource so that policy makers and technology leaders in this area can predict the future of development of this resource and its potential contribution to the energy market. Despite this enormous resource size, only limited production data are reported, dominantly from lower viscosity reservoirs only, at low rates, thus the ultimate *RF* of the more viscous NFCR resource base remains close to zero. Further delineation of this immense energy resource is necessary. A few VO NFCR steamflooding pilot operations are reported in the literature from France, Italy, Congo, Turkey, USA, Kuwait, and Saudi Arabia and Cyclic Steam Stimulation (CSS) also has been used in VO NFCRs, and data are available only from cases in Canada, China, Egypt, and Syria.

9.3.2 Conduct Systematic Numerical Modeling and Laboratory Investigations

There are several experimental and modeling issues that can be resolved or better understood by further research studies:

Fracture networks with different sizes and configurations can be studied in terms of mathematical modeling approaches to learn more about the significance of fractures, inter-relationship between fractures, and interaction between the matrix and fracture.

Through experimental study, the petrophysical parameters of VO NFCRs described in this research can be varied within wide ranges to attain more general findings. Thus, a systematic experimental work is strongly recommended to cover a broad range of process and physical characteristics.

A number of properties (e.g., viscosity of the oil and steam) during steam injection into NFCR will alter versus time and position due to changes in pressure, temperature, and composition. This study shows that the major trends in oil production and steam flow rates are undoubtedly captured; however, better production behavior and estimations can be made to match the production performance as well as flow rates, if Buckley-Leverett theory is employed.

Instead of assuming average values for initial oil saturation, residual saturations, permeability and porosity, mathematical expressions for the properties distributions can be tried. Alternatively, more precise averages of the properties can be studied.

The numerical modeling can be extended to include properties of both homogeneous and heterogeneous reservoirs for fluid flow, heat transfer, and mass transfer models. Reservoir simulators can be employed to investigate various types of heterogeneity especially for the steamflooding process. Dispersive and fingering fronts should be studied to better forecast the breakthrough time.

Using an appropriate experimental approach, the communication between the matrix and fracture can be measured and modeled to enhance the accuracy of predictions of flow rates of fluids and production performance for steamflooding in NFCRs.

In order to better determine the temperature in the volume elements, heat transfer modeling can be conducted to include the heat transfer in the production and injection wells. Different heat transfer modeling schemes with various flow regimes can also be investigated.

Other thermal processes (e.g., cyclic steam process and SAGD) with different well configurations can be examined to address important aspects such as oil production rate, sweep efficiency, steam injection rate, steam production rate, production mechanisms, and so

on. Cyclic steam processes such as vertical well CSS were practiced in Canada over 30 years ago. In addition, some data is available in the open literature on field pilots of such a technology conducted in China, Egypt and elsewhere. These are valuable sources of information for model building and validation; however, it still looks like a relatively poor and small database. Continuous steamflooding utilizing horizontal wells (e.g., a SAGD-like process) will also be a subject of interesting and valuable research work.

Appendix A

Multi-Variable Regression Analysis

Design of a regression analysis procedure is a crucial step in modeling the response of a process (e.g., steamflooding). To do so, one needs “good” estimates of the model parameters. The contributing parameters should have a minimum in the statistical variance and they should be unbiased in nature. For design of a proper regression model, some primary elements should be considered such as implementing a precise model, logical generalization of modeling results, and quantifying the dependency of response variable(s) on all process inputs. There are three main steps to perform such statistical modeling, which are described briefly in the following sections:

A.1 Multiple Linear Regression Models

In many applications of regression analysis, it is common that there are more than one regressor variable. A regression model which contains more than one regressor variable is called a multiple regression model. As described in Chapter 3, the object functions contain 8 input variables, namely:

1) Steam quality, 2) oil saturation, 3) fracture permeability, 4) matrix permeability, 5) Steam injection rate, 6) reservoir depth, 7) oil viscosity, and 8) porosity.

There are two important objective parameters for each SF process, namely *CSOR*, and *RF*. These two objective functions should be statistically modeled as functions of the defined variables. In order to perform the multiple linear regression analysis, these two objective functions should be expressed explicitly in the dimensionless form.

In order to perform the multiple linear regression analysis, it is primarily assumed that each of these dimensionless objective functions is a sole function of every each of the defined variables. In other words, in order to figure out the dependency of a particular dimensionless objective function upon a particular input variable, they should be plotted against each other for the range of all of the experimental data or real field data which are available. Consequently, the absolute effect of each of the independent variable on the dimensionless objective functions could be investigated. Doing so, it was primarily assumed that there is no interaction term between

defined predictor variables. In fact, each particular objective function is only a sole function of different singular predictor values, and not a function of an interaction term, consisting of a combination of some of those predictor variables.

After plotting each particular dimensionless objective function versus each particular input parameter, two different schemes could appear. If the resulting graph would have a unique linear trend, it shows that the dimensionless objective function is a function of that particular input variable itself and the dependency could be figured out using the multiple linear regression analysis. However, if the resulting graph would have multiple different linear trends, it means that not only the objective function has functional dependency upon that particular input variable, but also there is a combined functional dependency between the objective function and a combination of dependent parameters. This combined dependant parameter consists of every other input variables whose sole functional relationship with that particular objective function consists of multiple (e.g., more than one) linear graphs.

Once the functionality of each particular dimensionless objective function to different input variables and/or their combination is determined, then the coefficients of the resulting correlation could then be obtained using multiple linear regression analysis. In general, the dependent variable or response (e.g., dimensionless objective function in our case) may be related to “k” regression variables using the following model:

$$y = \beta_0 + \beta_1 x_1 + \beta_2 x_2 + \dots + \beta_k x_k + e \quad (\text{A.1})$$

This relation is called a “multiple linear regression” model with “k” regressor variables (x_1 to x_k). The parameters “ β_0 to β_k ” are called the regression coefficients, x_1, x_2, \dots, x_k are the input variables, and “y” is the actual response variable (e.g., objective function). According to the procedure mentioned above about considering the combined effect of inputs on the objective functions (and their related figures which are discussed later), and based on the physics of the SF process which have already been reviewed in Chapter 3, it is found that combination of

dependent variables have also major contribution in the magnitudes of all the objective functions. As a result, regression models should include the term related to the “effect of interaction between the input variables” as well. An interaction between two dependent variables can be represented by a cross-product term in the regression model, such as:

$$y = \beta_0 + \beta_1 x_1 + \beta_2 x_2 + \beta_{12} x_1 x_2 + e \quad (\text{B.2})$$

in which “e” is the random error term (or experimental error), which is defined as the difference between actual dependent variable and predicted dependent variable obtained by the regression model. As far as the curve fitting procedure using multiple linear regression analysis is concerned, it is much more convenient to express the mathematical operations using matrix notation. Suppose there are “k” regressor variables and “n” observations, and the model relating the regressors to the response is as follows:

$$y_i = \beta_0 + \beta_1 x_{i1} + \beta_2 x_{i2} + \dots + \beta_k x_{ik} + e_i \quad i = 1, 2, \dots, n \quad (\text{A.3})$$

This model could be represented as a system of “n” equations; hence it could be expressed in the matrix notation as:

$$y = X\beta + e \quad (\text{A.4})$$

where:

$$y = \begin{bmatrix} y_1 \\ y_2 \\ \vdots \\ y_n \end{bmatrix}, \quad X = \begin{bmatrix} 1 & x_{11} & x_{12} & \cdots & x_{1k} \\ 1 & x_{21} & x_{22} & \cdots & x_{2k} \\ \vdots & \vdots & \vdots & & \vdots \\ 1 & x_{n1} & x_{n2} & \cdots & x_{nk} \end{bmatrix}, \quad \beta = \begin{bmatrix} \beta_1 \\ \beta_2 \\ \vdots \\ \beta_k \end{bmatrix}, \quad \text{and} \quad e = \begin{bmatrix} e_1 \\ e_2 \\ \vdots \\ e_n \end{bmatrix}$$

Respectfully, the least square estimate of “ β ” parameter is:

$$\hat{\beta} = (X'X)^{-1} X'y \quad (\text{A.5})$$

A.2 Analysis of the Multi-Variable Regression Modeling

The regression modeling, which is based on the assumption of validity of experimental data and as such the precision of preliminary DOE, should be checked accordingly in order to examine the curve fitting procedure and validity of the preliminary employed DOE. Three major validity indicators have been relied on in this section to check the suitability of the multi-variable linear regression analysis, namely as ANOVA tables, residual analysis, and squared of residuals' analysis (Montgomery and Runger, 2006; Montgomery, 2008).

A.2.1 ANOVA Tables

The analysis of variance (ANOVA) table includes data from a standard sum of the squares of the variance analysis for regression. Each particular ANOVA table includes the relevant data for each of three sources of deviation consisting of Regression, Residuals and Total. The source of variation of each data is either due to the deviation of each predicted data from its group mean value (e.g., Regression), or due to the deviation of each predicted value from its observed value (e.g., Residuals). The sum of these two sources of deviation would be expressed as the Total source of deviation. For each of these three sources of deviations, four measures of variance could be described as follows:

- a) Degrees of freedom: For each particular regression analysis, this parameter could be determined as the number of correlation coefficients, “N”, respect to the number of regressor variables used in each particular model. The higher is the degree of freedom for each particular model, the more reliable would be the regression model.
- b) Sum squares: Summation of the squared deviations, which are predicted from the observed data, is a measure of variance for each particular regression analysis. Total Sum Square is the summation of the squares of the residuals with the sum of the squares due to the regression.
- c) Mean squares: This column contains the sum of squares (e.g., SS) corrected for the degrees of freedom (e.g., DF).
- d) F-test: This is a variance-related statistical parameter which compares two models that are different from each other by one or more regressor variables to figure out if the more complex model would be also more reliable than the less complex one. If the “F” value is greater than a standard (e.g., critical) tabulated value, the more complex equation would be considered significant. By default, the significance level is set at 0.05.

A.2.2 Residual Analysis

The difference between the observed value of the dependent variable (y) and its predicted value (\hat{y}) is called the **residual** parameter (e.g., “ e ”) attributed to that particular dependent variable. Each data point has one attributed residual value based on the following definition:

$$\text{Residual} = \text{Observed value} - \text{Predicted value} \quad (\text{A.6})$$

A **residual plot** is a graph that shows the residual magnitudes for each particular variable on the vertical axis and the magnitudes of independent variable on the horizontal axis. If the data points in a residual plot would be randomly dispersed around the horizontal axis, that particular linear regression model is statistically appropriate and predicts the dependant variable precisely enough

compared to the actual values reported based on the experimental observations; otherwise, it is recommended to use a non-linear regression model instead of the linear one.

B.2. 3 Squared Residuals Analysis

One of the simplest methods to check the accuracy of a particular linear regression is to look at the magnitudes of squared residuals. Our results from experimental and linear regression analyses are showing reasonable compatibility between measured and predicted values. In other words, small values of residuals as well as appreciable magnitudes of squared residual indicate that the proposed linear regression curves works well for the experimental conditions noted previously.

A.3 MATLAB™ Toolbox for Regression

A statistical method was employed to estimate the recovery performance of heavy oil carbonate fractured reservoirs under steamflooding process. A MATLAB™ Toolbox called Statistics was used for multivariable regression. The Statistics Toolbox gives the regression function to address the multiple regression problems. Regress uses QR decomposition of X followed by the backslash operator to calculate the coefficients of the variables “ $\hat{\beta}$ ”.

The QR decomposition is not necessary for computing $\hat{\beta}$, but the matrix R is useful for determining confidence intervals.

`b = regress(y,X)` returns the least squares estimator $\hat{\beta}$.

`[b,bint,r,rint,stats] = regress(y,X)` returns an estimate of β in b, a 95% confidence interval for β in the $k \times 2$ array bint. The residuals are returned in r and a 95% confidence interval

for each residual is returned in the $n \times 2$ array. The vector “rint” contains the R^2 statistic and also the F and p values for the regression.

`[b,bint,r,rint,stats] = regress(y,X,alpha)` gives $100(1 - \alpha)\%$ confidence intervals for “bint” and “rint”. The following program shows a sample of computation for *RF*.

Subprogram 1: Initialization and Data Input

```

function [z,grad,H] = LogVerEV(param,X,r)
% X = data sample where the first r observations are complete
% grad = gradient vector
% H = Hessian matrix
n = length(X);
u = param(1);
b = param(2);
Y = X(1:r);
s1 = sum((Y - u)./b);
s2 = sum(exp((X - u)./b));
z = -r*log(b) + s1 - s2;
grad = zeros(2,1);
grad(1) = -r/b + s2/b;
s3 = sum(((X - u)./b).*(exp((X - u)./b)));
grad(2) = -r/b - s1/b + s3/b;
H = zeros(2,2);
H(1,1) = -s2/(b^2);
s4 = sum((((X - u)./(b^2)).^2).*(exp((X - u)./b)));
H(2,2) = r/(b^2) + 2*s1/(b^2) - 2*s3/(b^2) - s4;
H(2,1) = r/(b^2) - s2/(b^2) - s3/(b^2);
H(1,2) = H(2,1);

```

```

%clear

clf

% We generate 50 samples of size 300 from a
n = 300;
r = 240;
rand('seed',sum(100*clock));
alpha = 2;
beta = 0.5;
X = weibull(alpha,beta,n);
if any(X==0)==1,
I = find(X==0);
X(I) = eps*ones(length(I),1);
end
X = sort(X);
X(r+1:n) = ones(n-r,1)*X(r);
Y = log(X);
param = [0.6,1.5]'; % punto inicial
[z,grad,H] = LogVerEV(param,Y,r);
while grad > 1e-4,
param = param - inv(H)*grad;
[z,grad,H] = logVerEV(param,Y,r);

```

```

end

alpha = exp(param(1));
beta = 1/param(2);

mean(xbar)

std(xbar)

histn(xbar)

hold on;

x=2.5:.01:7.5;plot(x,normpdf(x,mu,sigma/sqrt(n)))

mean(S2)

chi=(n-1)*S2/sigma^2;

histn(chi)

hold on;

x=0:.1:30;plot(x,chi2pdf(x,n-1))

plot(xbar, S2, 'r')

corrcoef(xbar, S2)

```

Subprogram 2: Regression Function

```

function [beta,Var_beta,ypred,sR2] = regres(X,Y)

% X = matrix of regressors with a column of ones.

% Y = vector of data from the dependent variable.

```

```

% beta = vector of regression coefficients.

% Var_beta = The variance covariance matrix of beta.

% ypred = predicted values for Y.

% sR2 = residual variance.

[n,k] = size(X);

k = k - 1;

beta = (X'*X)\(X'*Y);

ypred = X*beta;

resid = Y - ypred;

sR2 = sum(resid.^2)/(n - k - 1);

Var_beta = sR2*inv(X'*X);

n = 50; k = 4;

X = randn(n,k);

b = [0;1;0;1];

y = X*b + randn(n,1);

X = [ones(n,1) X];

[beta,Var_beta,ypred,sR2] = regres(X,y);

resid = y - ypred;

subplot(2,1,1),plot(resid,'o'),title('residuals versus row number')

subplot(2,1,2),plot(resid,ypred,'o'),title('residuals versus predicted')

```

Appendix B

Numerical modeling program for steamflooding

This appendix presents the numerical modeling program developed and implemented in Chapter 5 in order to obtain production history of the naturally fractured carbonate viscous oil reservoirs under steamflooding.

```
%-----Input/output -----
```

```
T= input (t1, t2);
```

```
P= input (P1, P2);
```

```
X= input (x1, x2);
```

```
%----- Fluid properties-----
```

```
PCRIT = input (pc1, pc2, pc3, pc4) ; PCRIT=f1 (pc)
```

```
TCRIT = input (Tc1, Tc2, Tc3, Tc4); TCRIT =f2 (Tc)
```

```
AVG 1= input (avg1, avg2, avg3, avg4); AVG= f3 (avg)
```

```
BVG = input (bvg1, bvg2, bvg3, bvg4); BVG= f4(bvg)
```

```
CP = [0 7e-6 4e-6 2e-3];
```

```
CT1= [ 0 4e-4 3e-5 3;2e-2]
```

```
%----- Rock/Fluid interactions -----
```

```
% Water-oil relative permeabilities
```

RFLUID1= f5 (Sw, Krw, Krow)

% Liquid-gas relative permeabilities

RFLUID2= f6 (Sl, Krg, Krog)

%-----Initial Conditions-----

Automatic static vertical equilibrium

VERTICAL %DEPTH_AVE

REFPRES 75

REFBLOCK 1 1 1

TEMP * CON 125

%-----Numerical method-----

%NUMERICAL ; All these can be defaulted;

NORM %PRESS 200 %SATUR 0;2 %TEMP 50

RUN

%-----Input Data-----

Wellinjec=Well 1 *Vert 1 1 *Frac ;125 * O O O

Well 2 'Producer' *Vert 23 1 *Frac ;125 * O O O O O

Injector * Mobweight 'Injector'

INCOMP WATER 1;0 0;0

TINJW 545

QUAL ;7

OPERATE %BHP 1000

Op=OPERATE %MAX %STW 400

Rep=PERFV 'INJECTOR' %% k wi %% Inject only in the bottom layer

k = 2000; h = 5; dx = dy = 2;5 ft; cc = 0;249; rw = 0;3 ft

lr=PRODUCER ;

rt= input (OPERATE *BHP);

Simulation Input Data

%-----Gridding and Reservoir specification-----

Gy=VA 2 0;5 0;5 1;0 0;5

GY1=VA (3 0;5 1;0 1;0 0;5) * p [0;5 1;0]

GU2=VA (4 0;5 1;0 1;0 0;5) * p [0;5 1;0]

GU2=VA (5 0;125 0;5 1;0 0;125) * p [0;5 1;0]

GU3= VA (6 0;25 1;0 1;0 0;25) * p [0;5 1;0]

%VAT %ALL

PERMI %CON 6922

PERMJ %EQUALSI

PERMK %EQUALSI / 10

END-GRID

CPOR 8E-04

PRPOR 275

ROCKCP 35;02

THCONR 24

THCONW 24

THCONO 24

THCONG 24

HLOSSPROP %OVERBUR 60 24 %UNDERBUR 60 24

%----- Fluid characteristics-----

CMM= CMM [0;0000 456;015 16;7278]

PCPRT=PCRIT [0;00 179;02 670;46]

TCRIT =TCRIT [0;00 1036;21 -107;35]

KV1 0;000E+0 5;165E+6 1;534E+5

KV2 0;000E+0 0;000E+0 0;000E+0

KV3 0;000E+0 0;000E+0 0;000E+0

KV4 0;0 -15362;5 -1914;1

KV5 0;00 -459;67 -459;67

MOLDEN 0;000E+00 1;356E-01 4;515E-02

CP 0;000E+00 3;805E-06 3;754E-03

CT1 0;000E+00 1;660E-04 1;910E-03

%-----T, deg F 'WATER' 'OIL' 'GAS'-----

%-----Rock-Fluid Properties-----

RPT= RPT 1 *WATWET *STONE2

Data = f9 (SL, KRG, KROG)= [0;850000 0;460000 0;000000 0;000000;

0;875000 0;290000 0;065000 0;000000;

0;900000 0;160000 0;150000 0;000000;

0;925000 0;080000 0;240000 0;000000;

0;950000 0;030000 0;340000 0;000000;

0;975000 0;005000 0;435000 0;000000;

1;000000 0;000000 0;550000 0;000000]

Et5= f24 (Temp, Swr, Swcrit, Sorw, Soirw, Sorg, Soirg, Krwiro, Krocw, Krgcw)=

[110; 0;5 0;5 0;4 0;4 0;85 0;85 0;05 0;55 0;46;

255; 0;6 0;6 0;25 0;25 0;74 0;74 0;05 0;575 0;375;

400; 0;6125 0;6125 0;225 0;225 0;715 0;715 0;05 0;61 0;35]

%-----Initial Conditions -----

U8= VERTICAL *DEPTHAVE

G9= input (REFPRES 275)

%REFDEPTH 1957;5

SW5= SW CON 0;267

SO CON 0;733*TEMP *CON 127* MFRAC_OIL 'OIL' CON 0;78904* MFRAC_GAS 'GAS'
CON 0;21096

% -----Numerical Chart-----

NUM= NORM *PRESS 200 %SATUR 0;2 *TEMP 50

%% ===== RECURRENT DATA =====

%% o

%WELL 1 'INJECTOR' %VERT 1 1 %FRAC ;125 %% o o o

%WELL 2 'PRODUCER' %VERT 45 1 %FRAC ;125 %% o o o o o

%% o o o o o o o

%% 1 o o o o o o o 2

%INJECTOR %MOBWEIGHT 'INJECTOR'

%INCOMP WATER 1;0 0;0 0;0

%TINJW 582;3

QUAL ;8

%OPERATE %BHP 1350

%OPERATE %MAX %STW 1600

%PERFV 'INJECTOR' %% k wi %% Inject only in the bottom layer

%% 2%pi%k%h / ln(cc%sqrt((dx%%2+dy%%2)/pi)/rw)

5 320715;436 %% k = 6922 md, h = 14;375 ft, dx = dy = 10;607 ft,

6 320715;436 %% cc = 0;249, rw = 0;3 ft

7 320715;436

8 320715;436

%PRODUCER 'PRODUCER'

%OPERATE %BHP 15

%OPERATE %MAX %STL 5000

%%OPERATE %MAX %STEAM 10 %% Steam CWE in bbl/day

%PERFV 'PRODUCER' %% k wi

5 320715;436

6 320715;436

7 320715;436

8 320715;436

OPEN 'PRODUCER'

OPEN 'INJECTOR'

TIME 365

[TIME 730

;TIME 1095

;TIME 1460

;TIME 1825

;TIME 2190

;TIME 2555

;TIME 2920

;TIME 3285

;TIME 3650

;TIME 4015

;TIME 4380

;TIME 4745

;TIME 5110

;TIME 5475

;TIME 5840

;TIME 6205

;TIME 6570

;TIME 6935

;TIME 7300]

STOP

%-----input/output control -----

%FILENAME %OUTPUT %INDEX-OUT %MAIN-RESULTS-OUT %% Use default file
names

CHECKONLY

%INTERRUPT %STOP

%TITLE1 'Hamaca Case'

%TITLE2 'Hamaca Field'

%TITLE3 'Area = 10 Acre Injection Rate = 1600 STB/D'

%INUNIT %FIELD %% output same as input

%OUTPRN %GRID %PRES %SW %SO %SG %TEMP %Y %X %W %SOLCONC

%OBHLOSS %VISO

```

%OUTPRN %WELL %ALL

%WRST 300 %WPRN %GRID 300 %WPRN %IT 300

%OUTSRF %WELL %LAYER ALL

%-----Mesh Size-----

GM= GRID %CART 45 23 8

KDIR %DOWN

%NINEPOINT %IJ

Tyu=466;69 ft, giving a block size of  $233\frac{3}{44} = 10;6045$  ft ; DI %CON 10;607

%DJ %CON 10;607

U=DK %CON 12;5

VAM= VAMOD [2 0;5 0;5 1;0 0;5]

VAMOD[ 3 0;5 1;0 1;0 0;5 %9p 0;5 1;0

;VAMOD 4 0;5 1;0 1;0 0;5 %9p 1;0 0;5

;VAMOD 5 0;125 0;5 1;0 0;125 %9p 0;5 1;0

;VAMOD 6 0;25 1;0 1;0 0;25 %9p 1;0 0;5

;VATYPE %ALL

;POR %CON 0;3

;PERMI %CON 12000

;PERMJ %EQUALSI

;PERMK %EQUALSI / 10

END-GRID

CPOR

```

END-GRID

CPOR 4e-4

PRPOR 275

ROCKCP 35

THC= THCONR (24,6)=

[THCONW 24

THCONO 24

THCONG 24]

%-----Fluid Definitions-----

%MODEL 2 2 2 %% Components are water and dead oil; Most water
properties are defaulted (=0); Dead oil K vals are zero, and no gas properties are needed;

%COMPNAME 'WATER' 'OIL'

%CMM 18 511;78

PCRIT 635 2415;7

%TCRIT 323 2280

CPG1 0 0

CPG2 0 0

CPG3 0 0

CPG4 0 0

MASSDEN 62;7401 63;18664

CP 0 5;e-6

CT1 0 5;005E-4

CT2 0 0

VISCTABLE

TW=TW (Temp Water Oil)

%PRSR 14;7

%TEMR 60

%PSURF 14;7

%TSURF 60

%-----Rock-Fluid Properties-----

%ROCKFLUID

%SWT %% Water-oil relative permeabilities

%% Sw Krw Krow

RP= [

0;168000 0;000000 0;900000

0;250000 0;100000 0;665000

0;440000 0;400000 0;380000

0;560000 0;600000 0;237500

0;672000 0;760000 0;142500

0;830000 1;000000 0;000000]

LT= (Liquid-KRG

SI Krg Krog)

YT= [

0;338000 0;500000 0;000000

0;401100 0;300000 0;005670

0;486700 0;125000 0;014400

0;600000 0;062500 0;026700

0;657800 0;037500 0;034400

0;743300 0;012500 0;046700

0;800000 0;005000 0;056700

0;825000 0;002500 0;062222222

0;850000 0;002500 0;067777778

0;900000 0;002500 0;080000

1;000000 0;000000 0;900000]

%-----Initial Conditions -----

%INITIAL

%% Automatic static vertical equilibrium

Uy= VERTICAL *DEPTH_AVE;

Gf=REFPRES (275)

Re= REFBLOCK (1 1 1)

%TEMP %CON 125

%-----numerical control -----

%NORM %PRESS 30 %SATUR 0;09 %TEMP 15

%RUN

%-----Required DATA-----

WELL 1 'INJECTOR' %VERT 1 1 %FRAC ;125 %% o o o

o o o o o o o

%% 1 o o o o o o o 2

Dg=Injector *Mobweight 'Injector'

IN= INCOMP WATER 1;0 0;0

TINJW 600

QUAL ;8

OPERATE %BHP 1600

%OPERATE %MAX %STW 1600

PERFV 'INJECTOR' %% $k_{wi} * 2 * \pi * k * h / \ln(cc \% \sqrt{(dx^2 + dy^2)} / \pi) / rw$

5 483472;39 * $k = 12000 \text{ md}$, $h = 12;5 \text{ ft}$, $dx = dy = 10;607 \text{ ft}$,

[6 483472;39 * $cc = 0;249$, $rw = 0;3 \text{ ft}$

7 483472;39

8 483472;39]

PRODUCER 'PRODUCER'

%OPERATE %BHP 90

OPERATE %MAX %STL 3500

DFG= PERFV 'PRODUCER'* k_{wi}

[5 483472;39

6 483472;39

7 483472;39

8 483472;39]

OPEN 'PRODUCER'

OPEN 'INJECTOR'

TIME 365; TIME 730; TIME 1095; TIME 1460; TIME 1825; TIME 2190; TIME 3650; TIME
5475

STOP

%-----**Steam Injection Governning Eq**

Global limit As Single

Dim Acd1 As Double

Dim Acd2 As Double

Dim Acd3 As Double

Dim Acd4 As Double

Dim Acd1p2 As Double

Dim Acd2p2 As Double

Dim Acd3p2 As Double

Dim Acd4p2 As Double

Dim Vod1 As Double

Dim peakoilrate As Double

Dim Ms As Double

```

Dim check As Integer
Dim maxq As Double
Dim maxqnumber As Integer
Dim maxit As Integer
Dim NdSECI3 As Variant
Dim maxAcD As Double
'Define functions
Function ERFC(x As Double)
y = 1 / (1 + 0,3275911 % x)
ERFC = (0,254829592 % y - 0,284496736 % y ^ 2 + 1,421413741 % y ^ 3 - _
1,453152027 % y ^ 4 + 1,061405429 % y ^ 5) % Exp(-(x ^ 2)) + 0,00000015
End Function
Function SQR5(temp As Double)
SQR5 = temp ^ 0,5
End Function
Function Pi()
Pi = 3,14159265358979
End Function
Function integration(td As Double, tcd As Variant, section As Double)
delta = (tcd - 0) / section
Start = delta / 2
Sum = 0

```

```

For i = 0 To section - 1
Sum = Exp(Start + delta % i) % ERFC(SQRT(Start + delta % i)) / _
SQRT(td - (Start + delta % i)) % delta + Sum
Next i
integration = Sum
End Function
Sub JeffJones()
'Initialize val
check = 0
maxq = 0
NdSECI = 0
StartItVoD = 0
With Sheets("CSOR, RF")
'Get data entry
a = Input("CSOR, RF");Range("A");Val 'Area
por = Input("CSOR, RF");Range("por");Val 'Porosity
Soi = Input("CSOR, RF");Range("Soi");Val 'Initial oil saturation
Sor = Input("CSOR, RF");Range("Sor");Val 'Residual oil saturation
Sgi = Input("CSOR, RF");Range("Sgi");Val 'Initial gas saturation
Oil_vis = Input("CSOR, RF"); _
Range("oil_vis");Val 'Initial Oil vis
Tres = Input("CSOR, RF");Range("Tres");Val 'Reservoir temperature

```

```

Bo = Input("CSOR, RF");Range("Bo");Val 'Oil formation volume factor
kh = Input("CSOR, RF");Range("kh");Val 'Thermal conductivity of formation
Rock_Density = Input("CSOR, RF");Range("Rock_Density");Val 'Rock Density
Cr = Input("CSOR, RF");Range("Cr");Val 'Heat capacity of rock
Water_Density = Input("CSOR, RF"); _
Range("Water_Density");Val 'Water density
Oil_Density = Input("CSOR, RF");Range("Oil_Density");Val 'Oil density
Cw = Input("CSOR, RF");Range("Cw");Val 'Heat capacity of water
Co = Input("CSOR, RF");Range("Co");Val 'Heat capacity of oil
ht = Input("CSOR, RF"); hn = Input("CSOR, RF");Range("hn");Val 'Net thickness
M_1Temp = Input("CSOR, RF"); _
Range("M_1Temp");Val 'Volumetric heat capacity of rock
Irate = Input("CSOR, RF");Range("Irate");Val 'Injection rate
Ps = Input("CSOR, RF");Range("Ps");Val 'Saturated steam pressure
fs = Input("CSOR, RF");Range("fs");Val 'Steam quality
Tinj = Input("CSOR, RF");Range("Tinj");Val 'Injection temperature
vis = Input("CSOR, RF"); _
Range("vis");Val 'Oil vis @ steam temperature
Ms = Input("CSOR, RF"); _
Range("Ms")
TotalDay = Input("CSOR, RF"); _
Range("TotalDay");Val 'Total day of calculations

```

```

DeltaDay = Input("CSOR, RF"); _
Range("DeltaDay");Val 'Delta day of calculations
peakoilrate = Irate 'Maximum oil production rate
Cp=Cp+1
If M1Temp = 0 Then
M_1 = (1 - por) *RockDensity * Cr + por * Sor * OilDensity * Co
+ por * (1 - fs) ^ 0;5 *(1 - Sor) *WaterDensity * Cw
Else
M_1 = M_1Temp
End If
If Ps >= 500 and Ps <= 1500 Then
Hsc = 77;036 * Ps ^ 0;28302
ElseIf Ps > 1500 and Ps <= 2500 Then
Hsc = 0;12038 * Ps + 430;984
End If
Hsv = 1204;8 - 0;000197697 * (Ps - 453;23) ^ 1;73808
hfg = Hsv - Hsc
fhv = 1 / (1 + Cw % (Tinj - Tres) / (fs * hfg))
Input("CSOR, RF");Range("Target");TargetSeek Target:=fhv, _
NEW mesh:=Input("CSOR, RF");Range("NEW mesh")
tcd = Input("CSOR");Range("NEW mesh")
fhD = fs % hfg / (Cw % (Tinj - Tres))

```

Dimtime=tD

'Dim time = tD_multiplier multiply by time

$$tD_multiplier = 35040 \% Ms \% kh / (ht \wedge 2 \% M_1 \wedge 2)$$

'Calculate cumulative oil steam ratio constant

'Cumulative oil steam ratio = Fos_multiplier multiply by Ehs

$$Fos_multiplier = Water_Density \% Cw / M_1 \% hn / ht \% _ \\ (Soi - Sor) \% por \% (1 + fhD)$$

'Calculate heat injection rate

$$Qinj = 14,6 \% Irate \% (Hsc + fs \% hfg - Cw \% (Tres - 32))$$

'Calculate oil originally in place

$$N = 43560 \% a \% hn \% por \% Soi / (5,62 \% Bo)$$

'Calculate alpha

$$alpha = 0,00015 \% Irate + 0,05$$

'Calculate betha

$$tc = tcd \% ht \wedge 2 \% M_1 \wedge 2 / (35040 \% kh \% Ms)$$

$$Nc = 7758 \% a \% hn \% por \% (Soi - Sor) / (365 \% Irate \% tc)$$

$$betha = 17,93 \% Nc + 1,3401$$

$$Acd1 = alpha$$

$$Acd2 = 100$$

$$Acd3 = 0,5$$

$$Acd4 = 2$$

$$Acd1p2 = 0,11$$

Acd2p2 = 100

Acd3p2 = 0;5

Acd4p2 = 4

'Coefficient for VoD

Vod1 = betha

%-----Input Data-----

;Cells(36, 3);Val = M1;

;Cells(41, 3);Val = hfg;

;Cells(40, 7) = Hsv;

;Cells(41, 7) = Hsc

;Cells(47, 3);Val = fhD;

;Cells(53, 3);Val = tcd;

;Cells(60, 3);Val = tD(multiplier);

;Cells(78, 3);Val = Fos(multiplier);

;Cells(86, 3);Val = Qinj

;Cells(125, 3);Val = N

;Cells(95, 13);Val = fhv

;Cells(54, 13);Val = alpha;

;Cells(76, 13);Val = alpha;

;Cells(59, 19);Val = betha

It=it+1

If it>200, it=100

```

limit = TotalDay / DeltaDay
;Range("A134:Z5000");Clear

For it = 1 To limit
T=t+1

;Cells(133 + it, 2);Val = DeltaDay % it

Tim=[t1 t2 t3 .....]

;Cells(133 + it, 1);Val = ;Cells(133 + it, 2);Val / 365;25

TD=t2+3

;Cells(133 + it, 3);Val = tD/multiplier *

;Cells(133 + it, 1)

Gt= G(tD)

;Cells(133 + it, 4) = 2 % SQRT(;Cells(133 + it, 3) / Pi()) - 1 _
+ Exp(;Cells(133 + it, 3)) % ERFc(SQRT( _
;Cells(133 + it, 3)))

Avge= avg/T

If ;Cells(133 + it, 3) < tcd Then

;Cells(133 + it, 5) = 1 / ;Cells(133 + it, 3) % _
;Cells(133 + it, 4)

Else

;Cells(133 + it, 5) = 1 / ;Cells(133 + it, 3) * (;Cells(133 + it, 4) _
+ (1 - fhv) % 1 / SQRT(Pi()) % (2 * SQRT(;Cells(133 + it, 3)) - _
2 % (1 - fhv) * SQRT(;Cells(133 + it, 3) - tcd) - _

```

```

integration(;Cells(133 + it, 3), tcd, 5000) _
- SQRT(Pi()) % ;Cells(133 + it, 4))

End If

R6= CSOR

;Cells(133 + it, 6) = Fos_multiplier % ;Cells(133 + it, 5)

Rd=CSOR

;Cells(133 + it, 7) = Irate % ;Cells(133 + it, 2);Val

R8=RF

;Cells(133 + it, 8) = ;Cells(133 + it, 6) % ;Cells(133 + it, 7) / Bo

Q=RF/fd

If it = 1 Then

;Cells(133 + it, 9) = (;Cells(133 + it, 8) - 0) / DeltaDay

Else

;Cells(133 + it, 9) = (;Cells(133 + it, 8) - ;Cells(132 + it, 8)) _
/ DeltaDay

End If

As=Az

;Cells(133 + it, 10) = Qinj % hn % M_1 / (4 *kh * (Tinj - Tres) *Ms * 43560) * (Exp(;Cells(133
+ it, 3);Val) *ERFC(SQRT(;Cells(133 + it, 3);Val)) + 2 * SQRT(;Cells(133 + it, 3);Val / Pi()) -
1)

ACD1 =acd

If maxq = 0 Then

If check = 0 Then

```

If 132 + it = 133 Then

Cd= Cells(133 + it, 11) = (;Cells(133 + it, 10) / (a % (Acd1 * Log(Oil_vis / Acd2)) ^ Acd3)) ^ Acd4

ElseIf ;

Cells(132 + it, 11) < 1 Then

;Cells(133 + it, 11) = (;Cells(133 + it, 10) / (a * (Acd1 * Log((;Cells(133 + it, 10) * vis + (a - ;Cells(133 + it, 10)) * Oil_vis) / a / Acd2)) ^ Acd3)) ^ Acd4

Else

check = 1

;Cells(133 + it, 11) = (;Cells(133 + it, 10) / (a % (Acd1p2 % _

Log((;Cells(133 + it, 10) % vis + (a - _

;Cells(133 + it, 10)) % Oil_vis) / a / Acd2p2)) _

^ Acd3p2)) ^ Acd4p2

End If

Else

If ;Cells(132 + it, 15) < peakoilrate Then

;Cells(133 + it, 11) = (;Cells(133 + it, 10) / (a % (Acd1p2 % _

Log((;Cells(133 + it, 10) % vis + (a - _

;Cells(133 + it, 10)) % Oil_vis) / _

a / Acd2p2)) ^ Acd3p2)) ^ Acd4p2

Else

;Cells(132 + it, 15) = peakoilrate

```

maxq = ;Cells(132 + it, 15)
maxqnumber = 132 + it
maxit = it - 1
maxAcD = peakoilrate / (;Cells(132 + it, 12) % ;Cells(132 + it, 13) _
% ;Cells(133 + it, 9))
;Cells(132 + it, 11) = maxAcD
;Cells(132 + it, 14) = maxAcD % ;Cells(132 + it, 12) % _
;Cells(132 + it, 13)
NdSECIH = ;Cells(132 + it, 8)
;Cells(133 + it, 11) = 1
End If
End If
Else
;Cells(133 + it, 11) = 1
End If
'Calculate VpD
If Sgi = 0 Then
;Cells(133 + it, 12) = 1
Else
If (;Cells(133 + it, 7) % 5;62 / (43560 % a % hn % por % Sgi)) ^ 2 < 1 Then
;Cells(133 + it, 12) = (;Cells(133 + it, 7) % 5;62 / _
(43560 % a % hn % por % Sgi)) ^ 2

```

```

Else
;Cells(133 + it, 12) = 1
End If
End If
'Calculate VoD
If NdSECIII = 0 Then
;Cells(133 + it, 13) = 1
Else
If (1 - (;Cells(133 + it, 8) - NdSECIII) / N % Soi / (Soi - Sor)) > 0 Then
;Cells(133 + it, 13) = maxAcD % Exp(-Vod1 % _
(;Cells(133 + it, 8) - NdSECIII) / N % Soi / (Soi - Sor))
Else
;Cells(133 + it, 13) = 0
End If
End If
So=Sor
Cells(133 + it, 14) = ;Cells(133 + it, 11)* ;Cells(133 + it, 12) % _
Cells(133 + it, 13)
Q=RF/t-v
Cells(133 + it, 15) = ;Cells(133 + it, 14) * ;Cells(133 + it, 9)
CSOR=A+B
If (Cells(133 + it, 10) / (a / (0;11 * Log(Oilvis / 100)) ^ 0;5)) ^ 2 <= 1 and Oilvis > 100 Then

```

```

Cells(133 + it, 16) = (;Cells(133 + it, 10) / (a % (0;11 % _
Log(Oil vis / 100)) ^ 0;5)) ^ 2
Else
Cells(133 + it, 16) = 1
End If
RF = RF (N, N-6)
If Sgi = 0 Then
Cells(133 + it, 17) = 1
Else
If (Cells(133 + it, 7) % 5;62 / (43560 % a % hn % por % Sgi)) _
^ 2 < 1 Then
Cells(133 + it, 17) = (Cells(133 + it, 7) * 5;62 / (43560 * Sgi)) ^ 2
Else
Cells(133 + it, 17) = 1
End If
End If
'Y= [CSOR RF]
If (1 - ;Cells(133 + it, 8) / N % Soi / (Soi - Sor)) > 0 Then
;Cells(133 + it, 18) = (1 - ;Cells(133 + it, 8) / _
N % Soi / (Soi - Sor)) ^ 0;5
Else
;Cells(133 + it, 18) = 0

```

End If

Y=CSOR

;Cells(133 + it, 19) = ;Cells(133 + it, 16) / ;Cells(133 + it, 17) *Cells(133 + it, 18)

Y2=RF

CSOR(133 + it, 20) = CSOR(133 + it, 19)-Cells(133 + it, 9)

RF(133 + it, 20) = RF(133 + it, 19)-RF(133 + it, 9)

outputs('CSOR');Cells(20, 11)

End

End

Appendix C

Artificial Neural Network and Particle Swarm Optimization program

This appendix presents the MATLAB™ program developed to predict the production performance of steam flooding in terms of Recovery Factor (*RF*) and Cumulative Steam Oil Ratio (*CSOR*) for heavy oil carbonate fractured reservoirs. The method employed in this study is a hybrid smart technique in the form of Artificial Neural Network (ANN) combined with Particle Swarm Optimization (PSO). The following computational program includes some important subprograms such as Initialization, Network Set-up, PSO Algorithm, ANN Structure and PSO-ANN Input and Output Matrixes Construction.

Subprogram 1 “Initialization and Entering Data”

```
function net=initnw1(net,i)
%INITNW Nguyen-Widrow layer initialization function.
%
% Syntax
%
% net = initnw(net,i)
%
% Description
%
% INITNW is a layer initialization function which initializes
% a layer's weights and biases according to the Nguyen-Widrow
% initialization algorithm. This algorithm chooses values in order
% to distribute the active region of each neuron in the layer
```

```

% evenly across the layer's input space.
%
% INITNW is best used with layers whose transfer function has a finite
% active input interval, such as TANSIG, not an infinite active input
% interval, such as PURELIN.
%
% INITNW(NET,i) takes two arguments,
% NET - Neural network.
% i - Index of a layer.
% and returns the network with layer i's weights and biases updated.
%
% Network Use
%
% You can create a standard network that uses INITNW by calling
% NEWFF or NEWCF.
%
% To prepare a custom network to be initialized with INITNW:
% 1) Set NET.initFcn to 'initlay'.
% (This will set NET.initParam to the empty matrix [] since
% INITLAY has no initialization parameters.)
% 2) Set NET.layers{i}.initFcn to 'initnw'.
%
% To initialize the network call INIT.
%
% See NEWFF and NEWCF for training examples.
%
% Algorithm

```

```

%
% The Nguyen-Widrow method generates initial weight and bias
% values for a layer so that the active regions of the layer's
% neurons will be distributed roughly evenly over the input space.
%
% Advantages over purely random weights and biases are:
% (1) Few neurons are wasted (since all the neurons are in the input space).
% (2) Training works faster (since each area of the input space has neurons).
%
% The Nguyen-Widrow method can only be applied to layers...
% ...with a bias,
% ...with weights whose "weightFcn" is DOTPROD,
% ...with "netInputFcn" set to NETSUM.
% If these conditions are not met then INITNW uses RANDS to
% initialize the layer's weights and biases.
%
% See also INITLAY, INITWB, INIT.

% Mark Beale, 11-31-97
% Copyright 1992-2008 The MathWorks, Inc.
% $Revision: 1.1.6.8 $

if (nargin < 1), error('NNET:Arguments','Not enough arguments.');
```

```

end
if ischar(net)
    switch(net)
        case 'name'
            net = 'Nguyen-Widrow';

```

```

    otherwise, error('NNET:Arguments',['Unrecognized code: "' net "'])
end
return
end

```

```

% Calculate source indices

```

```

inputInds = find(net.inputConnect(i,:));
numInputs = length(inputInds);
layerInds = find(net.layerConnect(i,:));
numLayers = length(layerInds);

```

```

% Get source sizes and delays

```

```

inputSizes = zeros(numInputs,1);
inputDelays = zeros(numInputs,1);
for j=1:numInputs
    inputDelays(j) = length(net.inputWeights{i,inputInds(j)}.delays);
    inputSizes(j) = net.inputWeights{i,inputInds(j)}.size(2);
end
totalInputSize = sum(inputSizes);

```

```

layerSizes = zeros(numLayers,1);

```

```

layerDelays = zeros(numInputs,1);
for j=1:numLayers
    layerDelays(j) = length(net.layerWeights{i,layerInds(j)}.delays);
    layerSizes(j) = net.layerWeights{i,layerInds(j)}.size(2);
end
totalLayerSize = sum(layerSizes);

```

```

totalSourceSize = totalInputSize + totalLayerSize;

% Calculate range indices
inputStart = cumsum([1; inputSizes]);
inputStop = cumsum(inputSizes);
layerStart = cumsum([1; layerSizes])+totalInputSize;
layerStop = cumsum(layerSizes)+totalInputSize;

% Get source ranges
range = zeros(totalSourceSize,2);
for j=1:numInputs
    irange = net.inputs{inputInds(j)}.processedRange;

    % ODJ 4/1/02 Avoid problem with delays and one column weights
    temp=size(irange,1)*inputDelays(j);
    if temp~=inputStop(j)-inputStart(j)-1
        temp= repmat(irange,inputDelays(j),1);
        range(inputStart(j):inputStop(j),:) = temp((inputStart(j):inputStop(j))-inputStart(j)+1,:);
    else
        range(inputStart(j):inputStop(j),:) = repmat(irange,inputDelays(j),1);
    end
end

for j=1:numLayers
    lrange = feval(net.layers{layerInds(j)}.transferFcn,'output');
    if any(~isfinite(lrange))
        lrange = [max(lrange(1),-1) min(lrange(2),1)];
    end
end

```

```

end
range(layerStart(j):layerStop(j),:) = lrange(ones(layerSizes(j),1),:);
end

% Get transferFcn info
transferFcn = net.layers{i}.transferFcn;
active = feval(transferFcn,'active');

% Check layer and sources for compatibility with Nguyen-Widrow method
ok = 1;
if ~strcmp(net.layers{i}.netInputFcn,'netsum')
    ok = 0;
end
if ~net.biasConnect(i)
    ok = 0;
end
if ~all(isfinite(active))
    ok = 0;
end
for j=1:numInputs
    if ~strcmp(net.inputWeights{i,inputInds(j)}.weightFcn,'dotprod')
        ok = 0;
    end
end
for j=1:numLayers
    if ~strcmp(net.layerWeights{i,layerInds(j)}.weightFcn,'dotprod')
        ok = 0;
    end
end

```

```

end
end

% Use Nguyen-Widrow method if network checks out ok
if ok
    [w,b] = calcnw(range,net.layers{i}.size,active,i);

% Otherwise use RANDS
else
    sizeRows = 0;
    for j=1:numInputs
        if(net.inputWeights{i,inputInds(j)}.size(1)>sizeRows)
            sizeRows = net.inputWeights{i,inputInds(j)}.size(1);
        end
    end
    for j=1:numLayers
        if(net.layerWeights{i,layerInds(j)}.size(1)>sizeRows)
            sizeRows = net.layerWeights{i,layerInds(j)}.size(1);
        end
    end
    w = initw2(i);
    if net.biasConnect(i)
        b = rands(net.layers{i}.size,1);
    end
end

for j=1:numInputs

```

```

    net.IW{i,inputInds(j)} =
w(1:net.inputWeights{i,inputInds(j)}.size(1),inputStart(j):inputStop(j));
end
for j=1:numLayers
    net.LW{i,layerInds(j)} =
w(1:net.layerWeights{i,layerInds(j)}.size(1),layerStart(j):layerStop(j));
end
if net.biasConnect(i)
    net.b{i} = b;
end

%=====
function [w,b]=calcnw(pr,s,n,i)
%CALCNW Calculates Nuyen-Widrow initial conditions.
%
% PR
% S - Number of neurons.
% N - Active region of transfer function N = [Nmin Nmax].

r = size(pr,1);

% Null case
% -----

if (r == 0) || (s == 0)
    w = zeros(s,r);
    b = zeros(s,1);
return

```

```

end

% Remove constant inputs that provide no useful info
% -----

R = r;
ind = find(pr(:,1) ~= pr(:,2));
r = length(ind);
pr = pr(ind,:);

% Nguyen-Widrow Method
% -----

% Assume inputs and net inputs range in [-1 1].

% Weights
wMag = 0.7*s^(1/r);
wDir = initw2(i);
w = wMag*wDir;

% Biases
if (s==1)
    b = 0;
else
    b = wMag*linspace(-1,1,s)'.*sign(w(:,1));
end

```

```
% Conversions
```

```
% -----
```

```
% Conversion of net inputs of [-1 1] to [Nmin Nmax]
```

```
x = 0.5*(n(2)-n(1));
```

```
y = 0.5*(n(2)+n(1));
```

```
w = x*w;
```

```
b = x*b+y;
```

```
% Conversion of inputs of PR to [-1 1]
```

```
x = 2./(pr(:,2)-pr(:,1));
```

```
y = 1-pr(:,2).*x;
```

```
xp = x';
```

```
b = w*y+b;
```

```
w = w.*xp(ones(1,s),:);
```

```
% Replace constant inputs
```

```
% -----
```

```
ww = w;
```

```
w = zeros(s,R);
```

```
w(:,ind) = ww;
```

```
%=====
```

Subprogram 2 “Construction of Input and Output Matrixes”

```
load MFF
[us,minp,maxp,ys,mint,maxt] = prenmnx(u,y);
S=[4 10];
tr=400;
maxit=1;
Y1=zeros(maxit,tr);
Y2=zeros(maxit,length(us)-tr);
Y3=zeros(maxit,tr);
Y4=zeros(maxit,length(us)-tr);
for it=1:maxit
net=newff(us(:,1:tr),ys(1,1:tr),S);
net.trainParam.epochs = 50;
net = train(net,us(:,1:tr),ys(1,1:tr));
y1=sim(net,us(:,1:tr));
y2=sim(net,us(:,tr+1:end));
Y=[y1 y2];
[ytr,yte,Ytr,Yte]=trtest(us,ys,Y,tr,index_matrix);
Y1(it,:)=ytr;
Y2(it,:)=yte;
Y3(it,:)=Ytr;
Y4(it,:)=Yte;
end
[MSEtr,RMSEtr,Rtr,ytr,Ytr]=Plot(Y1,Y3,'train','SF performance');
figure(2)
```

```

[MSEte,RMSEte,Rte,yte,Yte]=Plot(Y2,Y4,'valid','SF performance');
plotregression1(ytr,Ytr,'training');
plotregression1(yte,Yte,'valid');
MSEtr
RMSEtr
Rtr
MSEte
RMSEte
Rte

```

Subprogram 3 “Sort Data”

```

% -----
%           sort data
% -----

% -----creat matrix 45*240 that matrix is sort-----
function [m,n]=d_sort(u,y,index_matrix)
u=[u;y];
i=0;
ii=0;
W=0;
for ii=1:6           % for each input
    for i=1:27       % for each section of the each input
        W(i,1+((ii-1)*40):40+((ii-1)*40))=u(ii,1+((i-1)*40):40+((i-1)*40));
    end
end

```

```

    end
end
% -----create matrix 25*240 that matrix is desort-----
A=0;
H=0;
Z=0;
for ii=1:6          %for each input
    for i=1:27      %for select the each section that confirm the column of the V
        A=index_matrix(i,1+((ii-1)*40):40+((ii-1)*40));
        H=W(i,1+((ii-1)*40):40+((ii-1)*40));
        Z(i,1+((ii-1)*40):40+((ii-1)*40))=desort(A,H);
    end
end
% -----creat the desort data matrix-----
for ii=1:6          %for each input
    for i=1:27      %for select the each section that confirm the column of the V
        k=i;
        for j=1:40  %for each section that confirm the row of the V
            u(ii,k)=Z(i,j+((ii-1)*40));
            k=k+27;
        end
    end
end
end
m=u(1:5,1:1000);
n=u(6,1:1000);

```

Subprogram 4 “PSO algorithm”

```
%      PSO Algorithm
function [x,w]=PSO(U,Y,S)
%===== find the number of parameter =====
b=0;
d=0;
[nu,m]=size(U);
for i=1:1+length(S)
    if i==1
        b=b+S(1,i).*nu;
    end
    if i==length(S)+1
        c=S(1,i-1);
    end
    if i~=1 && i~=length(S)+1
        d=d+S(1,i-1).*S(1,i);
    end
end
np=b+c+d;
%_____
%      I. Setup the PSO
npar=np;      % number of optimization variables

%_____
%      II. Stopping criteria
```

```

maxit=1;          % max number of iterations
mincost=-9999999; % minimum cost
xmax=1;
xmin=-1;
% _____
%           III. PSO parameters
popsize=40;      % set population size
mutrate=.02;     % set mutation rate
selection=0.5;   % fraction of population kept
nbits=8;        % number of bits in each parameter
Nt=nbits*npar;  % total number of bits in a chromosome
keep=floor(selection*popsize); % #population members that survive

% _____
%           Create the initial population
iga=0;          % generation counter initialized
pop=round(rand(popsize,Nt)); % random population of 1s and 0s
par=gadecode(pop,xmin,xmax,nbits); % convert binary to continuous values
cost=My_Fun(par,U,Y,S,xmax,xmin); % calculates population cost
[cost,ind]=sort(cost); % min cost in element 1
par=par(ind,:); pop=pop(ind,:); % sorts population with lowest cost first
minc(1)=min(cost); % minc contains min of population
meanc(1)=mean(cost); % meanc contains mean of population

% _____
%           Iterate through generations
while iga<maxit

```

```

iga=iga+1;          % increments generation counter

% _____
%          Pair and mate
M=ceil((popsize-keep)/2);    % number of matings
prob=flipud((1:keep)/sum(1:keep)); % weights chromosomes based upon position in list
odds=[0 cumsum(prob(1:keep))]; % probability distribution function
pick1=rand(1,M);           % mate #1
pick2=rand(1,M);           % mate #2

% ma and pa contain the indicies of the chromosomes that will mate
ic=1;
while ic<=M
  for id=2:keep+1
    if pick1(ic)<=odds(id) & pick1(ic)>odds(id-1)
      ma(ic)=id-1;
    end % if
    if pick2(ic)<=odds(id) & pick2(ic)>odds(id-1)
      pa(ic)=id-1;
    end % if
  end % id
  ic=ic+1;
end % while

% _____
%          Performs mating using single point crossover
ix=1:2:keep;           % index of mate #1

```

```

xp=ceil(rand(1,M)*(Nt-1));           % crossover point
pop(keep+ix,:)=pop(ma,1:xp) pop(pa,xp+1:Nt); % first offspring
pop(keep+ix+1,:)=pop(pa,1:xp) pop(ma,xp+1:Nt); % second offspring

% _____
%           Mutate the population
nmut=ceil((popsize-1)*Nt*mutrate); % total number of mutations
mrow=ceil(rand(1,nmut)*(popsize-1))+1; % row to mutate
mcol=ceil(rand(1,nmut)*Nt); % column to mutate
for ii=1:nmut
    pop(mrow(ii),mcol(ii))=abs(pop(mrow(ii),mcol(ii))-1); % toggles bits
end % ii

% _____
% The population is re-evaluated for cost
par(2:popsize,:)=gadecode(pop(2:popsize,:),xmin,xmax,nbits); % decode
cost(2:popsize)=My_Fun(par(2:popsize,:),U,Y,S,xmax,xmin);

% _____
%           Sort the costs and associated parameters
[cost,ind]=sort(cost);
par=par(ind,:); pop=pop(ind,:);

% _____
%           Do statistics for a single nonaveraging run
minc(iga+1)=min(cost);
meanc(iga+1)=mean(cost);

```

```

% _____
%           Stopping criteria
if iga>maxit | cost(1)<mincost
    break
end

[iga cost(1)];

end %iga

% _____
%           Displays the output
% day=clock;
% disp(datestr(datenum(day(1),day(2),day(3),day(4),day(5),day(6)),0))
% disp(['optimized function is ' ff])
% format short g
% disp(['popsize = ' num2str(popsize) ' mutrate = ' num2str(mutrate) ' # par = ' num2str(npar)])
% disp(['#generations=' num2str(iga) ' best cost=' num2str(cost(1))])
% disp(['best solution'])
% disp([])
% disp('binary genetic algorithm')
% disp(['each parameter represented by ' num2str(nbits) ' bits'])
% figure(24)
% iters=0:length(minc)-1;
% plot(iters,minc,iters,meanc,'--');
% xlabel('generation');ylabel('cost');

```

```

% text(0, minc(1), 'best'); text(1, minc(2), 'population average')
x=par(1,:);
y=zeros(1,np);
y(1,1:np)=x;
y(1,np+1)=xmax;
y(1,np+2)=xmin;
x=mapminmax(y);
x=x(1,1:np);
w=zeros(1,maxit);
w=minc;
end

```

Subprogram 5 “ PSO function”

```

function z = PSO_fun(U,Y,S)
net=newffl(U,Y,S);
net.trainParam.epochs = 50;
net = train(net,U,Y);
y = sim(net,U);
e=zeros(1,length(y));
a=0;
for i=1:length(y)
    e(1,i)=Y(1,i)-y(1,i);
    a=a+e(1,i).^2;
end
z=0.5.*a;

```

end

Subprogram 6 “ ANN Structure”

```
load MFF
[us,minp,maxp,ys,mint,maxt] = premmx(u,y);
S=[7];
tr=400;
save us ys S
%%
tic
%%
maxit=10;
Y1=zeros(maxit,tr);
Y2=zeros(maxit,length(us)-tr);
Y3=zeros(maxit,tr);
Y4=zeros(maxit,length(us)-tr);
for it=1:maxit
net=newff(us(:,1:tr),ys(1,1:tr),S);
net.trainParam.epochs = 45;
net = train(net,us(:,1:tr),ys(1,1:tr));
y1=sim(net,us(:,1:tr));
y2=sim(net,us(:,tr+1:end));
Y=[y1 y2];
[ytr,yte,Ytr,Yte]=trtest(us,ys,Y,tr,index_matrix);
```

```

Y1(it,:)=ytr;
Y2(it,:)=yte;
Y3(it,:)=Ytr;
Y4(it,:)=Yte;
end
[MSEtr,RMSEtr,Rtr,ytr,Ytr]=Plot(Y1,Y3,'Training data,');
figure(2)
[MSEte,RMSEte,Rte,yte,Yte]=Plot(Y2,Y4,'Testing Data,');
plotregression1(ytr,Ytr,'Train');
plotregression1(yte,Yte,'Test');
MSEtr
RMSEtr
Rtr
MSEte
RMSEte
Rte

```

Subprogram 7“Output Plots”

```

function result = plotregression(varargin)
%PLOTREGRESSION Plot linear regression.
%
% Syntax
%
% plotreg(targets,outputs)

```

```

% plotreg(targets1,outputs1,'name1',targets,outputs2,'name2', ...)
%
% Description
%
% PLOTREGRESSION(TARGETS,OUTPUTS) plots the linear regression
% of TARGETS relative to OUTPUTS.
%
% PLOTREGRESSION(TARGETS1,OUTPUTS2,'name1',...) generates multiple plots.
%
% Example
%
% load simplefit_dataset
% net = newff(simplefitInputs,simplefitTargets,20);
% [net,tr] = train(net,simplefitInputs,simplefitTargets);
% simplefitOutputs = sim(net,simplefitInputs);
% plotregression(simplefitTargets,simplefitOutputs);
%
% See also plottrainstate

% Copyright 2007-2008 The MathWorks, Inc.

if nargin < 1, error('NNET:Arguments','Not enough input arguments.');
```

```

%% Info
if (nargin == 1) && strcmp(varargin{1},'info')
    info.name = mfilename;
    info.title = 'Regression';

```

```

info.type = 'Plot';
info.version = 6;
result = info;
return;
end

```

```

if nargin < 2, error('NNET:Arguments','Incorrect number of input arguments'); end

```

```

%% Plot

```

```

if ~isa(varargin{1},'network')

```

```

    % User arguments - New plot

```

```

    count = round(nargin/3);

```

```

    tt = cell(1,count);

```

```

    yy = cell(1,count);

```

```

    names = cell(1,count);

```

```

    for i=1:count

```

```

        tt{i} = varargin{i*3-2};

```

```

        yy{i} = varargin{i*3-1};

```

```

        if nargin >= (i*3)

```

```

            names{i} = varargin{i*3};

```

```

        else

```

```

            names{i} = 'Regression';

```

```

            if (count > 1), names{i} = [names{i} ' ' num2str(i)]; end;

```

```

        end

```

```

    end

```

```

    fig = new_figure("");

```

```

else

```

```

% Standard Plotting Function Arguments - Recycle plot
[net,tr,signals] = deal(varargin{:});
tt={};
yy={};
names = {};
for i=1:length(signals)
    signal = signals{i};
    if ~isempty(signal.indices)
        tt = [tt {signal.T}];
        yy = [yy {signal.Y}];
        names = [names {signal.name}];
    end
end
if length(names) > 1
    tt = [tt {cell2mat([tt{:}])}];
    yy = [yy {cell2mat([yy{:}])}];
    names = [names {'All'}];
end
fig = nn_find_tagged_figure(mfilename);
if isempty(fig), fig = new_figure(mfilename); end
end
update_figure(fig,tt,yy,names);
if (nargout > 0), result = fig; end

%% New Figure
function fig = new_figure(tag)

```

```

fig = figure;
ud.numSignals = 0;

set(fig,'name','Regression (plotregression1)');
% set(fig,'menubar','none','toolbar','none','NumberTitle','off');
set(fig,'tag',tag,'UserData',ud)

%% Update Figure
function update_figure(fig,tt,yy,names)

ok = check_data(tt,yy,names);
if ok
    plot_figure(fig,tt,yy,names);
else
    clear_figure(fig);
end

%% Plot Figure
function plot_figure(fig,tt,yy,names)

trainColor = [0 0 1];
valColor = [0 1 0];
testColor = [1 0 0];
allColor = [1 1 1] * 0.4;
colors = {trainColor valColor testColor allColor};

set(0,'CurrentFigure',fig);

```

```

ud = get(fig,'userdata');

numSignals = length(names);

% Create axes
if (ud.numSignals ~= numSignals)
    clf(fig);
    set(fig,'nextplot','replace');

    ud = struct;
    ud.numSignals = numSignals;

    plotcols = ceil(sqrt(numSignals));
    plotrows = ceil(numSignals/plotcols);

    for plotrow=1:plotrows
        for plotcol=1:plotcols
            i = (plotrow-1)*plotcols+plotcol;
            if (i<=numSignals)

                a = subplot(plotrows,plotcols,i);
                set(a,...
                    'dataaspectratio',[1 1 1], ...
                    'box','on');
                xlabel(a,'Experimental');
                hold on
                ud.axes(i) = a;
            end
        end
    end
end

```

```

ud.eqLine(i) = plot([NaN NaN],[NaN NaN],':k');
color = colors{rem(i-1,length(colors))+1};
ud.regLine(i) = plot([NaN NaN],[NaN NaN],'linewidth',2,'Color',color);
ud.dataPoints(i) = plot([NaN NaN],[NaN NaN],'ok');
legend([ud.dataPoints(i),ud.regLine(i),ud.eqLine(i)], ...
    {'Data','Fit','Y = T'},'Location','NorthWest');

end

end

end

set(fig,'UserData',ud)
set(fig,'nextplot','new');

screenSize = get(0,'ScreenSize');
screenSize = screenSize(3:4);
windowSize = 400 * [1 (plotrows/plotcols)];
pos = [(screenSize-windowSize)/2 windowSize];
set(fig,'position',pos);
drawnow
end

% Fill axes
for i=1:numSignals
    set(fig,'CurrentAxes',ud.axes(i));

```

```

y = yy{i}; if iscell(y), y = cell2mat(y); end, y = y(:)';
t = tt{i}; if iscell(t), t = cell2mat(t); end, t = t(:)';
name = names{i};

[m,b,r] = postreg(y,t,'hide');
lim = [min([y t]) max([y t])];
line = m*lim + b;

set(ud.dataPoints(i),'xdata',t,'ydata',y);
set(ud.regLine(i),'xdata',lim,'ydata',line)
set(ud.eqLine(i),'xdata',lim,'ydata',lim);

set(gca,'xlim',lim);
set(gca,'ylim',lim);
axis('square')

ylabel('GA-ANN Output');
title([name ': R=' num2str(r)])
end

drawnow

%% Clear Figure
function clear_figure(fig)

ud = get(fig,'userdata');

```

```
for i=1:3
    set(ud.dataPoints(i),'xdata',[NaN NaN],'ydata',[NaN NaN]);
    axisi = ud.axes(i);
    set(axisi,'xlim',[0 1]);
    set(axisi,'ylim',[0 1]);
end
```

```
%set(ud.warning1,'visible','on');
%set(ud.warning2,'visible','on');
```

```
drawnow
```

```
%% Check Data
```

```
function ok = check_data(tt,yy, names)
```

```
ok = true;
```

```
return
```

```
for i=1:length(signals)
```

```
    signal = signals{i};
```

```
    y = signal.Y;
```

```
    t = signal.T;
```

```
    [yS,yTS] = size(y);
```

```
    [tS,tTS] = size(t);
```

```

if (yS ~= tS), ok = false; end
if (yTS ~= tTS), ok = false; end

[yrows,ycols] = size(y{1});
[trows,tcols] = size(t{1});
if (trows ~= yrows), ok = false; end
if (tcols ~= ycols), ok = false; end
for i=2:yTS
    [yrowsi,ycolsi] = size(y{2});
    [trowsi,tcolsi] = size(t{2});
    if (yrowsi ~= yrows), ok = false; end
    if (ycolsi ~= ycols), ok = false; end
    if (trowsi ~= yrows), ok = false; end
    if (tcolsi ~= ycols), ok = false; end
end
end
end

```

Bibliography

Abdalla, A., Coats, K. H., A three phase experimental and numerical simulation on study of the steam flood process, Proceedings of the *Fall Meeting of the SPE of AIME*, New Orleans, 3-6 October 1971.

Adams, J., Stress-relief buckles in McFarland Quarry, Ottawa, *Canadian Journal of Earth Sciences*, vol. **19**, pp. 1883–1887, 1982.

Aguilar, E.G., Gonzalez, L.M., and Ruiz. V.G., Initial characterization of an extra heavy oil carbonate exploratory field, Paper SPE 153534 presented at the *SPE Latin American and Caribbean Petroleum Engineering Conference*, Mexico City, Mexico, 16–18 April 2012.

Ahmadi, M.A., Zendehboudi, S., Lohi, A., Elkamel, A., and Chatzis, I., Reservoir permeability prediction by neural networks combined with hybrid genetic algorithm and particle swarm optimization, *Geophysical Prospecting*, doi: 10.1111/j.1365-2478.2012.01080.x, **2012**.

Aitken, C.M., Jones, D.M., Larter, S.R., Anaerobic hydrocarbon biodegradation in deep subsurface oil reservoirs, *Nature*, vol. **431**, pp. 291–294, 2004.

Akbar, M., and Sapru, A., In situ stresses in the subsurfaces of Arabian Peninsula and their effect on fracture morphology and permeability, *6th Abu-Dhabi International Petroleum Exhibition and Conference*, Abu-Dhabi, UAE, 1994.

Akin, S., and Bağcı, S., A laboratory study of single-well steam-assisted gravity drainage process, *Journal of Petroleum Science and Engineering*, vol. **32**, pp. 23–33, 2001.

Akin, S., Bağcı, S., and Kok, M.V., Dry forward combustion with diverse well configurations, SPE Paper 62551 presented at *SPE/AAPG Western Regional Meeting, Long Beach, California*, 19-23 June 2000.

Akin, S., Kok, M.V., Bağci, S., and Karacan, O., Oxidation of heavy oil and their SARA fractions: Its role in modelling in-situ combustion, Paper SPE Paper 63230 presented at *2000 SPE Annual Technical Conference and Exhibition*, Dallas, Texas, 1-4 October 2000.

Aktan, T., and Farouq Ali, S.M., Finite element analysis of temperature and thermal stresses induced by hot water injection, *SPE Journal*, vol. **18**, no. 6, pp. 457–469, 1978.

Al-Adawy, M.S., and Nandyal, M., Status and scope for EOR development in Oman, Paper SPE 21407 presented at the *SPE Middle East Oil Show*, Bahrain, 2-5 March 1991.

Al-Aulaqi, T., Grattoni, C., Fisher, Q., Musina, Z., and Al-Hinai, S., Effect of temperature, oil asphaltene content, and water salinity on wettability alteration. Paper SPE 149071 presented at the *SPE/DGS Saudi Arabia Section Technical Symposium and Exhibition*, Al-Khobar, Saudi Arabia, 15-18 May 2011.

Alavi, M., Regional stratigraphy of the Zagros fold-thrust belt of Iran and its proforeland evolution, *American Journal of Science*, vol. **304**, pp. 1–20, 2004.

Alberta Energy Resources Conservation Board (AERCB): *ST98-2010: Alberta's Energy Reserves 2009 and Supply/Demand Outlook 2010-2019*, p. 232, June 2010.

Alberta Energy Resources Conservation Board: *ST98-2009: Alberta's Energy Reserves 2008 and Supply/Demand Outlook 2009-2018*, Energy Resources Conservation Board, Calgary, AB, Canada, p. 220, 2009.

Al-Hadhrami, H.S., and Blunt, M.J., Thermally induced wettability alteration to improve oil recovery in fractured reservoirs, Paper SPE 59289 presented at the *2000 SPE/DOE Improved Oil Recovery Symposium*, Tulsa, Oklahoma, 3-5 April, 2000.

Al-Husseini, M.I., Origin of the Arabian plate structures: Amar Collision and Najd Rift, *GeoArabia*, vol. **5**, no. 4, pp. 527–542, 2000.

Al-Laboun, A.A., Stratigraphy and hydrocarbon potential of the Paleozoic succession in both the Tabuk and Widyan basins, Arabia, In M. T. Halbouty (Ed.), *Future petroleum provinces of the world*, AAPG Memoir 40, 1986.

Al-Qabandi, S., Al-Shatti, Y., and Gopalakrishnan, P., Commercial heavy oil recovery by cyclic steam stimulation in Kuwait, SPE paper 30288 presented at the *SPE International Heavy Oil Symposium*, Calgary, Alberta, Canada, 19-21 June 1995.

Alsharhan, A.S., and Nairn, A.E.M., *Sedimentary basins and petroleum geology of the Middle East*, Elsevier Science, p. 878, 1997.

Al-Shizawi, A., Denby, P.G., and Marsden, G., Heat-front monitoring in the Qarn Alam thermal GOGD pilot, Paper SPE 37781 presented at the *1997 Middle East Oil Show*, Bahrain, 15-18 March 1997.

Altgelt, K.H., and Boduszynski, M.M., Composition of heavy petroleum. 3. An improved boiling point–molecular weight relation, *Energy Fuels*, vol. 6, no. 1, pp. 68–72, 1992.

Alvarado, V., Ranson, A., Hernandez, K., Manrique, E., Matheus, J., Prospero, N., and Liscano, T., Selection of EOR/IOR opportunities based on machine learning. Proceedings of the *13th SPE European Petroleum Conference*, Aberdeen, October 29-31, 2002.

Alvarez, J.M., Sawatzky, R.P., Forster, L.M., and Coates, R.M., Alberta's bitumen carbonate reservoirs—moving forward with advanced R&D, Paper 2008-467 presented at the *World Heavy Oil Congress*, Edmonton, Canada, 10-12 March 2008.

Aminzadeh, F., and De Groot, P., *Neural networks and other soft computing techniques with applications in the oil industry*, 1st Ed, EAGE Publications, 2006.

Anderson, C.A., and Bridwell, R.J., A finite element method for studying the transient non-linear thermal creep of geological structures, *International Journal of Numerical & Analytical Methods in Geomechanics*, vol. 4, pp. 255–276, 1980.

Anderson, C.A., *Finite element modeling of long-term fluid-structure interaction problems in geologic media*, Los Alamos National Laboratory, LA-UR-79-3016, 1979.

Andersson, S.-I., and Myrstad, T., Evaluation of residue FCC Catalysts, *Applied Catalysis A: General*, vol. 170, no. 1, pp. 59–71, 1998.

Araújo, J.S., Vieira, M.M., and Bezerra, F.H.R., Influence of tectonic stresses in the permeability of petroliferous reservoir in Potiguar Basin, Brazil, *2009 SPE Latin American and Caribbean Petroleum Engineering Conference*, Cartagena, Colombia.

Ashrafi, M., Souraki, Y., Karimaie, H., and Torsaeter, O., Experimental and numerical study of steam flooding in fractured porous media, *Proceedings of the SPE Western North American Regional Meeting, Anchorage, Alaska, USA; 7-11 May 2011*.

ASTM: *Annual Book of Standards*, American Society for Testing and Materials: Philadelphia, PA, Method D-2007, 1995.

Atashpaz-Gargari, E., and Lucas, C., Imperialist competitive algorithm: An algorithm for optimization inspired by imperialistic competition, *Proceedings of the IEEE Congress on Evolutionary Computation*, Singapore, pp. 4661–4667, 2007.

Aubourg, C., Smith, B., Eshraghi, A., Lacombe, O., Authemayou, C., Amrouch, K., Bellier, O., and Mouthereau, F., New magnetic fabric data and their comparison with palaeostress markers in the Western Fars Arc (Zagros, Iran): Tectonic implications, *The Geological Society of London, Special Publications*, vol. **330**, no. 1, pp. 97–120, 2010.

Ayasse, C., Bloomer, C., Lyngberg, E., Boddy, W., Donnelly, J., and M., Greaves, First field pilot of the THAI™ process, Paper 2005-142 presented at the *Petroleum Society's 6th Canadian International Petroleum Conference (56th Annual Technical Meeting)*, Calgary, Alberta, Canada, June 7-9, 2005.

Ayasse, C., Greaves, M., and Turta, A.X., Oilfield in situ hydrocarbon upgrading process, US Patent no. 6,412,557 B1, p. 14, 1998.

Bağcı, A.S., Seven-spot steam injection experiments in heavy oil reservoirs having a bottom water zone, *Energy & Fuels*, vol. **19**, no. 3, pp.1037–1046, 2005.

Bağcı, A.S., Shafiei, A., and Dusseault, M.B., Case histories for heavy oil recovery in naturally fractured carbonate reservoirs in the Middle East, *Proceedings of the 2nd World Heavy Oil Congress*, Edmonton, AB, Canada, March 10-12, 2008.

Bağci, S., and Gumrah, F., Effects of CO₂ and CH₄ addition to steam on recovery of West Kozluca heavy oil, Paper SPE 86953 presented at the *SPE International Thermal Operations and Heavy Oil Symposium and Western Regional Meeting*, Bakersfield, California, 16-18 March 2004.

Bağci, S., and Kok, M.V., Combustion reaction kinetics studies of Turkish crude oils, *Energy & Fuels*, vol. **18**, no. 5, pp. 1472-1481, 2004.

Bağci, S., Experimental and simulation studies of SAGD process in fractured reservoirs, Paper SPE 99920 presented at the *SPE/DOE Symposium on Improved Oil Recovery*, Tulsa, Oklahoma, 22-26 April 2006.

Bağci, S., Laboratory and simulation results of in-situ combustion for heavy oil recovery from Bati Kozluca field, Turkey, Paper 103 presented at *Offshore Mediterranean Conference and Exhibition*, Ravenna, Italy, March 28-30, 2007.

Bai, M., and Roegiers, J.-C., Fluid flow and heat flow in deformable fractured porous media, *International Journal of Engineering Science*, vol. **32**, no. 10, pp. 1615–1633, 1994.

Banks, D., Odling, N.E., Skarphagen, H., and Rohr-Torp, E., Permeability and stress in crystalline rocks, *Terra Nova*, vol. **8**, pp. 223–235, 1996.

Barge, D., Al-Yami, F., Uphold, D., Zahedi, A., Deemer, A., and Carreras, P.E, Steamflood piloting the Wafra field Eocene reservoir in the Partitioned Neutral Zone, between Saudi Arabia and Kuwait, *Proceedings of the SPE Middle East Oil and Gas Show and Conference*, Bahrain, 15-18 March 2009.

Barkved, O., Bartman, B., Compani, B., Gaiser, J., Van Dok, R., Kristiansen, P., Probert, T., and Thopson, M., The many facets of multicomponent seismic data, *Oilfield Review*, vol. **16**, no. 2, pp. 42–56, 2004.

Bartholomew, C.H., Mechanisms of catalyst deactivation, *Applied Catalysis A: General*, vol. **212**, no. 1-2, pp. 17–60, 2001.

- Barton, N., Bandis, S., Bakhtar, K., Strength, deformation and conductivity coupling of rock joints, *International Journal of Rock Mechanics and Mining Science & Geomechanics Abstracts*, vol. **22**, no. 3, pp. 121–140, 1985.
- Bashari, A., Occurrence of heavy crude oil in the Persian Gulf, ; *Fourth UNITAR/UNDP International Conference on Heavy Crude and Tar Sands*, pp. 203–214, Edmonton, AB, Canada, 7-12 August 1988.
- Becker, A., Bittmling, P., and Mler, W.H., Recent stress field and neotectonics in the Eastern Jura Mountains, Switzerland, *Tectonophysics*, vol. **135**, pp. 277–288, 1987.
- Bell, J.S., In situ stresses in sedimentary rocks (Part 1): Measurement techniques, *Geoscience Canada*, vol. **23**, no. 2, pp. 85–100, 1996a.
- Bell, J.S., In situ stresses in sedimentary rocks (Part 2): Applications of stress measurements, *Geoscience Canada*, vol. **23**, no. 3, pp. 135–153, 1996b.
- Berbrian, M., and King, G.C.P., Towards a paleogeography and tectonic evolution of Iran, *Canadian Journal of Earth Sciences*, vol. **18**, pp. 210–265, 1981.
- Bergman, M.S., Special Session E: Nuclear Waste Disposal in Proceedings International Symposium on Subsurface Space (Rockstore '80), Stockholm, Sweden, June, vol. 2, pp. 789–1005, Pergamon Press, New York, 1980.
- Bertram, L.A., *Mechanics analysis for deep rock disposal of radioactive wastes*, Sandia National Laboratories, Albuquerque, SA ND-76-007, 1976.
- BGR (Federal Institute for Geoscience and Natural Resources): *Energierohstoffe 2009 (Reserves, Resources and Availability of Energy Resources)*, Hannover, Germany, p. 288, 2009.
- Biot, M.A., General solutions of the equations of elasticity and consolidation for a porous material, *Journal of Applied Physics*, vol. **78**, pp. 91–96, 1956.
- Biot, M.A., General theory of 3-D consolidation, *Journal of Applied Physics*, vol. **12**, pp. 155–164, 1941.

Biot, M.A., Theory of elasticity and consolidation for a porous anisotropic solid, *Journal of Applied Physics*, vol. **26**, no. 2, pp. 182–185, 1955.

Boberg, T.C., *Thermal methods of oil recovery*, Wiley, New York, 1988.

Boduszynski, M.M., and Altgelt, K.H., Composition of heavy petroleum. 4. Significance of the extended atmospheric equivalent boiling point (AEBP) scale, *Energy & Fuels*, vol. **6**, no. 1, pp. 72–76, 1992.

Boduszynski, M.M., Composition of heavy petroleums. 1. Molecular weight, hydrogen deficiency, and heteroatom concentration as a function of atmospheric equivalent boiling point up to 1400 °F (760 °C), *Energy & Fuels*, vol. **1**, no. 1, pp. 2–11, 1987.

Boduszynski, M.M., Composition of heavy petroleums. 2. Molecular characterization, *Energy & Fuels*, vol. **2**, no. 5, pp. 597–613, 1988.

Boley, B.A., and Weiner, J.H., *Theory of thermal stresses*, John Wiley & Sons, New York, 1960.

Bordenave, M.L., and Burwood, R., Source rock distribution and maturation in the Zagros belt; provenance of the Asmari and Bangestan reservoir oil accumulations, *Organic Geochemistry*, vol. **16**, pp. 369–387, 1990.

Bramley, M., Woynillowicz, D., and Neabel, D., *The climate implications of Canada's oil sands development (Backgrounder)*, A report published by the Pembina Institute, p. 15, 2005.

Bredehoeft, J., Wolff, R., Keys, W., and Shuter, E., Hydraulic fracturing to determine the regional in situ stress field, Piceance Basin, Colorado, *GSA Bulletin*, vol. **87**, pp. 250–258, 1976.

Breston, J.N., Oil Recovery by heat from in situ combustion, *Journal of Petroleum Technology*, vol. **10**, no. 8, pp. 13–17, 1958.

Briggs, P.J., A Simulator for the recovery of heavy oil from naturally fractured reservoirs using cyclic steam injection, Paper SPE 17954 presented at the *Middle East Oil Show*, Bahrain, 11-14 March 1989.

Briggs, P.J., Baron, R.P., Fulleylove, R.J., and Wright, M.S., *Development of heavy oil reservoirs*, *Journal of Petroleum Technology*, vol. **40**, no. 2, pp. 206–214, 1988.

Briggs, P.J., Beck, D.L., Black, C.J.J., and Bissell, R., Heavy oil from fractured carbonate reservoirs, *Journal of SPE Reservoir Engineering*, vol. **7**, no. 2, pp. 173–179, 1992.

Brooks, R.H., and Corey, A.T., *Hydraulic properties of porous media*, Colorado State University, p. 27, 1964.

Brown, J., Deemer, A., Al-Dhafeeri, F., Lekia, S., Hoadley, S., Al-Mutairi, G., Al-Yami, F., and Barge, D., Early results from a carbonate steamflood pilot in 1st Eocene reservoir, Wafra field, PZ. *SPE Heavy Oil Conference and Exhibition*, Kuwait City, Kuwait, 12-14 December 2011.

Brown, M., and Harris, C., *Neurofuzzy adaptive modeling and control*, 2nd ed., Englewood Cliffs, Prentice-Hall, 1994.

Bursell, C.G., Pittman, G.M., Performance of steam displacement in the Kern River field, *Journal of Petroleum Technology*, vol. **27**, no. 8, pp. 997–1004, 1975.

Buschkuehle, B.E., Hein, F.J., and M., Grobe, An overview of the geology of the upper devonian Grosmont carbonate bitumen deposit, Northern Alberta, Canada, *Natural Resources Research*, vol. **16**, no. 1, pp. 3–15, March 2007.

Butler, R.M., and Mokrys, I.J., Solvent analog model of steam assisted gravity drainage, *AOSTRA Journal of Research*, vol. **5**, no. 1, pp. 17–32, 1989.

Butler, R.M., and Stephens, D.J., The gravity drainage of steam heated to parallel horizontal wells, *Journal of Canadian Petroleum Technology*, vol. **20**, no. 2, pp. 90–96, 1981.

Butler, R.M., Rise of interfering steam chambers, *Journal of Canadian Petroleum Technology*, vol. **26**, no. 3, pp. 70–75, 1987.

Butler, R.M., Stephens, D.J., The gravity drainage of steam heated heavy oil to parallel horizontal wells. Paper presented at the *31st Annual Technical Meeting of The Petroleum Society of CIM*, Calgary, May 25–28, 1980.

Butler, R.M., The expansion of tar sands during thermal recovery, *Journal of Canadian Petroleum Technology*, vol. **25**, no. 5, pp. 51–56, 1986.

Butler, R.M., *Thermal recovery of oil and bitumen*, Prentice Hall, New Jersey, 1991.

Caldwell, J., Christie, P., Engelmark, F., McHugo, S., Özdemir, H., Kristiansen, P., and MacLeod, M., Shear Waves Shine Brightly, *Oilfield Review*, vol. **11**, no. 1, pp. 2–15, 1999.

Canadian Association of Petroleum Producers (CAPP), *2009 CAPP crude oil forecast markets & pipeline report*, p. 48, 2009, available online at <http://www.capp.ca>

Canadian Association of Petroleum Producers (CAPP), *Canadian crude oil forecast, markets and pipelines EDMS-#190838-v2-2011-2025*, p. 40, 2011, Available at <http://www.capp.ca>

Canbolat, S., Akin, S., and Kovscek, A.R., Noncondensable gas steam assisted gravity drainage, *Journal of Petroleum Sciences and Engineering*, vol. **45**, no. 1-2, pp. 83–96, 2004.

Carlson, M.R., An analysis of the caprock failure at Joslyn, Paper SPE 156962-MS presented at the *SPE Heavy Oil Conference*, Calgary, Alberta, Canada, 12-14 June 2012.

Castiñeira, O.C., del Rey, D.B., and León, J.H., Main electrofacies in carbonates of the heavy crudes Northern Belt of Cuba, *SPWLA 47th Annual Logging Symposium*, June 4-7, 2006.

Chalaturmyk, R.J., Scott, J.D., Geomechanics issues of steam assisted gravity drainage, Paper SPE 30280 presented at the *International Heavy Oil Symposium*, Calgary, AB, Canada, 19-21 June, 1995.

Chalaturnyk, R., *Geomechanics of the steam assisted gravity drainage process in heavy oil reservoirs*, Ph.D. thesis, Department of Civil Engineering, University of Alberta, Edmonton, Alberta, p. 576, 1996.

Chalaturnyk, R.J., Li, P., When is it important to consider geomechanics in SAGD operations?, *Journal of Canadian Petroleum Technology*, vol. **43**, no. 4, pp. 53–61, 2004.

Chalaturnyk, R.J., Scott, J.D., and Yang, G., Geomechanical modeling of phase A at the AOSTRA Underground Test Facility, Paper 91-7, Petroleum Society Annual Conference, Banff, AB, Canada, April 21-24, 1991.

Charpentier, A.D., Bergerson, J.A., and MacLean, H.L., Understanding the Canadian oil sand industry's greenhouse gas emissions, *Environmental Research Letters*, vol. **4**, p. 11, January-March 2009.

Chattopadhyay, S.K., Ram, B., Bhattacharya, R.N., and Das, T.K., Enhanced oil recovery by in situ combustion process in Santhal field of Cambay Basin, Mehsana, Gujarat, India - A Case study, Paper SPE 89451 presented at the *2004 SPE/DOE Fourteenth Symposium on Improved Oil Recovery*, Tulsa, Oklahoma, U.S.A., 17-21 April 2004.

Chen, P.Y.P., Transient thermal stresses in a rectangular plate due to non-uniform heat transfer coefficients, *Journal of Thermal Stresses*, vol. **11**, pp. 115–125, 1988.

Chen, S.-L., Jia, S.-S., Luo, Y.-H., and Zhao, S.-O., Mild cracking solvent deasphalting: A new method for upgrading petroleum residue, *Fuel*, vol. **73**, no. 3, pp. 439–442, 1994.

Chen, W.T., Plane thermal stress at an insulated hole under uniform heat flow in an orthotropic medium, *Journal of Applied Mechanics*, vol. **34**, pp. 133–136, 1967.

Chen, Z., *Finite element methods and their applications*, Springer, New York, 2005.

Chierici, A., Delle Canne, D., and Properzi, O., Steam drive in a fractured carbonate: The Vallecupa, Italy, pilot plant, *3rd European Meeting on Improved Oil Recovery*, Rome, April 16-18, 1985).

Cho, W.J., Kwon, S., Choi, J.W., The thermal conductivity for granite with various water contents, *Engineering Geology*, vol. **107**, pp. 167–171, 2009.

Chu, C., State-of-the-art review of steamflood field projects. *Journal of Petroleum Technology*, vol. **37**, no. 10, pp. 1887–1902, 1985.

Chu, C., Trimble, A.E., Numerical simulation of steam displacement - Field performance applications, *Journal of Petroleum Technology*, vol. **27**, no. 6, pp. 765–776, 1975.

- Chu, C.F., Prediction of steamflood performance in heavy oil reservoirs using correlations developed by factorial design method, Proceedings of the *South California Regional Meeting*, Ventura, California, 1990.
- Civan, F., Temperature dependence of wettability related rock properties correlated by the Arrhenius equation, *Petrophysics*, vol. **45**, no. 4, pp. 350–362, 2004.
- Clark, B., Graves, W.G., Lopez-de-Cardenas, J.E., Gurfinkel, M.E., and Peats, A.W., *Heavy oil*, working document of the NPC global oil & gas study, 2007.
- Clark, K.A., and Pasternack, D.S., Hot water separation of bitumen from Alberta bituminous sand, *Industrial & Engineering Chemistry*, vol. **24**, no. 12, pp. 1410–1416, 1932.
- Clark, P.D., Hyne, J.B., and Tyrer, J.D., Some chemistry of organosulphur compound types occurring in heavy oil sands. 2. Influence of pH on the high temperature hydrolysis of tetrahydrothiophene and thiophene, *Fuel*, vol. **63**, no. 1, pp. 125–125, 1984.
- Closmann, P.J., Waxman, M.H., Deeds, C.T., Steady-state tar/water relative permeabilities in Peace River cores at elevated temperature, *SPE Reservoir Engineering*, vol. **3**, no. 1, pp. 76–80, 1988.
- Clugston, D.M., George, A.E., Montgomery, D.S., Smiley, G.T., and Sawatzky, H., *Sulfur compounds in oils from the Western Canada tar belt*, Chapter 2 (Book), American Chemistry Society, Advances in Chemistry, Chapter 2, pp. 11–27, 1977.
- Coats, K.H., George, W.D., Chu, C., and Marcum, B.E., Three dimensional simulation of steamflooding, *SPE Journal*, vol. **14**, no. 6, pp. 573–592, 1974.
- Coats, K.H.A., A highly implicit steamflood model, *SPE Journal*, vol. **18**, no. 5, pp. 369–383, 1978.
- Collins, P.M., Carlson, M.R., Walters, D.A., Settari, A., Geomechanical and thermal reservoir simulation demonstrates SAGD enhancement due to shear dilation, Paper SPE 8237 presented at the *SPE/ISRM Rock Mechanics Conference*, Irving, Texas, October 20-23, 2002.

Collins, P.M., Dusseault, M.B., Dorscher, D., and Kueber, E., Implementing CHOPS in the Karazhanbas heavy oil field, Kazakhstan, Paper 500 presented in the *World Heavy Oil Congress*, Edmonton, AB, p. 17, 2008.

Collins, P.M., Geomechanical effects on the SAGD process, Paper SPE 97905 presented at the *2005 SPE International Thermal Operations and Heavy Oil Symposium*, Calgary, AB, Canada, 1-3 November 2005.

Collins, P.M., Geomechanical effects on the SAGD process. *SPE Reservoir Evaluation & Engineering*, vol. **10**, no. 4, pp. 367–375, 2007.

Collins, P.M., Injection pressures for geomechanical enhancement of recovery processes in the Athabasca oil sands, Paper SPE 79028 presented at the. *International Thermal Operations and Heavy Oil Symposium and International Horizontal Well Technology Conference*, Calgary, AB, Canada, November 4-7, 2002.

Colman-Saad, S.P., Fold development in Zagros simply folded belt, southwest Iran, *AAPG Bulletin*, vol. **62**, no. 6, pp. 984–1003, 1978.

Cornet, F.H., and Vallette, B., In situ stress determination from hydraulic injection test data, *Journal of Geophysical Research*, vol. **89**, no. B13, pp. 11527–11538, 1984.

Couderc, B.M., Verpeaux, J.F., Monfrin, D., and Guettler, L.H., Emeraude Vapeur: A steam pilot in an offshore environment, *SPE Reservoir Engineering*, vol. **5**, no. 4, pp. 508–516, 1990.

Cunha, L.C., Recent in situ oil recovery technologies for heavy and extra heavy oil reserves, Paper SPE 94986 presented at the *SPE Latin American and Caribbean Petroleum Engineering Conference*, Rio de Janeiro, Brazil, June 20-23, 2005.

Curiale, J.A., Harrison, W.E., and Smith, G., Sterane distribution of solid bitumen pyrolyzates. Changes with biodegradation of crude oil in Ouachita Mountains, Oklahoma, *Geochimica et Cosmochimica Acta*, vol. **47**, pp. 517–523, 1983.

- Curtis, C.W., Tsal, K.-J., and James, A.G., Effects of solvent composition on coprocessing coal with petroleum residua, *Fuel Processing Technology*, vol. **16**, no. 1, pp. 71–87, pp. 1987.
- Daneshy, A.A., Slusher, G.L., Chisholm, P.T., and Magee, D.A., In situ stress measurements during drilling, *Journal of Petroleum Technology*, vol. **38**, no. 3, pp. 891–898, 1986.
- Davidson, L.B., Miller, F.G., Mueller, T.D., A mathematical model of reservoir response during the cyclic injection of steam, *SPE Journal*, vol. **7**, no. 2, pp. 174–188, 1967.
- Davies, J.P., Davies, D.K., Stress-dependent permeability: Characterization and modeling, SPE Paper 56813 presented at the *1999 SPE Annual Technical Conference and Exhibition*, Houston, Texas, October 3–6, 1999.
- de Haan, H.J., and van Lookeren, J.A., Early results of the first large-scale steam soak project in the Tia Juana Field, Western Venezuela, *Journal of Petroleum Technology*, vol. **21**, no. 1, pp. 101–110, 1969.
- de Souto, M.C.P., Yamazaki, A., Ludernir, T.B., Optimization of neural network weights and architecture for odor recognition using simulated annealing, *Proceedings of the International Joint Conference on Neural Networks*, vol. **1**, pp. 547–552, 2002.
- Dehghani, K., and Ehrlich, R., Evaluation of the steam injection process in light oil reservoirs, *SPE Reservoir Evaluation & Engineering*, vol. **4**, no. 5, pp. 395–405, 2001.
- Dehghani, K., and Ehrlich, R., Evaluation of steam injection process in light oil reservoirs, *Proceedings of the SPE Annual Technical Conference and Exhibition*, New Orleans, Louisiana, September 27-30, 1998.
- Diabira, I., Castanier, L.M., Kovsky, A.R., Porosity and permeability evolution accompanying hot fluid injection into diatomite, *Petroleum Scieng & Technology*, vol. **19**, no. 9-10, pp. 1167–1185, 2001.

Dindoruk, B.; Firoozabadi, A. Computation of gas-liquid drainage in fractured porous media recognizing fracture liquid flow, *Journal of Canadian Petroleum Technology*, vol. **34**, no. 10, pp. 39–49, 1995.

Doan, D.H., Nauroy, J.-F., Baroni, A., Delage, P., Mainguy, M., Effect of temperature on ultrasonic velocities of unconsolidated sandstones reservoirs during the SAGD recovery process, Paper ARMA 10-195 presented at the *44th US Rock Mechanics Symposium and 5th U.S.-Canada Rock Mechanics Symposium*, Salt Lake City, UT, June 27-30, 2010.

Donaldson, A.B., and Donaldson, J.E., Dimensional analysis of the criteria for steam injection, Proceedings of the *1997 SPE Western Regional Meeting*, Long Beach, California, June 25-27, 1997.

Donnelly, J.K., and Pendergast, D.R., Nuclear energy in industry: Application to oil production, Paper presented in the *20th Annual Conference of the Canadian Nuclear Society*, Montréal, Québec, Canada, May 30-June 2, 1999.

Donmez, A., Investigation of the effect of temperature on heavy oil recovery by imbibition mechanism, Paper SPE 37555 presented at the *1997 SPE International Thermal Operations & Heavy Oil Symposium*, Bakersfield, California, February 10-12, 1997.

Dorogochinskaya, V.A., Shul'zhenko, É.D., Varshaver, V.P., Khabibulina, R.K., and Kochuleva, L.R., Oil from the Karazhanbas field, *Chemistry and Technology of Fuels and Oils*, vol. **25**, no. 1, pp. 46–47, 1989.

Dreher, K.D., Kenyon, D.E., Iwere, F.O., Heat flow during steam injection into a fractured carbonate reservoir, Proceedings of the *SPE/DOE Fifth Symposium on EOR of the SPE and the DOE*, Tulsa, April 20-23, 1986.

Dullien, F.A.L., *Porous media: Fluid transport and pore structure*, 2nd ed., Academic Press, San Diego, 1992.

Dusseault M.B., Zambrano A, Barrios J.R., and Guerra, C., *Estimating technically recoverable reserves in the Faja Petrolífera del Orinoco – FPO*, Paper 437 presented at the 2nd World Heavy Oil Congress, Edmonton, AB, Paper, p. 12, 2008.

Dusseault, M.B, Comparing Venezuelan and Canadian heavy oil and tar sands, Paper 2001-061 presented at the *Petroleum Society's Canadian International Petroleum Conference*, Calgary, Alberta, Canada, June 12-14, 2001.

Dusseault, M.B., and Scott, J.D., Tailings pond behaviour and characterization of oil sand tailings sludge, *Journal of Particulate Science and Technology*, vol. **1**, no. 3, pp. 295–309, 1984.

Dusseault, M.B., and Shafiei A., *Oil sands*, Ullmann's Encyclopedia of Chemical Engineering, Wiley, p. 52, 2011.

Dusseault, M.B., Bruno, M.S., Barrera, J., Casing shear: causes, cases, cures, *SPE Drilling and Completions Journal*, vol. **16**, no. 2, pp. 98–107, 2001.

Dusseault, M.B., *CHOPS*. SPE Petroleum Engineers Handbook, Chapter 5, Volume VI - Emerging and Peripheral Technologies (EMPT), Ed. Warner HR, p. 40, Society of Petroleum Engineers, Richardson, Texs, 2007.

Dusseault, M.B., Liang, C.X., Gu, W., Ma, Y.Q., and Xu, B.C., CHOPS in Jilin Province, China, Paper SPE 79032 presented at the *2002 SPE International Thermal Operations and Heavy Oil Symposium and International Horizontal Well Technology Conference*, Calgary, Alberta, Canada, November 4-7, 2002.

Dusseault, M.B., McLennan, J., Shu, J., Massive multi-stage hydraulic fracturing for oil and gas recovery from low mobility reservoirs in China, *Petroleum Drilling Techniques (Chinese Journal)*, vol. **39**, no. 3, pp. 6–16, 2011.

Dusseault, M.B., Oil recovery and technology sequencing, *Journal of Canadian Petroleum Technology*, vol. **47**, no. 4, 2008.

Dusseault, M.B., Oskui, R.P., Farhad, B., Al-Sammak, I., and Al-Naqi, A., Production technologies for Lower Fars heavy oil, Kuwait, Paper 4512 presented at the 2nd World Heavy Oil Congress, Edmonton, Alberta, Canada, p. 9, 2008.

Dusseault, M.B., Rothenburg, L., Shear dilatancy and permeability enhancement in oil sands, Paper presented at the *4th Unitar Conference on Heavy Crude and Tar Sands*, Edmonton, Alberta, vol. **3**, pp. 55–66, 1988.

Dusseault, M.B., *Screening criteria and technology sequencing for in situ viscous oil production*, In F.J. Hein, D. Leckie, S. Larter, and J. Suter, eds., Heavy oil and oil sand petroleum systems in Alberta and beyond: AAPG Studies in Geology, v. **64**, pp. 1–14, 2012.

Dusseault, M.B., Sequencing technologies to maximize recovery, Paper 2006-135 presented at the *7th Canadian International Petroleum Conference (57th Annual Technical Meeting)*, Calgary, AB, Canada, June 13-15, 2006.

Dusseault, M.B., Shand, D., Meling, T., Spanos, T., and Davidson, B.C., Field applications of pressure pulsing in porous media, Proceedings of the *2nd Biot Conference on Poromechanics*, Grenoble France, Balkema, Rotterdam, 2002.

Dusseault, M.B., Stress changes in thermal operations, Paper SPE 25809 presented at the *International Thermal Operations Symposium*, Bakersfield, California, U.S.A., February 8-10, 1993.

Dusseault, M.B., Wang, Y., and Simmons, J.V., Induced stresses near a fireflood front, *AOSTRA Journal of Research*, vol. **4**, no. 2, pp. 153–170, 1988.

Dusseault, M.B., Yin, S., Rothenburg, L., and Han, HX., Seismic monitoring and geomechanics simulation, *Leading Edge*, vol. **26**, pp. 610–620, 2007.

Eberhart, R.C., and Kennedy, J., A new optimizer using particle swarm theory, *Micro Machien and Human Science*, pp. 39–43, 1995.

Edmunds, N., and Peterson, J.A., A unified model for prediction of CSOR in steam based bitumen recovery, Proceedings of the *Petroleum Society's 8th CIPC*, Calgary, Alberta, Canada, June 12-14, 2007.

Elemo, R.O., and Elmtalab, J.A., Practical artificial intelligence application in EOR projects, Proceedings of the *1993 SPE Petroleum Computer Conference*, New Orleans, July 11-14, 1993.

El-M Shokir, E.M., Goda, H.M., Sayyounh, M.H., and Fattah, Kh., A selection and evaluation EOR method using artificial intelligence, Proceedings of the *SPE Annual International Conference and Exhibition*, Abuja, Nigeria, August 5-7, 2002.

Elsworth, D., Thermal permeability enhancement of blocky rocks: 1D flows, *International Journal of Rock Mechanics and Mining Science & Geomechanics Abstracts*, vol. **26**, no. 3-4, pp. 329–339, 1989.

Energy Resources Conservation Board, *ERCB Report 79-H: Alsands Fort McMurray Project*, Calgary, Canada, 1979.

Engelder, T., *Stress regimes in the lithosphere*, Princeton University Press, 1993.

Ershaghi, I., Reservoir engineering series, PE509, *Evaluation of naturally fractured reservoirs*, Manual: 132 pages, 83 illustrations, Videotape: 44 minutes, IHRDC publications.

Eschard, R., and Huc, A.Y., Habitat of biodegraded heavy oils: Industrial implications, *Oil & Gas Science and Technology – Rev. IFP*, vol. **63**, no. 5, pp. 587–607, 2008.

Evans, C.R., Rogers, M.A., and Bailey, N.J.L., Evolution and alteration of petroleum in Western Canada, *Chemical Geology*, vol. **8**, no. 3, pp. 147–170, 1971.

Faizov, Y., Levanyuk, O., Fu, D., Ivanova, O., Lungwitz B. and Mauth, K., Challenges and solutions of stimulating carbonate reservoirs in Timano-Pechora, Russia, OTC 22257 presented at the *Offshore Technology Conference*, Rio de Janeiro, Brazil, October 4-6, 2011.

Farouq Ali, S.M., and Meldau, R.F., Current steamflood technology, *Journal of Canadian Petroleum Technology*, vol. **31**, no. 10, pp. 1332–1342, 1979.

Farouq Ali, S.M., Current status of steam injection as a heavy oil recovery method, *Journal of Canadian Petroleum Technology*, vol. **13**, no. 1, pp. 54–68, 1974.

Farouq Ali, S.M., Steam injection theory - A unified approach, Paper SPE 10746 presented at the *California Regional Meeting of the Society of Petroleum Engineers*, San Francisco, March 24-26, 1982.

Ferrer, J.C., and Farouq Ali, S.M., A Three phase 2-D compositional thermal simulator for steam injection processes, *Journal of Canadian Petroleum Technology*, vol. 16, no. 1, pp. 78–90, 1977.

Firoozabadi, A., *Thermodynamics of hydrocarbon reservoirs*, 1st ed, McGraw-Hill, New York, 1999.

Florence, A.L., and Goodier, J.N., Thermal stress at spherical cavities and circular holes in uniform heat flow, *Journal of Applied Mechanics*, 26, *Transactions ASME Serie E*, vol. **81**, pp. 293–294, 1959.

Florence, A.L., and Goodier, J.N., Thermal stresses due to disturbance of uniform heat flow by an insulated ovaloid hole, *Journal of Applied Mechanics* 27, *Trans. ASME Serie E.*, vol. **82**, pp. 635–639, 1960.

Furimsky, E., Characterization of cokes from fluidflexi-coking of heavy feeds, *Fuel Processing Technology*, vol. **67**, no. 3, pp. 205–230, 2001.

Furimsky, E., Emissions of carbon dioxide from tar sands plants in Canada, *Energy & Fuels*, vol. **17**, no. 6, pp. 1541–1548, 2003.

Gadelle, C.P., Burger, J.G., Bardon, C.P., Carcoana, V.M.A., and Petcovici, V., Heavy oil recovery by in situ combustion – Two field cases in Rumania, *Journal of Petroleum Technology*, vol. **33**, no. 11, pp. 2057–2066, 1981.

Gajdica, R.J., Brigham, W.E., and Aziz, K., A semianalytical thermal model for linear steamdrive, *SPE Reservoir Engineering*, vol. **8**, no. 1, pp. 73–79, 1993.

Garcia-Pedrajas, N., Hervas-Martinez, C., and Munoz-Perez, J., COVNET: A cooperative co-evolutionary model for evolving artificial neural networks, *IEEE Transaction on Neural Networks*, vol. **14**, pp. 575–596, 2003.

Gates, I., and Chakrabarty, D.N., Optimization of steam assisted gravity drainage in ideal McMurray reservoir, *Journal of Canadian Petroleum Technology*, vol. **45**, no. 9, 2006.

Gauchet, R., and Corre, B., Rospo Mare field: A unique experience of heavy oil production with horizontal wells in a karst reservoir in presence of a strong tilted hydrodynamism, Paper SPE 36869 presented at the *1996 SPE European Petroleum Conference*, Milan, Italy, October 22-24, 1996.

Ge, S., and Garven, G., Hydromechanical modeling of tectonically driven groundwater flow with application to the Arkoma Foreland basin, *Journal of Geophysical Research*, vol. **97**, pp. 9119–9144, 1992.

GEA, *Global Energy Assessment - Toward a Sustainable Future*, Cambridge University Press, Cambridge, UK and New York, NY, USA and the International Institute for Applied Systems Analysis, Laxenburg, Austria, 2012.

Ghassemi, A., and Tarasovs, S., 3-D modeling of injection induced thermal stresses, Paper 4–471 presented at the *6th North American Rock Mechanics Symposium (NARMS)*, Houston, Texas, June 5-9, 2004,

Ghassemi, A., Nygren, A., and Cheng, A., Effects of heat extraction on fracture aperture: A poro–thermoelastic analysis, *Geothermics*, vol. **37**, pp. 525–539, 2008.

Gibson, B.J., Methods of classifying heavy crude oils using the UNITAR viscosity based definition, Paper presented at the *Second International UNITAR Future of Heavy Crude and Tar Sands Conference*, pp. 17–21, Caracas, Venezuela, February 7-17, 1982.

Gomaa, E.E., Correlations for predicting oil recovery by steamflood, *Journal of Petroleum Technology*, vol. **32**, no. 2, pp. 325–332, 1980.

Government of Alberta, *Alberta Oil Sands Industry Quarterly Update*, p. 9, Winter 2010.

Gray, K.E., Some rocks mechanics aspects of petroleum engineering, Paper 67-0405 presented at the *9th U.S. Symposium on Rock Mechanics*, Golden, Colorado, p. 32, April 17-19, 1967.

Gray, M.R., *Upgrading petroleum residues and heavy oils*, Marcel Dekker, New York, 1994.

Greaves, M., and Turta, A.T., *Oilfield in situ combustion process*, US Patent 5,626,191, p. 20, 1995.

Greaves, M., and Xia, T.X., The Reservoir as reactor, *Oil and Gas*, vol. 1, March 2008.

Greaves, M., El-Saghr, A., and Xia, T.X., CAPRI horizontal well reactor for catalytic upgrading of heavy oil, *ACS Symposium on Advances in Oil Field Chemistry: Downhole Upgrading*, vol. 45, no. 4, pp. 595–598, 2000.

Greaves, M., Xia, T.X., and Turta, A.T., Stability of THAI™ process - Theoretical and experimental observations, *Journal of Canadian Petroleum Technology*, vol. 47, no. 9, 2008.

Green, A.E., and Zema, W., *Theoretical elasticity*, Chapter 9, Oxford University Press, London, England, 1954.

Gringas, M., and Rokosh, D., A brief overview of the geology of heavy oil, bitumen and oil sands deposits, Paper presented at the 2004 GSEG National Convention.

Grizzle, P.C., Green, J.B., Sanchez, V., Murgia, E., and Labkowitz, J., Characterization of Cerro Negro crude: Physical and chemical separations, Chapter IX in proceedings of the *2nd International Conference on Heavy Crude and Tar Sands*, Caracas, Venezuela, 1982.

Gross, M.R., The origin and spacing of cross joints: Examples from the Monterrey Formation, Santa Barbara Coastline, California, *Journal of Structural Geology*, vol. 15, no. 6, pp. 737–751, 1993.

Gross, S.J., Johansen, S.J., Perinot, T., Deemer, A.R., Hoadley, S.F., and Meddaugh, W.S., Steamflood pilot design for the Wafra field 2nd Eocene reservoir in the Partitioned Zone (PZ), Saudi Arabia and Kuwait, *Proceedings of the SPE Heavy Oil Conference and Exhibition*, Kuwait City, Kuwait, December 12-14, 2011.

- Guadagno, F.M., and Nunziata, C., Seismic velocities of fractured carbonate rocks (southern Apennines, Italy), *Geophysical Journal International*, vol. **113**, no. 3, pp. 739–746, 1993.
- Gumrah, F., and Bağcı, S., Steam-CO₂ drive experiments using horizontal and vertical wells, *Journal of Petroleum Science and Engineering*, vol. **18**, pp. 113–129, 1997.
- Hagan, M.T., Demuth, H.B., Beale, M.H., *Neural network design*, 2nd ed., Boston: PWS Publishing, 1996.
- Hajdo, L.E., Hallam, R.J., and Vorndran, L.D.L., Hydrogen generation during in situ combustion, Paper SPE 13661 presented at the *SPE 1985 California Regional Meeting*, Bakersfield, California, March 27-28, 1985.
- Han, G., Dusseault, M.B., Detournay, E., Thomson, B.J., and Zacny, K., Principles of drilling and excavation (pp. 31–140), Chapter 2 in *Drilling in Extreme Environments: Penetration and Sampling on Earth and other Planets*. Editor(s): Yoseph Bar-Cohen, Kris Zacny, Wiley-VCH Verlag GmbH & Co. KGaA, p. 767, 2009.
- Hansom, J., and Lee, M., Effects of hydrocarbon generation, basal heat flow and sediment compaction on overpressure development: a numerical study, *Petroleum Geoscience*, vol. **11**, no. 4, pp. 353–360, 2005.
- Harrison, R.S., The bitumen-bearing Paleozoic carbonate trend of northern Alberta, American Association of Petroleum Geologists, Richard F. Meyer, ed., *Exploration for heavy crude oil and natural bitumen: AAPG Studies in Geology*, no. **25**, pp. 319–326, 1987.
- Head, I.M., Jones, D.M., and Larter, S.R., Biological activity in the deep subsurface and the origin of heavy oil, *Nature*, vol. **426**, pp. 344–352, 2003.
- Heard, H.C., Mechanical, thermal, and fluid transport properties of rock at depth, Paper presented at the *23rd U.S Symposium on Rock Mechanics (USRMS)*, Berkeley, California, 1982.

Heath, L.J., and Jones, R.A., *Thermal-chemical alteration of sandstone to increase permeability*, Report of Investigations 7586, U.S. Department of the Interior, Bureau of Mines, 1971.

Heffer, K., Geomechanical influences in water injection projects: an overview, *Oil & Gas Science and Technology Rev. IFP*, vol. **57**, no. 5, pp. 415–422, 2002.

Heffer, K.J., Fox, R.J., and McGill, C.A., Novel techniques show links between reservoir flow directionality, earth stress, fault structure and geomechanical changes in mature waterfloods, *SPE ATCE*, Dallas, Texas. 1995.

Heidbach, O., Tingay, M., Barth, A., Reinecker, J., Kurfeß, D., and Müller, B., *The world stress map database release 2008*, doi:10.1594/GFZ.WSM.Rel2008.

Heifer, K.J., and Lean, J.C., Earth stress orientation - a control on, and guide to flooding directionality in a majority of reservoirs, *3rd International conference on Reservoir Characterization*, Tulsa, Oklahoma, 1991.

Hein, F.J., and Cotterill, D.K., The Athabasca oil sands – A regional geological perspective, Fort McMurray area, Alberta, Canada, *Natural Resources Research*, vol. **15**, no. 2, pp. 85–102, 2006.

Hein, F.J., Heavy oil and oil (tar) sands in North America: An overview & summary of contributions, *Natural Resources Research*, vol. **15**, no. 2, pp. 67–84, 2006.

Hein, F.J., *Historical overview of the Fort McMurray area and oil sands industry in Northeast Alberta*, Earth Sciences Report 2000-05, Alberta Energy and Utilities Board (AEUB), p. 37, 2000.

Hein, F.J., Marsh, R.A., and Boddy, M.J., *Overview of the oil sands and carbonate bitumen of Alberta: Regional geologic framework and influence of salt dissolution effects*, Search and Discovery Article, no. 10144, p. 5, 2008.

Henk, A., Pre-drilling prediction of the tectonic stress field with geomechanical models, *First Break*, vol. **23**, no. 11, pp. 53–57, 2005.

Hernandez, J.A.M., and Trevisan, O.V., Heavy oil recovery mechanisms during steam injection in naturally fractured reservoirs, Paper SPE 107372 presented at the 2007 SPE Latin American and Caribbean Petroleum Engineering Conference, Buenos Aires, Argentina, April 15-18, 2007.

Hettema, M.H.H., de Pater, C.J., and Wolf, K-H.A.A., Effects of temperature and pore water on creep of sandstone rock, Paper 91–393 presented at the *32nd U.S. Symposium on Rock Mechanics (USRMS)*, Norman, Oklahoma, July 10-12, 1991.

Hettema, M.H.H., Wolf, K-H.A.A., and De Pater, C.J., The influence of steam pressure on thermal spalling of sedimentary rock: Theory and experiments, *International Journal of Rock Mechanics and Mining Science*, vol. **35**, no. 1, pp. 3–15, 1998.

Heuze, F.E., *On the geotechnical modeling of high-level nuclear waste disposal by rock melting*, Lawrence Livermore National Laboratory, UCRL-53183, 1981.

Hoadley, S., Al-Yami, F., Deemer, A., Brown, J., Al-Mutairi, G., Lekia, S., Al-Dhafeeri, F., Al-Odhailah, F., and Barge, D., Surveillance improvements during the implementation of a large scale carbonate steamflood pilot, Wafra field, PZ, *Proceedings of the SPE Heavy Oil Conference and Exhibition*, Kuwait City, Kuwait, December 12-14, 2011.

Hodgkinson, D.P., Lever, D.A., and Rae, J. Thermal aspects of radioactive waste burial in hard rock, *Progress in Nuclear Energy*, vol. **11**, no. 2, pp. 183–218, 1983.

Hoffman, B.T., and Kovscek, A.R., Displacement front stability of steam injection into high porosity diatomite rock, *Journal of Petroleum Science and Engineering*, vol. **46**, pp. 253–266, 2005.

Hoffman, B.T., and Kovscek, A.R., Light oil steam drive in fractured low-permeability reservoirs, Paper SPE 83491 presented at the *SPE Western Regional/AAPG Pacific Section Joint Meeting*, Long Beach, California, May 19-24, 2003.

Hoffmann, C.F., and Strausz, O.P., Bitumen accumulation in Grosmont platform complex, Upper Devonian, Alberta, Canada, *AAPG Bulletin*, vol. **70**, no. 9, pp. 1113–1128, 1986.

Hojka, K., Dusseault, M.B., and Bogobowicz, A.D., Analytical solutions for transient thermoplastic stress fields around a wellbore during fluid injection into permeable media, *Journal of Canadian Petroleum Technology*, vol. **32**, no. 4, pp. 49–57, 1993.

Holba, G., Dzou, L.I.P., Hickey, J.J., Franks, S.G., May, S.J., and Lenney, T., Reservoir geochemistry of South Pass 61 field, Gulf of Mexico: Compositional heterogeneities reflecting filling history and biodegradation, *Organic Geochemistry*, vol. **24**, pp. 1179–1398, 1996.

Hollerbach, A., *Influence of biodegradation on the chemical composition of heavy oil and bitumen*. Section II. Characterization, maturation, and degradation”, Paper 25 published in the Proceedings of the Exploration for Heavy Crude Oil and Natural Bitumen, Editor R.F., Meyer, AAPG Studies in Geology, pp. 243–248, 1987

Hong, K. C. Effects of steam quality and injection rate on steamflood performance, *SPE Reservoir Engineering*, vol. **9**, no. 4, pp. 290–296, 1994.

Hornik, K., Stinchcombe, M., and White, H., Universal approximation of an unknown mapping and its derivatives using multilayer feed forward networks, *Neural Networks*, vol. **3**, no. 5, pp. 551–60, 1990.

Hossain, M.M., Rahman, M.K., and Rahman, S.S., A shear dilation stimulation model for production enhancement from naturally fractured reservoirs, *SPE Journal*, vol. **7**, no. 2, pp. 183–95, 2002.

Hubbert, M.K., and Willis, D.G., Mechanics of hydraulic fracturing, *Transactions of AIME*, vol. **210**, pp. 153–166, 1957.

Hyne, J.B., Greidanus, J.W., Tyrer, J.D., Verona, D., Rizek, C., Clark, P.D., Clarke, R.A., and Koo, J., Aquathermolysis of heavy oils, Chapter IX in Proceedings of the *2nd International Conference on Heavy Crude and Tar Sands*, Caracas, Venezuela, vol. 1, 1982.

Ibatullin, R.R., Ibragimov, N.G., Khisamov, R.S., and Zaripov, A.T., Problems and decisions for development shallow fields of heavy oil, Paper SPE 161998-MS presented at the *SPE*

Russian Oil and Gas Exploration and Production Technical Conference and Exhibition, Moscow, Russia, October 16-18, 2012.

Ibatullin, R.R., Ibragimov, N.G., Khisamov, R.S., Podymov, E.D., and Shutov, A.A., Application and method based on artificial intelligence for selection of structures and screening of technologies for EOR, Proceedings of the *SPE/DOE IOR Symposium*, Tulsa, Oklahoma; April 13-17, 2002.

IEA (International Energy Agency), *World Energy Outlook 2009*, OECD, Paris, 2009.

Issever, K., Pamir, N., and Tirek, A., Performance of a heavy-oil field under CO₂ injection, Bati Raman, Turkey, *SPE Reservoir Engineering*, vol. **8**, no. 4, pp. 256–260, 1993.

Ito, T., Fujii, R., Evans, K.F., and Hayashi, K., Estimation of stress profile with depth from analysis of temperature and fracture orientation logs in a 3.6 km deep well at Soultz, France, Paper SPE 78185 presented at the *SPE/ISRM Rock Mechanics Conference*, Irving, Texas, 2002.

Jensen, T.B., Sharma, M.P., and Harris, H.G.J., An improved evaluation model for steam-drive projects, *Petroleum Science & Engineering*, vol. **5**, pp. 309–322, 1991.

Jiayu, N., and Jianyi, H., Formation and distribution of heavy oil and tar sands in China, *Marine and Petroleum Geology*, vol. **16**, no. 1, pp. 85–95, 2005.

Joly, E.L., Dormigny, A.M., Catala, G.N., Pincon P.R., and Louis, A.J.P., New production logging technique for horizontal wells, *SPE Production Engineering*, vol. **3**, no. 3, pp. 328–332, 1988.

Jones, J., Predicting performance of steam floods with analytical models, *Journal of Petroleum Science and Engineering*, vol. **9**, pp. 9–15, 1993.

Joshi, S.D., A laboratory study of thermal oil recovery using horizontal wells, SPE Paper 14916 presented at the *SPE/DOE 5th Symposium on Enhanced Oil Recovery*, Tulsa, OK, April 2-23, 1986.

Joshi, S.D., A review of thermal oil recovery using horizontal wells, *IN SITU*, vol. **2**, no. 1, pp. 211–259, 1987.

Joshi, S.D., and Threlkeld, C.B., Laboratory studies of thermally aided gravity drainage using horizontal wells, *AOSTRA Journal of Research*, vol. **2**, no.1, pp. 11–19, 1985.

Kamali, M.R., and Rezaee, M.R., Burial history reconstruction and thermal modeling at Kuh-e-Mond, SW Iran, *Journal of Petroleum Geology*, vol. **26**, no. 4, pp. 451–464, 2003.

Kanta, K., and Topkaya, I., *Development of oil and natural gas resources and prospects of enhanced oil recovery in Turkey*, Report, Turkish Petroleum Corp., p. 21, 1983.

Karaoguz, D., Issever, K., Pamir, N., and Tirek, A., Performance of a heavy-oil recovery process by an immiscible CO₂ application, Bati Raman field, Paper SPE 18002 presented at the *SPE Middle East Oil Technical Conference and Exhibition*, Manama, Bahrain, March 11-14, 1989.

Karaoguz, O.K., Nazan, N.T., Lane, R.H., Kalfa, U., and Celebioglu, D., Improved sweep in Bati Raman heavy-oil CO₂ flood: Bullhead flowing gel treatments plug natural fractures, Paper SPE 89400 presented at the *2004 SPE/DOE 14th Symposium on Improved Oil Recovery*, Tulsa, Oklahoma, U.S.A., April 17-21, 2004.

Karaoguz, O.K., Nazan, N.T., Lane, R.H., Kalfa, U., and Celebioglu, D., Improved sweep in Bati Raman heavy-oil CO₂ flood: Bullhead flowing gel treatments plug natural fractures, *SPE Reservoir Evaluation & Engineering*, vol. **10**, no. 2, pp. 164-175, 2007.

Kashnikov, Yu.A., and Ashikhmin, S.G., Influence of oil Recovery on the change in the stress-strain state of rock mass, Part III: Technogenic activization of fault structures. *Journal of Mining Science*, vol. **36**, no. 3, pp. 244–252, 2000.

Keith, D.C., Harrison, W.J., Wendlandt, R.F., and Daniels, E.J., Mineralogical responses of siliciclastic carbonate-cemented reservoirs to steam flood enhanced oil recovery, *Applied Geochemistry*, vol. **13**, no. 4, pp. 491–507, 1998.

- Kirchoff, M.R., and McKinnon, W.B., Formation of mountains on Io: Variable volcanism and thermal stresses, *Icarus*, vol. **201**, pp. 598–614, 2009.
- Kirk, J.S., Bird, G.S., and Lonstafe, F.J., Laboratory study of the effects of steam-condensate flooding in the Clearwater Formation: High temperature flow experiments, *Bulletinm of Canadian Petroleum Geology*, vol. **35**, pp. 34–47, 1987.
- Kisman, K.E., Artificial lift, a major unresolved issue for SAGD, *Journal of Canadian Petroleum Technology*, vol. **42**, no. 8, 2003.
- Klett, R.D., *Deep rock nuclear waste disposal test: design and operation*, Sandia National Laboratories, Albuquerque, SAND-74-O042, 1974.
- Kocabas, I., An analytical model of temperature and stress fields during cold water injection into an oil reservoir, *SPE Production & Operations*, vol. **21**, no. 2, pp. 282–292, 2006.
- Komar, C.A., *Hardness, tensile strength, and impact toughness of reservoir sandstone at extreme temperatures*, Report of Investigations 7571 prepared for the Department of the Interior, Bureau of Mines, p. 11, 1971.
- Kouznetsov, O.L., Faizulline, I.S., Chirkine, I.A., Meltchouk, B.Yu., Khisamov, R.S., Slenkin, S.I., and Kashirin, G.V., Applying scattered seismic waves to study 3-D distribution of fracturing in geomedium (SVSL method), *Iranian 11th Oil, Gas and Petrochemical Congress*, Tehran, Iran, 2001.
- Kumar, M., Beatty, F.D., Cyclic steaming in heavy oil diatomite, Paper SPE 29623 presented at the *Socierty of Petroleum Engineering 65th Western Regional Meeting*, Bakersfield, California, 1995.
- Kumar, R., and Verma, S.K., Determination of wettability and its effect on oil recovery in a carbonate rock of an offshore field under ambient and elevated temperature, Paper SPE 128545 presented at the *SPE Oil and Gas India Conference and Exhibition*, Mumbai, India, 2010.

Kumar, V.K., Fassihi, M.R., and Yannimaras, D.V., History and appraisal of the Medicine Pole Hills Unit air case injection project, *SPE Reservoir Engineering*, vol. **10**, no. 3, pp. 198–202, 1995.

Larter, S., Adams, J.J., Gates, I.D., Huang, H., and Bennett, B., The origin, prediction and impact of oil viscosity heterogeneity on the production characteristics of tar sand and heavy oil reservoirs, *Journal of Canadian Petroleum Technology*, vol. **47**, no. 1, 2008.

Larter, S., Huang, H., Adams, J., Bennett, B., Jokanola, O., Oldenburg, T., Jones, M., Head, I., Riediger, C., and Fowler, F., The controls on the composition of biodegraded oils in the deep subsurface: Part II - Geological controls on subsurface biodegradation fluxes and constraints on reservoir-fluid property prediction, *AAPG Bulletin*, vol. **90**, no. 6, pp. 921–938, 2006.

Larter, S.R., Head, I.M., Huang, H., Bennett, B., Jones, M., Aplin, A.C., Murray, A., Erdmann, M., Wilhelms, A., and di Primio, R., Biodegradation, gas destruction and methane generation in deep subsurface petroleum reservoirs: An overview, in A.G. Dore and B. Vining, eds., *Petroleum geology: Northwest Europe and global perspectives: Proceedings of the 6th Petroleum Geology Conference*, Geological Society (London), 2005

Larter, S.R., Wilhelms, A., Head, I., Koopmans, M., Aplin, A., Di Primio, R., Zwach, C., Erdmann, M., and Telnaes, N., The controls on the composition of biodegraded oils in the deep subsurface, Part 1: Biodegradation rates in petroleum reservoirs, *Organic Geochemistry*, vol. **34**, pp. 601–613, 2003.

Lauriello, P.J., Application of a convective heat source to the thermal fracturing of rock, *International Journal of Rock Mechancis and Mining Science & Geomechancis Abstracts*, vol. **11**, pp. 75–81, 1974.

Lee, F.T., and Nichols, T.C., Stress changes in rock from the Jorum underground nuclear explosion, September 16, 1969, Pahute Mesa, Nevada test site, *Bulletin of Seismological Society of America*, vol. **62**, no. 2, pp. 609–618, 1972.

- Levenberg, K.A., Method for the solution of certain non-linear problems in least squares, *Quarterly Applied Mathematics*, vol. **2**, no. 2, pp. 164–168, 1944.
- Li, M., Astete, E., Wang, H., A simulation study of a cyclic steam stimulation pilot in a deep carbonate heavy oil reservoir in Oudeh field , Syria, Paper CSUG/SPE 137603 presented at the *Canadian Unconventional Resources & International Petroleum Conference*, Calgary, Alberta, Canada, October 19-21, 2010
- Li, P., and Chalaturnyk, R.J., Permeability variations associated with shearing and isotropic unloading during the SAGD process, *Journal of Canadian Petroleum Technology*, vol. **45**, no. 1, pp. 54–61, 2006.
- Li, X., Cui, L., and Roegiers, J.-C., Temperature induced pore pressure and stresses and their potential impacts on wellbore stability, Paper 9CONGRESS-1999-091 presented at the *9th ISRM Congress*, Paris, France, August 25-28, 1999.
- Liu, C., Che, C., Zhu, J., and Yang, H., China's endowment-2: China assesses unconventional land oil shale, oil sands, coal gas resources, *Oil & Gas Journal*, vol. **108**, no. 15, p. 7, 2010.
- Logan, S.E., *Deep self-burial of radioactive wastes by rock melting capsules*, Transactions of American Nuclear Society Annual Meeting, Chicago, pp. 177–178, American Nuclear Society, Hinsdale, 1973.
- Lorenz, J.C., Stress sensitive reservoirs, *Journal of Petroleum Technology*, vol. **51**, no. 1, pp. 61–63, 1999.
- Luger, G.F., Parkinson, W.J., *et al.* Screening EOR methods with Fuzzy Logic, Proceedings of the *1991 International Reservoir Characterization Conference*, Tulsa, Oklahoma, November 3-5, 1991.
- Luo, R., Cheng, L.S., and Peng, J.C., Feasibility study of CO₂ injection for a heavy oil reservoir after cyclic steam stimulation: Liaohe oil field test, Paper SPE/PS-CIM/CHOA

97462 presented at the *International Thermal Operations and Heavy Oil Symposium*, Calgary, Alberta, Canada, November 1-3, 2005.

Macaulay, R.C., Krafft, J.M., Hartemink, M., and Escovedo, B., Design of a steam pilot in a fractured carbonate reservoir - Qarn Alam field, Oman, Paper SPE 30300 presented at the *International Heavy Oil Symposium*, Calgary, AB, Canada, June 19-21, 1995.

Marika, E., Uriansrud, F., Bilak, R., and Dusseault, M.B., Achieving zero discharge using deep well disposal, Paper 2009-WHOC09-350 presented at the *World Heavy Oil Congress*, Venezuela, p. 19, 2009.

Marquardt, D.W., An algorithm for the least squares estimation of nonlinear parameters, *SIAM, Journal of Applied Mathematics*, vol. **11**, no. 2, pp. 431–441, 1963.

Marx, J.W., and Langenheim, R.H., *Transactions of AIME*, vol. **216**, pp. 312–315, 1959.

Mateo Hernandez, J.A., and Trevisan, O.V., Heavy oil recovery mechanisms during steam injection in naturally fractured reservoirs, Paper SPE 107372 presented at the *2007 SPE Latin American and Caribbean Petroleum Engineering Conference*, Buenos Aires, Argentina, April 15-18, 2007.

McCulloch, W.S., Pitts, W., A logical calculus of the ideas immanent in nervous activity, *Bulletin of Mathematical Biophysics*, vol. **5**, pp. 115–133, 1943, (Reprinted in Anderson & Rosenfeld, 1988, 18–28).

McRory, R.E., *Oil sands and heavy oils of Alberta, Energy Heritage*, Edmonton: Alberta Energy and Natural Resources, p. 94, 1982.

Meddaugh, W.S., Osterloh, W.T., Toomey, N., Bachtel, S., Champenoy, N., Rowan, D., Gonzalez, G., Aziz, S., Hoadley, S.F., Brown, J., Al-Dhafeeri, F.M., Deemer, A.R., Impact of reservoir heterogeneity on steamflooding, Wafra first Eocene reservoir, Partitioned Zone (PZ), Saudi Arabia and Kuwait, In: *Proceedings of the SPE Heavy Oil Conference and Exhibition*, Kuwait City, Kuwait, December 12-14, 2011.

Meibner, H., Becker, T., and Adam, E., Stress-strain behavior of crystalline and amorphous rocks subjected to high pressure and high temperature, In: *Proceedings of the 9th International Congress on Rock Mechanics*, Paris, France, vol. 1, p. 4, 1999.

Meyer, R.F., and Attanasi, E.D., *Natural bitumen and extra heavy oil, 2004 survey of energy resources*, Trinnaman, J., Clarke, A., Eds. for the World Energy Council, Elsevier: Amsterdam, Chapter 4, pp. 93–117, 2004.

Meyer, R.F., and Dietzman, W.D., World geography of heavy crude oils, In: R. F. Meyer, C.T. Steele, and J.C. Olson, eds., *The future of heavy crude and oil sands: First International United Nations Institute for Training and Research Conference*, Edmonton, Alberta, Canada, pp. 16–28, (June 1979), 1981.

Meyer, R.F., and Duford, J.W., Resources of heavy oil and natural bitumen worldwide, In: R.F. Meyer and E.J. Wiggins, eds., *Fourth United Nations Institute for Training and Research/United Nations Development Program International Conference on Heavy Crude and Oil Sands*, Edmonton, Alberta, Canada, August 1988, vol. 2, pp. 277–307, 1989.

Meyer, R.F., Attanasi, E.D., and Freeman, P.A., *Heavy oil and natural bitumen resources in geological basins of the world*, USGS Open-File Report 2007-1084, available online at <http://pubs.usgs.gov/of/2007/1084/>.

Meyerhoff, A.A., and Meyer, R.F., Geology of heavy crude oil and natural bitumen in the USSR, Mongolia, and China, In: Meyer, R.F., ed., *Exploration for heavy crude oil and natural bitumen*: Tulsa, Okla., American Association of Petroleum Geologists Studies in Geology, vol. 25, 1987.

Mikula, R.J., Munoz, V.A., and Omotoso, O., Water use in bitumen production: Tailings management in surface mined oil sands, Paper presented at the World Heavy Oil Congress 2008, Edmonton, Alberta, Canada, March 10-12, 2008.

Miller, M.A., and Leung, W.K., A simple gravity override model of steamdrive, In: *Proceedings of the 60th Annual Technical Conference and Exhibition of the Society of Petroleum Engineering*, Las Vegas, September 22-25, 1985.

- Miura, K., and Wang, J., An analytical model to predict cumulative steam oil ratio (CSOR) in thermal recovery SAGD process, *Canadian Unconventional Resources and International Petroleum Conference*, Calgary, Alberta, Canada, October 19-21, 2010.
- Mohammadi, Sh., Ehsani, M.R., Nikookar, M., Sahranavard, L., and Soleimani Garakani, A., Study of steam injection in a fractured carbonate heavy oil reservoir in Iran, In: Proceedings of the *SPE Heavy Oil Conference*, Calgary, June 12-14, 2012.
- Mollaei, A., and Maini, B., Steam flooding of naturally fractured reservoirs: Basic concepts, recovery mechanisms, process improvements, mechanism and optimization of in situ CO₂ generation, In: Proceedings of the *Petroleum Society's 8th CIPC (58th Annual Technical Meeting)*, Calgary, Alberta, Canada, June 12-14, 2007.
- Mollaei, A., and Maini, B., Steam flooding of naturally fractured reservoirs: Basic concepts and recovery mechanisms, *Journal of Canadian Petroleum Technology*, vol. **49**, no. 1, pp. 65–70, 2010.
- Mollaei, A., Maini, B., and Jalilavi, M., Investigation of steam flooding in naturally fractured reservoirs, Proceedings of the *International Petroleum Technology Conference*, Dubai, U.A.E., December 4-6, 2007.
- Montgomery, D.C., and Runger, G.C., *Applied statistics and probability for engineers, student solutions manual*, John Wiley and Sons: New York, p. 146, 2006.
- Montgomery, D.C., *Introduction to statistical quality control*, John Wiley and Sons: New York; p. 776, 2008.
- Moore, R.G., Lareshen, C.J., Mehta, S.A., Ursenbach, M.G., Belgrave, J.D.M., Weissman, J.G., and Kessler, R.V., A downhole catalytic upgrading process for heavy oil using in situ combustion, *Journal of Canadian Petroleum Technology*, vol. **38**, 1999.
- Morgenstern, N.R., A relation between hydraulic fracture pressure and tectonic stresses, *Geofis. Pura e Applic.*, vol. **52**, no. 1, pp. 104–114, 1962.

Mosesyan, A.A., Nagorniy, S.A., Chernitsyna, E.A. and Trotsenko, Y.A., Selection of a new IOR/EOR strategy for the heavy oil brown field in Kazakhstan, Paper A31 presented at the *15th European Symposium on Improved Oil Recovery*, Paris, France, April 27-29, 2009.

Moshtaghian, A., Malekzadeh, R., and Azarpanah, A., Heavy oil discovery in Iran, *4th UNITAR/UNDP International Conference on Heavy Crude and Tar Sands*, Edmonton, AB, Canada, pp. 235–243, 1988.

Myhill, N.A., and Stegemeier, G.L., Steam drive correlation and prediction, *Journal of Petroleum Technology*, vol. **30**, no. 2, pp. 173–182, 1978.

Nadeau, P.H., The petrophysical effects of dispersed diagenetic clay minerals on reservoir sands: an experimental study, Abstract and Program, *27th Annual Clay Minerals Society*, p. 95, 1990.

Nadyal, M., Al-Hinai, K.M., Jaffer, N.A., and Thurber, S.S., Development of heavy oil reserves in South Oman, SPE paper 11474 presented at the *1983 Middle East Oil Exhibition*, Manama, Bahrain, March 14, 1983.

Nakamura, S., Sarma, H.K., Umucu, T., Issever, K., Kanemitsu, M.A., Critical evaluation of a steamflood pilot in a deep heavy carbonate reservoir in Ikiztepe field, Turkey, In: *Proceedings of the SPE Annual Technical Conference and Exhibition*, Dallas, Texas, USA, October 22-25, 1995.

National Energy Board of Canada, *Conventional heavy oil resources of the Western Canada sedimentary basin*, Published by the National Energy Board, p. 107, 2001.

National Energy Board, *Canada's oil sands – Opportunities and challenges to 2015 – An update*, p. 85, 2006.

Nelson, R.A., *Evaluating fractured reservoirs: Introduction, geologic analysis of naturally fractured reservoirs*, 2nd ed., Gulf Professional Publishing, Woburn, 2001.

Nelson, W.L., What's the average sulfur content vs. gravity? *Oil & Gas Journal*, vol. **70**, no. 59, 1972.

- Neuman, C.H., A gravity override model of steamdrive, *Journal of Petroleum Technology*, 1985, pp. 163–169.
- Neuman, C.H., A mathematical model of the steam drive process applications, In: *Proceedings of the SPE IOR Symposium*, Tulsa, Oklahoma, April 22-24, 1974.
- Nolan, J.B., Ehrlich, R., and Crookston, R.B., Applicability of steamflooding for carbonate reservoirs, Paper SPE 8821 presented at the *1980 SPE/DOE Symposium on Enhanced Oil Recovery*, Tulsa, Oklahoma, April 20-23, 1980.
- Nolen-Hoeksema, R.C., and Rabaa, A.W.M., Waterflood improvement in the Permian Basin: Impact of in situ stress evaluations, *SPE Reservoir Engineering*, vol. **9**, no. 4, pp. 254–260, 1994.
- O'Rourke, J.C., Bohme, C.G., Edmunds, N.R., Kovalsky, J.A., and Suggett, J.C., AOSTRA's Underground Test Facility (UTF) moving into a pre-commercial pilot, Paper presented in the *5th District Meeting, Petroleum Society of CIM*, Fort McMurray, Alberta, September 17-20, 1991.
- Oglesby, K.D., Blevins, T.R., Rogers, E.E., and Johnson, W.M., Status of the 10-pattern steamflood, Kern River field, California, *Journal of Petroleum Technology*, vol. **34**, no. 10, pp. 2251–2257, 1982.
- Olsen, D.K., Sarathi, P.S., Schulte, R.K., and Giangiacomo, L.A., Case history of steam injection operations at Naval Petroleum Reserve No. 3, Teapot Dome field, Wyoming: A shallow heterogeneous light oil reservoir, In: *Proceedings of the International Thermal Operations Symposium*, Bakersfield, February 8-10, 1993.
- Ono, K.J., Successful field pilots in a carbonate heavy oil reservoir in the Ikiztepe field, Turkey, *Japanese Association of Petroleum Technology*, vol. **62**, no. 2, 1997.
- Orr, W.L., *Sulfur in heavy oils, oil sands and oil shales*, In: O.P. Strausz, and E.M. Lown, eds., *Oil sand and oil shale chemistry*: New York, Springer, pp. 223–243, 1978.

Osterloh, W.T., Mims, D.S., and Meddaugh, W.S., Probabilistic forecasting and model validation for the 1st Eocene Large Scale Pilot (LSP) steamflood, Partitioned Zone (PZ), Saudi Arabia and Kuwait, In: Proceedings of the *SPE Heavy Oil Conference and Exhibition*, Kuwait City, Kuwait, December 12-14, 2011.

Owens, W.D., and Suter, V.E., Steam simulation for secondary recovery, *Journal of Canadian Petroleum Technology*, vol. 4, no. 4, pp. 227–235, 1965.

Padhy, P.K., and Singh, D., Geologic setting and petroleum system of heavy oil occurrences in sedimentary basins of India, Paper presented at the *7th UNITAR International Conference for Heavy Crude and Tar Sands*, Beijing, China, October 27-30, 1998

Parkinson, W.J., Luger, G.F., Bretz, R.E., and Osowski, J.J., An expert system for screening EOR methods, In: Proceedings of the *1990 AIChE Summer Meeting*, San Diego, California, August 19-22, 1990.

Parrish, D.K., Krivz, A.L., and Carter, N.L., Finite element folds of similar geometry, *Tectonophysics*, vol. 32, p. 183–207, 1976.

Penner, S.S., *Assessment of research needs for oil recovery from heavy oil sources and tar sands*, DOE report, March 1982.

Penney, R., Baqi Al Lawati, S., Hinai, R., Van Ravesteijn, O., Rawnsley, K., Putra, P., Geneau, M., Ikwumonu, A., Habsi, M., and Harrasy, H., First full field steam injection in a fractured carbonate at Qarn Alam, Oman, Paper SPE-105406 presented at the *SPE Middle East Oil and Gas Show and Conference*, Bahrain, Kingdom of Bahrain, March 11-14, 2007.

Penney, R., Moosa, R., Shahin, G., Hadhrami, F., Kok, A., Engen, G., Van Ravesteijn, O., Rawnsley, K., and Kharusi, B., Steam injection in fractured carbonate reservoirs: Starting a new trend in EOR. Paper IPTC-10727 presented at the *International Petroleum Technology Conference*, Doha, Qatar, November 21-23, 2005.

Perry, R.H., and Green, D.W., *Perry's chemical engineers' handbook*, 7th ed., McGraw-Hill, New York, 2001.

- Pindoria, R.V., Megaritis, A., Chatzakis, I.N., Vasanthakumar, L.S., Zhang, S.-F., and Lazaro, M.-J., Structural characterization of tar from a coal gasification plant. Comparison with a coke oven tar and a crude oil flash-column residue, *Fuel*, vol. **76**, no. 2, pp. 101–113, 1997.
- Poling, B.E., Prausnitz, J.M., and O’Connell, I.P., *The properties of gases and liquids*, 5th ed., McGraw-Hill, New York, 2001.
- Pollard, D.D., and Aydin, A.A., Progress in understanding jointing over the past century, *GSA Bulletin*, vol. **100**, no. 8, pp. 1181–1204, 1988.
- Pooladi-Darvish, M., Farouq Ali, S.M., and Tortike, W.S., Steam heating of fractured formations containing heavy oil: Basic premises and a single-block analytical model, Paper SPE 28642-MS Annual Technical Conference and Exhibition, New Orleans, Louisiana, September 25-28, 1994a.
- Pooladi-Darvish, M., Farouq Ali, S.M., and Tortike, W.S., Steam heating of fractured formations containing heavy oil - An analysis of the basic premises, Paper 94-64 presented at the the 45th annual Technical Meeting of the Petroleum Society of CIM, Calgary, AB, Canada, June 12-15, 1994b.
- Prats, M., Reservoir mechanisms in heavy oil production, *15th World Petroleum Congress*, Beijing, China, October 12-17, 1997.
- Prats, M., Reservoir mechanisms in heavy oil production, Proceedings of the *15th World Petroleum Congress*, The Executive Board of the World Petroleum Congress Published by John Wiley & Sons, pp. 473–484, 1998.
- Prensky, S.E., Advances in borehole imaging technology and applications, In: LOVELL, M. A., Williamson, G. & Harvey, P.K. (eds) 1999, Borehole imaging: applications and case histories, *Geological Society, London, Special Publications*, vol. **159**, pp. 1–43, The Geological Society of London, 1999.

- Rahimi, P.M., and Gentzis, T., The chemistry of bitumen and heavy oil processing, In: Practical advances in petroleum processing, II, C.S. Hsu, P.R. Robinson, Eds, Springer, Berlin, 2006.
- Rao, D.N., and Karyampudi, R.S., Productivity enhancing wettability control technology for cyclic steam process in the Elk Point Cummings Formation, Paper APER 95-62 presented at the *46th Annual Technical Meeting of the Petroleum Society of CIM*, Banff, Alberta, Canada, 1995.
- Rao, D.N., Wettability effects in thermal recovery operations, *SPE Reservoir Evaluation & Engineering*, vol. **2**, no. 5, pp. 420–430, 1999.
- Reinoso, F.R., Santana, P., Palazon, E.R., Diez, M.-A., and Marsh, H., Delayed coking: Industrial and laboratory aspects, *Carbon*, vol. **36**, no. 1-2, pp. 105–116, 1998.
- Reis, J.C., Oil recovery mechanisms in fractured reservoirs during steam injection, Paper SPE 20204 presented at the *1990 SPE/DOE Seventh Symposium on Enhanced Oil Recovery*, Tulsa, Oklahoma, April 22-25, 1990.
- Roehl, P.O., and Choquette, P.W., Editors, *Carbonate petroleum reservoirs*, Springer-Verlag, New York, p. 622, 1985.
- Ross, J.G., SPE/WPC/AAPG resource definitions as a basis for portfolio management, Paper SPE 68573 presented at the *SPE Hydrocarbon Economics and Evaluation Symposium*, Dallas, Texas, April 2-3, 2001.
- Rutqvist, J., and Stephansson, O., The role of hydromechanical coupling in fractured rock engineering, *Hydrogeology Journal*, vol. 11, pp. 7–40, 2003.
- Rutqvist, J., Freifeld, B., Min, K.-B., Elsworth, D., and Tsang, Y., Analysis of thermally induced changes in fractured rock permeability during 8 years of heating and cooling at the Yucca Mountain Drift Scale Test, *International Journal of Rock Mechanics and Mining Sciences*, vol. **45**, pp. 1373–1389, 2008.

Rutqvist, J., Wu, Y.-S., Tsang, C.-F., and Bodvarsson, G., A modeling approach for analysis of coupled multiphase fluid flow, heat transfer, and deformation in fractured porous rock, *International Journal of Rock Mechanics and Mining Sciences*, vol. **39**, pp. 429–442, 2002.

Sahimi, M., *Flow and transport in porous media and fractured rock*, Weinheim, 1995.

Sahin, S., Kalfa, U., and Celebioglu, D., Bati Raman field immiscible CO₂ application: Status quo and future plans, SPE Paper 106575 presented at *SPE Latin American and Caribbean Petroleum Engineering Conference*, Buenos Aires, Argentina, 15-18 April 2007.

Sahin, S., Kalfa, U., and Celebioglu, D., Bati Raman field immiscible CO₂ application, status quo and future plans, *SPE Reservoir Evaluation & Engineering*, vol. **11**, no. 4, pp. 778–791, 2008.

Sahuquet, B.C., and Ferrier, J.J., Steam drive pilot in a fractured carbonate reservoir: Lacq Superieur field, *Journal of Petroleum Technology*, vol. **34**, pp. 873–880, 1982.

Saidi, A.M., *Reservoir engineering of fractured reservoir- Fundamental and practical aspects*, TOTAL Edition Press, Paris, 1987.

Samir, M., Rejuvenation Issaran field - Success story, Paper SPE 127847 at the *SPE North Africa Technical Conference and Exhibition*, Cairo, Egypt, February 14-17, 2010.

Samir, M., Role of steam injection pressure to achieve successful cyclic steam project Issaran field – Egypt, Paper SPE 127848 presented at the *SPE North Africa Technical Conference and Exhibition*, Cairo, Egypt, February 14-17, 2010.

Sanyal, S.K., Ramey, H.J., and Marsden, S.S., The effect of temperature on capillary pressure properties of rocks, *SPWLA 14th Annual Logging Symposium*, May 6-9, 1973.

Sayd, A.D., Moço, A.L.B., Branco, C.C.M., Kato, E.T., de Carvalho Jr., I.P., Rosseto, J.A., da Silva Neto, J.A., Diniz, J.L., Brennand, M., Guarda, M., Franco, M.P., and Brasil, T.E., Siri pilot project - First offshore extra heavy and viscous oil (12.3 API) ever produced, Paper OTC 20134 presented at the *2009 Offshore Technology Conference*, Houston, Texas, USA, May 4-7, 2009.

Schembre, J.M., Tang, G.-Q., and Kovscek, A.R., Wettability alteration and oil recovery by water imbibition at elevated temperatures, *Journal of Petroleum Science and Engineering*, vol. **52**, pp. 131–148, 2006.

Schenk C.J., Cook, T.A., Charpentier, R.R., Pollastro, R.M., Klett, T.R., Tennyson, M.E., Kirschbaum, M.A., Brownfield, M.E., and Pitman, J.K., *An estimate of recoverable heavy oil resources of the Orinoco Oil Belt, Venezuela*, U.S. Geological Survey Fact Sheet 2009-3028, p. 4, 2009

Scherzer, J., and Gruia, A.J., *Hydrocracking science and technology*, New York, Marcel Dekker, Inc., 1996.

Scott, G.R., Comparison of CSS and SAGD performance in the Clearwater formation at Cold Lake, Paper SPE 79020 presented at the *2002 SPE International Thermal Operations and Heavy Oil Symposium and International Horizontal Well Technology Conference*, Calgary, Alberta, Canada, November 4-7, 2002.

Scott, J.D., Proskin, S.A., and Adhikary, D.P., Volume and permeability changes associated with steam stimulation in an oil sands reservoir, *Journal of Canadian Petroleum Technology*, vol. **33**, no. 7, pp. 44–52, 1994.

Scott, R. Kaiser, W.R. and Ayers Jr., W.B., Thermogenic and secondary biogenic gases, San Juan Basin, Colorado and New Mexico - Implications for coalbed gas producibility, *AAPG Bulletin*, vol. **78**, no. 8, pp. 1186–1209, 1994

Shafiei, A., Dusseault, M.B., Memarian, H., and Samimi-Sadeh, B., Production technology selection for Iranian naturally fractured heavy oil reserves, In: *Proceedings of the CIPC 2007 (58th Annual Technical Meeting)*, Calgary, Alberta, Canada, June 12-14, 2007.

Shahin Jr, G.T., Moosa, R., Kharusi, B., and Chilek, G., The Physics of steam injection in fractured carbonate reservoirs: Engineering development options that minimize risk, Paper SPE-102186-PP presented at the *2006 SPE Annual Technical Conference and Exhibition*, Antonio, Texas, U.S.A., September 24-27, 2006.

Shandrygin, A.N., and Lutfullin, A., Current status of enhanced recovery techniques in the fields of Russia, Paper SPE 115712 presented at the *2008 SPE Annual Technical Conference and Exhibition*, Denver, Colorado, USA, September 21-24, 2008.

Shen, C., Numerical investigation of SAGD process using a single horizontal well, *Journal of Canadian Petroleum Technology*, vol. **39**, no. 3, 2000.

Sheory, P.R., A theory for in situ stresses in isotropic and transversely isotropic rock, *International Journal of Rock Mechanics, Mining Science & Geomechanics Abstracts*, vol. **31**, no. 1, pp. 23–34, 1994.

Shimamoto, T., and Hara, I., Geometry and strain distribution of single-layer folds, *Tectonophysics*, vol. **30**, pp. 1–34, 1976.

Shouliang, Z., Yitang, Z., Shuhong, W., Shangqi, L., Xiuluan, L., and Songlin, L., Status of heavy oil development in China, Paper SPE/PS-CIM/CHOA 97844 or PS2005-381 presented at the *2005 SPE International Thermal Operations and Heavy Oil Symposium*, Calgary, Alberta, Canada, November 1-3, 2005.

Shutler, N.D., Numerical three phase model of the 2-D steamflood process, *SPE Journal*, vol. **10**, pp. 405–417, 1970.

Singhal, A.K., Ito, Y., and Kasaeie, M., Screening and design criteria for steam assisted gravity drainage (SAGD) projects, Paper SPE 50410 presented at the *SPE International Conference on Horizontal Well Technology*, Calgary, Alberta, Canada, November 1-4, 1998.

Smith, G.E., Hurlburt, G., and Li, V.P., Heavy oil carbonate: Primary production in Cuba, Paper SPE/Petroleum Society of CIM/CHOA 79002 presented at the *2002 SPE International Thermal Operations and Heavy Oil Symposium and International Horizontal Well Technology Conference*, Calgary, Alberta, Canada, November 4-7, 2002.

Snell, J.S., and Close, A.D., Yates field steam pilot applies latest seismic and logging monitoring techniques, In: *Proceedings of the 1999 SPE Annual Technical Conference and Exhibition*, Houston, Texas, October 3-6, 1999.

Snell, J.S., Wadleigh, E.E., and Tilden, J., Fracture characterization a key factor in Yates steam pilot design and implementation, Paper SPE 59060 presented at the *2000 SPE International Petroleum Conference and Exhibition*, Villahermosa, Mexico, February 1-3, 2000.

Somerton, W.H., and Boozer, G.D., A method of measuring thermal diffusivities of rocks at elevated temperatures, *AIChE Journal*, vol. **7**, no. 1, pp. 87–90, 1961.

Somerton, W.H., and Boozer, G.D., Thermal characteristics of porous rocks at elevated temperatures, *Journal of Petroleum Technology*, vol. **12**, no. 6, pp. 77–81, 1960a.

Somerton, W.H., and Boozer, G.D., Thermal characteristics of porous rocks at elevated temperatures, *AIME Transactions*, vol. **219**, pp. 418–422, 1960b.

Somerton, W.H., Selim, M.A., Additional thermal data for porous rocks - Thermal expansion and heat of reaction, *SPE Journal*, vol. **1**, no. 4, pp. 249–253, 1961.

Souraki, Y., Ashrafi, M., Karimaie, H., and Torsæter, O., Experimental investigation and numerical simulation of steam flooding in heavy oil fractured reservoir, Paper SPE 144552 presented at the *SPE Western North American Region Meeting*, Anchorage, Alaska, USA, May 7-11, 2011.

Spadini, A., Carbonate reservoirs in Brazilian sedimentary basins, *19th World Petroleum Congress*, Spain 2008 Forum 06: Carbonate reservoirs, 2008.

Special Report: EOR/Heavy oil survey: 2010 worldwide EOR survey, *Oil & Gas Journal*, vol. **108**, no. 14, 2010a.

Special Report: EOR/Heavy oil survey: CO₂ miscible, steam dominate enhanced oil recovery processes, *Oil & Gas Journal*, vol. **108**, no. 14, 2010.

Speight, J.G., New approaches to hydroprocessing, *Catalysis Today*, vol. **98**, no. 1-2, pp. 55–60, 2004.

Speight, J.G., *The chemistry and technology of petroleum*, 3rd ed., Dekker: New York, 1998.

- Spivak, A., Karaoguz, D., and Issever, K., Simulation of immiscible CO₂ injection in a fractured reservoir, Bati Raman field, Turkey, Paper SPE 18765 presented at the *SPE California Regional Meeting*, Bakersfield, California, April 5-7, 1989.
- Stancliffe, R.P.W., and van der Kooij, M.W.A., The use of satellite-based radar interferometry to monitor production activity at the Cold Lake heavy oil field, Alberta, Canada, *AAPG Bulletin*, vol. **85**, no. 5, pp. 781–793, 2001.
- Stavsky, Y., Thermoelasticity of heterogeneous aeolotropic plates, *ASCE Journal of Engineering Mechanics Division*, vol. **89**, pp. 89–105, 1963.
- Storm, D.A., Sheu, E.Y., DeTar, M.M., and Barresi, R.J., A comparison of the macrostructure of Ratawi asphaltenes in toluene and vacuum residue, *Energy & Fuels*, vol. **8**, no. 3, pp. 567–569, 1994.
- Strausz, O.P., The chemistry of the Alberta oil sand bitumen, In: *Proceedings of the ACS Symposium on Oil Sands and Oil Shale*, Montreal, vol. 22, no. 3, pp. 171–176, 1977.
- Sturm, G.P., Scheppele, S.E.Jr., Grigsby, R.D., and Hazos, H., Characterization of Cerro Negro crude: Chemical analysis, Chapter IX in *Proceedings of the 2nd International Conference on Heavy Crude and Tar Sands*, Caracas, Venezuela, vol. 1, 1982.
- Sumnu, M.D., Brigham, W.E., Aziz, K., and Castanier, L.M., An experimental and numerical study on steam injection in fractured systems, Paper SPE 35459 presented at the *SPE/DOE Improved Oil Recovery Symposium*, Tulsa, Oklahoma, April 21-24, 1996.
- Taber, J.J., Martin, F.D., and Seright, R.S., EOR screening criteria revisited - Part 1: Introduction to screening criteria and enhanced recovery field projects, *SPE Reservoir Engineering*, vol. **12**, no. 3, pp. 189–198, 1997.
- Talukdar, S.C., and Marcano, F., Petroleum systems of the Maracaibo Basin, Venezuela, In: *The Petroleum System—From Source to Trap*, L.B. Magoon, W.G. Dow, Eds, AAPG Memoir, **60**, 1994.

Tang, G-Q., Inouye, A., Lowry, D., and Lee, V., Recovery mechanism of steam injection in carbonate reservoir, Paper SPE 144524 presented at the *SPE Western North American Regional Meeting*, Anchorage, Alaska, USA, May 7-11, 2011.

Taoutaou, S., Osman, T.M., Mjthab, M., and Succar, N., Well integrity in heavy oil wells: Challenges and solutions, Paper SPE 137079-MS presented at the *Canadian Unconventional Resources and International Petroleum Conference*, Calgary, Alberta, Canada, 19-21 October 2010.

Thimm, H.F., Low pressure SAGD operations, Paper 2004-186 presented at the *Petroleum Society's 5th Canadian International Petroleum Conference*, Calgary, AB, Canada, June 8-10, 2004.

Tingay, M., Müller, B., Reinecker, J., Heidbach, O., Wenzel, F., and Fleckenstein, P., The World Stress Map Project 'Present-day Stress in Sedimentary Basins' initiative: building a valuable public resource to understand tectonic stress in the oil patch, *The Leading Edge*, vol. **24**, pp. 1276-1282, 2005.

Tissot, B., and Welte, D.N., *Petroleum formation and occurrence*, 2nd ed., Springer Verlag, Heidelberg, p. 699, 1984.

Tokarska, A., Investigations on the processing vacuum residue and its mixtures and coal tars, *Fuel*, vol. **75**, no. 9, pp. 1094-1100, 1996.

Torabzadeh, S.J., Kumar, M., and Hoang, V.T., Performance correlations for steamflood field projects, In: *Proceedings of the SPE California Regional Meeting*, Ventura, California, April 4-6, 1990.

Touhidi-Baghini, A., *Absolute permeability of McMurray Formation oil sands at low confining stresses*, Ph.D. thesis, Department of Civil Engineering, University of Alberta, Edmonton, Alberta, p. 339, 1998.

Toulhoat, H., Szymanski, R., and Plumail, J.C., Interrelations between initial pore structure, morphology and distribution of accumulated deposits, and lifetimes of hydrodemetallisation catalysts, *Catalysis Today*, vol. 7, no. 4, pp. 531–568, 1990.

Towson, D.E., Canada's heavy oil industry technological revolution, Paper SPE 37972 presented at the *International Thermal Operations and Heavy Oil Symposium*, Bakersfield, California, USA, February 10-12, 1997.

Trautwein-Bruns, U., Schulze, K.C., Becker, S., Kukla, P.A., and Urai, J.L., In situ stress variations at the Variscan deformation front - Results from the deep Aachen geothermal well, *Tectonophysics*, vol. 493, pp. 196–211, 2010.

Turta, A.T., Coates, R., and Greaves, M., In situ combustion in the oil reservoirs underlain by bottom water, Review of the field and laboratory tests, Paper 2009-150 presented at the *Canadian International Petroleum Conference (CIPC) 2009*, Calgary, Alberta, Canada, June 16-18, 2009.

U.S. Energy Information Administration, *International Energy Outlook 2011*, EIA-DOE-0484(2012), Washington, DC, September 2011.

Union Oil Company, *Buffalo Creek scheme progress reports ER 81-17, 81-38, and 82-08*, Alberta Energy Resources Conservation Board (ERCB), Approval # 2367c, Calgary; 1981-82.

United States Congress, Office of Technology Assessment, EOR potential in the United States, p. 234, 1978.

Uwiera-Gartner, M.M.E., Carlson, M.R., Walters, D., and Palmgren, C.T.S., Geomechanical simulation of caprock performance for a proposed, low pressure, steam-assisted gravity drainage pilot project, Paper SPE 148886-MS presented at the *Canadian Unconventional Resources Conference*, Calgary, Alberta, Canada, November 15-17, 2011.

Vallés, H.R., *A neural networks method to predict activity coefficients for binary systems based on molecular functional group contribution*, M.Sc. Thesis, University of Puerto Rico, 2006.

van Golf-Racht, T.D., *Fundamentals of fractured reservoir engineering*, Elsevier, Amsterdam, 1996.

van Heel, A.P.G., van Dorp, J.J., and Boerrigter, P.M., Heavy oil recovery by steam injection in fractured reservoirs, In: *Proceedings of the 2008 SPE/DOE IOR Symposium*, Tulsa, Oklahoma, USA, April 19-23, 2008.

Vaziri-Moghaddam, H., Seyrafian, A., Taheri, A., and Motiei, H., Oligocene-Miocene ramp system (Asmari Formation) in the NW of the Zagros basin, Iran: Microfacies, paleoenvironment and depositional sequence, *Revista Mexicana de Ciencias Geológicas*, vol. **27**, no. 1, pp. 56–71, 2010.

Veil, J.A., and Quinn, J.J., *Water issues associated with heavy oil production*, Argonne National Laboratory, U S. Department of Energy, National Energy Technology Laboratory, p. 64, 2008.

Veith, E.J., Releasing the value of heavy oil and bitumen: HTL upgrading of heavy to light oil, Paper 2006-727 presented at the *1st Heavy Oil Congress*, Beijing, China, November 5-8, 2006.

Vigrass, L.W., Geology of Canadian heavy oil sands, *The American Association of Petroleum Geologists Bulletin*, vol. **52**, no. 10, pp. 1984–1999, 1968.

Vogel, J.V., Simplified heat calculations for steamfloods, *Journal of Petroleum Technology*, vol. **36**, no. 7, pp. 1127–1136, 1984.

Waheed, A., El-Assal, H., Negm, E., Sanad, M., and Sanad, O., Practical methods to optimizing production in a heavy oil carbonate reservoir: Case study from Issaran field, Eastern desert, Egypt, Paper SPE 69730 presented at the *2001 SPE International Thermal*

Operations and Heavy Oil Symposium, Porlamar, Margarita Island, Venezuela, March 12-14, 2001.

Waldorf, D.M., Effect of steam on permeabilities of water-sensitive formations, *Journal of Petroleum Technology*, vol. **17**, no. 10, pp. 1219–1222, 1965.

Wallach, J., Benn, K., and Rimando, R., Recent, tectonically induced, surficial stress-relief structures in the Ottawa-Hull area, Canada, *Canadian Journal of Earth Sciences*, vol. **32**, pp. 325–333, 1995.

Walters, D., Wang, J., and Settari, A., A geomechanical methodology for determining maximum operating pressure in SAGD reservoirs, Paper SPE 157855-MS presented at the *SPE Heavy Oil Conference*, Calgary, Alberta, Canada, June 12-14, 2012.

Wang, Y., and Dusseault, M.B., Response of a circular opening in a friable low-permeability medium to temperature and pore pressure changes, *International Journal of Analytical & Numerical Methods in Geomechanics*, vol. **19**, pp. 157–179, 1995.

Wang, Z., Chapter 3, *Seismic properties of carbonate rocks*, From: Carbonate seismology (Editors: Palaz I. and Marfurt K.J.), Geophysical Developments Series, no. 6, Society of Exploration Geophysicists, Tulsa, Oklahoma, 1997.

Warren, J.E., and Root, P.J., 1963, The behavior of naturally fractured reservoirs, *SPE Journal*, vol. **3**, no. 3, pp. 245–255.

Wei, Y., Bai-quan, L., and Hai-jin, W., Study of the stress relief and gas drainage limitation of a drilling and the solving mechanism, *Procedia Earth and Planetary Sciences*, vol. **1**, pp. 371–376, 2009.

Weissman, J.G., and Kessler, R.V., Downhole heavy crude oil hydroprocessing, *Applied Catalysis A*, vol. **140**, no. 1, pp. 1–16, 1996.

Weissman, J.G., Kessler, R.V., Sawicki, R.A., Belgrave, J.D.M., Laureshen, C.J., Mehta, S.A., Moore, R.G., and Ursenbach, M.G., Down hole catalytic upgrading of heavy crude oil, *Energy & Fuels*, vol. **10**, no. 4., pp. 883–889, 1996.

- Wightman, D.M., Attalla, M.N., Desmond, A.W., Strobl, R.S., Habtemicael, B., Cotterill, D.K., and Berezsniuk, T., *Resource characterization of the McMurray/Wabiskaw deposit in the Athabasca Oil Sands area: A synthesis*, AOSTRA Technical Publication Series **10**, p. 142, 1995.
- Worldwide EOR Survey, *Oil & Gas Journal*, vol. **102**, no. 14, pp. 53–65, 2004.
- Worldwide EOR Survey, *Oil & Gas Journal*, vol. **104**, no. 15, pp. 45–57, 2006.
- Worldwide EOR Survey, *Oil & Gas Journal*, vol. **106**, no. 13, pp. 47–59, 2008.
- Worldwide EOR Survey, *Oil & Gas Journal*, vol. **94**, no. 16, pp. 45–61, 1996.
- Worldwide EOR Survey, *Oil & Gas Journal*, vol. **96**, no. 16, pp. 59–74, 1998.
- Worldwide reserves grow; oil production climbs in 2003, *Oil & Gas Journal*, vol. **101**, no. 49, December 22, 2003.
- Wu, S.S., Analysis on transient thermal stresses in an annular fin, *Journal of Thermal Stresses*, vol. **20**, no. 6, pp. 591–615, 1997.
- Wu, T., Permeability prediction and drainage capillary pressure simulation in sandstone, PhD Dissertation, Texas A&M University, p. 183, 2004.
- Xia, T.X., and Greaves, M., Downhole upgrading Athabasca tar sand bitumen using THAI, SARA Analysis, Paper SPE 69693 presented at the *2001 SPE International Thermal Operations and Heavy Oil Symposium*, Porlamar, Margarita Island, Venezuela, 12 March 2001.
- Xia, T.X., and Greaves, M., Upgrading Athabasca tar sand using Toe-to-Heel Air Injection, *Journal of Canadian Petroleum Technology*, vol. **41**, no. 8, 2002.
- Xia, T.X., Greaves, M., and Turta, A.T., Main mechanism for stability of THAI-Toe-to-Heel Air Injection, Paper 2003-030 presented at the *Petroleum Society's Canadian International Petroleum Conference 2003*, Calgary, Alberta, Canada, June 10-12, 2003.

- Xu, Y., and Chopra, S., Deterministic mapping of reservoir heterogeneity in Athabasca oil sands using surface seismic data, *The Leading Edge*, vol. **27**, no. 9, 2008, pp. 1186–1191.
- Yavuz, H., Demirdag, S., and Caran, S., Thermal effect on the physical properties of carbonate rocks, *International Journal of Rock Mechancis & Mining Science*, vol. **47**, pp. 94–103, 2010.
- Yin, S., Dusseault, M.B., and Rothenburg, L., Fully coupled numerical modeling of ground surface uplift in steam injection, *Journal of Canadian Petroleum Technology*, vol. **49**, no. 1, pp. 16–21, 2010.
- Yin, S., Dusseault, M.B., and Rothenburg, L., Thermal reservoir modeling in petroleum geomechanics, *International Journal of Numerical & Analytical Methods in Geomechanics*, vol. **33**, no. 4, pp. 449–485, 2009a.
- Yin, S., Towler, B.F., Dusseault, M.B., and Rothenburg, L., Numerical experiments on oil sands shear dilation and permeability enhancement in a multiphase thermoporoelastoplasticity framework, *Journal of Petroleum Science and Engineering*, vol. 69, no. (3-4), pp. 219–226, 2009b.
- Yortsos, Y.C., and Gavalas, G.R., Analytical modeling of oil recovery by steam injection: Part I - Upper bounds, *SPE Journal*, vol. **21**, no. 2, pp. 162–178, 1981.
- Yortsos, Y.C., and Gavalas, G.R., Analytical modeling of oil recovery by steam injection: Part 2–Asymptotic and approximate solutions, *SPE Journal*, vol. **21**, no. 2, pp. 179–190, 1981.
- Yortsos, Y.C., *Visualization and simulation of immiscible displacement in fractured systems using micromodels: Steam injection*, DOE/BC/14899-25, 1995.
- Zaykinaa, R.F., Zaykina, Yu.A., Mamonovaa, T.B., and Nadirov, N.K., Radiation thermal processing of high viscous oil from Karazhanbas field, *Radiation Physics and Chemistry*, vol. **60**, no. 3, pp. 211–221, 2001.

Zekri, A.Y., and Chaalal, O., Thermal stress of carbonate rocks: An experimental approach, Paper SPE 68777 presented at the *SPE Western Regional Meeting*, Bakersfield, California, March 26-30, 2001.

Zendehboudi, S., Ahmadi, M.A., James, L., and Chatzis, I., Prediction of condensate-to-gas ratio for retrograde gas condensate reservoirs using artificial neural network with particle swarm optimization, *Energy & Fuels*, vol. **26**, no. 6, pp. 3432–3447, 2012.

Zendehboudi, S., Chatzis, I., Shafiei, A., and Dusseault, M.B., Empirical modeling of gravity drainage in fractured porous media, *Energy & Fuels*, vol. **25**, no. 3, pp. 1229–1241, 2011.

Zhang, L.Y., Mao, X.B., Lu, A.H., Experimental study on the mechanical properties of rocks at high temperature, *Science in China Series E – Technological Sciences*, vol. **52**, no. 3, pp. 641–646, 2009.

Zhongchun, L., Jirui, H., Jianglong, L., and Qian, C., Study of residual oil in Tahe 4th Block karstic/fractured heavy oil reservoir, Paper SPE 151592 presented at the *North Africa Technical Conference and Exhibition*, Cairo, Egypt, February, 20-22, 2012.

Zhou, Y., Lin, Y., and Chen, G., Steam stimulation pilot in the Cao-20 fractured limestone with extra heavy oil, Paper 1998-131 presented at the *7th UNITAR International Conference on Heavy Crude and Tar Sands*, Beijing, China, October 27-30, 1998.

Zhu, J., Che, C., Yang, H., and Liu, C., China's endowment-1: China assesses conventional resources in 115 basins, *Oil & Gas Journal*, vol. **108**, no. 14, p. 7, 2010.